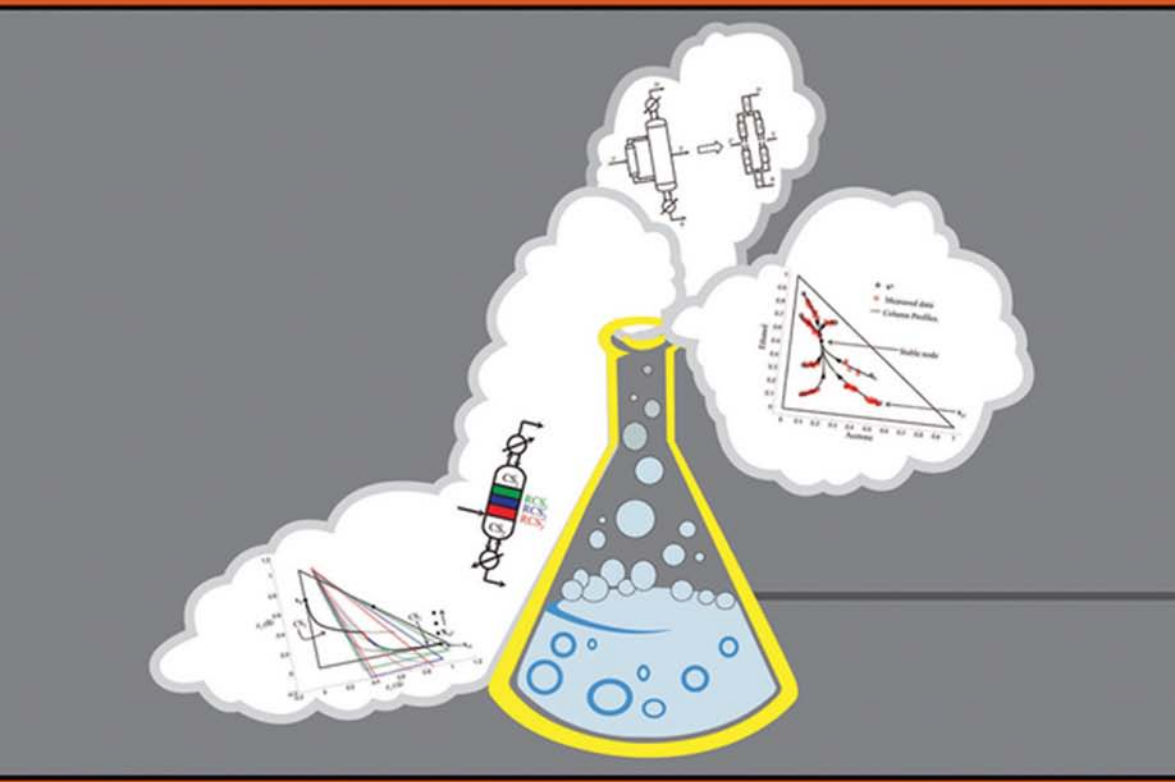
WWW.
LINK AVAILABLE

Understanding Distillation Using Column Profile Maps

Daniel Beneke, Mark Peters, David Glasser, and Diane Hildebrandt



WILEY

EBOOKS ACADÉMICOS

COMPS
CENTRE OF MATERIAL AND PROCESS SYNTHESIS

UNDERSTANDING DISTILLATION USING COLUMN PROFILE MAPS

UNDERSTANDING DISTILLATION USING COLUMN PROFILE MAPS

DANIEL BENEKE

MARK PETERS

DAVID GLASSER

DIANE HILDEBRANDT

Centre of Material and Process Synthesis (COMPS)
University of the Witwatersrand
Johannesburg, South Africa



A JOHN WILEY & SONS, INC., PUBLICATION

Copyright © 2013 by John Wiley & Sons, Inc. All rights reserved.

Published by John Wiley & Sons, Inc., Hoboken, New Jersey.
Published simultaneously in Canada.

No part of this publication may be reproduced, stored in a retrieval system, or transmitted in any form or by any means, electronic, mechanical, photocopying, recording, scanning, or otherwise, except as permitted under Section 107 or 108 of the 1976 United States Copyright Act, without either the prior written permission of the Publisher, or authorization through payment of the appropriate per-copy fee to the Copyright Clearance Center, Inc., 222 Rosewood Drive, Danvers, MA 01923, (978) 750-8400, fax (978) 750-4470, or on the web at www.copyright.com. Requests to the Publisher for permission should be addressed to the Permissions Department, John Wiley & Sons, Inc., 111 River Street, Hoboken, NJ 07030, (201) 748-6011, fax (201) 748-6008, or online at http://www.wiley.com/go/permission.

Limit of Liability/Disclaimer of Warranty: While the publisher and author have used their best efforts in preparing this book, they make no representations or warranties with respect to the accuracy or completeness of the contents of this book and specifically disclaim any implied warranties of merchantability or fitness for a particular purpose. No warranty may be created or extended by sales representatives or written sales materials. The advice and strategies contained herein may not be suitable for your situation. You should consult with a professional where appropriate. Neither the publisher nor author shall be liable for any loss of profit or any other commercial damages, including but not limited to special, incidental, consequential, or other damages.

For general information on our other products and services or for technical support, please contact our Customer Care Department within the United States at (800) 762-2974, outside the United States at (317) 572-3993 or fax (317) 572-4002.

Wiley also publishes its books in a variety of electronic formats. Some content that appears in print may not be available in electronic formats. For more information about Wiley products, visit our web site at www.wiley.com.

Library of Congress Cataloging-in-Publication Data:

Beneke, Daniel, 1985-
Understanding distillation using column profile maps / Daniel Beneke, Mark Peters, David Glasser, Diane Hildebrandt, Centre of Material and Process Synthesis (COMPS), University of the Witwatersrand, Johannesburg.
pages cm
Includes bibliographical references and index.
ISBN 978-1-118-14540-1 (cloth)
1. Distillation–Simulation methods. 2. Distillation apparatus–Design and construction. I. Title.
TP156.D5B46 2013
660'.28425–dc23

2012023640

Printed in the United States of America

10 9 8 7 6 5 4 3 2 1

CONTENTS

PREFACE xiii

NOMENCLATURE AND ABBREVIATIONS xix

ABOUT THE AUTHORS xxiii

1 INTRODUCTION 1

1.1 Context and Significance / 1
1.2 Important Distillation Concepts / 4
1.2.1 A Typical Column / 5
1.2.2 Complex Columns / 6
1.2.3 Vapor–Liquid Equilibrium / 7
1.3 Summary / 12
References / 12

2 FUNDAMENTALS OF RESIDUE CURVE MAPS 15

2.1 Introduction / 15
2.2 Batch Boiling / 16
2.3 The Mass Balance Triangle (MBT) / 17
2.4 The Residue Curve Equation / 19
2.4.1 Derivation / 19
2.4.2 Approximation to Equilibrium / 20

2.5 Residue Curve Maps / 21
2.5.1 Constant Relative Volatility Systems / 21
2.5.2 Nonideal Systems / 24
2.5.3 Numerical Integration / 24
2.6 Properties of Residue Curve Maps / 25
2.6.1 Separation Vector Field / 25
2.6.2 Stationary Points / 26
2.6.3 Isotherms / 29
2.6.4 Other Properties of RCMs / 30
2.7 Applicability of RCMs to Continuous Processes / 30
2.7.1 Total Reflux Columns / 30
2.7.2 Infinite Reflux Columns / 33
2.7.3 Bow-Tie Regions / 35
2.7.4 Column Sequencing at Infinite Reflux / 38
2.8 Limitations of RCMs / 39
2.8.1 Applications / 39
2.9 Residue Curve Maps: The Bigger Picture / 40
2.9.1 Extending the Axes / 40
2.9.2 Discontinuity / 43
2.9.3 Thermodynamic Models in Negative Space / 43
2.9.4 Use of Negative Compositions / 44
2.10 Summary / 46
References / 47

3 DERIVATION AND PROPERTIES OF COLUMN PROFILE MAPS 48

3.1 Introduction / 48
3.2 The Column Section (CS) / 49
3.3 The Difference Point Equation (DPE) / 51
3.3.1 The Generalized CS / 51
3.3.2 Constant Molar Overflow / 52
3.3.3 Material Balances / 52
3.4 Column Profile Maps / 54
3.4.1 Constant Relative Volatility Systems / 55
3.4.2 Nonideal Systems / 59
3.5 The Effect of CPM Parameters / 61
3.5.1 The Net Flow (Δ) / 61
3.5.2 The Difference Point (X_Δ) / 62
3.5.3 The Reflux Ratio (R_Δ) / 66

3.6 Properties of Column Profile Maps / 67
3.6.1 The Relationship Between RCMs and CPMs / 67
3.6.2 Vector Fields / 68
3.6.3 Pinch Points / 69
3.6.4 Isotherms / 71
3.6.5 Transformed Triangles / 72
3.7 Pinch Point Loci / 75
3.7.1 Analytical Solutions / 75
3.7.2 Graphical Approach / 79
3.8 Some Mathematical Aspects of CPMs / 80
3.8.1 Eigenvalues and Eigenvectors / 80
3.8.2 Nature of Pinch Points / 83
3.9 Some Insights and Applications of CPMs / 84
3.9.1 Column Stability / 85
3.9.2 Node Placement / 87
3.9.3 Sharp Splits / 88
3.10 Summary / 89
References / 89

4 EXPERIMENTAL MEASUREMENT OF COLUMN PROFILES 91

4.1 Introduction / 91
4.2 The Rectifying Column Section / 92
4.2.1 The Batch Analogy / 92
4.2.2 Experimental Setup and Procedure / 94
4.2.3 Experimental Results / 96
4.3 The Stripping Column Section / 98
4.4 Validation of Thermodynamic Models / 103
4.5 Continuous Column Sections / 105
4.5.1 Apparatus / 106
4.5.2 Experimental Results / 112
4.5.3 Temperature Inversion / 113
4.6 Summary / 114
References / 115

5 DESIGN OF SIMPLE COLUMNS USING COLUMN PROFILE MAPS 116

5.1 Introduction / 116
5.2 Absorbers and Strippers / 117

5.2.1 Absorption Towers / 118
5.2.2 Stripping Towers / 124
5.2.3 Discussion / 128
5.3 Simple Column Design / 128
5.3.1 External Mass Balance / 128
5.3.2 Internal Mass Balance: Column Section Interaction / 130
5.3.3 Finite Reflux Design / 132
5.3.4 Design Offshoots / 137
5.4 Azeotropic Systems / 141
5.5 Constant Relative Volatility Systems / 145
5.5.1 Minimum Reflux Design Using TTs / 145
5.5.2 Design Using Eigenvectors / 153
5.6 Summary / 154
References / 155

6 DESIGN OF COMPLEX COLUMNS USING COLUMN PROFILE MAPS 157

6.1 Introduction / 157
6.2 Distributed Feed Addition / 158
6.2.1 Column Section Breakdown / 158
6.2.2 The Effect on the Reflux Ratio (R_{Δ}) / 159
6.2.3 The Effect on the Difference Point ($\mathbf{X}_{\Delta}$) / 160
6.2.4 Feasible Designs / 162
6.2.5 Potential Benefits and Limitations / 166
6.2.6 Discussion / 173
6.3 Sidestream Withdrawal / 175
6.3.1 Refluxes and Difference Points / 176
6.3.2 Preliminary Design Considerations / 177
6.3.3 Design Procedure / 180
6.4 Thermally Coupled Columns: Side Rectifiers and Strippers / 184
6.4.1 Column Section Breakdown / 185
6.4.2 Degrees of Freedom / 186
6.4.3 Difference Points / 186
6.4.4 Refluxes and Net Flow / 187
6.4.5 General Design Procedure / 190
6.4.6 Design with Transformed Triangles / 193
6.5 Summary / 205
References / 205

7 DESIGN OF FULLY THERMALLY COUPLED COMPLEX COLUMNS USING COLUMN PROFILE MAPS 206

7.1 Introduction / 206
7.2 A Simplified Infinite Reflux Case / 208
7.2.1 All CSs at Infinite Reflux / 208
7.2.2 Overall Infinite Reflux / 213
7.3 General Petlyuk Design / 216
7.3.1 Degree of Freedom Analysis and Variable Selection / 217
7.3.2 Net Flow Patterns / 218
7.3.3 Difference Point Behavior and Placement / 223
7.3.4 Reflux Ratios / 228
7.3.5 Properties of Variables in Φ-Space / 230
7.3.6 Feasibility Conditions / 234
7.3.7 Putting it all Together / 236
7.4 Sharp Split Petlyuk Design Using TTs / 240
7.4.1 Feasibility Criteria Using TTs / 240
7.4.2 Design Implications / 245
7.5 Insights into Kaibel Column Design / 250
7.5.1 Structure and CS Breakdown / 252
7.5.2 Similarities to the Petlyuk / 252
7.5.3 Net Flow Patterns / 253
7.5.4 Sharp Split Constraints / 256
7.6 Summary / 258
References / 259

8 REACTIVE DISTILLATION DESIGN USING COLUMN PROFILE MAPS 261

8.1 Introduction / 261
8.2 Simple Reactive Distillation / 262
8.2.1 Extending the Residue Curve Map / 262
8.2.2 Characteristics of the Reaction Vector Field / 265
8.2.3 Overall Reactive Distillation Vector Field / 266
8.2.4 Simple Reactive Distillation Design / 269
8.2.5 Zero-Order Reactions—An Interesting Analogy / 273
8.3 Reactive Column Sections / 275
8.3.1 Definition / 275
8.3.2 The Reactive Difference Point Equation / 276
8.3.3 RCS Transition / 281

8.3.4 Conserved Moles and Low Reaction Heat—A Simplified Case / 284
8.3.5 Column Design / 285
8.3.6 Column Stability / 292
8.4 Summary / 293
References / 294

9 APPLICATION OF COLUMN PROFILE MAPS TO ALTERNATIVE SEPARATION PROCESSES: MEMBRANE PERMEATION 296

9.1 Introduction / 296
9.2 Membrane Permeation / 297
9.3 Generalized Membrane Column Sections / 299
9.4 Theory / 299
9.4.1 Membrane Column Sections / 299
9.4.2 The Difference Point Equation for an MCS / 300
9.4.3 Permeation Modeling / 301
9.4.4 Properties of the MDPE / 303
9.5 MCS Profiles: Total Reflux / 304
9.5.1 Operating Conditions / 304
9.5.2 Mathematics / 304
9.5.3 Membrane Residue Curve Map / 304
9.6 Column Section Profiles: Finite Reflux / 306
9.6.1 Operating Conditions / 306
9.6.2 Mathematics / 307
9.6.3 Membrane Column Profile / 308
9.6.4 Pinch Point Loci / 308
9.6.5 Analysis of Column Profile / 309
9.6.6 Pinch Points / 311
9.6.7 Further Column Profiles / 312
9.6.8 Variations in $\mathbf{X}_{\Delta}$ and r_{Δ} / 312
9.7 Conclusions / 314
9.8 Example: Design of Hybrid Systems Using Distillation-Membrane Processes / 315
9.8.1 Introduction / 315
9.8.2 The Methanol/Butene/MTBE System / 316
9.8.3 Design of a Hybrid Configuration / 318
9.8.4 Conclusion / 325
References / 326

10 CONCLUDING REMARKS **328**

10.1 Overall Conclusions / 328
10.2 Limitations / 329
10.3 Extensions and the Way Forward / 330
References / 330

APPENDIX A: DODS SOFTWARE PACKAGE **331**

APPENDIX B: NRTL PARAMETERS AND ANTOINE COEFFICIENTS **345**

INDEX **349**

PREFACE

BACKGROUND

The Centre of Materials and Process Synthesis (COMPS) was founded in 1998 by Professors Hildebrandt, Glasser, and Moys as a research group within the University of the Witwatersrand that would provide a platform for interaction between university expertise and industry. With the initiative being to reduce financial dependence of research on grant-awarding foundations, COMPS was set up as a channel to enhance scientific expertise through consulting, corporate training, and process development with industry. This endeavor has proven to be extremely beneficial to the research output of the group, at one time supporting as many as 40 graduate students, mostly supervised by Professors Hildebrandt and Glasser. The group has been at the forefront of several key areas of the field of process engineering, including reaction engineering and the attainable region, comminution, biosystems, Fischer–Tropsch synthesis, process synthesis, and of course separation synthesis.

This book is a culmination of approximately 15 years of research in the field of separation synthesis from the COMPS team. Many graduate students have passed through COMPS' doors during these times that have made valuable contributions to the work presented in this book. In particular, Simon Holland and Michaela Vrey developed much of the early work and fundamentals of what is now known as column profile maps (CPMs), which forms the heart of this book. These maps are thought to be a new take on distillation, allowing a designer the freedom to design virtually any distillation structure. The refined form of the work that is presented in this book is the result of countless research meetings, arguments, debates, and scribbling. Through all of this, however, all that have been involved with the work

have found it to be stimulating, exciting, and thought provoking, and the authors hope that this has been transferred to the reader.

The origin of our research into column profile maps began (inadvertently) due to a project initiated by John Marriot from Sasol. The project was to look at the design and optimization of divided wall columns. We originally started trying to simulate these columns on Aspen Plus® and found that we could not get converged designs easily (or even at all!). We went back to the drawing board and developed code to model a section of the column. Simon Holland worked on this as a graduate student for his M.Sc. Every week his supervisors, Professors David Glasser and Diane Hildebrandt, would meet with the separations research group and Simon would show his plots where his liquid composition profiles predicted negative mole fractions! David and Diane disbelieved his results and sent him back week after week to check his code—it was obviously wrong! After some months, seeing Simon's predicting negative mole fractions in the liquid composition (again) and after him claiming (again) that there was no fault in his code, Diane sat down one evening to prove to Simon why his code had to be wrong, and indeed found that there was no mathematical reason why mole fractions had to stay positive. After drawing many triangles and mixing and separation vectors, it eventually dawned on us that there was a beautiful geometry sitting behind the column profiles, and further more that Simon's code was, in fact, correct.

We eventually were able to answer the question that was posed to us initially, namely, the design and optimization of divided wall columns, and indeed were able to answer many other interesting and important questions in the field of separations. We are very grateful to John Marriot and Sasol for inadvertently setting us on this exciting and important area of research.

TARGET AUDIENCE

This book has been written from the point of view that the student/reader is familiar with basic distillation and vapor–liquid equilibrium concepts. The material is suitable for use in chemical engineering curriculums as an advanced undergraduate, or a graduate level course. COMPS has used and adapted some of this material for these purposes as well as for industrial short courses, and the feedback has been largely positive. We have found that engineers with a more industrial background also find the concepts and ideas expressed in the book enlightening. There are many instructive examples and tutorials on problem solving, and many of them include use of the DODS software package. This too is a useful learning tool.

EXPECTED OUTCOMES

The authors hope that with this book the reader is comfortable with the design of a variety of distillation columns. We have attempted to include and present solutions for many of the most prevalent problems encountered in academic and industrial

literature. This includes distillation by simple columns, side rectifiers/strippers, multiple feed columns, and fully thermally coupled columns. Moreover, advanced topics such as reactive distillation, membrane permeation, and validation of thermodynamic models are also dealt with. For each of the aforementioned processes we present design techniques, solution strategies and insights that may be gained when using the CPM technique.

It should be mentioned that the majority of the work presented here is graphically based simply because it is easier to grasp column interactions and behavior when approached from this point of view. However, this need not be a limitation for the methods. The authors would also like to stress that it is not necessarily the specific material and problems presented in the book that are important, but more the tools that the reader should be equipped with. The concepts we present simply put tools into the designer's hand for him/her to create a unique column or separation structure that may solve his/her particular separation problem. For instance, both distributed feed and reactive distillation columns are discussed independently, although it is of course entirely possible to conceive of a reactive distributed feed system, which is not discussed. The tools in this book will thus first allow the reader understand, analyze, and design well-known and frequently encountered distillation problems. Second, the tools can be used to synthesize and develop new systems that perhaps have not even been thought of yet. This principle applies to virtually all the work in this book and the reader is urged to explore such concepts.

EXAMPLES AND TUTORIALS

The primary purpose of this book is to teach the column profile map method to students and engineers alike. As such, the text includes numerous examples (with solutions) that elucidate clearly how a particular problem should be solved using the column profile map method. In many, but not all, of these examples it is possible for the user to reproduce or follow the principles of the example at hand using the appropriate software package (as discussed in Section "Software").



Tutorials are indicated with the www symbol to the left, and all additional text will be available at booksupport.wiley.com by entering ISBN 9781118145401. The main purpose of each tutorial is for the user to become familiarize with the ideas discussed in this book through experimentation with the appropriate DODS software package (as discussed in Section "Software"). When coming across the tutorial symbol in the book, the user should then try and reproduce the applicable figure using one of the DODS packages. This will simultaneously assist the user in becoming comfortable with the ideas in text body as well as the accompanying software.

SOFTWARE

Most of the examples and tutorials found in this book have been written to be used in conjunction with the Design and Optimization of Distillation Systems (DODS)

software package. This package has been developed specifically for this book and should assist the reader in understanding sometimes complex behavior quicker. In all, there are five subcomponents of the package:

(1) DODS-ProPlot (A *Pro*file *Plot*ting tool that allows one to construct CPMs and find pinch points)
(2) DODS-SiCo (A tool for designing *Si*mple *Co*lumns)
(3) DODS-DiFe (A tool for designing *Di*stributed *Fe*ed columns)
(4) DODS-SiSt (A tool for designing *Si*de *St*rippers)
(5) DODS-SiRe (A tool for designing *Si*de *Re*ctifiers).

The DODS package is fairly intuitive and easy to use once the fundamental concepts of each package are grasped. In Appendix A, a manual is provided that gives the user instructions on how the DODS package should be installed and operated.

ACKNOWLEDGMENTS

This book comprises of the work and ideas of many talented researchers who have worked at COMPS, without whom this manuscript would not have been possible. Specifically we, the authors, would like to mention, chapter by chapter, the following persons who were involved with the original development of the work:

- *Chapter 3*: Simon Holland, Michaela Vrey
- *Chapter 4*: Tsepho Modise, Jean Mulopo, Cameron Wilson
- *Chapter 6*: Simon Holland, Chan Yee Ma
- *Chapter 7*: Simon Holland, Ronald Abbas
- *Chapter 8*: Jean Mulopo

Furthermore, the authors would like to thank the following graduate and post-doctoral students for their patience, suggestions, and discussions, all of which have contributed to writing a clear manuscript: Emmanuel Kasese, Naadhira Seedat, Edmund Bono, Celestin Sempuga, Chan Yee Ma, and Neil Stacey. A very special thanks to Dr. Brendon Hausberger for his valuable contributions in making certain that the message we are trying to convey is unambiguous and concise. We would also like to thank Darryn Peters for his contributions in the preparation of the cover artwork, as well as the editing of every figure within the book.

Several organizations have supported this work financially, both directly and indirectly, and we are grateful to them. These include the University of the Witwatersrand, Johannesburg, South Africa, The National Research Foundation (NRF) of South Africa, Sasol Technology, the South African Research Chair

Initiative (SARChI) for Sustainable Process Engineering, and the Technology and Human Resources for Industry Programme (THRIP).

Daniel Beneke
Mark Peters
David Glasser
Diane Hildebrandt

Johannesburg, South Africa

NOMENCLATURE AND ABBREVIATIONS

Scalars are given in *italics*.

Vectors are given in **bold**.

Symbols		
a	Activity	–
A	Dimensionless membrane area	–
B	Bottoms flowrate	mol/s
$\dot{B}$	Product (bottoms) removal rate	mol/s
C_P	Specific heat capacity at constant pressure	kJ/mol K
D	Distillate flowrate	mol/s
$\dot{D}$	Distillate (feed) addition rate	mol/s
$\mathbf{e}$	Eigenvector	–
F	Feed flowrate	mol/s
$\dot{F}$	Feed addition rate	mol/s
H	Liquid hold-up	mol
ΔH_{RXN}	Molar heat of reaction at 298 K	kJ/mol
ΔH_{VAP}	Molar latent heat of vaporization at normal pressure	kJ/mol
$\mathbf{I}$	Identity matrix	–
J	Flux through a membrane	mol/s m^2
$\mathbf{J}$	Jacobian matrix	–
k_f	Reaction rate constant	s^{-1}
K	Separation equilibrium constant	–
K_{eq}	Reaction equilibrium constant	–
L	Liquid flowrate	mol/s

$\mathbf{M}$	Mixing vector	–
N	Number of stages, or position	–
N	Total number of CSs in a Distributed Feed Column	–
P	Pressure	Pa
$P(A)$	(Chapter 9) Permeate flowrate, as a function of position	mol/s
P'_i	Permeability of component i	mol m/s m^2 Pa
P^{VAP}	Vapor pressure	Pa
PS	Total number of product streams	–
Q	Liquid fraction of the feed	–
Q	Heat load or duty	kW
$Q(t)$	Heat input rate	kW
R	(Chapter 4) Reflux ratio [batch processes]	–
R	(Chapter 8) Reaction rate	s^{-1}
$\underline{R}$	Dimensionless reaction rate	–
r_Δ	(Chapter 9) Reflux ratio, as a function of position	–
$R(A)$	Retentate flowrate, as a function of position	mol/s
$\mathbf{R}$	Reaction vector	–
R_Δ	Reflux ratio	–
S	Reboil ratio	–
S	Sidestream flowrate	mol/s
$\mathbf{S}$	Separation vector	–
T	Time	s
T	Temperature	K
V	Stoichiometric coefficient	–
$\mathbf{V}$	(vector of) Stoichiometric coefficients	–
V	Vapor flowrate	mol/s
$\dot{V}$	Vapor removal rate	mol/s
X	Liquid phase molar fraction (individual species)	–
$\mathbf{X}$	(vector of) Liquid phase molar fractions	–
$\mathbf{x}^p$	Pinch points (or stationary points, or nodes) in liquid phase	–
$\mathbf{X_\Delta}$	Difference point	–
y	Vapor phase molar fraction (individual species)	–
$\mathbf{y}$	(vector of) Vapor phase molar fractions	–
$\mathbf{y}^p$	Vapor composition in equilibrium with $\mathbf{x}^p$	–
Δz	Height of packing, or position	m
z'	Dimensionless position	–

Greek Letters

α	Relative volatility	–
$\boldsymbol{\alpha}$	Vector of relative volatilities	–
α^M	Relative permeability	–
$\boldsymbol{\alpha}^M$	Vector of relative permeabilities	–
β	Mixing coefficient	–
δ	Effective membrane thickness	m
$\boldsymbol{\delta}$	Difference vector	–
Δ	Net flow in a CS	mol/s
ε	Reaction extent	mol/s

Φ_L	Liquid split ratio	–
Φ_V	Vapor split ratio	–
γ	Liquid phase activity coefficient	–
κ	Dimensionless reaction coefficient	–
λ	Eigen value	–
π	(Chapter 9) Pressure	Pa
θ	Reaction coefficient	s
$\boldsymbol{\theta}$	Zero matrix	–
τ	Ratio of enthalpies ($\Delta H_{\mathrm{VAP}}/\Delta H_{\mathrm{RXN}}$)	–
ξ	Warped, or dimensionless, time	–
ω	(Chapter 4) Warped, or dimensionless, time	–

Subscripts

Symbol	*Designates*
B	Bottom
D	Distillate
F	Final
F	Feed
I	Component *i*
J	Component *j*
K	Column section
K	Stream
Max	Maximum
MIN	Minimum
N	Stage, or position, *n*
nc	Number of components
P	Permeate
R	Reference component
R	Rectifying section
R	Retentate (Chapter 9)
S	Stripping section
S	Sidestream
SR	Side-rectifier
SS	Side-stripper
T	Total (Chapter 6)
T	Top
RXN	Reaction

Superscripts

Symbol	*Designates*
B	Bottom
O	Initial condition
T	Top

Abbreviations

Symbol	*Designates*
BP	Boiling point
BVM	Boundary value method
CMO	Constant molar overflow
CPM	Column profile map
CS	Column section
DODS	Design and optimization of distillation systems
DPE	Difference point equation
FP	Flow pattern
HETP	Height equivalent theoretical plate
LLE	Liquid–liquid equilibrium
MBT	Mass balance triangle
MCS	Membrane column section
MRF	Minimum reflux at feed
MTBE	Methyl tertiary-butyl ether
NRTL	Nonrandom two liquid
RCM	Residue curve map
RCS	Reactive column section
RCPM	Reactive column profile map
RDPE	Reactive difference point equation
R-RCM-M	Reactive residue curve map with mixing
R-RCM	Reactive residue curve map
TT	Transformed triangle
TT^4	Transformed tetrahedron
VLE	Vapor–liquid equilibrium

ABOUT THE AUTHORS

Daniel Beneke obtained an undergraduate degree in Chemical Engineering from the North West University, Potchefstroom (NWU-PUK), South Africa in 2007, and a Ph.D. in Chemical Engineering from the University of the Witwatersrand, Johannesburg, South Africa, in 2011, focusing on distillation synthesis using column profile maps. He has authored or coauthored seven papers and has also presented papers at numerous international conferences on this topic, and spent two semesters at the University of Illinois at Chicago (UIC), Chicago, IL, USA, as a visiting research scholar focusing on computational methods for column profile map design. In 2011, he received a Graduate Student Award from the Separations Division of the AIChE for his work in the field of distillation. Currently, Daniel is a Process Engineering Consultant at the Centre of Material and Process Synthesis (COMPS), based at the University of the Witwatersrand, where he is involved with process design for liquid fuel processes and separations research.

Mark Peters has authored a book in the field of industrial separations, entitled *Membrane Process Design Using Residue Curve Maps* (Wiley, 2011). He obtained his undergraduate degree in Chemical Engineering *cum laude* in 2003 and his Ph.D. in 2008 from the University of the Witwatersrand, Johannesburg, South Africa. Mark has spent time at the University of Illinois at Chicago (UIC), Chicago, IL, USA, as a research scholar. He has authored two scientific articles in the field of membrane separation, and has presented work at numerous internationally recognized conferences. He previously worked as a research process engineer at Sasol Technology, focusing on low-temperature Fischer–Tropsch (LTFT) gas-to-liquids (GTL) conversion. He is currently a Separations Consultant and Research engineer at the Centre of Material and Process Synthesis (COMPS), based at the University of the

Witwatersrand, where he is actively involved in separation research as well as innovative waste-to-energy processes.

David Glasser is a Professor of Chemical Engineering and director of the Centre of Material and Process Synthesis (COMPS) at the University of the Witwatersrand, Johannesburg, South Africa. He obtained his B.Sc. (Chemical Engineering) from the University of Cape Town and his Ph.D. from Imperial College in London. Along with Diane Hildebrandt, he pioneered the work in the attainable region (AR) approach for process synthesis and optimization. He has been awarded an A1 rating as a scientist in South Africa by the National Research Foundation (NRF) of South Africa. He coauthored the book *Membrane Process Design Using Residue Curve Maps* (Wiley, 2011). He has authored or coauthored more than 100 scientific papers and was editor-in-chief of the new book series on Chemical Engineering and Technology, published by Kluwer Academic Publishers of the Netherlands. He has authored a chapter published in *Handbook of Heat and Mass Transfer, Vol. 4, Advances in reactor design and combustion science*. He has worked in a very wide range of research areas, including optimization, chemical reactors, distillation, and process synthesis.

Diane Hildebrandt is the codirector for the Centre of Material and Process Synthesis (COMPS) at the University of the Witwatersrand, Johannesburg, South Africa. She obtained her B.Sc., M.Sc., and Ph.D. from the University of the Witwatersrand. She coauthored the book *Membrane Process Design Using Residue Curve Maps* (Wiley, 2011), and has authored or coauthored over 90 scientific papers and has supervised 60 postgraduate students. She has been both a plenary speaker and invited speaker at numerous local and international conferences. In 2005, she was recognized as a world leader in her area of research when she was awarded A rating by the National Research Foundation (NRF) of South Africa. She has been the recipient of numerous awards, including the Bill Neale-May Gold Medal from the South African Institute of Chemical Engineers (SAIChE) in 2000, and Distinguished Women Scientist Award presented by the Department of Science and Technology (DST), South Africa in 2009, and she was the first winner of the African Union Scientific Continental award Basic Science, Technology and Innovation category in the same year. In 2010, she was awarded the ASSAf "Science-for Society" Gold Medal Award. She has worked at Chamber of Mines, Sasol and the University of Potchefstroom and has spent a sabbatical at Princeton.

CHAPTER 1

INTRODUCTION

1.1 CONTEXT AND SIGNIFICANCE

In virtually any chemical process, whether it is in the food, pharmaceutical, biological or fuel industries, one or more chemical reactions take place to manufacture a wide range of products. Unfortunately, as nature would have it, these reactions invariably produce by-products which severely affect the quality and therefore the final market value of the final product. This generally means that some sort of separation scheme has to be devised to remove unwanted impurities and to upgrade the purity of the wanted component(s). Over the course of the past few decades, many technologies have become available and have been sufficiently developed to accomplish this task, including distillation, membrane separation, crystallization, and solvent extraction, among others. However, of all these methods of separations, distillation remains by far the most common, mainly because it is (relatively) well understood, and its economic properties on a large scale are at the present moment the most favorable. In short, distillation is a method of purifying binary and multicomponent mixtures into purer products by exploiting the difference in boiling points between the respective components.

In order to exploit the difference in boiling point temperatures (or vapor pressures), a distillation column generally requires heating. On a large scale this heating is not insignificant. In fact, Soave and Feliu have reported that in 1995 there were approximately 40,000 distillation columns in the United States [1], accounting for 90% of all industrial separations and consuming around 2.87×10^{18} J (2.87 million TJ), which is equivalent to 54 million tons of crude oil or a continuous

Understanding Distillation Using Column Profile Maps, First Edition. Daniel Beneke, Mark Peters, David Glasser, and Diane Hildebrandt.
© 2013 by John Wiley & Sons, Inc. Published 2013 by John Wiley & Sons, Inc.

power consumption of 91 GW [2]. In another study, it has been estimated that energy inputs into distillation columns in the United States accounts for approximately 3% of the entire country's energy consumption [3]. It is evident that by saving or recovering only 1% of the energy used by distillation columns, the impact would be significant. Apart from the obvious opportunities in reducing the energy requirements of a distillation train, it is also important to consider the capital investments associated to a particular separation, that is, the cost to physically construct the column, which is a strong function of the steel price at the time of construction. Capital and energy costs are generally opposing objectives, namely an energy-intensive column usually requires a smaller capital investment, and vice versa. A typical *simple*, one-feed-two-product continuous distillation column is shown in Figure 1.1.

The column shown in Figure 1.1 generally accepts an impure or mixed feed, and purifies it into two product streams, namely the *distillate* and *bottoms* streams. The distillate stream has a higher purity in low-boiling components while the bottoms stream is richer in high-boiling components.

Due to the tremendous costs associated to distillation, it is essential that a design engineer fully knows and understands the phenomena and processes at work. As such, graphical methods for designing distillation schemes have been especially

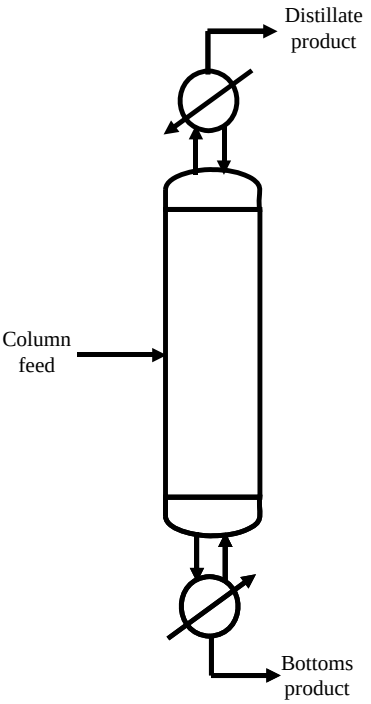


FIGURE 1.1 A typical continuous distillation column.

popular. In 1925, McCabe and Thiele published a landmark paper on a graphical design method for binary distillation [4], still used today as a quick means of understanding the relationship between energy and capital costs for simple distillation. Multicomponent distillation columns have been traditionally designed through the Underwood set of equations [5]. These equations assume constant relative volatility between all components, constant molar overflow, and a sharp separation between product streams, that is, one or more of the components are completely depleted in at least one of the products (sharp splits) [6]. These assumptions are very good approximations for a large number of industrial applications and these equations have been applied by numerous authors to a plethora of distillation structures [7–16].

Residue curve maps and distillation line maps have also been a useful graphical technique for screening ternary separation feasibility, especially for simple columns [17]. These maps are basically a range of trajectories that track the liquid compositions of the chemical species over time in a simple batch distillation operation and conveniently present the relationship between liquid and vapor phases, allowing one to quickly analyze potential splits, even for highly nonideal systems. Although these maps can tell much about the feasibility of separation, they have limitations in that they only give information at rather impractical conditions for the design engineer: infinite energy requirements when in continuous operation. This will become apparent especially in Chapters 2 and 3.

Numerous other design techniques have evolved over the years with varying degrees of complexity. One of these is the shortest stripping line method proposed by Lucia et al. [18], which states that the shortest stripping line will generally lead to the structure with lowest heat duty. Another technique, proposed in the 1980s by Doherty and coworkers, modeled sections above and below the feed stage of a simple column with a set of ordinary differential equations [19–23]. This approach, named the boundary value method, is relatively simple to employ (with modern day computers and mathematical software) and accepts virtually any phase equilibrium behavior and product distributions.

Other, so-called nonequilibrium models or rate-based models [24–28] have also received considerable attention. In short, these models do not assume perfect equilibrium on each stage in the distillation column, but rather use mass and heat transfer coefficients to compute the degree of fractionation. Although the nonequilibrium model is unquestionably more rigorous and precise, it may not allow the same insight and understanding afforded by its simpler, equilibrium counterpart. For the vast majority of distillation problems, the equilibrium model is quite sufficient, especially when the designer is still in the conceptual or "idea-generation" stage of the design.

Even advanced simulation packages such as Aspen Plus® or Hysys, although having undoubted modeling capabilities, have not provided much insight into the design of complex distillation systems. This is largely due to the fact that these packages require precise initialization values to ensure convergence to the specified product purities. Furthermore, because of the "black box" nature of these packages, the user often does not have any insight into the final solution and how one might go about improving it. Without the necessary experience or advanced knowledge of the

problem at hand, rigorously determining a column's feasibility or optimal point(s) of operation is a time-consuming, if not impossible, task.

Recently, in a series of papers by the Centre of Material and Process Synthesis (COMPS) at the University of the Witwatersrand, Johannesburg, a new distillation design technique was proposed, Column Profile Maps (CPMs) [29,30]. CPMs were derived from an adaptation of ordinary differential equations for simple columns first proposed by Doherty and coworkers [19–23]. The graphical, generalized CPM method has been shown to be extremely useful for designing and analyzing distillation systems, especially complex distillation systems [31,32]. As with the boundary value method, the CPM method is an equilibrium model, and does not require any simplifying assumptions regarding the phase equilibrium behavior, that is, the ideality of the liquid–vapor phase or the product distribution. Furthermore, highly insightful design parameters, such as the feed and product placements, are a product of the design and do not require the designer to specify them blindly beforehand. However, it is thought that the CPM method is perhaps most useful in devising new, previously unthought-of structures, since it is completely generalized and not limited to any particular piece of equipment.

The CPM method is furthermore not only confined to classical distillation schemes like those mentioned above but also the distillation research group at COMPS have used the original CPM ideas to design and analyze reactive distillation systems (Chapter 8) [33], hybrid membrane-distillation systems (Chapter 9) [34,35], experimental validation of thermodynamic models and column behavior (Chapter 4) [36–38], and fundamental work in the behavior of columns [39,40]. This book aims to summarize some of the key ideas the group have developed over the past few years, with the hope that other researchers, students, and engineers may come up with new and interesting configurations, or at the very least, understand the underlying workings of a particular distillation column.

Although this book primarily advocates distillation synthesis using the CPM method and can be read on its own, the reader should be aware that it is by no means an all encompassing text on distillation. Among the books that are considered by the authors to be a useful addition to this book are *Distillation Design* [41] and *Distillation Operation* by Henry Kister [42], *Conceptual Design of Distillation Systems* by Doherty and Malone [43], *Separation Process Principles* by Seader and Henley [44], and *Distillation Theory and its Application to Optimal Design of Separation Units* by Petlyuk [45]. All these works present different perspectives on the separation synthesis problem. Specifically, the book by Doherty and Malone shows the fundamental roots of the CPM method, that is modeling distillation columns with differential equations.

1.2 IMPORTANT DISTILLATION CONCEPTS

This book has been compiled for the student, engineer, or researcher that understands the fundamental concepts of distillation, or has at least attended an introductory course on the subject. The reader should be familiar with key vapor–liquid

equilibrium concepts, how industrial distillation is performed and basic design techniques such as the McCabe–Thiele method. For the sake of completeness and clarity however, we give a brief overview here of core concepts that the reader should be aware of and that are often used in this book.

1.2.1 A Typical Column

As evident from Figure 1.1, heat is added to the column through a *reboiler*, which vaporizes material and causes a vapor stream to travel upward in the column. Moving upward in the column, this vapor stream becomes richer in low-boiling component (s). For an efficient separation to occur, the vapor stream at the top of the column is condensed, at the *condenser*, and a portion of the condensed liquid is sent back down the column. This recycling of material is a key design parameter in distillation and is known as *reflux*, or the *reflux ratio*, and is directly proportional to the energy requirement of the column, that is, the higher the reflux ratio of the column, the higher the heating and cooling loads of the column are. Therefore, from a purely energetic perspective, one would like to operate as close to the minimum column reflux as possible.

A column can be either *packed* or *trayed*, as shown in Figure 1.2a and b, respectively. Separation occurs continuously throughout the length of a packed column, and occurs in a more step-by-step fashion in trayed columns. In general, this book deals with packed columns but the behavior of these two types of columns are fundamentally similar and the results can be interpreted interchangeably. We will refer to the spatial coordinate representing the position down the length of the column as stage number, represented by the variable n. The total number of stages

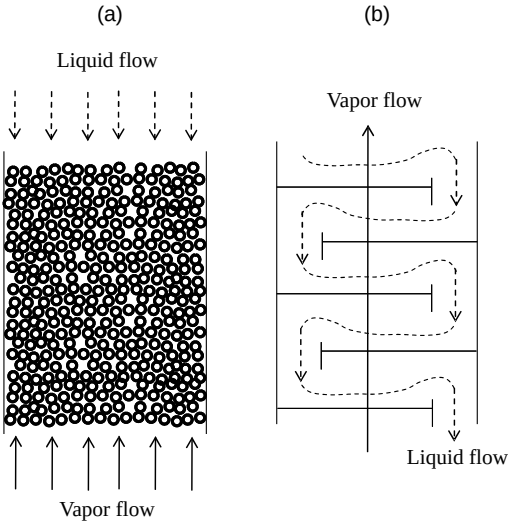


FIGURE 1.2 (a) Packed column and (b) trayed column.

required to affect the separation is thus related to the height of the column, which is indicative of the capital costs. It should be noted that the entry point of the feed stream occurs at the *feed stage*. Determining the feed stage is also an important design factor as it has a significant impact on the final product distribution of the column.

1.2.2 Complex Columns

Complex columns are in a broad sense all columns that are not simple columns, like the column shown in Figure 1.1. Complex columns may have multiple feeds, side product streams, stream transfers between two column units (thermally coupled columns), simultaneous chemical reaction(s) within the column body, hybrid membrane-distillation columns, and so on. Each of these columns present unique opportunities for cost saving. Typical complex columns are shown in Figure 1.3a–d.

Due to the tremendous costs associated to distillative separations, many alternate schemes to the simple column shown above have been proposed over the past several years both to improve on some of its inherent costs. Traditionally, when purifying a multicomponent mixture, an entire series of distillation columns are used in series, and the way in which these columns are sequenced may make a tremendous difference in the eventual process costs. However, due to the large energy requirements of even the most optimal sequence, more complex column arrangements have been proposed and subsequently utilized. These arrangements include thermally coupled columns such as side rectifiers and strippers, the fully thermally coupled columns (often referred to as the Petlyuk and Kaibel columns),

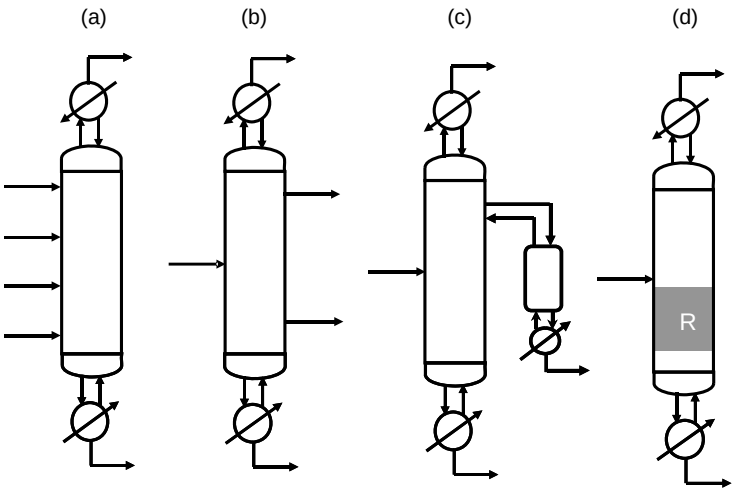


FIGURE 1.3 Examples of complex columns (a) distributed feed, (b) side-draw columns, (c) thermally coupled side stripper, (d) reactive distillation column with reaction zone (R).

prefractionating columns, and multieffect arrangements [9,10]. Up to 50% savings in energy expenditures have been reported with these thermally coupled arrangements [10,11,46–48].

Side stripping columns have found widespread use in the petrochemical industry to produce various cuts of petroleum products [49]. On the other hand, side rectifying columns have found application in air separation [45] as well as replacing entrainer regeneration columns in extractive distillation operations [50]. Even more complex columns such as the Petlyuk column or dividing wall column for separating a given feed into three products in a single distillation unit, requires only a single heat addition and removal, thereby reducing the energy costs of the separation. Despite the apparent advantages that these complex configurations offer, simple distillation columns are overwhelmingly more utilized in industry. One factor contributing to the underutilization of the complex arrangements is, possibly, a lack of understanding of these columns. Simple columns, on the other hand, are extremely well understood. Current research in distillation has therefore largely been directed toward complex column design.

1.2.3 Vapor–Liquid Equilibrium

The fundamental driving force for a separation to occur via distillation is that a mixture of components has different vapor and liquid compositions due to differences in vapor pressures. In other words, low-boiling components tend toward the vapor phase quicker than high-boiling components. Obviously, this difference in composition across coexisting vapor and liquid phases is dependent on the mixture being dealt with. From a modeling and design point of view, the relationship between the vapor composition of component i (y_i) and its liquid compositions (x_i) are centrally important, as it is ultimately this relationship which determines the design and operation of a distillation structure. In general, the relationship between vapor and liquid compositions can be expressed as

$$y_i = K_i x_i \tag{1.1}$$

Depending on the system at hand, the equilibrium ratio K_i may be either constant (as in Henry's law), or a function of temperature, pressure, and/or composition. In this book, the following phase equilibrium models are primarily models dealt with (1) constant relative volatilities, (2) ideal solutions using Raoult's law, and (3) nonideal solutions using a modified Raoult's law and the NRTL activity coefficient model, although other activity coefficient models are also applicable. Each of these three models is briefly discussed here.

(1) *Constant Relative Volatilities.* The constant relative volatility model is the simplest model for relating vapor and liquid compositions with each other. Essentially, this model assumes that the volatility of components with respect

to each other remain constant, and are independent of temperature or composition. The relative volatility (α_i) of a component i is defined simply as

$$\alpha_i = \frac{K_i}{K_r} \tag{1.2}$$

where r is a reference component in the system and α_i is a constant. The reference component is usually taken as the highest boiling component and its relative volatility will be unity, subsequently all other relative volatilities in the system will be greater than one. This is the convention used in this book, but any component can of course be taken as the reference component. Using the unity summation properties of both vapor and liquid compositions, elucidated in Equation 1.3, the relationship in Equation 1.4 can be derived

$$\sum_{i=1}^{nc} x_i = 1 \quad \text{and} \quad \sum_{i=1}^{nc} y_i = 1 \tag{1.3}$$

$$y_i = \frac{\alpha_i x_i}{\sum_{j=1}^{nc} \alpha_j x_j} \tag{1.4}$$

where nc is the total number of components in the system. Equation 1.4 shows that the vapor composition in equilibrium with its liquid composition is only a function of the liquid composition and the relative volatilities that have been assumed. Obviously, the higher the value for α is for a particular component, the greater its tendency is to escape to the vapor phase. The assumption of constant relative volatility is generally, but not always, acceptable when the species being dealt with are all from the same functional group. For example, benzene and toluene have constant volatilities of approximately 5.28 and 2.24 with respect to the higher boiling *p*-xylene, respectively. Figure 1.4 shows the effect of the relative volatility on vapor and liquid compositions for binary systems. Here, component 1 is the low-boiling component, that is, most volatile, and component 2 is the highest boiling component, that is, least volatile with volatility of 1.

Figure 1.4 clearly indicates that higher the volatility is between two components, the greater the difference is between vapor and liquid compositions at equilibrium. Since it is exactly this difference between liquid and vapor compositions, that is, the driving force for distillative separation, higher volatility mixtures are consequently "easier" to separate than low volatility mixtures.

(2) *Ideal Solutions.* The constant relative volatility assumption is often very good for a large number of systems. However, in many systems the equilibrium ratio is not constant but a function of temperature and pressure. Such a system may be modeled with Raoult's law, assuming that the vapor phase is an ideal

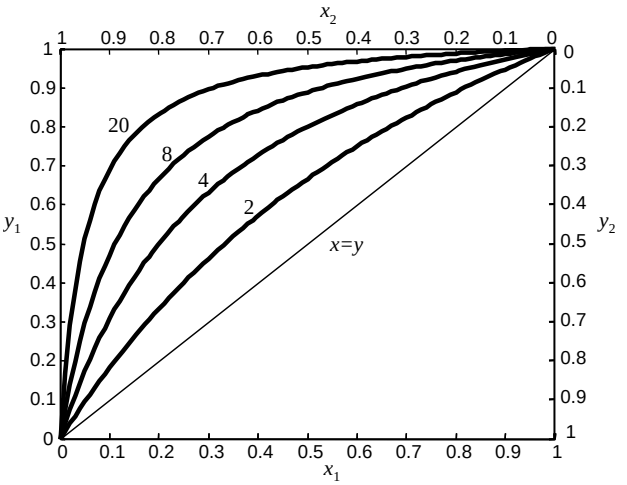


FIGURE 1.4 The effect of the relative volatility (α) on vapor and liquid compositions in a binary system.

gas and the liquid is an ideal solution (typically when liquid phase molecules are of the same size and chemically similar). In such instances, the equilibrium ratio is given by

$$K_i = \frac{P_i^{\mathrm{VAP}}}{P} \tag{1.5}$$

where P is the total system pressure, and P_i^{VAP} is the vapor pressure of species i and a function of temperature using the familiar Antoine equation, which has the general form shown in Equation 1.6

$$\ln\left(P_i^{\mathrm{VAP}}\right) = A_i - \left(\frac{B_i}{T + C_i}\right) \tag{1.6}$$

Coefficients A_i, B_i, and C_i are constants unique to specie i, and T is the boiling (or bubble) temperature of the mixture. The temperature at which a liquid with a particular composition is in equilibrium with its vapor may be calculated by combining Equations 1.1, 1.3, 1.5, and 1.6, ultimately yielding Equation 1.7

$$\sum_{i=1}^{nc} y_i = 1 = \sum_{i=1}^{nc} K_i x_i = \frac{1}{P}\sum_{i=1}^{nc} P_i^{\mathrm{VAP}} x_i \tag{1.7}$$

If the system pressure (P), the liquid composition and the Antoine coefficients are known for all components, temperature is the only remaining variable in Equation 1.7. Solving for the temperature in Equation 1.7 requires an iterative numerical technique. Once the temperature (and therefore the equilibrium ratio) is known, the vapor in equilibrium with its liquid may be obtained quite

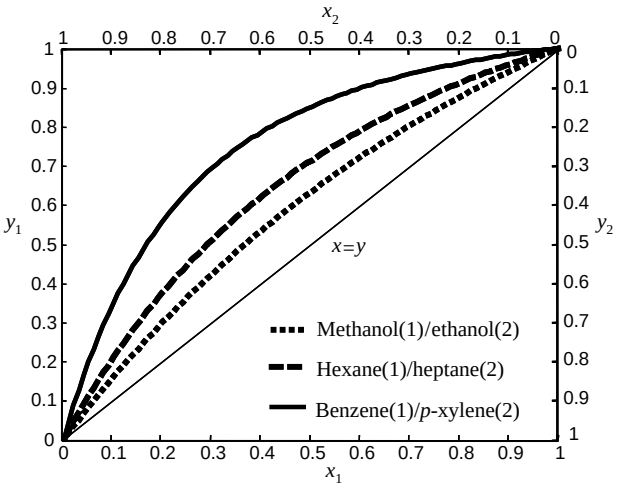


FIGURE 1.5 Behavior of selected binary systems' vapor and liquid compositions using Raoult's law at 1 atm.

simply through Equation 1.1. Examples of selected binary systems are shown in the $x - y$ diagram in Figure 1.5

(3) *Nonideal Solutions.* The final level of complexity for modeling the relationship between vapor and liquid compositions accounts for nonideal interactions in the liquid phase. The equilibrium ratio is still used for such systems, but in this instance it is defined as

$$K_i = \frac{\gamma_i P_i^{\mathrm{VAP}}}{P} \tag{1.8}$$

where γ_i is known as the activity coefficient of component i, and takes into account deviations from ideal, Raoult's law behavior. It is evident that Raoult's law in Equation 1.5 is a special case of Equation 1.8 where the activity coefficients are assumed to be one. Thus, Equation 1.8 is known as the modified Raoult's law. The activity coefficient is a function of both temperature and composition and calculating it can be quite intricate. There are many models used to calculate activity coefficients (Wilson, Margules, UNIQAUC, NRTL, and so on), and certain models may be better suited to a certain system than others. In this book, however, we primarily focus on the NRTL (nonrandom-two-liquid) model because it is quite widely applicable to a large number of systems. The NRTL activity coefficient may be modeled through Equations 1.9 and 1.10

$$\gamma_i = \exp\left[\frac{\sum_j x_j \tau_{ji} G_{ji}}{\sum_k x_k G_{ki}} + \sum_j \frac{x_j G_{ij}}{\sum_k x_k G_{kj}}\left(\tau_{ij} - \frac{\sum_m x_m \tau_{mj} G_{mj}}{\sum_k x_k G_{kj}}\right)\right] \tag{1.9}$$

$$\text{where} \quad \tau_{ij} = a_{ij} + \left(\frac{b_{ij}}{T(\text{K})}\right) \quad \text{and} \quad G_{ij} = \exp(-c_{ij}\tau_{ij}) \tag{1.10}$$

The coefficients a_{ij}, b_{ij}, and c_{ij} are binary interaction parameters specific to components i and j. A list of binary interaction parameters and Antoine coefficients for systems prominently featured systems in the book are given in Appendix B. Evidently, modeling nonideal systems can be rather laborious and computationally intensive, but the solution strategy is exactly the same to the one outlined for ideal solutions in Equation 1.7, and simply incorporating the activity coefficients. Activity coefficient models can account for azeotropes, that is, where vapor and liquid compositions are equal, while neither Raoult's law nor the constant volatility model is able to. Examples of binary nonideal systems modeled with the NRTL equation are shown in Figure 1.6.

Figure 1.6 shows a very different curvature when compared to the "well-behaved" mixtures in Figures 1.4 and 1.5. Specifically, the acetone/chloroform and ethyl acetate/water systems form azeotropes where the vapor and liquid compositions become equal and the equilibrium curve intersects the $y = x$ line. Systems with azeotropes present challenging design problems because it is no longer possible to obtain two high purity products in a single distillation unit. There are of course ways to overcome this problem, notably through adjusting the pressure for so-called pressure swing distillation (notice from Equation 1.8 that the $y - x$ relationship is system pressure dependent), or through creative material recycling [43]. The acetone/water system, on the other hand, does not have azeotropic behavior, but it is still quite nonideal, as evident from the asymmetric nature of its $y - x$ curve.

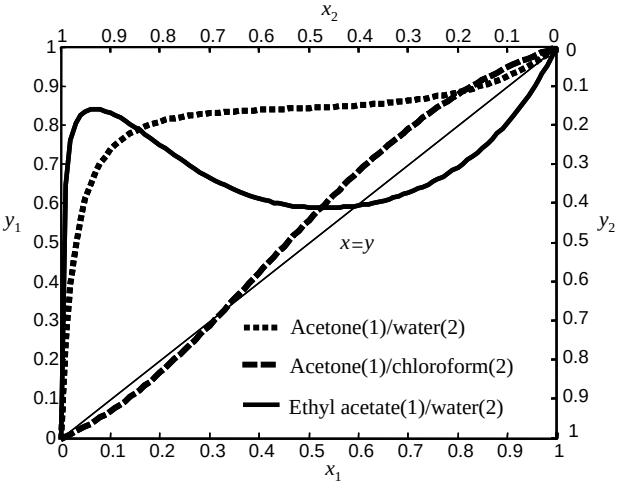


FIGURE 1.6 Behavior of selected binary systems' vapor and liquid compositions using a modified Raoult's law at 1 atm.

None of the systems in Figure 1.6 are, therefore, good candidates for modeling with either constant volatility or ideal solution models.

1.3 SUMMARY

It is hoped that from this chapter the reader understands the context and importance of industrial distillation, and realizes why efficient and insightful design techniques are so important. Although it is a comparatively old separation technique, there is still much room for improvement, especially in the area of complex distillation. The CPM technique that is presented in this book will aid in understating simple and complex distillation systems more clearly. Although the premise of the CPM technique is reasonably easy to follow and comprehend, it is a rather advanced technique, not recommended as a reader's first introduction to the field of distillation.

REFERENCES

[1] Humphrey, J.L., Separation processes: Playing a critical role. *Chemical Engineering Progress*, 1995, **91**(10):31–41.

[2] Soave, G. and J.A. Feliu, Saving energy in distillation towers by feed splitting. *Applied Thermal Engineering*, 2002, **22**(8):889–896.

[3] Mix, T.W. and J.S. Dweck, *Conserving Energy in Distillation*. 1982, Cambridge, MA: MIT Press. p. 104.

[4] McCabe, W.L. and E.W. Thiele, Graphical design of fractionating columns. *Industrial and Engineering Chemistry*, 1925, **17**(6):606–611.

[5] Underwood, A.J.V., Fractional distillation of multi-component mixtures—Calculation of minimum reflux ratio. *Institute of Petroleum – Journal*, 1946, **32**(274):614–626.

[6] Huss, R.S. and A.W. Westerberg, Collocation methods for distillation design. 1. Model description and testing. *Industrial & Engineering Chemistry Research*, 1996, **35**(5):1603–1610.

[7] Halvorsen, I.J. and S. Skogestad, Minimum energy consumption in multicomponent distillation. 1. $V_{\min}$ diagram for a two-product column. *Industrial & Engineering Chemistry Research*, 2003, **42**(3):596–604.

[8] Halvorsen, I.J. and S. Skogestad, Minimum energy consumption in multicomponent distillation. 2. Three-product Petlyuk arrangements. *Industrial & Engineering Chemistry Research*, 2003, **42**(3):605–615.

[9] Engelien, H.K. and S. Skogestad, Minimum energy diagrams for multieffect distillation arrangements. *AIChE Journal*, 2005, **51**(6):1714–1725.

[10] Engelien, H.K. and S. Skogestad, Multi-effect distillation applied to an industrial case study. *Chemical Engineering and Processing*, 2005, **44**(8):819–826.

[11] Wolff, E.A. and S. Skogestad, Operation of integrated three-product (Petlyuk) distillation columns. *Industrial & Engineering Chemistry Research*, 1995, **34**(6):2094–2103.

[12] Fidkowski, Z. and L.W. Krolikowski, Minimum energy requirements of thermally coupled distillation systems. *AIChE Journal*, 1987, **33**(4):643–653.

[13] Alstad, V., I.J. Halvorsen, and S. Skogestad, Optimal operation of a Petlyuk distillation column: Energy savings by over-fractionating, in *Computer Aided Chemical Engineering*, A. Barbosa-Póvoa and H. Matos, editors. 2004, Elsevier. pp. 547–552.

[14] Carlberg, N.A. and A.W. Westerberg, Temperature-heat diagrams for complex columns; Underwood's method for side strippers and enrichers. *Industrial & Engineering Chemistry Research*, 1989, **28**(9):1379–1385.

[15] Glinos, K. and M.F. Malone, Minimum vapor flows in a distillation column with a sidestream stripper. *Industrial & Engineering Chemistry, Process Design and Development*, 1985, **24**:1087–1090.

[16] Glinos, K.N. and M.F. Malone, Design of sidestream distillation columns. *Industrial & Engineering Chemistry, Process Design and Development*, 1985, **24**(3):822–828.

[17] Kiva, V.N., E.K. Hilmen, and S. Skogestad, Azeotropic phase equilibrium diagrams: A survey. *Chemical Engineering Science*, 2003, **58**(10):1903–1953.

[18] Lucia, A., A. Amale, and R. Taylor, Energy efficient hybrid separation processes. *Industrial & Engineering Chemistry Research*, 2006, **45**(25):8319–8328.

[19] Van Dongen, D.B. and M.F. Doherty, Design and synthesis of homogeneous azeotropic distillations. 1. Problem formulation for a single column. *Industrial & Engineering Chemistry, Fundamentals*, 1985, **24**(4):454–463.

[20] Doherty, M.F. and G.A. Caldarola, Design and synthesis of homogeneous azeotropic distillations. 3. The sequencing of columns for azeotropic and extractive distillations. *Industrial & Engineering Chemistry, Fundamentals*, 1985, **24**(4):474–485.

[21] Levy, S.G., D.B.Van Dongen, and M.F. Doherty, Design and synthesis of homogeneous azeotropic distillations. 2. Minimum reflux calculations for nonideal and azeotropic columns. *Industrial & Engineering Chemistry, Fundamentals*, 1985, **24**(4):463–474.

[22] Levy, S.G. and M.F. Doherty, Design and synthesis of homogeneous azeotropic distillations. 4. Minimum reflux calculations for multiple-feed columns. *Industrial & Engineering Chemistry, Fundamentals*, 1986, **25**(2):269–279.

[23] Knight, J.R. and M.F. Doherty, Design and synthesis of homogeneous azeotropic distillations. 5. Columns with non-negligible heat effects. *Industrial & Engineering Chemistry, Fundamentals*, 1986, **25**(2):279–289.

[24] Krishnamurthy, R. and R. Taylor, Simulation of packed distillation and absorption columns. *Industrial & Engineering Chemistry, Process Design and Development*, 1985, **24**(3):513–524.

[25] Taylor, R., H.A. Kooijman, and J.S. Hung, A second generation nonequilibrium model for computer simulation of multicomponent separation processes. *Computers & Chemical Engineering*, 1994, **18**(3):205–217.

[26] Kooijman, H.A. and R. Taylor, Nonequilibrium model for dynamic simulation of tray distillation columns. *AIChE Journal*, 1995, **41**(8):1852–1863.

[27] Kooijman, H., Dynamic nonequilibrium column simulation, in *Chemical Engineering*. 1995, Potsdam, NY: Clarkson University. p. 144.

[28] Taylor, R., R. Krishna, and H. Kooijman, Real-world modeling of distillation. *Chemical Engineering Progress*, 2003, **99**(7):28–39.

[29] Holland, S.T., et al., Column profile maps. 2. Singular points and phase diagram behaviour in ideal and nonideal systems. *Industrial & Engineering Chemistry Research*, 2004, **43**(14):3590–3603.

[30] Tapp, M., et al., Column profile maps. 1. Derivation and Interpretation. *Industrial & Engineering Chemistry Research*, 2004, **43**(2):364–374.

[31] Holland, S.T., et al., Complex column design by application of column profile map techniques: Sharp-split Petlyuk column design. *Industrial & Engineering Chemistry Research*, 2010, **49**(1):327–349.

[32] Holland, S.T., et al., Novel separation system design using "moving triangles". *Computers & Chemical Engineering*, 2004, **29**(1):181–189.
[33] Mulopo, J.L., D. Hildebrandt, and D. Glasser, Reactive residue curve map topology: Continuous distillation column with non reversible kinetics. *Computers & Chemical Engineering*, 2008, **32**(3):622–629.
[34] Peters, M., et al., Derivation and properties of membrane residue curve maps. *Industrial & Engineering Chemistry Research*, 2006, **45**(26):9080–9087.
[35] Peters, M., et al., Application of membrane residue curve maps to batch and continuous processes. *Industrial & Engineering Chemistry Research*, 2008, **47**(7):2361–2376.
[36] Mulopo, J.L., et al., Experimental simulation of distillation column concentration profiles using a batch apparatus: Columns stripping section. *Chemical Engineering Science*, 2005, **60**(24):6815–6823.
[37] Modise, T., et al., Experimental simulation of distillation column section profiles using a batch apparatus. *Industrial & Engineering Chemistry Research*, 2005, **44**:7511–7519.
[38] Modise, T., et al., Experimental measurement of the saddle node region in a distillation column profile map by using a batch apparatus. *Chemical Engineering Research and Design*, 2007, **85**(1):24–30.
[39] Hömmerich, U. and R. Rautenbach, Design and optimization of combined pervaporation/distillation processes for the production of MTBE. *Journal of Membrane Science*, 1998, **146**(1):53–64.
[40] Tapp, M., et al., Make distillation boundaries work for you! in *Computer Aided Chemical Engineering*, A. Barbosa-Póvoa and H. Matos, editors. 2004, Elsevier. pp. 499–504.
[41] Kister, H.Z., *Distillation Design*. 1992, McGraw-Hill.
[42] Kister, H., *Distillation Operation*. 1990, McGraw-Hill Professional.
[43] Doherty, M.F. and M.F. Malone, *Conceptual Design of Distillation Systems. 1st ed.* 2001, New York, NY: McGraw-Hill. p. 568.
[44] Seader, J.D. and E.J. Henley, *Separation Process Principles*. 2nd ed. 2006, Hoboken, NJ: Wiley. p. 756.
[45] Petlyuk, F.B., *Distillation Theory and its Application to Optimal Design of Separation Unit*. 2004, Cambridge: Cambridge University Press.
[46] Agrawal, R. and Z.T. Fidkowski, Are thermally coupled distillation columns always thermodynamically more efficient for ternary distillations? *Industrial & Engineering Chemistry Research*, 1998, **37**(8):3444–3454.
[47] Fidkowski, Z.T. and R. Agrawal, Multicomponent thermally coupled systems of distillation columns at minimum reflux. *AIChE Journal*, 2001, **47**(12):2713–2724.
[48] Brüggemann, S. and W. Marquardt, Rapid screening of design alternatives for nonideal multiproduct distillation processes. *Computers & Chemical Engineering*, 2004, **29**(1):165–179.
[49] Watkins, R.N., *Petroleum Refinery Distillation*. 1979, Houston: Gulf Pub. Co.
[50] Emmrich, G., H. Gehrke, and U. Ranke, The progressive extractive distillation arrangement for the morphylane extractive distillation process. *Chemie Ingenieur Technik*, 2001, **73**(6):715.

CHAPTER 2

FUNDAMENTALS OF RESIDUE CURVE MAPS

2.1 INTRODUCTION

Residue curve maps (RCMs) have been long used as a tool for analyzing a given ternary system's phase equilibrium behavior. These maps, originally pioneered by Schreinemakers in 1902 [1], enable design engineers to quickly scan possible separation trains or sequences, and also to identify areas of difficult separation due to azeotropes.

In this chapter, the derivation of RCMs from simple batch boiling, as well as the fundamental properties behind RCMs, are discussed. Thereafter, the application of RCMs to continuous processes is explored. However, as will be shown, this application has limitations and these will also be addressed.

A reader familiar with distillation research will find much of the material in this chapter to be familiar. However, RCMs do form the fundamental backbone of column profile maps (CPMs), and thus the need for this chapter is important. Readers that are experienced with distillation may find Section 2.9, particularly interesting and useful when some not-so-common ways of looking at RCMs are discussed.

It should be noted that only the information needed for the development of the material in the book is included in this chapter. Hence, some parts of the RCM theory are omitted since it is out of the scope of context for this particular text, but interested readers can consult the reference list for more detailed information [2–7].

Understanding Distillation Using Column Profile Maps, First Edition. Daniel Beneke, Mark Peters, David Glasser, and Diane Hildebrandt.
© 2013 by John Wiley & Sons, Inc. Published 2013 by John Wiley & Sons, Inc.

2.2 BATCH BOILING

The idea of the RCM arises from a simple batch experiment, whereby a beaker is filled with a mixture of components in the liquid phase. The liquid mixture is brought to its boiling point, producing a vapor in equilibrium with the liquid mixture, as shown in Figure 2.1.

In this batch experiment,

H represents the liquid holdup within the beaker (mol),

$\dot{V}$ is the removal rate of vapor leaving the beaker (mol/s), and

$\mathbf{x}$ and $\mathbf{y}$ are the liquid and vapor molar fractions, respectively, in vector form.

One may assume that $\mathbf{y}$ is in equilibrium with $\mathbf{x}$, but this will be discussed in Section 2.4.

The molar fractions are defined using the following vector notation (as indicated in bold):

$$\mathbf{x} = [x_1, x_2, \ldots, x_{n_c}] \quad \text{and} \quad \mathbf{y} = [y_1, y_2, \ldots, y_{n_c}] \tag{2.1}$$

where x_i is the mole fraction of component i in the liquid phase, y_i is the mole fraction of component i in the vapor phase, and n_c is the total number of components in the system.

Furthermore, since the entries in these compositional vectors are mole fractions, it is then a necessary requirement that

$$\sum_{i=1}^{n_c} x_i = 1 \quad \text{and} \quad \sum_{i=1}^{n_c} y_i = 1 \tag{2.2}$$

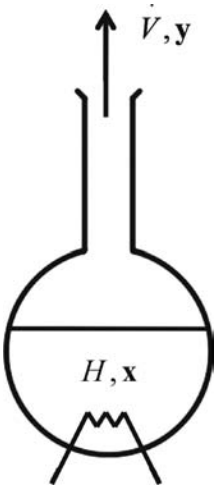


FIGURE 2.1 A simple batch boiling experiment.

With this condition, only $(n_c - 1)$ entries in a compositional vector are needed to fully define it. Thus, for example, a 3-component system only requires mole fractions of two components for it to be fully specified. The remaining component is inferred by unity summation property in Equation 2.2.

When the initial charge of liquid, of composition $\mathbf{x^o}$, is brought to its boiling (bubble) point, vapor will be produced in equilibrium with $\mathbf{x^o}$. By removing this vapor from the still as soon as it is formed, continual vaporization will occur. As separation proceeds, the more volatile components will vaporize quicker than the lower volatile components. The remaining liquid, or residue, will thus become progressively more concentrated in the less volatile species, thereby increasing the boiling point of the residue. Thus, in order for boiling to continue, the temperature of the system needs to be raised. If this increase in temperature occurs very slowly, and the liquid is well mixed, one can assume that near-perfect vapor–liquid equilibrium (VLE) is attained. It should be noted that the experiment, as shown in Figure 2.1, is conducted under isobaric conditions. A similar experiment can be set up for an isothermal process whereby the pressure is reduced to bring about vaporization. The reader is referred to Chapter 4 for more details regarding the various forms of boiling experiments.

Suppose the still is charged with a ternary mixture comprising of arbitrary components such that

Component 1 is a low-boiling (or most volatile) component,

Component 2 is a high-boiling (or least volatile) component, and

Component 3 is an intermediate-boiling component.

If one continuously analyzes the composition of the residual liquid in the still with time, until the last trace of liquid vaporizes, one is able to plot the change in both liquid and vapor composition over time. Figure 2.2 shows this plot for the least volatile component—plots for the other species are not shown but can easily be generated. In this instance, vapor and liquid compositions have been plotted against so-called reduced time defined as the instantaneous time of the experiment (t) divided by some final time (t_f) when the experiment has reached completion.

As boiling progresses, the liquid becomes richer in the least volatile component, namely component 2. A result of this is that the vapor (in equilibrium with this liquid) also gradually becomes richer in this component too, but tends to trail behind the liquid compositional change. After sufficient experimental time, the liquid phase tends to contain only the pure low-volatility component, that is, the lower boiling components have been boiled off. However, the amount of this remaining liquid has been greatly reduced since the commencement of boiling. Although the remaining liquid in the beaker has a higher purity of component 2 as the experiment progresses, the total amount of liquid is also gradually diminished.

2.3 THE MASS BALANCE TRIANGLE (MBT)

Another related, but more important plot is that of the change of each species' composition with each other, where each point along the profile is measured as time

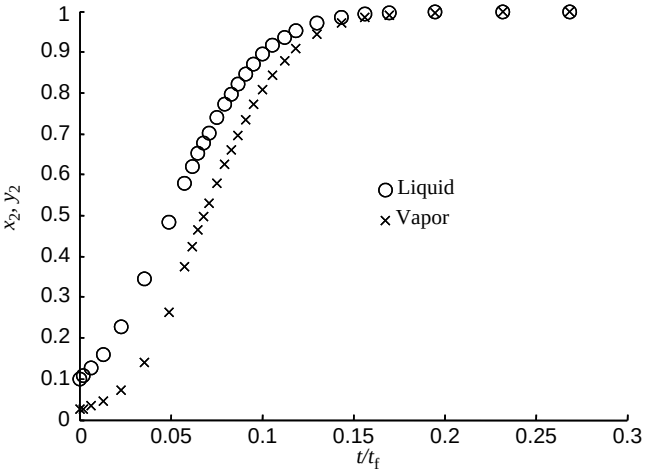


FIGURE 2.2 Schematic showing the compositional change with time of the least volatile component in both vapor and liquid phases during a simple boiling experiment.

proceeds during the experimental run. For a ternary mixture, such a plot is shown in Figure 2.3. The label $\mathbf{x^o}$ represents the initial composition in the still, that is, the composition at $t = 0$, as can be confirmed in Figure 2.2.

Such a set of axes (or triangle) is known as a mass balance triangle (MBT), or sometimes referred to as a Gibbs Triangle, and is typically used for ternary systems. The region enclosed by the triangle represents all the physically attainable compositions in a ternary system, that is, $0 \leq x_i \leq 1$ for $i = 1$, 2, and 3. Also, Equation 2.2

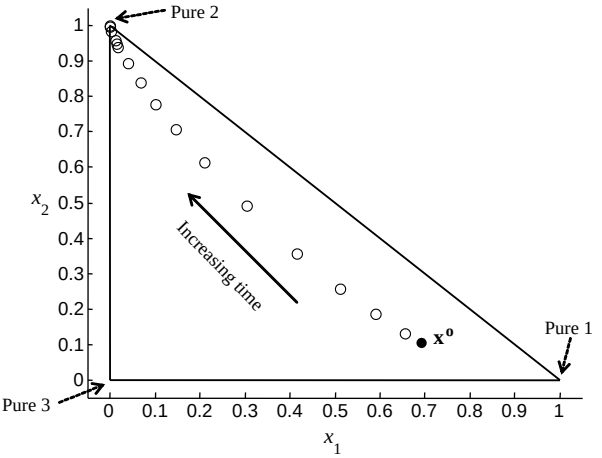


FIGURE 2.3 Schematic showing the compositional change of the residual liquid during batch experimentation. The axes are collectively known as the mass balance triangle.

applies. The boundaries of the triangle are graduated for molar compositions (fractions) for each component (some plots may use mass fractions, but only mole fraction plots will be used in this book). As an example, the point labeled as $\mathbf{x^o}$ has the following composition (as read from Figure 2.3) of $\mathbf{x^o} = [0.7, 0.1, 0.2]$. However, as explained in Section 2, the last component can be inferred by material balance, and writing the composition vector as $\mathbf{x^o} = [0.7, 0.1]$ is sufficient to fully define a ternary composition. Note that composition vectors presented here, and throughout the book, are arranged in accordance with their volatilities in the form $[x_1, x_2] = [\text{low boiling, high boiling}]$.

The vertices of the triangle indicate the location of individual pure components, as labeled in Figure 2.3. Each of the boundaries of the triangle physically represents the three binary mixtures that can exist, that is, the 2–3 binary is the vertical boundary, the 1–3 binary is the horizontal boundary, and the 1–2 binary is the diagonal boundary. The MBT is plotted in Figure 2.3 as a right-angled triangle, but can easily be adapted to an equilateral triangle, as is done in some texts. In this book and in the DODS software bundle accompanying the book, however, only right-angled triangles will be used.

It must be noted that in this plot, the composition of one component is plotted against that of another component, both in the same phase (i.e., liquid). This is different from the *x–y* plot typically used in McCabe–Thiele type examples where compositions of the same component in different phases (liquid and vapor) are plotted against each other. In accordance with the definition of a residue curve plot, the change in the liquid phase (only) is tracked. Of course, the change in the vapor composition can be similarly tracked—this is not shown, but can be easily generated from the data given in Figure 2.2.

2.4 THE RESIDUE CURVE EQUATION

2.4.1 Derivation

Rather than relying on an intuitive understanding of the batch boiling experiment shown in Figure 2.1, let us consider a more mathematical description of the process. In order to do this, we start with an unsteady state component mass balance (in vector form) around the beaker, resulting in

$$\frac{dH\mathbf{x}}{dt} = -\dot{V}\mathbf{y} \tag{2.3}$$

The product rule from differential calculus can be applied to obtain

$$H\frac{d\mathbf{x}}{dt} + \mathbf{x}\frac{dH}{dt} = -\dot{V}\mathbf{y} \tag{2.4}$$

Noting that the overall mass balance is equivalent to

$$\frac{dH}{dt} = -\dot{V} \tag{2.5}$$

Equation 2.5 may be replaced into Equation 2.4, which, upon rearrangement yields

$$\frac{d\mathbf{x}}{dt} = \frac{\dot{V}}{H}(\mathbf{x} - \mathbf{y}) \tag{2.6}$$

This is the well-known Rayleigh equation [2]. In order to proceed from this point, one may wish to relate the time-dependence of V, H, and $\mathbf{x}$ via an energy input rate $Q(t)$ (kW). This would then require an appropriate energy balance to be written. However, in order to assess the separation traits of a given system, one is generally only interested in the relation of all the compositions with each other, rather than time. This then allows us to simplify the equations as follows: by transforming the time variable, t in Equation 2.6 into a warped, or dimensionless time, ζ, defined as

$$d\zeta = \frac{\dot{V}}{H}dt \tag{2.7}$$

Using the transformation in Equation 2.7, the familiar residue curve equation may be obtained

$$\frac{d\mathbf{x}}{d\zeta} = \mathbf{x} - \mathbf{y} \tag{2.8}$$

All the compositions given here are in vectorized form. It is worth noting that only $(n_c - 1)$ equations need to be solved since the remaining composition can be determined by the unity summation properties of compositions (see Equation 2.1).

By combining Equations 2.7 and 2.8, and integrating with the initial condition $\zeta = 0$, and $H = H^{\circ}$ at $t = 0$, the solution for ζ at time t is

$$\zeta(t) = \ln\left(\frac{H^{\circ}}{H(t)}\right) \tag{2.9}$$

The advantage of using this transformed time variable is that it is related to real time, yet it is dimensionless. Further, rather than having bounds of 0 and t_f (where t_f is the time at which the still runs dry), it has more specific bounds of 0 and $+\infty$.

2.4.2 Approximation to Equilibrium

It is important to note that the residue curve equation (Equation 2.8) is simply a *mass balance*. In deriving it, there were no pre-defined notions regarding how the vapor phase is related to that of the liquid. The equation is merely providing a mathematical means of determining the composition of the residual liquid phase after an amount of material has transferred to the vapor phase. Solving the residue curve equation, however, requires knowledge about how the two compositions are related to each other. Such a relationship depends on the manner in which the boiling is conducted.

One could, for example, boil extremely rapidly, even possibly producing droplets in the vapor phase. The relationship for $\mathbf{y}(\mathbf{x})$ would, in that case, be very different from a very slow boiling scenario, for example. During slow boiling, one may justifiably assume that phase equilibrium is sufficiently approached, and we can thus model $\mathbf{y}$ using an appropriate thermodynamic model.

With that said, it was traditionally believed that residue curve equation (and the resulting maps) were only suitable for *equilibrium-based* separations and could not be used for the representation of kinetically based processes [3]. However, the differential equations which describe a residue curve are merely a combination of *mass balance equations*. Because of this, the inherent nature of residue curves is such that they can be used for equilibrium- as well as nonequilibrium-based processes.

We, therefore, assume slow boiling here, and thus at any given liquid composition $\mathbf{x}$, the vapor in equilibrium with it may be solved through the bubble point equation:

$$\sum_{i=1}^{n_c} y_i = \sum_{i=1}^{n_c} K_i x_i = 1 \tag{2.10}$$

where for the general case $K = f(\mathbf{x}, P, T)$ is the equilibrium constant relating vapor and liquid compositions (see Chapter 1).

2.5 RESIDUE CURVE MAPS

By simply knowing the phase equilibrium behavior and the composition within the beaker at the start of the experiment ($\mathbf{x}^{\mathbf{o}}$), one can easily construct a residue curve by integrating Equation 2.8. Such integration is usually performed with the use of a numerical integration method (see later, Section 2.5.3), such as Runge–Kutta type methods, remembering that at each function evaluation, a bubble point calculation must be performed in order to determine $\mathbf{y}(\mathbf{x})$.

2.5.1 Constant Relative Volatility Systems

Figure 2.4 shows the residue curve for an arbitrarily chosen initial charge, $\mathbf{x}^{\mathbf{o}}$, under constant relative volatility behavior (see Chapter 1). The following volatilities have been assumed:

$$a_1 = 5, a_2 = 1, \quad \text{and} \quad a_3 = 2, \tag{2.11}$$

or written in vector form,

$$\boldsymbol{\alpha} = [5, 1, 2] \tag{2.12}$$

It is important to point out that, although only two differential equations have to be solved for the ternary case (Equation 2.2), phase equilibrium data for *all three* components need to be known since the y_1–x_1 relationship, for instance, is a function of both components 2 and 3.

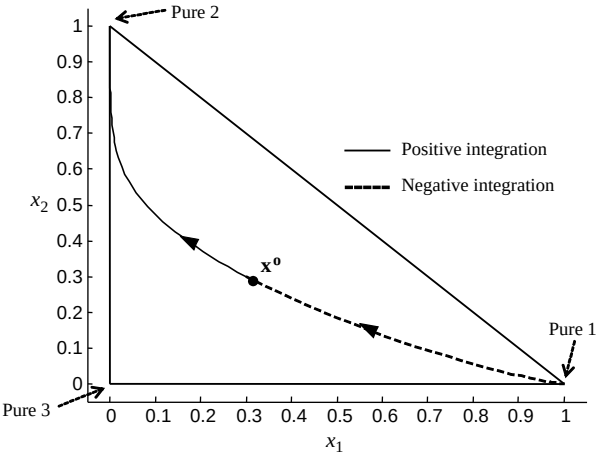


FIGURE 2.4 Residue curve for an initial charge in the still of $\mathbf{x^o} = [0.3, 0.3]$ with $\boldsymbol{\alpha} = [5,1, 2]$.

WWW

TUTORIAL 2.1

Try this for yourself: Reproduce Figure 2.4 with DODS-ProPlot using the given parameters. Try generating similar figures with different values for $\mathbf{x^o}$ and $\boldsymbol{\alpha}$.

The profile, as shown, gives a pathway or trajectory that the residual liquid would follow during batch boiling, tracking the changes in the liquid composition. The integration mimics the experimental procedure, in that it begins at zero time increasing toward positive infinity.

The relative volatility values (Equation 2.12) inform us about the behavior of the system. Component 1 has the highest rate of boiling, and thus the liquid is depleted of component 1 the fastest. This can be seen graphically—the curve is moving in a direction away from pure 1. Component 2, on the other hand, has the lowest boiling rate, implying that the liquid will become richer in 2, hence the residue curves move toward pure 2, eventually terminating there. Component 3 has a relative volatility that lies in between that of 1 and 2, thus profile neither propagates away from nor into pure 3, but does tend to curve or bend toward pure 3, before moving toward component 2.

Although impossible to achieve in the actual experiment discussed in Section 2.2, it is mathematically possible to begin with the same feed composition ($\mathbf{x^o}$) and perform the integration in the negative direction, that is, from zero toward negative infinity. This is shown in the dashed profile in Figure 2.4. Performing negative integration merely completes the residue curve and informs one what initial composition may be chosen in the still that will result in the same residue curve. In other words, any composition point on a residue curve is a potential initial composition that would result in the same curve. Thus, an entire residue curve can be generated by performing the integration in both positive and negative directions.

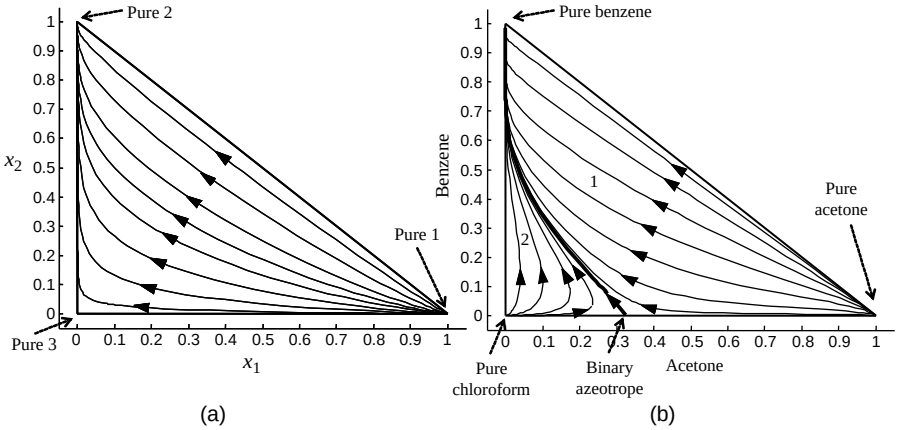


FIGURE 2.5 A residue curve map for (a) a constant relative volatility system with $\boldsymbol{\alpha} = [5,2,1]$ and (b) the nonideal acetone/benzene/chloroform system using the NRTL model at $P = 1$ atm.

It is also customary to show the positive direction of movement of the residue curves on the maps [3]. This direction corresponds to the way the trajectory would be generated during batch boiling, and is therefore related to forward integration towards positive infinity. Thus, the profiles move from the low-boiling component to the high-boiling component, as indicated.

Furthermore, other residue curves can be produced in the same manner by simply altering the initial charge composition, and integrating Equation 2.8. The entire MBT can then be populated with residue curves. However, it is logical to only show a few curves, as is done in Figure 2.5a. Such a collection of residue curves is known as a residue curve map. Figure 2.5a shows a three component RCM for a constant relative volatility system, as indicated.

WWW

TUTORIAL 2.2

Try this for yourself: Reproduce Figure 2.5a and b with DODS-ProPlot using the given parameters. Try generating (a) with other $\boldsymbol{\alpha}$ values and (b) at different pressures.

From Figure 2.5a, one may quickly scan which separation is feasible or not on a batch scale, remembering that the profiles show the behavior of the liquid compositions. The constant volatility system shows that one may produce a pure high-boiling component in the still once all the light and intermediate-boiling components have been boiled off. However, the actual amount of the high-boiling component remaining would decrease with an increase in purity. The vapor leaving the beaker is initially richer in the low-boiling component, but as boiling proceeds, the other, less volatile components report to the vapor phase too.

It should be noted that in systems with constant relative volatility, as well as ideal thermodynamic behavior, the profiles that result all have similar behavior irrespective of the initial composition. In other words, profiles will move in such a way that the liquid is rapidly decreased of the low-boiling specie, moving toward the intermediate component, but ultimately terminating at the high-boiling specie. Thus, we may say that a region within the MBT with these properties form a distillation region. That is, a region where the trajectories collectively behave in the same topological manner. A distillation boundary is more formally defined with the use of stationary points—this is given in Section 2.6.2.

2.5.2 Nonideal Systems

In exactly the same manner, one could both experimentally and mathematically determine the liquid trajectories for ternary systems that exhibit thermodynamically nonideal behavior. As an example, Figure 2.5b, shows the RCM for the nonideal acetone/benzene/chloroform at 1 atm pressure. This map was generated using the NRTL thermodynamic model (see Chapter 1). The necessary parameters used in these equations can be found in Appendix B.

Unlike ideally behaved systems, the acetone/benzene/chloroform system exhibits an azeotrope. An azeotrope is a point in the compositional space where a liquid mixture has a constant boiling point because the vapor has the same composition as the liquid. Azeotropes can occur between two or more species, and the boiling temperature determines the nature of the azeotrope. In this case (refer to Figure 2.5b), the azeotrope is a high (or maximum) boiling binary azeotrope between acetone and chloroform.

The presence of the single azeotropic point in Figure 2.5b alters the entire topology of the map (when compared to that of the ideal map). Rather than a single region of possible operation that occupies the entire MBT, there are two distinct distillation regions created within the map (labeled 1 and 2) where one may perform a separation. These regions are characterized by the collective nature of the profiles within them, and are separated by the *distillation boundary* (represented by the solid bold line connecting the azeotrope to pure benzene). This boundary, although imaginary, signifies the division between the regions.

If one were to conduct batch boiling with an initial charge composition located in region 1, the initial vapors produced would be rich in acetone, while the liquid would become richer in benzene. Operation in region 2 would result in a benzene-rich liquid as well; however, the vapor produced will be more concentrated in chloroform. Furthermore, it should be noted that the nature of the profiles, and hence the distillation regions formed, are dependent on the system and type of azeotrope(s) present (either minimum or maximum boiling).

2.5.3 Numerical Integration

As mentioned previously, numerical integration of the residue curve equation can be done with Runge–Kutta type methods. Fortunately, mathematical software packages

such as Matlab® are able to perform this integration extremely quickly and it is no longer the painstaking process it used to be. In fact, an entire RCM for a constant relative volatility system can be produced in a matter of a few seconds. More complex systems that require a more detailed thermodynamic model such as the NRTL activity coefficient model may take slightly longer, but nevertheless it is still quite fast. All the maps generated and shown in this book, and with all DODS packages, are generated by a fourth order, single step Runge–Kutta method in Matlab.

For a specific system, all that is required to generate a RCM is specification of the phase equilibrium parameters and an initial integration composition. The integration limits for the time are taken from zero to a sufficiently large number (for both positive and negative integration), $\zeta = 30$ usually suffices. This upper integration limit ensures that integration calculations will proceed sufficiently close to the intended termination point of the profile (see Section 2.6.2), that is, a pure component vertex or in some instances, an azeotropic composition. The integration steps are usually taken smaller than 1 to generate a smooth profile. Packages such as Matlab automatically adjust the integration step size to ensure rapid computation. For instance, when the profiles approach a point of profile termination, Matlab automatically makes larger jumps in integration steps since the composition does not change by any significance in these areas, until the upper integration limit has been reached.

2.6 PROPERTIES OF RESIDUE CURVE MAPS

In the preceding sections, the concept of a residue curve map was introduced. While these maps provide information about the separation of a particular mixture via boiling, they also yield some very interesting mathematical and topological behavior. Analysis of the residue curve equation (Equation 2.8) gives insight into the properties of these maps.

2.6.1 Separation Vector Field

The degree of separation obtained at any time during boiling would be the difference between the vapor and liquid compositions at that time. Formally, one may refer to this as the *separation vector* or *equilibrium vector*:

$$\mathbf{S} = (\mathbf{x} - \mathbf{y}) \tag{2.13}$$

As can be seen, $\mathbf{S}$ is simply the right-hand side of Equation 2.8 in vector form. Furthermore, it can be deduced that $\mathbf{S}$ is *tangent* to a residue curve at the liquid composition, $\mathbf{x}$. Figure 2.6 gives a graphical representation of the separation vector with respect to a residue curve. A distillation curve, also shown, is the vapor-equivalent of a residue curve.

The separation vector is only a function of $\mathbf{x}$ at that particular point. This means that a separation vector can be defined at every point within the MBT, resulting in the entire space termed the *separation vector field*.

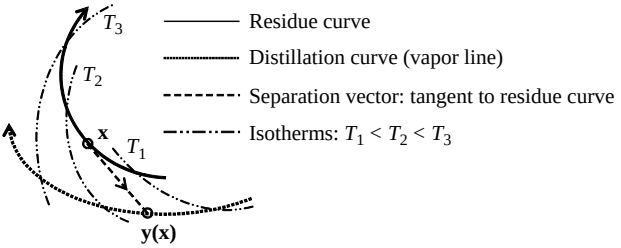


FIGURE 2.6 The difference between the vapor composition, **y**, in equilibrium with the liquid composition, **x**, is the separation vector, which is tangent to the residue curve at **x**. The isotherms increase in magnitude as boiling proceeds.

2.6.2 Stationary Points

Figure 2.5a and b show points at which the composition profiles originate from, terminate at, and tend toward. These points, interchangeably referred to as stationary points, pinch points or nodes, represent compositional steady states in the beaker where the liquid composition within the beaker is no longer changing with time, and may be determined by solving the system of nonlinear algebraic equations (see Equation 2.8) such that

$$\frac{d\mathbf{x}}{d\zeta} = 0 \tag{2.14}$$

In terms of the residue curve equation, this means algebraically solving for points where $\mathbf{x} = \mathbf{y}$. Generally speaking, these stationary points may be classified into three main types: a stable node, an unstable node, and a saddle point, depicted in Figure 2.7a–c, respectively.

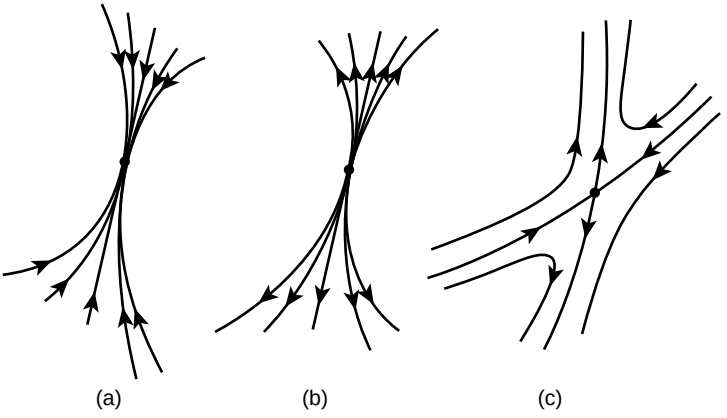


FIGURE 2.7 Topological representation of (a) a stable node, (b) an unstable node, and (c) a saddle point.

Although from a mathematical point of view there are other types of nodes that exist, the three nodes depicted in Figure 2.7 are the most prevalent. All profiles initiate from the unstable node, terminate at the stable nodes, and are attracted by the saddle point(s). In general, a *distillation region* contains at least these three nodes. For some highly nonideal systems, a distillation region may for instance contain two saddle points, but the region will still have only a single unstable and single stable node present.

From a different point of view, the unstable node indicates the most volatile point within a distillation region, and the stable node, indicates where the liquid composition in the beaker will tend to, represents the least volatile point. Thus, the stable node will always have the highest temperature in its distillation region, while the unstable node will have the lowest. The saddle point(s) will always be at some intermediate temperature within the region. One could track how the temperature is increasing along a residue curve, or set of residue curves, and plot contours of constant temperature across them, as shown by the isotherms in Figure 2.6.

Notice specifically that the profiles for the constant volatility system shown in Figure 2.5a originate and terminate exactly on the pure component vertices and experience the highest curvature near the intermediate boiling vertex. For systems that have nonideal phase equilibrium behavior containing azeotropes, stationary points are also situated at the azeotropic compositions, as shown in Figure 2.5b. The nature of the azeotropic node depends on the type of azeotrope (maximum- or minimum-boiling). A more thorough investigation on the nature of pinch points is discussed in Chapter 3 (Section 3.8.1).

In summary,

- Residue curves cannot intersect with each other.
- Residue curves begin at unstable nodes.
- Residue curves end at stable nodes.
- Residue curves move from low temperature to high temperature, that is, the temperature increases along a residue curve.

WWW

Example 2.1: Given the Aspen Plus®-generated RCMs for the acetone/ethanol/methanol system at 1 and 10 atm in Figure 2.8a and b, respectively:

(1) Reproduce these plots using the DODS-ProPlot program and
(2) Identify the different node types in each RCM.

Solution 2.1: Using the manual in Appendix B for the DODS-ProPlot package, RCMs can be generated fairly easily. Figure 2.9a and b shows the RCM at 1 and 10 atm, respectively, using DODS-ProPlot. Clearly, there is an excellent agreement Aspen Plus®-generated RCMs and those generated in DODS-ProPlot. Subsequently, given the RCM of this system with profile directions it is simple to intuitively infer different node types. Here follows all nodes with a brief statement regarding each

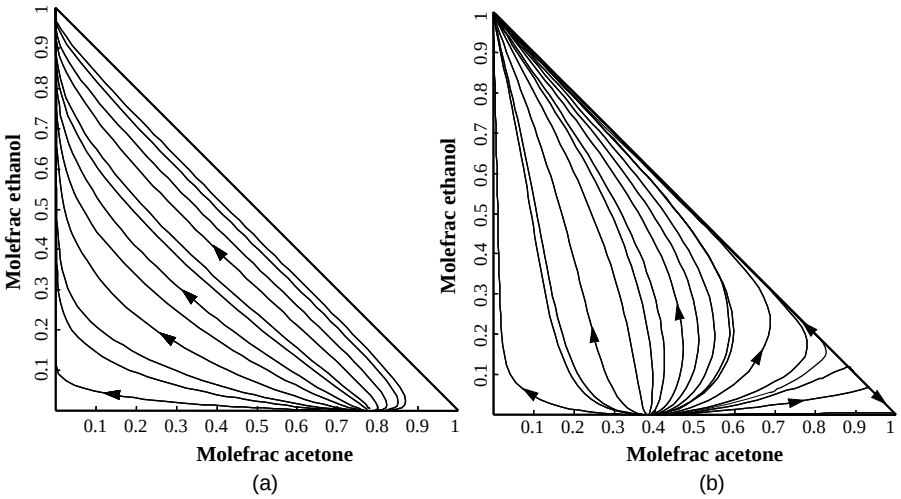


FIGURE 2.8 RCM plots generated in Aspen Plus® for the acetone/ethanol/methanol system using the NRTL thermodynamic model at (a) $P = 1$ atm and (b) $P = 10$ atm.

For the RCM at 1 atm

- The binary azeotrope between acetone and methanol is the point with the lowest temperature on the map, and all profiles originate from this point. Thus, the azeotrope is an unstable node.
- Pure ethanol is a stable node, since all profiles terminate at this point.
- Pure acetone and pure methanol both have profile moving toward them, but never terminating there. This implies that they are both saddle points.

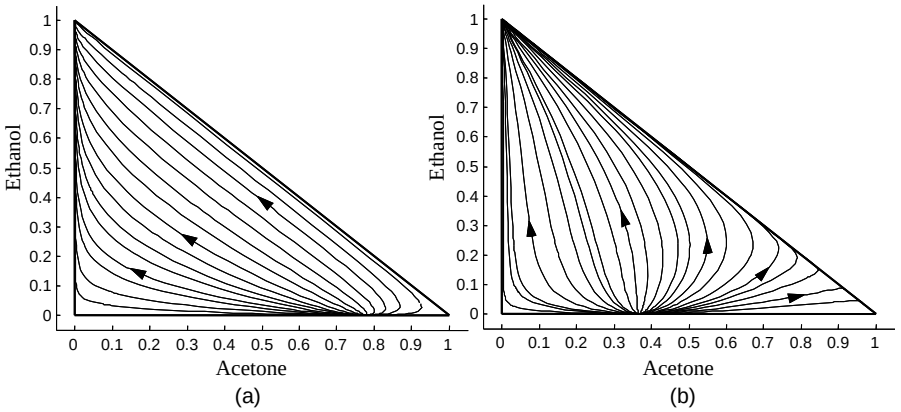


FIGURE 2.9 RCM plots generated with DODS-ProPlot for the acetone/ethanol/methanol system using the NRTL thermodynamic model at (a) $P = 1$ atm and (b) $P = 10$ atm.

For the RCM at 10 atm

- The acetone/methanol azeotrope is still the unstable node.
- Ethanol remains the stable node.
- Pure methanol is still a saddle point.
- Pure acetone has now become a stable node.
- An azeotrope between acetone and ethanol has now emerged—this azeotrope does not exist in the 1 atm map! Looking at the behavior of the profiles around this point, we can classify it as a saddle point.

Comparing the two plots in Figure 2.8a and b, it can be seen that the composition of the low-boiling binary azeotrope that exists between acetone and methanol has a strong dependence on pressure, moving from about 80 mol% acetone at 1 atm to 40 mol% at 10 atm. More importantly, however, is to notice the change in the node type at pure acetone: at 1 atm, pure acetone is a saddle point, while at 10 atm, this point becomes a stable node. Further, there is now also a saddle node in the form of a binary azeotrope between acetone and ethanol at 10 atm that never existed at 1 atm.

One could attempt to understand these phenomena by looking at the system behavior at the respective operating conditions. However, with the current knowledge of RCMs and their topology, that is, up to this point in the book, there is no formal way of explaining how a node can appear in one RCM, and not in another, and also how a node can change its properties, thereby altering the entire topology of the RCM. In Section 2.9, some very interesting topological aspects of RCMs will be shown, where after this obscure behavior in the RCMs in Figure 2.8a and b can be better understood and explained.

2.6.3 Isotherms

As discussed, the temperature increases along a residue curve as it moves from the lowest boiling point in the map (unstable node) to the highest boiling point (stable node). Every point along a residue curve has a corresponding equilibrium vapor composition, and thus, a unique temperature associated with it, as depicted in Figure 2.6. This temperature is calculated when performing the appropriate VLE calculation, given in Equation 2.10. Notice the tangency of the separation vectors at any **x** that exists for any isotherm that connects an **x** and **y** data pair. Collectively, taking an entire RCM, one is able to connect points of the same temperature with contours, thereby creating a map of isotherms. An example of an isotherm plot is shown in Figure 2.10 for the acetone/benzene/chloroform system at 1 atm.

This plot allows one to identify nodes from a different perspective. Rather than tracking the origin, direction, and termination of residue curves, one can now analyze the temperature contours to classify nodes. For the system at hand, the lowest temperature is observed at pure acetone, while the highest is at pure benzene. Also, the binary azeotrope is a maximum-boiling binary azeotrope between acetone and chloroform, and this is the point of highest temperature along that binary boundary (horizontal boundary of MBT). However, this temperature is still lower

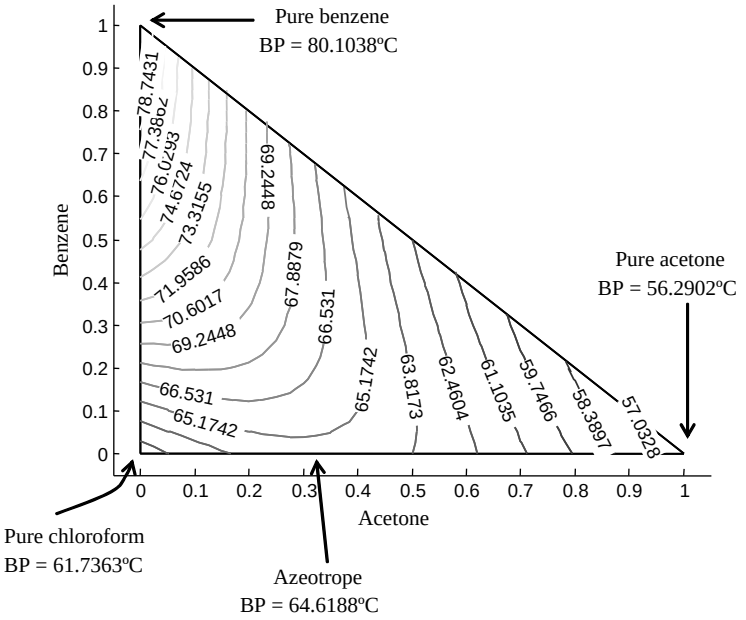


FIGURE 2.10 Isotherm plot for the acetone/benzene/chloroform system at $P = 1$ atm using the NRTL thermodynamic model. Temperatures indicated in °C.

than that of pure benzene, and thus residue curves do not terminate at the azeotrope. Also notice how the isotherms get closer together near the stable node (pure benzene). This indicates that separation by boiling will become a lot slower as the experiment progresses toward pure benzene.

2.6.4 Other Properties of RCMs

There are numerous other properties related to RCMs that one can delve into, such as classification of RCMs, rules of azeotropy, and unidistribution and univolatility lines. Although interesting in their own right, these are not the focus of this book and are therefore not discussed here. An interested reader is strongly urged to refer to the review works of Fien and Liu [3] as well as Kiva et al. [4] to gain a deeper understanding into these topics.

2.7 APPLICABILITY OF RCMs TO CONTINUOUS PROCESSES

2.7.1 Total Reflux Columns

Consider the total reflux simple column shown in Figure 2.11, where the following nomenclature applies:

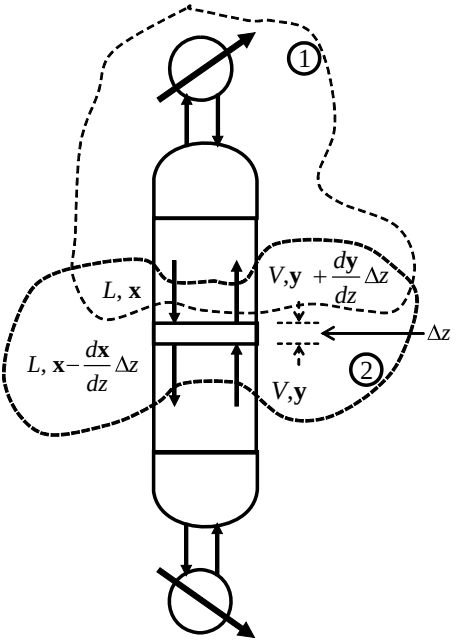


FIGURE 2.11 Total reflux distillation column. Packing segment of height Δz shown, with associated flows and compositions as indicated.

L is the total liquid flow rate (mol/s),
V is the total vapor flow rate (mol/s),
$\mathbf{x}$ is the composition of the liquid, as a function of position,
$\mathbf{y}$ is the composition of the vapor, as a function of position, and
Δz is an arbitrarily chosen packing height, or change in position (m).

In a total reflux column, all the vapor leaving the top of the column is completely condensed and then returned to the column. Similarly, all the liquid at the bottom of the column is completely vaporized and sent back to the column. Thus, there are no products from the column, and hence no feed is required. It is obvious then that such a column has no practical use. However, as will be shown here, analysis of this column gives great insight into both infinite and finite reflux operation.

Consider a section of packing of height Δz within the simple column. Liquid and vapor streams enter this section at flows of L and V, and compositions of $\mathbf{x}$ and $\mathbf{y}$, respectively. With the mass transfer that occurs between the two phases, it is assumed the total flows do not change, but the respective compositions do. The compositional change is as indicated in Figure 2.11.

A material balance around the boundary labeled 1 gives

$$V = L \quad \text{and} \quad V\left(\mathbf{y} + \frac{d\mathbf{y}}{dz}\Delta z\right) = L\mathbf{x} \tag{2.15}$$

Thus,

$$\left(\mathbf{y} + \frac{d\mathbf{y}}{dz}\Delta z\right) = \mathbf{x} \tag{2.16}$$

A material balance around boundary 2 yields

$$V\mathbf{y} + L\mathbf{x} = V\left(\mathbf{y} + \frac{d\mathbf{y}}{dz}\Delta z\right) + L\left(\mathbf{x} - \frac{d\mathbf{x}}{dz}\Delta z\right) \tag{2.17}$$

Substituting Equation 2.16 into Equation 2.17 gives

$$V\mathbf{y} + L\mathbf{x} = V\mathbf{x} + L\mathbf{x} - L\frac{d\mathbf{x}}{dz}\Delta z \tag{2.18}$$

Rearranging

$$L\frac{d\mathbf{x}}{dz}\Delta z = V(\mathbf{x} - \mathbf{y}) \tag{2.19}$$

Defining dimensionless position as $z' = z/\Delta z$, Equation 2.20 is obtained

$$\frac{d\mathbf{x}}{dz'} = (\mathbf{x} - \mathbf{y}) \tag{2.20}$$

This is the residue curve equation, since it is mathematically analogous to Equation 2.8. It can also be seen that the dimensionless time variable, ζ in the batch set-up is replaced with an equivalent position variable in Equation 2.20 in the column.

As discussed in Section 2.4, the residue curve equation is merely a mass balance, and can be used for any relationship between **x** and **y**. In this scenario, however, it is logical and common practice to assume that the streams emerging from a tray, or packing segment, are in equilibrium with each other. This then allows **y** to be defined by the appropriate thermodynamic phase equilibrium model.

It can then be stated that *the liquid profile along a continuously operated packed distillation column operating under total reflux conditions will follow a residue curve*. The exact residue curve will depend on the composition of the liquid at any point in the column. Furthermore, in accordance with the temperature profile along a residue curve, it can be deduced that the hottest temperature in a column occurs in the reboiler, while the coldest temperature is in the condenser.

This is a remarkable result it is showing that a certain type of continuous column can be modeled exactly using a simple batch experiment. In other words, the exact trajectory mapped out when boiling a liquid of a certain mixture is exactly the same path followed by the liquid down a continuously operated total reflux column.

2.7.2 Infinite Reflux Columns

If one further assumes that the internal flows of the column are infinitely large, then drawing off finite amounts of overheads and bottoms products (as done in normal operation of a simple column, refer to Figure 1.1) will have a negligible effect on the internal flows. Of course, doing this then warrants the need for a feed stream to the column in order to obey mass balance. However, it can still be assumed that the internal flows are much larger than either the feed or products, and thus the same material balances put forward for total reflux operation apply, as shown in Equations 2.15–2.17. Thus, it can be stated that the path followed by the liquid in an infinite reflux column will follow a residue curve as well, with the temperatures in the column dictated by the profile.

Although an infinite reflux column is still impractical, it does have feed and product streams associated with it. Thus, unlike the total reflux column, the infinite reflux column has an external mass balance. The mass balance is for the column shown in Figure 1.1 is very simple, and can be summarized as

$$F = D + B \tag{2.21}$$

$$\text{and } F\mathbf{x}_F = D\mathbf{x}_D + B\mathbf{x}_B \tag{2.22}$$

where F is the feed rate to the column (mol/s), D is the distillate, or overheads, product rate (mol/s), B is the bottoms product rate (mol/s), and $\boldsymbol{x}_M$ is the molar composition of stream M.

From a geometric perspective, the mass balance is a straight line with $\mathbf{x}_F$ lying between $\mathbf{x}_D$ and $\mathbf{x}_B$. Furthermore, since the liquid profile is following a residue curve, then both the distillate composition ($\mathbf{x}_D$) and bottoms composition ($\mathbf{x}_B$) have to lie on the *same* residue curve.

In short, when designing an infinite reflux column, two criteria have to be met

- $\mathbf{x}_F$, $\mathbf{x}_D$, and $\mathbf{x}_B$ have to lie on a straight line (material balance), with $\mathbf{x}_F$ in the middle, and
- $\mathbf{x}_D$ and $\mathbf{x}_B$ have to lie on the same residue curve (equilibrium), with $\mathbf{x}_D$ being at the lower temperature.

Let us consider, as an example, the ideally behaved benzene/*p*-xylene/toluene system. It is applicable, in this scenario, to model the phase equilibrium using Raoult's law. The RCM for this system (which can be constructed using DODS-ProPlot) at 1 atm is shown in Figure 2.12.

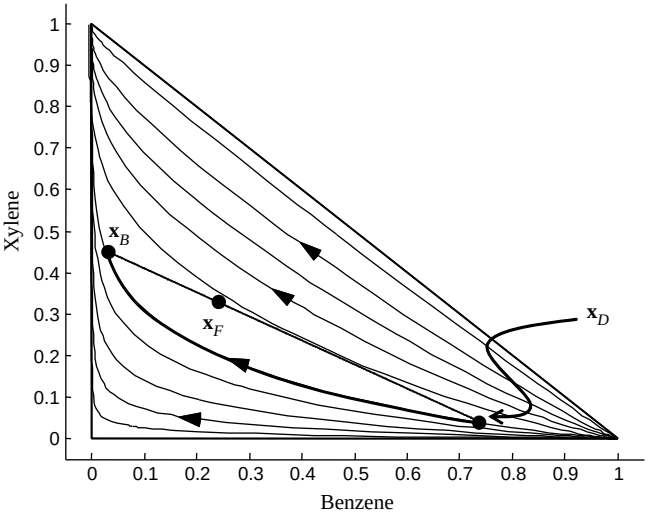


FIGURE 2.12 RCM for the benzene/*p*-xylene/toluene system at $P = 1$ atm with a possible feasible design for an infinite reflux column.

WWW

TUTORIAL 2.3

Try this for yourself: Reproduce the RCM in Figure 2.12 with DODS-ProPlot using the given parameters. Try generating another RCM at different pressures and find other feasible design solutions.

An example of a feasible infinite reflux column is also shown in Figure 2.12 where we have arbitrarily chosen a 1 mol/s feed of composition $\mathbf{x}_F = [0.25,\ 0.33]$ and distillate product to be $\mathbf{x}_D = [0.74,\ 0.05]$. Identifying a feasible design entails drawing a straight line from the distillate composition through the feed and finding the point where this line intersects the residue curve that runs through the distillate too.

With this example, it should be obvious that there are other combinations of $\mathbf{x}_D$ and $\mathbf{x}_B$ that can be sought for a fixed $\mathbf{x}_F$: these can be achieved by either altering the length of the mass balance line and/or by rotating the line, by pivoting about $\mathbf{x}_F$. Of course, there are limits as to how much the line can be lengthened and rotated. The line has to remain within the MBT for the products to be real, and its direction has to be such that the products still remain on the same residue curve. With this, one can identify the following two important mass balance lines:

(1) A *direct split* mass balance line connects the feed composition and the unstable node in a region, indicating a sharp split with the low-boiling component as the pure top product of a column.

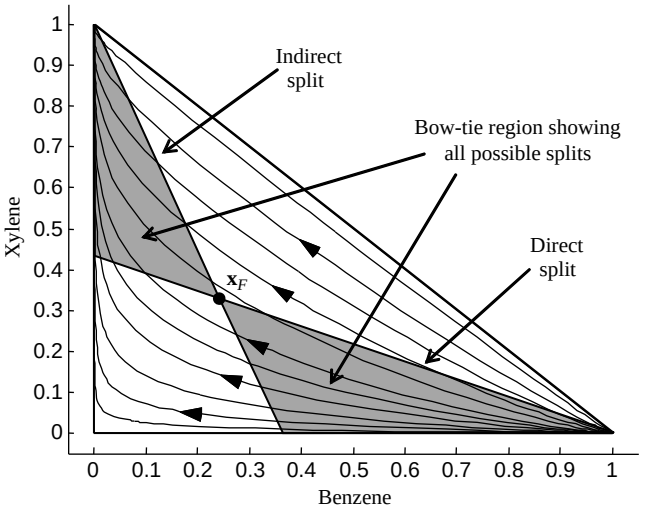


FIGURE 2.13 Bow-tie region bounded by the direct and indirect mass balance lines for the benzene/*p*-xylene/toluene system at $P = 1$ atm for an arbitrary feed composition.

(2) An *indirect split* mass balance line connects the feed composition and the stable node, indicating a sharp split with the highest boiling component as the pure bottoms product of a column.

Graphical representations of these sharp splits are shown in Figure 2.13.

2.7.3 Bow-Tie Regions

These two "split" lines form boundaries of an entire region of possible feasible infinite reflux columns. This region is shown in Figure 2.13 too, and by the nature of its shape has been given the name "bow-tie region." Any mass balance lines outside this region would not intersect the same residue curve twice due to the nature of the curvature of the profiles, and are thus infeasible. In azeotropic systems, the same two criteria still apply when looking for feasible infinite reflux columns. Some design scenarios for azeotropic systems at infinite reflux are depicted in Figure 2.14a and b.

WWW

TUTORIAL 2.4

Try this for yourself: Reproduce the RCMs in Figure 2.14a and b with DODS-ProPlot using the given parameters. Try generating using RCMs at different pressures and find other feasible design solutions.

An interesting observation in azeotropic systems (that hence exhibit multiple distillation regions) is that while the feed composition may lie in one region, the

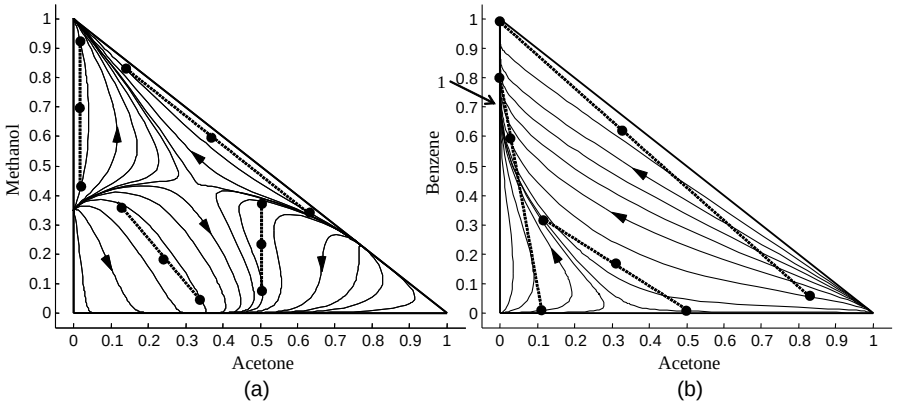


FIGURE 2.14 An example of feasible designs at infinite reflux for (a) the acetone/methanol/chloroform system and (b) the acetone/benzene/chloroform system both operating at $P = 1$ atm.

product compositions can lie in another region. Consider the line marked 1 in Figure 2.14b where the feed is in the bigger region and the products are in the smaller region, but both criteria have been adhered to. This occurs because of the shape of the distillation boundary, and the location of the feed composition in relation to it. Of course, if the distillation boundary was a straight line, or if it curved the other way, then this phenomenon would not occur. Thus, not all azeotropic systems show this behavior. Furthermore, it should be appreciated that when at these operating conditions of infinite reflux, it is never possible to have the two products in two different regions—they always have to lie on the same residue curve, hence be in the same region. Thus, although the feed may be in a different region to the products, the profile tracked out by the liquid in an infinite reflux column can never "cross" the distillation boundary. However, we will see in the chapters that follow that these regions can in fact be overcome in columns operating at finite reflux. It is therefore important to realize that RCMs can be used to give quick insights into potential solutions to overcome distillation boundaries, such as shown in the following example. The reader is referred to Fien and Liu [3] for further insight into bow-tie regions.

WWW

Example 2.2: Suppose an acetone/ethanol/methanol mixture of composition [0.3, 0.3] is to be fed to a distillation column for separation. Determine

(a) All possible products for this feed at RCM conditions
(b) What feed is required to obtain higher purity acetone in the distillate
(c) Whether it is possible to obtain pure methanol in the distillate or bottoms stream

Solution 2.2:

(a) To answer this problem, we produce an RCM for this system. It is immediately obvious that this system has an azeotrope between acetone and methanol with composition of approximately [0.77, 0.23], creating two distinct distillation regions as shown in Figure 2.15. Now, for this feed, it is then possible to identify possible splits through a bow-tie region that pivots around the feed, shown in the shaded area in Figure 2.15. In this case, the presence of the azeotrope reduces the possible attainable splits, because there is no way for distillate and bottoms products to lie in different distillation regions as they cannot be linked by a single residue curve. Thus, in this case, the bow-tie region is partially defined by the curvature of residue curves. The purest attainable distillate composition is therefore the azeotropic acetone/methanol composition, but the purest attainable bottoms composition is pure ethanol. With the given feed, however, these products cannot be obtained simultaneously.

(b) As evident from Figure 2.15's bow-tie region it is impossible, under infinite reflux conditions, to obtain pure acetone in the distillate stream using the feed outlined in the problem statement. In order to obtain high purity acetone in the distillate, the feed would have lie in the other distillation region. Notice, however, that acetone is a saddle point, that is, all profiles swerve away from it, and is impossible to obtain a 100% pure acetone mixture if the feed contains all the components, because it is impossible to satisfy the residue curve and mass balance criteria simultaneously.

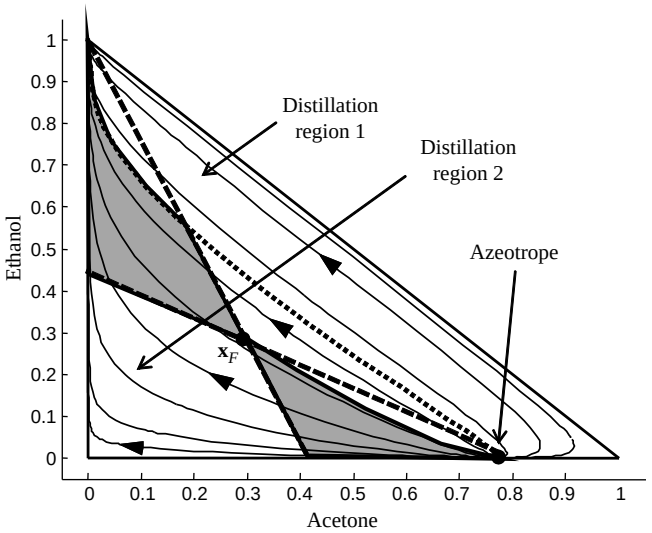


FIGURE 2.15 RCM for the acetone/ethanol/methanol system, showing the unique distillation regions and a bow-tie region.

(c) As evident from the discussion in (b), the saddle node at the acetone vertex prevents one from obtaining pure acetone. Similarly, it is impossible to obtain pure methanol at infinite reflux conditions, regardless of the feed composition.

2.7.4 Column Sequencing at Infinite Reflux

For the ideally behaved system shown in Figure 2.12, the order of volatility from highest to lowest is benzene–toluene–*p*-xylene. There are three possible ways of sequencing units at infinite reflux in order to achieve a separation of all three components. The first method requires two units, the first of which performs the direct split to produce pure benzene, as shown in Figure 2.16a, after which the second separates the remaining binary mixture of toluene and *p*-xylene. Figure 2.16b follows a similar sequence, but incorporates the indirect split, resulting in the distillate needing to be further purified, as shown. In Figure 2.16c, the first column follows neither the direct nor indirect split, but rather performs a split within the bow-tie region, resulting in both the distillate and bottoms products of this column requiring further purification in order to obtain the pure products.

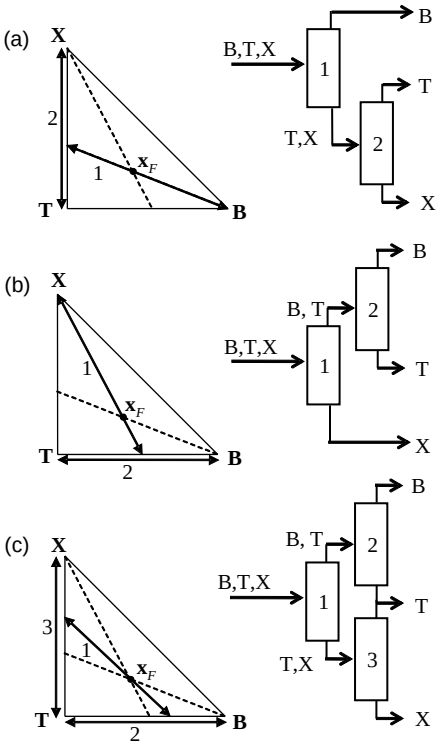


FIGURE 2.16 Sequencing of infinite reflux columns for the benzene [B]/*p*-xylene [X]/toluene [T] system at $P = 1$ atm using (a) a direct split followed by a binary separation, (b) an indirect split followed by a binary separation, and (c) a mixed split followed by two binary separations.

Sequencing infinite reflux columns for azeotropic systems is not as trivial. While methods involving stream splitting and mixing can be applied, this is not the focus of this book, and is not discussed here. For more information regarding this topic, the reader is referred to Fien and Liu [3].

What is evident, however, is that at least two columns are needed to perform a separation of an ideal system of three components—even more would be needed for azeotropic systems. This now gives rise to some important questions which a designer should be asking:

- How does the column sequencing change when operating at *finite* reflux? Remember, operation at finite reflux has $V \neq L$, and thus the material balances derived for infinite reflux no longer hold true.
- Is it possible to perform the entire separation, that is, purify *all* components, in a single column? If so, at what operating conditions, and how does one go about designing such a configuration?

These are topics that will be discussed at length in this book. What can be said at this point, however, is that synthesizing columns at infinite reflux, although insightful, does not offer any practical value.

The principle of RCM-based design techniques have been shown here. Although the residue curve is a single profile, it should be clearly understood that this curve in reality consists of two parts—that of the rectifying and stripping sections, that is, lengths of column above and below the feed entry point, respectively. This will become clearer in subsequent chapters. As mentioned, RCM-based design techniques are impractical because they only reveal information at infinite reflux (and thus require an infinite amount of energy to vaporize and condense material), but they do offer a very good starting point in establishing which designs are feasible and which are not. This is especially true in more complex, azeotropic systems where it is not always immediately obvious what separations can and cannot be achieved.

The reader should also be aware that infinite reflux columns are the smallest attainable columns in terms of column height; however, they do require infinitely large internal flows and hence have operating expenses that are infinitely large to ensure continuous vaporization and condensation. This is the one extreme mode of operation, the other mode being minimum reflux which requires an infinitely high column to be built (and therefore have an initial capital investment that is infinitely large), but the smallest internal flows necessary for a desired separation. This is discussed in more detail in Chapter 4.

2.8 LIMITATIONS OF RCMs

2.8.1 Applications

Despite the ability of RCMs to give a rapid account of potential separation designs, they are, however, derived from a batch experiment and only have applicability to

total and infinite reflux continuous operations, as shown in the preceding sections. Although this limitation may not be entirely obvious at present, it will become apparent in the development of the difference point equation (DPE) in Chapter 3. Infinite reflux in distillation implies infinite energy costs and is therefore an impractical design condition. For separating a continuous feed stream at practical finite reflux conditions, an alternate technique is required that will preferably still retain the most valuable trait of RCMs: to rapidly determine or synthesize a separation path or sequence. Chapter 3 will extend the ideas put forward by the RCM to continuous networks of distillation column sections that ultimately constitute a distillation column operating at finite reflux.

With that said, there is one final aspect of RCMs that needs to be looked at: the analysis of topological behavior of profiles in the space surrounding the MBT. Of course, this is not a standard practice in distillation design, and the reason for looking at this may not be all that apparent at this stage, but will become clear in subsequent chapters. The next section introduces the necessary theory; the application of it will be seen from Chapter 3 onwards.

2.9 RESIDUE CURVE MAPS: THE BIGGER PICTURE

2.9.1 Extending the Axes

As discussed in Section 2.3, the MBT or Gibbs triangle represents the region of physically achievable profiles in ternary systems. One may define this triangular region mathematically as $0 \leq x_i \leq 1$ for all components i, with every point obeying the unity summation constraint of Equation 2.2.

Although the RCM describes a real process it is nonetheless only a set of mathematical differential equations (as given by Equation 2.8). These equations are not bound by any physically relevant initial conditions, and therefore it is possible to evaluate this equation at initial compositions with entries greater than one and less than zero, that is, outside the MBT, with the summation of the individual compositions still equating to one. Mathematically, the residue curve equation can be solved for $-\infty < x_i < \infty$ for all i, provided that unity summation of all components is still maintained. Furthermore, it is taken that the phase equilibrium model permits these negative compositions—this is discussed in Section 2.9.3. By simply selecting initial compositions outside the MBT and integrating in both positive and negative directions, it is possible to construct the entire RCM, as shown in Figure 2.17a and b for a constant relative volatility and nonideal system, respectively.

WWW

TUTORIAL 2.5

Try this for yourself: Reproduce the RCMs in Figure 2.17a and b with DODS-ProPlot using the given parameters. Try generating (a) with other $\boldsymbol{\alpha}$ values and (b) at different pressures.

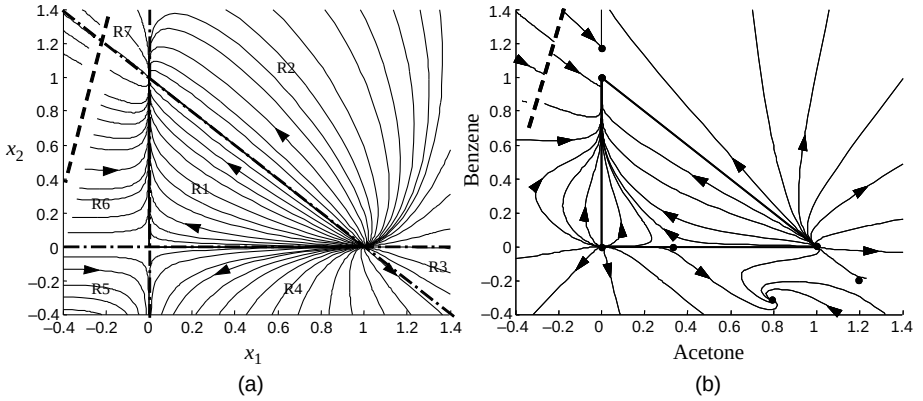


FIGURE 2.17 Entire residue curve maps for (a) a constant relative volatility system with $\boldsymbol{\alpha} = [5,1,2]$ and (b) the nonideal acetone/benzene/chloroform system using the NRTL model at $P = 1$ atm. The black dots indicate stationary points.

It is evident from Figure 2.17a that there are seven different distillation regions, numbered R1–R7, corresponding to the extended axes of the MBT. The extension of the MBT axes are represented by dashed lines in Figure 2.17a. The profiles within each of these regions are qualitatively similar in behavior. In other words, in each of these regions the general profile curvature is similar. This is a phenomenon unique to constant relative volatility systems. In the nonideal acetone/benzene/chloroform system Figure 2.17b, and in fact all nonideal systems, it is more difficult to identify such unique regions because of the existence of multiple nodes both inside and outside the MBT.

WWW

Example 2.3: In Example 2.1, we looked at plots produced in Aspen Plus® for the acetone/ethanol/methanol system at 1 atm. These plots were limited to the bounds of the MBT. Now, given the entire RCM for this same system (generated using DODS-ProPlot) in Figure 2.18 with numbered nodes, identify the different node types as elucidated from Figure 2.7.

Solution 2.3: Given the RCM of this system with profile directions it simple to intuitively infer different node types. Here follows all nodes with a brief statement regarding each of the following:

1. *Stable Node*: All profiles run toward this point. Highest boiling point in the RCM and the liquid composition will tend to this point after infinite boiling of a batch experiment.
2. *Saddle Point*: Profiles initially run toward and then veer away from this point. For any ternary initial composition in a batch experiment, obtaining this composition is impossible.

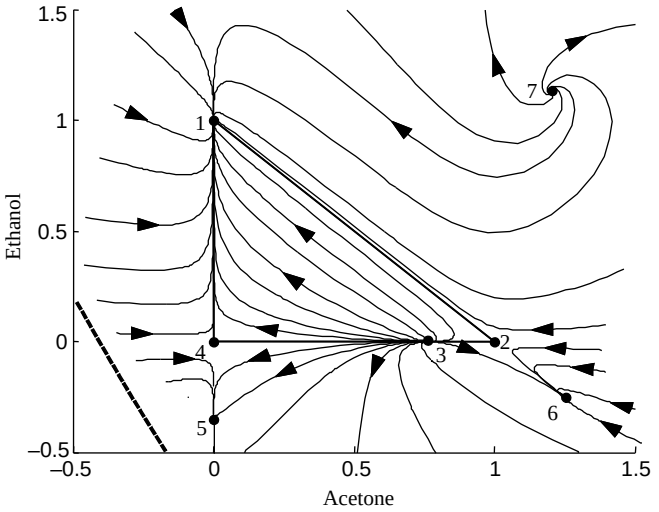


FIGURE 2.18 Entire residue curve map for the nonideal acetone/ethanol/methanol system (with numbered nodes) using the NRTL model at $P = 1$ atm.

3. *Unstable Node*: All profiles diverge from this point. Causes very different profile curvature if initial composition of batch experiment is started on either side of this point.
4. *Saddle Point*: As with 2.
5. *Stable Node*: All profiles run toward this point, even though located in negative composition space.
6. *Stable Node*: As with 5.
7. This node behaves as an unstable node since profiles originate from it. Mathematically, however, it is classified as an unstable focus due to characteristic spiraling (see Section 3.8.1).

From Example 2.3, the question that now arises is this: What is the purpose of generating profiles that exist in a space that is physically unachievable to obtain? Section 2.9.4 and Example 2.4 will partially answer this question, and this issue is also covered more broadly in Chapter 3. It is, however, important to note here that viewing negative compositions is by no means standard practice in distillation design, and since thermodynamic models have not been constructed to include these compositions, some oddities may arise such as discontinuous regions or complex roots. It is also fair to ask whether which thermodynamic models are fit to handle the expanded view of composition space. The following section addresses some of these topics.

2.9.2 Discontinuity

Expanding the view of the composition space to include negative compositions brings with it some inherent mathematical oddities since thermodynamic models were not designed for negative compositions. Along with new stationary points that may be found in negative composition space, there are also areas of discontinuity, or in other words, areas where a denominator in the residue curve equations tends to zero. In the residue curve equation (Equation 2.8), there is only one possible source of discontinuity: the phase equilibrium relationship. In order to determine where these discontinuous regions are located, consider the case where the denominator of the vapor composition (**y**) of the constant volatility system shown in Equation 1.3 is equal to zero.

$$\alpha_1 x_1 + \alpha_2 x_2 + \alpha_3(1 - x_1 - x_2) = 0 \tag{2.23}$$

Rearranging

$$x_1 = \frac{\alpha_2 - \alpha_3}{\alpha_1 - \alpha_3} \quad x_2 - \frac{\alpha_3}{\alpha_1 - \alpha_3} \tag{2.24}$$

Geometrically, Equation 2.24 represents a straight line in x_1–x_2 space and is only a function of the volatilities of the system. An example of the discontinuity for a constant relative volatility system is shown in Figure 2.17a through a dashed line on the outside of the MBT.

Unfortunately, however, determining discontinuous regions for nonideal models is somewhat more complex and very difficult to obtain a simple relationship as given in Equation 2.24. The principle for finding the discontinuity, however, remains the same: it is simply a region in composition space where a denominator in the thermodynamic model tends to zero. In general, most, if not all, real systems will contain discontinuous regions in the negative composition space. It is important to note that discontinuous regions are fixed for a certain set of components, and they always occur outside the MBT.

It should be noted that as trajectories approach areas of discontinuity, the integration procedure should be stopped to avoid excessive computation. This can easily be done by specifying that the absolute difference between vapor and liquid compositions do not exceed a certain tolerance. This tolerance has to be greater than one, since a tolerance less than one may cause profiles to terminate within positive composition space at points that are not pinch points. The choice of tolerance depends somewhat on the system, but a value of 2 will usually suffice.

2.9.3 Thermodynamic Models in Negative Space

In the preceding discussions, we have presented the idea of viewing the entire composition space, both positive and negative. However, it is reasonable to question whether these negative compositions are thermodynamically consistent and if

profiles located outside the composition space allow any insight at all. First, it is worth noting that phase equilibrium models such as UNIQUAC or UNIFAC can immediately be excluded because both contain logarithms of compositions, which are therefore undefined for negative compositions. However, other models such as van Laar, Margules, Wilson, and the NRTL model can safely be extrapolated to negative compositions, as they do not contain such mathematical restrictions.

All phase equilibrium thermodynamic models have to obey, and are constructed according to, the *Gibbs–Duhem* relationship shown in Equation 2.25 [8].

$$\sum_{i=1}^{n_c} x_i \frac{d\ln(\gamma_i)}{dx_j} = 0, \quad \text{for} \quad j = 1, 2, \ldots, n_c \tag{2.25}$$

Intuitively, all vapor–liquid equilibrium models obey this relationship in positive composition space, but in order to be sure that it is useful, and valid, to analyze negative compositions, the *Gibbs–Duhem* relationship should be maintained for negative composition too. Since $\gamma_i = 1$ for the ideal and constant relative volatility cases, this condition is always valid for the entire composition spectrum, since the derivative of a constant is zero. Fortunately, it can be shown that all other models where γ_i is a function of composition (NRTL, Wilson, and so on) obey this rule, except in areas of discontinuity. Therefore, it is safe and thermodynamically sound, to analyze and interpret these negative compositions as they still obey fundamental thermodynamic rules.

2.9.4 Use of Negative Compositions

Once the underlying properties and concepts of the negative composition space have been understood, it is now convenient to explore the applications of viewing negative compositions. Example 2.4 shows how nodes placed in negative composition space at 1 atm can in fact be moved.

WWW

Example 2.4: Following on from Example 2.3 using negative compositions, examine the difference in the overall RCM topology when changing system pressure from 1 to 10 atm for the nonideal acetone/ethanol/methanol system.

Solution 2.4: Figure 2.18 already illustrates a RCM for the acetone-/ethanol/methanol system at 1 atm. Fortunately, nodes have been numbered in this diagram enabling one to track the movement of specific nodes at 10 atm. Figure 2.19 shows a RCM for the same system, but at 10 atm pressure with nodes again being numbered in accordance with Figure 2.18.

Figure 2.19 illustrates that node number 6, previously located in negative composition space at 1 atm in Figure 2.18, has in fact been moved into the MBT and lies on the acetone vertex at 10 atm. Node number 2 has now become a binary

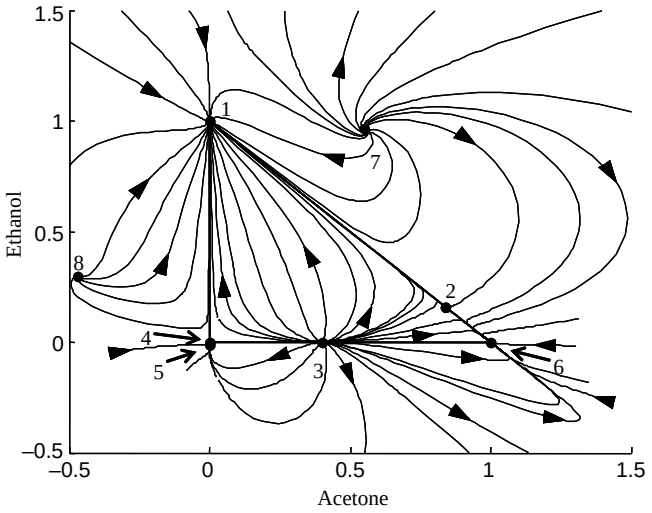


FIGURE 2.19 Entire residue curve map for the nonideal acetone/ethanol/methanol system (with numbered nodes) using the NRTL model at $P = 10$ atm.

azeotrope at 10 atm. Similarly, node number 4 has also become a binary azeotrope by being displaced by node number 5 that was previously in negative space. Furthermore, another node, number 8, has also come into view although it does not have an effect on the profiles within the MBT.

Example 2.4 illustrates a fascinating result. Residue curves in negative space, which are meaningless in a physical sense, can be used to identify and predict topological changes at different pressures. By allowing negative compositions at 1 atm, a designer is given an *a priori* insight into a system's behavior. In other words, the somewhat mysterious appearance and disappearance of azeotropes at different pressures can be understood and predicted more clearly.

To reiterate what was said at the start of this section, certain thermodynamic models cannot be used when plotting outside the MBT due to the presence of logarithms of composition which cannot be evaluated for negative values. However, we can still use these models to see if the same or similar behavior is experienced *within* the MBT. As an example, consider the RCM plot for the acetone/ethanol/methanol system operating at 10 atm as shown in Figure 2.20. This plot was generated in Aspen Plus® using the UNIQUAC thermodynamic model.

Comparing the plot in Figure 2.20 with that obtained using the NRTL model at the same pressure, shown in Figure 2.8b, we immediately see the same behavior of the nodes and topology. Although we cannot produce the profiles outside the MBT using the UNIQUAC model, our knowledge is such that we are in a position to explain how these nodes came to be. We now know that the binary azeotrope between acetone and ethanol, for example, did not just "appear," but in fact was always there (at 1 atm, for example), it just happened to lie outside the MBT!

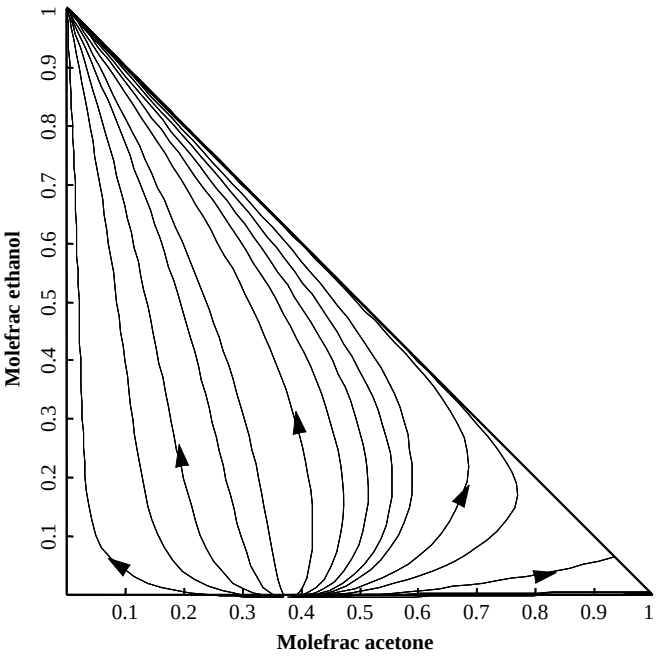


FIGURE 2.20 CM plot generated in Aspen Plus® for the acetone/ethanol/methanol system using the UNIQUAC thermodynamic model at $P = 10$ atm.

In the next chapter, an equivalent node-shifting principle will be shown for continuous distillation column sections: at the appropriate operating conditions, pinch points can be shifted. Some pinch points move from real space (within the MBT) to negative space (outside the MBT), and vice versa. Thus, the mode of operation of the piece of equipment can be used to shift unwanted topological features outside the MBT.

2.10 SUMMARY

This purpose of this chapter is to introduce the reader to describing and designing distillation columns using a differential equation. This differential equation can easily be graphed, thereby making the design and analysis procedure fairly straightforward and intuitive. However, the graphs presented in this chapter, RCMs, only allow one to glean information at infinite or total reflux, a rather impractical operating condition. Nonetheless, these ideas are the foundation for "real" column design, as will be shown in the subsequent chapters. Finally, the notion of viewing negative compositions has been introduced in this chapter. Although compositions outside the MBT are unrealistic and never physically realizable, they do lend some insight into real-world problems.

REFERENCES

[1] Schreinemakers, F.A.H., Einige bemerkungen ueber dampfdruecke ternaerer gemische. *Journal of Physical Chemistry*, 1902, **43**:671–685.

[2] Rayleigh J.W.S., On the distillation of binary mixtures. *Philosophical Magazine*, 1902, **6** (4):521–537.

[3] Fien, G.-J.A.F. and Y.A. Liu, Heuristic synthesis and shortcut design of separation processes using residue curve maps: A review. *Industrial & Engineering Chemistry Research*, 1994, **33**(11):2505–2522.

[4] Kiva, V.N., E.K. Hilmen, and S. Skogestad, Azeotropic phase equilibrium diagrams: A survey. *Chemical Engineering Science*, 2003, **58**(10):1903–1953.

[5] Doherty, M.F. and J.D. Perkins, On the dynamics of distillation processes—I: The simple distillation of multicomponent non-reacting, homogeneous liquid mixtures. *Chemical Engineering Science*, 1978, **33**(3):281–301.

[6] Doherty, M.F. and J.D. Perkins, On the dynamics of distillation processes—II. The simple distillation of model solutions. *Chemical Engineering Science*, 1978, **33**(5):569–578.

[7] Doherty, M.F. and J.D. Perkins, On the dynamics of distillation processes—III: The topological structure of ternary residue curve maps. *Chemical Engineering Science*, 1979, **34**(12):1401–1414.

[8] Smith, J.M., H.C.Van Ness, and M.M. Abbott, *Introduction to Chemical Engineering Thermodynamics*. 7th ed. McGraw-Hill Chemical Engineering Series. 2005, Boston: McGraw-Hill. xviii, p. 817.

CHAPTER 3

DERIVATION AND PROPERTIES OF COLUMN PROFILE MAPS

3.1 INTRODUCTION

As highlighted in the introduction to the book, distillation is an enormous consumer of energy. Process engineers are thus required to seek new and alternative methods for large-scale separations that are more energy efficient. This needs to be done by critically reexamining distillation and identifying areas of improvement, or synthesizing new distillation schemes. At present, however, most other means of industrial scale separation are either too expensive or not well understood to be employed immediately. Therefore, improving our understanding of distillation design and improving industrial scale separations appears to be the most pragmatic alternative. In order to achieve this goal, a design tool is required that allows a designer to freely and creatively synthesize any structure, and not be confined by any predetermined ideas about optimal configurations.

Over the past several decades, residue curve maps (RCMs) have gained interest, by design engineers and academics alike, as a useful tool when assessing and understanding a particular separation system. The previous chapter explained the ideas behind RCMs, and their applications to continuous processes. However, it was shown that RCMs are limited in that they are only directly applicable to the impractical total and infinite reflux operation scenarios. While one could guess or estimate how finite reflux columns may behave, a more fundamental and reliable method needs to be developed for process design simulations that require finite reflux operating conditions.

Understanding Distillation Using Column Profile Maps, First Edition. Daniel Beneke, Mark Peters, David Glasser, and Diane Hildebrandt.
© 2013 by John Wiley & Sons, Inc. Published 2013 by John Wiley & Sons, Inc.

The advent of rigorous process simulation packages, such as Aspen Plus® and HYSYS®, has significantly enhanced the performance of processes through rigorous optimization. However, despite these packages' unquestionable modeling capabilities, they are almost exclusively "black-box" type design simulators, meaning that the user specifies certain operating conditions of a given process and a set of results are returned corresponding to the input. Although useful, this black-box type approach has the drawback that the user has limited insight into the final design solution and it is often difficult to grasp the important subtleties hidden within the results.

This chapter introduces a novel tool that allows design engineers to gain further insight into distillation systems. This technique gives the freedom to not only design distillation processes but also to *synthesize* them. In other words, the method gives the opportunity to explore more creative distillation systems, and does not confine to a set design.

3.2 THE COLUMN SECTION (CS)

Most of the complexity in modeling and designing distillation processes arises from the fact that it is difficult to derive a single, continuous model that includes the points of material and/or energy addition and/or removal in a distillation column, no matter how simple its configuration. The addition and removal of material and energy instantly changes the flowrates and compositional fluxes from one section of a column to the next, making it difficult to interpret the effects of this with a single, continuous model for an entire column. For example, in a simple distillation column comprising of two column sections (CSs), the addition of the feed stream changes the mode of operation from rectifying in one section to stripping in the next section. The inclusion of this transition in a single mathematical model for the entire column is thus difficult to express.

A more pragmatic approach is to break down a distillation configuration into a series of CSs [1], where a CS is defined as *a length of column located between points of material and/or energy addition or removal.*

A simple column (i.e., one with a single feed and two products) will thus have two CSs, one below and one above the feed, as shown in Figure 3.1a. These particular CSs are more commonly referred to as the rectifying section (1) and stripping section (2). Figure 3.1b extends the idea of CS breakdowns to an arbitrarily chosen distillation configuration.

The concept of a CS is by no means a new one, but importantly the breakdown approach shown in Figure 3.1a and b is generalized. This allows one to break down *any* distillation configuration, irrespective of its complexity, into simpler units that are easier to model, instead of trying to model the entire column as a whole. One now has the building blocks to analyze different configurations while not being constrained to a single predefined structure. In other words, the designer now has the ability to *synthesize* the system using almost any imaginable distillation structure subject to counter current vapor–liquid separation using this simple building block. Subsequent chapters in this book deal with column design using this very idea of

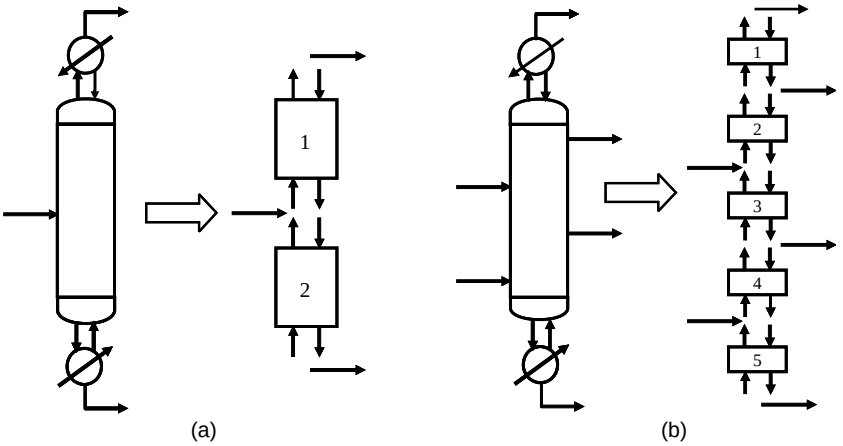


FIGURE 3.1 A CS breakdown of (a) a simple column into the rectifying [1] and stripping sections [2], and (b) an arbitrary column into a sequence of column sections.

generalized CSs, as well as extending it to include other phenomena such as chemical reactions and membrane permeation.

Example 3.1: Given the distillation structures in Figure 1.3a and b, perform a CS breakdown on each and count the total number of CSs used in each configuration.

Solution 3.1: Following the examples laid out in Figure 3.1a and b, one can perform similar breakdowns for the structures shown in Figure 1.3a and b. These breakdowns are shown in Figure 3.2a and b.

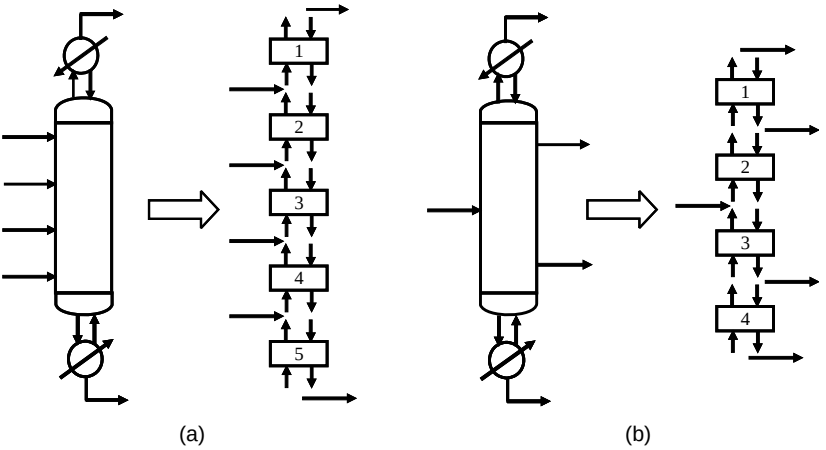


FIGURE 3.2 CS breakdown for the (a) distributed feed column having five CSs and (b) side-draw column with four CSs.

3.3 THE DIFFERENCE POINT EQUATION (DPE)

3.3.1 The Generalized CS

The generalized CS definition conveniently puts one in a position to concentrate on a single piece of equipment at a time, and not consider the entire column from the onset. A magnified view of a CS is shown in Figure 3.3, along with the definitions of all entering and exiting streams, allowing a mass balance across the section to be written.

In Figure 3.3, the following nomenclature applies

L and V are liquid and vapor streams, respectively (mol/s),
$\mathbf{x}$ is the molar fraction composition of the liquid $(-)$,
$\mathbf{y}$ is the molar fraction composition of the vapor $(-)$,
n is a representation of position in column section length $(-)$, and
superscript (T) merely references the top of the CS.

The following assumptions have been applied to Figure 3.3:

- All flows and compositions at the top (T) of a CS are known and constant. This assumption is completely arbitrary and can be altered accordingly, if necessary.
- Flows L and V are assumed constant throughout the CS. This is a result of the constant molar overflow (CMO) assumption (see Section 3.3.2).
- The column internals are either trays or packing. In a CS with trays, the vapor and liquid only come into contact at discreet points (i.e., on the trays). In a packed CS, there is continuous contact between vapor and liquid streams. The principle of "height equivalent theoretical plate (HETP)" is therefore used, which allows to model both packed and trayed CSs using the same position variable, n. Thus, the position variable, n, is often referred to as the "number of trays" or "stage number." However, since it may represent a continuous packing rather than discreet points, $n \in \mathbb{R}$.

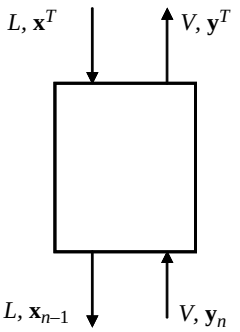


FIGURE 3.3 A general CS with all entering and exiting stream definitions.

In Figure 3.3, the two top streams with composition $\mathbf{x}^T$ and $\mathbf{y}^T$ are considered *passing* liquid and vapor streams, respectively, meaning that these streams are not in equilibrium with each other and merely pass one another. Since it was assumed that all flows and compositions are known at the top of the CS, it is logical to set $n = 0$ at this point. However, this is arbitrary and one could have equivalently chosen the bottom of the CS for this reference point. Therefore, as one progresses downward in the CS, the stage numbers (n) increase. On the $(n-1)$th stage in the CS, the vapor flowing into this stage comes from the stage below, that is, the nth stage. The liquid exiting stage $n-1$ is then the liquid feed to stage n. On any particular stage n, it is assumed that vapor ($\mathbf{y}_n$) and liquid ($\mathbf{x}_n$) streams are in equilibrium with each other, at the bubble-point temperature of the mixture. It is important to note that the stream notation could have been reversed, that is, with passing streams $\mathbf{x}^T$ and $\mathbf{y}^T$ at the bottom of the CS and streams $\mathbf{x}_{n-1}$ and $\mathbf{y}_n$ entering and exiting from the top of the CS, respectively. The subsequent derivation, however, does not depend on this convention.

3.3.2 Constant Molar Overflow

An important assumption has been made in the definition of streams: the total vapor and liquid flowrates (V and L, respectively) remain unchanged along the CS, even though the respective compositions are changing with position. This assumption is often referred to as the CMO assumption, and is quite a common practice in distillation design. The CMO assumption effectively replaces the energy balance around the CS. The assumption is exact when the latent heats and heat capacities of all components are equal, and when mixing effects and heat transfer through the column walls are negligible. The relaxation of the CMO assumption would require to simultaneously solve both mass and energy balances, making computation and interpretation of results considerably more complex. However, for most systems encountered in industrial distillation, the CMO assumption is generally very good, and only extreme cases need to be dealt with otherwise. Guidelines for solving such extreme cases can be found in a paper by Knight and Doherty [2]. The CMO assumption will be employed throughout this book, unless otherwise stated.

3.3.3 Material Balances

With the streams and compositions across the CS now defined, a material balance yields

$$V\mathbf{y}_n + L\mathbf{x}^T - V\mathbf{y}^T - L\mathbf{x}_{n-1} = 0 \tag{3.1}$$

It is now convenient to define three important parameters. These parameters will ultimately dictate the operation of a CS.

First, the *net flow* through the CS [1]

$$\Delta = V - L \tag{3.2}$$

From Equation 3.2, it can be seen that Δ is the difference between the internal flows of a CS, and thus gives information regarding the overall net movement of material (up or down) in a CS. Δ is, obviously, not an actual flow in the CS, but can nonetheless be regarded as a pseudo flow. Further, being a difference in two flows, it is obvious that Δ can exhibit either positive or negative values.

Second, the composition of the net flow, or *difference point*, is defined as

$$\mathbf{X}_{\boldsymbol{\Delta}} = \frac{V\mathbf{y}^T - L\mathbf{x}^T}{\Delta}; \quad \Delta \neq 0 \tag{3.3}$$

To fully define a stream, both its total flow and composition are required (e.g., F and $\mathbf{x}_F$ completely define the feed stream to a distillation column). Thus, if one were to regard Δ as a pseudo real flow, then its composition would be $\mathbf{X}_{\boldsymbol{\Delta}}$. $\mathbf{X}_{\boldsymbol{\Delta}}$ can thus be viewed as a pseudo composition. The sum of the elements of $\mathbf{X}_{\boldsymbol{\Delta}}$ is unity, similar to real compositions, that is,$\sum_{i=1}^{nc} X_{\Delta i} = 1$. As with real compositions, one only needs to specify *nc*–1 entries in the $\mathbf{X}_{\boldsymbol{\Delta}}$ vector to fully define it—the last composition is inferred by the unity summation property. This is explained more deeply in Section 3.5.2.

Lastly, a generalized *reflux ratio* is

$$R_\Delta = \frac{L}{\Delta} \tag{3.4}$$

This parameter is the ratio of liquid flow in a CS to the net flow. Since $\boldsymbol{\Delta}$ may be negative, it is perfectly acceptable that R_Δ may exhibit either positive or negative values.

A brief discussion on the physical meanings of these parameters has been given here—a more detailed discussion regarding the same, and their implications on operation, is given in Section 3.5.

Replacing the definition of the $\mathbf{X}_{\boldsymbol{\Delta}}$ into Equation 3.1 gives

$$\mathbf{x}_{n-1} = \frac{V}{L}\mathbf{y}_n - \frac{\Delta}{L}\mathbf{X}_{\boldsymbol{\Delta}} \tag{3.5}$$

Furthermore, using the definition of reflux ratio, Equation 3.5 can be written as

$$\mathbf{x}_{n-1} = \left(1 + \frac{1}{R_\Delta}\right)\mathbf{y}_n - \frac{1}{R_\Delta}\mathbf{X}_{\boldsymbol{\Delta}} \tag{3.6}$$

Now, expanding $\mathbf{x}_n$ around stage n using a Taylor series gives

$$\mathbf{x}_n = \mathbf{x}_{n-1} + \frac{d\mathbf{x}}{dn}\Delta n + \frac{d^2\mathbf{x}}{dn^2}\Delta n^2 + \cdots \tag{3.7}$$

Assuming that only the first-order derivative is significant [3,4] and noting that $\Delta n = n-(n-1) = 1$, Equation 3.7 reduces to

$$\frac{d\mathbf{x}}{dn} = \mathbf{x}_n - \mathbf{x}_{n-1} \tag{3.8}$$

Replacing $\mathbf{x}_{n-1}$ in Equation 3.6 by the definition in Equation 3.8 results in

$$\frac{d\mathbf{x}}{dn} = \left(1 + \frac{1}{R_\Delta}\right)(\mathbf{x}_n - \mathbf{y}_n) + \left(\frac{1}{R_\Delta}\right)(\mathbf{X}_\Delta - \mathbf{x}_n) \tag{3.9}$$

Finally, we can drop the subscript n, resulting in

$$\frac{d\mathbf{x}}{dn} = \left(1 + \frac{1}{R_\Delta}\right)(\mathbf{x} - \mathbf{y}) + \left(\frac{1}{R_\Delta}\right)(\mathbf{X}_\Delta - \mathbf{x}) \tag{3.10}$$

Equation 3.10 is known as the difference point equation (DPE). It is a first-order differential equation that governs the change in liquid composition, $\mathbf{x}$, with progressing stage numbers, n, in a single, general CS. Although derived under the assumption that flows and compositions at the top of the CS are known, the same result would emerge if an assumption pertaining to the bottom of the CS was used.

It is worth noting that the DPE is based on the pioneering work by Doherty and coworkers [2–6] for conventional (nongeneralized) rectifying and stripping sections, as found in simple columns. It will be shown in Chapter 5 how the generalized DPE can be applied to these conventional distillation sections, and in fact produce the same result.

The DPE is not restricted to a specific VLE model and is also not configuration specific. Integration of the DPE can easily be done numerically with a Runge–Kutta type method (as was done when generating RCMs). All that is required from the user to determine the change in liquid composition through a CS are the values for $\mathbf{X}_\Delta$,R_Δ, a model for the VLE relationship, and a boundary condition (liquid composition at stage 0) from where integration can commence.

3.4 COLUMN PROFILE MAPS

As seen with the RCMs in Chapter 2, a greater understanding can often be gleaned into abstract, mathematical problems by representing the problem visually. Although the DPE is an elegant means of tracking compositional changes as stages progress in a CS, many insights can be gained by plotting the compositional changes against each other—similarly to RCMs. Although interpreting the DPE graphically is much more difficult for higher order systems, it is especially useful for three- and four-component systems, which can be represented in a two- and three-dimensional space, respectively.

In this section, column profiles and eventually entire column profile maps (CPMs) will be generated. The discussions and interpretations that are given relate somewhat to the operation of a CS, but are mostly done from a mathematical and topological perspective. Once understood, these aspects of CPMs will be used to appreciate the physical operation of various CSs.

3.4.1 Constant Relative Volatility Systems

Consider a ternary system with arbitrarily chosen process parameters of $\mathbf{X}_{\boldsymbol{\Delta}} = [0.2, 0.3]$, $R_{\Delta} = 5$, $\boldsymbol{\alpha} = [5, 1, 2]$, and an initial integration composition of $\mathbf{x}^T = \mathbf{x}^{\mathbf{0}} = [0.8, 0.1]$. This initial integration composition is the liquid composition on stage $n = 0$, and is simply the boundary value required to solve the set of differential equations. The independent integration variable (n) is taken from zero to a sufficiently large number of positive stages, thus portraying the change in composition downward in the CS. Using these parameters and integrating the DPE, the profile shown in Figure 3.4 is obtained.

WWW

TUTORIAL 3.1

Try this for yourself: Reproduce Figure 3.4 with DODS-ProPlot using the given parameters. Try generating similar figures with different values for $\mathbf{X}_{\boldsymbol{\Delta}}$, $\mathbf{x}^{\mathbf{0}}$, R_{Δ}, and $\boldsymbol{\alpha}$.

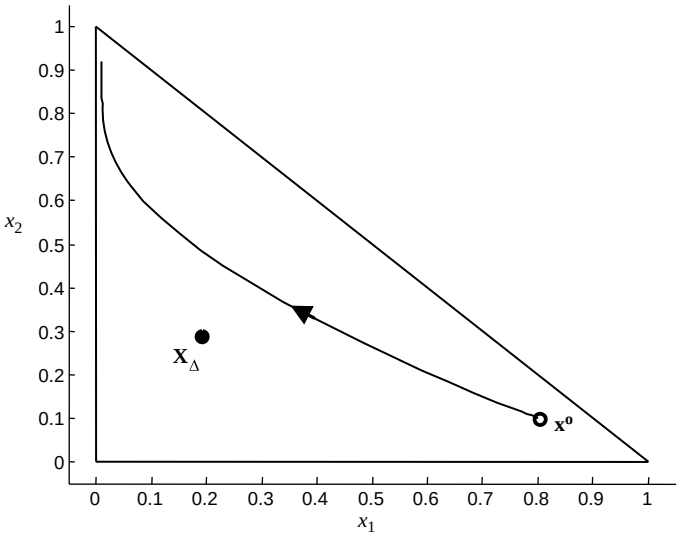


FIGURE 3.4 A column profile indicating the change in composition for a constant relative volatility system with $\boldsymbol{\alpha} = [5, 1, 2]$ along a CS with arbitrarily specified conditions $\mathbf{X}_{\boldsymbol{\Delta}} = [0.2, 0.3]$, $R_{\Delta} = 5$, and $\mathbf{x}^{\mathbf{0}} = [0.8, 0.1]$.

The curve in Figure 3.4 is known as a *column profile* or a *liquid composition profile*. This trajectory originates from the topmost composition, $\mathbf{x}^{\mathbf{0}}$, and terminates, in this case, at a location near (but not at) the high boiler vertex. A large enough integration parameter, n, has been used to allow the profile to reach its termination, or pinch, point.

As is done when producing RCMs, the integration may be performed in both positive and negative directions: from zero to both a sufficiently large positive and negative n. Integrating in a negative direction is equivalent to determining the change in composition from the bottom of the CS upward, and vice versa. Furthermore, the DPE, like the residue curve equation, is also not bound, mathematically, by physically obtainable compositions. One may, in fact, choose initial integration compositions to lie anywhere in the composition space, as was done when constructing entire RCMs in Chapter 2. With this in mind one can populate the entire composition space with profiles, for the same process parameters as given in Figure 3.4. The resulting map, shown in Figure 3.5, is known as a CPM.

WWW

TUTORIAL 3.2

Try this for yourself: Reproduce Figure 3.5 with DODS-ProPlot using the given parameters. Try generating similar figures with different values for $\mathbf{X}_{\mathbf{\Delta}}$, R_{Δ}, and $\boldsymbol{\alpha}$.

From Figure 3.5, it is apparent that a CPM has the same topological characteristics as an RCM (refer to Figure 2.17a). However, remembering that the MBT is fixed in the

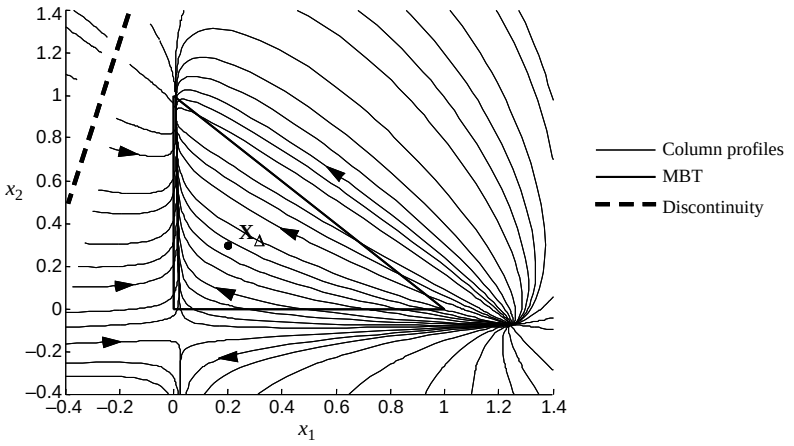


FIGURE 3.5 A CPM for a constant relative volatility system with $\boldsymbol{\alpha} = [5, 1, 2]$ using arbitrarily specified conditions $\mathbf{X}_{\mathbf{\Delta}} = [0.2, 0.3]$ and $R_{\Delta} = 5$. The MBT is shown as solid black lines. The discontinuity is indicated by the dashed line.

composition space, it can be seen that all the original stationary points are still present but have been shifted away from the pure component locations. When compared to the RCM plot, the CPM plot is just a rotation and resizing of its accompanying RCM! With this, it can be stated that *a CPM is a simple linear transform of the RCM*. It is important, however, to note that the discontinuity discussed in Section 2.9.2 present in the RCM does not move and is unaltered by the linear transformation of the DPE, and is thus in the same position in the CPM in Figure 3.5.

All the profiles depicted in the CPM have different entering liquid compositions but were all generated with the same operating parameters, namely $\mathbf{X_\Delta}$ and R_Δ, that is, all the profiles still obey the CS mass balance. The physical meaning and implications of these parameters on operation will be discussed in subsequent sections. Each trajectory represents the compositional change along a CS for a set R_Δ and $\mathbf{X_\Delta}$ from different entering liquid compositions, $\mathbf{x}^T$ or $\mathbf{x}^B$, to a pinch point. The arrows indicated on the profiles show the direction of positive integration, that is, from the top of a CS down. Therefore, commencing integration at $\mathbf{x}^T$ will follow the profile in the direction of the arrow, as shown. Starting at $\mathbf{x}^B$, on the other hand, implies that the profile obtained will move in a direction opposite to that shown on the map.

WWW

Example 3.2: Using the DODS-ProPlot program, generate CPM plots for the following constant relative volatility system with $\boldsymbol{\alpha} = [5, 1, 2]$:

(1) $\mathbf{X_\Delta} = [1.2, 0.3]$, $R_\Delta = 5$
(2) $\mathbf{X_\Delta} = [1.2, -0.3]$, $R_\Delta = 5$
(3) $\mathbf{X_\Delta} = [0.4, -0.2]$, $R_\Delta = 5$

Compare these plots with the RCMs for the same system (refer to Figure 2.17a).

Solution 3.2: Figure 3.6 shows the plots one should obtain from the program. Note that the plots shown include dashed, straight lines which trace the movement of pinch points. Collectively these lines produce a triangle, known in the context of CPMs as a transformed triangle (TT). The importance and use of the TTs are discussed in greater detail in Section 3.6.5.

Notice in Example 3.2 that the reflux ratio used is the same in all CPM plots, including the one shown in Figure 3.5. It is thus interesting to note that the resulting trajectories inside the MBT follow very different paths depending on the position of the difference point. The $\mathbf{X}_\Delta$ position in Figure 3.6c, for instance, shifts a saddle and a stable node inside the MBT which changes the path and the directions of certain profiles dramatically. Similar changes in the profiles from RCM conditions are also seen in the other plots.

It is of importance to understand that the CPMs in Figures 3.5 and 3.6 are showing all possible trajectories that can be achieved mathematically. From a

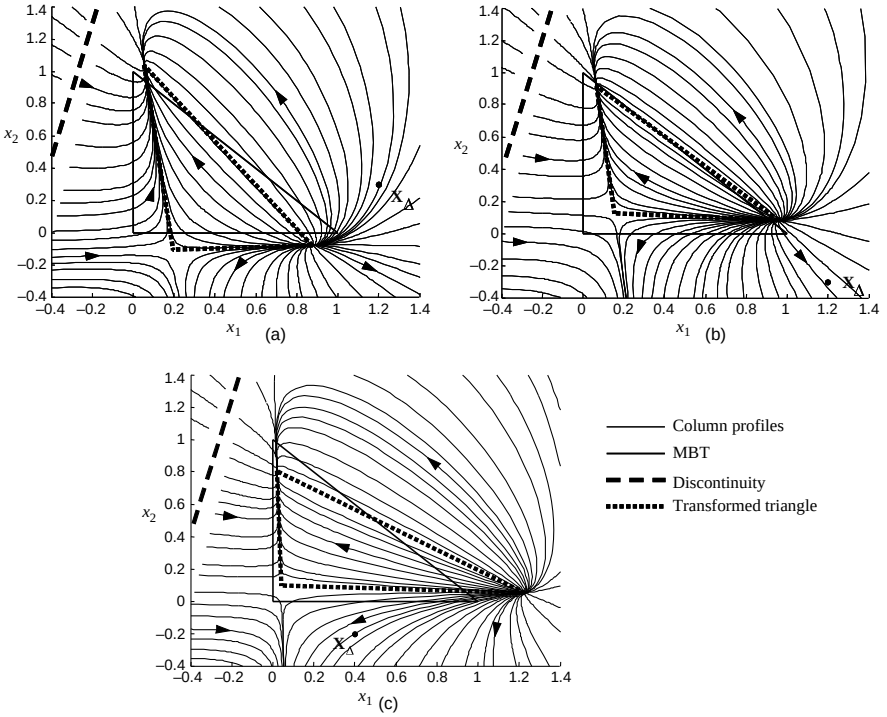


FIGURE 3.6 CPMs for a constant relative volatility system with $\boldsymbol{\alpha} = [5,\ 1,\ 2]$ using arbitrarily specified conditions (a) $\mathbf{X}_{\boldsymbol{\Delta}} = [1.2,\ 0.3]$ and $R_\Delta = 5$, (b) $\mathbf{X}_{\boldsymbol{\Delta}} = [1.2,\ -0.3]$ and $R_\Delta = 5$, and (c) $\mathbf{X}_{\boldsymbol{\Delta}} = [0.4,\ -0.2]$ and $R_\Delta = 5$.

physical point of view, however, only the profiles within the MBT are obtainable. However, notice that when compared to the RCM in Figure 2.17a, some profiles (or parts thereof) that are in the MBT under RCM conditions have shifted outside the MBT, and are no longer achievable at the operating conditions specified for the CPM. With that said, there are also numerous profiles that are in the negative space at RCM conditions that are now suddenly physical profiles since they are in the MBT. The manner in which these profiles, and their associated nodes, shift is dependent on the operating parameters $\mathbf{X}_{\boldsymbol{\Delta}}$, R_Δ, and the operating column pressure (P).

By populating the entire composition space with profiles, one now has a global topological view of the separation at hand and it is possible to construct any particular CS to suit the needs of a desired separation. At this stage, it is important to emphasize that the designer has freedom in choosing these parameters, and in doing so can shift topology within the composition space as he/she desires. The potential of this is rather staggering: it may be possible to shift unwanted topology (such as azeotropes) located within the real composition space to lie outside it, or

alternatively, to move desirable topology (perhaps a stable node) from the negative composition to lie in positive composition space.

3.4.2 Nonideal Systems

Nonideal systems are very interesting to study with the CPM technique. The traditional view in distillation was that nonideal mixtures are difficult to study and therefore even more difficult to design. Classic design techniques are for the most part lacking in this area, and often large simplifications and assumptions are made merely to suit the design method. Fortunately, the CPM technique may be used to model any form of nonideal behavior with the same amount of effort as simpler systems (apart from a slightly longer computational time). Somewhat counter-intuitively, nonideal systems containing multiple azeotropes may even hold advantages for the designer because there are more points to manipulate and hence more opportunities for creative designs. This is a unique attribute of the CPM design technique.

Figure 2.17b gives the entire RCM for the acetone/benzene/chloroform system at 1 atm. Examination of this map indicates that there are several nodes to be found even outside the physically realizable composition space. Clearly, the presence of additional stationary points gives more room for manipulation. A situation where the acetone/chloroform azeotrope in the acetone/benzene/chloroform system has been shifted into negative composition space is shown in Figure 3.7, with the relevant parameters indicated.

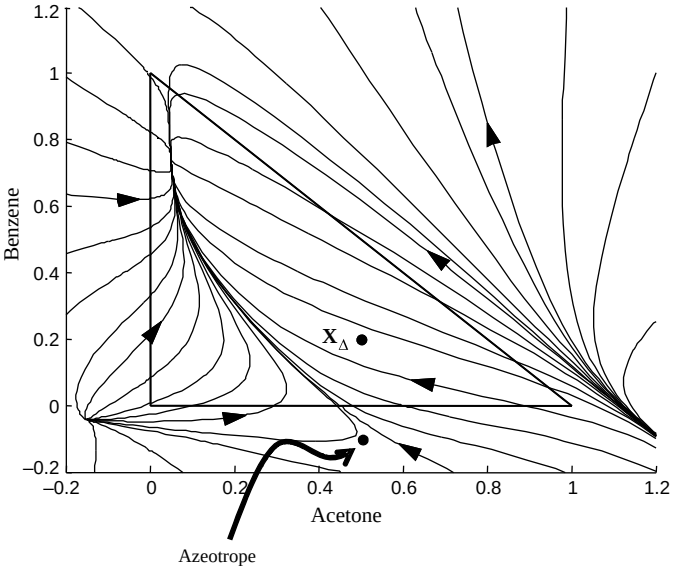


FIGURE 3.7 A CPM for the acetone/benzene/chloroform system at $R_\Delta = 5$ and $\mathbf{X}_\Delta = [0.5, 0.2]$. The NRTL model was used at $P = 1$ atm.

WWW

TUTORIAL 3.3

Try this for yourself: reproduce Figure 3.7 with DODS-ProPlot using the given parameters. Try generating similar figures with different values for $\mathbf{X_\Delta}$, R_Δ, and P.

Figure 3.7 shows that profiles have been considerably altered from the RCM conditions by this choice of parameters. Since the azeotropic point has been altered, the distillation boundary identified in the RCM has also changed. Thus, separations that were previously thought to be infeasible due to the distillation boundary using the RCM technique may in fact be feasible at finite reflux conditions. There is, of course, also the possibility that the choice of parameters for the CPM could in fact shift azeotropic points into the MBT, potentially complicating the separation. Such a case is shown in Example 3.3.

WWW

Example 3.3: Considering the RCM for acetone/benzene/chloroform system in Figure 2.17b, investigate and comment on how the azeotropic composition between acetone and chloroform is shifted with $\mathbf{X_\Delta} = [0.1, 0.8]$ for $R_\Delta = \pm 15$ using DODS-ProPlot. As with the RCM in Figure 2.17b the NRTL model at $P = 1$ atm may be used.

Solution 3.3: As with the Example 3.2, it is very easy to create a CPM for these conditions using DODS-ProPlot. Figure 3.8a and b shows the two cases requested in the problem statement.

Figure 3.8a shows that the azeotropic node has moved outside the MBT. In fact, all nodes, except for the stable node (near the benzene vertex), have been shifted beyond the enclosures of the MBT. On the other hand, with a reflux of $R_\Delta = -15$ in Figure 3.8b, the azeotropic composition as well two unstable nodes are located within the MBT. Clearly, Figure 3.8b represents a more complex distillation problem and the designer may want to seek alternative modes of operation, if possible.

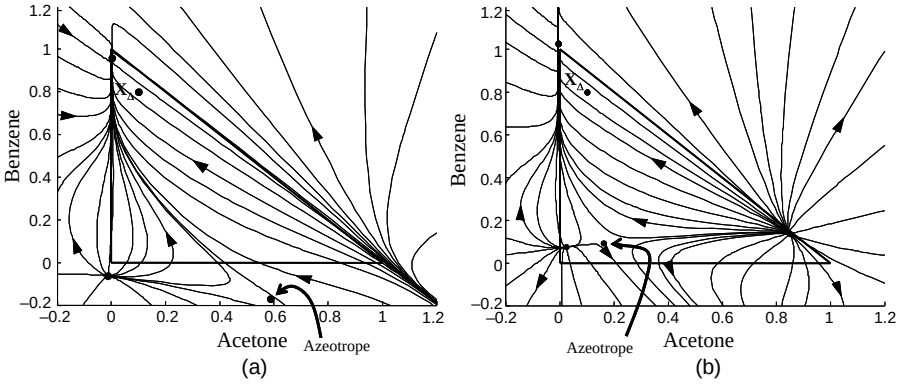


FIGURE 3.8 CPMs for the acetone/benzene/chloroform system for $\mathbf{X_\Delta} = [0.1, 0.8]$ and (a) $R_\Delta = 15$, and (b) $R_\Delta = -15$ generated using the NRTL model at $P = 1$ atm.

3.5 THE EFFECT OF CPM PARAMETERS

3.5.1 The Net Flow (Δ)

The net flow in a CS, $\Delta = V - L$, governs the direction of the flow of the bulk material. By definition, it is implied that if $V > L$, then $\Delta > 0$ and the net flow in a CS is upward, while if $L > V$, then $\Delta < 0$ and the bulk flow is downward. Although the net flow does not explicitly appear in DPE and need not be specified in order to construct a CPM, it is important to realize its significance in terms of actual column operation. Consider for a moment a simple one-feed-two-product distillation setup as shown in Figure 3.1a, consisting of a rectifying and a stripping CS across the feed stage, as presented in Figure 3.9a and b, respectively. The rectifying section produces a distillate product with a flowrate of D and the stripping section a bottoms product with a flowrate of B.

A mass balance around the condenser above the rectifying CS shows that

$$V_R - L_R = D = \Delta_R \tag{3.11}$$

where the subscript R indicates quantities in a rectifying section.

Equation 3.11 shows that since the distillate flowrate, D, is always positive, the net flow, Δ_R, is too. Rectifying sections are thus, by definition, characterized by a positive (upward) net flow, as indicated in Figure 3.9a.

A mass balance around the stripping section in Figure 3.9b gives

$$V_S - L_S = -B = \Delta_S \tag{3.12}$$

where the subscript S indicates quantities in a stripping section.

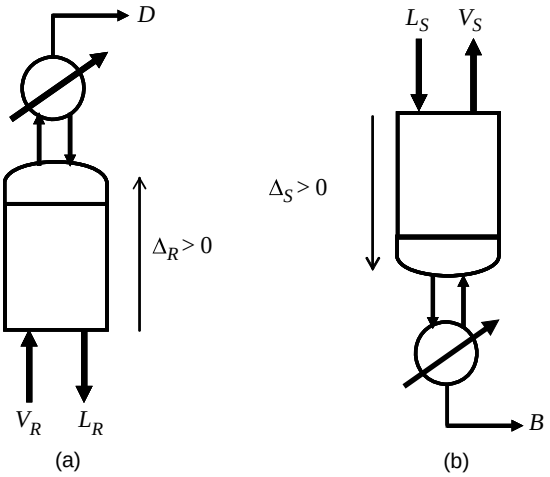


FIGURE 3.9 (a) A conventional rectifying section, and (b) a conventional stripping section.

Unsurprisingly, the net flow in the stripping CS, Δ_S, is always negative, indicating overall net movement of material down the CS. Stripping CSs are thus identified as CSs where the bulk material flows downward.

Notice that in both the rectifying and stripping CSs, the magnitude of the net flow is equivalent to the product flowrate. This is a property of CSs that are terminated by condensers or reboilers. The sign of the net flow thus gives an indication in which direction the bulk of the material is flowing in a CS, either upward with the vapor or downward with the liquid stream.

Although the conclusions drawn from Equations 3.11 and 3.12 seem somewhat trivial, the importance of the net flow in CSs becomes especially prevalent in complex columns, that is, columns that have internal CSs that are not terminated by a condenser or reboiler (such as the general CS shown in Figure 3.3), and do not necessarily produce a product stream. In such internal CSs, it is imperative to realize in which direction the bulk fluid is travelling as this has an effect on the operation of other CSs. This will become more apparent in Chapters 6 and 7 which address complex column design.

It should also be appreciated that Δ is constant for a CS, irrespective of whether the CMO assumption is employed or not. This result is trivial and can be deduced from material balance around the general CS in Figure 3.3.

3.5.2 The Difference Point (X_Δ)

Any general CS has associated with it four streams, namely two inlet and two outlet streams, as shown in Figure 3.3. In order to reduce these streams and thus simplify and generalize any calculations associated with a CS, a single net flow stream (Δ) along with the CMO assumption was defined in Section 3.3.3. While Δ is not an actual stream that exists in the CS, it provides essential information about the resulting direction of the overall material movement in a CS. However, like any stream, both a flow and composition are required to fully define it. Thus, by definition, $\mathbf{X_\Delta}$ is the composition of the net flow stream. Each entry in the $\mathbf{X_\Delta}$ vector is found by calculating the difference between the vapor flowrate of a particular species and the liquid flowrate of the same species.

$\mathbf{X_\Delta}$ is a vector of compositions which, like real compositions, is subject to the constraint that its individual components sum to unity [1]. This can be easily shown by considering the definition of $\mathbf{X_\Delta}$ for individual components 1, 2, and 3, shown in Equation 3.13.

$$\mathbf{X_\Delta} = [X_{\Delta 1}, X_{\Delta 2}, X_{\Delta 3}] = \left[\frac{Vy_1^T - Lx_1^T}{V-L}, \frac{Vy_2^T - Lx_2^T}{V-L}, \frac{Vy_3^T - Lx_3^T}{V-L}\right] \tag{3.13}$$

Since components $\mathbf{y^T}$ and $\mathbf{x^T}$ are compositions subject to the constraint that they have to sum to unity, we can rewrite the definition of $X_{\Delta 3}$ in terms of components 1 and 2:

$$X_{\Delta 3} = \frac{V(1 - y_1^T - y_2^T) - L(1 - x_1^T - x_2^T)}{V-L} \tag{3.14}$$

Equation 3.14 can be rewritten such that

$$X_{\Delta 3} = \frac{V-L}{V-L} - \frac{Vy_1^T - Lx_1^T}{V-L} - \frac{Vy_2^T - Lx_2^T}{V-L} \tag{3.15}$$

which reduces to

$$X_{\Delta 3} = 1 - X_{\Delta 1} - X_{\Delta 2} \tag{3.16}$$

Therefore, in a ternary system, for example, specifying only the two entries of the difference point enables to infer the remaining third component. This can be extended to systems of *nc* components: (*nc*–1) difference point compositions would have to be specified, with the remaining species being inferred by unity summation.

Although $\mathbf{X_\Delta}$ displays the summation properties of real compositions, it should in fact be interpreted as a net composition. Closer examination of its definition reveals that it is a compositional difference between vapor and liquid streams. Hence, it is referred to as the difference point for any particular CS. In other words, an individual element of the $\mathbf{X_\Delta}$ vector dictates the net composition of that specific component in the CS.

3.5.2.1 X_Δ in CSs with Condensers/Reboilers When considering the individual CSs of a simple column in Figure 3.9, it can easily be shown by mass balance that for a rectifying section terminated by a condenser, the difference point is equivalent to the distillate product composition

$$\mathbf{X}_{\Delta R} = \mathbf{x}_D \tag{3.17}$$

Similarly, for any stripping section terminated by a reboiler, its difference point is equal to the bottoms product composition

$$\mathbf{X}_{\Delta S} = \mathbf{x}_B \tag{3.18}$$

Therefore, one can conclude that for all CSs terminated by either a reboiler or a condenser (even in complex configurations), the difference point for these sections will be equal to the product composition that is being produced. Since a physical product has to result from either a stripping or rectifying section, it is then obvious that $\mathbf{X_\Delta}$ has to lie in the MBT for these CSs.

3.5.2.2 X_Δ in General CSs Since $\mathbf{X_\Delta}$ deals with the net composition of each species, it is not necessarily an actual composition within a CS. Furthermore, being a difference of compositions, it is completely conceivable that it may have negative element entries, even though the mole fractions associated with the actual streams in the CS (namely, $\mathbf{x}$ and $\mathbf{y}$) lie between 0 and 1, for each individual component. CPMs that show this possibility are illustrated in Figure 3.6b and c. These operating conditions may be found in CSs that are not terminated by either a reboiler or a

condenser, such as those found within complex columns. Example 3.4 illustrates this idea. Further, when a single element of $\mathbf{X_\Delta}$ is negative, at least one of the other elements of $\mathbf{X_\Delta}$ is forced to be positive since unity summation has to be maintained.

It is also important to realize that since no material is added or withdrawn from a CS, the net composition in the CS stays constant, or put otherwise:

$$\mathbf{X}_\Delta = \frac{V\mathbf{y}^B - L\mathbf{x}^B}{V - L} = \frac{V\mathbf{y}^T - L\mathbf{x}^T}{V - L} \tag{3.19}$$

where superscripts T and B are streams at the top and the bottom of the CS, respectively. The example below illustrates a case where $\mathbf{X_\Delta}$ entries are negative and greater than 1, but the CS is still perfectly valid.

WWW

Example 3.4: Suppose the operating characteristics of a particular CS within a complex column are to be validated. The system in question is benzene/*p*-xylene/toluene operating at $P = 1$ atm, and assuming constant relative volatilities. Preliminary mass balances and design intuition have indicated that the CS should operate with $V = 60$ mol/s, $L = 50$ mol/s, $\mathbf{x}^T = [0.7, 0.2]$, $\mathbf{y}^T = [0.8, 0.1]$. Confirm that this design is realistic by using the DODS-ProPlot profile simulation tool and, where possible, validate these findings on Aspen Plus®.

Solution 3.4: Using the preliminary data, quick calculations show that (from Equations 3.2 to 3.4)

$$\Delta = 10\,\text{mol/s}, \mathrm{X}_\Delta = [1.3, -0.4, 0.1], \text{and}\, R_\Delta = 5.$$

Notice the negative entry in $\mathbf{X_\Delta}$, despite the real compositions being positive. Since $\mathbf{X_\Delta}$, R_Δ, and the starting point of integration of the DPE (liquid composition at the top of the CS) are known, a profile may easily be constructed on DODS-ProPlot. Such a profile, starting from $\mathbf{x}^T$, is shown in Figure 3.10. This profile was generated by using a large n such that it would approach its pinch point, positioned at a composition of $\mathbf{x}^B = [0.068, 0.913]$. However, each point on this profile represents a possible exit liquid composition at the bottom of the CS after a certain number of stages; the larger n is, the closer the profile moves to the stable pinch. Since $\mathbf{X_\Delta}$ is known throughout the entire column (Equation 3.19), it is relatively simple to compute the entering vapor stream (if the column had infinite stages) as $\mathbf{y}^B = [0.273, 0.694]$. The rigorous RADFRAC CS simulation block in Aspen Plus® only requires specification of the number of stages (taken here to be 20), net flowrates (given), and entering streams' compositions ($\mathbf{x}^T$ and $\mathbf{y}^B$). The simulation was allowed to run, and the extracted is plotted in Figure 3.10 as well.

Example 3.4 highlights two important facts regarding the CPM technique. First, the fit between the rigorous stage-by-stage calculations in Aspen Plus® and the approximate DPE are quite good (approximate because of the CMO assumption and that higher order differential terms are negligible in Equation 3.7). In fact, the profile

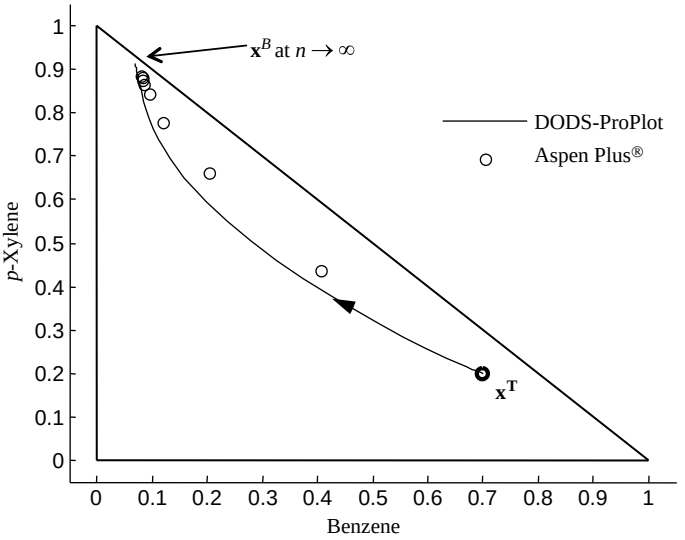


FIGURE 3.10 Composition profile produced in DODS-ProPlot, and validation of profile using Aspen Plus®.

pinches are virtually identical in these two cases. Second, CSs with negative individual $\mathbf{X}_{\mathbf{\Delta}}$ elements, or elements that are greater than 1, occur quite naturally in standard separation columns, as shown in this example. Absorption or stripping towers and distributed feed columns, which all form part of the chemical engineer's vapor–liquid separation toolbox (see Chapter 5), display negative $\mathbf{X}_{\mathbf{\Delta}}$ elements and can, therefore, also be modeled by the CPM technique. One can furthermore begin to envision that it is possible to manipulate the entries of $\mathbf{X}_{\mathbf{\Delta}}$, and it is associated with CPM, to suit the needs of the separation.

3.5.2.3 Individual Component Flows Since Δ is the net flow and $\mathbf{X}_{\mathbf{\Delta}}$ is the net composition within a CS, it then follows that the product, $\Delta\mathbf{X}_{\mathbf{\Delta}}$, is a vector of the net flowrates of each component. In the vector $\Delta\mathbf{X}_{\mathbf{\Delta}}$, a negative element entry merely implies that the net flow of that particular component is downward in the CS. The opposite can be said for positive entries implying upward flow. In Figure 3.11, a graphical representation of all possible $\mathbf{X}_{\mathbf{\Delta}}$ vectors and the associated net species flows are given in a single CS for a ternary system. Figure 3.11a shows the direction of each species flow for $\Delta > 0$, while Figure 3.11b gives the directions for $\Delta < 0$. The seven possible combinations of net flows in a CS with three components that exist follow on from the regions originally defined for the entire RCM shown in Figure 2.17a.

CSs terminated by a reboiler or condenser are CSs that produce actual compositions that must be equivalent to $\mathbf{X}_{\mathbf{\Delta}}$, thus their compositions are all positive (refer to Equations 3.11 and 3.12), forcing $\mathbf{X}_{\mathbf{\Delta}}$ to lie in region 1 (or within the MBT). Thus,

Region		1 (MBT)		2		3	
Flow	$\mathbf{X}_\Delta$ elements	↑↑↑	$\mathbf{X}_\Delta$= [+,+,+]	↑↑↓	$\mathbf{X}_\Delta$= [+,+,–]	↑↓↓	$\mathbf{X}_\Delta$= [+,–,–]
4		5		6		7	
↑↓↑	$\mathbf{X}_\Delta$= [+,–,+]	↓↓↑	$\mathbf{X}_\Delta$= [–,–,+]	↓↑↑	$\mathbf{X}_\Delta$= [–,+,+]	↓↑↓	$\mathbf{X}_\Delta$= [–,+,–]

(a)

Region		1 (MBT)		2		3	
Flow	$\mathbf{X}_\Delta$ elements	↓↓↓	$\mathbf{X}_\Delta$= [+,+,+]	↓↓↑	$\mathbf{X}_\Delta$= [+,+,–]	↓↑↑	$\mathbf{X}_\Delta$= [+,–,–]
4		5		6		7	
↓↑↓	$\mathbf{X}_\Delta$= [+,–,+]	↑↑↓	$\mathbf{X}_\Delta$= [–,–,+]	↑↓↓	$\mathbf{X}_\Delta$= [–,+,+]	↑↓↑	$\mathbf{X}_\Delta$= [–,+,–]

(b)

FIGURE 3.11 All possible flow types associated to entries of $\mathbf{X}_\Delta$ for a ternary system when (a) $\Delta > 0$, (b) $\Delta < 0$. The sign of the entries in $\mathbf{X}_\Delta$ depends on the region it is placed, as shown in Figure 2.17a. The order of the arrows is component 1 (low boiler), component 2 (high boiler), component 3 (intermediate boiler).

flow type 1 in Figure 3.11a and b is typical of CSs in simple distillation columns with a rectifying and stripping section where *all* components flow either up or down in the CS.

The other flow patterns (regions 2–7) can thus only ever be found in non-terminating CSs. It is only ever possible to have these CS somewhere in the middle of a column. This implies that if a designer wants to explore more creative designs (that move away from region 1), complex columns need to be looked at.

3.5.3 The Reflux Ratio (R_Δ)

The generalized reflux ratio (R_Δ) in a CS is a parameter that fixes the ratio of the liquid stream to the net flow in the CS, defined as

$$R_\Delta = \frac{L}{\Delta} = \frac{L}{V - L} \tag{3.20}$$

The general definition given in Equation 3.20 can be written specifically for a simple column rectifying section using Equation 3.11 to give the familiar definition of reflux

$$R_{\Delta R} = \frac{L_R}{\Delta_R} = \frac{L_R}{D} \tag{3.21}$$

Equation 3.21 is in fact equivalent to the standard definition of a reflux ration used throughout distillation literature. It is not usually common practice to refer to a reflux ratio for a stripping section, but with the general definition it can be defined by incorporating Equation 3.12

$$R_{\Delta S} = \frac{L_S}{\Delta_S} = \frac{L_S}{-B} \tag{3.22}$$

Since the net flow can be positive or negative depending on the directional flow of the bulk material, R_Δ is also allowed to be both positive and negative. As with the net flow, the sign of R_Δ is characterized by the type of CS under consideration (rectifying or stripping). Negative reflux ratios imply stripping sections where $L > V$ and vice versa positive refluxes are associated with rectifying sections where $V > L$.

R_Δ is allowed to lie between zero and infinity on the positive spectrum, and between -1 and negative infinity on the negative spectrum. Values of $-1 < R_\Delta < 0$ are not permissible since this reflux range implies a cocurrent mode of operation because the liquid flowrate is proportional to the negative vapor flowrate, conditions for which the DPE are not defined for.

3.6 PROPERTIES OF COLUMN PROFILE MAPS

3.6.1 The Relationship Between RCMs and CPMs

Having established that there are topological similarities between CPMs and RCMs, it is of interest to determine what the exact relationship between the two is. In Section 2.6.2, it was shown that a liquid profile in a total reflux column follows a residue curve exactly, and that the liquid composition in an infinite reflux column will sufficiently approximate a residue curve too. Thus, it should come as no surprise then that when taking the limit in the DPE such that $R_\Delta \to \infty$, we observe that the DPE reduces to the residue curve equation discussed in Chapter 2.

$$\lim_{R_\Delta \to \pm\infty} \left[\left(1 + \frac{1}{R_\Delta}\right)(\mathbf{x} - \mathbf{y}) + \left(\frac{1}{R_\Delta}\right)(\mathbf{X}_\Delta - \mathbf{x}) \right] = \mathbf{x} - \mathbf{y} \tag{3.23}$$

This result was first highlighted by Doherty and coworkers [3] using their boundary value method for rectifying and stripping sections of simple columns. Thus, the DPE and the residue curve equation are related by the limiting condition of a CS operating at (positive and negative) infinite reflux, which corresponds to $L = V$ in a CS. Therefore, for all finite choices of reflux, one can expect a shifting of nodes in the composition space, and at infinite reflux the nodes will fall exactly on their positions in the RCM. This relationship forms a link between the batch process which is time-dependent and the continuous process that is equipment or stage dependent. Even though the dependent variables differ in these equations, they are, from a mathematical sense, equivalent. Interestingly, this link between time-dependent and

equipment-dependent processes is by no means a new concept in the field of chemical engineering. For instance, in reactor theory, there exists a similar analogy between a batch reactor and a continuous plug flow reactor.

One may then say that CPMs, which are affected by various parameters, can be classified for general operation, while an RCM is for more specific operation. The RCM is a single, special member of the family of CPMs that can possibly describe the workings of a CS.

The fact that the DPE at infinite reflux conditions simply reduces to the residue curve equation has an additional implication of just that: RCMs can only give us information at infinite reflux, as emphasized in Chapter 2. Although RCMs may give us a good idea about potential synthesis pathways, they do not show the influence of finite refluxes or the effect of placement of $\mathbf{X_\Delta}$s. Both these parameters are critical in shifting topology and by only considering RCMs for design, the designer severely limits his/her design freedom. With knowledge of both R_Δ and $\mathbf{X_\Delta}$ the designer has the opportunity to be creative in designing a separation, and certainly opens the doors to a much wider range of possibilities.

3.6.2 Vector Fields

In Section 2.5.1, the separation vector was defined by the right-hand side of the residue curve equation. Examining the right-hand side of the DPE, it can be seen that two vector fields now exist. The separation vector is still present, as one would expect

$$\mathbf{S} = (\mathbf{x} - \mathbf{y}) \tag{3.24}$$

The individual influence of $\mathbf{S}$ on the DPE thus results in an RCM, an example of which is shown in Figure 3.12a for a constant volatility system.

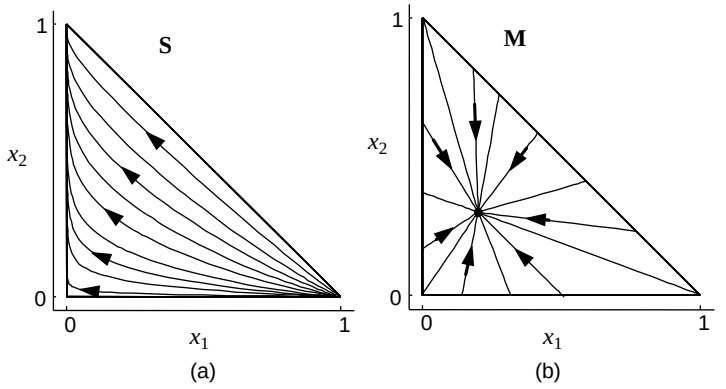


FIGURE 3.12 Maps arising from the individual vector fields of (a) separation, **S**, and (b) mi**x**ing, **M**.

The other vector present is

$$\mathbf{M} = (\mathbf{X}_{\Delta} - \mathbf{x}) \tag{3.25}$$

$\mathbf{X}_{\Delta}$ remains constant throughout a particular CS, and thus it can be deduced that **M** is a *mixing vector*. If one were to ignore the **S** vector in the DPE and only plot **M** in the composition space, it would result in a map consisting of straight lines moving radially from all directions to a single node located at $\mathbf{X}_{\Delta}$ (which is not a function of **x**). An example of such a plot can be seen in Figure 3.12b. This plot can be generated using a simple batch experiment where by a liquid of composition **x** is charged to a still, and then an amount of material of composition $\mathbf{X}_{\Delta}$ is added at discrete times to the still. The resulting composition of the mixture would, as time goes by, tend toward $\mathbf{X}_{\Delta}$ as more and more material is added to the system. Thus, both **M** and **S** vectors in the DPE have an equivalent batch analogy.

When it comes to the behavior of a CS, the DPE dictates that profiles are influenced by both **S** and **M**, and the vector addition of these two results in the movement of the column profiles. Figure 3.13 graphically displays nature of these vectors. Notice how the vector sum is tangent to the column profile.

3.6.3 Pinch Points

As mentioned earlier, although the entire CPM appears to have shifted, the nature of the profiles is similar to those in an RCM. It is then no surprise that the identification and classification of pinch points in a CPM follows the same procedure as that for RCMs.

In summary

- Column profiles cannot intersect with each other.
- Column profiles begin at unstable nodes.

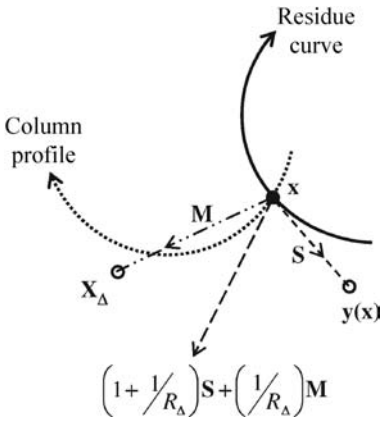


FIGURE 3.13 The separation vector, **S**, is tangent to the residue curve at **x**. The mixing vector, **M**, points in the direction of $\mathbf{X}_{\Delta}$. The vector sum is tangent to the column profile at **x**.

- Column profiles end at stable nodes.
- Column profiles, in general, move from low temperature to high temperature, although this is not always true. Refer to Section 3.6.4 for more information, as well as Section 4.5.3 for experimental validation of this.

At a pinch point the composition is no longer changing with respect to changes in the position in a CS. Mathematically, these pinch points may be found by solving

$$\frac{d\mathbf{x}}{dn} = 0 \tag{3.26}$$

Rearranging the DPE in Equation 3.10

$$(1 + R_{\Delta})(\mathbf{x} - \mathbf{y}) = \mathbf{x} - \mathbf{X}_{\boldsymbol{\Delta}} \tag{3.27}$$

From Equations 3.24 and 3.25, it can be seen that at a pinch point, the vectors **S** and **M** point in opposite directions to each other. Furthermore, since **S** is tangent to a residue curve at **x**, it then follows that at a pinch point, **M** is also tangent to the residue curve at **x**. This can be seen in the illustration shown in Figure 3.14. Equation 3.27 further tells us that this common tangent point, **x**, on the residue curve is in fact a pinch point in the CPM.

Figure 3.14 shows that a pinch point occurs in the CPM even though the residue curve has not pinched. Remembering that a residue curve will, in most cases, pinch at the vertices of the MBT (and elsewhere if azeotropes are present), it can be seen how it is possible that a column profile will then pinch at a different location. What is more, the example shown is for a single residue curve—in a RCM there are many profiles, and suddenly there are numerous locations for pinch points. However, all these pinch points do not occur simultaneously: for a fixed $\mathbf{X}_{\boldsymbol{\Delta}}$, the scalar term, involving R_{Δ}, in Equation 3.27 determines the exact pinch locations by the familiar lever-arm rule. Therefore, it should be apparent how the combination of $\mathbf{X}_{\boldsymbol{\Delta}}$ and R_{Δ} sets the pinch points not only graphically but mathematically too. A change in one or both these values alters the locations of the pinch points, implying a shift in the profiles to form a different CPM. A designer could easily determine the positions of

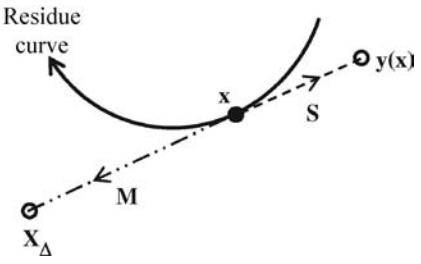


FIGURE 3.14 Tangency conditions of both **S** and **M** vectors on a residue curve at a CPM pinch point, **x**.

all pinch points at set values of $\mathbf{X}_{\boldsymbol{\Delta}}$ and R_{Δ} and solving Equation 3.27. However, rather counter-intuitively, one may also determine what values of $\mathbf{X}_{\boldsymbol{\Delta}}$ and R_{Δ} result in a desired pinch point location, thus allowing a CS to be synthesized, rather than designed.

3.6.4 Isotherms

Every point in the liquid composition space has an associated equilibrium vapor composition. A temperature can also be calculated at every point in the composition space. Closer inspection of the DPE reveals that this temperature is, in fact, only a function of the equilibrium model used, and is not influenced by the parameters $\mathbf{X}_{\boldsymbol{\Delta}}$ and R_{Δ}. In other words, the isotherm plots that can be generated at RCM conditions will still hold true for any CPM, regardless of the operating parameters used.

This topic was discussed in some detail in Section 2.5.3, and the reader is referred there for more information. The isotherm plot given in Figure 2.9 for the acetone/benzene/chloroform at $P = 1$ atm thus remains fixed in its position, that is, regardless of value of parameters in the DPE, this map will remain the same. As we have done for composition profiles, we are now again in a position to extend the isotherms to outside the MBT, as shown in Figure 3.15. Such plots can be generated for any system, provided the thermodynamic model holds for negative compositions.

Up to this point in the chapter, it has been established how the CPMs are a strong function of $\mathbf{X}_{\boldsymbol{\Delta}}$ and R_{Δ} and consequently are able to shift topology in the composition

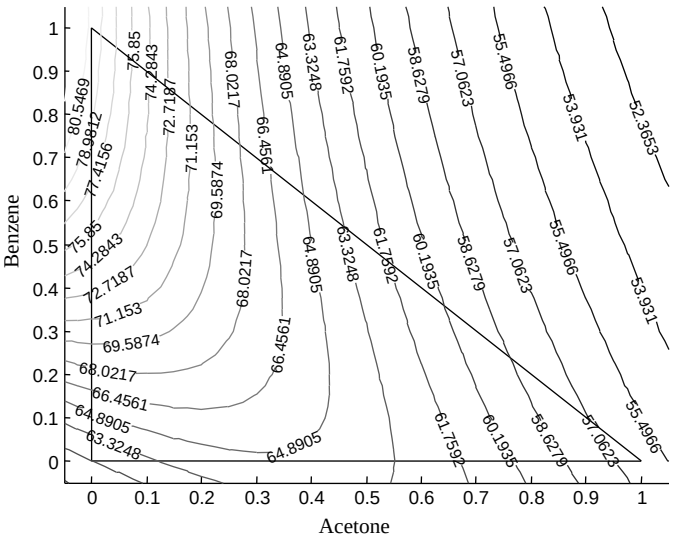


FIGURE 3.15 Extended isotherm plot for the acetone/benzene/chloroform system at $P =$ 1 atm using the NRTL thermodynamic model. Temperatures indicated in °C.

space. It has also now known that the isotherm plot, which represents the temperature profile along any column profile, is fixed in its location, and does not move irrespective of the operating conditions. Thus, it should become clear that while most profiles will move in a direction with increasing temperature, there are some cases where the profiles do the opposite, having a direction equating to decreasing temperature. Examples of this can be sought by superimposing the CPM plots in Figure 3.8a and b on the isotherm plot in Figure 3.15.

This superimposition is quite a remarkable result. It implies that at some operating conditions and initial compositions, a CS will have its hottest temperature at the top of the CS, thereby creating an inverse temperature profile (remember, in conventional simple columns the coldest temperature is at the top). While an inverse temperature profile is not necessarily desired in simple columns, it may very well be a feasible mode of operation in complex columns that have CSs that are neither rectifying nor stripping CSs found in simple columns. This result of an inverse temperature profile in a CS has further been validated experimentally, and the reader is referred to Section 4.5.3 for the details.

3.6.5 Transformed Triangles

A closer inspection of the ideally behaved CPMs in Figures 3.5 and 3.6 reveals another underlying, but very useful, result: there are three shifted nodes that may all be connected by straight lines. This result can intuitively be arrived at by examining the movement of the profiles in the vicinity of the stationary points. There is, however, a more fundamental mathematical reason why the nodes can be connected by straight lines—this is discussed in Section 3.8.1. For now, the usefulness of this phenomenon will be shown. The result of this unique characteristic of being able to connect all the nodes with straight lines is a so-called TT. These linear transforms are however only valid for systems that obey constant relative volatility behavior, since, in nonideal systems, there is significant curvature between stationary points as shown in Figures 3.7 and 3.8. An example of a TT with its associated CPM is given in Figure 3.16. The TTs are also indicated in Figure 3.6a–c.

WWW

TUTORIAL 3.4

Try this for yourself: Reproduce Figure 3.16 with DODS-ProPlot using the given parameters. Try generating similar figures with different values for $\mathbf{X}_{\Delta}$, R_{Δ}, and P.

The term "transformed" is used to indicate the shift in the nodes from infinite reflux conditions, where the nodes all lie on the vertices of the MBT (i.e., at the pure components) to their current positions in the CPM.

WWW

Example 3.5: Using the DODS-ProPlot package, produce a CPM with parameters outlined in (a)–(d) for the benzene/*p*-xylene/toluene system (1 atm pressure) using a constant relative volatility model. Identify and comment on the position

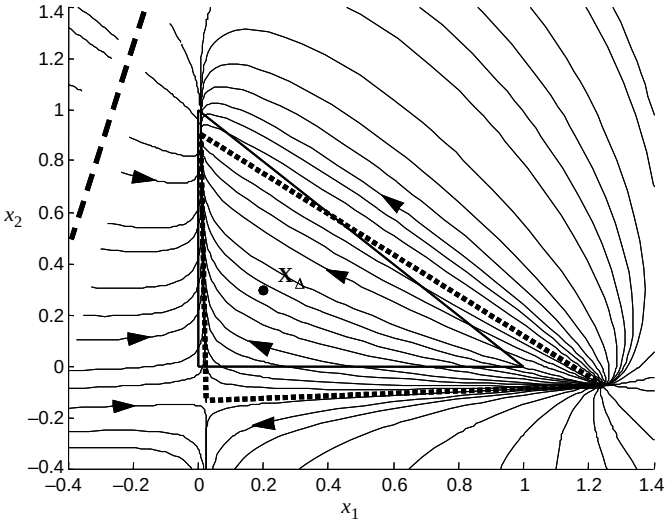


FIGURE 3.16 A CPM with a TT (dashed lines) for a constant relative volatility system with $\boldsymbol{\alpha} = [5, 1, 2]$ using arbitrarily specified conditions $\mathbf{X}_{\boldsymbol{\Delta}} = [0.2, 0.3]$ and $R_{\boldsymbol{\Delta}} = 5$. The MBT is shown as solid black lines.

of the nodes and TT relative to the RCM and MBT, respectively, for this system shown in Figure 2.11.

(a) $\mathbf{X}_{\boldsymbol{\Delta}} = [0.95,0.02]$, $R_\Delta = 3$
(b) $\mathbf{X}_{\boldsymbol{\Delta}} = [0.03,0.92]$, $R_\Delta = -6$
(c) $\mathbf{X}_{\boldsymbol{\Delta}} = [-0.2,-0.1]$, $R_\Delta = 5$
(d) $\mathbf{X}_{\boldsymbol{\Delta}} = [-0.35, 1.2]$, $R_\Delta = -70$

Solution 3.5: The user-friendly DODS-ProPlot package enables one to plot CPMs for an array of chemical systems and thermodynamic models quite easily and efficiently. Instructions for using this package can be found in Appendix A. Figure 3.17 shows CPMs of scenarios (a)–(d), followed by some discussions on each of these CPMs' node placements.

(a) As shall be seen in subsequent chapters on column design, these specifications are typical of a standard rectifying CS in a simple column, where the actual column's profile originates from $\mathbf{X}_{\boldsymbol{\Delta}}$ moving in the direction of the profile arrows. It is noticeable here that the stable node, which was at pure *p*-xylene in the RCM, is now located within the MBT, meaning that this CS will pinch, whereby no separation will occur beyond this point.

(b) Conversely to the situation depicted in (a), these specifications are typical of a standard stripping CS in a simple column, where the actual column's profile originates from $\mathbf{X}_{\boldsymbol{\Delta}}$ moving against the direction of the profile arrows. Here, the unstable node is found within the MBT, resulting in a similar pinch point for

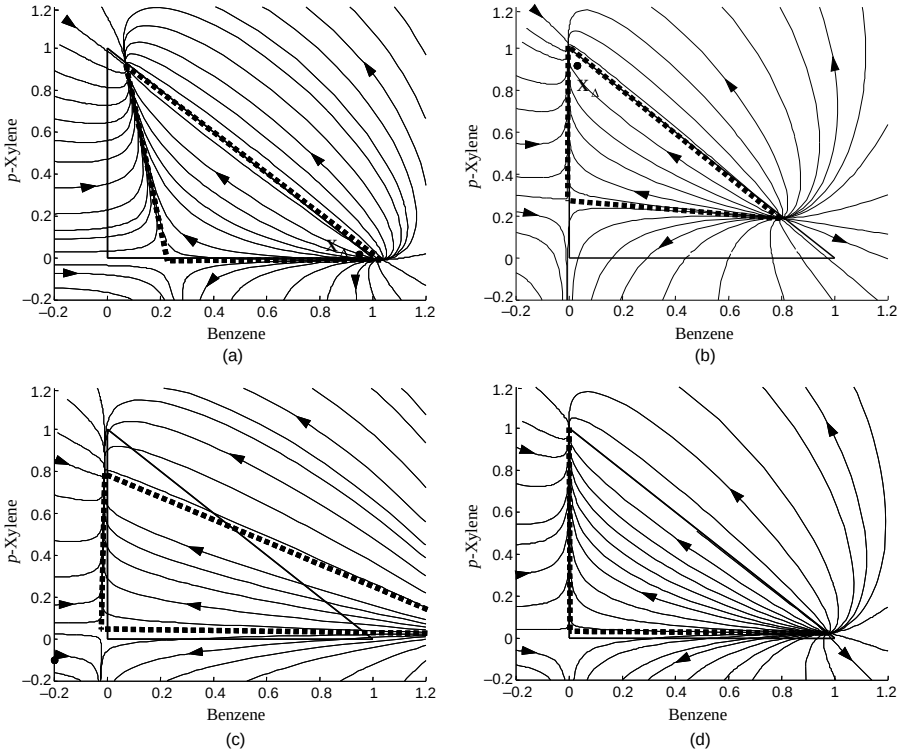


FIGURE 3.17 CPMs for Example 3.5 for the benzene/*p*-xylene/toluene system at $P = 1$ atm at (a) $\mathbf{X_\Delta} = [0.95, 0.02]$ and $R_\Delta = 3$, (b) $\mathbf{X_\Delta} = [0.03, 0.92]$ and $R_\Delta = -6$, (c) $\mathbf{X_\Delta} = [-0.2, -0.1]$ and $R_\Delta = 5$, and (d) $\mathbf{X_\Delta} = [-0.35, 1.2]$ and $R_\Delta = -70$. The MBT is shown as solid black lines, TT shown as dashed lines.

the stripping CS. Again, no pinch occurs at the saddle point as it is positioned outside the MBT.

(c) This case has significance in that none of the pinch points (and hence TT vertices) are actually located within the MBT, meaning that separation can take place from one end of the MBT to the other, without the column pinching!

(d) Here, the TT almost resembles the MBT (for reasons that will become apparent later). Thus, the stable, unstable, and saddle nodes lie close to the high, low, and intermediate boiling vertices of the MBT, respectively, and the map looks very much the RCM (Figure 2.11). This implies that the operation of the CS sufficiently approximates infinite reflux.

Notice from Example 3.5 how the overall topology of the map is influenced by the parameters $\mathbf{X_\Delta}$ and R_Δ. For example, in Figure 3.17b, there has been a shift of profiles that lay below the MBT in the RCM to well within the MBT. Not only are these profiles now achievable when operating at the conditions specified for this map, but looking closer shows that there is in fact a profile that moves right through pure

toluene (i.e., the [0, 0] vertex of the MBT). This implies that one can potentially have a CS that would produce the intermediate boiler. Further, the pure toluene point is no longer near any nodes, thus producing it will not pose any difficulty.

What is even more remarkable is that the location of the pinch points, and hence the TT, can be identified *without* having to plot the entire CPM. This is simply done by solving the DPE equated to zero, as in Equation 3.26. With this, we have significantly simplified the analysis of constant relative volatility systems. A large amount of the theory presented in this chapter and those that follow hinge on the knowledge of the TTs, as they present an easy means of tracking pinch points and delineating the CPM. The TT simplification can also be extended to quaternary mixtures where a transformed tetrahedron (TT^4) can be formed—these will be used in the design of complex columns in Chapter 7.

3.7 PINCH POINT LOCI

3.7.1 Analytical Solutions

In separation science, a pinch point may be defined as any point where the driving force for separation has diminished to zero. The location of pinch points can be determined mathematically by equating the DPE to zero, and solving the resulting equation, as shown in Equation 3.26. Pinch points correspond to nodes or stationary points on the CPM.

For a fixed $\mathbf{X_\Delta}$ there exists a unique set of pinch points for a specific R_Δ, as illustrated in Figure 3.5. As R_Δ changes, so do the locations (and sometimes the number) of the pinch points for a fixed $\mathbf{X_\Delta}$. Pinch point loci can therefore be defined as "the loci of all pinch points obtained by varying the reflux ratio, R_Δ, for a set $\mathbf{X_\Delta}$" [7]. Pinch loci help describe the path that the TTs follow as R_Δ is varied because the nodes for every CPM have to lie on the respective pinch curve. In this section, we will show how the behavior of the pinch point loci affects the topology of CPMs.

As shown in Figure 3.18a, keeping $\mathbf{X_\Delta}$ constant and varying R_Δ (for $R_\Delta > 0$) allows to draw a set of TTs, the vertices of which correspond to the pinch points associated with the values of R_Δ chosen. The same can be done for negative values of R_Δ, as shown in Figure 3.18b. Thus, for a fixed $\mathbf{X_\Delta}$, there exists a unique set of pinch points for a specific R_Δ.

It is apparent from Figure 3.18 that the movements of the TTs form a clear pattern. Connecting each of the subsequent vertices of the TTs, that is, the pinch points, with each other at different reflux values allows to construct a pinch point locus. Pinch point loci then describe the path that the TTs move on as R_Δ is varied because the nodes for every CPM have to lie on the respective pinch point curve. Figure 3.19 illustrates this movement of TTs along the pinch point loci for the same conditions as Figure 3.18. Although not discussed here, the reader should be aware that finding these pinch loci quickly and reliably is not necessarily a trivial matter, especially when the phase-equilibrium behavior is nonideal. The reader is referred to Felbab

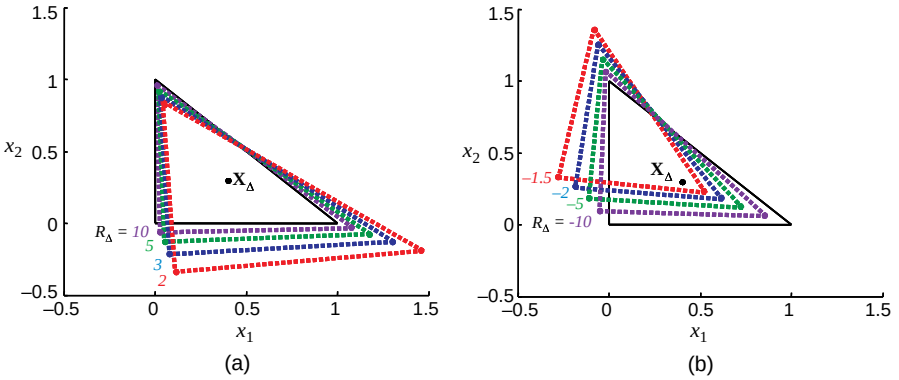


FIGURE 3.18 Movement of TTs for a constant volatility system with $\boldsymbol{\alpha} = [5, 1, 2]$, $\mathbf{X}_\Delta = [0.2, 0.3]$ with (a) positive values of R_Δ, and (b) negative values of R_Δ.

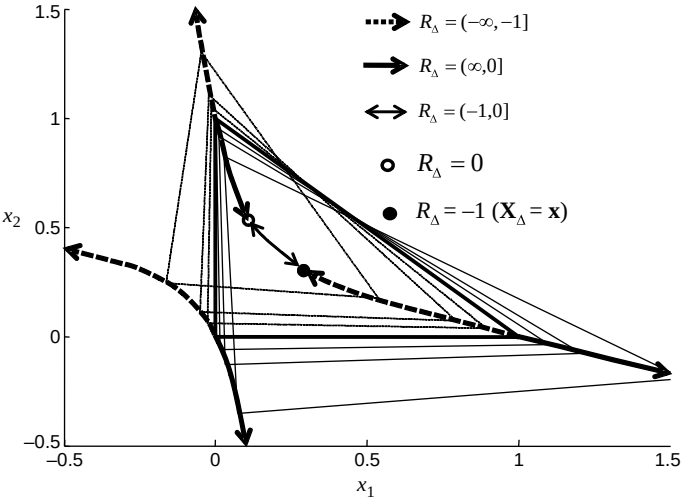


FIGURE 3.19 Movement of TTs for a constant relative volatility system with $\boldsymbol{\alpha} = [5, 1, 2]$ for a set $\mathbf{X}_\Delta = [0.2, 0.3]$ and varying reflux along the pinch point curve.

et al. where a reasonably effective means of finding the pinch point loci for nonideal systems is presented [7].

WWW

TUTORIAL 3.5

Try this for yourself: Reproduce Figure 3.18 with DODS-ProPlot using the given parameters. Try generating similar figures with different values for $\mathbf{X}_\Delta$, R_Δ, and $\boldsymbol{\alpha}$.

The smaller the refluxes become, the larger the differences between L and V become and simultaneously the greater the departure from RCM conditions become. As shown in Section 3.6.1, the other extreme reflux condition, infinite reflux, results in the residue curve equation and at these conditions the TT and the MBT will coincide with each other exactly.

Mathematically, $R_\Delta = -1$ represents a special case where Equation 3.27 reduces to

$$\mathbf{X}_\Delta = \mathbf{x} \tag{3.28}$$

This special case in Equation 3.28 is valid for any system, regardless of the phase equilibrium properties of the system. The significance of $R_\Delta = -1$ is that this represents the point where the vapor flowrate in the CS tends to zero, and can be seen as the switching point from a counter-current mode of operation to a cocurrent operation mode. The only pinch point at these conditions is thus at $\mathbf{X}_\Delta$ and profiles will resemble the "mixing only" process shown in Figure 3.12b. More importantly, though, this shows that any pinch point loci will always move through $\mathbf{X}_\Delta$, irrespective of phase equilibrium.

Another special case arises when $R_\Delta = 0$ where the liquid flowrate tends to zero, and also represents a switch from counter-current to cocurrent mode. At these conditions, the DPE becomes

$$\mathbf{X}_\Delta = \mathbf{y} \tag{3.29}$$

Equation 3.29 implies that, in the x_1–x_2 space, a CS will pinch at the equilibrium vapor point of $\mathbf{X}_\Delta$ if operated at $R_\Delta = 0$.

It is quite obvious from Figure 3.19 that the placement of $\mathbf{X}_\Delta$ significantly affects the pinch point loci and therefore the general movement of TTs. What is more important is that, as discussed in previous sections, $\mathbf{X}_\Delta$ need not lie within the MBT. In fact, $\mathbf{X}_\Delta$ can be placed anywhere in the composition space. It is interesting to note that the seven flow types depicted in Figure 2.17a correspond to the extended axes of the MBT. These seven regions are also significant in terms of the behavior of the pinch loci, illustrated in Figure 3.20a–g . Each of these discrete regions in fact displays qualitative unique pinch point loci. Notice, however, that all pinch point curves, regardless of $\mathbf{X}_\Delta$ placement and shape of the loci, pass through the pure component vertices (at infinite reflux), and also through $\mathbf{X}_\Delta$ (at $R_\Delta = -1$).

Figure 3.20a shows the pinch point loci for $\mathbf{X}_\Delta$s in the MBT, also shown in detail in Figure 3.19. In Section 3.5.2, it was discussed that CSs terminated by a reboiler or condenser which produce product streams will have the composition of the product equal to $\mathbf{X}_\Delta$ for the CS. In other words, for these CSs, the design is limited to $\mathbf{X}_\Delta$s in the MBT, and the associated pinch point loci (Figure 3.20a). Thus, the behavior of the pinch points in simple columns is constrained to only these flow patterns and their associated topological behavior.

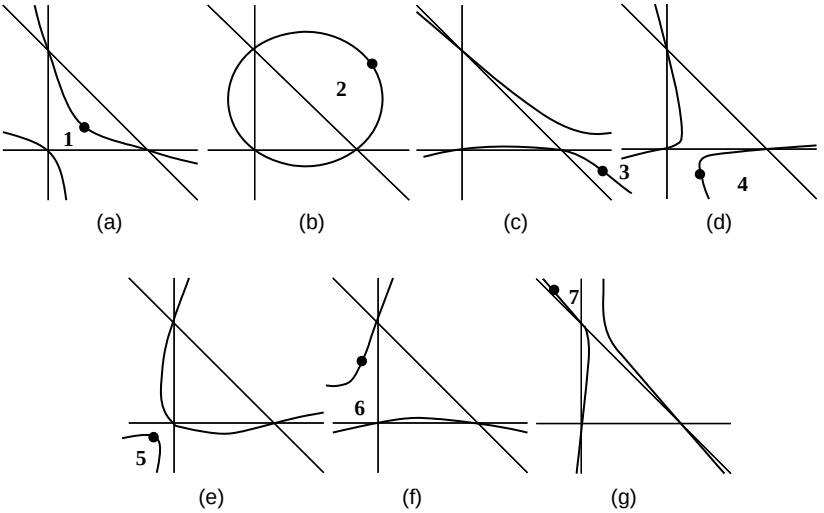


FIGURE 3.20 A geometric description of possible flow types associated with entries of $\mathbf{X}_{\Delta}$, with their associated pinch point loci for a constant volatility system with $\boldsymbol{\alpha} = [5, 1, 2]$ for the seven different regions (labeled) depicted in Figure 2.17a.

However, the remaining images in Figure 3.20 show some interesting possibilities that are open to the designer by permitting some counter-intuitive or unusual flow patterns, not found in so-called simple columns. For example, if one were able to manipulate a CS to operate with a $\mathbf{X}_{\Delta}$ lying in region 2 (Figure 3.20b) or 5 (Figure 3.20e), one would have a CS that does not have any stationary points within the MBT! Thus, there would not be any compositional steady states or pinch points inside the MBT for these flow types. Some preliminary applications of creative $\mathbf{X}_{\Delta}$ placement are discussed in Section 3.9.

Although these discrete regions of similar pinch point behavior are easily identifiable in constant volatility systems, they are more difficult to interpret and identify in nonideal systems where more stationary points occur. Nevertheless, manipulating net flows even in these nonideal systems permits the designer much more flexibility to the design. Figure 3.21 gives an example of a pinch point loci generated for the acetone/benzene/chloroform system using the NRTL model at $P = 1$ atm and $\mathbf{X}_{\Delta} = [0.1, 0.2]$.

Figure 3.21 shows a very different behavior in the pinch point loci from those given for the constant relative volatility system. However, the same properties still exist: at infinite reflux the nodes are at their RCM positions, and at $R_{\Delta} = -1$ the only solution is $\mathbf{X}_{\Delta} = \mathbf{x}$. As with the ideally behaved systems in Figures 3.18 and 3.19, this pinch point locus is of course unique to the chosen $\mathbf{X}_{\Delta}$ coordinate. Different loci will be obtained for alternate $\mathbf{X}_{\Delta}$ placement, and again some useful features may arise by allowing $\mathbf{X}_{\Delta}$ to lie outside the MBT. The reader is referred to Holland et al. [9] for more information regarding this.

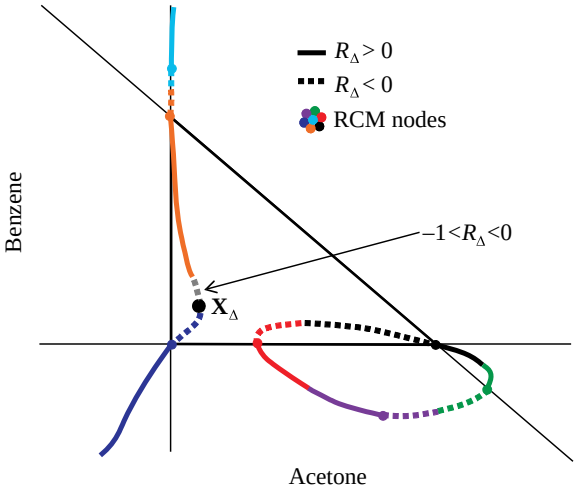


FIGURE 3.21 Pinch point loci for the acetone/benzene/chloroform system at $P = 1$ atm (NRTL) with $\mathbf{X}_\Delta = [0.1, 0.2]$.

3.7.2 Graphical Approach

The previous section gives the mathematical background necessary to produce a pinch point loci analytically. There is, however, a more elementary way that one could roughly generate these curves. Revisiting the pinch point equation (Equation 3.26), as well as Figure 3.14, it can be seen that pinch points can be sought by locating tangency points on the residue curves using straight lines originating from a fixed $\mathbf{X}_\Delta$. This is essentially taking the **S** map in Figure 3.12a and superimposing the **M** map in Figure 3.12b on it, and identifying all tangent points. Figure 3.22a gives an

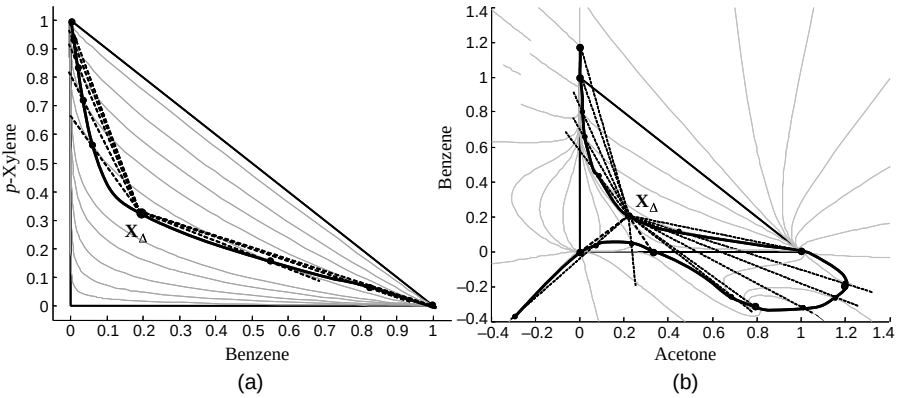


FIGURE 3.22 Pinch point loci produced by tangent conditions between and arbitrarily chosen $\mathbf{X}_\Delta$ and the residue curves. The RCM for the system is given, with the tangent lines displayed as dashed lines. The pinch point loci are drawn by connecting all tangent points for the (a) benzene/*p*-xylene/toluene system, and (b) acetone/benzene/chloroform system.

example of this for the benzene/*p*-xylene/toluene system at 1 atm and arbitrary placement of $\mathbf{X}_{\boldsymbol{\Delta}}$.

This method is simple and easy to use, and all that is required is the RCM for the system in question. However, the accuracy of the method depends on the number of residue curves used. Of course, the same method can be used directly to locate pinch point loci outside the MBT, as is done in the example in Figure 3.22b for the acetone/benzene/chloroform system at 1 atm. Thus, by understanding the graphical nature of the DPE, one is able to gather a plethora of information, and many insights can be gained from this.

3.8 SOME MATHEMATICAL ASPECTS OF CPMs

3.8.1 Eigenvalues and Eigenvectors

By this stage, it is hoped that the reader has a geometric understanding of node types (stable, unstable, saddle, and so on) and what they represent in terms of possible separation paths. However, it is imperative that one understands the mathematical traits of these nodes and how they are defined from a mathematical point of view. In order to discriminate between nodes, in a mathematical sense, it is necessary to delve into the field of topological mathematics, specifically Lyupunov's theorem of dynamic stability. The first step is to arrange the DPE in a square matrix by determining the Jacobian matrix (J) of the set of DPEs. Writing the DPE of component i in terms of a function, f_i, results in

$$f_i = \left(1 + \frac{1}{R_\Delta}\right)(x_i - y_i) + \left(\frac{1}{R_\Delta}\right)(X_{\Delta i} - x_i), \text{ for } i = 1, 2, ..., (nc-1) \tag{3.30}$$

Due to the unity summation relationship we only need $(nc-1)$ DPE equations to fully define the system. The resulting Jacobian system of equations is a matrix of size $(nc-1) \times (nc-1)$ where entry ij is the first partial derivative of f_i with respect to component x_j:

$$\mathbf{J} = \begin{pmatrix} \dfrac{\partial f_1}{\partial x_1} & \cdots & \dfrac{\partial f_1}{\partial x_{(nc-1)}} \\ \vdots & \ddots & \vdots \\ \dfrac{\partial f_{(nc-1)}}{\partial x_1} & \cdots & \dfrac{\partial f_{(nc-1)}}{\partial x_{(nc-1)}} \end{pmatrix} \tag{3.31}$$

The Jacobian matrix is a square matrix from which one may compute eigenvalues. To solve the eigenvalue problem it is necessary to compute the scalar values, λ, that satisfy the equation

$$\det(\mathbf{J} - \lambda \mathbf{I}) = 0 \tag{3.32}$$

where **I** is the identity matrix. For the special case of a ternary system, Equation 3.32 results in

$$(J_{11} - \lambda)(J_{22} - \lambda) - J_{12}J_{21} = 0 \tag{3.33}$$

Equation 3.33 is a simple quadratic equation, known as the characteristic equation, with two unique solutions (λ_1 and λ_2), where λ_1 and λ_2 are known as the eigenvalues. It is the nature of these eigenvalues that allow us to identify nodes, according to Lyapunov's theorem. These nodes can be classified as follows [10]:

1. The roots λ_1 and λ_2 of the characteristic equation are distinct and real:
   (a) $\lambda_1 < 0$ and $\lambda_2 < 0$. The singular point is asymptotically stable (stable node).
   (b) $\lambda_1 > 0$ and $\lambda_2 > 0$. The singular point is asymptotically unstable (unstable node).
   (c) $\lambda_1 < 0$ and $\lambda_2 > 0$. The singular point is asymptotically unstable (saddle point).
2. The roots of the characteristic equation are complex and in the form $\lambda_{1,2} = p \pm iq$:
   (a) $p < 0$ and $q = 0$. The singular point is asymptotically stable (stable focus).
   (b) $p > 0$ and $q = 0$. The singular point is asymptotically unstable (unstable focus).
   (c) $p = 0$ and $q \neq 0$. The singular point is asymptotically stable (midpoint).
3. The roots of the characteristic equation are real but not distinct:
   (a) $\lambda_1 = \lambda_2 < 0$. The singular point is an asymptotically stable node.
   (b) $\lambda_1 = \lambda_2 > 0$. The singular point is an asymptotically unstable node.
4. The roots of the characteristic equation have one zero value:
   (a) $\lambda_1 = 0$ and $\lambda_2 < 0$. The singular point is an asymptotically stable half-node/saddle node.
   (b) $\lambda_1 = 0$ and $\lambda_2 > 0$. The singular point is an asymptotically unstable half-node/saddle.

Noticeably there are far more nodes than just the stable, unstable, and saddle nodes listed under heading 1. There are in fact, in total, 10 unique types. However, except for the complex nodes under heading number 2, all these other nodes are closely related to, or a combination of, stable, unstable, and saddle nodes.

A useful tool to enhance the understanding of eigenvalue theory is an eigenvalue map [9], which shows discreet regions of similar node behavior at a set reflux. An example is depicted in Figure 3.23.

Figure 3.23 shows that there is a complex region (black and cyan regions) situated outside the MBT. This complex region stays fixed, regardless of the reflux because it is defined by the eigenvectors which are independent of reflux. By choosing different refluxes all regions in Figure 3.23 will be shifted, even so that one may, for instance,

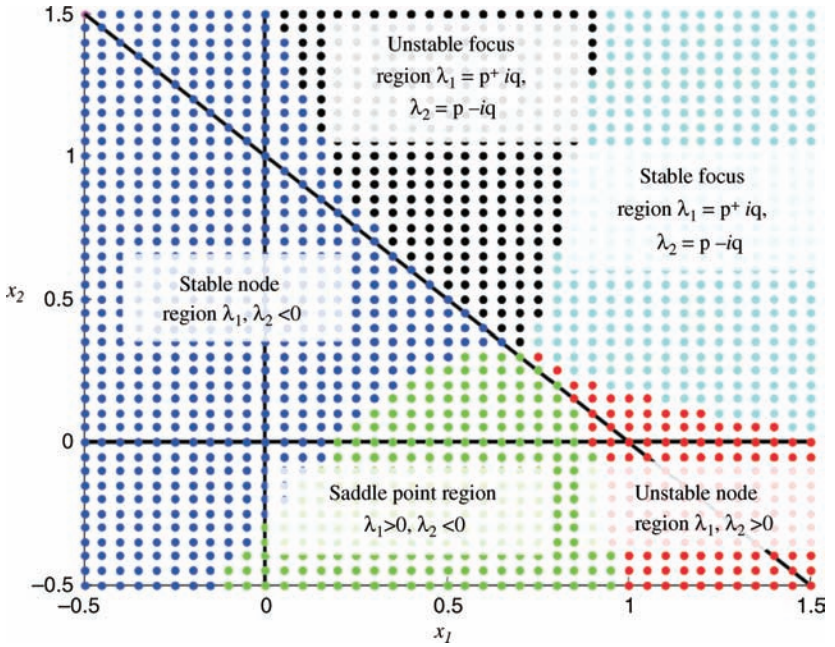


FIGURE 3.23 An eigenvalue map at $R_\Delta = 2$ for $\boldsymbol{\alpha} = [5, 1, 2]$.

put a stable node region on the intermediate boiling component! Although doing this may require an extreme or impractical operation of the CS, it does suggest that there are potential opportunities to devising counter-intuitive separations. The following section elaborates on where these types of nodes may be encountered and how they are represented in composition space.

It is important to take cognizance of the fact that since we are taking first-order derivatives (through the Jacobian matrix) of the DPE to calculate the eigenvalues, the eigenvalues are independent of the positioning of $\mathbf{X}_\Delta$ as it appears as a constant in Equation 3.30. Eigenvalues thus are only a function of R_Δ and the thermodynamic model describing the phase equilibrium.

Eigenvectors, on the other hand, are determined by solving for the vector $\mathbf{e}$ in the following equation:

$$(\mathbf{J} - \lambda\mathbf{I})\mathbf{e} = \boldsymbol{\theta} \tag{3.34}$$

where $\boldsymbol{\theta}$ is the zero matrix and $\mathbf{I}$ is the identity matrix. Interestingly, the eigenvectors are independent of both R_Δ and $\mathbf{X}_\Delta$ and depend solely on the thermodynamic model, that is, $\mathbf{e} = f[\mathbf{y}(\mathbf{x})]$. The proof of this is left to the reader for enrichment. For a ternary system, the size of the vector $\mathbf{e}$ is 2×1, and in general for the system with nc components the size of the eigenvector is $(nc - 1) \times 1$. Thus, every point within the composition space in a ternary system has two eigenvectors associated with it. Thus, by specifying a

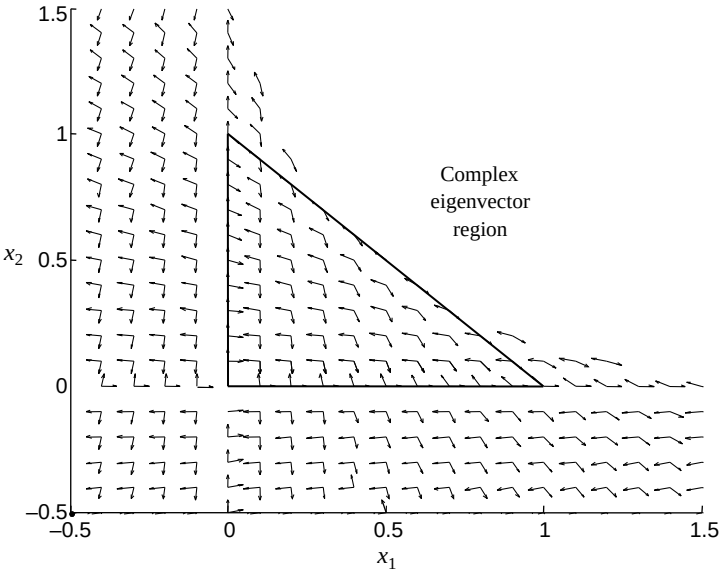


FIGURE 3.24 An eigenvector map for $\boldsymbol{\alpha} = [5, 1, 2]$.

series of discrete composition coordinates, it is possible to generate an eigenvector map [9], shown in Figure 3.24. This map characterizes the asymptotic direction of the profiles in the neighborhood of the stationary point.

Figure 3.24 shows a blank region where the eigenvectors are complex. This complex region is caused by roots of the DPE that are also complex. Since the eigenvectors are independent of operating conditions, this map is fixed for a given set of thermodynamic properties.

Although the concept of eigenvectors may seem somewhat abstract, it is a very useful property in constant relative volatility system design: it is the eigenvectors which allow one to connect the stationary points with straight lines, thus forming the TT. The eigenvectors at a node will always be orientated in such a way that they point to the other nodes, thus allowing for a straight line connection. In fact, if one were to determine the eigenvectors at various compositions along the straight line connecting two nodes, it will be found that one of the eigenvectors will always be collinear to the line. This can be seen for the infinite reflux (RCM) case where the TT is in fact the MBT, as shown in Figure 3.19. Thus, if we know the coordinate of one stationary point in an ideal system, we can easily determine the remaining stationary points by letting the eigenvectors line up to form a TT.

3.8.2 Nature of Pinch Points

The preceding section shows that there are in fact many types of nodes to consider, each with their own mathematical description. It is, however, useful to have an understanding of when one may expect a certain stationary to be of a certain nature.

TABLE 3.1 Three Different Cases of Pinch Point Solutions for a Constant Relative Volatility Ternary System

Case Number	Nature of Solutions	Type of Nodes	Real Roots
1	$\mathbf{x}^p = [\mathbb{R}_1, \mathbb{R}_2, \mathbb{R}_3]$	Stable, unstable, saddle node	3
2	$\mathbf{x}^p = [\mathbb{R}_1, \mathbb{R}_2, \mathbb{R}_3]$ with $\mathbb{R}_2 = \mathbb{R}_3$	Asymptotically stable/unstable node + half unstable saddle/half stable saddle node	2
3	$[\mathbf{x}^p = [\mathbb{R}_1, \mathbb{C}_1, \mathbb{C}_2]$	Stable/unstable focus or midpoint	1

Furthermore, due to the fact that negative compositions are permissible, we have to account for all types of steady-state solutions to the DPE, including complex solutions. In fact, complex solutions are not that rare in CPMs, and CSs displaying these properties are perfectly normal. For a constant relative volatility ternary system which only has three roots, there are three unique cases that may occur, as summarized in Table 3.1.

Table 3.1 indicates the roots one may expect for particular solutions. The asymptotically stable/unstable nodes classified as type 2 nodes in the preceding section are special cases of case 1 in Table 3.1 and behave accordingly. Interestingly, when there are three distinct real roots, a shifted triangle is formed (Case 1), as shown in Figure 3.25a. When two of the roots are equal the shifted triangle collapses to a line and a hybrid node is formed (Case 2), as shown in Figure 3.25b. These types of nodes, found on the boundary between the discrete eigenvalue regions in Figure 3.23, behave as a saddle on the one side, but as a stable/unstable node on the other side. The formation of the hybrid node also brings the asymptotically stable/unstable node to the fore, which behaves exactly like a normal stable and unstable node from a topological point of view. Finally, when parameters $\mathbf{X}_{\boldsymbol{\Delta}}$ and R_Δ are chosen such that the roots of the DPE are complex, there is only one stationary point in the real composition space and thus no TT to speak of (Case 3)—Figure 3.25c serves as an example of this. These complex roots only occur in the region of complex solutions indicated in Figure 3.24. Thus when $\mathbf{X}_{\boldsymbol{\Delta}}$ lies in region 1 (see Figure 2.17a), it is impossible to obtain complex roots since the pinch point curves do not run through this region at all.

WWW

TUTORIAL 3.6

Try this for yourself: Using DODS-ProPlot, find combinations of $\mathbf{X}_{\boldsymbol{\Delta}}$, R_Δ, and $\boldsymbol{\alpha}$ that will result in each of the cases depicted in Figure 3.25.

3.9 SOME INSIGHTS AND APPLICATIONS OF CPMs

Now that a fundamental understanding of the importance and relevance of CPM parameters has been obtained, the next logical question is how this is of use or what

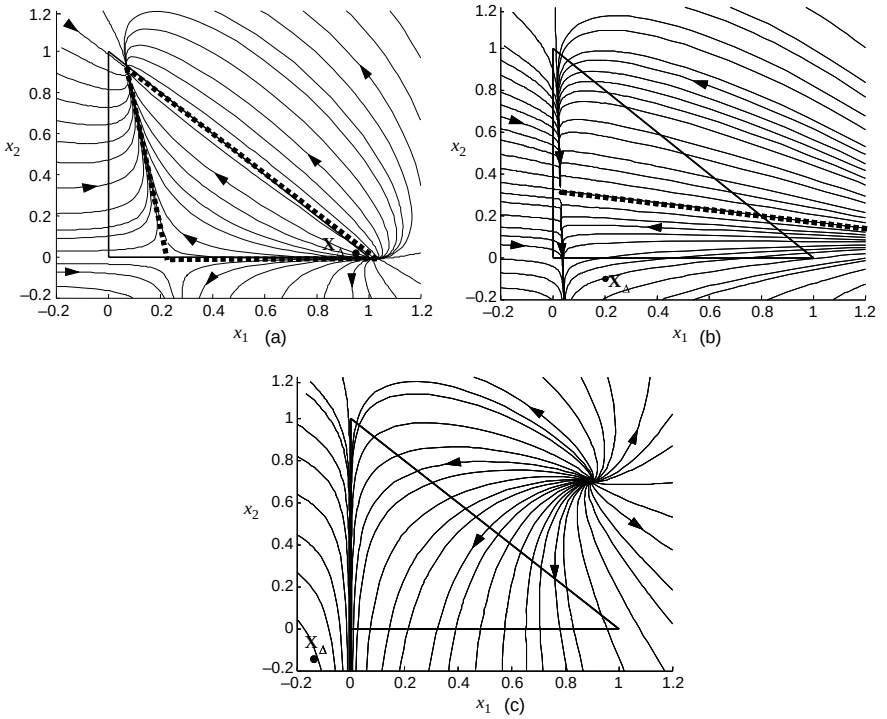


FIGURE 3.25 Constant relative volatility CPMs with $\boldsymbol{\alpha} = [5, 1, 2]$ at appropriate $R_{\boldsymbol{\Delta}}$ values showing (a) Case 1 with three real solutions and a TT, (b) Case 2 with three real solutions but two equal roots, and (c) Case 3 with one real solution and two complex solutions. The black dots indicate $\mathbf{X}_{\boldsymbol{\Delta}}$ placement.

might be inferred from a CPM. Although CPM's primary use is in designing columns or networks of CSs, this section attempts to highlight some important preliminary insights and applications that can be gleaned by the designer in a single CS, and how the design may be affected.

3.9.1 Column Stability

When designing a single CS, and ultimately a network of CSs that constitute a complete distillation column, it is often not only important to know that a design is feasible, but also, perhaps more importantly, that it is flexible and it can handle a certain degree of uncertainty or variance. CPMs are especially useful in this regard because they show all possible separation paths. Consider a CPM and its accompanying CS for the isobutene/methanol/MTBE system with $\mathbf{X}_{\boldsymbol{\Delta}} = [0.8,\ 0.07]$ and $R_{\Delta} = 2$, assuming that the CS is terminated by a condenser, thus $\mathbf{X}_{\boldsymbol{\Delta}} = \mathbf{x}^T$, as shown in Figure 3.26.

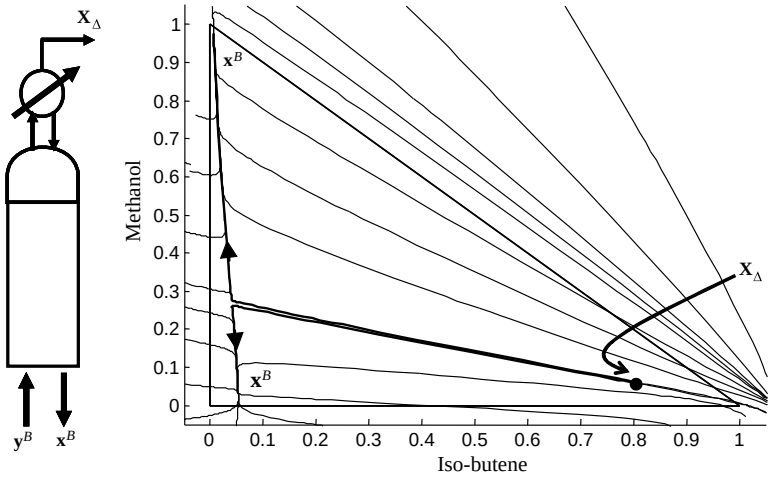


FIGURE 3.26 A CPM for the isobutene/methanol/MTBE system at $P = 1$ atm (NRTL) using $\mathbf{X_\Delta} = [0.8, 0.07]$ and $R_\Delta = 2$ with accompanying CS.

WWW

TUTORIAL 3.7

Try this for yourself: Reproduce Figure 3.26 with the given parameters using DODS-ProPlot. Try and find other systems and operating conditions that will result in similar column instability.

Figure 3.26 reveals that the profile running precisely through $\mathbf{X_\Delta}$ will eventually pinch near the pure methanol vertex. However, by selecting a profile slightly below $\mathbf{X_\Delta}$ (note with the naked eye it actually looks like the same profile), the eventual pinch coordinate is changed drastically and found near the MTBE vertex. This is a result of both profiles running very close to a saddle point; the saddle deflects the profile depending on which side of the saddle point the profile approaches. Thus, it is possible to conclude that if operating conditions in this particular CS were to change ever so slightly, the resulting profiles could run in completely different directions! The instability of this CS can be easily inferred using the CPM method, whereas running a single simulation on a simulation package would only reveal a half truth of a realizable design.

This illustration should also give the reader some insight into what topology is sought after for a "good" design. Saddle points generally, but not always, represent areas of caution because they can cause profiles to deviate around them. Stable and unstable nodes are in general, but not always, much better because all profiles are attracted to these points either in the positive or negative integration directions, irrespective of the starting point. One can expect that a column containing a CS operating under the conditions outlined in Figure 3.26 to be unstable to operate: changing the column's reflux slightly or having slightly

different feeds to the column may cause the column to operate well away from the desired specifications.

3.9.2 Node Placement

If it is possible to specify parameters $\mathbf{X}_{\Delta}$ and R_{Δ} and from this algebraically calculate all the pinch points in a CPM, then the inverse calculation must also hold: by specifying a reflux and a pinch point composition, one can determine what $\mathbf{X}_{\Delta}$ placement will satisfy this pinch point [11]. This statement is very powerful from a synthesis point of view, as it implies that the designer may in fact position the map and construct a CS to suit the needs of the exact separation required. This result is illustrated perhaps most effectively with the highly nonideal acetone/methanol/chloroform system. This particular system is notorious in distillation literature for its multiple azeotropes at RCM conditions, four in fact, and seven stationary points in all when counting the pure components, shown in Figure 3.27a. It would certainly be useful if we could shift the nonideal topology located within positive composition space to lie outside it. This is shown in Figure 3.27b, where we have specified the position of a pinch point outside the composition space (labeled 1) at $R_{\Delta} = 3$, calculated its accompanying difference point, and constructed a CPM.

WWW

TUTORIAL 3.8

Try this for yourself: Reproduce Figure 3.27a and b with the given parameters using DODS-ProPlot. Try and find other cases in other systems where azeotropes at RCM conditions are shifted into or out of the MBT.

Figure 3.27b shows that all the stationary points have been shifted outside the positive composition space, without having to operate the CS at particularly

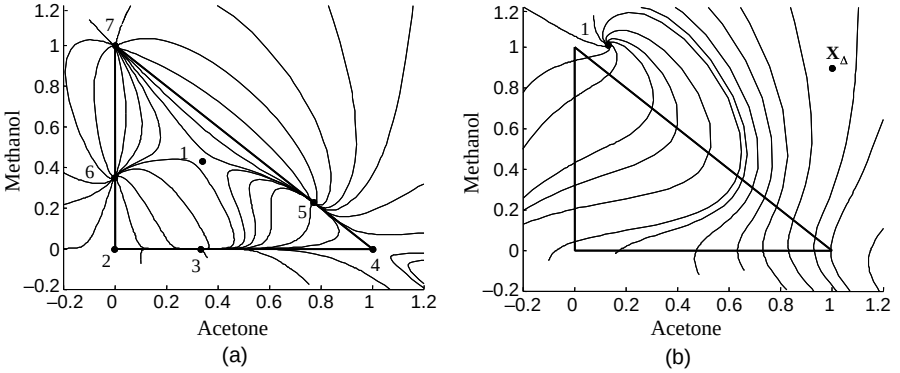


FIGURE 3.27 The acetone/methanol/chloroform system at (a) RCM conditions and (b) a CPM at $R_{\Delta} = 3$ and $\mathbf{X}_{\Delta} = [1.0, 0.9]$. The NRTL model was used at $P = 1$ atm.

extreme conditions. This is a staggering topological transform, especially if one considers that it is only achieved by a combination of mixing and vapor–liquid phase separation. One is thus able to cross several distillation boundaries given by the RCM. Although the operating conditions for the CS shown in Figure 3.27b may not be practical because of the feed requirements to such a CS, it does show that there are opportunities open to the engineer, much more than previously thought. If one were to only consider the RCM in Figure 3.27a, there would have been little to no hope for achieving certain product specifications. However, using the CPM technique with a global view of the composition space has put us in a position to at least consider some alternatives, by positioning nodes and the difference point. It should be noted that vast topological transforms, as depicted here, are not always possible for all systems at all refluxes. In other words, some nonideal systems may simply not be as sensitive to such transforms by merely adjusting the flow patterns in the CS—it is thus completely system dependent. Moreover, Figure 3.27 provides very good motivation for extending our view to negative composition space.

3.9.3 Sharp Splits

To further demonstrate the insight that may be gained from CPMs, sharp splits present an interesting mathematical study because they are cases where at least one element of $\mathbf{X_\Delta}$ is zero. It should be clear that even though an element of $\mathbf{X_\Delta}$ has a value of zero, it does not necessarily mean that the component is not present; it merely implies that its net flow is zero, that is, equal molar flowrates of that component in the vapor and liquid streams. This restriction forces a pinch point (mathematically) to lie on the same axis where $\mathbf{X_\Delta}$ is fixed. In other words, when $\mathbf{X_\Delta}$ is restricted to lie on a single axis (or extended axis) of the MBT, at least one pinch point is restricted to lie on this axis too. This gives us a unique opportunity to manipulate profiles in a desired direction on that specific axis where one entry of $\mathbf{X_\Delta}$ is zero. This is easily seen in a constant relative volatility system, where the TT lies on the $x_1 = 0$ axis, in Figure 3.28a.

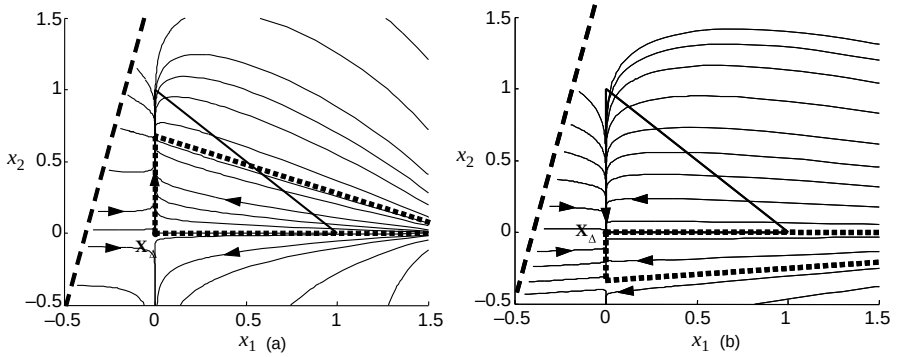


FIGURE 3.28 A TT for the constant relative volatility system with $\boldsymbol{\alpha} = [5, 1, 2]$ at $\mathbf{X_\Delta} = [0, 0]$ (a) $R_\Delta = 2$ and (b) $R_\Delta = 0.6$.

Figure 3.28a shows that one of the edges of the TT has been lodged to an axis at an arbitrarily chosen finite reflux value. Since the value of R_Δ may significantly affect the positioning of nodes and the fact that it is still a free design parameter, we can expect that very different TTs for our choice of a sharp split $\mathbf{X}_\Delta$ may come about. However, mathematics dictates that one side of the TT still be fixed to the $x_1 = 0$ axis. Thus, we witness a radical change in the direction of profiles in positive composition space by merely changing reflux, as shown in Figure 3.28b.

A comparison between Figure 3.28a and b shows that TTs have in fact flipped around their bases and in so doing have significantly altered the behavior of the system. The saddle point in Figure 3.28a has been replaced by a stable node. This means all profiles are running into the intermediate boiling vertex corner and implies that one could sample the intermediate boiling component as a bottoms product! This is a phenomenon termed "node-bumping" in previous works, and particularly interesting cases were shown for higher order sharp splits where more than one $\mathbf{X}_\Delta$ element has a value of zero [12].

3.10 SUMMARY

In this chapter, the reader should be comfortable with some of the basic concepts of CPMs. We have derived the DPE and shown that it is topologically similar to classic RCMs. However, unlike RCMs, which only give information at infinite reflux conditions, we now have the tools to comprehend, and graphically visualize, the effects of finite refluxes and the net compositional flows. We have shown what the basic effects of these parameters are on a given system and how they should be interpreted. The mathematics regarding CPM theory, that is, eigenvalues, eigenvectors, and so on, has also been presented. Although we have not yet discussed full column design, that is, the interconnection of multiple CSs, we have shown some preliminary insights into what the maps imply, and what they may be used for. Specifically, additional insight can be gained by relaxing the constraint that compositions need only be placed within the MBT, so much so that multiple stationary points found inside composition space can be shifted outward. Moreover, the CPMs lean some insight into CS stability and indicate areas where the design may change rapidly. Perhaps the most important message that the reader should take from this chapter is that it is possible to devise new separation paths by creatively placing $\mathbf{X}_\Delta$ or choosing R_Δ. It is easy to succumb to the idea that certain separations are possible and certain are not. Here, we have shown that it is indeed possible to synthesize almost any type of separation! This chapter should serve as a foundation for subsequent chapters which address the actual design of columns, each of which consist of networks of CSs.

REFERENCES

[1] Tapp, M., et al., Column profile maps.1. Derivation and interpretation. *Industrial and Engineering Chemistry Research*, 2004, **43**(2):364–374.

[2] Knight, J.R. and M.F. Doherty, Design and synthesis of homogeneous azeotropic distillations. 5. Columns with non-negligible heat effects. *Industrial and Engineering Chemistry, Fundamentals*, 1986, **25**(2):279–289.

[3] Van Dongen, D.B. and M.F. Doherty, Design and synthesis of homogeneous azeotropic distillations. 1. Problem formulation for a single column. *Industrial and Engineering Chemistry, Fundamentals*, 1985, **24**(4):454–463.

[4] Levy, S.G., D.B.Van Dongen, and M.F. Doherty, Design and synthesis of homogeneous azeotropic distillations. 2. Minimum reflux calculations for nonideal and azeotropic columns. *Industrial and Engineering Chemistry, Fundamentals*, 1985, **24**(4):463–474.

[5] Doherty, M.F. and G.A. Caldarola, Design and synthesis of homogeneous azeotropic distillations. 3. The sequencing of columns for azeotropic and extractive distillations. *Industrial and Engineering Chemistry, Fundamentals*, 1985, **24**(4):474–485.

[6] Levy, S.G. and M.F. Doherty, Design and synthesis of homogeneous azeotropic distillations. 4. Minimum reflux calculations for multiple-feed columns. *Industrial and Engineering Chemistry, Fundamentals*, 1986, **25**(2):269–279.

[7] Felbab, N., D. Hildebrandt, and D. Glasser, A new method of locating all pinch points in nonideal distillation systems, and its application to pinch point loci and distillation boundaries. *Computers and Chemical Engineering*, 2011, **35**(6):1072–1087.

[8] Ruiz, G.J., et al., Rigorous synthesis and simulation of complex distillation networks. *AIChE Journal*, 2011, **57**(1):136–148.

[9] Holland, S.T., et al., Column profile maps. 2. Singular points and phase diagram behaviour in ideal and nonideal systems. *Industrial and Engineering Chemistry Research*, 2004, **43**(14):3590–3603.

[10] Doherty, M.F. and J.D. Perkins, On the dynamics of distillation processes III: The topological structure of ternary residue cure maps. *Chemical Engineering Science*, 1979, **34**:1401–1414.

[11] Holland, S.T., et al., Novel separation system design using “moving triangles”. *Computers and Chemical Engineering*, 2004, **29**(1):181–189.

[12] Hildebrandt, D., et al., Column profile maps as a tool for synthesizing complex column configurations. *Computers and Chemical Engineering*, 2010, **34**(9):1487–1496.

CHAPTER 4

EXPERIMENTAL MEASUREMENT OF COLUMN PROFILES

4.1 INTRODUCTION

The techniques discussed in the first few chapters are all theoretical, based on simple chemical engineering tools such as mass balances and phase equilibrium. It has been shown, thus far, that the CPM technique is, for example, extremely useful in the assessment of column stability in particular CSs. It has also been shown that nodes can be shifted throughout the composition space by merely adjusting parameters such as the reflux ratio, R_{Δ}, and difference point, $\mathbf{X}_{\boldsymbol{\Delta}}$. In subsequent chapters, the CPM technique will be applied to identifying potential separation networks, whether it be in designing complex distillation structures such as fully thermally coupled columns, membrane, or reactive columns. Unfortunately, all the techniques presented so far make one fundamental assumption: the phase equilibrium data is known and accurate, and therefore the resulting CPM is also accurate. There are of course a multitude of systems which do not have either known or accurate equilibrium data, and thus it becomes very difficult to trust that stationary points are in fact moving in the way which the thermodynamic model predicts, ultimately making the final design of the process extremely difficult.

To address this concern, one needs to have some sort of experimental procedure that allows one to measure column profiles at finite reflux. One could decide to erect a pilot scale distillation column to do this, but this has the drawback that it may be difficult to start-up and control, potentially wasting valuable engineering time without getting the needed insight, not to mention the huge costs involved. In

Understanding Distillation Using Column Profile Maps, First Edition. Daniel Beneke, Mark Peters, David Glasser, and Diane Hildebrandt.
© 2013 by John Wiley & Sons, Inc. Published 2013 by John Wiley & Sons, Inc.

contrast to this, a batch still, such as the one used to generate RCMs (see Section 2.1), although only giving information at infinite reflux, is reasonably simple and inexpensive to set-up and operate.

In this chapter we introduce techniques that modify the batch experiment, in order to allow one to assimilate information regarding a finite reflux column. Numerous papers from the COMPS group have been published on this topic for both rectifying and stripping CSs, and have been shown to be extremely useful in validating the theoretical node-shifting predicted through CPMs, as well as to compare different thermodynamic models at finite reflux [1–6].

4.2 THE RECTIFYING COLUMN SECTION

4.2.1 The Batch Analogy

Describing a continuous rectifying CS producing a set distillate product with a batch experiment was pioneered by Modise et al. [3–5] in the COMPS group, from which most of this section is based on. The conventional continuous rectifying CS in a simple column is characterized by a net flow of material upward and is generally located above the feed stage, producing a distillate product at its upper end. A typical rectifying CS is depicted in Figure 4.1.

The composition changes in the CS from the bottom toward the distillate product, $\mathbf{X}_{\Delta D}$, at the top as the stages progress upward. The change in composition is described by a modified version of the DPE for a rectifying CS

$$\frac{d\mathbf{x}}{d\rho} = (R_\Delta + 1)(\mathbf{x} - \mathbf{y}) + (\mathbf{X}_{\Delta D} - \mathbf{x}) \tag{4.1}$$

where ρ is a warped stage variable such that $dn = (1/V)d\rho$. The reader is urged to derive the expression in Equation 4.1. The transformation of the independent

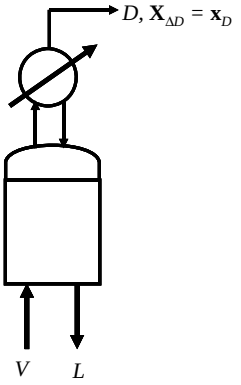


FIGURE 4.1 A typical continuous rectifying CS in a simple column, producing a distillate $\mathbf{X}_{\Delta D}$.

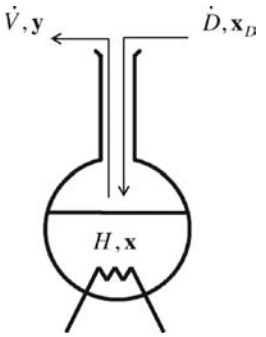


FIGURE 4.2 A simple batch distillation configuration with a constant feed stream addition of $\mathbf{x}_{\boldsymbol{D}}$.

position variable from n to ρ only affects the length of integration and not the direction of the profiles or shifted stationary points in the CPM. In other words, the form of the CPM will remain the same but the limits of the integration coordinate will change. Furthermore, the difference point ($\mathbf{X}_{\boldsymbol{\Delta D}}$) and distillate composition are exactly equivalent ($\mathbf{x}_{\boldsymbol{D}} = \mathbf{X}_{\boldsymbol{\Delta D}}$) this CS as shown in Section 3.5.2. Recall too that the reflux ratio in a rectifying CS is always positive (see Section 3.5.3).

Consider now a modified version of the simple batch distillation setup portrayed in Chapter 2 (see Figure 2.1), but in this instance the addition of a feed stream with a fixed composition ($\mathbf{x}_{\boldsymbol{D}}$) is permitted, as shown in Figure 4.2.

In this batch experiment

H represents the liquid holdup within the beaker (mol),
$\dot{V}$ is the removal rate of vapor leaving the beaker (mol/s),
$\dot{D}$ is the addition rate of feed (distillate) to the beaker (mol/s), and
$\mathbf{x}$ and $\mathbf{y}$ are the liquid and vapor molar fractions, respectively, in the vector form.

The unsteady-state mass balance over the liquid in the still results in

$$\frac{d\mathbf{x}}{dt} = \left(\frac{\dot{V}}{H}\right)(\mathbf{x} - \mathbf{y}) + \left(\frac{\dot{D}}{H}\right)(\mathbf{x}_{\boldsymbol{D}} - \mathbf{x}) \tag{4.2}$$

Equation 4.2 describes the change in composition with time in the still. This equation can also be further modified by dividing it by D/H to obtain a differential equation in terms of a warped time variable $dt = \left(\dot{D}/H\right)d\zeta$ and letting $\left(\dot{V}/\dot{D}\right) = r + 1$, where r is the reflux ratio, resulting in Equation 4.3:

$$\frac{d\mathbf{x}}{d\zeta} = (r + 1)(\mathbf{x} - \mathbf{y}) + (\mathbf{x}_{\boldsymbol{D}} - \mathbf{x}) \tag{4.3}$$

Equation 4.3 is mathematically equivalent to Equation 4.1 when taking $r = R_\Delta$ and $\mathbf{X}_\Delta = \mathbf{x}_D$, even though the equipment used to realize the changes in composition are very different: the one being a continuously operated CS, while the other is a simple batch experiment. The independent integration variable (ζ) is time-dependent in Equation 4.3, while in Equation 4.1 it reflects the number of stages down the length of the CS. Collecting data through the batch setup shown in Figure 4.2 is comparatively easy, simple and cheap, and mimics the real CS exactly, thus preventing the need for piloting a continuous column. The composition of the feed stream $\mathbf{x}_D$ is essentially the difference point composition, implying that only difference points with positive elements, that is, product producing CSs, can be measured.

4.2.2 Experimental Setup and Procedure

In order to approximate column profiles by collecting experimental data points, it is important that the experimental equipment and procedure be carefully laid out, such that results are easily obtainable, but more importantly that they are reliable. The setup used for profile validation of rectifying sections throughout this chapter can be seen in Figure 4.3.

4.2.2.1 Distillate Addition Before discussing the experimental setup, it is important to first interpret the underlying mathematics of Equation 4.3. Through the variable transformations used to obtain Equation 4.3, it can be shown that the reflux ratio r and the distillate flowrate $\dot{D}$ can be related to each other as follows:

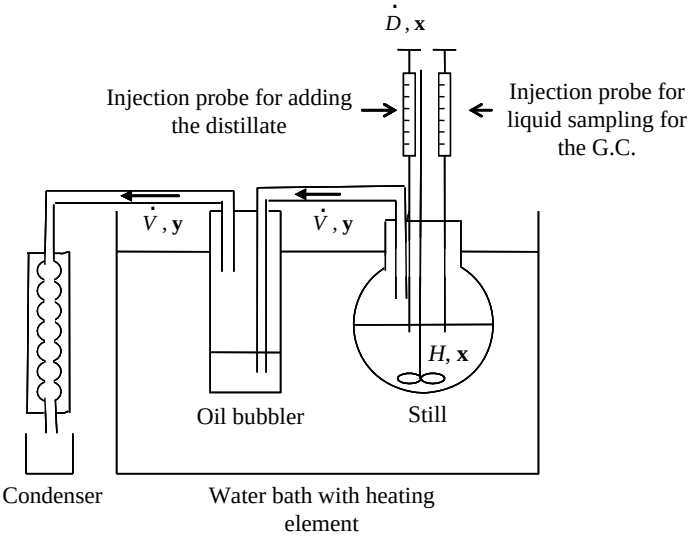


FIGURE 4.3 Experimental setup to generate column profiles of a rectifying CS.

$$\dot{D} = \frac{\dot{V}}{r+1} \tag{4.4}$$

By combining Equation 4.4 with an overall material balance across the still, we can obtain

$$\dot{D} = \frac{dH/dt}{r} \tag{4.5}$$

$$\dot{D} = \frac{\Delta H/\Delta t}{r} \tag{4.6}$$

Equation 4.6 indicates that in these experiments the distillate $(\dot{D})$ can be added incrementally rather than continuously. Thus, for a fixed reflux ratio (r), the amount of distillate to be added to the still can be calculated through Equation 4.6, by observing how much the liquid level has dropped (ΔH) after a time interval Δt. The smaller the time interval and the smaller the change in liquid level in the still, the more accurately the batch experiment will approximate the actual column profiles.

4.2.2.2 Apparatus The still shown in Figure 4.3 was submersed in a heated water bath to first ensure even heating, and second to ensure that the liquid residue would be at its boiling point. It was graduated in such a way that the level of the liquid inside the still can be measured and the volume calculated. In these experiments the still is typically charged with a liquid of known composition of about 200 mL. The still also contains four ports, two of which are for sampling of the liquid in the still and injection of the distillate, respectively. The other two ports are for the thermocouple probe and to keep the pressure constant by releasing vapor below the oil level in a bubbler. The oil bubbler was also used to measure the rate of vaporization $(\dot{V})$. A magnetic stirrer was used to ensure that the liquid in the still was well mixed, along with boiling stones to assist nucleation. A condenser was attached to the other end of the bubbler to capture the vapor from the system.

A Hewlett Packard gas chromatograph, HP6890, was used for the analysis of liquid samples. A small quantity of the distillate with the distillate composition was kept in a fridge to be used as a feed solution.

It should be noted that since the temperature of the liquid in the still is continuously changing as volatiles are boiled off, the water bath temperature must also be changed continuously to maintain a temperature driving force. In these experiments, we have chosen to maintain a temperature difference of 6°C between the contents of the still and the water bath. It is important to note that in order to maintain a reasonable approach to equilibrium between vapor and liquid in the still, the boiling process has to occur very slowly. Thus, the temperature of the water bath was increased in small increments, and then held for a substantial time before changing it.

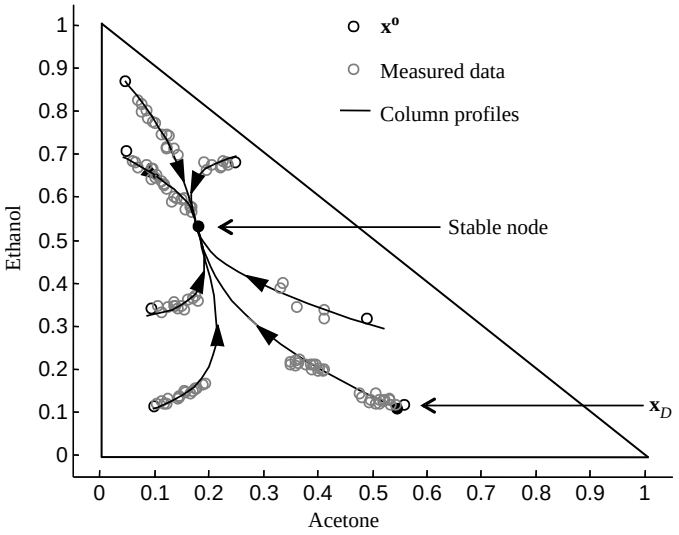


FIGURE 4.4 Experimental validation of column profiles for the acetone/ethanol/methanol system with the reflux ratio $r = R_{\Delta} = 1$ and $\mathbf{x}_{\boldsymbol{D}} = \mathbf{X}_{\boldsymbol{\Delta D}} = [0.54, 0.11]$. Theoretical profiles were generated using the NRTL thermodynamic model.

4.2.3 Experimental Results

4.2.3.1 Stable Node In CPMs, many different entering liquid compositions may be chosen for fixed values of $\mathbf{X}_{\boldsymbol{\Delta}}$ and R_{Δ}. In the same way, the still may be charged with different initial compositions ($\mathbf{x}^{\mathbf{0}}$) and the subsequent compositions resulting from boiling may be traced to eventually generate an experimental version of the CPM. This is illustrated in Figure 4.4 for the acetone/ethanol/methanol system with a reflux ratio of $r = R_{\Delta} = 1$ and a distillate composition of $\mathbf{x}_{\boldsymbol{D}} = \mathbf{X}_{\boldsymbol{\Delta D}} = [0.54, 0.11]$. The theoretical column profiles were generated using the NRTL thermodynamic model at the operating (atmospheric) pressure of 0.825 atm. This is the atmospheric pressure of Johannesburg, South Africa, situated at roughly 1500 m above sea level.

In the RCM for this system, the stable node is located at pure ethanol, being the high-boiling component (see the RCMs in Figure 2.8a, or Figure 2.17). Figure 4.4 shows that the CPM predicts that the stable node has moved into positive composition space from its position at the ethanol vertex at RCM conditions. The experimental data generally agrees very well with this prediction from a range of different initial compositions. Data points that show significant deviation from the theoretical profiles could be attributed to inaccurate feed addition that may arise from the manual injection. Another possible reason for deviation from the theoretical curve could be due to superheating of the liquid mixture leading to deviation from equilibrium. It can also be observed that at areas of high-profile curvature, the experimental points appear to be very close to each other, suggesting that the profiles were moving slowly around these areas, implying that the separation becomes more difficult in these regions.

Figure 4.4 shows that it is possible to simulate CPMs experimentally and, more importantly, that the node-shifting phenomenon observed theoretically in Chapter 3 can be verified relatively easily using simple batch equipment. Topology that had been in negative composition space in the RCM has now been shifted into the positive domain in the CPM. The three upper profiles in Figure 4.4 above the stable node were originally outside the MBT at infinite reflux, but at the chosen operating conditions now lay well within the physical region, and are thus measurable. Likewise, topology originally lying in positive composition space at RCM conditions has been shifted to outside. Figure 4.4 portrays the behavior of profiles near the stable node region, where all profiles are attracted.

4.2.3.2 Saddle Point Perhaps more importantly from a column stability point of view, is verifying the existence of a saddle node, since these nodes have profiles moving into and away from it. Figure 4.5 shows such an RCM for such a case for the diethyl ether/benzene/methanol system. This map was generated using the NRTL thermodynamic model at $P = 0.825$ atm

This RCM has a saddle azeotropic point on the benzene–methanol axis, which tends to move into the positive composition space at positive finite reflux values. Thus, this is a point of concern from an operational point of view in rectifying CSs operating at finite reflux values. As discussed in the previous chapter (see Section 3.9.1), operating either side of the saddle point results in drastic changes in profile behavior. Figure 4.6 depicts the behavior of profiles in the near-lying neighborhood of the saddle point at $R_\Delta = r = 3$ and $\mathbf{X}_{\boldsymbol{\Delta D}} = \mathbf{x}_{\boldsymbol{D}} = [0.694,\ 0.066]$.

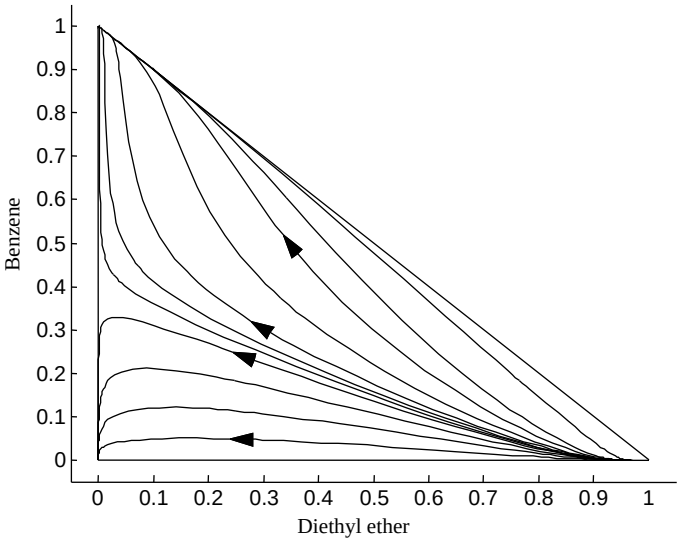


FIGURE 4.5 A residue curve map for the diethyl ether/benzene/methanol system generated using the NRTL thermodynamic model at $P = 0.825$ atm.

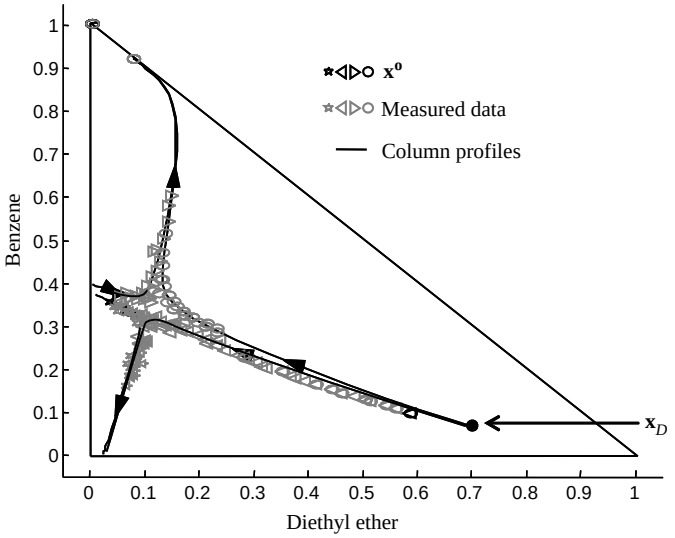


FIGURE 4.6 Experimental validation of rectifying column profiles for the benzene/diethyl ether/methanol system with the reflux ratio $r = R_\Delta = 3$ and $\mathbf{x}_D = \mathbf{X}_{\Delta D} = [0.694, 0.066]$ using the NRTL thermodynamic model at $P = 0.825$ atm.

Figure 4.6 shows clearly that extremely small changes in the initial charge composition of the still results in very different profile behavior. For instance, one can see that the two points originating near the distillate composition (the left-facing triangle and circle) are virtually identical. Both the data sets follow each other quite closely, until they approach the (shifted) saddle node where they veer off in opposite directions. In both instances (Figures 4.4 and 4.6) we can thus deduce that the thermodynamic model (NRTL) is a relatively good fit to the data.

Measuring rectifying column profiles can thus be done quite easily using a batch apparatus. The advantages of verifying profiles in this manner are, among others, that only a small amount of material is required to simulate profiles and that valuable engineering time can be saved when looking to verify or theoretical profiles. However, a disadvantage of the method is that it is not possible to simulate composition profiles where $\mathbf{X}_{\Delta D}$ is placed outside the positive composition space, since it is only possible to add a "real" distillate composition with these properties to the still. In other words, using the described apparatus and procedure is only applicable for CS which operates such that all the entries of $\mathbf{X}_\Delta$ lies within the MBT.

4.3 THE STRIPPING COLUMN SECTION

The preceding section deals with the experimental validation of column profiles in rectifying CSs. However, it is just as important to be able to model stripping sections, as these operating conditions may shift topology inside the MBT in ways that

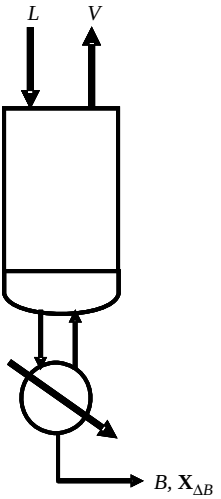


FIGURE 4.7 A typical stripping CS in a simple column, producing a bottoms product $\mathbf{X}_{\boldsymbol{\Delta B}}$.

rectifying sections do not. This section is based on work by Mulopo et al. [2]. A typical stripping CS can be seen in Figure 4.7.

However, the development of a stripping model is slightly more involved than the rectifying model because by definition, the operating reflux is negative. The mathematics of the DPE for stripping CSs thus implies that the batch equivalent is in fact the reverse process of vaporization, namely condensation. This, however, brings with it some experimental difficulties due to the nature of controlling and maintaining a vapor mixture at its dew point and then selectively condensing high-boiling components. Thus, it would be preferable to follow well-known boiling experiment as closely as possible. With this in mind, consider then a modified version of the DPE for a stripping section, as shown in Equation 4.7:

$$\frac{d\mathbf{x}}{dn} = \left(\frac{V}{L}\right)(\mathbf{y} - \mathbf{x}) + \left(\frac{B}{L}\right)(\mathbf{X}_{\boldsymbol{\Delta B}} - \mathbf{x}) \tag{4.7}$$

which may be rewritten as

$$\frac{d\mathbf{x}}{d\psi} = (\mathbf{x} - \mathbf{y}) - \left(\frac{B}{V}\right)(\mathbf{X}_{\Delta \boldsymbol{B}} - \mathbf{x}) \tag{4.8}$$

where $dn = (-V/L)d\psi$. The negative sign introduced into this variable transformation has the effect of reversing the direction of integration, that is, profiles head into opposite direction from the initial integration composition, but the shape of the profiles in the composition space still remains the same. In order to simulate stripping column profiles in a batch still, we now need to find a differential equation that can be

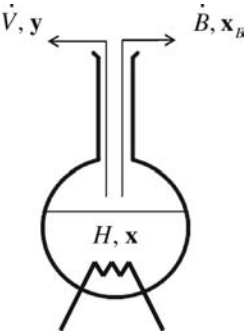


FIGURE 4.8 A simple batch distillation configuration with a constant material removal addition of $\mathbf{x}_B$.

related to Equation 4.8. The setup shown in Figure 4.8 does exactly this, where the liquid in the still is boiled off and removed at its vapor equilibrium composition, and where a stream with composition $\mathbf{x}_B$ is continuously being removed at a rate of $\dot{B}$.

The time-dependent differential equation describing the composition transformation in this still can easily be shown to be

$$\frac{d\mathbf{x}}{d\zeta} = (\mathbf{x} - \mathbf{y}) - \left(\frac{\dot{B}}{\dot{V}}\right)(\mathbf{x_B} - \mathbf{x}) \tag{4.9}$$

Although the mathematics of the continuous column and the batch still are now beautifully aligned with each other, it is not practical to remove material at a constant composition from an experimental point of view. It is much easier to *add* material at a constant composition, as shown in Figure 4.2. In order to apply the feed-addition experiment in Figure 4.2 to model stripping CSs, Equations 4.8 and 4.3 have to be equivalent to each other. Hence, it is convenient to rewrite Equation 4.3 for the feed-addition experiment in a form comparable to Equation 4.8, as shown in Equation 4.10:

$$\frac{d\mathbf{x}}{d\omega} = (\mathbf{x} - \mathbf{y}) + \left(\frac{\dot{D}}{\dot{V}}\right)(\mathbf{x_D} - \mathbf{x}) \tag{4.10}$$

where $d\omega = \left(\dot{V}/H\right)dt$. This is a different variable transformation than used previously to obtain Equation 4.3, but Equations 4.8 and 4.10 are now mathematically similar, as both have a separation vector term and a mixing vector term. Although the independent integration constants differ in these equations, if they are both plotted in concentration space, which is independent of the integration variable, they are equivalent. Thus, for the feed-addition experiment to simulate stripping composition profiles, Equations 4.8 and 4.10 need to be equivalent to each other. Since the separation vectors are already equivalent, this is the case if and only if the mixing vectors in each of these equations are identical, that is,

$$\left(\frac{\dot{B}}{\dot{V}}\right)(\mathbf{x} - \mathbf{X}_{\boldsymbol{\Delta B}}) = \left(\frac{\dot{D}}{\dot{V}}\right)(\mathbf{x}_{\boldsymbol{D}} - \mathbf{x}) \tag{4.11}$$

In our stripping CS, the ratio of $\dot{B}/\dot{V}$ can easily be converted into the generalized definition of $R_\Delta = L/(V - L)$, such that Equation 4.11 may be rewritten, in the vectorized form as

$$(-1 - R_\Delta)(\mathbf{x} - \mathbf{X}_{\boldsymbol{\Delta B}}) = \left(\frac{\dot{D}}{\dot{V}}\right)(\mathbf{x} - \mathbf{x}_{\boldsymbol{D}}) \tag{4.12}$$

remembering that R_Δ is always negative in stripping CSs. The relationship expressed in Equation 4.12 relates a certain composition in the still or in the stripping CS ($\mathbf{x}$) with the difference point in a stripping CS ($\mathbf{X}_{\Delta B}$) and a distillate feed composition in the batch setup ($\mathbf{x}_{\boldsymbol{D}}$). Equation 4.12 is essentially the lever-arm rule, and can be expressed geometrically as shown in Figure 4.9. Note that $\mathbf{X}_{\Delta B}$ can, but need not be, the bottoms or even a real composition within the CS. It is simply the difference point in the CS, and Figure 4.9 simply illustrates a case where $\mathbf{X}_{\Delta B} = \mathbf{x}_B$.

If we choose to add the distillate incrementally rather than continuously, the vapor flowrate leaving the still is equivalent to the drop in the liquid level in the still, thus

$$(-1 - R_\Delta)(\mathbf{x} - \mathbf{X}_{\boldsymbol{\Delta B}}) = \left(\frac{\dot{D}}{dH/dt}\right)(\mathbf{x} - \mathbf{x}_{\boldsymbol{D}}) = \left(\frac{\dot{D}}{\Delta H/\Delta t}\right)(\mathbf{x} - \mathbf{x}_{\boldsymbol{D}}) \tag{4.13}$$

Generally, profiles need to be generated/validated for a specified R_Δ and $\mathbf{X}_{\boldsymbol{\Delta B}}$, and therefore it is assumed in Equation 4.13 that both these are known variables. Thus, for a ternary system there are two independent equations but three unknown variables

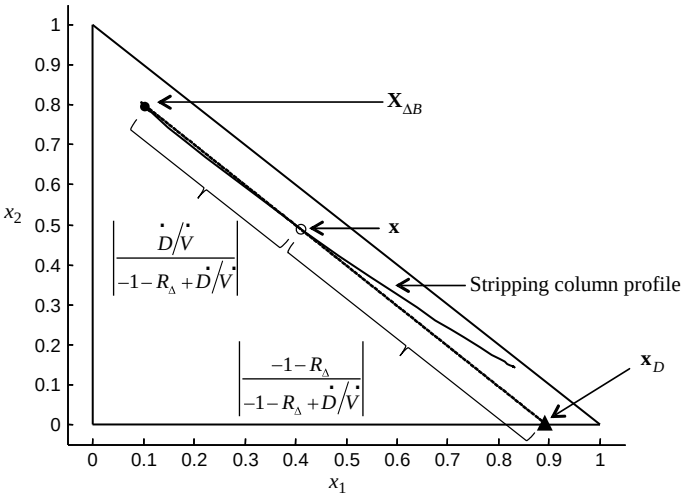


FIGURE 4.9 A geometric description of the lever arm rule portrayed in Equation 4.12.

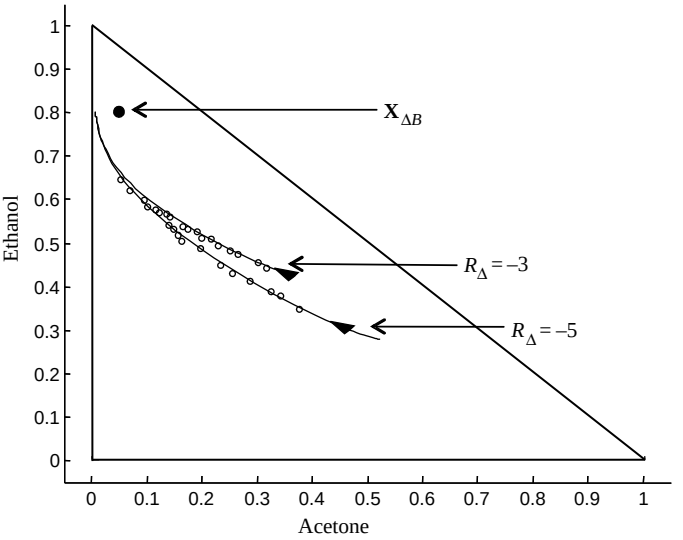


FIGURE 4.10 Experimental validation of stripping column profiles for the acetone/ethanol/methanol system with the reflux ratios $R_\Delta = -3$ and -5, and $\mathbf{X}_{\boldsymbol{\Delta B}} = [0.05,\ 0.80]$. Theoretical profiles were generated using the NRTL model at 0.825 atm.

($\dot{D}$ and two elements of the distillate composition vector $\mathbf{x}_{\boldsymbol{D}}$), and there is only one variable remaining to be specified. A simple case is then, for instance, to stipulate that $\mathbf{x}_{\boldsymbol{D}}$ is only a binary mixture, that is, $x_{D,i} = 0$ for one particular component i in a ternary system. It is then straightforward to determine the distillate composition ($\mathbf{x}_{\boldsymbol{D}}$) and flowrate ($\dot{D}$) that needs to be added to the still from Equation 4.13 once the composition ($\mathbf{x}$) and level-drop (ΔH) has been quantified after a certain time interval (Δt), again assuming both R_Δ and $\mathbf{X}_{\boldsymbol{\Delta B}}$ have been specified. Although one may choose to specify the distillate addition rate rather than a single composition for $\mathbf{x}_{\boldsymbol{D}}$, we have found it easier and more convenient to change the distillate rate, rather than make a completely new feed solution, according to Equation 4.13 after each measurement in the still. Figure 4.10 shows a set of experimental results for emulating a stripping CS for the acetone/ethanol/methanol system. Here, two cases are shown with operating refluxes of -3 and -5, respectively, while the bottoms composition in the CS ($\mathbf{X}_{\boldsymbol{\Delta B}}$) was taken as [0.05, 0.80] in both cases.

Figure 4.10 confirms a good agreement between the theoretically predicted profiles and the experimental data points, with a standard variance of less than 3%. Notice again that any initial composition in the still can be chosen, a range of which will eventually result in a CPM. One should also take cognizance of the fact that the experiment starts with a low-boiling mixture and the continually tracks how the liquid becomes richer in high-boiling components (thus, in terms of a stripping CS, from the top-down). $\mathbf{X}_{\boldsymbol{\Delta B}}$ is simply the chosen difference point of the CS; it need not be the final product of the experiment, as is the case in Figure 4.10 where profiles do not pinch at $\mathbf{X}_{\boldsymbol{\Delta B}}$. In fact, one may choose any $\mathbf{X}_{\Delta B}$ vector within the MBT and

validate stripping profiles as described in this section. Other considerations that should be kept in mind during these experiments are as follows:

- The experiment needs to be aborted after a long run because the distillate feed composition moves further away from the still composition and the ratio $\dot{D}/\dot{V}$ becomes very small (by lever-arm rule).
- Experimental points tend to deviate from the theoretical curve if the time interval between material additions increases because the differential equation followed by the experiment is not a good approximation of the theoretical first-order differential equation of the CS.
- Deviation is observed in the region of high curvature due to the local behavior of the separation and the mixing vectors.

Thus, we have shown here that, although slightly more complex, it is possible to simulate stripping composition profiles experimentally through a modified version of the batch boiling experiment. Although the mathematics indicate that the stripping CS requires a stream removal of constant composition, it was shown how this was modified to accommodate the easier feed-addition route, yet still generate results that closely approximate the desired profile.

4.4 VALIDATION OF THERMODYNAMIC MODELS

Thus far, simple experimental techniques have been presented for validating column profiles in both rectifying and stripping CSs. However, one may question how to put this knowledge, and that of node movement at finite reflux, to use in terms of discriminating between thermodynamic models. Choosing the right thermodynamic model for a particular system of components is of great importance to a designer, as a design is only as good as the model used. Even at the conceptual design stage of a distillation system, one still requires a model that sufficiently describes the system so that preliminary decisions can be made regarding column sequencing and structuring. There are numerous models for predicting vapor–liquid equilibrium in the literature, such as the NRTL model (used frequently in this book), as well as UNIFAC and UNIQUAC models, to mention few. Often, especially with nonideally behaved systems, it is difficult to assess which model is predicting the phase equilibrium correctly. While literature provides insights with regards to phenomena such as the existence of azeotropes, and two liquid phase regions, it is only given for systems that are well studied. Further, two thermodynamic models may predict considerably different behavior for the same system. For ambiguous cases, one requires an inexpensive method to ascertain which thermodynamic model is best for the system at hand. With this in mind, consider the following example.

In a nonideal system such as ethyl acetate/water/ ethanol, for instance, there exists considerable complexity from a phase equilibrium point of view because of the presence of a liquid–liquid-equilibrium (LLE) envelope, as well as the presence of three binary azeotropes and a single ternary azeotrope. Attempts have been made to

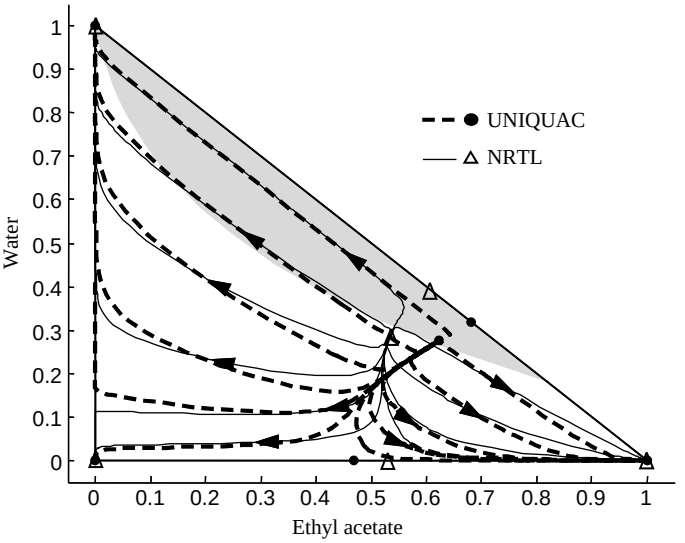


FIGURE 4.11 Superimposed RCMs for the ethyl acetate/water/ethanol system using the NRTL and UNIQUAC phase equilibrium models at a pressure of 0.825 atm. Shaded LLE region also shown.

model this particular system with the UNIFAC model, but the ternary azeotrope could not be located [7]. Here we shall investigate two other models, NRTL and UNIQUAC, to discriminate which is better suited to model the system. Figure 4.11 shows this envelope as well as predicted stationary points and the superimposed RCMs using the NRTL and the UNIQUAC thermodynamic models. The parameters for both models were obtained through data regression in Aspen Plus®.

Although both models shown in Figure 4.11 indicate the same qualitative behavior in terms of the general direction profiles run toward (and the number of stationary points), they show significant deviation in the prediction of the ternary azeotrope composition near the LLE boundary. In fact, the NRTL model predicts an unstable azeotropic node to lie on the outside of the LLE region, while the UNIQUAC model predicts that this azeotrope lies within the LLE region. This of course begs the question: which one of these models is correct? Unfortunately, the answer to this question is not as simple as one might think, that is, "just boil a mixture in a simple batch still with a composition near the predicted azeotropic point and see which model fits better." Because the azeotropic point lies near (or in?) the LLE region, it is very difficult to experimentally obtain reliable VLE data in this region. Thus, merely measuring the appropriate residue curves will not suffice.

A simple alternative to the problem is to use our knowledge of CPMs to shift the appropriate nodes away from the LLE region. Once these nodes have been shifted satisfactorily, one can simply measure these profiles using the techniques described in Sections 4.2 and 4.3. Such a case where nodes have been shifted is shown in Figure 4.12 where finite reflux profiles have been constructed such that

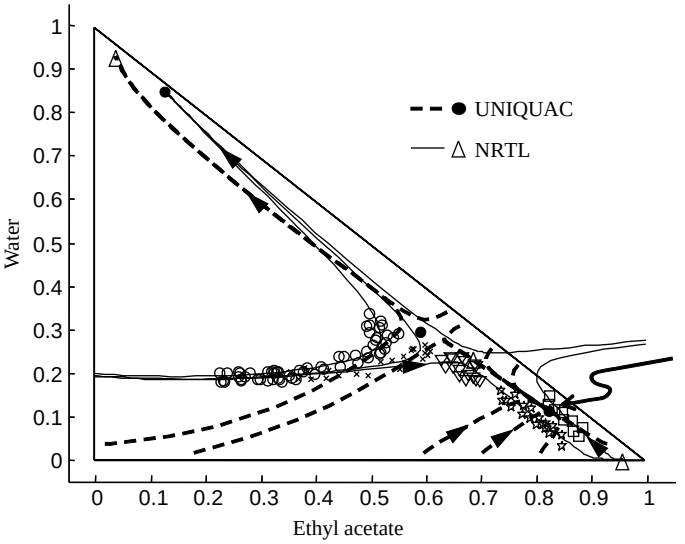


FIGURE 4.12 Superimposed CPMs for the ethyl acetate/water/ethanol system at a $R_{\Delta} = 1$ and $\mathbf{x}_{\boldsymbol{D}} = \mathbf{X}_{\boldsymbol{\Delta D}} = [0.8, 0.1]$ using the NRTL and UNIQUAC phase equilibrium models at $P = 0.825$ atm. Experimental data points have also been plotted.

the concerned azeotropic points are far away from the LLE region and can consequently be easily measured. In this case, the operating reflux was chosen to be 1 (hence a rectifying CS as in Section 4.2), while the distillate feed composition was $\mathbf{x}_{\boldsymbol{D}} = \mathbf{X}_{\boldsymbol{\Delta D}} = [0.8, 0.1]$. These operating points cause the desired change in the position for the nodes of interest. Data points for the equivalent batch experiment have been superimposed on the corresponding CPMs predicted by both thermodynamic models.

It is evident from the superimposed data points in Figure 4.12 that they are very closely aligned with the predictions of the NRTL model. The experimental results indicate that the profiles in fact move past the stable node predicted by the UNIQUAC model (highlighted by the curved arrow), and do not pinch at this point as one would expect if using this model. The predictions of the location of stationary points made by the UNIQUAC model are therefore false and those made by the NRTL are much better suited to this particular system.

The results shown in this section points out that not only can CPMs be measured experimentally in simple, small-scale, batch setups, they can also be used to discriminate between thermodynamic models in a quick and efficient manner.

4.5 CONTINUOUS COLUMN SECTIONS

The preceding sections in this chapter mainly present batch-wise experimental techniques to model continuous CPMs, thereby mimicking real distillation columns

in a relatively simple experiment. Although these small-scale experiments are very useful in that they are comparatively simple and do not require large amounts of material, it is often necessary to assess the workings of a *real* CS, by sampling liquid composition at various points along the length of the CS. It would be very useful, and indeed comforting, if the profiles predicted with the CPM technique can be verified experimentally in a packed or trayed column, especially when there is uncertainty in thermodynamic models or when the CPMs predict peculiar or counterintuitive results (like moving azeotropes into/out of the MBT). In this section, techniques will be presented that allow to measure column profiles in continuous CSs, specifically for the acetone/ethanol/methanol system at atmospheric pressure of 0.825 atm.

4.5.1 Apparatus

In the design of this experiment it is essential that the ultimate goal of the column, namely to validate composition profiles for a continuous CS, always be kept in mind. It is important to note that when integrating the DPE to generate CPMs it was assumed that both flows and compositions at either the top or bottom of the CS were known. This then allowed one to determine the Δ and $\mathbf{X}_{\Delta}$ of the CS, and hence solve the DPE. Experimentally, however, it is not always possible to know the flows and composition of both streams at either the top or bottom of the CS, especially if one is trying to simulate a general CS. One would have control over the flow and composition of the entering streams, namely the liquid feed at the top, as well as the vapor feed at the bottom. However, the exiting vapor (top) and liquid (bottom) streams are determined according to the mass transfer that occurs within the CS. Thus, material balance around the entire column would dictate when steady state has been reached. This is easily done by comparing measured values of Δ and $\mathbf{X}_{\Delta}$ at both the top and bottom of the CS (remembering that these parameters are constant throughout a CS—refer to Sections 3.5.1 and 3.5.2): once the values at the top are comparable to those at the bottom, the CS is at steady state, and liquid samples along the column length can commence.

Figure 4.13 illustrates the physical apparatus used within the COMPS Separations Group at the University of the Witwatersrand for these continuous CS experiments. The following key points within the experiment have been identified which will enable one to eventually achieve the aforementioned experimental goals and objectives, each of which will be subsequently discussed:

- column shell and packing;
- vapor feed at bottom of column (composition and flowrate required);
- liquid feed at top of column (composition and flowrate required);
- vapor exit at column top (composition and flowrate measurement);
- liquid exit at column bottom (composition and flowrate measurement);
- sampling equipment (thermocouples, sampling probes, and so on); and
- physical property measurement.

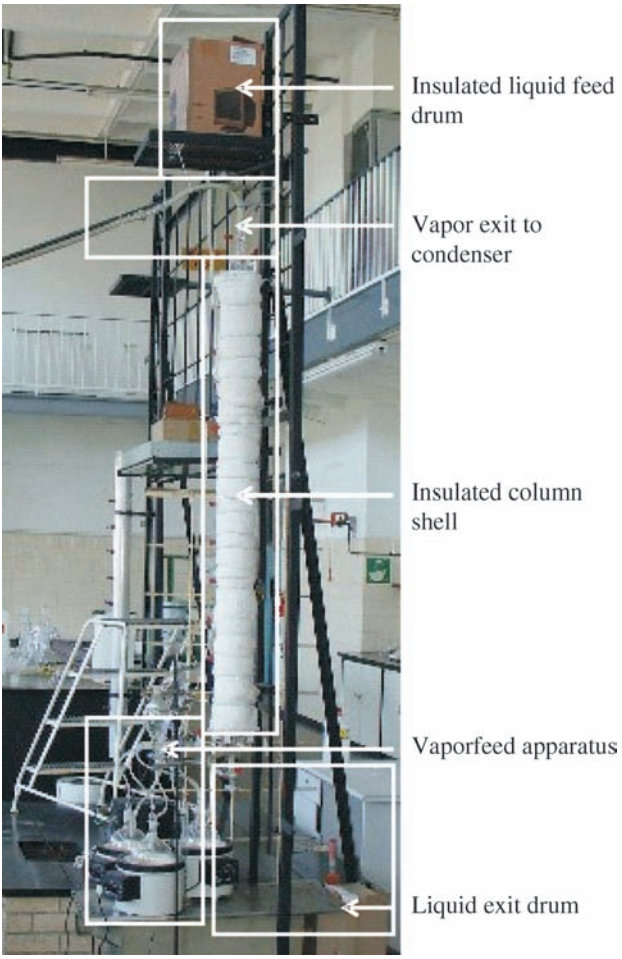


FIGURE 4.13 Photograph of complete column apparatus showing various column function areas.

4.5.1.1 Column Shell and Packing For the column shell and packing design, it is important to consider materials of construction, packing type and support structure, sampling ports along the length of the CS, and heating mechanisms.

When choosing the materials of construction, it is apparent that the column shell and its packing must be able to withstand all expected operation temperatures within the CS. In this particular case, the normal boiling points are relatively mild, between 50 and 80°C. The column shell is basically a pipe containing packing material, and aluminum was used in this case because

- It is relatively cheap.
- There is no need for the shell to be transparent.

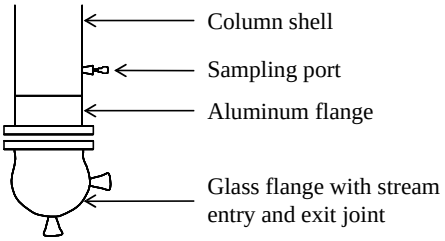


FIGURE 4.14 Schematic of column shell end (identical top and bottom), showing sample ports and flanges.

- Support for packing is easily implemented by inserting flat circular discs above and below the packing that also served to ensure efficient distribution of the liquid and vapor streams.
- The strength of aluminum affords the use of liquid sample ports that need to be moved or orientated fairly often without having to worry about breaks.

Of course, there are many other materials (glass, stainless steel, and so on) that may be used efficiently. An aluminum flange was machined to fit on either end of the shell. A corresponding glass flange was made for each aluminum end. The glass flange has two ground glass female joints to accommodate the entering and exiting streams at the top and bottom of the column. A schematic of the column shell ends is shown in Figure 4.14.

For the packing, two types were considered: ceramic Rashig rings and stainless steel Intalox saddles. The flooding (excessive retention of liquid within the CS) and loading (flux of liquid and vapor streams) characteristics of both types of packing were tested in a pre-existing column made of Perspex with a linked water and compressed air supply. The behavior of both packing types may be compared in a plot of pressure drop for increasing gas velocity, as shown in Figure 4.15.

It is evident from Figure 4.15 that the Intalox saddles behave consistently at both high and low liquid flowrates with no appreciable difference in the flooding or loading characteristics. The Rashig rings tend to flood at lower gas velocities for increasing liquid flowrates. This difference is due to the volume difference of the two packing types; there is far more free surface area available in the case of the Intalox saddles for vapor–liquid contact. There is a higher pressure drop associated with the Rashig rings for equivalent gas velocities when compared to the Intalox saddles. This is again due to the volume difference between the two types. The increased surface area per volume of the Intalox saddles compared to the Rashig rings results in a far more stable response to operating conditions, and was therefore chosen for this experiment. Furthermore, perforated aluminum plates above and below the packing provided a means of support and fluid distribution for the entering vapor and liquid streams.

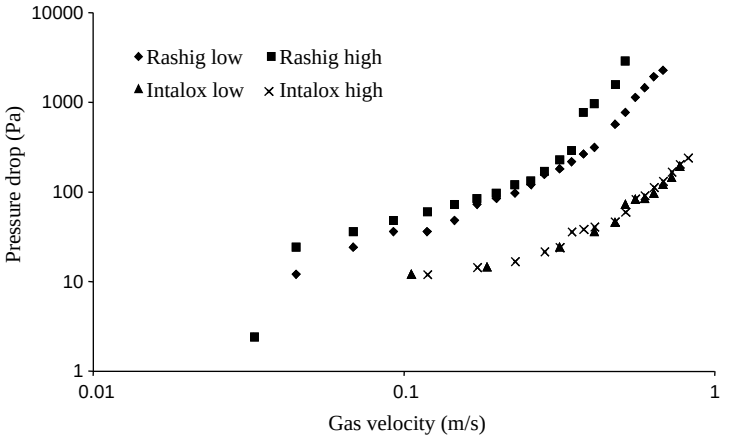


FIGURE 4.15 Flooding and loading characteristic graph for Rashig ring and Intalox saddle in identical apparatus for high and low liquid flowrates.

Ports for sampling liquid flowrates are placed along the length of the column shell. The ports are simply drilled holes into which customized liquid sampling tubes are placed. A sampling tube is shown in Figure 4.16. The rubber plug provides a tight seal in the column shell. The flared end inside the column maximizes the liquid sample catchment area, which then collects at the end where the rubber syringe seal is located.

In the derivation of the CPM equations, constant molar overflow has been assumed throughout, that is, vapor and liquid flowrates remain constant in a CS. This assumption is quite good for most systems, and essentially implies that the column is operated adiabatically with no heat loss through the column walls. If heat were to be added or removed down the length of a CS, the assumption would strictly no longer be valid since localized vaporization or condensation will occur and either the vapor or liquid stream flowrates may change considerably. Thus, for an honest comparison between experimental results and theoretical prediction, the CS should be completely insulated. Deviations from the constant molar overflow will manifest as discrepancies in the calculation of the bottom and top difference points for the CS. For a column operating strictly at constant molar overflow, the top and bottom

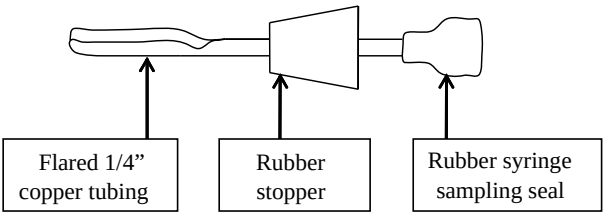


FIGURE 4.16 Schematic of sampling port in column shell.

difference points will be exactly equivalent by mass balance. Thus by comparing the calculated difference points at the top and bottom of the column, one has a good measure of how adiabatic the column was for the experimental run.

Moreover, one should realize that thermal equilibrium has to be reached in the column before accurate measurements can be made. Upon initial operation of the column shell, the column acts as a heat sink until it has reached a steady state whereby the column wall is roughly the same temperature as the equilibrium temperature along the length of the CS. In order to reach this steady state quickly, one may simply apply heating tape to the shell of the column underneath the insulation material. For this particular experiment with these particular components, the heating tape was kept at a mid-range temperature of 60°C according to the component boiling points of the acetone/ethanol/methanol system at 0.825 atm pressure. The column can be heated to this temperature and the heating tape can then be switched off just prior to the introduction of the feed streams for a particular run, whereby a thermal steady state is achieved in about 5 min.

4.5.1.2 Vapor Feed The simplest method of providing a vapor feed to the column is simply to heat a liquid to its boiling point and provide some means of transport to the column. However, the experiment requires a vapor feed at constant flowrate and of constant composition, to simulate a situation that will be encountered in a real column. If one were to use one mantle and simply charge it with a mixture of the required composition, the composition of the vapor would follow that of a residue curve and would thus be continually changing with time. This problem is easily surmountable if one uses three pure components, each in their own heating mantles. The composition of the resulting vapor-feed mixture can be controlled by simply manipulating the temperature control of the mantles. In this study, three identical mantles were sourced with capacities of 3 L and 450 W, and are temperature controlled by means of a variable resistor graded as a percentage of the total mantle heat output. It is important to note that using this individual mantle approach that the composition *and* flowrate of the resulting mixture is set once a heating strategy has been decided upon, as evident from Figure 4.17, showing the effect of heating mantle duty on the molar evaporation rates of each component.

4.5.1.3 Liquid Feed Since the vapor flowrate has already been specified by choosing its composition, the flowrate of to be fed at the top of the column may be easily determined for finite reflux CSs by using the definition of R_Δ, given here again:

$$R_\Delta = \frac{L}{V - L} \tag{4.14}$$

Positive refluxes indicate that the column is in rectifying mode and require a vapor flowrate larger than that of the liquid. In this case, however, the heating capacity of the mantles is the limiting factor and in order to achieve positive refluxes, very small liquid flowrates relative to the size of the column have to be used, resulting in insufficient wetting of the packing and inconsistent liquid sampling. Thus, in this

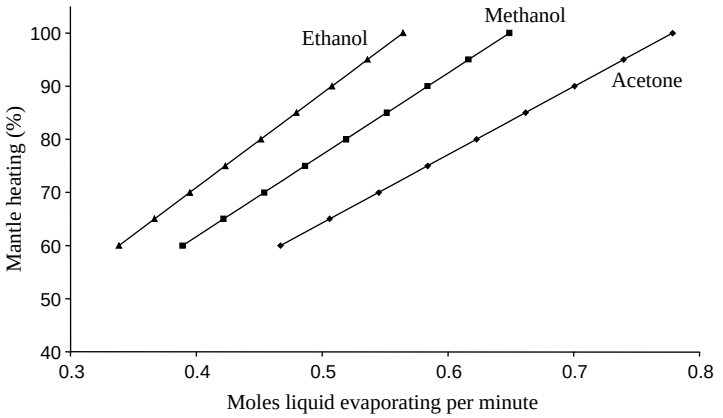


FIGURE 4.17 Moles of pure components evaporated for different heat settings on heating mantles.

particular study, only stripping CSs will be considered. The general experimental procedure is, however, not limited to stripping columns only; one merely needs either larger heating mantles or a smaller column to achieve useful and practical liquid and vapor flowrates. The liquid flowrate to be fed at the top of the column can easily be determined with a rotameter.

The temperature at which the liquid stream is to be added to the column is also an important variable to consider and control. One should keep in mind that the purpose of the experiment is to replicate a CS within a column. Thus, the liquid added to the CS should be at its bubble point, which may be easily determined from theoretical calculations or by simply heating a liquid mixture and noting at which temperature the first bubble starts to form. Once the boiling temperature of liquid feed has been established, heating tape may again be applied to the liquid reservoir to maintain that temperature.

4.5.1.4 Vapor Exit Once the column is in full operational mode, vapor will be produced at the top of the column. The flowrate and composition of this exiting vapor stream are both important variables that need to be known. The vapor is sampled at the top of the column above the liquid feed entry point. For ease of handling, this vapor should be condensed with cooling water. Analysis of the resulting liquid gives an overall average exiting vapor composition for the experiment. The vapor exiting at the top of the column is an instantaneous composition, thus comparing this to the average gives an idea whether a constant vapor composition was maintained. A burette prior to the flask provides a means of measuring the instantaneous flowrate of vapor through the column. This may then be compared to the average flowrate calculated from the total condensed liquid and the total experiment time.

4.5.1.5 Liquid Exit The liquid exiting the column acts as a liquid seal to the entering vapor feed stream by means of a sump. The instantaneous liquid

composition may be sampled in the sump. The average composition is sampled from the insulated drum at the base of the column at the end of the experiment. A valve and incremented glass tube provide a means to compare the instantaneous flowrate with the average flowrate. The average bottoms liquid flowrate is the total bottoms liquid volume divided by the total experiment time.

4.5.1.6 Sampling Equipment The liquid was sampled with a syringe and sample points are located along the length of the column. All sample ports should be sealed with a rubber syringe seal. In this experiment, vapor samples were taken with a vacuum syringe designed to condense the vapor as the sample is taken. All samples were cooled in a cooler bag with ice packs prior to being injected into 1.5-mL sample vials.

4.5.2 Experimental Results

Once there is certainty that constant molar overflow has been achieved to a reasonable extent in the CS (through analysis of the top and bottom difference point, and entering liquid and vapor flowrates), and that steady state has been reached in the column, it is possible to compare the measured compositions and the theoretically predicted CPM. Such a comparison is shown in Figure 4.18, with $\mathbf{X_\Delta} = [0.303, 0.294]$ and $R_\Delta = -2$.

Clearly, there is a reasonably good agreement between the CPM and the measured points. The labels T and B indicate the top and the bottom of the CS, respectively. At these particular operating conditions there is an unstable node

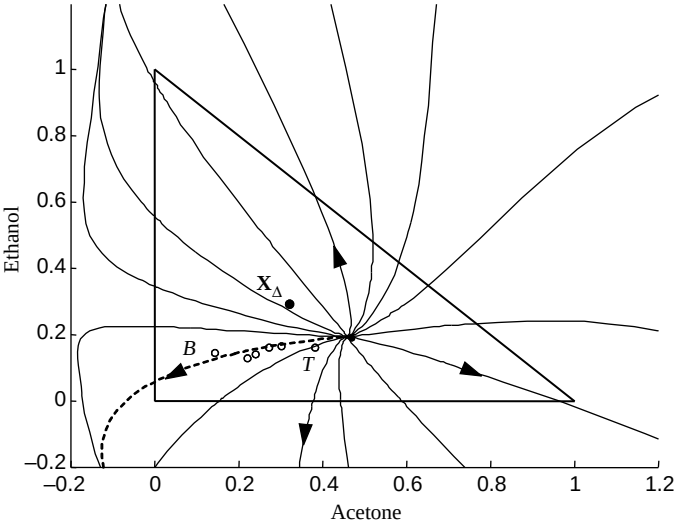


FIGURE 4.18 Comparison between experimental measurements (dots) and corresponding theoretical CPM (lines) with $\mathbf{X_\Delta} = [0.303, 0.294]$, and $R_\Delta = -2$.

within the positive composition space forcing all profiles away from it. The profiles predicted using the CPM method are thus quite representative of what is happening in an actual column. This experiment can obviously be repeated for a different set of operating conditions and a similar agreement between theory and practice can be found. As mentioned previously, experimental validation is especially important where one may be uncertain of, perhaps counterintuitive, behavior predicted by the CPMs. Such a case is shown in the following section, where a so-called temperature inversion occurs.

4.5.3 Temperature Inversion

Sections 2.5.3 and 3.6.4 introduce and discuss the properties of isotherm plots. Each isotherm represents all combinations of compositions that have equivalent boiling temperatures. For ideal systems these isotherms are linear, while nonideal systems are somewhat curved. An isotherm diagram for the nonideal acetone/methanol/ethanol system studied above is shown in Figure 4.19.

Figure 4.19 shows, as one would expect, that the lowest boiling temperatures are near the low-boiling acetone vertex, while the higher boiling isotherms are near the high-boiling ethanol vertex. The azeotrope between methanol and acetone cause profiles to have some curvature. It is important to point out that the location of these isotherms are fixed for a certain pressure, and that neither $\mathbf{X}_{\Delta}$ nor R_{Δ} will shift them (refer to Section 3.6.4).

In terms of classic, simple distillation columns like those depicted in Chapter 3, one can infer from the isotherm plot that the lowest temperature in the column is at

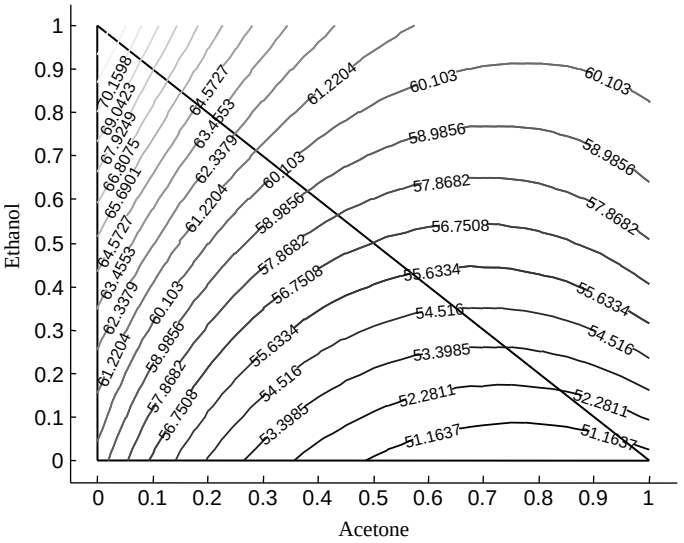


FIGURE 4.19 Isotherms for the acetone/methanol/ethanol system at 0.825 atm (temperatures in °C).

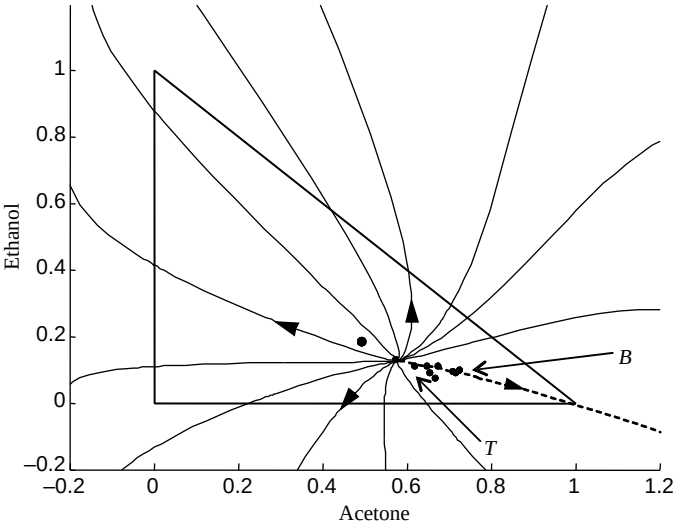


FIGURE 4.20 Comparison between experimental measurements (dots) and corresponding theoretical CPM (lines) with $\mathbf{X}_{\mathbf{\Delta}}$= [0.492, 0.188], and $R_{\Delta} = -1.96$.

the condenser, where the majority of the low-boiling components are removed, and conversely the highest temperature in the column is located at the reboiler. Classic simple columns, therefore, have a monotonic rise in temperature from the bottom of the column upward. However, situations may arise (especially in complex columns) where this may not be the case. In other words, some CPM designs may actually predict that the top of the column be hotter than the bottom! This somewhat strange prediction is therefore a perfect candidate for experimental verification. Such a case is shown in Figure 4.20.

Again, there is a good agreement between the CPM and experimental points. Notice that, when comparing Figure 4.20 with the isotherm diagram in Figure 4.19, it is clear that the top of the column is actually hotter than the bottom. The temperature of the bottoms and distillate products were measured to confirm this. It is important to note that there is nothing particularly strange in the operating conditions of this CS, and may occur quite naturally in a column.

4.6 SUMMARY

In this chapter, techniques have been introduced to experimentally measure and verify CPMs—for rectifying and stripping CSs. The rectifying section, in particular, is relatively easy to simulate since the mathematics describing the batch setup is equivalent to the continuous CS. The stripping CS, on the other hand, is not as simple since the mathematics of batch and continuous systems are not in complete agreement. This can, however, be overcome through a slight modification of the

experimental procedure. By merely altering the addition material's composition and flowrate, the batch experiment mimics the stripping CS very well. Furthermore, these techniques can be used to verify thermodynamic models as shown in the ethyl acetate/water/ethanol system. Here, it is easily shown that a particular model, the UNIQUAC model in this case, does not predict profiles correctly as the actual measured profiles in the batch system behave very differently. The NRTL model does, however, provide a good fit for this system. Finally, it is shown how one may validate CPMs using a continuous lab-scale CS. This particular technique is very useful for verifying profile behavior in a *real* CS that resembles what may be encountered in an actual column. This allows one to easily validate strange or counterintuitive behavior predicted by the CPM technique.

REFERENCES

[1] Tapp, M. and S. Kauchali, et al., An experimental simulation of distillation column concentration profiles using a batch apparatus. 2003, *Chemical Engineering Science*. **58**:479–486.

[2] Mulopo, J.L, et al., Experimental simulation of distillation column concentration profiles using a batch apparatus: Columns stripping section. 2005, *Chemical Engineering Science*, **60**(24):6815–6823.

[3] Modise, T., et al., Experimental simulation of distillation column section profiles using a batch apparatus. 2005, *Industrial and Engineering Chemistry Research*, **44**:7511–7519.

[4] Modise, T., et al., Experimental measurement of the saddle node region in a distillation column profile map by using a batch apparatus. 2007, *Chemical Engineering Research and Design*, **85**(1):24–30.

[5] Modise, T. D., Experimental simulation of distillation column profile maps, *Chemical and Metallurgical Engineering*. 2008, Johannesburg: University of the Witwatersrand.

[6] Mulopo, J., A study of vector formulations for distillation processes, *Chemical and Metallurgical Engineering*. 2008, Johannesburg: University of the Witwatersrand.

[7] Furzer, I. A., Critical distillation experiments in a region near the homogeneous ternary azeotrope in the system ethyl acetate−ethanol−water. 2001. *Industrial and Engineering Chemistry Research*, **40**(3):990–992.

CHAPTER 5

DESIGN OF SIMPLE COLUMNS USING COLUMN PROFILE MAPS

5.1 INTRODUCTION

At this point, the reader should have an understanding of the basic concepts of the CPM technique, from both a theoretical and experimental perspective. The DPE has been derived for a generalized CS using a general reflux ratio and a difference point ($\mathbf{X}_{\Delta}$). The underlying mathematical implications and potential practical applications were shown for single CSs, and that additional insight may be gained when using the CPM technique. A valuable attribute of the technique is CS synthesis, where one may position nodes and profiles to suit a specific separation and thus design separation equipment accordingly. Although we have unearthed several valuable conclusions from single CSs using the CPM method, we have not yet explored actual (entire) column design.

This chapter deals with the design of absorbers and strippers (which, in essence, are single CSs), and simple column design (one feed-two product columns, with two CSs). Although both these topics are well established in the literature, the CPM method is a quick (and generalized) means of finding feasible designs. Using this method, one does not need a new set of equations or a new technique to design a different or more complex column. Simple columns are one of the most prevalent pieces of equipment in the chemical industry, yet they are often poorly understood—especially when complex phase equilibrium behavior is present. Classical methods such as the Underwood equations assume constant relative volatilities and sharp splits between products and are thus not always applicable. Techniques based on

Understanding Distillation Using Column Profile Maps, First Edition. Daniel Beneke, Mark Peters, David Glasser, and Diane Hildebrandt.
© 2013 by John Wiley & Sons, Inc. Published 2013 by John Wiley & Sons, Inc.

RCMs also have limitations in that they only give information at infinite reflux (see Section 2.7).

To tackle this problem, Doherty and coworkers [1–3] devised the boundary value method (BVM) for, among others, designing simple columns for any phase-equilibrium relationship and any product distribution through first-order differential equations. The BVM is so named because the distillation synthesis problem is solved by specifying the *ends* (or boundaries) of the column, that is, the product specifications [4]. The governing equations in these works were derived for conventional rectifying and stripping sections only, and are the foundation for the derivation of the DPE. In this chapter an approach similar to the BVM is used, but showcasing its applicability and versatility to the CPM technique. Therefore a reader that is familiar with work by Doherty and coworkers will find this chapter a useful revision and supplement to the BVM.

5.2 ABSORBERS AND STRIPPERS

Absorption and stripping towers are a simple and effective means of removing impurities from a gas or liquid stream using an appropriate solvent. These impurity levels are generally very small, in the order of parts per million, but a very high recovery can be achieved. Absorption usually implies that the impurities are in the vapor phase, which is purified by passing a liquid stream over it, while the stripping process implies that an impure liquid stream is to be purified by passing a vapor stream over it. The hardware needed for absorption and stripping often consists of towers with vapor and liquid inlet streams, at the bottom and top, respectively, over a sequence of either equilibrium stages, or packing (structured or random). Fortunately, this is exactly the definition of a CS described in Chapter 2. The absorption/stripping problem is usually defined by a specified stream of impurities, an absorption or stripping agent, and the fractional recovery of the impurities, that is, the amount of impurity that has to be removed to satisfy the separation objective. Critical design parameters are the liquid-to-vapor ratio in the CS and the number of stages (or packing height) needed to obtain a desired purity in either the liquid or vapor product streams. Fortunately, again, all these parameters may be inferred using the DPE. It is however important to emphasize that the DPE relies on an equilibrium relationship between vapor and liquid phases, as do other simplified absorption and stripping design methods such as the Kremser equations [5]. That is to say, it is assumed that on each theoretical stage (or equivalent packing height) equilibrium is reached. For a more detailed design, one may opt to take into account other factors such as mass transfer limitations (by using so-called nonequilibrium models), but for the purpose of a first design approximation, an equilibrium relationship will suffice.

In this section, we will look at both absorption and stripping towers as stand-alone separation units. However, because of the configuration of these units being single CSs, they do also offer important information and ideas about complex columns, which consist of internal CSs that in essence behave similarly to either a stripper or absorber.

5.2.1 Absorption Towers

The most fundamental pieces of vapor–liquid separation equipment in the chemical engineer's toolbox are either an absorption or stripping tower. In this section, absorption design will be investigated. Absorption operations have found considerable application in chemical industries, some of which include air purification and removing catalyst poisons from reactive gas mixtures. A typical absorption tower is shown in Figure 5.1.

It is interesting to note that a typical absorption tower is merely a staged or packed column with no entering or exiting material/energy streams along its length—exactly the definition of the generalized CS introduced in Chapter 3. The entering streams to the tower are a liquid absorbent stream to the top of column ($\mathbf{x}^T$), and a "dirty" vapor stream to the bottom ($\mathbf{y}_{\text{in}}$). This dirty inlet stream contains impurities while the liquid inlet stream is usually a pure substance such as water, or some other specialized absorbent. The vapor and liquid streams are passed counter-currently over each other to produce an exiting vapor stream ($\mathbf{y}^T$) that has been cleaned of most of the impurities. The exiting liquid stream at the bottom of the column ($\mathbf{x}_{\text{out}}$) contains most of the impurities that were originally present in the entering vapor stream.

In order to solve the problem by means of the DPE, the two critical parameters, namely R_Δ and $\mathbf{X}_\Delta$, have to be specified. By merely specifying the flowrate of vapor and liquid streams it is simple to determine the reflux ratio. It is important to emphasize again that constant molar overflow (CMO) is assumed, meaning that the vapor and liquid flows remain constant throughout the column (see Section 3.3.2). This is a standard assumption in absorber and stripper design, and is generally a very good one, but it can be relaxed if the situation calls for it [5,6]. Recall that the reflux ratio is defined as

$$R_\Delta = \frac{L}{V - L}; \quad V \neq L \tag{5.1}$$

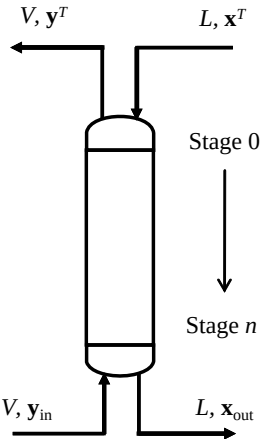


FIGURE 5.1 A typical absorption tower.

The remaining parameter, $\mathbf{X_\Delta}$, requires by definition that the flowrates and compositions of streams either at the top or the bottom of the column be specified. Since the vapor and liquid flowrates are assumed to remain constant throughout the column, the streams entering and leaving the column can be determined by specifying R_Δ. We need only specify the compositions of the streams at the top or the bottom of the column to determine $\mathbf{X_\Delta}$. Again, the definition of $\mathbf{X_\Delta}$ is given as

$$\mathbf{X_\Delta} = \frac{V\mathbf{y}^T - L\mathbf{x}^T}{V - L} = \frac{V\mathbf{y}_{\text{in}} - L\mathbf{x}_{\text{out}}}{V - L}; \quad V \neq L \tag{5.2}$$

For the absorption problem it is convenient to use the top of the column for specifying $\mathbf{X_\Delta}$, since one usually knows the composition of the clean absorbent (usually a pure liquid) and also the desired impurity composition that the exiting vapor stream at the top of the column has to achieve. Thus, through these compositions and flowrates all the parameters for integrating the DPE have now been specified.

Furthermore, numerical integration of the DPE requires that an initial composition be specified, that is, at stage 0, but this has been already specified by setting the liquid composition at the top of the column (the clean absorbent). By integrating the DPE to the *n*th stage, it is now possible to determine what the exiting liquid stream's composition, $\mathbf{x}_{\text{out}}$, at the bottom of the column is (at stage n), that is, the amount of impurities absorbed into the absorbent. Perhaps more importantly, it is then possible to determine what the entering vapor composition, $\mathbf{y}_{\text{in}}$, at the bottom of the column has to be to satisfy the mass balance. The entering vapor composition can be determined by rearranging Equation 5.2 as

$$\mathbf{y}_{\text{in}} = \frac{(V - L)\mathbf{X_\Delta} + L\mathbf{x}_{\text{out}}}{V} \tag{5.3}$$

Calculating $\mathbf{y}_{\text{in}}$ is equivalent to determining what the maximum impurities are that an absorption column operating at a set R_Δ, $\mathbf{X_\Delta}$, and n, can handle. Obviously, the more stages one specifies, the better the separation will be and the more impurities the column will be able to handle. Similarly, a higher absorbent flowrate (L) relative to the vapor flowrate (V) will increase the reflux ratio and therefore the absorption capability of the column. The amount of absorbent used and the height of the column are the dominant factors in deciding on the overall feasibility of the column, that is, whether the particular design specifications of the column can be met. As is evident from the derivation of the DPE in Chapter 2, any vapor–liquid equilibrium relationship may be assumed, although for the dilute mixtures typically encountered in absorption processes a simple model such as constant relative volatilities (or even using Henry's law) is usually sufficient. The general design procedure described here is likely to be understood more clearly through examples, shown below.

WWW

Example 5.1: An absorption tower is to be designed to remove ammonia (NH_3) from air using water as an absorbent. The design requires that the final air stream should not have more than 0.02 mol% NH_3. The tower operates at 1-atm pressure. At these

conditions, and as a first-design estimate, the components can be approximated with a constant relative volatility model where the volatilities of air, NH_3, and water with respect to water are 28,000, 400, and 1, respectively. For the purposes of this example, we will neglect evaporation of water into air. The reader should note that the DODS-ProPlot package may be used for this example.

(a) Determine the relationship between the absorbent (water) flowrate and number of stages, n, such that the process can handle an air–ammonia feed mixture of 2 mol% at a flowrate of 1 mol/s.
(b) Suppose we decide on operating at $L = 3$ mol/s of absorbent for the $V = 1$ mol/s air feed, requiring approximately six stages (see (a) solution) to "overdesign" the column. What is the effect of additional stages on the allowable inlet concentration of NH_3?

Solution 5.1

(a) The initial step in absorption calculations using the DPE is identifying all the parameters, that is, $\mathbf{X}_{\mathbf{\Delta}}$, R_{Δ}, and the initial integration composition. The initial integration composition has already been given as the entering liquid composition that is pure water, which is also $\mathbf{x}^T$. The problem asks to determine the effect of the absorbent flowrate, L, on the stage number required to ensure that the exiting vapor stream ($\mathbf{y}^T$) will have a purity of 0.02 mol% NH_3 when the inlet vapor stream contains 2 mol% NH_3. The stream compositions at the top of the column are thus (in the form [NH_3, water, air])
   - $\mathbf{x}^T = [0, 1, 0]$ (pure water)
   - $\mathbf{y}^T = [0.0002, 0, 0.9998]$ (assuming no water is transferred to the vapor phase)

   A strategy for solving this problem is as follows:
   - Choose a value for the liquid flowrate (L),
   - Calculate $\mathbf{X}_{\mathbf{\Delta}}$ and R_{Δ} through Equations 5.1 and 5.2 using the specified values for $\mathbf{x}^T$, $\mathbf{y}^T$, L, and V,
   - Integrate the DPE to a large stage number (say, $n = 20$) from $\mathbf{x}^T$,
   - Calculate $\mathbf{y}_{\text{in}}$ with Equation 5.3 at each stage n,
   - Determine the stage number where $\mathbf{y}_{\text{in}}$ is equal to the maximum allowable limit (2 mol% NH_3 in this case),
   - Repeat the procedure and plot the trend.

   This procedure can easily be implemented into an algorithm and solved with a computer. This allows one to establish the trend, as shown in Figure 5.2.
(b) The solution of problem (a) shows that to obtain 0.02 mol% ammonia–air product purity from an original ammonia–air purity of 2 mol%, we need approximately six stages for an absorbent flowrate of 3 mol/s, to be on the

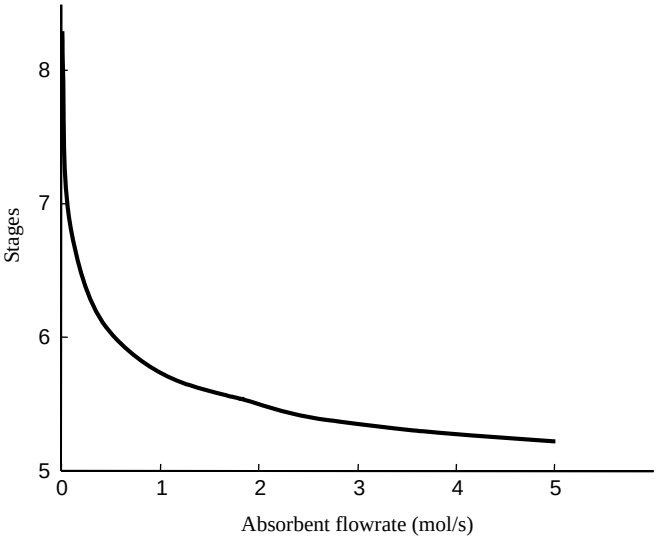


FIGURE 5.2 Stage number versus absorbent flowrate to ensure a 0.02 mol% ammonia–air stream is obtained from an inlet purity of 2 mol%.

"safe side" of the design. The solution of problem (b) is relatively simple once this is known, as we merely have to integrate the DPE to a sufficiently large number of stages and determine how the inlet vapor composition changes. The composition of the entering vapor stream is very sensitive to the stage number as shown in Figure 5.3.

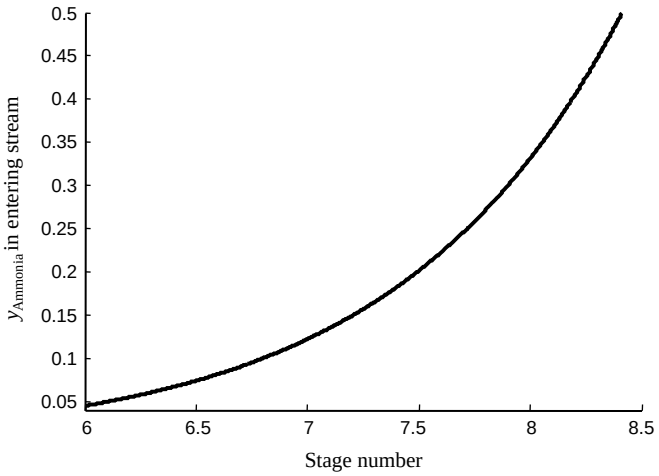


FIGURE 5.3 The effect of stage number on the entering ammonia–air purity to obtain a 0.2–mol% ammonia–air stream.

WWW

Example 5.2: Suppose there exists 1 mol/s liquid off-stream from a process containing a mixture of acetone/benzene/chloroform of composition [0.7, 0.1] that we wish to purify to 20 mol% acetone, with a final benzene concentration of less than 20 mol%. Using the DODS-ProPlot program, explore what operating conditions can be used in single absorber, operating at a pressure of 1 atm, with the off-stream liquid entering from the top. Use the NRTL thermodynamic model. Assume, for the purposes of this example, that any vapor stream can be made available to perform the separation.

Solution 5.2: The system in question is a nonideal, azeotropic system, exhibiting a distillation boundary. The location of this boundary with respect to the liquid feed and product locations is plotted in Figure 5.4.

Since the feed ($\mathbf{x}^T$) and product composition ($\mathbf{x}^B$) lie in different distillation regions, it is evident that this boundary will need to be crossed if the desired product is to be achieved. Also shown in Figure 5.4a is the residue curve passing through the

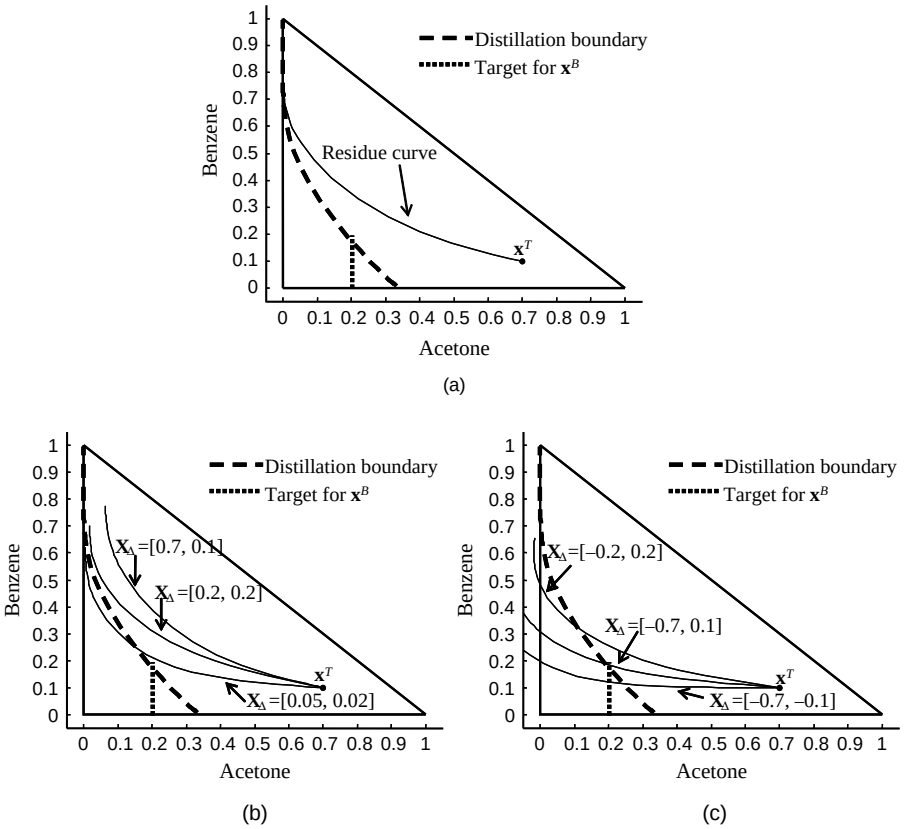


FIGURE 5.4 (a) Column profiles originating at $\mathbf{x}^T$ generated with (a) a residue curve, (b) $\mathbf{X}_\Delta$'s within the MBT at $R_\Delta = 6$, and (c) $\mathbf{X}_\Delta$'s outside the MBT at $R_\Delta = 6$.

feed composition. Thus, if we were to operate the absorber at infinite reflux (which implies that $V = L = 1$ mol/s), the desired product purity will never be obtained. Thus, operation at finite reflux is needed.

One could, for example, set a finite value of R_Δ (say, 6), and try different $\mathbf{X_\Delta}$s, thereby allowing the DPE to be integrated and generating a column profile for the absorber in each case. Once the operating parameters have been set, the unknown flows and compositions can be determined for a fixed feed rate and composition (see later). One may wish to try each of the feed or product specifications as $\mathbf{X_\Delta}$ or any other value too. This is shown in Figure 5.4b. The reader is encouraged to generate other profiles for different $\mathbf{X_\Delta}$s too.

Notice in Figure 5.4b that $\mathbf{X_\Delta}$s have been chosen to lie within the bounds of the MBT, and it appears that at the operating conditions chosen it is still not possible to reach the desired purity. Thus, we need to explore other options: keeping the same R_Δ, but using $\mathbf{X_\Delta}$ values that lie outside the MBT. Figure 5.4c shows examples of some profiles generated at the given $\mathbf{X_\Delta}$s.

It can now be seen that the profiles obtained in Figure 5.4c all cross the distillation boundary, and that utilizing the idea of $\mathbf{X_\Delta}$ to its full potential has its advantages from a topological perspective. Of course, reaching the actual required product specification does entail some manipulation. If we were to choose, $\mathbf{X_\Delta} = [-0.7, -0.1]$, for example, then using Equations 5.1–5.3 we can determine the unknown flows and compositions associated with the absorber. It can be shown that

$$V - L = \Delta = \frac{L}{R_\Delta} = \frac{1}{6} = 0.1667 \text{ mol/s} \tag{5.4}$$

$$V = L + \Delta = 1 + 0.1667 = 1.1667 \text{ mol/s} \tag{5.5}$$

$$\mathbf{y}^T = \frac{\Delta \mathbf{X_\Delta} + L\mathbf{x}^T}{V} = [0.5,\ 0.0714] \tag{5.6}$$

Using DODS-ProPlot it can also be seen that, in fact, only two stages are needed to get to $\mathbf{x}^B = [0.2,\ 0.1202]$. $\mathbf{y}^B$ can thus be calculated as

$$\mathbf{y}^B = \frac{\Delta \mathbf{X_\Delta} + L\mathbf{x}^B}{V} = [0.0714,\ 0.0887] \tag{5.7}$$

We see that, although using an $\mathbf{X_\Delta}$ that lies outside the space, all flows and compositions needed to achieve the separation are physically realizable.

While Example 5.2 may seem very different from the traditional ideas of absorption, it does give incredible insight as to what can be done in a single CS. While such a CS may not necessarily operate on its own, it may very well form part of an arrangement of CS in a complex column. This then gives a designer incredible freedom, especially when a number of these CSs have to be linked. Such considerations are discussed in Chapters 6 and 7.

It is worthwhile noting that both Examples 5.1 and 5.2 are ternary problems, and profile behavior can as such be easily visualized in a two-dimensional space. It is also entirely possible, in the case of Example 5.1 where constant volatilities have been assumed, to plot the transformed triangles (TTs) for the problem to interpret where a particular profile will tend toward, or whether there may be instability issues because the profile is closely approaching a saddle node. Analogous analyses can be performed for nonideal systems too, as shown in Example 5.2. Generating profiles and pinch points with DODS-ProPlot is rather simple for such systems and is not shown explicitly here.

5.2.2 Stripping Towers

Stripping, by definition, is the purification of an impure liquid stream by passing a vapor stream counter-currently over it. It can therefore, in principle, be seen as the reverse process of absorption and hence can be approached in the same way as shown in Section 5.2.1. A typical stripping tower can be seen in Figure 5.5, showing an impure liquid entering from the top of the column and a gas stripping agent entering from the bottom. The products are then a purified stripped liquid from the bottom and a contaminant-rich vapor stream at the top of the column.

Although it may seem that the DPE can be applied directly to predicting the behavior of the stripping tower, it is important to bear in mind that we are now dealing with trace amounts of *liquid* impurities. Notice that the classic form of the DPE tracks the compositional change in the liquid phase per stage and therefore requires an initial liquid composition for integration. In our case this would mean specifying the exact composition of the trace elements in the purified liquid stream. When dealing with trace amounts of substances as the initial integration condition, the DPE is known to be very sensitive to the composition of these components [2,4]. Therefore, if this specification is off by the smallest amount (even to the 8th decimal

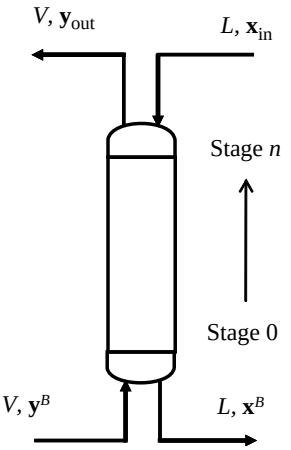


FIGURE 5.5 A typical stripping tower.

place), profiles will veer off into completely different directions which may not be useful for the design.

Thus, a more pragmatic approach is to track the compositions of a stream which we know the definite entering conditions of. In the case of stripping, this would be the entering or clean vapor stream from the bottom of the column. This implies that we have to track the compositional changes of the vapor stream as the stage numbers vary. The DPE for vapor compositions can be deduced in much the same way as the classical DPE for liquid compositions, and is given in Equation 5.8.

$$\frac{d\mathbf{y}}{dn} = \left(\frac{R_\Delta}{R_\Delta + 1}\right)(\mathbf{x} - \mathbf{y}) + \left(\frac{1}{R_\Delta + 1}\right)(\mathbf{X_\Delta} - \mathbf{y}) \tag{5.8}$$

The parameters R_Δ and $\mathbf{X_\Delta}$ retain the definitions they had for the liquid-phase DPE, and the liquid composition ($\mathbf{x}$) may now be modeled with respect to the vapor composition ($\mathbf{y}$) with an appropriate phase-equilibrium model, with the mixture still at its boiling point. Notice that the two streams we will use to define $\mathbf{X_\Delta}$ are now located at the bottom of the column, the vapor stream being the pure stripping agent $\mathbf{y}^B$ (usually a pure component) and the desired purity of the stripped liquid $\mathbf{x}^B$. We will thus be determining the vapor compositions along the length of the column in Figure 5.5, starting from the entering vapor composition at the bottom ($n = 0$) toward the top of the column to an arbitrary stage $n > 0$. The bottom of the column is completely specified and the composition of the exiting vapor stream at stage n is also known ($\mathbf{y}_{\text{out}}$), allowing one to determine the entering liquid composition at the top of the column too ($\mathbf{x}_{\text{in}}$), by mass balance:

$$\mathbf{x}_{\text{in}} = \frac{(V - L)\mathbf{X_\Delta} - V\mathbf{y}_{\text{out}}}{L} \tag{5.9}$$

To summarize, specifying the compositions and flowrates of the bottom vapor and liquid streams allows one to determine both $\mathbf{X_\Delta}$ and R_Δ. Using the entering stripping agent's composition as the boundary composition to initialize integration, we can determine both liquid and vapor compositions at the top of the column after n stages. Since we are mostly concerned with the allowable purity of the liquid stream at the top of the column, this approach allows to specify the desired liquid stream composition and calculate what liquid composition should enter the column. This procedure is illustrated more effectively through Example 5.3.

Example 5.3: One of the most important applications of stripping tower is the purification of both groundwater and industrial water from upstream chemical processes to produce clean water that may be safely discarded into natural water sources. An example of such a process is the removal of the volatile organic compounds dichloroethane, trichloroethylene, and trichloroethane from groundwater by stripping with air. Environmental agencies have specified that for safe disposal to the environment, the concentrations of (1) dichloroethane, (2) trichloroethylene, and (3) trichloroethane should not exceed 0.005 ppm by mass (each), corresponding to molar

fractions of 9.1×10^{-10}, 6.8×10^{-10}, and 3.5×10^{-10}, respectively. Also, the relative volatilities of these substances with respect to water are 3.5, 3.3, and 5.5, respectively, while the volatility of air with respect to water is extremely high at 28,000. The only economic constraint we have is that the column should not exceed 16 equilibrium stages. Determine the minimum air flowrate required for a groundwater flowrate of 1 mol/s, when the maximum tolerance for all three components in the groundwater (in mol fraction) is

(a) 10^{-4}
(b) 6×10^{-5}
(c) 2×10^{-5}

Solution 5.3: The problem requires that we find the flowrate of air entering the column that will strip the water to a certain concentration by not exceeding 16 stages. As the minimum air flowrate will occur at maximum number of stages, we have to determine what the flowrate will be when all impurity concentrations surpass these levels at 16 stages. Thus, for problem (a), let us guess a vapor flowrate of say 0.5 mol/s. This results in

$$R_{\Delta} = \frac{1}{0.5 - 1} = -2 \tag{5.10}$$

$$\mathbf{X_{\Delta}} = \frac{0.5(0,0,0,0,1) - 1(9.1 \times 10^{-10}, 6.8 \times 10^{-10}, 3.5 \times 10^{-10}, 1, 0)}{0.5 - 1} \tag{5.11}$$

$$\mathbf{X_{\Delta}} = [1.8 \times 10^{-9}, 1.4 \times 10^{-9}, 7.0 \times 10^{-9}, 2, -1] \tag{5.12}$$

The phase equilibrium may be modeled through

$$x_i = \frac{y_i/\alpha_i}{\sum y_i/\alpha_i}, \text{where } \boldsymbol{\alpha} = \left[3.5,\ 3.3,\ 5.5,\ 1,\ 28 \times 10^3\right]$$

All the significant parameters in the vapor phase DPE have now been specified, thus integrating from $\mathbf{y}^B$ to determine $\mathbf{y}_{\text{out}}$ and consequently $\mathbf{x}_{\text{in}}$ through Equation 5.9, results in Figure 5.6.

Figure 5.6 shows that at the specified operating conditions, two of the impurities' concentrations in the groundwater are lower than 10^{-4}. Thus, at these conditions, the water will not be sufficiently purified. We require somewhat more air to ensure that all the impurities entering the stripping tower are above 10^{-4}. After a few trial-and-error guesses, we arrive at a vapor flowrate of 0.85 mol/s, resulting in $R_{\Delta} = -6.67$. The change in concentrations at these conditions is depicted in Figure 5.7, showing that all the contaminants entering the column are above a molar fraction of 10^{-4}. Thus, if the actual groundwater's impurity mole fractions are less than 10^{-4}, the

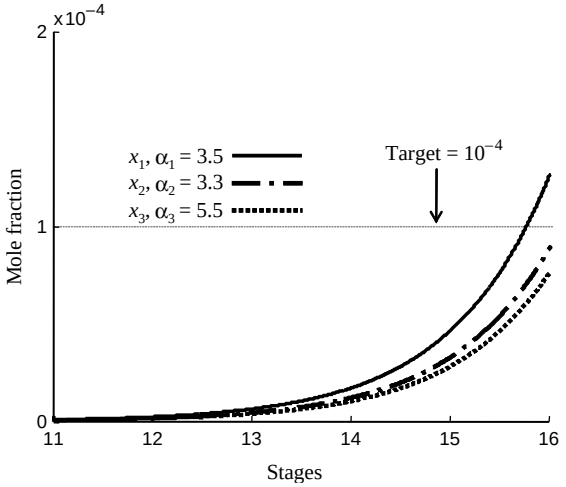


FIGURE 5.6 Change in groundwater impurity composition versus stage number at $R_\Delta = -2$.

current operating conditions will ensure, at the very least, that the specifications for the "clean water" are met.

In a similar way, we can determine the vapor flowrate for problems (b) and (c):

(a) 0.85 mol/s ($R_\Delta = -6.67$)
(b) 0.31 mol/s ($R_\Delta = -1.45$)
(c) 0.035 mol/s ($R_\Delta = -1.036$)

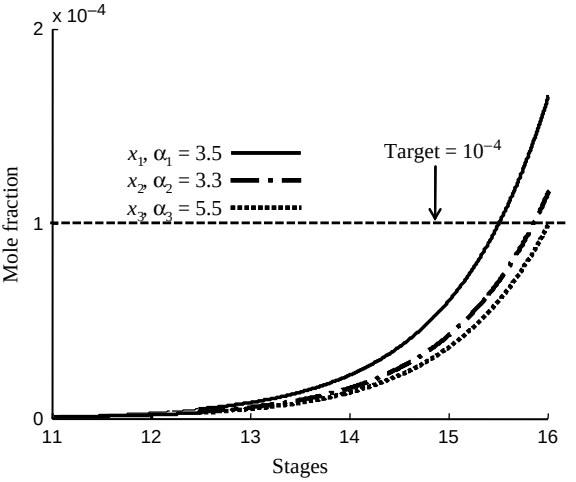


FIGURE 5.7 Change in groundwater impurity composition versus stage number at $R_\Delta = -6.67$.

5.2.3 Discussion

Interestingly, both the absorber and the stripper configurations are not restricted or defined by net flows directions. In other words, it is perfectly legitimate for either an absorber or stripper to have a positive ($V > L$) or negative ($V < L$) net flow—it is entirely dependent on the problem at hand. In the case of the absorber, as alluded to in Example 5.1, we operate with an absorbent flowrate that is greater than the flowrate of the vapor. Of course, the more absorbent we have the better the separation will become. An analogous argument can be made for stripping towers with regard to stripping agent. The fact that these towers can operate in either rectifying or stripping mode is a unique property, as it will become apparent in the subsequent chapters and discussions that the designer does not always have a choice in this regard.

Moreover, it should be noted that since we are generally dealing with very dilute mixtures in absorbing and stripping operations, that there is an extreme sensitivity to both R_Δ as well as the number of fractionation stages. As depicted in both Figures 5.6 and 5.7, a considerably better separation may be achieved by merely adding one or two additional equilibrium stages. The design parameters obtained using the DPE for absorption and stripping towers are by no means rigorous since the simplifying assumptions of constant molar overflow and complete equilibrium may not always hold, but it should nevertheless give a very good design estimate in much the same way as the classic Kremser equations [5,7]. It is also relatively straightforward to transfer the outputs from the CPM procedure to a more rigorous process simulation package such as Aspen Plus®.

5.3 SIMPLE COLUMN DESIGN

5.3.1 External Mass Balance

As mentioned in the introduction to this chapter, the design of simple columns using the CPM method stems from pioneering work done by Doherty and coworkers on the BVM. However, before determining ultimate design feasibility, it is important to know what constraints the mass balance places on our system, that is, what component *must* go to a specified product stream to satisfy the column's mass balance. Knowing the mass balance of the column is critical to the design since this enforces the boundary values for the design. A typical simple column is shown in Figure 5.8.

An overall material balance around the simple column gives

$$F = D + B \tag{5.13}$$

And a component balance

$$F\mathbf{x}_F = D\mathbf{x}_D + B\mathbf{x}_B \tag{5.14}$$

It can be shown that substituting Equations 5.13 and 5.14 into each other and using the fact that each of the compositions sum to unity, there is a linear dependence

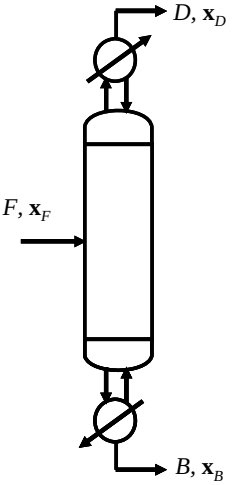


FIGURE 5.8 Simple-column setup with entering and exiting streams.

between products. Thus for a ternary system, we are able to represent this relationship in a two-dimensional space as straight lines as shown in Chapter 2, which subsequently leads to constructing a bow-tie region. Therefore, for a ternary system, if the feed is specified and one takes the liberty of completely specifying a single product stream's compositions, the other product composition will lie somewhere on the straight line defined by the specified composition and the feed composition. One only needs to specify one more variable, either a product flowrate or a single, additional composition for the mass balance to be completely specified. In general, it can be shown that a column with PS number of product streams and nc components in the feed requires that $nc(PS-1)$ mass balance variables be specified such that the entire column's mass balance be known. This is known as the column's external mass balance, or the external degrees of freedom. Section 2.6.3 deals with this topic more thoroughly.

As shown in Chapter 2 and again in Figure 5.9 all potential splits associated to a particular feed can be easily established. For the feed specification shown in the bow-tie region, it is possible for products to lie anywhere inside the shaded region, and be joined to each other by a straight line. Notice, however, that the bow-tie region has not yet considered phase-equilibrium behavior; it merely shows what is possible by the external mass balance. Chapter 2 showed how one may incorporate phase equilibrium through RCMs for the limiting infinite reflux case. However, it is still not entirely clear how this relates to a finite reflux scenario through the use of the DPE in Chapter 4. Furthermore, since we are dealing with two product-producing CSs in a simple column (CSs with a reboiler or condenser), we know from our understanding in Chapter 3 (see Section 3.5.2) that these product specifications are in fact the $\mathbf{X}_{\boldsymbol{\Delta}}$s of these sections. The following sections discuss how one may perform realistic simple column design by using DPE parameters such as R_Δ and $\mathbf{X}_{\boldsymbol{\Delta}}$.

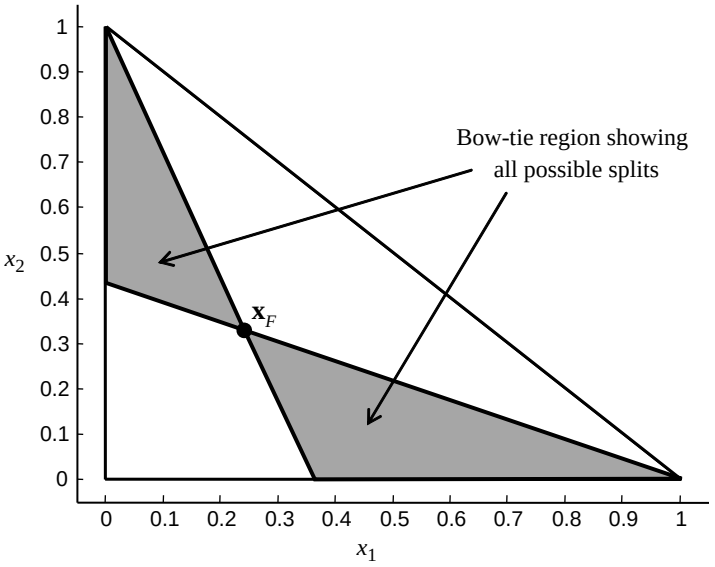


FIGURE 5.9 Bow-tie region for a certain feed $\mathbf{x}_F$.

5.3.2 Internal Mass Balance: Column Section Interaction

As discussed in Chapter 3, for the simple column shown in Figure 5.8, the rectifying section is characterized by a net flow upward (see Figure 3.9a) and is primarily responsible for carrying low-boiling components to the top of the column toward the distillate stream. Conversely, the stripping section has a net downward flow (see Figure 3.9b) and its main function is carrying higher boiling components toward the bottoms product. Thus, the rectifying section will have a positive reflux value while that in the stripping section will be negative. These CSs rely on each other to operate as an entire column, and naturally cannot be removed from each other. It is easy to see that the operating condition of the one is directly dependent on the other. By examining the feed stage shown in Figure 5.10, we can determine exactly how they are linked.

By assuming that the vapor portion of the feed mixes only with the vapor streams in the column, and likewise for the liquid, a mass balance for the vapor streams around this section gives (subscripts S and R indicate stripping and

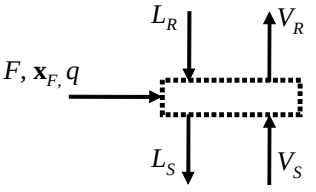


FIGURE 5.10 The feed stage of a simple distillation column.

rectifying CSs, respectively)

$$V_S = V_R - F(1-q) \tag{5.15}$$

where q is the liquid fraction of the feed, defined as L_F/F, also referred to as the feed quality. $q=1$ thus represents a saturated liquid feed, $q=0$ a saturated vapor feed, and $0<q<1$ is a two-phase feed.

Similarly, for the liquid stream

$$L_S = L_R + F(q) \tag{5.16}$$

We also know that in the rectifying (R) section

$$V_R - L_R = \Delta_R = D, \quad \text{and} \quad R_{\Delta R} = \frac{L_R}{\Delta_R} = \frac{L_R}{V_R - L_R} \tag{5.17}$$

And in the stripping (S) section

$$V_S - L_S = \Delta_S = -B, \quad \text{and} \quad R_{\Delta S} = \frac{L_S}{\Delta} = \frac{L}{V - L_S} \tag{5.18}$$

Using all the definitions given in Equations 5.15–5.18 and rewriting them in terms of a reflux ratio in the stripping section, yields Equation 5.19

$$R_{\Delta S} = \frac{L_S}{V_S - L_S} = \frac{L_R + F(q)}{-B} = \frac{DR_{\Delta R} + F(q)}{-B} \tag{5.19}$$

This gives the relationship between reflux in the rectifying section, $R_{\Delta R}$, and stripping section, $R_{\Delta S}$, and is known as the internal mass balance of the column. Notice that the stripping section is *always* negative (since $R_{\Delta R}$ and all flowrates are positive), and furthermore, the two reflux ratios in a simple column are linked by mass balances and cannot be chosen independently of each other. Once feed conditions and the external mass balance have been set for the column, the reflux in either CS is inherently linked to its neighbor. The relationship obtained in Equation 5.19 can also be obtained by performing an energy balance over the column and applying all the constant molar overflow assumptions.

It is also useful to note that the generalized reflux in the rectifying section, $R_{\Delta R}$, reduces to exactly the classical reflux ratio of $r = L/D$. However, the reflux ratio in the stripping section, $R_{\Delta S}$, is almost always expressed as a reboil ratio in classical column design as $s = V/B$. In this case, the relationship between the classical parameter and our generalized one is given as $R_{\Delta S} = -s - 1$.

Thus, by determining the overall mass balance around a simple column we can obtain all the $\mathbf{X_\Delta}$ values for each CS. By performing a mass balance over the feed stage, we can determine how the reflux ratios of the CSs are linked to each other. Therefore, by knowing the product specifications and specifying one reflux value we have all we need to start synthesizing a complete column because all CPM parameters in all CSs have been specified.

5.3.3 Finite Reflux Design

Consider the zeotropic benzene/*p*-xylene/toluene system. This system behaves quite ideally and may be designed using Raoult's law for ideal solutions. The same basic principles that were applied for infinite reflux column design (see Section 2.6) also apply for finite reflux design: we have to find a rectifying and stripping profile that connects the two product specifications in one continuous path of liquid composition profiles, while the feed, distillate, and bottoms products all lie on the same straight mass balance line. At infinite reflux operation, this task was simpler since both the rectifying and stripping sections shared a common profile, namely the residue curve. At finite reflux, the profiles no longer follow residue curves, but rather the appropriate column profiles for each CS.

Let us set the product specification such that $\mathbf{X}_{\boldsymbol{\Delta D}} = \mathbf{x}_{\boldsymbol{D}} = [0.700, 0.010]$ for an equimolar feed of 1 mol/s and pure liquid ($q = 1$). There is only one remaining design variable to completely specify the external mass balance for the system. This may be either a product flowrate (D or B) or the composition of one component in the bottoms (x_{Bi}). For simplicity, the composition of the low-boiling component (benzene) is specified to be 0.010 in the bottoms stream. The mass balance of the column has now been completely specified and all product flowrates and compositions can now be calculated using Equations 5.13 and 5.14.

The next step in the design is choosing a finite reflux value for the rectifying section and to construct the appropriate composition profiles from each product specification. For this design, we will choose an initial reflux value of $R_{\Delta R} = 2$ in the rectifying section. Recall that by doing this we have automatically specified the reflux in the stripping section by material balance (thus $R_{\Delta S} = -3.640$ in this case, by Equation 5.19) and we can now construct the appropriate profiles for each section using the $\mathbf{X}_{\boldsymbol{\Delta}}s$ as the initial integration composition. The integration of each profile initiates from the initial composition ($\mathbf{X}_{\boldsymbol{\Delta}}s$) at $n = 0$ to a sufficiently large number for n such that the profiles approach their pinch points ($n = 50$ is usually sufficient). This is depicted in Figure 5.11.

WWW

TUTORIAL 5.1

Try this for yourself: reproduce the feasible design in Figure 5.11 with the given parameters using DODS-SiCo. Investigate the effect of pressure and product compositions on feasibility.

Figure 5.11 clearly shows that this design is feasible because the two profiles intersect each other even at this finite reflux value. The bold parts of the respective profiles are the relevant parts of the profiles since these represent the actual changes in composition from the product specifications. The thinner, dashed parts of the profiles are merely each profile's continuation past the intersection point, moving toward their respective pinch points, and have no significance to the actual column. There is however an underlying insight that may be drawn from constructing the

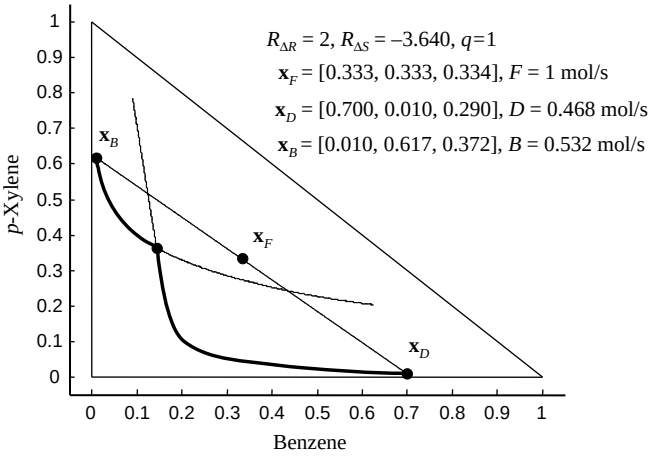

$R_{\Delta R}$ = 2, $R_{\Delta S}$ = –3.640, q=1
$\mathbf{x}_F$ = [0.333, 0.333, 0.334], F = 1 mol/s
$\mathbf{x}_D$ = [0.700, 0.010, 0.290], D = 0.468 mol/s
$\mathbf{x}_B$ = [0.010, 0.617, 0.372], B = 0.532 mol/s
$\mathbf{x}_B$
$\mathbf{x}_F$
$\mathbf{x}_D$
p-Xylene
Benzene
0 0.1 0.2 0.3 0.4 0.5 0.6 0.7 0.8 0.9 1

FIGURE 5.11 Feasible design for the benzene/*p*-xylene/toluene system at $P = 1$ atm at a reflux of 2 using Raoult's law (ideal solution).

profiles past the intersection point: it gives a qualitative indication of how far the design is from infeasibility. In this particular illustration, the reflux that we have chosen still allows for the profiles to continue somewhat past the intersection point, implying that we can still lower the reflux a fair bit before the continuous path between product specifications is not sacrificed and the column becomes infeasible. With this in mind, let us choose a new, lower reflux value for the rectifying section of say, 0.5, as shown in Figure 5.12.

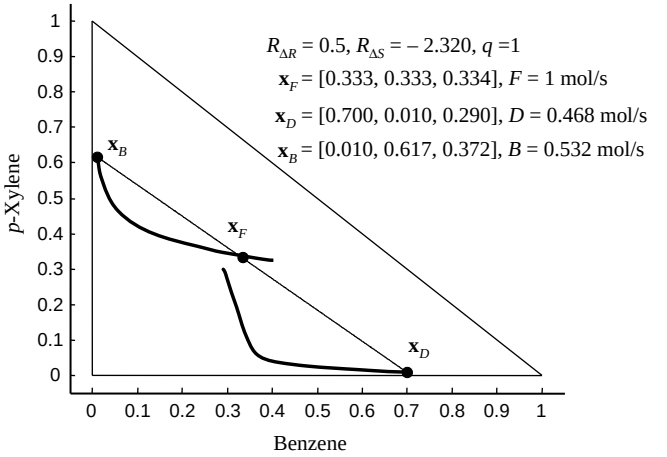

$R_{\Delta R}$ = 0.5, $R_{\Delta S}$ = – 2.320, q =1
$\mathbf{x}_F$ = [0.333, 0.333, 0.334], F = 1 mol/s
$\mathbf{x}_D$ = [0.700, 0.010, 0.290], D = 0.468 mol/s
$\mathbf{x}_B$ = [0.010, 0.617, 0.372], B = 0.532 mol/s
$\mathbf{x}_B$
$\mathbf{x}_F$
$\mathbf{x}_D$
p-Xylene
Benzene
0 0.1 0.2 0.3 0.4 0.5 0.6 0.7 0.8 0.9 1

FIGURE 5.12 Infeasible design for the benzene/*p*-xylene/toluene system at $P = 1$ atm at a reflux of 0.5 using Raoult's law (ideal solution).

WWW

TUTORIAL 5.2

Try this for yourself: reproduce the infeasible design in Figure 5.12 with the given parameters using DODS-SiCo. Investigate the effect of pressure and product compositions on feasibility.

On this occasion, we have chosen $R_{\Delta R}$ too low and the design is not feasible because the profiles do not meet each other. Both profiles have reached their pinch points (see Chapter 3, Section 3.6.3) before reaching the point of intersection and even an infinite number of stages will not make the design feasible, that is, the column's product specifications cannot be met at this reflux value. Thus, we know that the other operating extreme, minimum reflux, must lie between our "over-refluxed" value of 2 and the "under-refluxed" value of 0.5. With trial-and-error, we can find the reflux that causes the respective profiles to just touch each other, thereby completing the path between distillate and bottoms compositions. For this particular problem, the minimum reflux was found to be 0.544, shown in Figure 5.13.

WWW

TUTORIAL 5.3

Try this for yourself: reproduce the infeasible design in Figure 5.13 with the given parameters using DODS-SiCo. Investigate the effect of pressure and product compositions on the minimum reflux.

5.3.3.1 Minimum Reflux We have thus now determined the minimum energy requirement for this column because minimum reflux corresponds to the least amount of vaporization, that is, reboiler duty, and condensing to yield the specified

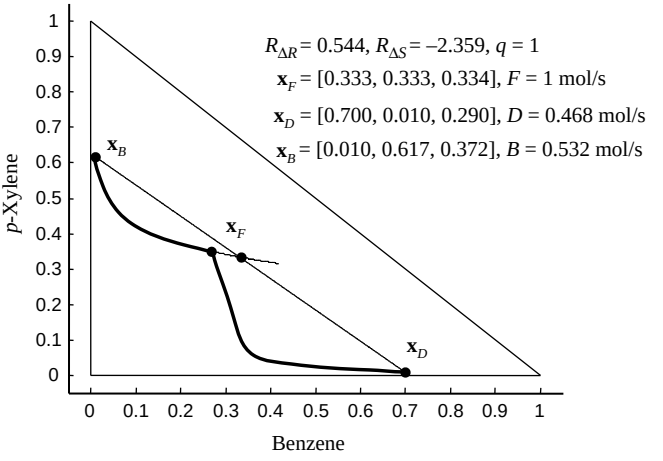


FIGURE 5.13 Feasible design for the benzene/*p*-xylene/toluene system at a (minimum) reflux of 0.544 using Raoult's law (ideal solution).

products. This operating mode does, however, come with a penalty of requiring a large number (infinite, in fact) of stages and is thus also an impractical operating condition. However, we now know the minimum criterion for feasibility in terms of the reflux requirement. Knowing minimum reflux is integral from a design point of view, and at the end of this chapter we introduce rapid means of finding this operating condition for the special case of sharp splits (see Section 5.4.1).

It is also worth mentioning that in the case of simple columns, there are in fact three cases where minimum reflux can occur. Recall that minimum reflux is obtained where one composition profile pinches, or terminates, on the other. The three cases are therefore as follows:

(a) the rectifying profile pinches on the stripping profile (thus the rectifying profile will have infinitely many stages), as shown in Figure 5.13;
(b) the stripping profile pinches on the rectifying profile (thus the stripping profile will have infinitely many stages); and
(c) Both profiles pinch on each other at the same composition, both having infinitely many stages.

For the special case of sharp splits, scenario (c) is known as the *double-feed pinch*, as this mutual pinch point will occur at the feed composition (illustrated in Section 5.4.1). These three cases are dependent on the product and feed compositions one chooses, and are illustrated in Figure 5.14a–c.

WWW

TUTORIAL 5.4

Try this for yourself: find all the cases shown Figure 5.14a–c using DODS-SiCo, by manipulating product compositions, R_{Δ}, or system pressure.

5.3.3.2 Maximum Reflux Interestingly, there is also a *maximum* reflux associated to any given product specifications, that is, an upper reflux limit above which there will also be no profile intersections. The only case where there isn't an upper bound on the choice of $R_{\Delta R}$ is when the product specifications happen to lie exactly on the same residue curve, that is, at infinite reflux.

5.3.3.3 Profile Intersection It is important to point out here that only liquid composition profiles have been constructed for finding feasible columns. Strictly speaking, however, we have to consider the intersection of vapor profiles when evaluating a liquid feed, because at the feed addition stage the liquid composition of the rectifying and stripping sections cannot be equal since we are adding material at this stage (see Figure 5.10). In the case of a liquid feed, the vapor profiles will intersect each other exactly and one should actually construct vapor profiles to evaluate the feasibility of the design. Conversely, when considering a vapor feed, one should then look for a liquid profile intersection as the vapor streams at the feed stage

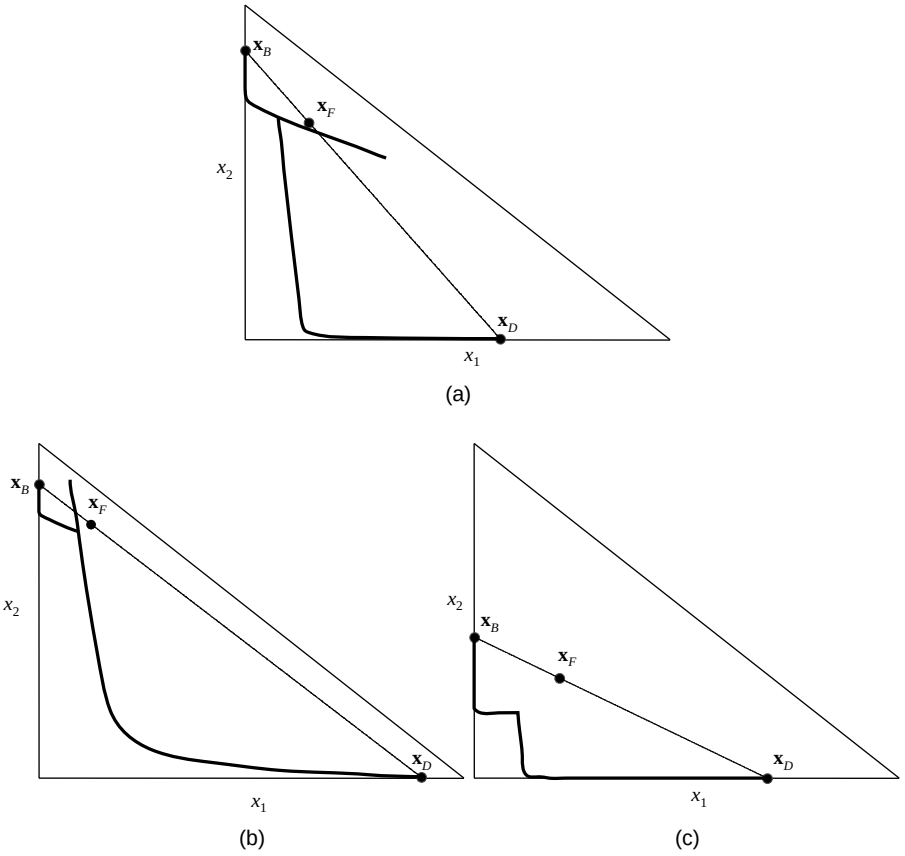


FIGURE 5.14 Three cases of minimum reflux: (a) rectifying profile pinches on the stripping profile; (b) stripping profile pinches on the rectifying profile; and (c) both profiles pinch on each other at the same composition.

will have different compositions due to feed mixing. For mixed feed columns ($0<q<1$), the problem of finding matching compositions for feasibility becomes even more complex. It is quite plain to see that by using different composition matching criteria for each different feed quality that one may encounter the CPM method loses some simplicity which makes this method so useful.

Fortunately, however, the curvature of vapor and liquid composition profiles follow each other quite closely [1], and in general we can assume that *if there is a continuous liquid composition path between bottoms and distillate products, then the design is considered feasible*. This approximation may be slightly off in the approximation of minimum reflux since one may find, for a liquid feed, that the liquid profiles just intersect each other but the vapor profiles miss each other (or vice versa). Nonetheless, liquid profile intersection still gives an excellent approximation and the design parameters found using this approach are very closely aligned with

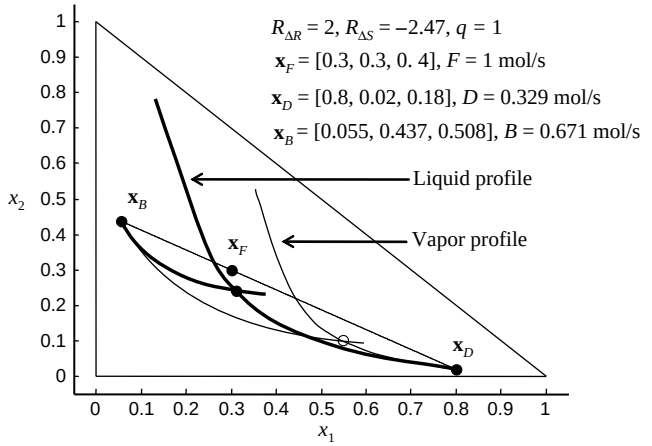

$R_{\Delta R}$ = 2, $R_{\Delta S}$ = –2.47, q = 1
$\mathbf{x}_F$ = [0.3, 0.3, 0. 4], F = 1 mol/s
$\mathbf{x}_D$ = [0.8, 0.02, 0.18], D = 0.329 mol/s
$\mathbf{x}_B$ = [0.055, 0.437, 0.508], B = 0.671 mol/s
Liquid profile
Vapor profile
$\mathbf{x}_B$
$\mathbf{x}_F$
$\mathbf{x}_D$
x_2
x_1
0 0.1 0.2 0.3 0.4 0.5 0.6 0.7 0.8 0.9 1

FIGURE 5.15 Vapor and liquid profile intersection, rendering a feasible design.

other, more rigorous and exact methods. In fact, other researchers have shown that design parameters found by only considering the liquid profiles, for any feed condition, can be used as initialization into rigorous process simulation packages such as Aspen Plus®, leading to a good agreement between the CPM-based predictions and rapid convergence of the simulator [8–10].

To illustrate this assumption more clearly, a feasible design for a constant relative volatility system ($\boldsymbol{\alpha} =$ [5, 1, 2]) is shown in Figure 5.15 where both the liquid and vapor profiles intersect each other, rendering a feasible design. As evident from this illustration, it is generally sufficient to only consider the intersection of liquid profiles, and we will do so in all the subsequent discussions on column feasibility and design parameter estimation in this book. However, the designer should be aware that this condition may not be completely exact in a few special cases, as shown in Figure 5.16.

Figure 5.16 shows that for a liquid feed, the minimum reflux calculated through liquid profile intersection is found to be 1.58. However, at this particular reflux value, the vapor profiles do not intersect and the design should be classified as infeasible because the feed is liquid. Searching for the lowest reflux where the vapor profiles will intersect each other will be the actual minimum reflux for this liquid feed column, and we have found this reflux value to be 1.66 in this case. One can see that the minimum reflux values obtained for these two intersection matching conditions are very close to each other. Only considering liquid intersections is therefore sufficient and it also has the additional advantage of simplifying the mixed feed quality ($0<q<1$) case.

5.3.4 Design Offshoots

Besides being able to determine the column feasibility and reflux conditions for a column with any phase-equilibrium behavior and product specifications, using this

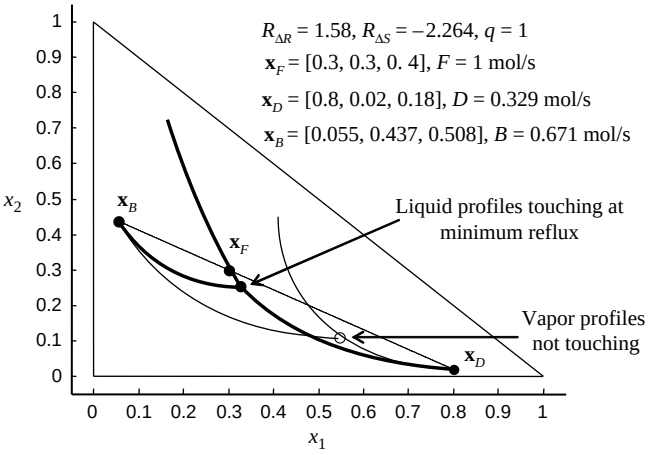

$R_{\Delta R}$ = 1.58, $R_{\Delta S}$ = −2.264, q = 1
$\mathbf{x}_F$ = [0.3, 0.3, 0. 4], F = 1 mol/s
$\mathbf{x}_D$ = [0.8, 0.02, 0.18], D = 0.329 mol/s
$\mathbf{x}_B$ = [0.055, 0.437, 0.508], B = 0.671 mol/s
Liquid profiles touching at minimum reflux
Vapor profiles not touching
$\mathbf{x}_B$
$\mathbf{x}_F$
$\mathbf{x}_D$
x_2
x_1
0 0.1 0.2 0.3 0.4 0.5 0.6 0.7 0.8 0.9 1

FIGURE 5.16 Liquid profile intersection, rendering a feasible design, but no vapor profile intersection.

BVM-based approach has other distinct advantages over other design methods. Notably, because the DPE is stage dependent, we can calculate the exact number of equilibrium or theoretical stages needed in each CS to go from the product specifications to the point of intersection by simply tracking the progression of stages (integration parameter). This allows one to infer exactly where the feed stage lies by merely counting the stages from either the top or bottom of column to the intersection point. Furthermore, the point where the composition profiles cross is also the composition on the feed stage. Although there are correlations that allow one to estimate these parameters, they often require a significant amount of insight or design experience to determine exactly, especially in nonideal systems. It should be noted that in this and all subsequent chapters, stage numbers are generally numbered from the top of the column downward. Thus, if the feed stage was given as the 5th stage, for instance, this implies that the feed is added at the 5th stage from the top of the column. Furthermore, columns are assumed to be packed, and stage counting thus starts from 0 at the top of the column.

Although these parameters may easily be inferred, their interpretation should be approached carefully, since distillation columns usually consist of a *partial* reboiler and a *total* condenser. When the energy input to a column falls under the class of total, as in a total condenser, it implies that all the vapor flowing into it is being condensed to liquid. Thus, the vapor and liquid composition entering and exiting the condenser are exactly the same. For partial utilities, as in a partial reboiler, only a part of the liquid entering it is vaporized, mostly because it is expensive to vaporize all the material entering the reboiler, and much more useful and practical to handle a liquid product stream. The bottoms product is thus (usually) drawn off as liquid from the reboiler. Therefore, the liquid and vapor entering and exiting a partial reboiler do not have the same compositions—the vapor leaving the condenser is in fact in equilibrium with the bottoms product. This type of reboiler, also known as a kettle

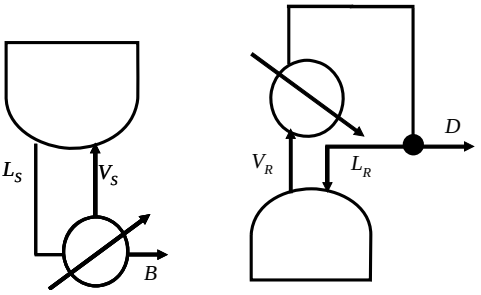


FIGURE 5.17 A partial reboiler and total condenser.

reboiler, thus acts as an equilibrium stage, while the total condenser does not, and this should be taken account for when counting the stage numbers. When the condenser is a partial type, then the same design procedure will hold but the condenser will be considered an equilibrium stage. This is graphically summarized in Figure 5.17. Notice, however, that regardless of total/partial condensers/reboilers, $\mathbf{X}_{\boldsymbol{\Delta}}$ is still equivalent to the product specification in CSs terminated by either one.

The DODS-SiCo software package accompanying this book allows one to simply search for feasible designs in a ternary simple column (with a total condenser and partial reboiler) by specifying the products and a reflux ratio. It is very useful for gaining an understanding of the design trade-off between reflux (energy requirement) and stage numbers (capital investment), and it also shows the exact feed stage. Furthermore, it is also very useful as an initialization tool for more rigorous packages such as Aspen Plus®. Although process simulation packages such as these have unquestionable modeling capabilities, they only permit limited insight into the problem, and often require numerous hours of fiddling to find the right design. Using the DODS-SiCo package allows one to quickly assess feasibility and the relevant parameters and if the column happens to be infeasible, the designer knows how far he/she is from feasibility (and vice versa). The parameters obtained using the CPM-based techniques through DODS-SiCo can be fed into Aspen Plus® very easily and the agreement between the simplified CPM approach and Aspen Plus® is generally very good. We thus recommend using DODS-SiCo and packages such as Aspen Plus® in cohesion to rigorously and quickly design columns. This is illustrated in the following example.

WWW

Example 5.4: Design a column for a 1 mol/s, equimolar benzene/*p*-xylene/toluene system with $\mathbf{x}_D = [0.700,\ 0.010]$ and a bottoms benzene composition of 0.010, assuming an equimolar feed (the same problem shown in Figures 5.11–5.13) using DODS-SiCo. The mixture may be assumed to behave ideally and phase equilibrium may be modelled with Raoult's law. Assume that we wish to operate at a factor of 1.34 times minimum reflux.

(a) What are the total number of stages and the feed stage for this design?
(b) Validate the design with Aspen Plus® (or any other suitable simulation package) using the results from DODS-SiCo as initialization.

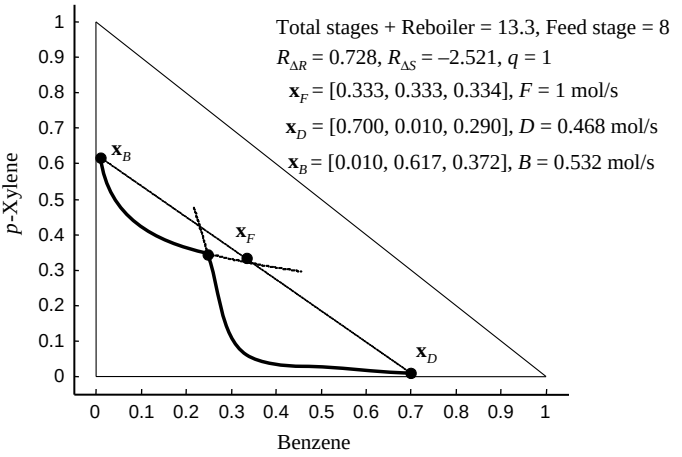


FIGURE 5.18 A feasible design at 1.34 times minimum reflux for the benzene/*p*-xylene/toluene system using profile intersection.

Solution 5.4

(a) In order to estimate the total number of stages and the feed stage for a column operating at 1.34 times minimum reflux, it is necessary to first determine minimum reflux. Fortunately, minimum reflux for this particular system has already been established as $R_{\Delta R} = 0.544$ (refer to Figure 3.16). The operating reflux ratio for this column is therefore 0.729. With these product specifications and reflux ratio, it can be found that the column requires 13.3 theoretical stages (including the reboiler), and that the feed stage should be located on the 8th stage from the top of the column. This design is shown in Figure 5.18.

(b) Aspen Plus®' rigorous distillation calculation block (RADFRAC) can determine the compositions on each stage in a distillation column through stage-by-stage calculations without making simplifying assumptions such as CMO. The only user inputs needed are a single-product flowrate, the column reflux, the total number of stages, and the feed stage location. The product compositions are not required as this is a result of the stage-by-stage calculations. Fortunately, all these input values are available to us from part (a). It should be noted that the Aspen Plus® column starts stage numbering from 1, while the CPM calculations started at 0. Thus, 1 stage number should be added to the value obtained from the CPM method when transporting the stage numbers to Aspen Plus®. Allowing Aspen Plus® to converge and extracting the composition on each stage allows to compare the rigorous profiles of Aspen Plus® and the CPM method. This comparison is shown in Figure 5.19.

Clearly, the profiles match reasonably well, but importantly, the product specifications have been met very closely, remembering that these were not specified in the

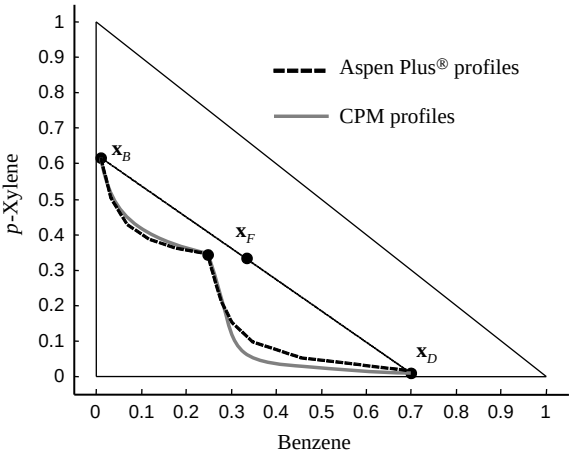


FIGURE 5.19 A comparison of the CPM design shown in Figure 5.18 and Aspen Plus®, using input from the CPM method.

initiation of the Aspen Plus® simulation. This gives a good indication that the design generated by the (approximate) CPM method is closely aligned with real column behavior. The deviation of the CPM profiles from those predicted by Aspen Plus® can be attributed to the inclusion of the CMO assumption in our methods. This assumption can be relaxed if necessary, but it should be clear that approximating the profiles in this manner is sufficient, especially for rapid conceptual designs. Deviations may also be attributed to the fact that, when deriving the DPE, only the first-order differential term in the Taylor expansion was assumed significant.

This example shows a very useful aspect of the CPM design method in that data generated with this relatively simple method corresponds very well to more rigorous simulation packages. If one were given the same separation task as shown in the example but resorted straight to Aspen Plus®, there is no telling how long one may have fiddled or optimized to find the right number of stages, the feed stage or the column reflux. It is evident that in the example shown, the designs generated via CPMs and Aspen Plus® agree very well with each other. It should however be noted that scenarios may arise where the CPM assumptions are not as good (specifically highly nonideal systems with large heating/mixing effects) and there may be a greater discrepancy between the two designs. Nevertheless, in such instances the CPM method will still provide a reasonably good guess from where one may optimize from.

5.4 AZEOTROPIC SYSTEMS

The design of separation systems to produce desirable products from azeotropic mixtures is a very active area of research. Classic methods such as those developed by Fenske [11] and Underwood [12] have limited application because they are based on the assumption that the mixtures behave ideally. Thus far, we have laid down the

fundamentals for synthesizing simple columns using the CPM technique. Although we have only addressed a near-ideal system in the form of benzene/*p*-xylene/toluene, the CPM method extends naturally to the design of even the most complex mixtures. The only factor that is important to consider for azeotropic systems is the directions of the profiles, that is, which directions rectifying and stripping profiles will run. Recall that for the rectifying section, integration proceeds from a low-boiling mixture at the distillate product toward a higher boiling one (toward the stable node). Conversely for the stripping section, integration is initialized at the high-boiling bottoms product and should tend toward a lower boiling product, that is, toward the unstable node. Put in another way, the rectifying profile has to be integrated in the positive direction from the distillate product, while the stripping section has to be integrated in the negative direction when starting from the bottoms product. The RCM is a useful means of assessing profile directions when deciding on a certain split. We illustrate a feasible design here for a nonideal acetone/water/methanol system using the NRTL phase equilibrium model at 1 atm, which has a minimum boiling binary azeotrope between acetone and methanol. The design has been superimposed on this system's distillation boundary in Figure 5.20.

WWW

TUTORIAL 5.5

Try this for yourself: using DODS-SiCo, reproduce the design shown in Figure 5.20 with the given parameters. Investigate the effect of changing the system pressure, column reflux, and feed/product compositions.

The design procedure for an azeotropic system is thus exactly the same as for simpler, ideal mixtures. We have again chosen to operate this column at a reflux of 2

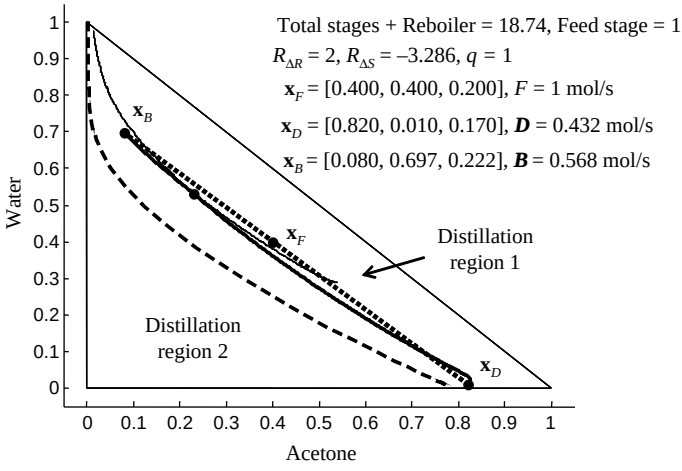


FIGURE 5.20 A feasible design for the acetone/water/methanol system showing unique distillation regions, using the NRTL phase equilibrium model at 1 atm.

which requires 18.74 equilibrium stages, one of which is the reboiler. The feed stage is also easily inferable along with the composition on the feed stage (where profiles intersect). In this particular design we have chosen to stay in one distillation region to perform the separation, that is, the distillate, bottoms, and feed compositions lie in a single distillation region. The traditional school of thought for designing azeotropic systems was that one cannot transgress the distillation regions defined in the RCMs in Chapter 2, because it is impossible for the distillate and bottoms products to lie on the same residue curve when they lie in different distillation regions. However, as we have shown in Chapter 3, both the choices for $\mathbf{X}_{\Delta}$ and R_{Δ} have significant influences on the topology—so much so that we can transform the topology almost at will. Although in the design of simple columns we are somewhat constrained by our choices of $\mathbf{X}_{\Delta}$ since they have to be set to the product specifications, finite reflux values will still have major impact on the overall topology.

This begs the question: could finite reflux values enable to cross distillation boundaries in a simple column that were previously thought impossible using RCM-based methods? There is no simple answer to this question as it is system dependent, but, in principle, it is possible. Such a case has been illustrated by Wahnschafft and coworkers [13] for the acetone/benzene/chloroform system as shown in Figure 5.21.

Figure 5.21 shows that the distillation boundary has indeed been crossed (only just) by merely operating at a finite reflux value (note $\mathbf{x}_D$ and $\mathbf{x}_B$ lie on opposite ends of the distillation boundary). Wahnschafft and coworkers have attempted to explain this phenomenon and have concluded for distillation boundary crossing to be possible that (1) the distillation boundary has to display considerable curvature, (2) a distillate or bottoms composition has to close to or on the concave side of the boundary, and (3) the distillation column needs to operate at a certain range of reflux ratios for it to be feasible as over-refluxing the column will cause the topology to resemble that of the RCM, hence rendering the product specifications to be infeasible.

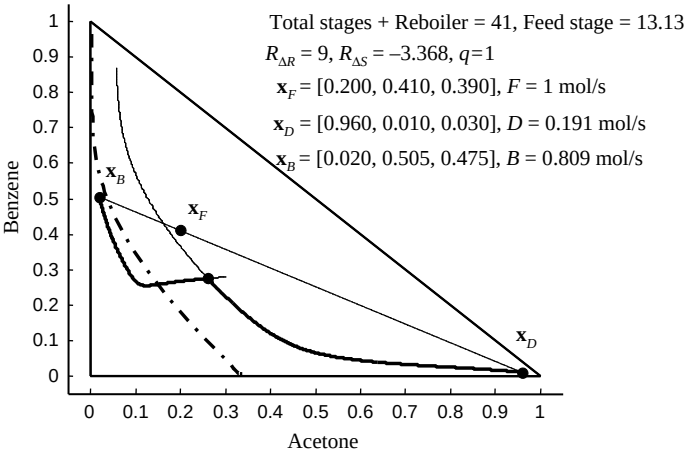


FIGURE 5.21 A feasible design crossing the distillation boundary for the acetone/benzene/chloroform system superimposed on its distillation boundary.

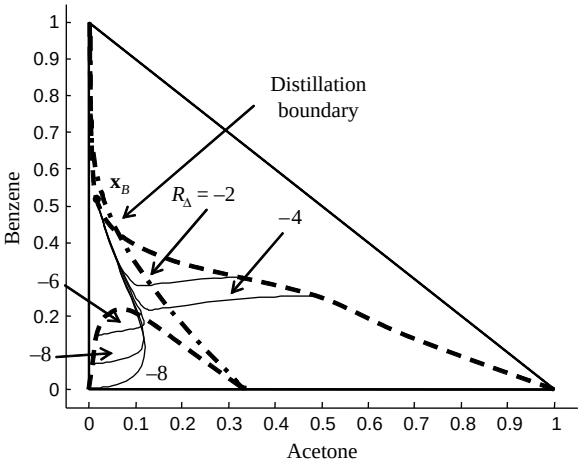


FIGURE 5.22 Movement of pinch points and their associated profiles with varying R_Δ at a certain $\mathbf{X}_\Delta$ for the acetone/benzene/chloroform system.

Wahnschafft explained this phenomenon by a so-called flipping over of profiles at certain reflux values that would realize the design. Although this is a good assessment of what has happened, this can be explained in another way in terms of our understanding of CPMs: at certain reflux values, the nodes in composition space (and the accompanying distillation boundary) have been shifted in such a way to change the direction of profiles, as shown in Figure 5.22. Here, profiles for the stripping section are shown, all with the same initial point ($\mathbf{x}_B = \mathbf{X}_{\Delta B}$), but at different refluxes.

The $\mathbf{X}_\Delta$ of the bottoms product lies close to the boundary on the concave side of the distillation boundary. The residue curve through this $\mathbf{X}_\Delta$ pinches at the pure chloroform node and goes through high curvature at the saddle located at chloroform/acetone azeotropic point. Decreasing the reflux ratio moves the unstable chloroform node and the azeotropic saddle node toward each other along the pinch point curve. At $R_\Delta = -4$, the CPM has shifted so much that the profiles originating from $\mathbf{x}_B$ run toward the unstable node at the previously located pure acetone vertex. These drastic changes, known as bifurcations, in the direction of the profiles imply an important underlying effect that can be easily verified using CPMs: the chosen column, although feasible, may be unstable and sensitive to change in operation, as discussed in Chapter 3. For instance, for the conditions that the stripping section is operating at in Figure 5.21 ($\mathbf{X}_{\Delta B} = [0.020, 0.505]$, $R_\Delta = -3.368$), we can construct a CPM to show this instability, illustrated in Figure 5.23.

WWW

TUTORIAL 5.6

Try this for yourself: reproduce Figure 5.21 using DODS-SiCo and the given parameters. Try and find more such instable designs.

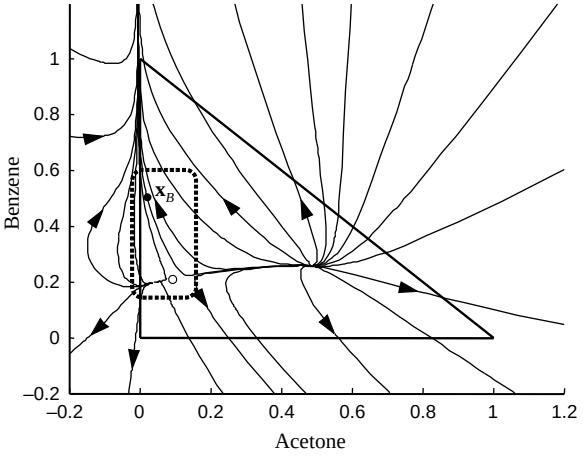


FIGURE 5.23 A CPM at $\mathbf{X}_{\Delta B} = [0.020, 0.505]$ and $R_\Delta = -3.368$ for the acetone/ benzene/ chloroform system showing an area of potential instability.

The highlighted area in Figure 5.23 shows that the profile running through $\mathbf{X}_\Delta$ is very close to running in a different direction. In this case, the profile running through the $\mathbf{X}_\Delta$ is deflected by the saddle point in a direction that is favorable for crossing the distillation boundary. However, a slight change in reflux or product specification would cause the profile to deviate in another direction, rendering the design infeasible.

Although the crossing of this distillation boundary seems somewhat trivial since it has not been crossed by a great deal, it does highlight an important fact: there are no hard and fast rules for determining feasibility of products for complex systems and the designer should explore *all* possibilities that may seem relevant—even those beyond the distillation boundary. It will become evident in subsequent chapters that complex columns may greatly aid in crossing distillation boundaries because of their ability to accommodate different, and useful, positions of $\mathbf{X}_\Delta$.

5.5 CONSTANT RELATIVE VOLATILITY SYSTEMS

5.5.1 Minimum Reflux Design Using TTs

The CPM technique has thus far proven to be an insightful tool for synthesizing distillation systems for even the most nonideal mixture of components. Unfortunately, searching for feasible designs using these techniques requires some degree of trial-and-error to eventually find a profile intersection between neighboring CSs. The designer has to specify the product streams and reflux value and subsequently produce column profiles to judge feasibility. Other researchers have addressed this problem by a *temperature collocation* technique, which allows the user to rapidly determine feasibility in a temperature domain using a bubble point distance objective function [9,10,14,15]. These techniques have proven to be quite successful in modeling nonideal and high-order systems computationally. However,

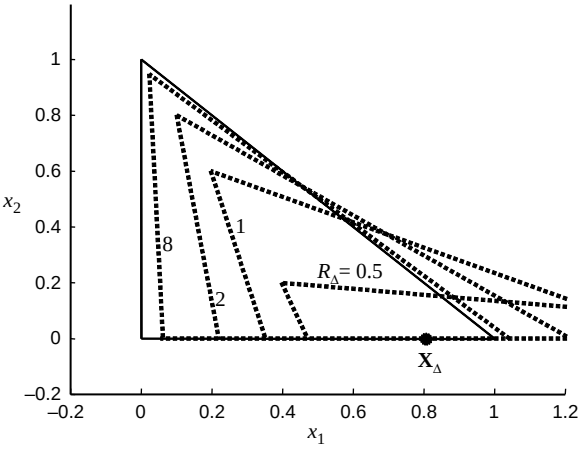


FIGURE 5.24 A TT for a sharp-split $\mathbf{X}_\Delta = [0.8, 0]$ with $\boldsymbol{\alpha} = [5, 1, 2]$.

the design procedure is still trial-and-error based in that the actual profiles have to be constructed for feasibility to be attained. What is really needed is a simple, non-iterative means of assessing, or approximating, feasibility.

Finding analytical solutions to even the simplest of nonideal models can be quite a challenge, if not entirely impossible. Fortunately, when we limit ourselves to only consider constant relative volatility systems, the problem becomes significantly easier to solve and interpret, as evident from Chapter 3 and the TT phenomenon (see Section 3.6.5). Furthermore, we know that when confining one even further to sharp splits only, that is, one of the elements of $\mathbf{X}_\Delta$ are zero, the base of the TT will lie exactly on the MBT axis to which $\mathbf{X}_\Delta$ is fixed. This means that a composition profile (through the base of the TT) runs exactly through the product specification. This is elucidated in Figure 5.24 for a system with $\boldsymbol{\alpha} = [5, 1, 2]$ and $\mathbf{X}_\Delta = [0.8, 0]$, with varying refluxes.

Figure 5.24 shows that with decreasing reflux, the TT becomes further departed from RCM conditions and that regardless of the reflux value there is always a base of the TT fixed to the same side as where $\mathbf{X}_\Delta$ is fixed, implying that there is always a profile running through the product specification. By lowering the reflux even further than shown here, the TTs eventually flip over, resulting in some of the interesting sharp split phenomena discussed in Section 3.9.3. This trend can be witnessed for any sharp split product specification on any edge of the MBT. Note that the profile running through $\mathbf{X}_\Delta$ along the TT edge requires infinitely many stages as the profile has to pass through the saddle point where $n \to \infty$. All sharp split problems thus require an infinite number of stages.

As discussed in the preceding section for the design of general nonideal systems, minimum reflux is the point where the two profiles of the rectifying and stripping sections just touch each other. Immediately one begins to realize that the use of triangles makes searching for this condition significantly easier because the profiles are just straight lines formed by the edges of the TT. This is illustrated in Figure 5.25 for arbitrarily set feed and product compositions.

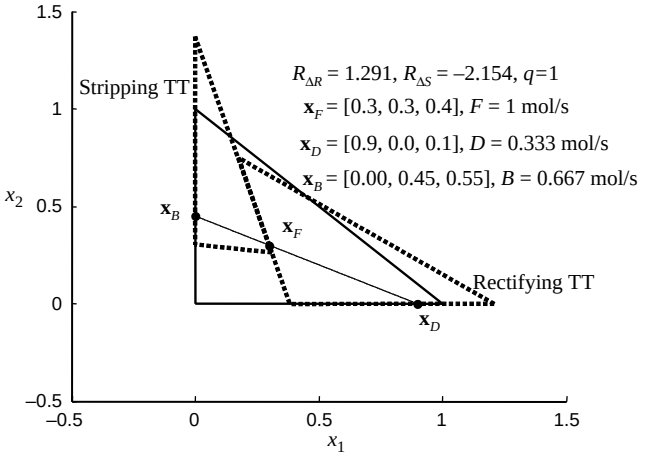


FIGURE 5.25 A feasible design at minimum reflux for $\boldsymbol{\alpha} = [5, 1, 2]$ using TTs.

WWW

TUTORIAL 5.7

Try this for yourself: using DODS-SiCo and the TT design option, design minimum reflux simple columns, trying various $\boldsymbol{\alpha}$ values, and product specifications.

Recall from Chapter 3 that the TTs may be calculated very easily and do not require integration. Thus, we can assess feasibility by employing simple, linear geometric techniques. The minimum reflux essentially entails meeting a colinearity condition between the two TTs of adjacent CSs. Doherty and coworkers were the first to point out this geometrical colinearity relationship for minimum reflux, but not in terms of TTs. The results are however the same. Interestingly, Doherty and Levy also showed that this special colinear condition for finding minimum reflux is essentially the same principle that Underwood used for finding minimum reflux [12]. Notice that it is impossible to use this TT phenomenon to design systems with nonsharp product specifications because the edges of the TTs do not run precisely through the product compositions. This is illustrated in Figure 5.26 where the profiles running through the product specification do not intersect each other but the TTs do. There is thus no feasibility criterion for nonsharp separations using TTs.

Apart from being limited to sharp splits, the TT design method cannot be applied to nonideal systems since the boundaries between pinch points are not precisely linear and therefore there is no basis for a colinearity condition.

Now that the key concepts of this design method have been illustrated, it is convenient to formulate a proof that will give us a minimum reflux. First, let us consider a generic feasible design using the TT concept as in Figure 5.25. We choose to label three pinch points that will meet the colinearity condition as A, B, and C, respectively, as shown in Figure 5.27. These points correspond to the stable pinch point in the rectifying section (A), the unstable pinch point in the stripping section

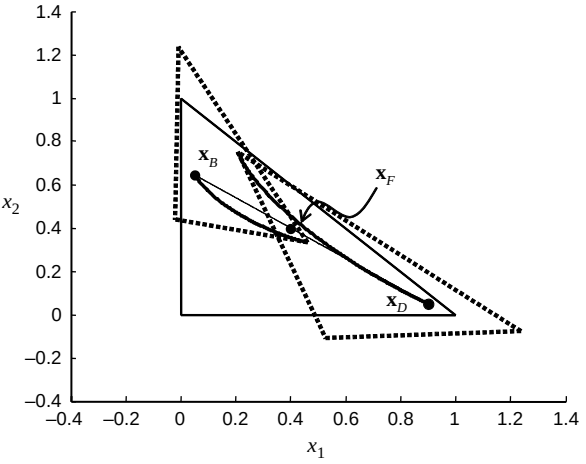


FIGURE 5.26 Infeasible design for nonsharp product specifications using TTs.

(B), and the saddle pinch point in the rectifying section (C). Note that the stable node in the stripping section could also have been chosen for the colinearity condition.

Consider now point A, one of the pinch points in the rectifying section. Since this point corresponds to a compositional steady state, it must satisfy the condition where $d\mathbf{x}/dn = 0$. Thus, we can write for point A in a vectorized form:

$$0 = (1 + R_{\Delta R})(\mathbf{x}_A - \mathbf{y}_A) + (\mathbf{X}_{\Delta D} - \mathbf{x}_A) \tag{5.20}$$

In a similar way, we can write the pinch equations for the DPE for points B and C:

$$0 = (1 + R_{\Delta S})(\mathbf{x}_B - \mathbf{y}_B) + (\mathbf{X}_{\Delta B} - \mathbf{x}_B) \tag{5.21}$$

$$0 = (1 + R_{\Delta R})(\mathbf{x}_C - \mathbf{y}_C) + (\mathbf{X}_{\Delta D} - \mathbf{x}_C) \tag{5.22}$$

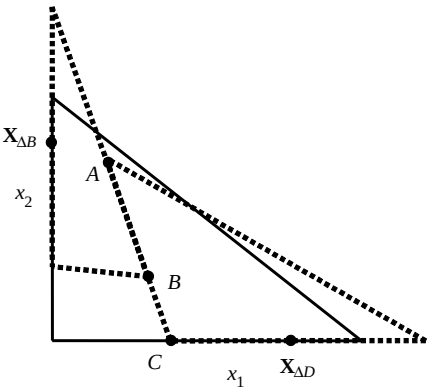


FIGURE 5.27 Co-linear points of TTs labeled A, B, and C.

Equations 5.20–5.22 essentially consist of six independent equations in total because there are two independent compositions in each vector for a ternary system. The vapor equilibrium compositions are completely specified for a set of volatilities using the constant relative volatility relationship, and the reflux in the stripping section is directly related to that in the rectifying section by Equation 5.19 once the external mass balance have been set to compute the mass balance. Whence, there are six compositions (from A, B, and C) and one reflux value ($R_{\Delta R}$), seven variables in total, to compute in this system of six nonlinear equations. An additional equation is thus required to solve this system, and for this the colinearity condition can be used, which essentially states that the slope of line *AB* must be equivalent to the slope of line *BC*. This can be formally expressed as

$$0 = (x_{1A} - x_{1B})(x_{2B} - x_{2C}) - (x_{1B} - x_{1C})(x_{2A} - x_{2B}) \tag{5.23}$$

Now, there are seven independent nonlinear equations and seven independent variables from which one can calculate the minimum reflux required to realize the separation which may be easily solved using a numerical solver. Although the graphical attributes of the method are lost in higher dimensions, the system of equations formulated in Equations 5.19–5.22 can easily be extended to higher order systems—although the number of equations increases rapidly, a system of *nc* components generally requiring $nc(nc-1)+1$ nonlinear equations to compute the minimum reflux. It is worthwhile to note that by determining the minimum reflux using the TT technique is exactly equivalent to finding minimum reflux using the classical Underwood method, and it suffers from the same constraints of Underwood's method by only being able to handle constant relative volatility systems at sharp split conditions since these are the only conditions where the profiles run through the product specifications and the connection between stationary points are straight lines.

Notice that here we have only shown the case where the stripping profile pinches on the rectifying profile. These equations are equally valid for any of the other two cases depicted in Figure 5.14. However, it is worth emphasizing the special case where both profiles pinch on each other, known as the *double-feed pinch* case. As the name might suggest, this special case occurs where both TTs pinch at the feed composition, a unique case for sharp split liquid feed columns. Such a case is shown in Figure 5.28.

WWW

TUTORIAL 5.8

Try this for yourself: using DODS-SiCo and the TT design option, find a combination of product distribution for a set $\boldsymbol{\alpha}$ that will result in the double-feed pinch.

The double-feed pinch case occurs only at a specific selection of product purities. Although it may seem like a trivial condition, the double-feed pinch scenario

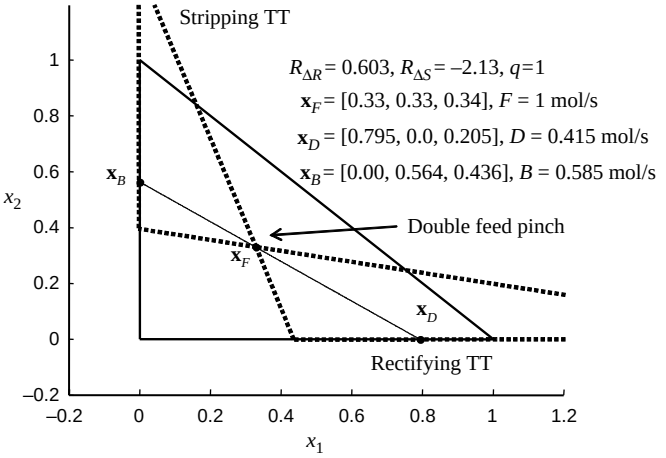


FIGURE 5.28 A feasible design at minimum reflux for $\boldsymbol{\alpha} = [5, 1, 2]$ using TTs, at the double-feed pinch.

represents the "turnover-point" between the stripping TT pinching on the rectifying TT, and the rectifying TT pinching on stripping TT. Thus, on either side of the double-feed pinch product compositions one would encounter either of these pinching scenarios. Furthermore, the real significance about the double-feed pinch case is that it represents the lowest possible reflux one may achieve to obtain sharp products from a given feed. In other words, if one were to pose the question "for a given feed, what is the lowest possible reflux to give a sharp separation between products?, the answer would be the double-feed-pinch reflux. This is qualitatively illustrated in Figure 5.29.

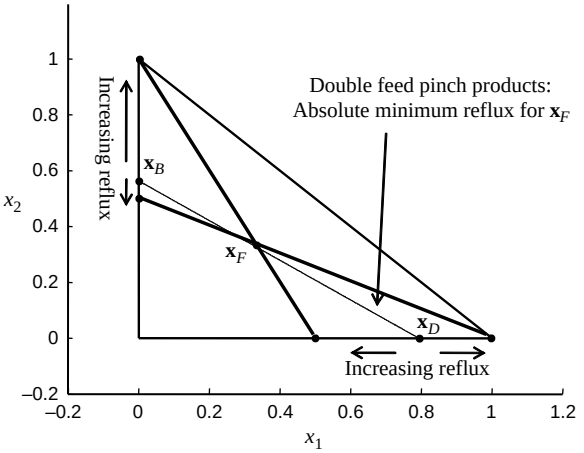


FIGURE 5.29 Illustration of minimum reflux increase for a given feed and for product specifications laying either side of the double-feed pinch product specifications.

Although one may think this simplified technique using TTs has limited application, it is very useful for obtaining quick design estimates in the early stages of the design phase as well as being used for an estimate for reflux ratios for more nonideal and/or nonsharp split systems. We illustrate this simple design procedure using TTs through an example below.

WWW

Example 5.5: A benzene/*p*-xylene/toluene separation problem has recently come to the fore in your design company, and answers regarding feasibility and operating conditions are needed very quickly. The design requires that a distillate product with a purity of 0.98 benzene and negligible *p*-xylene, and a bottoms product with negligible benzene be produced. The feed to the column can be assumed to be of composition [0.3, 0.3, 0.4]. Determine:

(a) approximately what is the minimum reflux of the column;
(b) total number of stages and feed stage for operating at 1.2 times minimum reflux; and
(c) whether rigorous models (such as Aspen Plus®) agree with the findings in (b).

Solution 5.5:

(a) It is quite clear that the problem can be approximated as a sharp split type problem (negligible benzene in bottoms, negligible *p*-xylene in distillate). Moreover, this particular mixture behaves quite ideally, and the volatilities of the mixture may be assumed to be constant. Both criteria for designing the column with the TT technique are thus met. Using DODS-SiCo and the TT design feature, it is quick to establish what the minimum reflux for such a column is. It is consequently found that $R_{\Delta R} = 1.789$. These TTs for this design are shown in Figure 5.30.
(b) In (a), we have found what the minimum reflux for a column is, that is, infinite stages. In (b) however, we want to progress toward a more realistic design with a finite number of stages and knowledge of the feed stage—thus implying design via profile intersection. Since it is impossible to achieve a finite number of stages at sharp split conditions (profiles pass exactly through saddles), we simply relax the sharp split condition slightly. Instead of specifying that there is zero benzene in the bottoms and zero *p*-xylene in the distillate, we allow a small amount of each to pass to the relevant product stream, say compositions of 10^{-5} in each respective stream, but still letting the benzene in the distillate be 0.98.

These conditions are still very close to those in (a), so we use the minimum reflux in (a) as an initial guess for finding minimum reflux using profile intersection, instead of searching for profile intersection by trial-and-error starting from an arbitrary reflux. Fortunately (using the DODS-SiCo package), it turns out that $R_{\Delta R} = 1.789$ is also the minimum reflux for the "real" problem, thus the TT method provides a very

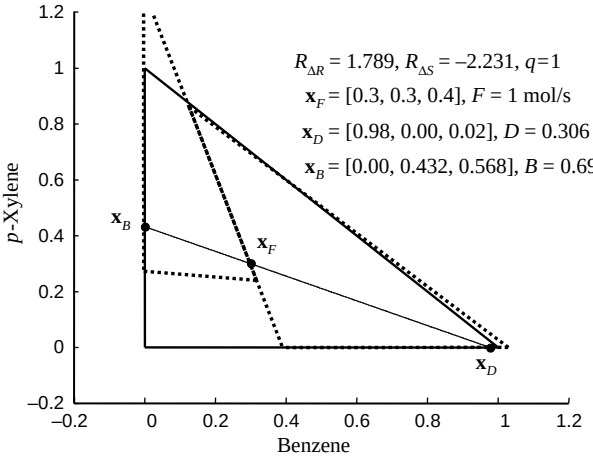


FIGURE 5.30 A feasible design at minimum reflux for the benzene/*p*-xylene/toluene system using TTs.

good initial guess (intuitively, if the sharp split constraint is relaxed further, this guess becomes progressively worse).

The design asks to determine the number of stages required and feed stage location when operating at 1.2 times minimum reflux—thus $R_{\Delta R} = 2.147$. Again using the DODS-SiCo package, the aforementioned specifications result in about 34.9 total number of stages, with the feed stage location at 15.4 (from the top). This feasible design is shown in Figure 5.31. The continuation of the profiles past the intersection point is also shown, confirming that the design has passed minimum reflux.

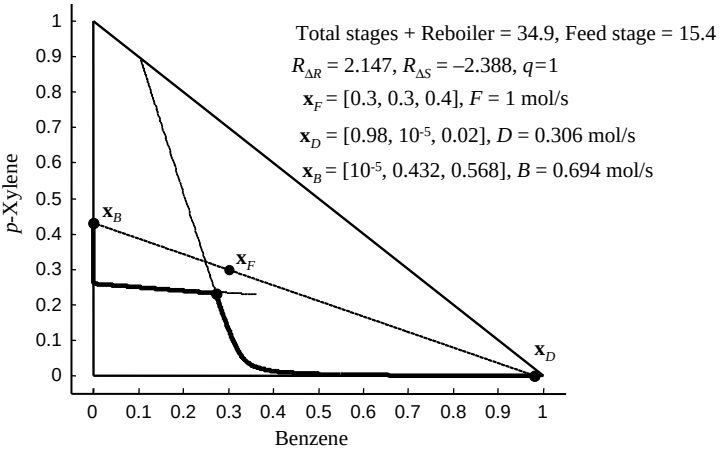


FIGURE 5.31 A feasible design at 1.2 times minimum reflux for the benzene/*p*-xylene/toluene system using profile intersection.

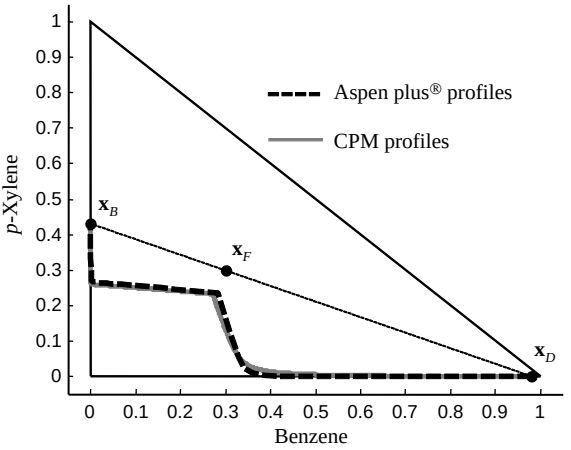


FIGURE 5.32 A comparison of the CPM design shown in Figure 5.31 and Aspen Plus®, using input from the CPM method.

(c) Finally, once these values have been estimated, it is relatively straightforward to export the design figures obtained in (b) to a more rigorous process simulation packages. For the Aspen Plus® simulation (using the RADFRAC distillation block), we specify that the column requires 34 stages (reboiler counts 1) and that the feed stage is on stage 15, the column reflux is 2.147 and the distillate flowrate is 0.306 mol/s (assuming 1 mol/s feed). As with our CPM design, the column is assumed to be isobaric at 1 atm. A comparison of the design found with CPMs and a more rigorous Aspen Plus® solution using input data from Figure 5.31 is shown in Figure 5.32.

As in the previous example, the product specifications are met very closely using Aspen Plus®. This particular case also shows that profiles match each other very closely.

5.5.2 Design Using Eigenvectors

An additional phenomenon that may be seen using the TT method is that, for a feasible design at minimum reflux conditions for a liquid feed, the edges of the TT of both rectifying and stripping CSs run through the feed composition, as shown in Figure 5.25. This leads to ponder what the feed composition tells us about feasibility, as clearly, there is some sort of relationship. As mentioned in the preceding chapter (see Section 3.8.1), eigenvectors represent the asymptotic direction of profiles entering stationary points. Whence, since the TTs edges are straight, the eigenvectors evaluated at the feed should also tell us something about feasibility. Recall too that the eigenvectors are solely a function of the phase-equilibrium model, and not of the reflux or difference points. Knowing the eigenvectors at the feed composition,

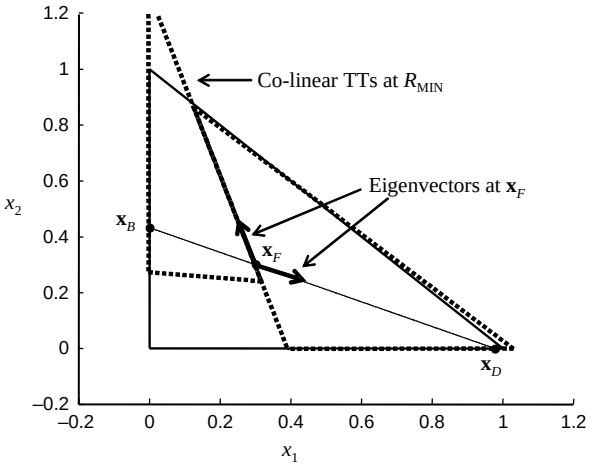


FIGURE 5.33 Eigenvectors at $\mathbf{x}_F$ are collinear to at least one TT.

therefore, already specifies the colinearity condition, that is, the slope of the colinear sides of the TTs, as explained earlier and shown in Figure 5.33 . Then, by knowing the product specifications in each CS ($\mathbf{X}_\Delta$), one only needs to solve for the unique reflux value that will cause the TTs of each CS to lie on the colinear line.

Determination of minimum reflux via the eigenvector method amounts to the exact same solution as described earlier in this section, and using classic methods such as the Underwood method. It also suffers from the same constraints in that it is only valid for constant volatility and sharp split systems. The advantage of using the eigenvector method is that solution for minimum reflux may be determined algebraically, that is, without numerical root finding methods, which may obviously be useful in certain instances. Abbas et al. [16] pioneered this eigenvector method and have produced regions of column feasibility and product distribution limits. However, encountering nonliquid feeds requires a different handling of the problem since the colinear edge of the (liquid) TTs will no longer go through the nonliquid feed composition. Moreover, this method may be somewhat cumbersome when one desires a quick assessment of a distillation structure. For these reasons, subsequent TT design problems encountered later in this book will be addressed using the method in this section, although the reader should be aware of the usefulness and applicability of the eigenvector method in certain cases.

5.6 SUMMARY

In this chapter, we have presented the application of CPMs to the most common pieces of distillation equipment, absorbers/stripping towers, and simple columns. The versatility of the CPM method can already be seen even in these basic structures,

as it is not bound by phase-equilibrium properties or the product specifications. The designer is able to draw several valuable conclusions from the CPM design technique, including among others:

- the exact total number of equilibrium stages;
- the feed stage, which is generally a parameter requiring significant insight/experience; and
- minimum reflux.

The efficacy of the methodology is perhaps demonstrated best with an azeotropic example where we have crossed the distillation boundary—a feat thought to be impossible using other methods such as RCMs. Furthermore, the usefulness of TTs is shown with respect to design. For the special case of constant relative volatilities and sharp splits, the minimum reflux required to render the design feasible requires only an algebraic colinearity calculation, and not the integration of the DPE. Another important outcome is that the design parameters estimated using the CPM method can be exported into more rigorous "black-box calculation" type models. In such models, one often has a very limited idea of what products are achievable because parameters such as the total number stages, feed stage, or column reflux are chosen blindly. Although not as rigorous, the CPM method is able to give very good initial values for design with these black-box models.

REFERENCES

[1] Van Dongen, D.B. and M.F. Doherty, Design and synthesis of homogeneous azeotropic distillations. 1. Problem formulation for a single column. *Industrial and Engineering Chemistry, Fundamentals*, 1985, **24**(4):454–463.

[2] Levy, S.G., D.B.Van Dongen, and M.F. Doherty, Design and synthesis of homogeneous azeotropic distillations. 2. Minimum reflux calculations for nonideal and azeotropic columns. *Industrial and Engineering Chemistry, Fundamentals*, 1985, **24**(4):463–474.

[3] Levy, S.G. and M.F. Doherty, Design and synthesis of homogeneous azeotropic distillations. 4. Minimum reflux calculations for multiple-feed columns. *Industrial and Engineering Chemistry Fundamentals*, 2002, **25**(2):269–279.

[4] Doherty, M.F. and M.F. Malone, *Conceptual Design of Distillation Systems*. 1st ed. 2001, New York, NY, USA, McGraw-Hill. p. 568.

[5] Kremser, A., Theoretical analysis of absorption process. *National Petroleum News*, 1930, **22**(21):43–49.

[6] Knight, J.R. and M.F. Doherty, Design and synthesis of homogeneous azeotropic distillations. 5. Columns with non-negligible heat effects. *Industrial and Engineering Chemistry, Fundamentals*, 1986, **25**(2):279–289.

[7] Seader, J.D. and E.J. Henley, *Separation Process Principles*. 2nd ed. 2006, Hoboken, NJ: Wiley. p. 756.

[8] Ruiz, G.J., et al., Robust thermodynamically-guided algorithms for synthesis of energy efficient separation networks, in *Computer Aided Chemical Engineering*. S. Pierucci and G.B. Ferraris, Editors. 2010, The Netherlands: Elsevier. pp. 1117–1122.

[9] Ruiz, G.J., et al. Design and optimization of energy efficient complex separation networks, in *7th International Conference on the Foundations of Computer-Aided Process Design*. 2009, New York: Taylor & Francis Group.

[10] Zhang, L. and A.A. Linninger, Temperature collocation algorithm for fast and robust distillation design. *Industrial and Engineering Chemistry Research*, 2004, **43**(12):3163–3182.

[11] Fenske, M.R., Fractionation of straight-run Pennsylvania gasoline. *Industrial and Engineering Chemistry*, 1932, **24**(5):482–485.

[12] Underwood, A.J.V., Fractional distillation of multi-component mixtures—Calculation of minimum reflux ratio. *Institute of Petroleum—Journal*, 1946, **32**(274):614–626.

[13] Wahnschafft, O.M., et al., The product composition regions of single-feed azeotropic distillation columns. *Industrial and Engineering Chemistry Research*, 1992, **31**(10):2345–2362.

[14] Linninger, A. Industry-Wide Energy Saving by Complex Separation Networks, in FOCAPO, Cambridge, MA, 2008.

[15] Zhang, L. and A.A. Linninger, Towards computer-aided separation synthesis. *AIChE Journal*, 2006, **52**(4):1392–1409.

[16] Abbas, R., S.T. Holland, and I.J. Halvorsen, Novel minimum reflux calculation using eigenvector maps, in *Distillation and Absorption 2010*, G.K. de Haan, editor. 2010, Eindhoven, The Netherlands: Eindhoven University of Technology.

CHAPTER 6

DESIGN OF COMPLEX COLUMNS USING COLUMN PROFILE MAPS

6.1 INTRODUCTION

The separation of a mixture of components into products with a higher purity via distillation is a very effective and reliable means of separation. This reason, and the fact that distillation is economically attractive for large scale separations, has lead to distillation becoming a relatively mature research field. However, despite the popularity of distillation as a means of separation, it is nonetheless an expensive operation from both a capital and an operating cost point of view. This has contributed to designers seeking more creative means of designing distillation schemes than simple columns (see Chapter 5) in an attempt to reduce or optimize the associated costs. These alternate distillation schemes, known as complex distillation columns, can be categorized as any column other than a single-feed-two-product column discussed in the preceding chapter.

Examples of such complex distillation structures are thus columns that have more than one feed point and/or more than two product streams, like distributed material addition/removal columns, and thermally coupled columns. Obviously, as the complexity of the distillation structure increases, so does the design itself thereof. This chapter will, as an introduction to complex column design, treat the design of "elementary" complex columns such as distributed feed and sidestream withdrawal columns, and side rectifiers, and strippers, before discussing more intricate complex columns like fully thermally coupled columns (sometimes referred to as the Petlyuk and Kaibel columns) in the subsequent chapter. Despite

Understanding Distillation Using Column Profile Maps, First Edition. Daniel Beneke, Mark Peters, David Glasser, and Diane Hildebrandt.
© 2013 by John Wiley & Sons, Inc. Published 2013 by John Wiley & Sons, Inc.

the perceived difficulty of complex column design, it is particularly in these columns where the most important application of the CPM design method lies, since the technique is entirely generalized to *all* types of CSs, not only conventional rectifying and stripping sections. Thus, the design procedure of complex structures is a mere extension of the design of simple columns and no new equations have to be derived for each new structure.

6.2 DISTRIBUTED FEED ADDITION

The first significant work for addressing the design of distributed material addition/removal was done by McCabe and Thiele [1] for binary systems. Although the McCabe–Thiele construction has been very successful in designing and understanding binary separation systems it does not address multicomponent systems where the effects of feed material distribution are not as obvious. In fact, most of the current design rules for the placement of the feed tray in simple columns are based on heuristics [2,3] and do not even address the distributed material case. Using the CPM method, these effects can be easily and rationally interpreted. The systematic design and potential benefits of such systems will be addressed in this chapter.

The preceding chapter put forward the fundamental ideas for designing feasible *simple* columns. Although simple columns are probably the most common pieces of separation equipment found in industrial plants, they do not allow creative placement of $\mathbf{X}_{\boldsymbol{\Delta}}$'s or R_{Δ}'s, since both these parameters are set by external mass and energy balances. Thus, the designer cannot use some of the interesting topology that may be generated with, for instance, $\mathbf{X}_{\boldsymbol{\Delta}}$'s located outside the positive composition space. One way of "creating" unusual, yet useful or interesting $\mathbf{X}_{\boldsymbol{\Delta}}$'s is by not insisting that all the feed be added on a single tray, but to distribute the feed along the column. This practice would create additional CSs and, depending on the relative compositions and flowrates of the particular stream, adjust R_{Δ} and $\mathbf{X}_{\boldsymbol{\Delta}}$ and open the door to new separation possibilities.

6.2.1 Column Section Breakdown

Before we start searching for feasible designs and interpreting the effects of $\mathbf{X}_{\boldsymbol{\Delta}}$'s and R_{Δ}'s, we first have to define our column and break it into a series of CSs. Consider then a two product distillation column terminated at the top by a condenser and at the bottom by a reboiler, as shown in Figure 6.1. We shall define the total feed to the column as F_T, which is to be distributed at multiple points down the length of the column. For the general case where the feed is to be split into $N-1$ substreams, at $N-1$ feed points, the result will be a column consisting of N CSs.

The CS situated at the top of the column, terminated by a condenser, is a standard rectifying section, while the bottommost CS, terminated by the reboiler, is a standard stripping section. These are the product producing CSs and behave in the same way to the product producing CSs in simple columns (see Section 5.3). All the remaining CSs are internal CSs which do not produce products but are created by the addition of

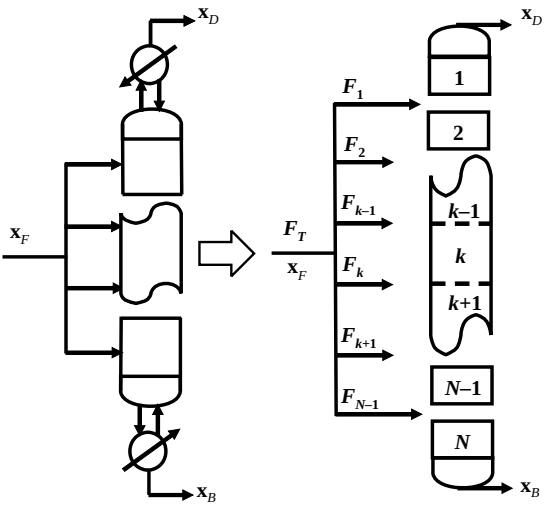


FIGURE 6.1 CS breakdown of a distributed feed column.

material. They may behave as either an equivalent rectifying or stripping section depending on the directional flow of material.

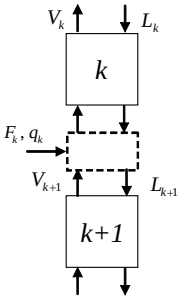
Note that we limit our discussions in this book to a single liquid feed that is split and distributed at various points along the column length. The method described can easily be adapted for vapor feeds, as well as for different feed compositions at each addition point.

6.2.2 The Effect on the Reflux Ratio (R_Δ)

Intuitively, spreading the feed to different points throughout the column will change the reflux ratio in each new CS. For each CS k in Figure 6.1, a different reflux ratio will come about, which we will define as

$$R_{\Delta k} = \frac{L_k}{\Delta_k} \tag{6.1}$$

In the same way as conventional CSs, the sign of R_Δ (which is set by the sign of Δ, since L is always positive) defines the operating mode of the CS, a negative R_Δ implies stripping mode while a positive R_Δ implies rectifying mode. The mode of operation tells us the direction of the net or bulk flow in any CS (see Section 3.5.1). In determining the refluxes of CSs in the column, it is convenient to define a "reference" reflux from which to work. In this case, we shall use the topmost rectifying CS to keep with the convention of simple columns, although this choice is completely arbitrary. If we only consider for the moment two generic CSs located across a feed point between CS_k and CS_{k+1}, we can perform a mass balance, as shown in Figure 6.2.



Overall material balance:

$$L_k + V_{k+1} + F_k = L_{k+1} + V_k$$

Rearranging:

$$V_{k+1} - L_{k+1} + F_k = V_k - L_k$$

$$\Delta_{k+1} = \Delta_k - F_k$$

Overall liquid balance:

$$L_{k+1} = L_k + F_k q_k$$

FIGURE 6.2 Magnified view of CS_{k+1} and CS_k with all stream definitions and an overall material balance.

We now have streams in CS_{k+1} written in terms of the stream of CS_k, which allows us to relate their refluxes (and net flows) using the definition of a R_Δ in Equation 6.1, for $k \geq 1$:

$$R_{\Delta k+1} = \frac{R_{\Delta k}\Delta_k + F_k q_k}{\Delta_k - F_k} \tag{6.2}$$

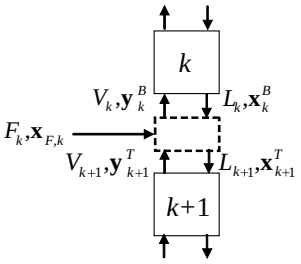
$$\Delta_{k+1} = \Delta_k - F_k \tag{6.3}$$

Recall from the previous chapters that the net flow (Δ) is simply equal to the product flowrate in product producing CSs. Simply put, in the top CS (rectifying section), $\Delta = D$. Thus, by defining a reflux ratio for the top CS (our reference CS), and knowing the flow of each feed substream and the product flowrates, we are able to calculate R_Δ's for the entire column. From the top of the column downward, each subsequent feed addition (assuming a pure liquid feed) has the effect of increasing the reflux, as the net flow term $(V - L)$ becomes smaller. When enough liquid feed material has been added, the CS switches to stripping mode as L becomes larger than V.

Interestingly, the reflux ratio in the bottommost (stripping) CS is exactly the same in the simple column where all the feed was added in a single stream (refer to Section 5.3.2), assuming the overall feed and product flowrates and compositions are the same in both instances. This is because all the feed, no matter how it is distributed along the column, will eventually accumulate to the bottommost CS making it operate at the same conditions as if all the feed has been added just above it.

6.2.3 The Effect on the Difference Point (X_Δ)

Although the concept of the difference point has thus far only been applied to simple columns where it is simply equal to the product specifications of the column, the true usefulness of using $\mathbf{X_\Delta}$ will become apparent in studying complex columns. Let us again consider generalized CSs k and $k+1$ above and below a feed stream F_k, as shown in Figure 6.3 with an accompanying mass balance.



$$L_k\mathbf{x}_k^B + V_{k+1}\mathbf{y}_{k+1}^T + F_k\mathbf{x}_{F,k} = L_{k+1}\mathbf{x}_{k+1}^B + V_k\mathbf{y}_k^T$$

Rearranging:

$$V_{k+1}\mathbf{y}_{k+1}^T - L_{k+1}\mathbf{x}_{k+1}^B + F_k\mathbf{x}_{F,k} = V_k\mathbf{y}_k^B - L_k\mathbf{x}_k^T$$

$$\Delta_{k+1}\left(\frac{V_{k+1}\mathbf{y}_{k+1}^T - L_{k+1}\mathbf{x}_{k+1}^T}{\Delta_{k+1}}\right) + F_k\mathbf{x}_{F,k} = \Delta_k\left(\frac{V_k\mathbf{y}_k^B - L_k\mathbf{x}_k^B}{\Delta_k}\right)$$

Therefore,

$$\Delta_{k+1}\boldsymbol{X}_{\Delta k+1} + F_k\mathbf{x}_{F,k} = \Delta_k\boldsymbol{X}_{\Delta k}$$

FIGURE 6.3 Magnified view of CS_k and CS_{k+1} with all stream definitions and a component balance for a generic feed.

The mass balance in Figure 6.3 highlights an important result: $\mathbf{X}_{\boldsymbol{\Delta}}$'s across a feed addition point are linearly related to the feed—they, in fact, behave as real compositions. Geometrically, this means that the $\mathbf{X}_{\boldsymbol{\Delta}}$'s of adjacent CSs across a feed point, and the feed composition, will all lie on the same straight line, analogously to the bottoms, distillate and feed compositions in simple columns. However, the question still remains, where do these new difference points lie? If the net flow in adjacent CSs are positive, that is, both CSs are in rectifying mode, then the internal $\mathbf{X}_{\boldsymbol{\Delta}}$'s tend to move outward, away from the distillate composition. As soon as enough material has been fed to the column to change the operating modes of the CSs from rectifying to stripping, the linear trend continues, but, from the outside inward toward the bottoms products. This is perhaps better understood graphically, shown in Figure 6.4. Thus, the internal difference points first move away from the distillate composition, but then return from the other side and head toward the bottoms composition.

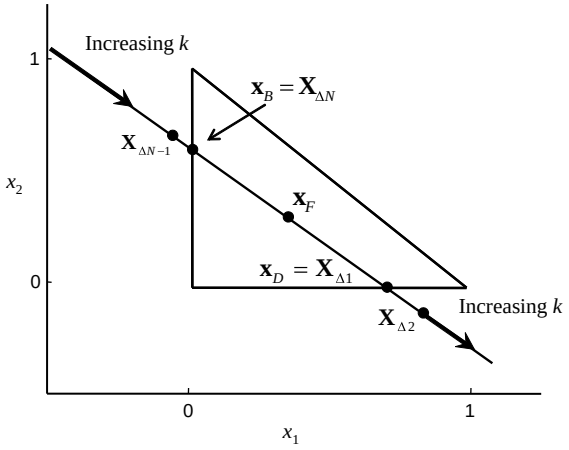


FIGURE 6.4 Movement of difference points for distributed feed columns.

As discussed in Chapter 3, the extended axes of the MBT correspond to different modes of operation in a CS. If $\mathbf{X}_{\Delta}$ crosses one of these extended axes, the compositional net flow has changed in the column and a component that was moving upward has started moving downward (when performing the analysis from top-down in the column). Thus, by adjusting the feed flowrate to be sent at different points in the column, we can manipulate the movement of $\mathbf{X}_{\Delta}$ and in so doing expose some of the interesting topology we have shown in Chapter 3.

It is also interesting to note that, from a mathematical point of view, these strange positions of $\mathbf{X}_{\Delta}$ that may be created through distributed feed addition allow the roots of the DPE to be complex. The profiles are in such cases, of course, still perfectly valid and it is still possible to design a feasible column if the roots of the DPE happen to be complex in a particular CS.

6.2.4 Feasible Designs

The true beauty of the CPM method is that the design procedure and criteria for feasibility stays largely the same, even when working with complex columns. Once the feed distribution policy has been set, assuming an initial reflux for the topmost CS (the reference reflux) and knowing the product specifications, we have essentially set the difference points and reflux ratios for each CS and have everything we need for producing CPMs for each respective CS. However, we do not know the specific initial integration compositions of the internal CSs, only CSs at the column ends, or the termination CSs, as the initial integration composition is again equal to the product specification. Thus, these product producing profiles have been fixed and cannot be manipulated once R_{Δ}'s and $\mathbf{X}_{\Delta}$'s have been specified. In other words, for the rectifying and stripping sections on either end of the column, we can generate the exact profiles which they will follow (and thus need not produce the entire CPM for these sections). However, at this point, it has not yet been decided where to terminate one section, and (through feed addition) start the next section. Thus, since we do not know the exact profile for each internal CS, it is more convenient to produce entire CPMs for each of the internal CSs which originate from different initial points. Thereafter, a continuous liquid profile can be sought.

As an example, consider the plot shown in Figure 6.5 for a constant relative volatility system. Here, we have chosen to split the feed into two equal parts, thereby creating only one internal CS. The total feed stream has a composition $\mathbf{x}_F = [0.3, 0.4]$ and flowrate 1 mol/s. The product specifications are: $\mathbf{x}_D = [0.990,\ 0.001]$ and $\mathbf{x}_B = [0.001,\ 0.573]$, and the reflux ratio in the uppermost CS is $R_{\Delta 1} = 4$.

In order to generate the individual profiles for the rectifying (CS_1) and stripping (CS_3) sections, as well as the CPM for the internal CS (CS_2), both external and internal material balances around the entire column as well as each point of feed addition had to be performed. The details of the calculations are left to the reader. A summary of the results for each CS is given in Figure 6.5.

Figure 6.5 makes reading very interesting, because it shows that the addition of a feed stream and the subsequent CS that has been created, and gives one a considerable amount of freedom. Recall that for a design to be feasible a continuous

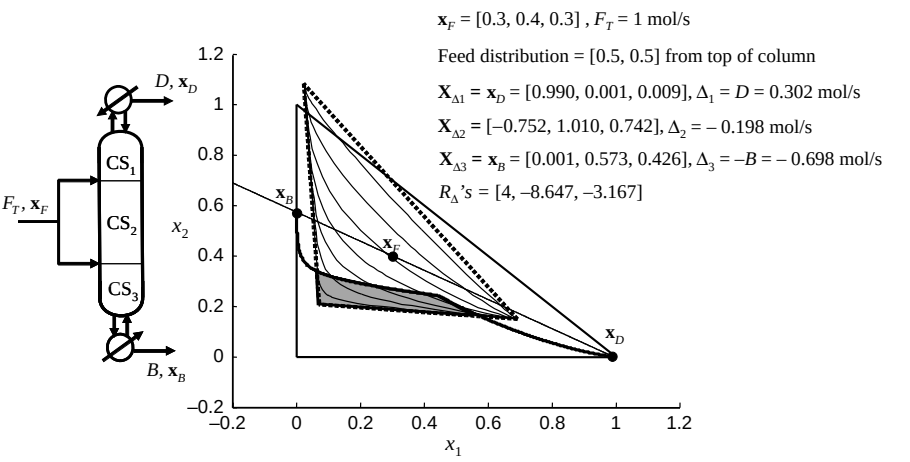


FIGURE 6.5 A distributed feed column for $\mathbf{x}_D = [0.990,\ 0.001]$, $\mathbf{x}_B = [0.001,\ 0.573]$, $\mathbf{x}_F = [0.3,\ 0.4]$, and $R_{\Delta 1} = 4$, with a CPM and TT for the internal section and $\boldsymbol{\alpha} = [5,\ 1,\ 2]$.

composition path must exist between all product compositions. Notice firstly that if all the feeds were added at one point, this particular column would still be feasible since the column termination profiles (those of the rectifying and stripping sections, namely CS_1 and CS_3) still intersect one another. By producing a CPM for the internal CS, we are, in fact, able to assess multiple profiles that will also result in a feasible design, highlighted in the shaded area. In this region, internal CS profiles intersect both termination profiles, in the "correct direction." By "correct direction," it is meant that all profiles are consistently aligned toward the same point. For instance, starting at the low-boiling distillate product and travelling toward the bottom of the column, *all* profiles should move toward their stable nodes. If this criterion is not met, profile intersection is meaningless.

The designer may choose any profiles in the feasible region in Figure 6.5 and a feasible design will be found. The shaded area is enclosed by the edges of the internal CSs' TT, representing the last profile that will allow for a feasible design using distributed feed. Viewed from another angle, if one were to add the distributed at the wrong point along the length of the column, the profiles will not intersect. Thus, the TT does not only show regions of feasibility, but also indicates the first point at which a distributed feed stream may be added. In this example, if the rectifying section is terminated too early (i.e., before the TT of the internal CS), then the profile of the internal CS will head in the incorrect direction, and will consequently never intersect with the terminating stripping profile, thereby making the design infeasible.

Furthermore, notice that the position of the feed points in the column cannot be chosen independently of one another—by selecting a certain operating profile in the internal CS, the feed points at the top *and* bottom of the column have been set, illustrated in Figure 6.6. The bold profiles in Figure 6.6 show a final column design with an arbitrarily chosen operating profile for CS_2, while the thinner profiles are merely the continuation of the profiles past the respective point of intersection. Note

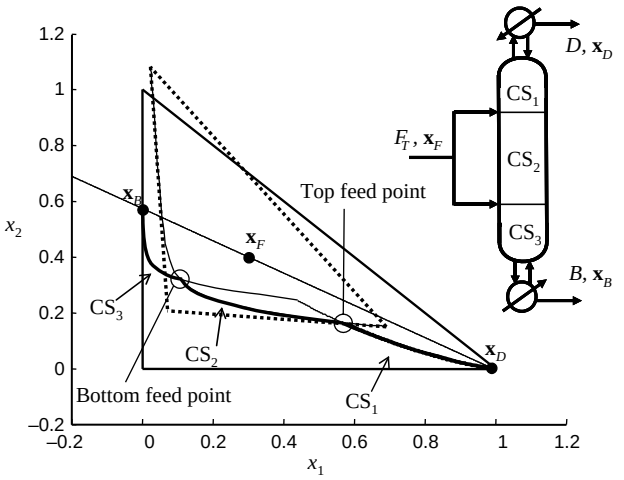


FIGURE 6.6 A distributed feed column for $\mathbf{x}_D = [0.990,\ 0.001]$, $\mathbf{x}_B = [0.001,\ 0.573]$, $\mathbf{x}_F = [0.3,\ 0.4]$, and $R_{\Delta 1} = 4$, with a CPM and TT for the internal section and $\boldsymbol{\alpha} = [5,\ 1,\ 2]$.

that any profile within the shaded area in Figure 6.5 would also have resulted in a feasible design, but simply with different feed locations.

WWW

TUTORIAL 6.1

Try this for yourself: Reproduce Figure 6.5 using DODS-DiFe and the given parameters. Assess the effect of changing key parameters such as $\boldsymbol{\alpha}$, $R_{\Delta 1}$, and feed and product compositions.

It is clear from Figure 6.5 that even one distributed stream split has a significant impact on the design. This however leads to one to ponder how any subsequent stream splitting and addition will impact the design. A feasible column using the same product specifications as the one shown above, but with five equal stream splits, is shown in Figure 6.7.

It is evident from Figure 6.7 that the feasible region has increased considerably from the scenario where the feed was only divided into two equal parts. There are considerably more profiles that the designer may choose in order to link the two terminating profiles with one another. The limit is again the edges of each TT on the one end and the single feed column profiles on the other end.

It is apparent that the single feed column is the one "limit" on the distributed feed column. At the other end of the design spectrum, one may theoretically choose to split the feed stream in infinitely many substreams, resulting in infinitely many CSs. Although this may seem like a purely academic or impractical limit, it does have some use because the feasible region resulting from this will show us *all* possibilities when deciding on a column. Thus, the profiles of any feed stream division will lie in

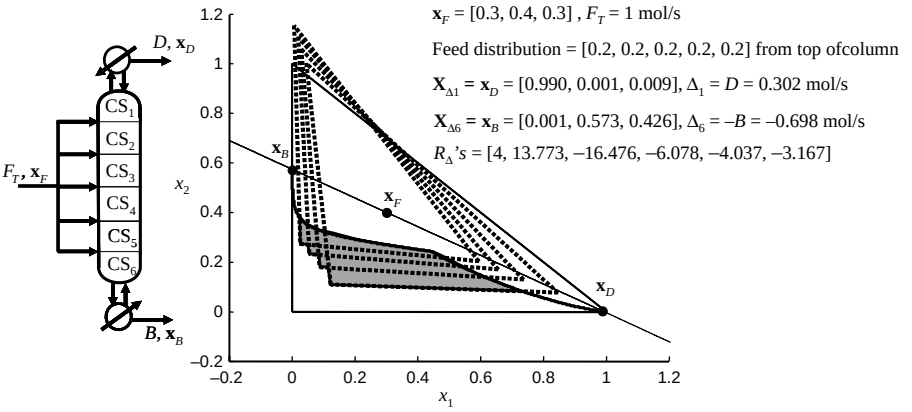


FIGURE 6.7 A multiple (5) distributed feed column for $\mathbf{x}_D = [0.990, 0.001]$, $\mathbf{x}_B = [0.001, 0.573]$, $\mathbf{x}_F = [0.3, 0.4]$, and $R_{\Delta 1} = 4$, with a TT for all the internal sections and $\boldsymbol{\alpha} = [5, 1, 2]$.

this region. Again, for the same product and operating conditions as the previous illustrations, an infinitely distributed column is depicted in Figure 6.8.

For the infinitely distributed feed column the feasible region is as large as it can possibly be, bound by the locus of saddle nodes of the internal CSs' TTs. Notice that roles of the two product producing CSs have been increasingly diminished as the number of feed points are increased. They are *almost* not needed at all in Figure 6.8!

What should be clear from the illustrations presented in Figures 6.5–6.8 is that the concept of distributed feed addition columns presents unique opportunities to the designer. Each stream addition gives the designer an additional degree of freedom that may be used to manipulate profiles to suit the separation. However, although

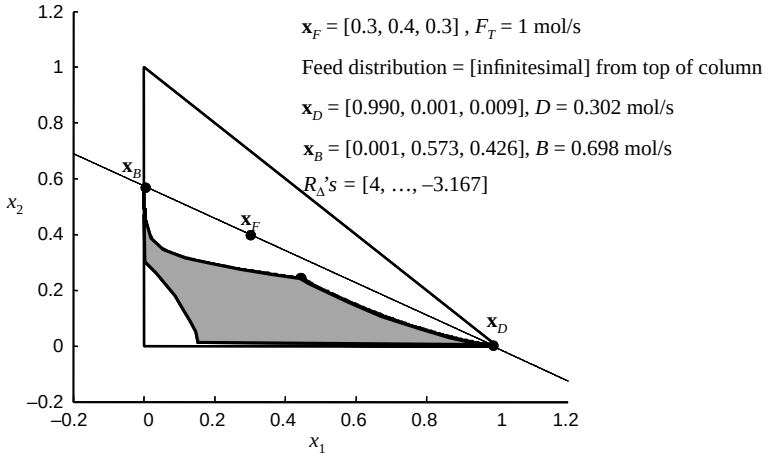

$\mathbf{x}_F$ = [0.3, 0.4, 0.3] , F_T = 1 mol/s
Feed distribution = [infinitesimal] from top of column
$\mathbf{x}_D$ = [0.990, 0.001, 0.009], D = 0.302 mol/s
$\mathbf{x}_B$ = [0.001, 0.573, 0.426], B = 0.698 mol/s
R_Δ's = [4, …, –3.167]
$\mathbf{x}_B$
$\mathbf{x}_F$
$\mathbf{x}_D$
x_1
x_2

FIGURE 6.8 An infinitely distributed feed column for $\mathbf{x}_D = [0.990, 0.001]$, $\mathbf{x}_B = [0.001, 0.573]$, $\mathbf{x}_F = [0.3, 0.4]$, and $R_{\Delta 1} = 4$, and $\boldsymbol{\alpha} = [5, 1, 2]$.

there are more design degrees of freedom open to the designer, it is not immediately evident whether distributed feed actually constitute an improvement in the process operating conditions. This is discussed in more detail in the following sections.

6.2.5 Potential Benefits and Limitations

Traditionally, distillation has two main cost variables associated to it:

1. The vapor flowrate in the column which is proportional to the reflux ratio. This variable is linked to the operating costs of a column, as the amount of vapor required sets the reboiler duty.
2. The number of stages required. This is associated with the capital cost of the column.

Thus, if we could improve either of these cost measures, distributed feed addition will certainly be a worthwhile consideration. First, let us consider whether a reduction in the reflux ratio may be achieved.

6.2.5.1 Reflux Ratio Chapter 5 introduced the concept of minimum reflux for simple columns as the reflux condition where rectifying and stripping profiles just touch one another. This condition is equivalent to the minimum vapor flow in the column, and anything lower than the minimum reflux will result in an infeasible column because a continuous path between the products will not exist, by definition. The question is: Can we manipulate the feed addition policy such that we can decrease the reflux ratio required for a simple column to perform a specific separation task? To answer this, consider a simple column at minimum reflux conditions of $R_{\Delta 1} = 1.56$ with a product specification of $\mathbf{x}_D = [0.970, 0.001]$, $\mathbf{x}_B = [0.001, 0.578]$, represented in Figure 6.9 by bold profiles originating from the product specifications.

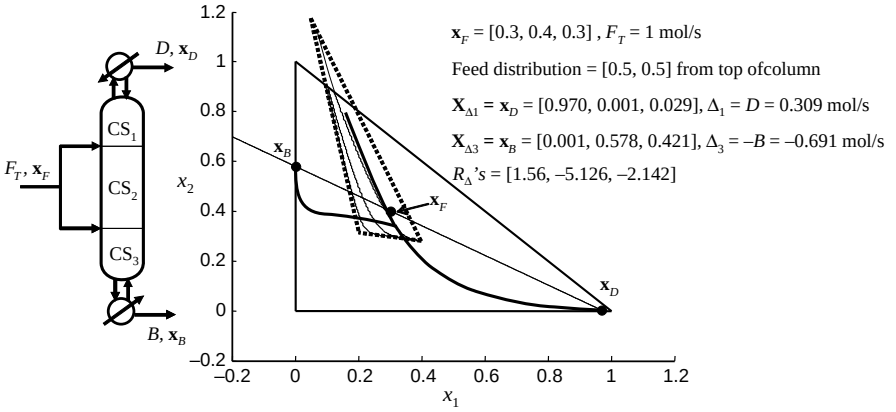


FIGURE 6.9 Profiles for a single distributed feed column for $\mathbf{x}_D = [0.970, 0.001]$, $\mathbf{x}_B = [0.001, 0.578]$, $\mathbf{x}_F = [0.3, 0.4]$, and $R_{\Delta 1} = 1.56$, and $\boldsymbol{\alpha} = [5, 1, 2]$.

Figure 6.9 also shows a TT for the internal CS that has been created by splitting the feed into two equal parts.

WWW

TUTORIAL 6.2

Try this for yourself: Reproduce Figure 6.9 using DODS-DiFe and the given parameters. Assess the effect of changing key parameters such as $\boldsymbol{\alpha}$, $R_{\Delta 1}$, and feed and product compositions.

Once more, there is a feasible region given by the boundaries of the TT. However, note here that the TT of the internal CS provides an additional insight because its vertices have gone significantly past each of the profiles, that is, the TT does not pinch on either profile. This means that there is some degree of maneuvering that may still be done before an infeasible column is reached. When a vertex (or pinch point) of the TT lies exactly on one of the product producing profiles, a new minimum reflux has been achieved. If the TT vertex has been shifted past one of the termination profiles, there is no way a continuous profile path can be achieved. Thus, this condition represents the lowest reflux where a column is still feasible. The minimum reflux for the distributed feed column in Figure 6.9 is shown in Figure 6.10. Notice that one of the TT's vertices lies precisely on the rectifying profile.

WWW

TUTORIAL 6.3

Try this for yourself: Reproduce Figure 6.10 using DODS-DiFe and the given parameters. Try and find other minimum reflux designs for a distributed feed column by changing parameters such as $\boldsymbol{\alpha}$, $R_{\Delta 1}$, and feed and product compositions.

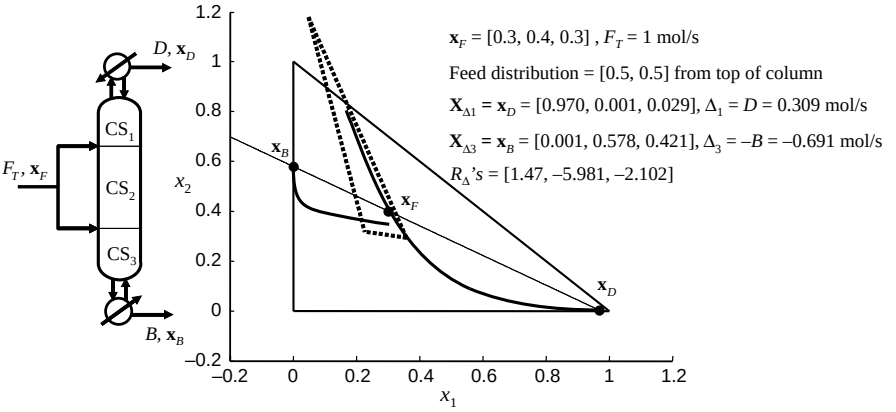


FIGURE 6.10 Profiles for a single distributed feed column for $\mathbf{x}_D = [0.970,\ 0.001]$, $\mathbf{x}_B = [0.001,\ 0.578]$, $\mathbf{x}_F = [0.3,\ 0.4]$, and $R_{\Delta 1} = 1.47$ (minimum), and $\boldsymbol{\alpha} = [5,\ 1,\ 2]$.

Comparing Figures 6.9 and 6.10 shows an incredible result. We were able to drop the minimum reflux, and the accompanying energy requirement, by almost 6% (compare $R_{\Delta 1}$ in each case). This is quite a remarkable result because it has been obtained within a few seconds by just adjusting the feed entry points. This illustration merely serves to indicate that there are definite potential benefits to material distribution. There are almost certainly even greater savings to be achieved with different product specifications or by adjusting number of feed points or the flowrates of each subdivided stream, as shown in the example at the end of this section. In general, for constant relative volatility systems, the more feed points one has, the lower the minimum reflux of the column is required to be, up to an upper limit of about six or seven distributions where after the benefits begin to asymptote. This is illustrated in Figure 6.11 for a column with the same product specifications as in Figures 6.9 and Figure 6.10, but with the feed distributed five times down the length of the column.

Notice again in Figure 6.11 that the TT adjacent to the topmost rectifying CSs' profile has a vertex located precisely on top of it. Any further reduction in column reflux will move this vertex to the left, thereby making the column infeasible. In Figure 6.11, we have reduced the minimum reflux even further to a value of 1.05, reducing the overall energy demand from the simple column by a staggering 33%. Again, this is without any sort of optimization or a search for an optimal distribution policy. Although the distributed feed column evidently has plenty to offer in terms of energy savings, the operability of such multiple distributed feed columns may be questionable since one has to exactly match feed entry points with one another to obtain the desired product specifications. In other words, the profile one chooses to operate on in one of the internal CSs has an exact feed position that it is required to lie on in two different profiles. Obviously, the more feed entry points one has, the more difficult this becomes.

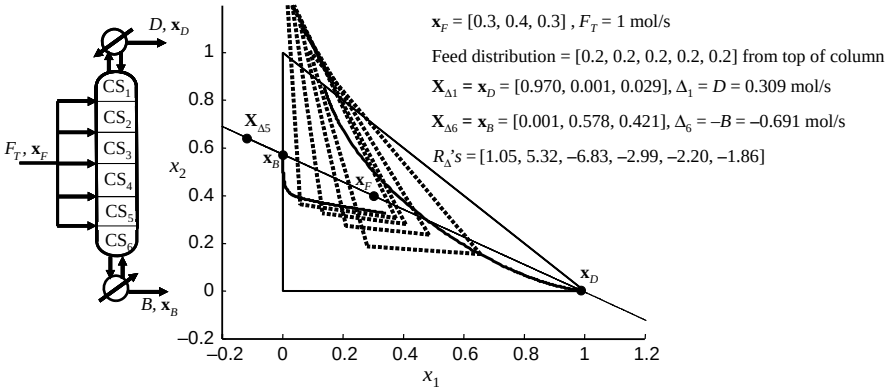


FIGURE 6.11 A multiple (5) distributed feed column for $\mathbf{x}_D = [0.970, 0.001]$, $\mathbf{x}_B = [0.001, 0.578]$, $\mathbf{x}_F = [0.3, 0.4]$, and $R_{\Delta 1} = 1.05$ (minimum), and $\boldsymbol{\alpha} = [5, 1, 2]$.

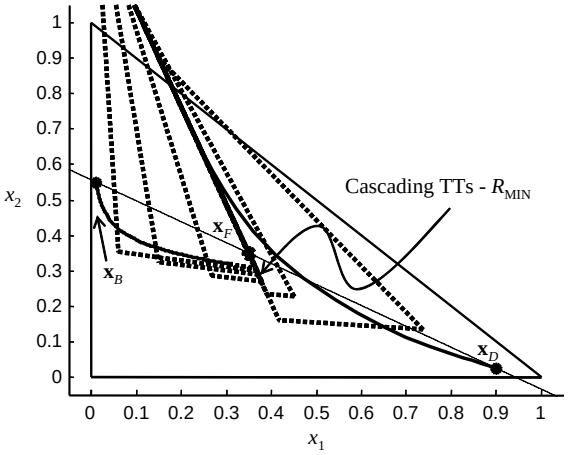


FIGURE 6.12 A multiple (5) distributed feed column where TTs cascade around a line.

The reader should be aware that the minimum reflux scenarios presented here are just one of three possible ways the minimum reflux limit can be obtained in distributed feed columns. The designs shown thus far all depicted minimum reflux when the vertex of the internal CS adjacent to the topmost rectifying section lies exactly on its profile, that is, a pinch occurs on the topmost rectifying CS. It is perfectly valid for the minimum reflux condition to be determined by the bottommost stripping profile, or indeed where the TTs of the internal CSs do not overlap one another. The latter case is shown in Figure 6.12 where the column reflux has been reduced and TTs cascade around one another, thereby limiting any further column reflux reduction. The general requirement for minimum reflux is however the same as for simple columns: any reflux value below the minimum reflux value will lead to a discontinuous path of profiles, and minimum reflux is therefore the last reflux where a continuous path is still maintained.

6.2.5.2 Stage Requirement The benefits of the overall energy requirements of a column for a certain separation using distributed feed addition have been clearly shown above. The recent trend in distillation design, and process design, in general, is to design for minimum energy usage. However, we have not investigated whether there are benefits in terms of stage reduction. The first instinct one may have is that feed division will increase the number of stages required since we are essentially creating a CS for each stream subdivision. Exploring this subject a bit further reveals that there may be benefits, especially if the feed could be distributed such that one can "move around" areas where columns start to pinch and the stage numbers approach infinity. Consider for example Figure 6.9 once more. This simple column operates at a minimum reflux of 1.56. It is to be noted that minimum reflux corresponds to an infinite number stages since the one profile is pinching on the other one, and as the profiles approach its pinch point the stages tend to infinity. By distributing the feed only once, it is possible to "sidestep" the area where the simple

columns pinch, thus resulting in a finite number of stages. The further one can stay from pinched columns, the better the overall stage requirement will become. Choosing any one of the profiles in the TT in Figure 6.11 allows one to move around the region where the stripping profile terminates. There are thus both energetic and capital advantages to be had by distributing the feed, although these effects are again opposing because lowering the reflux even more (toward minimum reflux) for the distributed feed case (as in Figure 6.10) will again lead to a tendency toward infinitely many stages.

6.2.5.3 Feasibility Another result that stems from both Figures 6.10 and 6.11 is that a design that was originally considered infeasible using a simple column has been made feasible with feed distribution. One can see that the two terminating profiles in both these figures do not intersect one another (making the simple column infeasible), but by distributing the feed a continuous path between the product specification has been found. Obviously, this has implications for azeotropic distillation when certain product specifications may seem unobtainable based on distillation boundaries seen in RCMs. An example of such a scenario can be seen in Figure 6.13 for the acetone/benzene/chloroform, where distributing the feed only once has made an apparently impossible separation, possible.

Clearly, the CS created by the feed distribution serves as a link between the rectifying and stripping profiles to cross the distillation boundary. For the CPM simulations, the following design parameters were used: $F = 1$ mol/s, $q = 1$, $\mathbf{x}_F = [0.35, 0.35]$, $\mathbf{x}_D = [0.95, 0.01]$, $\mathbf{x}_B = [0.02, 0.57]$, and $R_{\Delta R} = 2.6$. In order to validate these findings, data generated from CPM calculations have been exported to a more rigorous simulation program, Aspen Plus®. For input into Aspen Plus®, the same feed conditions were used with the following input data $D = 0.382$ mol/s, $R_{\Delta R} = 2.65$ with 15 stages in the first, uppermost CS, five stages in the second CS,

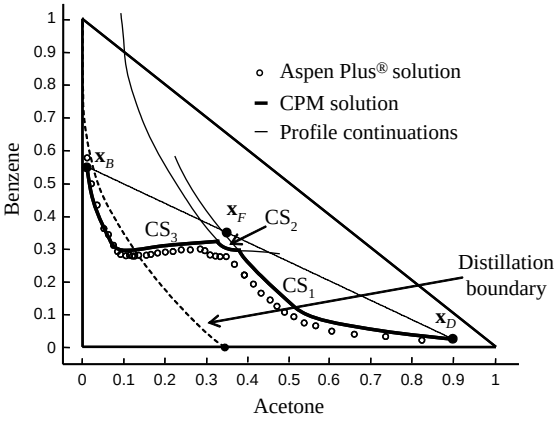


FIGURE 6.13 A distributed feed column at minimum column reflux for acetone/ benzene/ chloroform system with a feed distribution of [0.5, 0.5]. Solid profiles indicate CPM profiles while circles indicate Aspen generated compositions.

and 20 stages in the bottommost CS. Compositions generated on each stage using the RADFRAC distillation simulation block agrees quite well with the CPM profiles, indicated by the circles. The reader is urged to also validate these results in Aspen Plus®, or any other appropriate simulation package.

Discrepancies between the two designs may be attributed to the assumption of constant molar overflow in the CPMs or that the feed stages have not been exactly matched. Although it is not a general rule that distributed feed columns will make apparent infeasible separations feasible, it is evident that there are significant opportunities. It should be noted that although the agreement is strong between the Aspen Plus® and CPM predictions, it is difficult to identify interesting designs by solely relying on Aspen Plus® due to its black-box approach. Again, one should not discount the potential of a particular design based on the properties of an RCM or the behavior of a simple column.

6.2.5.4 Limitations Although it seems that distributed feed columns are a simple means for obtaining savings across the board, it is important to point out that there are limitations to its applicability. These limitations pertain specifically to sharp split product specifications. Firstly, the sharper the product specifications become, that is, the closer the products move to the edges of the MBT, the more the composition profiles lie on the TTs of the respective CSs. If the product specifications lie exactly on the edges of the MBT, the column can be designed without constructing profiles by integrating the DPE as one only has to consider the overlapping of TTs, as discussed in Chapter 5 and shown in Figure 6.14.

WWW

TUTORIAL 6.4

Try this for yourself: Find similar sharp split designs like that shown in Figure 6.14a using DODS-DiFe or DODS-SiCo and the TT design option.

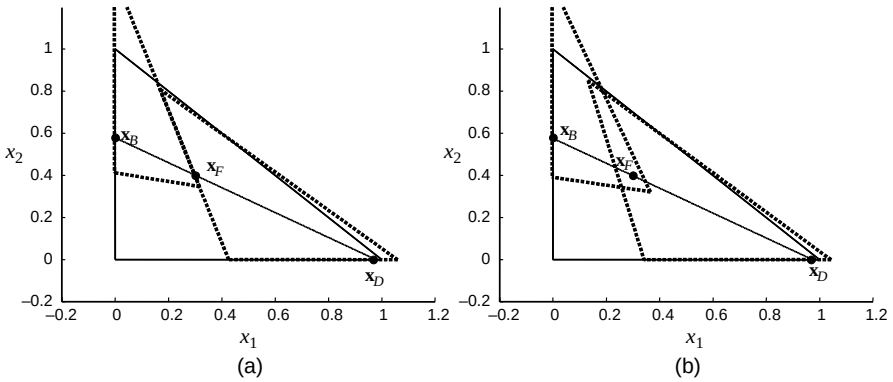


FIGURE 6.14 Feasible sharp split simple column designs at (a) minimum reflux and (b) above minimum reflux.

Notice that the profiles running from both product specifications in Figure 6.14a and b run along the edges of the respective TTs and, thus, run exactly through their saddle points too. These profiles that run straight through the saddle points require an infinite number of stages because the saddle point is a pinch point. Since these profiles *always* have to run through the saddle points, regardless of the feed policy, this infinite stage condition is unavoidable. This is true even when the column is operating above minimum reflux (Figure 6.14b) Thus, for sharp splits, there are no advantages in terms of stage reduction and distributing the feed is futile.

The second limitation is associated with lowering the minimum reflux ratio or making infeasible separations feasible at sharp split conditions. We have shown for the general case in Figures 6.9 and 6.10 that these conditions are achievable in non-sharp columns. For sharp split columns, however, if the column reflux ratio is such that the boundaries of the rectifying and stripping TTs border each other (minimum reflux), a situation is reached where a reduction of this minimum reflux ratio will prevent any feasible separation—irrespective of the feed distribution policy. This condition is the absolute two-product column minimum reflux ratio and no feed addition strategy will lower this value. To better explain this, a distributed feed column at sharp split conditions is depicted in Figure 6.15.

WWW

TUTORIAL 6.5

Try this for yourself: Find similar sharp split designs like that shown in Figure 6.15 using DODS-DiFe and the TT design option. Convince yourself of the benefits (if any) of feed distribution in sharp split columns.

Figure 6.15a illustrates that, at minimum reflux conditions, any additional feed stream will merely lie on the boundary where the TTs border each other for the

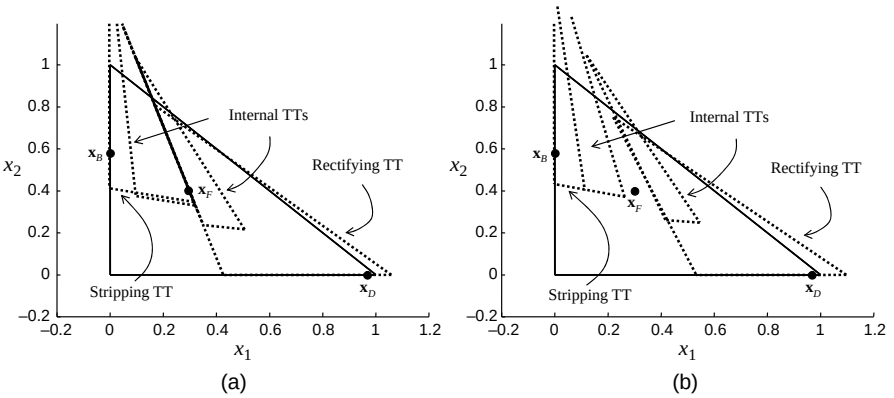


FIGURE 6.15 Distributed feed column at (a) minimum reflux and (b) below minimum reflux.

simple column. For a distributed feed column to be of use the TT of the internal CSs must overlap both product producing CSs. This is never the case for sharp splits at minimum reflux, and Figure 6.15a represents the very best one can do at these conditions. Decreasing the column reflux below minimum reflux has the effect of no bordering or intersection of any TT from any CS whatsoever, thus the column will not be feasible. It is thus impossible to operate below the minimum reflux of a simple column for sharp splits, regardless of feed distribution.

6.2.6 Discussion

This section attempts to highlight the interesting alternatives that may be open to the designer by merely considering alternative feed policies. There are significant benefits from both a reflux and stage requirement perspective in creating CSs which allow for extra degrees of freedom to manipulate profiles. We have even made apparent infeasible simple column designs feasible, by showing a case where it is possible to separate past a distillation boundary. Importantly, using the CPM method, we are able to attain very useful design information that would traditionally have taken very long. For instance, even with the multiple feed problems, we can determine the exact location of all the feed points by simply tracing the stage number down the length of the column, without expending much computational effort. Even very advanced and rigorous simulation packages require some insight into the location of feed streams. Thus, the CPM design method is very well suited to be used either on its own or in conjunction with simulation packages.

It should be noted that we have only looked at evenly distributed feed columns, that is, the feed stream is divided into equal substreams. Feed streams can, of course, be split into different fractions, and sometimes, different compositions, and liquid fractions too. A case where there are different quantities of feed distributed is discussed in the following example.

WWW

Example 6.1: Suppose you have two incoming process streams with the same purity of [0.4, 0.3] but with flowrates of $F_1 = 0.7$ mol/s and $F_2 = 0.3$ mol/s. We would like to obtain a distillate stream with a purity of [0.95, 0.01] and the bottoms product should only contain 0.01 of lights. From purely an energy point of view, is it better to (a) combine the streams and purify them in a simple column or (b) feed a distributed feed column in their given proportions? Note that to test option (b), both alternatives should be considered – that is, which stream should be sent to the top of the column, F_1 or F_2? The relative volatilities can be assumed as [5, 1, 2]. Use the DODS-DiFe package to solve this problem.

Solution 6.1: The first step in this design is determining the overall material balance so that the exact product compositions may be known from which to construct profiles. Doing this we find that

- $D = 0.415$ mol/s, $\mathbf{x}_D = [0.95,\ 0.01]$, and
- $B = 0.585$ mol/s, $\mathbf{x}_B = [0.01,\ 0.51]$.

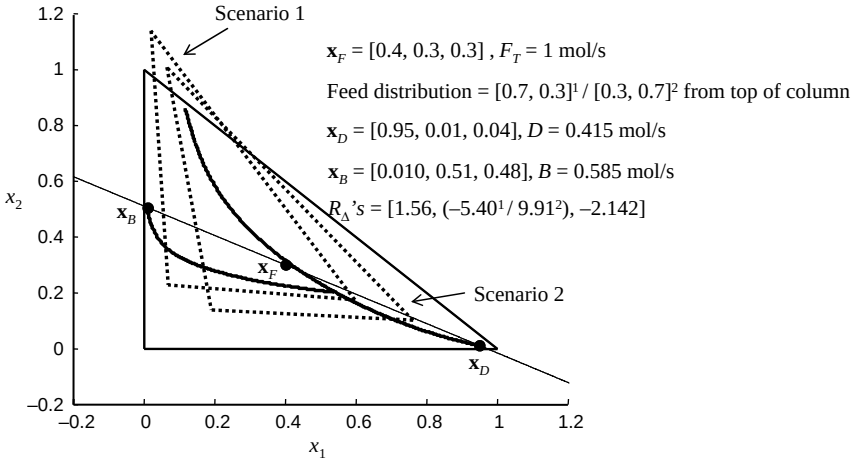


FIGURE 6.16 A simple column at minimum reflux with $\mathbf{x}_D = [0.95, 0.01]$, $\mathbf{x}_B = [0.01, 0.51]$, and [0.4, 0.3], together with the TTs of two different distributed feed cases (superscripts denote each respective scenario).

From this we can determine all the remaining internal column variables such as R_Δ's and $\mathbf{X}_\Delta$'s by choosing a reference reflux. Since we are only concerned here with comparing the energy demand, which relates to the reflux ratio, it is important to know what the minimum reflux is of the simple column. The simple column is essentially a column producing the aforementioned products but with a single feed of 1 mol/s. Using the techniques laid out in Chapter 5, along with the accompanying DODS-SiCo package, we find that minimum reflux in the simple column corresponds to $R_{\Delta R} = 2.02$. Thus, using now the DODS-DiFe package, we need to determine whether distributed feed offers any reduction on this number and if so, how the feed should be distributed. Figure 6.16 shows the profiles of the simple column at minimum reflux as well as both distributed feed scenarios. Scenario 1 is where stream F_1 is fed to the top of the column, while scenario 2 is where stream F_2 is fed to the top.

It is blatant that both scenario 1 and 2 are feasible as both the TTs from the internal CSs overlap the product producing profiles. The vertices of both these TTs are located some way from the profiles; therefore, a reduction in the reflux for both scenarios will have energetic advantages and still be feasible. However, it would seem that the second scenario may be more beneficial than the first, because its TT's vertex is located further away from the profiles. We can proceed to determine what the minimum reflux conditions of the distributed feed columns are. We thus have to find the reflux values that will result in either of TT's vertices lying precisely on a profile. This is shown in Figure 6.17a and b for Scenario 1 and 2, respectively.

Scenario 2 is able to achieve minimum reflux value of 1.37, considerably lower than both the simple column with a minimum reflux of 2.02 or Scenario 1 with a minimum reflux of 1.83. This constitutes a considerable energy saving. It should

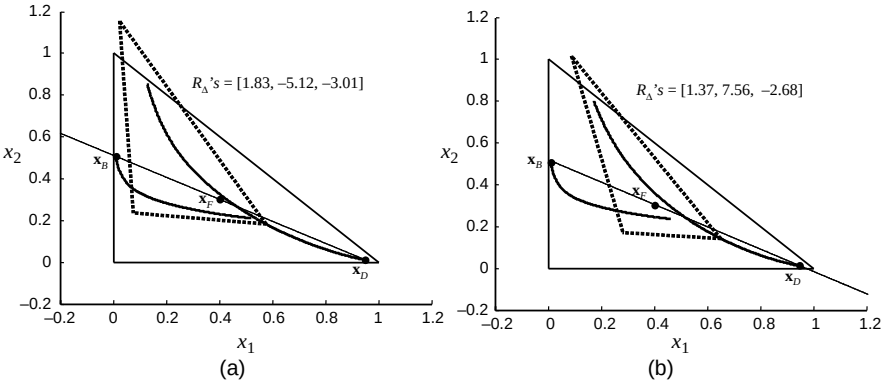


FIGURE 6.17 Minimum reflux designs for (a) Scenario 1 and (b) Scenario 2 in Example 6.2b.

however be mentioned that these designs represent pinched designs, meaning that they would require an infinite number of stages.

6.3 SIDESTREAM WITHDRAWAL

In all the systems considered so far, we have only been concerned with obtaining a relatively pure distillate or bottoms stream. However, in ternary systems, for example, it is often desirable to obtain three relatively pure products. The traditional approach for achieving this has been with a sequence of simple columns, although this has obvious disadvantages to it, because to achieve this separation at least two separate columns have to be erected (refer to Section 2.6.4); meaning an increase in both capital and operating costs. The removal of a sidestream product from the main column may however be more advisable in certain instances.

Sidestream removal is, in principle, the reverse process of distributed feed addition and can as such be treated in much the same way. Other works have in fact shown that a relatively high purity of intermediate component(s) can be achieved by drawing off a sidestream from the main column body [4]. With this being said, the energy expenditures associated with obtaining a high-purity sidestream product are relatively high, as will become apparent in this section. Sidestreams may be located either above or below a feed point, which will accordingly influence the presence of impurities in the sidestream. Drawing product from above the feed, adjacent to the topmost rectifying section, will result in a higher impurity level of lighter components, while drawing product from below the feed, adjacent to the bottommost stripping section, will result in the sidestream product containing heavier components [5]. In this section, only liquid stream withdrawals will be treated as these are the most common due to the ease of handling and transporting liquid streams, although the arguments can easily be extended to vapor stream removal columns. A

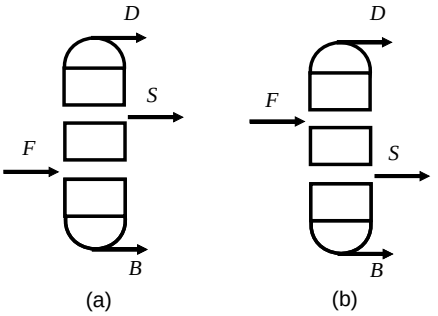


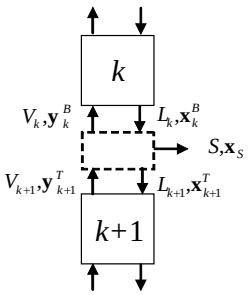
FIGURE 6.18 A schematic representation of a sidestream column and accompanying CS breakdown with the side-products located (a) above and (b) below the feed stream.

sidestream withdrawal column is shown in Figure 6.18a and b where the side product, *S*, is located above and below the feed point, respectively.

6.3.1 Refluxes and Difference Points

The sidestream column can be broken into a series of CSs in an analogous manner to Figure 6.1. Since sidestream withdrawal is essentially the reverse of multiple feed additions, the difference points obey the same linear mixing laws as shown in Figure 6.19. Therefore, all difference points and compositions are linked to each other via straight lines in composition space.

Although the movement $\mathbf{X}_{\mathbf{\Delta}}$ seems directly analogous to the distributed feed case, the behavior is quite different in composition space, mainly because the removal of sidestream product restricts the movement of $\mathbf{X}_{\mathbf{\Delta}}$ to lie within certain bounds. For example, if we consider Figure 6.18a along with the component balances across the feed and sidestream points in Figure 6.3 and Figure 6.19, respectively, it may be seen that the $\mathbf{X}_{\mathbf{\Delta}}$ of the internal CS located between the stream addition and removal have to satisfy two linear constraints imposed by



$$L_k\mathbf{x}_k^B + V_{k+1}\mathbf{y}_{k+1}^T - S\mathbf{x}_S = L_{k+1}\mathbf{x}_{k+1}^T + V_k\mathbf{y}_k^B$$

Rearranging:

$$V_{k+1}\mathbf{y}_{k+1}^T - L_{k+1}\mathbf{x}_{k+1}^T - S\mathbf{x}_S = V_k\mathbf{y}_k^B - L_k\mathbf{x}_k^B$$

$$\Delta_{k+1}\left(\frac{V_{k+1}\mathbf{y}_{k+1}^T - L_{k+1}\mathbf{x}_{k+1}^T}{\Delta_{k+1}}\right) - S\mathbf{x}_S = \Delta_k\left(\frac{V_k\mathbf{y}_k^B - L_k\mathbf{x}_k^B}{\Delta_k}\right)$$

Therefore,

$$\Delta_{k+1}\mathbf{X}_{\Delta k+1} - S\mathbf{x}_S = \Delta_k\mathbf{X}_{\Delta k}$$

FIGURE 6.19 Magnified view of CS_{k+1} and CS_k with all stream definitions and a component balance for a generic sidestream withdrawal.

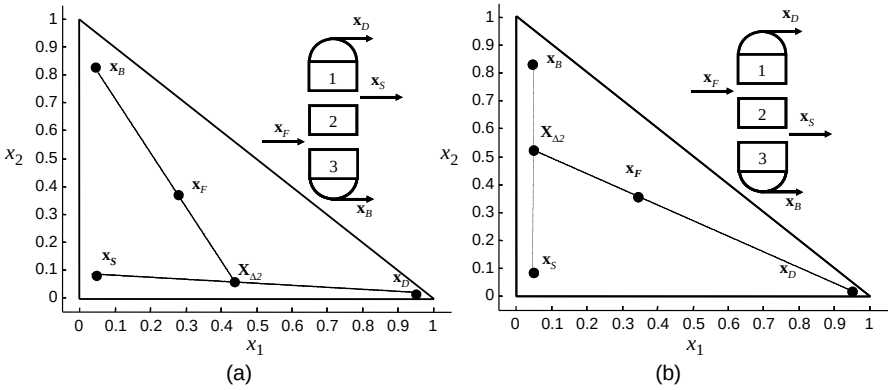


FIGURE 6.20 Geometric representation of $\mathbf{X}_{\Delta}$ movement for a sidestream withdrawal column with the side-products located (a) above and (b) below the feed stream.

adjacent CSs. First, this $\mathbf{X}_{\boldsymbol{\Delta}}$ has to lie on the straight line running through the distillate and the sidestream product compositions (Figure 6.19). Second, the same $\mathbf{X}_{\boldsymbol{\Delta}}$ has to lie on the straight line running through the feed composition and the bottoms product compositions. Therefore, it may be said that side-draw systems are somewhat more constricted in terms of creative $\mathbf{X}_{\boldsymbol{\Delta}}$ placement—all $\mathbf{X}_{\boldsymbol{\Delta}}$'s are required to lie inside the MBT. A geometric representation of the $\mathbf{X}_{\boldsymbol{\Delta}}$ behavior explained here is shown in Figure 6.20.

Assuming that only liquid products are being drawn off, it is also possible to obtain a qualitative understanding of the effect of sidestream withdrawal on the reflux ratio. Each liquid withdrawal increases the net flow from one CS to the next, as the quantity $V - L$ becomes larger.

6.3.2 Preliminary Design Considerations

While the similarities between distributed feed and sidestream withdrawal columns are evident, they do have a fundamental difference which makes the design procedure somewhat different. In essence, the sidestream column requires that a profile from a terminating CS has to run through the sidestream composition. This complicates matters somewhat because from a certain initial integration composition, say the distillate product, there is not necessarily a single profile that will satisfy the product specification in the sidestream too. We cannot adopt the traditional boundary value method approach [6] because, in this case, all the product streams are not boundary conditions. For example, if we consider the structure in Figure 6.18a, note that the profile running from the distillate composition has to also run through the sidestream composition. Thus, it is impractical to specify all the products *a priori*, since the profile running from the distillate composition may be nowhere near the specification we would like to achieve for the sidestream. We have to therefore devise a new design strategy to combat this. To visualize the problem at

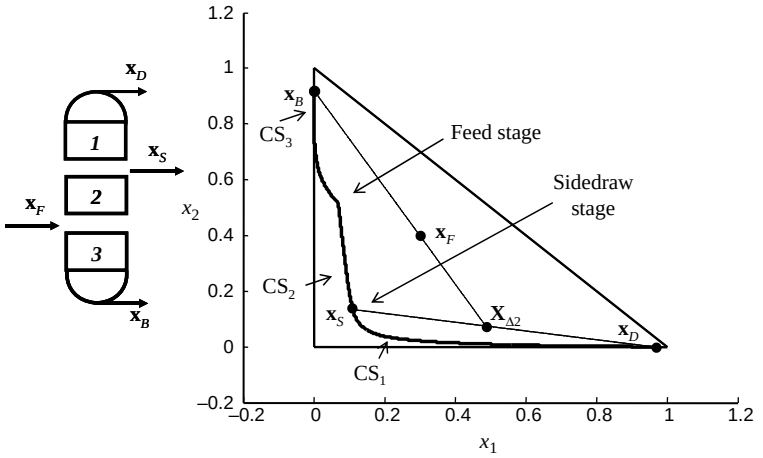


FIGURE 6.21 A feasible sidestream withdrawal column.

hand more clearly, Figure 6.21 shows a realizable sidestream withdrawal column indicating all difference points and product specifications.

Figure 6.21 illustrates more clearly what the problem is that we are faced with, as the sidestream composition lies exactly on the distillate terminating profile and cannot be arbitrarily chosen before the profile is known. Once the sidestream composition has been established by viewing the neighboring profile, integration can be initialized from this point and an intersection can be found with the bottoms termination profile. The bottom half of the column is essentially equivalent to designing a simple column—with the sidestream product acting as a distillate product. There is however a fundamental difference because the sidestream composition is not equal to $\mathbf{X}_{\Delta}$ of the internal CS in this case because its CS is not terminated by a reboiler/condenser. Thus, integration does not initiate from $\mathbf{X}_{\Delta}$, but from $\mathbf{x}_S$.

Moreover, it is obvious that the distillate and sidestream compositions are closely linked to each other, and therefore, the operating reflux of the topmost CS too (in the case where the sidestream is above the feed). In this case, the topmost CS has to, in fact, produce two products, namely $\mathbf{x}_D$ from its top and $\mathbf{x}_S$ from its bottom. Therefore, the column profile for the rectifying section has to pass through both these compositions. While $\mathbf{x}_D$ may be fixed, the trajectory of the profile, and hence the location of $\mathbf{x}_S$ is affected by the reflux ratio used. Figure 6.22a shows the effect of reflux on the potential sidestream composition from a certain distillate composition. Note that the higher the reflux becomes, more pure intermediate products are attainable. The extreme case of infinite reflux corresponds to the purest attainable sidestream product from a particular, set distillate composition (or equivalently, the bottoms composition in Figure 6.18b scenario). The shaded triangular region is a region where x_3 is greater than 0.9. Figure 6.22b shows, for the same distillate composition in Figure 6.22a, what the best attainable intermediate component purity

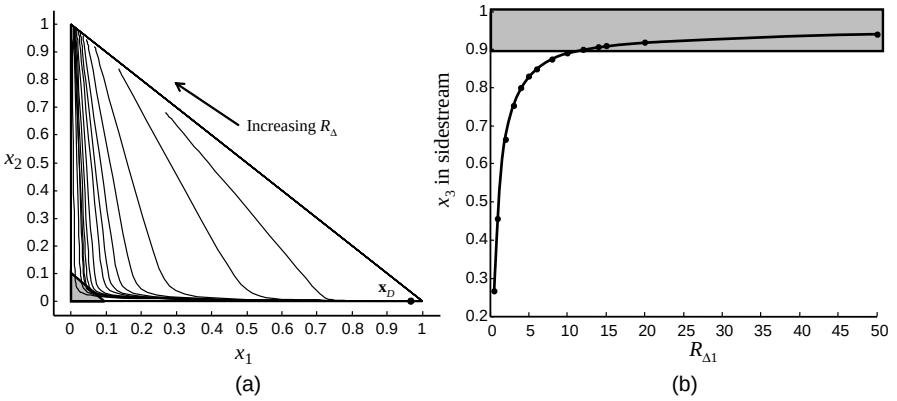


FIGURE 6.22 For $\boldsymbol{\alpha} = [6, 1, 3]$ and $\mathbf{x}_D = [0.95, 0.005]$: (a) The effect of reflux on the composition profiles and (b) the ma**x**imum purity of x_3 in the sidestream.

(x_3) is in the sidestream. The shaded area in Figure 6.22b shows refluxes where the same criterion of $x_3 > 0.9$ in the sidestream has been met.

WWW

TUTORIAL 6.6

Try this for yourself: Reproduce the relationship depicted in Figure 6.22a using the given parameters. Try and establish similar relationships for different product compositions and $\boldsymbol{\alpha}$ values.

It is evident from Figure 6.22a and b why it expensive to obtain a high-purity sidestream composition from a single column shell. Additionally, note that it is imperative that the right number of equilibrium stages is selected for this CS. If there are too few stages, the profiles will not reach the desired intermediate composition because the profile coming from the distillate will have terminated too early. On the other hand, if there are too many stages before the sidestream is removed, the profile may run past the desired product composition. Therefore, the stage numbers are an important design variable to be aware of, perhaps more important than in other designs. Again, this can be easily determined by tracking the stage progression along the profile.

Another insight that may be gleaned from Figure 6.22 is that in order to achieve a high-purity sidestream product, it is important that the distillate stream, in the case where the feed is below the side draw, be greatly depleted in high boiling components. The closer we can push the distillate composition to the x_1 (light component) axis, the "easier" it becomes for profiles to reach the necessary intermediate composition. Figure 6.23 shows how the best possible intermediate composition in the sidestream, that is, at infinite reflux, changes as a function of the mole fraction of high-boiling component in the distillate stream. Thus, in order to achieve a

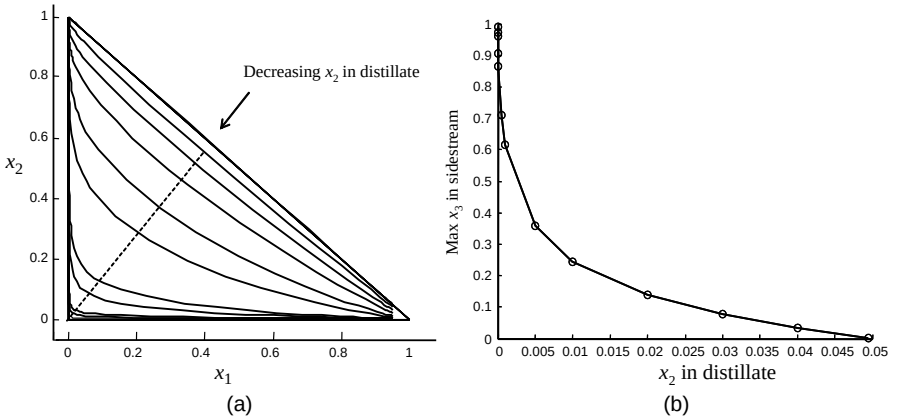


FIGURE 6.23 For $\boldsymbol{\alpha} = [6, 1, 3]$ and $x_{D1} = 0.95$: (a) The effect of distillate product purity on the best potential sidestream composition and (b) the maximum purity of x_3 in the sidestream from a set distillate at different x_2 impurities in the distillate.

high-purity intermediate product specification in the sidestream, it is advisable that the distillate stream be quite depleted of high-boiling components, or else one may need to operate at excessively high reflux ratios. A similar argument can be made for the bottoms product specification in Figure 6.18b.

6.3.3 Design Procedure

The preceding discussions put forward the fundamental ideas and issues involved in sidestream column design. We can now formulate a design procedure based on these discussions. The first step is to determine whether the feed should be located above or below a feed stream. This is important because we need to know which product producing CS is adjacent to the sidestream product. When the sidestream is drawn above the feed, the distillate product should be set and profiles constructed from this composition (as shown in Figure 6.22) at varying refluxes, to determine which reflux gives satisfactory intermediate compositions. In the case where the sidestream is below the feed and adjacent to the bottom CS, profiles should be constructed from the bottoms composition toward the appropriate intermediate purity in the sidestream. In the latter case, one should remember that the bottommost CS is a stripping section and therefore negative refluxes have to be selected.

Once a suitable reflux has been chosen that will produce the desired sidestream purity, the design procedure is very much the same as for simple columns. The sidestream product is then known and we can proceed to determine the mass balance for the entire column, that is, calculate the bottoms, sidestream(s), and distillate compositions and flowrates. In general, for a system containing nc components with a product stream for each component, there are nc^2 free variables. There are however nc independent mass balances which can be written and therefore there are then

generally $nc(nc-1)$ degrees of freedom that need to be set, assuming the feed composition is known. For the ternary system under consideration here, there are thus six variables to be set—typically the compositions of each stream.

Having determined all the product compositions and flowrates allows one to also determine all the refluxes and difference points of the entire column, and the design can commence with the same basic procedure as simple columns. We simply have to integrate from the sidestream composition and see whether there is an intersection with the profile of the remaining CS. To summarize this procedure and put it more clearly, a stepwise procedure is shown below:

1. Specify the structure and CS breakdown and decide whether the feed should be above or below the feed stream, based upon which impurity (low or high boiling component) is less desirable in the feed.
2. Identify the product composition of the product producing CS adjacent to the sidestream.
3. Determine which reflux (positive for rectifying and negative for stripping CSs) will result in a suitable intermediate product composition by integrating the DPE from top/bottommost CSs product composition.
4. Identify the exact composition where the profile produced in nr.3 should terminate (or alternatively, specify the stage number where the profile should terminate)
5. Specify and determine all remaining product compositions and flows.
6. Determine all remaining R_Δ's and $\mathbf{X}_\Delta$'s
7. Determine whether all remaining profiles intersect one another. If there is no intersection, return to the previous steps until a feasible design is found.

One significant difference between sidestream columns and all of the other columns encountered thus far, is that R_Δ's affect the product compositions and flows. By choosing a different reflux in step 3 of the design procedure given above, a different intermediate composition will arise and therefore all the other associated mass balance traits of the system. It is also important to note that due to the removal of product, the top and bottommost CSs reflux ratios are not proportional to each other, as with simple columns. In simple columns, a low reflux in the rectifying CS (low condensing load) implies a low reflux in the stripping section (low reboiler load). This relationship does not necessarily hold because it is dependent on how much product is being removed from the column in the side draw. One should be wary of this fact when discriminating between designs. Below is a worked example which outlines the design procedure more clearly.

Example 6.2: Suppose an upstream reactor produces, due to kinetic limitations, a rather impure product with a composition of approximately [0.3, 0.3] at an overall flowrate of 1 mol/s of a certain system that can be modeled using constant relative volatilities. Each of these components is however valuable in their own right when they are relatively pure, and hence need to be separated. Investigate which of the two

configurations in Figure 6.18 will result in a lower reboiling load, given the following data:

- $\mathbf{x_D}$ should have a purity of [0.92, 10^{-5}]
- $\mathbf{x_B}$ should have a purity of [10^{-5}, 0.90]
- The sidestream should have a purity of *at least* 0.9 intermediate
- Volatilities can be assumed as [3, 1, 2]

Solution 6.2: We first consider the scenario where the feed is below the sidestream product. Thus, we use the distillate purity as the initial integration composition from the top of the column. By guessing ever increasing values for the reflux ratio in the topmost CS, it is possible to eventually find a reflux ratio that will allow this profile to enter the sidestream purity level. This is illustrated in Figure 6.24. Figure 6.24 shows that the first reflux that achieves a composition of 0.9 intermediate is extremely high at 65. The exact composition where this specification is met is: $\mathbf{x}_S = [0.064,\ 0.036,\ 0.900]$.

The mass balance for the column has now been completely specified since all the compositions in all the product streams are known. All product flowrates can therefore also be calculated. In this specific example, it can be shown that: $D = 0.299$, $B = 0.318$, and $S = 0.383$ mol/s. It can then be shown through Figure 6.19 that the difference point of the internal CS, CS_2, is

$$X_{\Delta 2} = \frac{S\mathbf{x}_S + \Delta_1 X_{\Delta 2}}{\Delta_2} = \frac{0.383 \times [0.064, 0.036] + 0.299 \times [0.920, 10^{-4}]}{0.383 + 0.299} \tag{6.4}$$

$$X_{\Delta 2} = [0.440, 0.020] \tag{6.5}$$

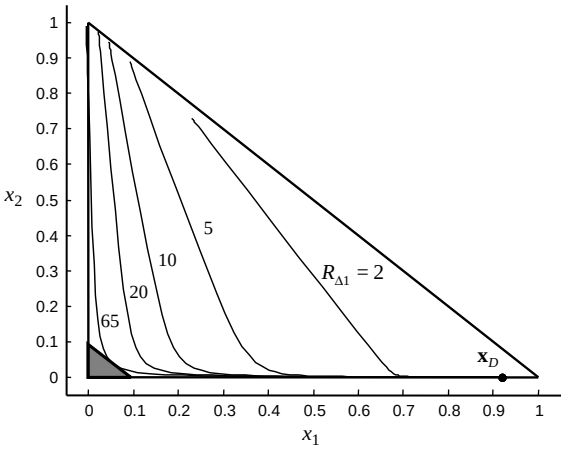


FIGURE 6.24 Effect of reflux ratio on the best attainable sidestream purity.

And that reflux ratio of the internal CS is

$$R_{\Delta 2} = \frac{L_2}{\Delta_2} = \frac{R_{\Delta 1}\Delta_1 - S}{\Delta_1 + S} = 27.98 \tag{6.6}$$

It is also useful to state here the reflux ratio of the bottommost CS as

$$R_{\Delta 3} = \frac{L_3}{\Delta_3} = \frac{R_{\Delta 2}\Delta_2 + Fq}{\Delta_2 - F} = -63.12 \tag{6.7}$$

Remember that the difference point for the bottommost stripping CS is simply equal to its product specification. It is now possible to produce profiles for all CSs because the difference points and reflux ratios for all CSs have been specified, as well as their respective initial integration compositions. It is important to reiterate that the profile for the internal CS, CS_2, will not originate from its difference point, but from the sidestream composition. All that remains now is to check whether the profiles from CS_2 and CS_3 intersect. Indeed these two profiles intersect on another; the final design is shown in Figure 6.25.

Clearly a feasible design has been found for this system. It is now necessary to check whether the case when the feed is above the sidestream offers any advantages. The design procedure is in fact exactly the same as the one described here. The only significant difference is that we have to work our way from the bottom of the column upward. Thus, starting with the bottoms product specification, a reflux in the bottommost CS is found by trial and error that satisfies the sidestream product specification. The first value for $R_{\Delta 3}$ that satisfies this condition is approximately -40, resulting in a sidestream composition of $\mathbf{x}_S = [0.023, 0.077, 0.900]$. Again, all parameters in the column are now automatically specified once this composition is known. All that remains now is to check whether there is a profile intersection between the internal and the topmost CS, as shown in Figure 6.26.

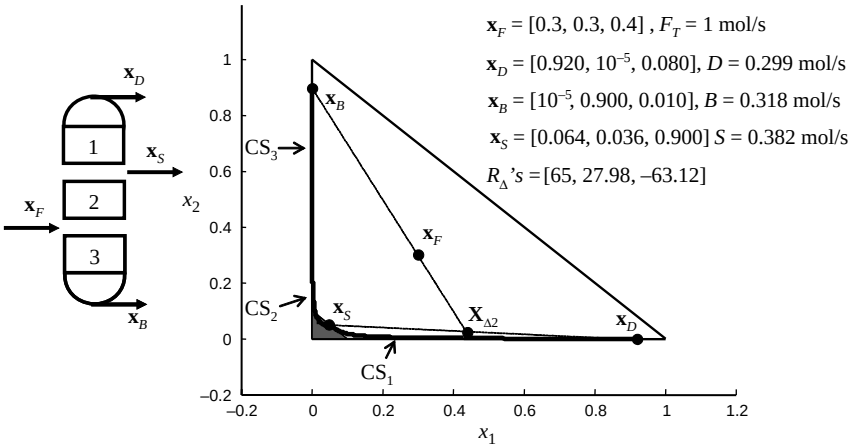


FIGURE 6.25 Final design for the feed below the sidestream.

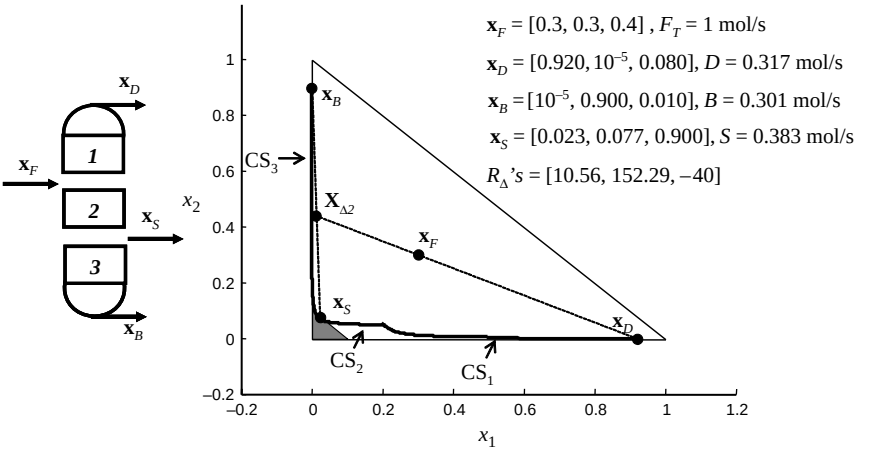


FIGURE 6.26 Final design for the feed above the sidestream.

Since the problems asks to identify the design shown with the lowest reboiling load, such that a composition in the sidestream be 0.90 irrespective of high/low boiling impurities, it is clear that the design shown in Figure 6.26 is superior because the reflux ratio in the structure's bottommost CS is −40, compared to that of Figure 6.25's of −63.12. Notice also the impurity levels in the sidestream for each structure—in Figure 6.25 there is more of x_1 in the sidestream, while in Figure 6.26 there is more x_2.

6.4 THERMALLY COUPLED COLUMNS: SIDE RECTIFIERS AND STRIPPERS

Another area in distillation that has received considerable attention for its ability to reduce both capital and operating costs is thermally coupled distillation. Thermally coupled distillation essentially entails transferring vapor and liquid streams between columns, allowing one to eliminate one or multiple energy inputs to obtain pure intermediate component(s). Although intermediate components may be removed from one column, as shown in the preceding section on sidestream withdrawal columns, it is particularly expensive to obtain a high purity of intermediate component(s) in a single column structure. Thermally coupled distillation thus offers another alternative, apart from the traditional column sequences, to this common problem in separation synthesis. The simplest means of thermal coupling is a side rectifying or stripping unit attached to a main column which allows for this transfer of material, but many more complex structures using this same principle exists, most notably the Petlyuk-type column (Chapter 7). The side stripping column has been extensively employed in petroleum refineries [7], while the side rectifier columns have found application in air separation [8] as well as replacing entrainer regeneration columns in extractive distillation operations [9].

6.4.1 Column Section Breakdown

As with the other configurations discussed so far, the first step in applying the CPM technique is breaking the proposed structure into a sequence of CSs. The CS breakdown for both the side stripper and rectifier configurations is shown in Figure 6.27.

Both configurations can be divided into four CSs for the case of a ternary system where we wish to obtain relatively pure distillate, bottoms, and sidestream products. For the sake of consistency, the side unit has been numbered as CS_4 while the internal CS is labeled as CS_2 in both configurations. In the side-stripper unit, the liquid coming from CS_1 is divided into two streams—one that is directed to the main column body and another one that is directed toward the side-stripping unit. The vapor flow in CS_1 is also the sum of the vapor flows from the side stripping unit and the main column. Similarly, the vapor flow from CS_3 in the side rectifier is directed toward the main column and the rectifying unit, while the liquid flowrate in CS_3 is the sum of the liquid flowrates in the main column and the rectifier. The location of the sidestream withdrawal and addition at the thermally coupled junction are assumed to take place at the same location. This assumption can be relaxed; however, an additional CS would be created and this case will not be further discussed in this text.

Note that in each structure there are only three utility inputs: two reboilers and a condenser in the side stripper and two condensers and a reboiler in the side rectifier. The classic means for obtaining high-purity intermediate components via a column sequence requires in total four utility inputs, that is, a condenser and reboiler for each column in the sequence. This reduction in utility inputs may result in both a capital and energy saving. It is furthermore interesting to note that both these configurations contain four CSs, the exact number of CSs that the simple column sequence would have had. In fact, any thermally coupled arrangement such as those depicted in Figure 6.27 will have the same number of CSs regardless of the number of

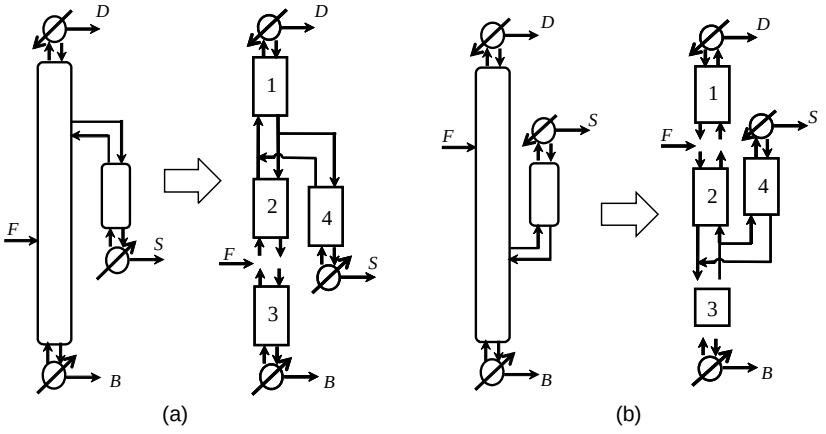


FIGURE 6.27 CS breakdown of a (a) side-stripper column and (b) a side rectifier configuration.

components. An *nc* component system requires $2(nc-1)$ CSs in both the simple column sequence and the side rectifier/stripper arrangement to obtain *nc* product streams. Note that this rule does not apply to fully thermally coupled arrangement discussed in Chapter 7.

6.4.2 Degrees of Freedom

In terms of CPM distillation design, there are generally two distinguishable types of degrees of freedom. First, there are external degrees of freedom which are generally product compositions or flowrates. The total number of external degrees of freedom is dependent on the number of components that are present and the number of desired product streams. Since these thermally coupled systems are equivalent to the side-draw column with regard to input and output streams, the external degrees of freedom in both these systems are equivalent. The reader is thus referred to Section 6.3.3.

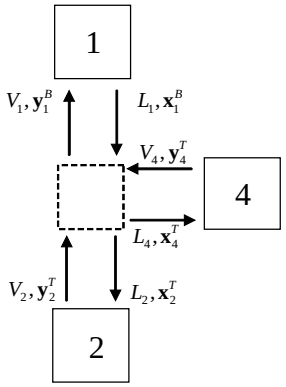
The internal degrees of freedom, on the other hand, are concerned with the internal workings of the column. The columns we have dealt with up to this point only had one internal degree of freedom—a single reflux ratio of a particular CS, which then allows one to infer all remaining column parameters. However, thermally coupled columns are fundamentally different from this point of view because there is a degree of freedom associated with each side unit. In other words, the designer may specify the reflux in the side unit's CS as well as the reflux of a CS in the main column independently of one another, which will subsequently specify the flows and refluxes in the remainder of the column. Thus, a three component thermally coupled system with one thermally coupled unit requires two refluxes to be specified.

6.4.3 Difference Points

The complex columns discussed thus far, although different structurally, all have a recurring property in that the difference points of adjacent CSs are linearly linked to one another. Since the thermally coupled junction is also merely a stream addition and removal operation, we can expect similar behavior for these types of structures too. The relationship between thermally coupled sections is derived in Figure 6.28a for a side stripper, and Figure 6.28b for a side rectifier (with the CSs as numbered in Figure 6.27) with a mass balance around the dashed control volume. Again, the $\mathbf{X}_{\Delta}$ relationship between neighboring CSs is linear, mimicking real compositions. A geometric representation of a typical $\mathbf{X}_{\Delta}$ placement for both the side rectifier and stripper is shown in Figure 6.29, including the mass balance around the feed addition point in each scenario.

Interestingly, the placement for $\mathbf{X}_{\Delta}$ in the thermally coupled arrangements is qualitatively similar to the sidestream withdrawal columns (refer to Figure 6.20). The difference point of the internal CS ($\mathbf{X}_{\Delta 2}$), in both cases, has to lie between to product producing CSs (by mass balance—see Figure 6.28) and therefore has to lie in positive composition space since real compositions are naturally forced to. Again, this means that the design is somewhat more constricted by potentially useful CPM

(a) Side stripper:



$$L_1\mathbf{x}_1^B + V_2\mathbf{y}_2^T + V_4\mathbf{y}_4^T = L_2\mathbf{x}_2^T + V_1\mathbf{y}_1^B + L_4\mathbf{x}_4^T$$

Rearranging:

$$V_2\mathbf{y}_2^T - L_2\mathbf{x}_2^T = V_1\mathbf{y}_1^B - L_1\mathbf{x}_1^B - V_4\mathbf{y}_4^T + L_4\mathbf{x}_4^T$$

$$\Delta_2\left(\frac{V_2\mathbf{y}_2^T - L_2\mathbf{x}_2^T}{\Delta_2}\right) = \Delta_1\left(\frac{V_1\mathbf{y}_1^B - L_1\mathbf{x}_1^B}{\Delta_1}\right) - \Delta_4\left(\frac{V_4\mathbf{y}_4^B - L_4\mathbf{x}_4^B}{\Delta_4}\right)$$

Therefore,

$$\Delta_2\mathbf{X}_{\Delta 2} = \Delta_1\mathbf{X}_{\Delta 1} - \Delta_4\mathbf{X}_{\Delta 4}$$

Now

$$\Delta_1 = V_1 - L_1 = D \text{ and } \Delta_4 = V_4 - L_4 = -S$$

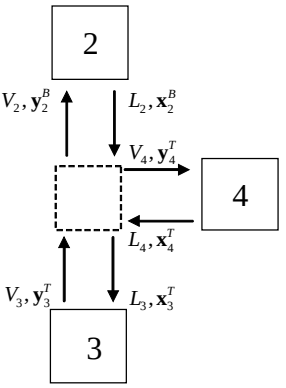
And

$$\mathbf{X}_{\Delta 1} = \mathbf{x}_D \text{ and } \mathbf{X}_{\Delta 4} = \mathbf{x}_S$$

Hence,

$$\Delta_2\mathbf{X}_{\Delta 2} = D\mathbf{x}_D + S\mathbf{x}_S$$

(b) Side rectifier



$$L_2\mathbf{x}_2^B + V_3\mathbf{y}_3^T + L_4\mathbf{x}_4^T = L_3\mathbf{x}_3^T + V_2\mathbf{y}_2^B + V_4\mathbf{y}_4^T$$

Rearranging:

$$V_3\mathbf{y}_3^T - L_3\mathbf{x}_3^T = V_2\mathbf{y}_2^B - L_2\mathbf{x}_2^B + V_4\mathbf{y}_4^T - L_4\mathbf{x}_4^T$$

$$\Delta_3\left(\frac{V_3\mathbf{y}_3^T - L_3\mathbf{x}_3^T}{\Delta_3}\right) = \Delta_2\left(\frac{V_2\mathbf{y}_2^B - L_2\mathbf{x}_2^B}{\Delta_2}\right) + \Delta_4\left(\frac{V_4\mathbf{y}_4^B - L_4\mathbf{x}_4^B}{\Delta_4}\right)$$

Therefore,

$$\Delta_3\mathbf{X}_{\Delta 3} = \Delta_2\mathbf{X}_{\Delta 2} + \Delta_4\mathbf{X}_{\Delta 4}$$

Now

$$\Delta_3 = V_3 - L_3 = -B \text{ and } \Delta_4 = V_4 - L_4 = S$$

And

$$\mathbf{X}_{\Delta 3} = \mathbf{x}_B \text{ and } \mathbf{X}_{\Delta 4} = \mathbf{x}_S$$

Hence,

$$-\Delta_2\mathbf{X}_{\Delta 2} = B\mathbf{x}_B + S\mathbf{x}_S$$

FIGURE 6.28 Magnified view of a (a) side stripper and (b) side rectifier with all stream definitions and a mass balance around the dashed control volume.

topology since all $\mathbf{X}_\Delta$'s have to lie in positive composition space. Importantly, the placement of $\mathbf{X}_\Delta$ does not depend on the chosen operating R_Δ's, only on the product specification of the column.

6.4.4 Refluxes and Net Flow

The parameter R_Δ is particularly difficult to interpret and comprehend in thermally coupled structures since there is a transfer of both liquid and vapor streams at the thermally coupled junction. Although the direction of the bulk material is obvious for the product producing CSs, it is not immediately obvious whether CS_2, for either structure, is in rectifying or stripping mode. In general, it can be shown that there is only one realizable flow pattern for each structure, such that the structure has to

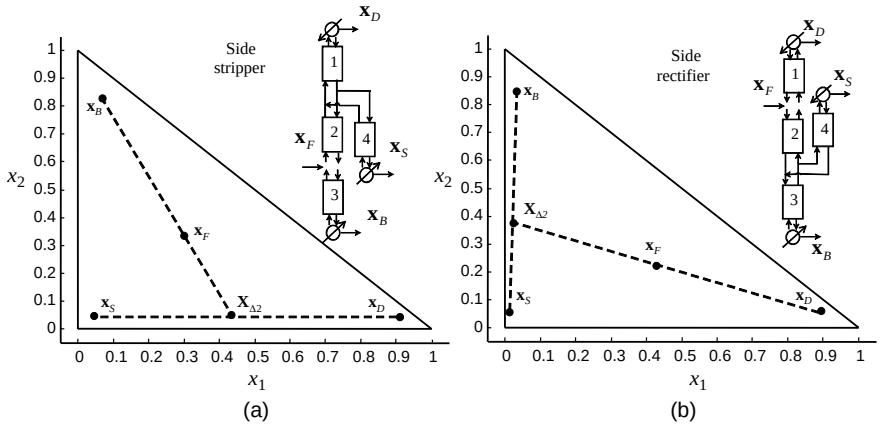


FIGURE 6.29 Geometric representation of $\mathbf{X}_\Delta$ movement for a thermally coupled side (a) stripper and (b) rectifier column.

consist of pairs of rectifying and stripping CSs, meaning that there has to be as many equivalent rectifying CSs as stripping CSs. The proof for this is rather simple:

For the side stripper, it can be shown that

$$\Delta_2 = F + \Delta_3 \tag{6.8}$$

Furthermore, a mass balance around the reboiler results in

$$\Delta_3 = -B \tag{6.9}$$

Since the feed to the column has to be greater than or equal to any product stream ($F \geq B$), one finds that

$$\Delta_2 \geq 0 \tag{6.10}$$

Therefore, the net flow direction in each CS in the side-stripper arrangement shown in Figure 6.30 is the only one that is physically realizable. Furthermore, it can be shown fairly easily that in the side stripper the feed has to lie below the thermally coupled junction. Analogous mass balance arguments can be made for the side rectifier, and its only viable flow pattern is shown in Figure 6.30b.

While the net flows patterns for each structure are now clearer, it still remains difficult to comprehend the effects of changing the reflux in one CS in the rest of the column. The reflux ratio in a specific CS is an important parameter in finding feasible structures and therefore it is necessary to fully understand these effects. As shown in previous chapters, the reflux in a specific CS is a limitless parameter valid anywhere from negative to positive infinity. Notice however that in the side-stripper configuration, for example, that the liquid stream is split into two parts.

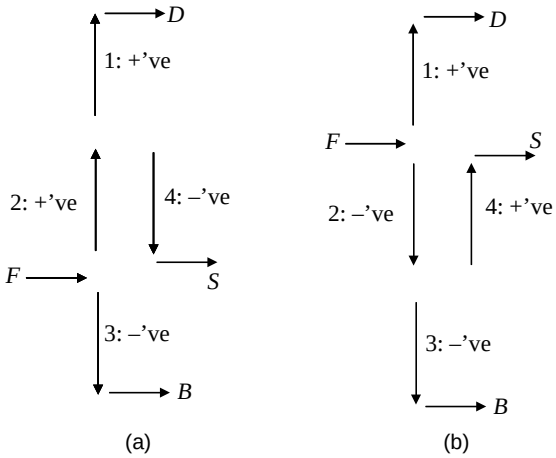


FIGURE 6.30 Net flow directions of respective CSs for the (a) side stripper and (b) side rectifier column.

Thus, it is more suitable to define the flows of the thermally coupled parts of the column in terms of a liquid split ratio, Φ_L. For the side stripping unit, we define a liquid split ratio as

$$\Phi_L = L_4/L_1 \tag{6.11}$$

Similarly for the side rectifying column, a vapor split ratio

$$\Phi_V = V_4/V_3 \tag{6.12}$$

Both these split ratios govern the amount of material sent to the side column and are bound between 0 and 1. Thus, for the side stripper, the refluxes of all the remaining CSs can be determined by specifying the reflux of the topmost CS ($R_{\Delta 1}$), and its associated liquid split ratio, as shown in Equations 6.13–6.15

$$R_{\Delta 2} = \frac{DR_{\Delta 1}(1 - \Phi_L)}{D + S} \tag{6.13}$$

$$R_{\Delta 3} = \frac{Fq + DR_{\Delta 1}(1 - \Phi_L)}{-B} \tag{6.14}$$

$$R_{\Delta 4} = \frac{DR_{\Delta 1}\Phi_L}{-S} \tag{6.15}$$

In the same way, for the side rectifier, all refluxes can be written in terms of the bottommost reflux ($R_{\Delta 3}$) and the vapor split ratio, given in Equations 6.16–6.18

$$R_{\Delta 4} = \frac{S + B\Phi_V(1 + R_{\Delta 3})}{-S} \tag{6.16}$$

$$R_{\Delta 2} = \frac{S + B\Phi_V(1 + R_{\Delta 3}) - BR_{\Delta 3}}{-B - S} \tag{6.17}$$

$$R_{\Delta 1} = \frac{S - Fq + B\Phi_V(1 + R_{\Delta 3}) - BR_{\Delta 3}}{D} \tag{6.18}$$

The two internal degrees of freedom of each column have been specified through the appropriate split ratio and a single, reference reflux. Both $R_{\Delta 1}$ in the side stripper and $R_{\Delta 3}$ in the side rectifier have been chosen as the respective reference refluxes since they lie the closest to the thermally coupled sections. This choice is of course arbitrary, and one may equivalently choose any CS to serve as the reference CS.

6.4.5 General Design Procedure

The criterion for a feasible design in thermally coupled configurations is slightly more involved than other structures, as strictly speaking, one has to take into account whether we are dealing with a vapor or liquid split. Columns that involve a liquid split, as side strippers do, require only finding liquid profile intersections. The reason for this particular composition-matching constraint can easily be seen in Figure 6.27a, where the liquid stream exiting the bottom of CS_1 is split into two fractions, one fraction toward CS_4, and the other toward CS_3. Since the compositions of all these streams have to be the same, it is sufficient to state that we need only consider the liquid composition profiles in these CSs for determining feasibility. Thus, side-stripper design requires no modification to the general design procedures discussed thus far, that is, searching for liquid profile intersection.

As one might suspect, in side rectifier design where there is a vapor split, the design is not necessarily as simple. The vapor split occurring at the top of CS_3 means that *vapor* compositions have to match at this point. Thus, thermally coupled sections, where a vapor split occurs, require that vapor composition profiles match one another. It is to be noted that for the rest of the column, beyond the thermally coupled section, it is still sufficient to find liquid profile intersections. It is evident that switching between vapor and liquid composition profiles diminishes the ease and efficacy of the CPM design method somewhat, especially in columns that have both liquid and vapor splits, like the fully thermally coupled columns (see Chapter 7). However, because the curvatures of vapor and liquid profiles follow each other quite closely we will again, as in the design of simple columns, approximate feasibility by only searching for liquid profile intersections. As shown in Section 5.3.3, this is in general an excellent assumption and significantly reduces the complexity of

calculation and interpretation, especially in more complex columns such as those dealt with here. It has been shown that designs obtained by this assumption still produce an excellent agreement between Aspen Plus® and those generated by the CPM technique [10]. Thus, in all the subsequent designs discussed here, we will only search for liquid profile intersections.

Furthermore, it should be noted that in thermally coupled columns, finding profile intersections is somewhat different from those we have become accustomed to thus far, because at a thermally coupled junction, there are not only two neighboring CSs, but three. Consequently, three profiles, not two, all have to intersect one another at the same point. A typical feasible design for a side-stripper configuration is shown in Figure 6.31.

Figure 6.31 indicates that there is an intersection of the profiles of CS_1, CS_2, and CS_4 at a single point, highlighted by the shaded circle. This point corresponds to the liquid composition at the precise location of the thermal coupling and one can infer the exact stage where this takes place by simply tracking the stage progression along a profile. This is an important consequence of the design because the exact location of the feed stage and thermally coupled stages often requires a significant amount of time and design experience to determine accurately. We are thus able to rationally establish the precise location of the thermally coupled section. Note that the internal CS mainly serves as a link between the remaining product producing profile and this profile. The reader is urged to use the DODS-SiSt package to reproduce this design.

An interesting result that stems from Figure 6.31 is that since there are essentially two points of profile intersection, there are also two possibilities of a pinched column. If either of these intersections is brought about by one profile *just* touching the other, this section would be at minimum reflux and require an infinite number of

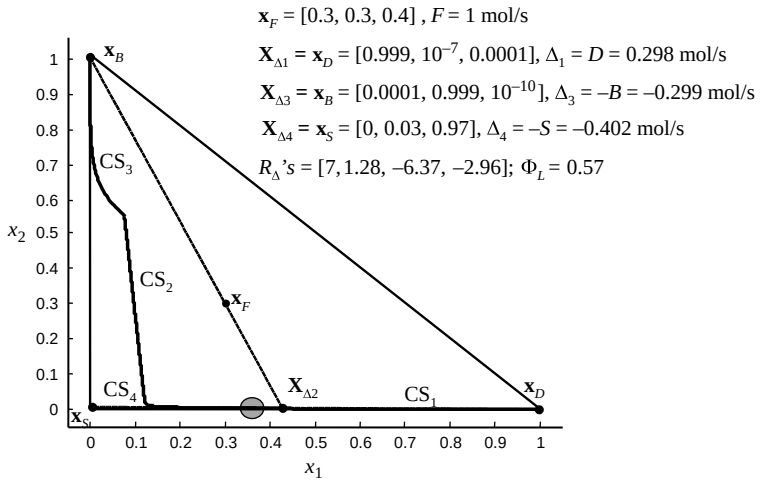


FIGURE 6.31 A typical feasible design for a side-stripper configuration with $\boldsymbol{\alpha} = [5, 1, 2]$.

stages or said to have pinched. Thus, there are a plethora of minimum reflux solutions, although not all of them correspond to the minimum energy requirement as with simple columns. For example, one may choose a very high reflux in $R_{\Delta 1}$, but choosing a certain split ratio will lead to some CSs tending toward pinched designs.

It is evident that thermally coupled columns are more difficult to design than other complex columns discussed in this chapter because firstly, there are additional degrees of freedom making finding a feasible design more difficult, and secondly, changing either one of these degrees of freedom has multiple effects on the column. The design therefore has to be approached with some caution. Here, we give a stepwise procedure for finding a feasible design by searching for profile intersections in a ternary system:

1. Identify the structure and break it into CSs.
2. Specify and calculate all variables to satisfy the external mass balance, that is, product compositions and/or flowrates.
3. Determine $\mathbf{X}_{\mathbf{\Delta}2}$.
4. Specify the reference reflux and a split ratio ($R_{\Delta 1}$ and Φ_L in side stripper, and $R_{\Delta 3}$ and Φ_V in the side rectifier).
5. Determine through the appropriate Equations 6.13–6.18 R_Δ's for the remainder of the column.
6. Plot composition profiles for all product producing CSs.
7. If there is an intersection of profiles of neighboring CSs, continue. If not, return to step 2 or 4 and try new values.
8. Use the intersection point obtained in step 7 as the initial integration composition for CS_2 operating with $R_{\Delta 2}$ and $\mathbf{X}_{\mathbf{\Delta}2}$, and construct a profile for CS_2.
9. If there is an intersection between the profiles of CS_2 and its remaining neighboring CS, a feasible design has been found. If not, return to step 2 or 4 and try new values.

The stepwise design procedure listed here has also been incorporated into DODS-SiSt and DODS-SiRe, but it is important that the designer fully understands it. Finding a feasible design can be quite difficult since changing one parameter has multiple effects on the column, and a trial and error approach is often required. Generally, one should start with a relatively high absolute reflux value and work downward. Although the design procedure is trial and error based, plotting the profiles and seeing the effect of each parameter on the feasibility of design aids the designer tremendously. Other works have shown a computational approach to also be successful in identifying feasible designs [10]. The general design procedure is illustrated by means of an example for an azeotropic, nonsharp system.

Example 6.3: A rival engineering company has claimed that they have designed a side rectifier for the acetone/benzene/chloroform system whereby separation is

achieved beyond the distillation boundary. The claim to achieve the following from $\mathbf{x}_F = [0.3, 0.3, 0.4]$:

- $\mathbf{x}_D = [0.9, 0.001, 0.099]$
- $\mathbf{x}_B = [2 \times 10^{-10}, 0.9, 0.099]$
- $\mathbf{x}_S = [0.1, 0.1, 0.8]$

They claim that this column operates with a reboil ratio ($s = V_3/B$) of 14. Investigate whether their claim holds water with the DODS-SiRe package. What range of split ratios has likely been used?

Solution 6.3: The DODS-SiRe Package makes this problem fairly easy to solve. The product specifications and a reboil ratio have been given, but not a split ratio. It can be shown, and inferred from Chapter 4 that $R_{\Delta 3} = -s - 1$. Thus, all that is required to do is find Φ_V values where the design will be considered feasible. Unfortunately, this procedure is somewhat trial and error, and there is no simple way, especially for azeotropic systems, to make an educated guess for Φ_V. Thus, we arbitrarily choose Φ_V values of 0.4, 0.5, and 0.6, and use the NRTL model. Each of these designs is shown in Figure 6.32a–c. Here, the dashed profiles are merely profile continuation past an intersection point. The distillation boundary is represented by a thin solid curve.

Figure 6.32a and b are both feasible as there are profile intersections between all neighboring CSs. These two designs are very similar; there are only slight differences in the exact areas of profile intersection. Notice that products lie on either side of the distillation boundary. However, Figure 6.32c is an infeasible design as CS_2's profile pinches before reaching an intersection with CS_1. Thus, the rival's split ratio is likely not as high as 0.6, but Figure 6.32a and b has given us a good idea where the region of feasible designs is located. Through some iteration, we find that the actual range for s Φ_V lies between 0.36 and 0.58.

6.4.6 Design with Transformed Triangles

6.4.6.1 Overall Minimum Reflux As we have shown in the previous chapter, studying the simplified sharp split constant relative volatility problem is very useful in terms of obtaining a first design approximation and can provide valuable insights before elevating the complexity of the problem to incorporate non-sharp product distributions. As will be demonstrated in the section, the TT phenomenon is a simple and effective means of understanding CS interaction—even for complex arrangements such as the side rectifier or stripper. As with simple columns, applying the TT ideas to these thermally coupled columns should also increase our intuitive understanding by "decoupling" CSs to gain a sense of the CS interaction, and at the very least serve as a guide for more realistic nonsharp, nonideal problems. Let us start our analysis of thermally coupled columns by examining the CSs located above and below the feed stream. In both instances, one of these CSs is the internal CS, CS_2, as shown in Figure 6.33a and b.

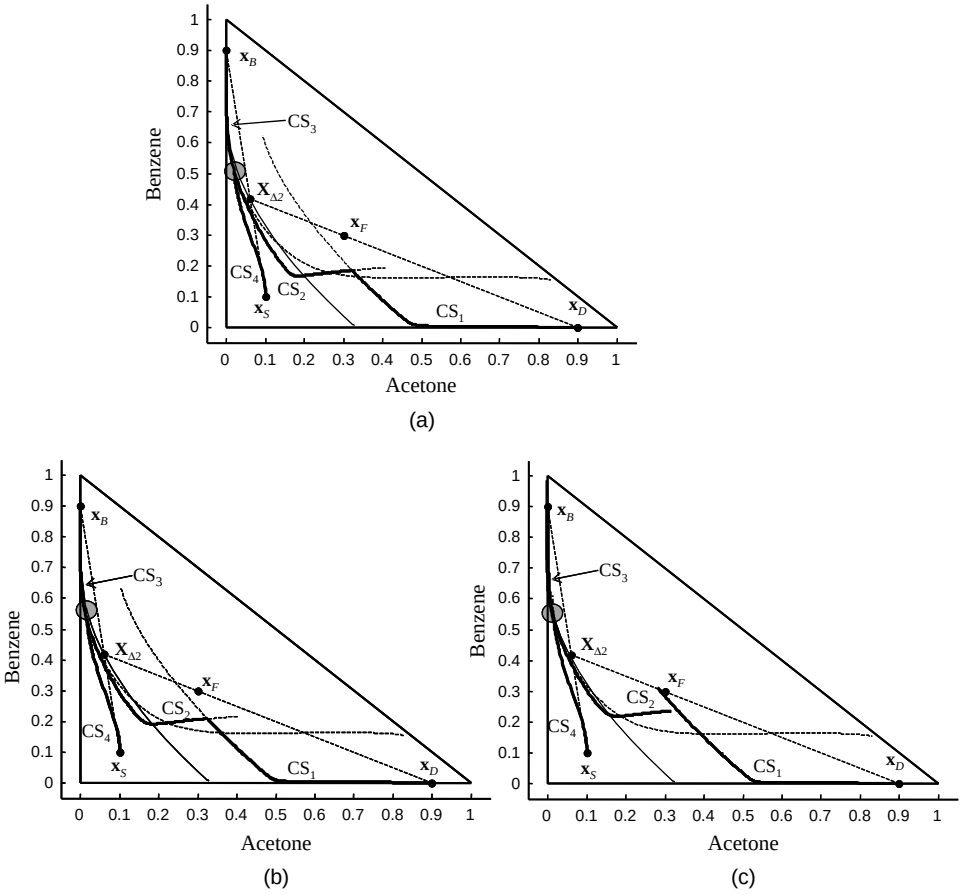


FIGURE 6.32 Side rectifier designs for the acetone/benzene/chloroform system using the NRTL model at 1 atm with $\mathbf{x}_F = [0.3, 0.3, 0.4]$, $\mathbf{x}_D = [0.9, 0.001, 0.099]$, $\mathbf{x}_B = [2 \times 10^{-10}, 0.9, 0.099]$, $\mathbf{x}_S = [0.1, 0.1, 0.8]$, $R_{\Delta 3} = -15$ and (a) $\Phi_V = 0.4$, (b) $\Phi_V = 0.5$, and (c) $\Phi_V = 0.6$.

Notice that in both configurations that they are very closely related to simple columns. For the side stripper, for instance, the simple column has a feed of flowrate F and quality q, a bottoms product of flowrate B and composition $\mathbf{x}_B$. One can show by mass balance that CS_2 produces a "distillate product," or a pseudo distillate, of flowrate $\Delta_2 = V_2 - L_2$ and composition $\mathbf{X}_{\Delta 2}$. Thus, for all practical purposes the CS above and below the feed is just a simple column with one feed and two products. One can in a similar way deduce that the CS_2 in the side rectifier acts as a conventional product producing stripping section with a flowrate of $-\Delta_2 = L_2 - V_2$ (since product flowrates have to be positive) and bottoms composition of $\mathbf{X}_{\Delta 2}$.

Recall that the $\mathbf{X}_{\Delta}$ placement for both configuration display linear properties. Thus, it makes sense that $\mathbf{X}_{\Delta 2}$ can be viewed as a product since it displays the same mass balance properties as any normal product. Thus, the CPM parameters extend

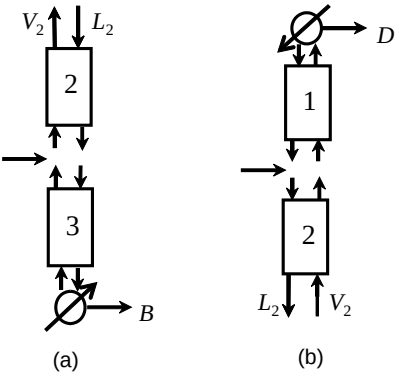


FIGURE 6.33 Column section breakdown across the feed stage for (a) a side stripper and (b) a side rectifier.

naturally to internal CSs as though they were terminating CSs that produce actual products. Both the side rectifier and stripping scenarios across the feed stage are summarized in Table 6.1.

Since the CSs above and below the feed stream merely reduce to a pseudo simple column, it follows that we should be able to find the minimum reflux for it, just as we would do for a conventional simple column. The reflux in the CS below the feed (a stripping CS) can, exactly like simple columns (refer to Section 5.3.2), also be related to the reflux in a CS above the feed through:

$$R_{\Delta 3} = \frac{Fq + \Delta_2 R_{\Delta 2}}{\Delta_2 - F} = \frac{Fq + (F - B)R_{\Delta 2}}{-B} \tag{6.19}$$

for the side stripper, and through

$$R_{\Delta 2} = \frac{Fq + DR_{\Delta 1}}{D - F} \tag{6.20}$$

for the side rectifier.

If we only concern ourselves with sharp splits and constant relative volatilities, we can solve this problem by the TT approach. It is worthwhile noting that $\mathbf{X}_{\mathbf{\Delta 2}}$ is also a sharp split product if we choose all products to be sharp (i.e., each product stream be completely depleted of at least one component) due to mass balance restrictions (see Figure 6.29). Thus, following the same approach used for simple columns in

TABLE 6.1 Summary the Pseudo Simple Column Across the Feed Stream

	Distillate		Bottoms	
Structure	Flowrate	Composition	Flowrate	Composition
Side stripper	$\Delta_2 = V_2 - L_2 = F - B$	$\mathrm{X}_{\Delta 2}$	B	x_B
Side rectifier	D	x_D	$\mathbf{X}_{\Delta 2}$	$-\Delta_2 = L_2 - V_2 = D - F$

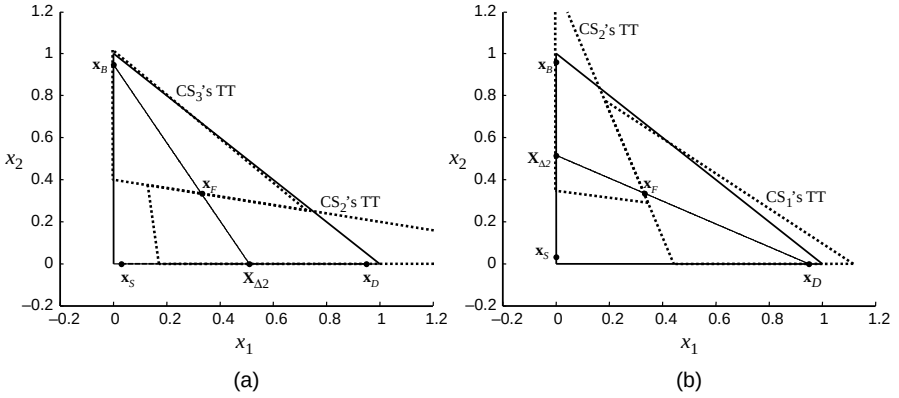


FIGURE 6.34 The two CSs across the feed stage operating at minimum reflux for the (a) side stripper and (b) side rectifier.

Chapter 5, we can find the minimum reflux for this pseudo simple column using the parameters in Table 6.1. For the simplified sharp split, constant relative volatility problem this means that the TTs of both CSs have to just touch one another, effectively an algebraic colinearity condition. This is shown in Figure 6.34 for arbitrary product specifications using the TT technique.

Figure 6.34 indicates that both these CS are operating at their minimum reflux, meaning reflux below this point will cause the TTs not to touch one another and the pseudo simple column, as well as the overall thermally coupled configuration, will be infeasible. A subtlety that can be picked up in comparing Figure 6.34a and b with one another is that the constraint that each structure places on the intermediate product compositions. For example, for the problem to be considered a sharp split problem, *all* $\mathbf{X}_{\mathbf{\Delta}}$'s have to lie on an axis of the MBT, and so does the $\mathbf{X}_{\mathbf{\Delta}}$ of the internal CS. Thus, in the side-stripper configuration, the side-draw composition cannot contain a high-boiling component since $\mathbf{x}_S$, $\mathbf{x}_D$, and $\mathbf{X}_{\mathbf{\Delta}2}$ have to lie on a straight line, by material balance (Figure 6.29). Analogously, the side-draw composition in the side rectifier cannot contain any low-boiling component because $\mathbf{x}_S$, $\mathbf{x}_B$, and $\mathbf{X}_{\mathbf{\Delta}2}$ have to lie on the same straight line. This observation provides some insight into the limitations of each column—if it is important that the sidestream contains little to no low-boiling components, the side rectifier will be preferable. Conversely, the side stripper is better suited to situations where the sidestream specification is such that there are negligible high-boiling components present.

Once the minimum reflux across the feed stage has been determined, the following point that needs to be addressed is determining the operating conditions for the remainder of the column. As mentioned, these thermally coupled columns have two internal degrees of freedom, that is, two reflux values that specify the rest of the column. We have essentially determined one of these refluxes thus far. The remaining minimum reflux is concerned with the operating reflux of the thermally coupled sections of each configuration. So, let us attempt to find a similar simple column

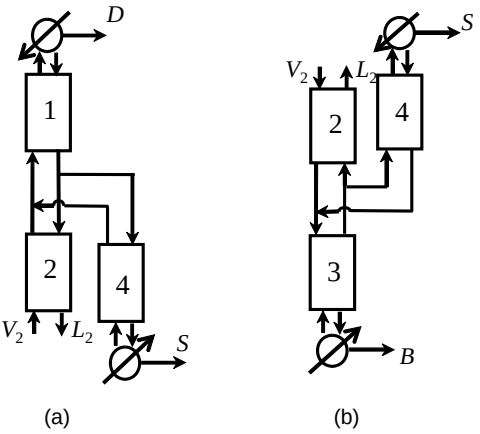


FIGURE 6.35 Column section breakdown across the feed stage for (a) a side stripper and (b) a side rectifier.

analogy that will allow us to employ the TT technique. Consider then the thermally coupled section of both the side stripper and rectifier, showed in Figure 6.35.

It is worthy to note that in both structures in Figure 6.35, $\mathbf{X}_{\mathbf{\Delta}2}$ as well as V_2 and L_2 have been determined by the minimum reflux calculation across the feed stage (discussed above). The simple column analogy required is not as straightforward to infer as the CSs across the feed stages, as in this instance there is no obvious "feed" stream. However, we have mentioned that one of the assumptions we have made with the thermal couplings is that stream withdrawal and addition take place on the same stage. Thus, although there are both stream addition and withdrawal, the column only "sees" the effect of a net stream addition or removal. It is therefore possible to view the streams of CS_2 as a feed stream to the remaining product producing CSs, where the feed stream is effectively the material going in minus the material going out. Thus, for both configurations, the feed stream to the product producing CSs would be

$$F = |V_2 - L_2| = |\Delta_2| \tag{6.21}$$

Since we know the product compositions of each product producing CS, the only parameters that still need to be defined in order to completely specify the pseudo simple column are the feed composition ($\mathbf{x}_F$) and the feed quality (q). For the feed composition, we have to find the net composition being added to our defined simple column, or in other words, the net composition being added to the pseudo column. It can be shown for both the side rectifier and side stripper that this average feed composition reduces to

$$\mathbf{x}_F = \frac{V\mathbf{y}_2^T - L\mathbf{x}_2^T}{V - L} = \frac{V\mathbf{y}_2^B - L\mathbf{x}_2^B}{V - L} = \mathbf{X}_{\mathbf{\Delta}2} \tag{6.22}$$

Remarkably, the pseudo feed composition and flowrate are both directly related to our CPM parameters. The only remaining variable to be determined is the feed

quality, which dictates the fraction of liquid in the feed. Thus

$$q = \frac{L_F}{F} = \frac{L_2}{|\Delta_2|} \tag{6.23}$$

Again, even the feed quality to the thermally coupled section can be simply related to the CPM parameters. However, it should be noted that, in the side stripping configuration, the liquid is being drawn out of the simple column, and this has to be taken into account, such that, for a side stripper:

$$q = \frac{L_F}{F} = \frac{-L_2}{|\Delta_2|} = -R_{\Delta 2} \tag{6.24}$$

In a similar way, feed quality can be determined for the side rectifier. It is important to point out however that the net flow in CS_2 is always negative in this case, leading to

$$q = \frac{L_F}{F} = \frac{L_2}{|\Delta_2|} = \frac{L_2}{-\Delta_2} = -R_{\Delta 2} \tag{6.25}$$

Interestingly, since $R_{\Delta 2}$ is always negative in the side rectifier, the feed quality is always pseudo superheated. Conversely, the feed to the thermally coupled junction in the side stripper is pseudo subcooled because $R_{\Delta 2}$ is always positive. Everything in the pseudo column has been specified and we can proceed with the minimum reflux calculations in the same manner as shown previously for simple columns. For the same arbitrarily chosen product specifications as Figure 6.34, the minimum reflux of the thermally coupled CSs can be represented using the TTs technique, as depicted in Figure 6.36.

We have now demonstrated quick and relatively simple algebraic method to design thermally coupled columns at minimum reflux conditions. All relative

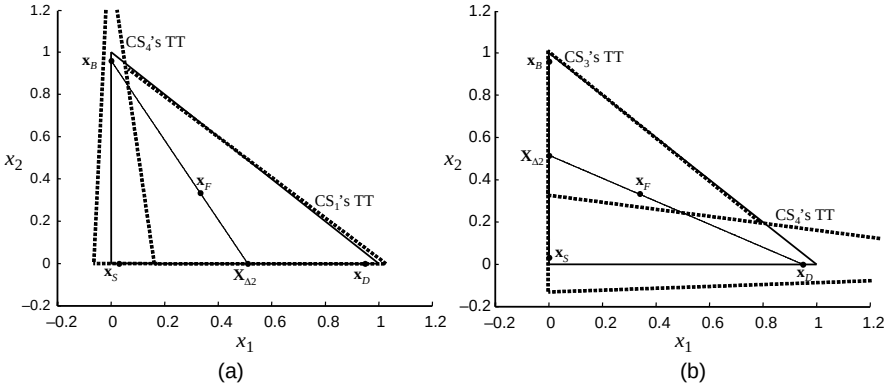


FIGURE 6.36 The thermally coupled CSs at minimum reflux for (a) side stripper and (b) side rectifier.

TABLE 6.2 Summary of the Pseudo Simple Column at the Thermally Coupled Units

Structure	Feed			Distillate		Bottoms	
	F	x_F	q	D	x_D	B	x_B
Side stripper	$-\Delta_2$	$\mathbf{X}_{\Delta 2}$	$-R_{\Delta 2}$	Δ_1	$\mathbf{X}_{\Delta 1}$	$-\Delta_4$	$\mathbf{X}_{\Delta 4}$
Side rectifier	Δ_2	$\mathbf{X}_{\Delta 2}$	$-R_{\Delta 2}$	Δ_4	$\mathbf{X}_{\Delta 4}$	$-\Delta_3$	$\mathbf{X}_{\Delta 3}$

parameters for thermally coupled designs are shown in Table 6.2. The methods can in principle be easily extended to higher order system with multiple thermally coupled units. Piecing the final design in terms of TTs together can be seen in Figure 6.37, which is basically a superimposition of the two simple column designs depicted in Figures 6.34 and 6.36. The bold lines depict the path of the composition profiles along the edges of the relevant TTs, while the arrows and accompanying labels show the primary function of each CS and how it affects composition profiles. Both these structures are said to be operating at overall minimum reflux.

Notice that the nonsharp side-stripper design shown in Figure 6.31 is qualitatively similar to the one depicted here. Although the TT method is only applicable to the idealized case of sharp splits and constant relative volatilities, it is very useful for initial design estimates for the minimum energy demands of a structure and comparison. Once R_Δ values have been determined for each CS, it is fairly simple to convey these values in terms of the previously defined split ratios. For the side stripper:

$$\Phi_L = \frac{-SR_{\Delta 4}}{DR_{\Delta 1}} \tag{6.26}$$

And side rectifier:

$$\Phi_V = \frac{S(1 + R_{\Delta 4})}{-B(1 + R_{\Delta 3})} \tag{6.27}$$

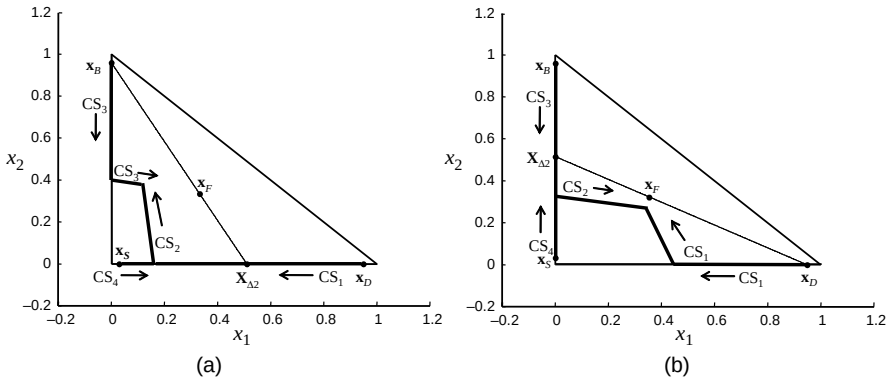


FIGURE 6.37 Overall minimum reflux design for (a) side stripper and (b) side rectifier.

6.4.6.2 Over-Refluxed Designs While it is extremely important to know what is the minimum energy demand of a column, it is also important to know of alternate, perhaps more practical, operating modes that exist in a column. In an arbitrarily chosen simple column with azeotropic behavior and sharp splits this task is rather trivial because one may operate at virtually any column reflux value that is higher than the minimum reflux. However, in columns such as these that have dependent variables linked to the choice of our column reflux, it is not as straightforward. For instance, if one chooses to operate at a slightly higher column reflux than the minimum determined for the column, it is conceivable that the rest of the column will also be affected by this choice. In fact, as will be shown in this section, an entire region of operability options becomes available when operating at higher than minimum column refluxes (note from the previous section that there is only a single permissible value of Φ_V or Φ_L that will cause TTs to be collinear with another). These new operability options may be important for assessing the controllability or stability of a particular column. Again, the same TT ideas can be used constructing these regions.

So let us examine the side stripper first. Suppose we have determined the minimum reflux for this column through the techniques shown previously. Suppose now that we would like to operate above this minimum reflux; thus it can be said that we are operating at a $R_{\Delta 1} > R_{\Delta 1 \mathrm{MIN}}$. Since CS_1 and CS_4 can be seen as a rectifying and stripping section of a pseudo simple column, respectively, it is obvious to see that when specifying a value for $R_{\Delta 1}$ above its minimum there is an associated $R_{\Delta 4}$ value that will cause the TTs of CS_1 and CS_4 to be collinear with one another. Effectively this means that there is a Φ_L value that will satisfy this colinearity requirement. It is again quite easy to calculate this colinearity condition using the TT technique for $R_{\Delta 1} > R_{\Delta 1 \mathrm{MIN}}$. It is also convenient to represent this interaction between $R_{\Delta 1}$ and Φ_L graphically, as shown by the appropriately labeled curve in Figure 6.38.

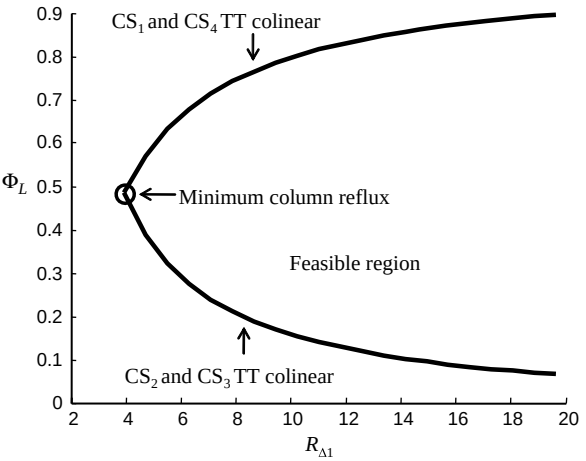


FIGURE 6.38 Feasible operating region for a side stripper.

It follows quite logically too that when $R_{\Delta 1}$ is changed, so to do the colinearity conditions for the TTs in CS_2 and CS_3 change. Again, there is a unique Φ_L value associated with the choice of $R_{\Delta 1}$ that causes the TTs in CS_2 and CS_3 to line up with one another, which is very easily computable. The dependence of $R_{\Delta 1}$ and Φ_L ensure colinearity between CS_2 and CS_3 is also shown by the appropriately labeled curve in Figure 6.38.

WWW

TUTORIAL 6.7

Try this for yourself: Using DODS-SiSt and the TT design option generates a feasible operating region for a side stripper, similar to Figure 6.38. Try using different feed/product compositions and other $\boldsymbol{\alpha}$ values.

The area enclosed by the set of curves gives a very useful indication of allowable values of Φ_L that may be chosen at a certain $R_{\Delta 1}$. These regions can be easily verified to constitute feasible designs using both the DODS-SiSt and -SiRe packages. Moreover, Beneke and Linninger showed that very similar regions can be generated rigorously through numerical methods for nonsharp splits [10]. In general, the higher the column operates above minimum reflux, the greater the freedom is in choosing the parameter Φ_L that still results in a feasible design. Furthermore, when Φ_L is chosen to lie within the region (and not on the curve), all TTs overlap one another (and do not touch). When Φ_L is chosen to lie on either one of these curves, the TTs associated with that curve will be colinear to one another (again easily verified with the DODS-SiSt and -SiRe packages). It is important to point out that these curves intersect one another at exactly the minimum column reflux point, where only one Φ_L value will constitute a feasible design. Similar plots can be generated for the side rectifier arrangement, using $R_{\Delta 4}$ and Φ_V as the control variables, shown in Figure 6.39. Examples of the TT overlapping in overrefluxed columns can be seen in Figure 6.40.

WWW

TUTORIAL 6.8

Try this for yourself: Using DODS-SiRe and the TT design option generates a feasible operating region for a side rectifier, similar to Figure 6.39. Try using different feed/product compositions and other $\boldsymbol{\alpha}$ values.

WWW

TUTORIAL 6.9

Try this for yourself: Using either DODS-SiRe or DODS-SiSt and the TT design option generates a feasible TT design for a side rectifier/stripper, similar to Figure 6.40a and b. Try using different feed/product compositions and other $\boldsymbol{\alpha}$ values.

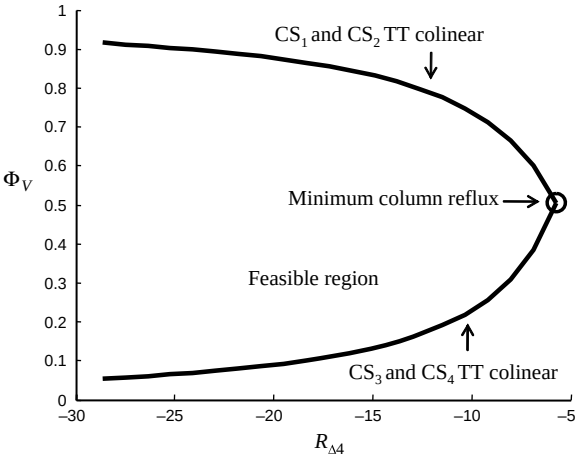


FIGURE 6.39 Feasible operating region for a side rectifier.

WWW

Example 6.4: A mixture of [benzene, *p*-xylene, toluene] is to be separated into three relatively pure product streams. The targets for these products require a high-purity benzene stream containing no *p*-xylene, a high-purity *p*-xylene stream containing no benzene and a toluene rich stream that may contain either benzene or p-xylene. The exact product specifications are given as

- $\mathbf{x}_F = [0.4,\ 0.3,\ 0.3]$, $F = 1$ mol/s, $q = 1$;
- $\mathbf{x}_D = [0.999,\ 0,\ 0.001]$,
- $\mathbf{x}_S =$ toluene has to be 0.97,
- $\mathbf{x}_B = [0,\ 0.995,\ 0.005]$

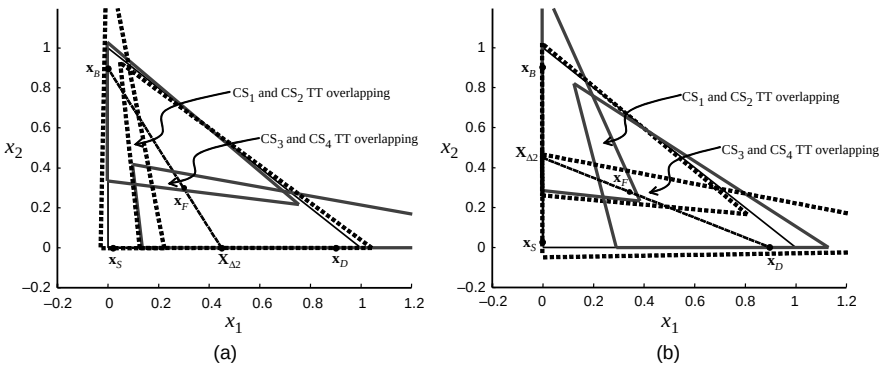


FIGURE 6.40 TT overlapping in an overrefluxed column for (a) side stripper and (b) side rectifier.

We have narrowed the design alternatives down to using either a side rectifier or side-stripper configuration. Using the DODS-SiSt or -SiRe packages accompanying the book determines which structure is better from a reboiler duty point of view, as this is generally the highest operating expense in a column. Also, determine which structure is better from an operability point of view if one operates at 1.2 times the minimum energy requirement for the column.

Solution 6.4: There are two important factors to point out in this design:

1. The product specifications are sharp
2. The benzene, *p*-xylene, and toluene are near ideal and can be approximated quite well with constant relative volatilities.

Thus, in order to gain a quick assessment of which design is superior, we can use the TT approach outlined in this section, which can be simply done with the DODS package. The DODS package estimates the relative volatilities of benzene and toluene with respect to *p*-xylene as 5.28 and 2.24, respectively. We shall first consider the side-stripper unit in our evaluation; the sidestream therefore cannot contain any *p*-xylene as this is the bottoms product. The sidestream composition is therefore: $\mathbf{x}_S = [0.03, 0, 0.97]$.

The overall design, with all refluxes, determined by the TT technique is given in Figure 6.41.

Since we are concerned by the energy usage in the reboiling sections we have to consider the duties in both $R_{\Delta 3}$ and $R_{\Delta 4}$. CS_3 and CS_4 produce products B and S, respectively, and since we know the reflux ratios in these sections we know the vapor flowrates too, which are directly proportional to the heat duty. Thus, in CS_3

$$\Delta_3 = -B = V_3 - L_3 = V_3 + BR_{\Delta 3} \tag{6.28}$$

$$V_3 = -B(1 + R_{\Delta 3}) \tag{6.29}$$

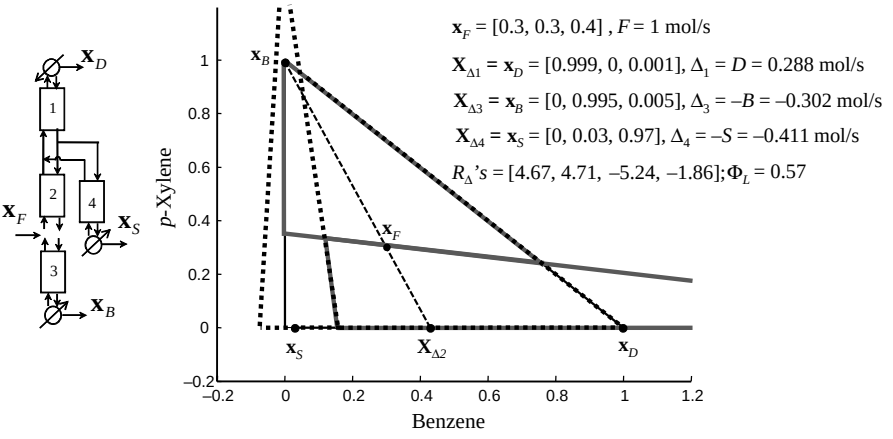

$\mathbf{x}_F$ = [0.3, 0.3, 0.4] , F = 1 mol/s
$\mathbf{X}_{\Delta 1} = \mathbf{x}_D$ = [0.999, 0, 0.001], $\Delta_1 = D$ = 0.288 mol/s
$\mathbf{X}_{\Delta 3} = \mathbf{x}_B$ = [0, 0.995, 0.005], $\Delta_3 = -B$ = –0.302 mol/s
$\mathbf{X}_{\Delta 4} = \mathbf{x}_S$ = [0, 0.03, 0.97], $\Delta_4 = -S$ = –0.411 mol/s
R_Δ's = [4.67, 4.71, –5.24, –1.86]; Φ_L = 0.57
$\mathbf{x}_D$
$\mathbf{x}_F$
$\mathbf{x}_S$
$\mathbf{x}_B$
1
2
3
4
p-Xylene
Benzene
$\mathbf{x}_{\Delta 2}$

FIGURE 6.41 A side stripper for the [benzene, *p*-xylene, toluene] system at minimum reflux using the TT technique.

and similarly for CS_4:

$$V_4 = -S(1 + R_{\Delta 4}) \tag{6.30}$$

Applying Equations 6.22 and 6.30 gives $V_3 = 1.200$, and $V_4 = 0.354$ mol/s. If we assume that the latent heat of vaporization (ΔH_{VAP}) of all components is equal, we obtain

$$Q = \Delta H_{VAP} \sum V \tag{6.31}$$

Leading to the heat demand of the column being $Q_{SS} = 1.554\Delta H_{VAP}$ for the side stripper, where the subscript *SS* indicates the side stripper. Following the same procedure, we are able to calculate the minimum reflux conditions for the side rectifier noting that in this case: $\mathbf{x}_S = [0, 0.03, 0.97]$. The design with all relevant reflux values is depicted in Figure 6.42. In this particular case there is only one section with a reboiler attached to it, CS_3. Following the same procedure for calculating reboiler heat duty for the side stripper and assuming equivalent latent heats of vaporization, we obtain $Q_{SR} = 1.570\Delta H_{VAP}$ for the side rectifier, where the subscript *SR* indicates the side stripper.

It is evident that the side stripper will achieve a slightly lower reboiler duty, thus we should choose the side stripper. In order to finally determine which one of these structures has a wider range of operability, we simply need to determine the upper and lower bounds of Φ for each structure at the chosen operating reflux. If the side stripper operates at 1.2 times the minimum reboiling load (equivalent to 1.2 times $R_{\Delta 1}$), it is easily found on the Φ–$R_{\Delta 1}$ diagram that the range of feasible operation is: of $0.452 \leq \Phi_L \leq 0.641$ giving a feasibility range of 0.189. Analogously, operating the side rectifier at 1.2 times the reboiling load (equivalent to 1.2 times $R_{\Delta 3}$), gives $0.356 \leq \Phi_V \leq 0.575$ and a feasibility range of 0.219, slightly higher than the side

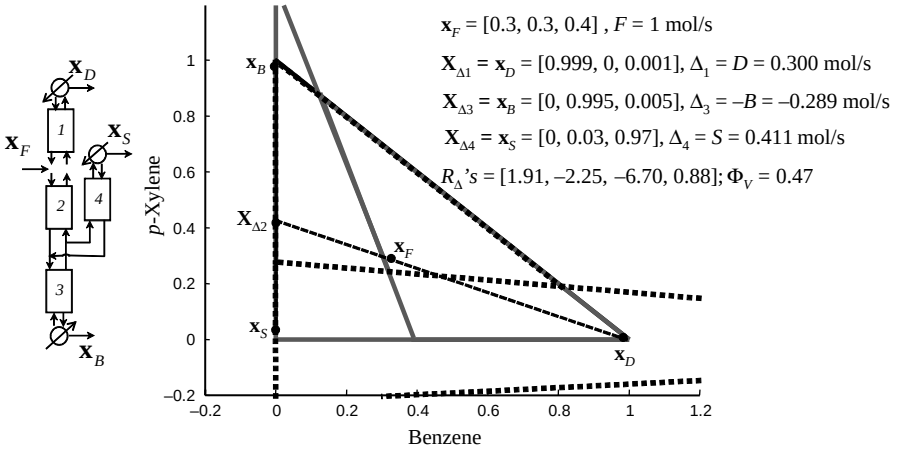


FIGURE 6.42 A side rectifier for the [benzene, *p*-xylene, toluene] system at minimum reflux using the TT technique.

stripper. It may therefore be easier to operate the side rectifier since it offers better flexibility, but it consumes slightly more energy.

6.5 SUMMARY

This chapter has introduced the designer to the fundamental concepts of complex column design. The designs of multiple feed/product columns, as well as thermally coupled columns, were covered using a single, all-encompassing CPM technique. While these columns appear to be difficult to understand and grasp at first sight, we have shown that they are all mere extensions of simple columns. Special focus was given to simplified constant relative volatility systems which allows one to construct TTs. The TTs are a very useful tool for attaining minimum reflux solutions in thermally coupled column (for sharp split columns), for assessing column stability, as well as for assessing the feasibility of multiple feed columns. The true value of the CPM technique perhaps begins to become apparent in this chapter, more so than others, in the sense that its main parameters, $\mathbf{X}_{\mathbf{\Delta}}$ and R_{Δ}, are generalized. Thus, no new equations have to be derived nor have any new parameters be defined for each structure. Virtually any structure, irrespective of complexity may be modeled with the same generalized tool.

REFERENCES

[1] McCabe, W.L. and E.W. Thiele, Graphical design of fractionating columns. *Industrial and Engineering Chemistry*, 1925, **17**(6):606–611.

[2] Akashah, S., J.H. Erbar, and R.N. Maddox, Optimum feed plate location for multicomponent distillation separations. *Chemical Engineering Communications*, 1979, **3** (6):461–468.

[3] Fenske, M.R., Fractionation of straight-run Pennsylvania gasoline. *Industrial and Engineering Chemistry*, 1932, **24**(5):482–485.

[4] Doherty, M.F. and M.F. Malone, *Conceptual Design of Distillation Systems*. 1st ed. 2001, New York, NY: McGraw-Hill. p. 568.

[5] Glinos, K.N. and M.F. Malone, Design of sidestream distillation columns. *Industrial and Engineering Chemistry, Process Design and Development*, 1985, **24**(3):822–828.

[6] Levy, S.G., D.B.Van Dongen, and M.F. Doherty, Design and synthesis of homogeneous azeotropic distillations: 2. Minimum reflux calculations for nonideal and azeotropic columns. *Industrial and Engineering Chemistry, Fundamentals*, 1985, **24**(4):463–474.

[7] Watkins, R.N. *Petroleum Refinery Distillation*. 1979, Houston, TX: Gulf Pub. Co.

[8] Petlyuk, F.B., *Distillation Theory and its Application to Optimal Design of Separation Unit*. 2004, Cambridge: Cambridge University Press.

[9] Emmrich, G., H. Gehrke, and U. Ranke, The progressive extractive distillation arrangement for the morphylane extractive distillation process. *Chemie Ingenieur Technik*, 2001, **73**(6):715.

[10] Beneke, D.A. and A.A. Linninger, Graphical design and analysis of thermally coupled sidestream columns using column profile maps and temperature collocation. *AIChE Journal*, 2010.

CHAPTER 7

DESIGN OF FULLY THERMALLY COUPLED COMPLEX COLUMNS USING COLUMN PROFILE MAPS

7.1 INTRODUCTION

As evident from the previous chapters, the energy demands of a specific separation problem may have a substantial influence on the profitability of a process. The energy demands of even the simplest binary distillation problem can be massive, not even to mention a multicomponent system where one may require a sequence of simple distillation columns to achieve the final desired product cuts. As shown in Chapter 6, there are some innovative ways of overcoming this large energy load by, among others, the thermal coupling of CSs as in side rectifiers and strippers. Thermal coupling of CSs essentially utilizes an interconnection of streams between neighboring CSs to eliminate a utility input, either a reboiler or condenser. However, there exists another class of thermally coupled columns, colloquially known as fully thermally coupled columns. Two of the most prominent examples of fully thermally coupled columns are the so-called Petlyuk column and the Kaibel column both of which are looked at in this chapter.

The idea of a fully thermally coupled column was first reported in 1949 in a patent by Wright [1] although the groundbreaking work and analysis of it comes from its namesake, Felix Petlyuk [2]. Although many variants have been proposed throughout the years, Petlyuk-type columns essentially have two areas of thermal coupling, thus allowing one to eliminate an additional utility input stream. The three-

Understanding Distillation Using Column Profile Maps, First Edition. Daniel Beneke, Mark Peters, David Glasser, and Diane Hildebrandt.
© 2013 by John Wiley & Sons, Inc. Published 2013 by John Wiley & Sons, Inc.

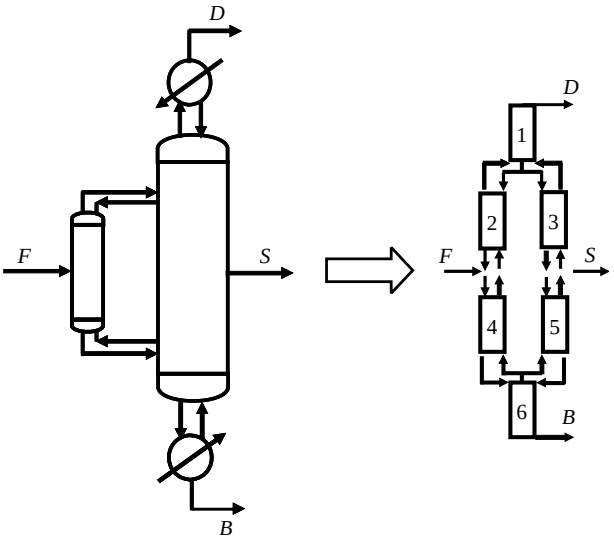


FIGURE 7.1 CS breakdown of a Petlyuk column.

component separation problem thus only requires one reboiler and one condenser to achieve high-purity distillate, bottoms, and side-draw products. Much of the chapter is centered on the design of a Petlyuk column, but a portion thereof is also dedicated to the Kaibel Column design (Section 7.5).

The Petlyuk column essentially consists of a prefractionating unit that partially separates the mixture, which is then fed to a product-producing column, as shown in Figure 7.1. It has been shown that even further savings in capital cost can be achieved [1,3] not by constructing separate prefractionating and product-producing column shells, but by inserting a dividing wall inside a single main column shell (known as a divided wall column). However, from a conceptual design point of view (i.e. CS breakdown and composition matching criteria), the divided wall column reduces to exactly the Petlyuk column and will be treated as such in this chapter. Due to these large promises of cost savings, the Petlyuk column has become arguably one of the most studied problems in distillation design over the past few years, using a variety of design techniques [3–20]. Savings with respect to energy costs have been reported to be in the region of 30%, and as high as 50%, depending on the nature of the mixture to be separated [3,12,21] although Agrawal pointed out that these configurations may not be the most efficient from a thermal efficiency point of view [22].

Kaibel columns, first introduced at BASF [23], are columns whereby four purified product streams are produced through a thermal couplings. It can therefore be seen as the four-component equivalent of the Petlyuk column, with savings of 35, 25, and 40% having been reported for operating cost, investment cost, and plot space, respectively [24]. This column gets its name from Gerd Kaibel, the person who first suggested the benefits of such an arrangement.

Although its cost saving properties is apparent, the industrial implementation of the Petlyuk column has been rather scarce. This is largely attributed to complex control and operational problems which have been well reported throughout the literature [16,20,25]. This, in turn, may be ultimately traced back to insufficient insight into the design of the column, because rigorous simulation software packages do not, at present, have a simple way of modeling a Petlyuk column, and other simplified techniques tend to be configuration specific that often requires a transformation of variables thereby not permitting one to draw quick and meaningful design conclusions. As mentioned in the previous chapter, this is exactly where the CPM design method has some advantage, because it is completely generalized. Designing a Petlyuk column is thus a simple extension of simple column design using the CPM technique.

As with the design of any structure, we first need to define the structure and determine its CS breakdown. The breakdown of the Petlyuk column into a sequence of CSs can be seen in Figure 7.1. The CS breakdown consists of six unique CSs, where CS_1 is a standard rectifying section, terminated by a total or partial condenser, with its function to predominantly produce a high purity low-boiling product. Conversely, CS_6 is a standard stripping section terminated by a total or partial reboiler which aims to purify the high-boiling component. The intermediate-boiling component can be removed either as a liquid from CS_3 or a vapor from CS_5, while the feed stage is located in between CS_2 and CS_4. Furthermore, notice that CS_1, CS_2, and CS_3 are thermally linked to one another at the top of the column and CS_4, CS_5, and CS_6 are thermally linked at the bottom of the column.

7.2 A SIMPLIFIED INFINITE REFLUX CASE

As we have seen in the design of simple columns, infinite reflux columns, although impractical, allow one to draw meaningful conclusions for the eventual design of finite reflux columns. The infinite reflux column is thus merely a special mode of operation in the global spectrum of feasible operating modes. Therefore, before diving in head first into the somewhat complex design procedure of finite reflux Petlyuk columns, let us first study the infinite reflux case. There are in fact two possibilities to consider: (1) all CSs operate at infinite reflux, and (2) only CS_1 and CS_6 operate at infinite reflux, while $CS_{2–5}$ do not. We will treat case 1 first.

7.2.1 All CSs at Infinite Reflux

A Petlyuk column operating with all CSs operating at infinite reflux essentially means negligible or infinitesimal feed to the column, as well as no or infinitesimal products drawn off from the column. In other words, the internal flowrates are so large that any addition of feed or removal of product has little to no effect on the internal flows. This operation mode has consequences with regard to our CS breakdown in Figure 7.1, because now CS_2 and CS_4 have identical operating conditions and can thus be seen as one CS. The same argument can be made for CS_3 and CS_5. CS_1 and CS_6 are

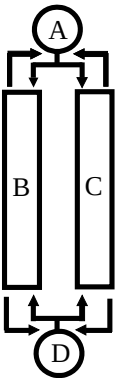


FIGURE 7.2 CS breakdown for the Petlyuk column operating at infinite reflux.

terminated by a total condenser and reboiler, respectively. These sections operate with $V = L$ and $X^T = Y^T$ and therefore they simply operate on their respective residue curves. We have labeled the merger of CS_2 and CS_4 as CS_B and that of CS_3 and CS_5 as CS_C.

For the remaining CSs, the first instinct one may have when specifying that all CSs operate at infinite reflux is that the operating profiles of these CSs will also merely lie on the residue curves as $\Delta = 0$ ($V = L$). This is, however, not necessarily the case. Consider expanding the DPE shown in Chapter 3 (Equation 3.9) as follows:

$$\frac{d\mathbf{x}}{dn} = \left(\frac{V}{L}\right)(\mathbf{x} - \mathbf{y}) + \left(\frac{\Delta}{L}\right)\left(\frac{V\mathbf{y}^T - L\mathbf{x}^T}{\Delta} - \mathbf{x}\right) \tag{7.1}$$

We can see that for the special case when $V = L$ that

$$\frac{d\mathbf{x}}{dn} = (\mathbf{x} - \mathbf{y}) + \left(\mathbf{y}^T - \mathbf{x}^T\right) = (\mathbf{x} - \mathbf{y}) + \boldsymbol{\delta} \tag{7.2}$$

The term $\boldsymbol{\delta} = (\mathbf{y}^T - \mathbf{x}^T)$ is known as the difference vector. $\boldsymbol{\delta}$ is the difference between vapor and liquid compositions in a CS and remains constant down the length of the CS. For CSs terminated by a reboiler or condenser (CS_1 and CS_6 in the Petlyuk), Equation 5.19 reduces to the classic residue curve equation because $\mathbf{y}^T = \mathbf{x}^T$. $\boldsymbol{\delta}$ can be understood in much the same way as $\mathbf{X}_{\boldsymbol{\Delta}}$: a negative value implies that a component is moving downward in the CS, and vice versa. However, unlike $\mathbf{X}_{\boldsymbol{\Delta}}$, it is important to note that

$$\sum \delta_i = \sum \left(y_i^T - x_i^T\right) = \sum y_i^T - \sum x_i^T = 1 - 1 = 0 \tag{7.3}$$

This implies that the individual elements of $\boldsymbol{\delta}$ cannot all have the same sign—if one of the entries in $\boldsymbol{\delta}$ is positive, then at least one other entry has to be negative to obey

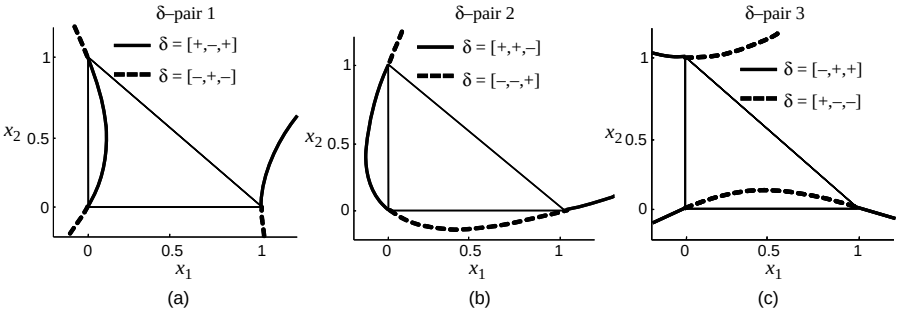


FIGURE 7.3 Regions of unique pinch point curve behavior the different placements of $\boldsymbol{\delta}$: (a) $\boldsymbol{\delta}$-pair 1, (b) $\boldsymbol{\delta}$-pair 2, and (c) $\boldsymbol{\delta}$-pair 3.

the summation to zero. This means that all components cannot simultaneously be in either rectifying or stripping mode in a particular CS—some components will be moving up a CS (rectifying mode), while others will be moving down (stripping mode). Seen from another point of view, the placement of $\boldsymbol{\delta}$ in the composition space can never be inside the MBT. A qualitative behavior of the pinch point curves for each $\boldsymbol{\delta}$ placement in composition space can be seen in Figure 7.3. The pinch points were generated here by arbitrarily choosing a coordinate for $\boldsymbol{\delta}$, that is, a vector direction, and then varying the magnitude of the vector.

Notice that there are six possibilities of positive and negative net flow combinations, each producing unique pinch point curves, but their pinch point curve behavior suggests that these six different flow possibilities can be divided into three pairs because of the continuation of these curves. A pair essentially consists of two opposite flow patterns. These three pairs are imperative for the design of this simplified system, since a mass balance around the thermally coupled junction in Figure 7.2 gives

$$V_B\mathbf{y}_B^T + V_C\mathbf{y}_C^T + L_A\mathbf{x}_A^B = L_B\mathbf{x}_B^T + L_C\mathbf{x}_C^T + V_A\mathbf{y}_A^B \tag{7.4}$$

Since $V_B = L_B$, $V_C = L_C$, $V_A = L_A$, and $\mathbf{x}_A^B = \mathbf{y}_A^B$ at infinite reflux, Equation 7.4 reduces to

$$\boldsymbol{\delta}_B = -\boldsymbol{\delta}_C \tag{7.5}$$

Thus, CS_B and CS_C operate with opposite difference vectors, that is, one pair of the three conceivable flow patterns pairs. Placing either difference vector automatically specifies the other. Physically, this means that components that are in rectifying mode in CS_B, are in stripping mode in the other CS_C. In other words, a component will have a net movement upwards in one CS, and downwards in the other—this is expected from the coupled CSs configuration in Figure 7.2. A CPM for the simplified DPE in Equation 7.2 is shown in Figure 7.4.

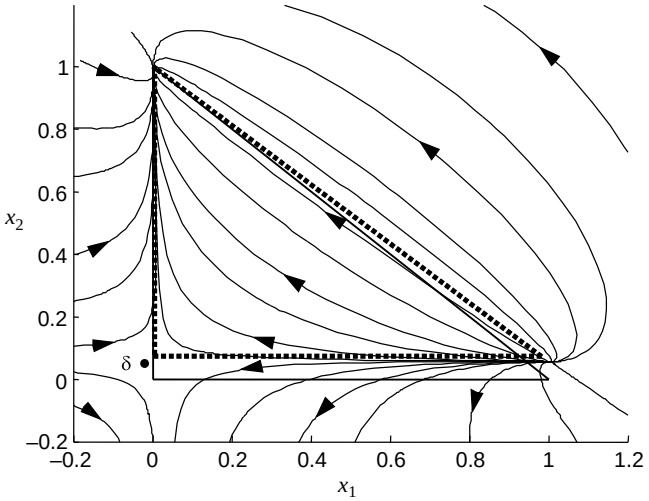


FIGURE 7.4 A CPM for the simplified DPE in Equation 7.2 with $\boldsymbol{\delta} = [-0.02, 0.05]$ and $\boldsymbol{\alpha} = [5, 1, 2]$. The TT is represented by the dashed lines.

Figure 7.4 shows that the simplified DPE with the difference vector behaves in much the same way as the original DPE where profiles have been altered and nodes have been shifted—even outside the positive composition space. As before, with constant relative volatility systems, we are able to connect the (shifted) nodes with straight lines to form a transformed triangle (TT).

Now that the mass balance characteristics of the column have been determined, we now focus on feasibility. In other words, in order for this simplified design to be considered feasible, what do we need to achieve? Remember that CS_A and CS_D operate at infinite reflux (on the residue curves), and the designer thus has no choice in choosing the operating conditions of this column. It is evident from the both structures in Figures 7.1 and 7.2 that we are dealing with a liquid and a vapor split at the top and bottom of the column, respectively. This means there has to be a common liquid composition at the top of the column where the liquid streams are split, and common vapor composition at the bottom of the column where the vapor stream is split. Consequently, this implies that one has to find vapor profile intersections at the bottom of the column, and liquid profile intersections at the topmost thermally coupled point. This is however cumbersome and insight becomes very limited if one has to plot both liquid and vapor profiles to search for profile intersections. Thus, as with all our other designs, we can approximate feasibility by solely searching for liquid profile intersections because the general trajectory of liquid and vapor profiles are the same and, in general, one can state that if there is a liquid profile intersection, there is likely to be a vapor profile intersection too (refer to Section 5.3.3 and Figure 5.15). Since profiles need to intersect at the bottom and the top of the column, we thus need to find profiles in CS_B that intersect profiles in CS_C twice. Furthermore, this intersection has to, of course, occur within the bounds of the MBT. This can be

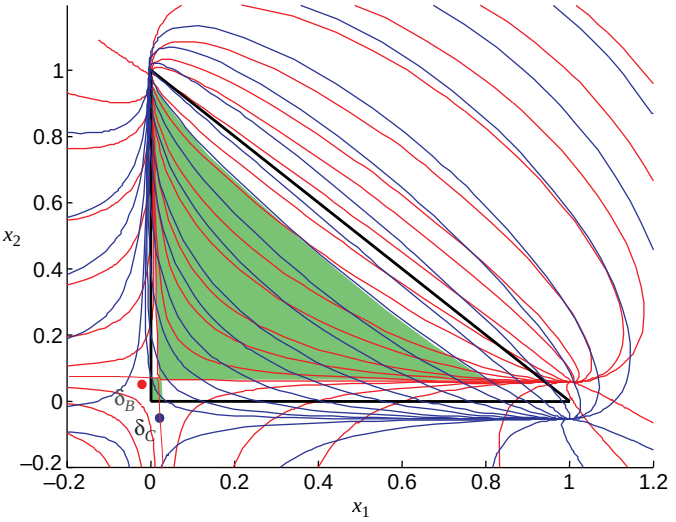


FIGURE 7.5 Superimposed CPMs with the associated region of double intersections with $\boldsymbol{\delta}_B = [-0.02, 0.05]$ and $\boldsymbol{\delta}_C = [0.02, -0.05]$ and $\boldsymbol{\alpha} = [5, 1, 2]$.

easily achieved by merely superimposing two CPMs (as the one in Figure 7.4) upon one another, remembering that mass balance dictates that the CS_B and CS_C operate with opposite difference vectors. Such a superimposition of CPMs to find a feasible design is shown in Figure 7.5, where the region of double profile intersections has been highlighted. For this specific design, we have arbitrarily chosen to operate with $\boldsymbol{\delta}_B = [-0.02, 0.05] = -\boldsymbol{\delta}_C$ indicated by the red and blue dots in Figure 7.5 (see color insert). Under these operating conditions, there is an entire region of double intersections, suggesting that even in this simplified problem there are multiple steady state solutions to the Petlyuk column.

The feasible region of double profile intersection always has a bow-tie type shape, which is formed by the overlapping of the two TTs of CS_B and CS_C. The TTs of each CS has not been plotted here because the space becomes too cluttered. One may choose to operate on any one of the profiles enclosed by the shaded feasible region. Notice in the CS breakdown that CS_C is a merger of the CSs across the side-draw stage (CS_3 and CS_5), meaning that the profile of CS_C is indicative of the product purity in the sidestream. Since a part of the shaded feasible region is on the pure intermediate-boiler axis it is possible, theoretically, to achieve a pure intermediate boiling sidestream composition in this column although the actual flowrate of this sidestream is infinitesimal.

Interestingly, in general only $\boldsymbol{\delta}$-pairs 1 and 3 produce profiles where double intersection may occur. The reason that region 2 does not produce such a feasibility condition can be qualitatively understood through Figure 7.3b, where the there is no possibility of TT vertices occurring within the MBT, which is clearly a necessary

condition for double intersections by viewing Figure 7.5. A feasible design for a system such as the one describe is qualitatively similar to the one depicted in Figure 7.7.

7.2.2 Overall Infinite Reflux

The second infinite reflux condition in the Petlyuk column is where CS_1 and CS_6 operate at infinite reflux, but we do not specify that CS_{2-5} operate under these conditions, that is, the vapor and liquid flowrates in CS_{2-5} are finite values and are not equal to each other. Since the overall reflux is infinite, there is still no effect from feed addition or product removal on the column. Therefore, the CS breakdown for this structure is equivalent to the one shown in Figure 7.2. We can again apply the mass balance around the thermally coupled junction at the top of the column as in Equation 7.4. In this case, we again have the condition that $V_A = L_A$ and $\mathbf{x}_A^B = \mathbf{y}_A^B$, but in this case $V_B \neq L_B$, $V_C \neq L_C$. Under these conditions, we find that Equation 7.4 reduces to

$$\Delta_B \mathbf{X}_{\Delta B} = -\Delta_C \mathbf{X}_{\Delta C} \tag{7.6}$$

And also

$$\Delta_B = -\Delta_C \tag{7.7}$$

Equations 7.6 and 7.7 suggest that CS_B and CS_C operate with the same difference point but opposite net directional fluxes. As with the previous infinite reflux case, this suggests that components that are in rectifying mode in CS_B, operate in stripping mode in CS_C, and vice versa. Since we are now dealing with finite reflux CSs, we have to employ the full DPE, which is dependent on both the reflux ratio and the difference point. In the previous example, the designer was only required to set the direction of the difference vector, but in this case, the designer is required to specify the difference point of either CS_B or CS_C (since they are equal), and the reflux ratios of both CS_B and CS_C. In specifying the reflux ratios for these two CSs, one must bear in mind that the net flows of these CSs have to be in the opposite direction (Equation 7.7), which directly implies that their respective reflux ratios also have to operate with opposite signs.

Let us suppose for this design, we would like to obtain a sidestream product of at least a 90% purity of the intermediate-boiling component. Even though a negligible sidestream is being drawn off from the column, we would still like to find a combination of profiles that would realize this specification. The question is, however, how we choose parameters such as $\mathbf{X}_{\boldsymbol{\Delta}}$ and R_Δ that will achieve this? In Chapter 3 (Section 3.9.2), it was shown how one can deliberately position pinch points in composition space by merely specifying a reflux value and calculating the resulting $\mathbf{X}_{\boldsymbol{\Delta}}$ values, essentially the reverse pinch point calculation. In symbolic form this reduces to (refer to Equations 3.25 and 3.26)

$$\mathbf{X}_\Delta = \mathbf{x}^p - (R_\Delta + 1)(\mathbf{x}^p - \mathbf{x}^p) \tag{7.8}$$

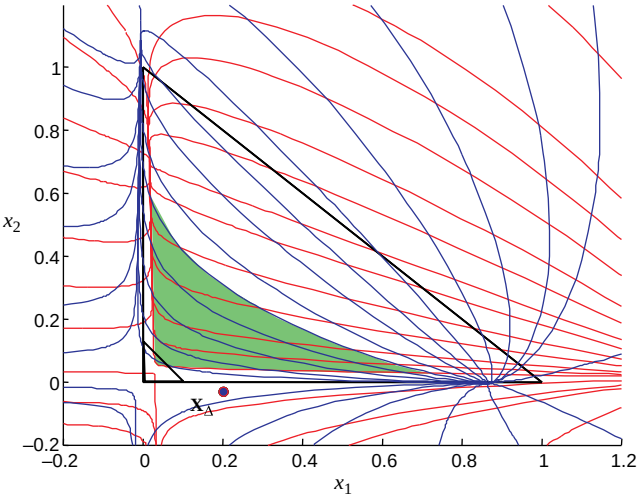


FIGURE 7.6 Superimposed CPMs with the associated region of double intersections with $\mathbf{X}_{\Delta B} = \mathbf{X}_{\Delta C} = [0.201, -0.031]$, with $R_{\Delta C} = 3$ (red) and $R_{\Delta B} = -10$ (blue) with $\boldsymbol{\alpha} = [5, 1, 2]$.

where $\mathbf{x}^p$ is a pinch point and $\mathbf{y}^p$ is the vapor composition in equilibrium with the liquid pinch point. With this in mind, we select to specify a sidestream composition of [0.03, 0.03] and an arbitrary reflux of 3 for CS_C. The purity of the intermediate-boiling component is chosen to be greater than the product specification of 90% in order do better than the theoretical target; the reasons behind this will become evident as we proceed. With this sidestream composition and a constant relative volatility system of [5, 1, 2], we find that $\mathbf{X}_{\Delta C} = [0.201, -0.031]$. This is the difference point of both CS_B and CS_C, and since the reflux ratio of CS_C has already been specified all that is needed now is to specify a reflux ratio for CS_B. Remembering that the reflux in CS_C has to have an opposite sign to the one in CS_B, we arbitrarily choose to operate this CS at a reflux of -10. The resulting superimposition of the CPMs of CS_B and CS_C can then be seen in Figure 7.6.

Here, it is shown that the region of double intersections fall within the product specification target area of 90% intermediate (depicted by the bold triangle on the intermediate boiling vertex on the MBT). This design can consequently be considered feasible. Notice that the location of the saddle point of the red CPM in Figure 7.6 is located on the exact pinch coordinates that were chosen for this CS. Moreover, note that the attainable region shown here is again partly enclosed by TTs. As mentioned in the previous infinite reflux case, we can choose to operate on any of the profiles in the shaded region. However, the intermediate product specification will only be achieved when the red profiles enter the product specification region. With knowledge that the two termination CSs (CS_A and CS_D) merely operate on their residue curves, we can tentatively propose a design, shown in Figure 7.7.

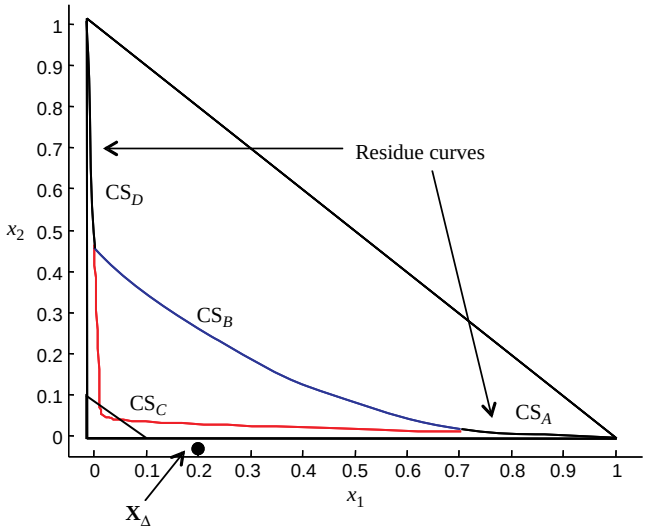


FIGURE 7.7 A possible design for the infinite reflux Petlyuk in Figure 7.2 column (with CS_B and CS_C at finite reflux) achieving $> 90\%$ intermediate-boiling component in the sidestream.

This design shows that the red profile enters the intermediate product specification region from where the sidestream product can be sampled. Notice that we could have very well chosen any combination of double intersecting profile. It is quite evident now why a pinch composition for CS_C better than the product specification was chosen: choosing the pinch composition to lie exactly on the boundary of the product specification region would mean that there would be only one double intersecting profile pair that would result in CS_C achieving the desired product purity. The fact that one may choose any one of a number of profiles running through the product specification region again alludes to the fact that there are multiple steady-state solutions in Petlyuk columns. Furthermore, it should be made clear that the two termination profiles (CS_A and CS_D) operate on their residue curves and thus both of them originate at their respective pure component vertices.

This section has thus presented a quick synthesis and analysis method for two simplified infinite reflux cases. Just like simple columns, it can be generally stated that if a design is considered feasible at infinite reflux conditions, then a feasible design can be found at finite reflux too. This fact is particularly useful for nonideal systems. An illustration of a more complex infinite Petlyuk column example is given in the following example for the azeotropic acetone/benzene/chloroform system.

Example 7.1: Determine whether it is feasible to obtain a sidestream product of 90% chloroform for the azeotropic acetone/benzene/chloroform system in an infinite reflux Petlyuk column with $R_{\Delta C} = 8$ and $R_{\Delta B} = -10$.

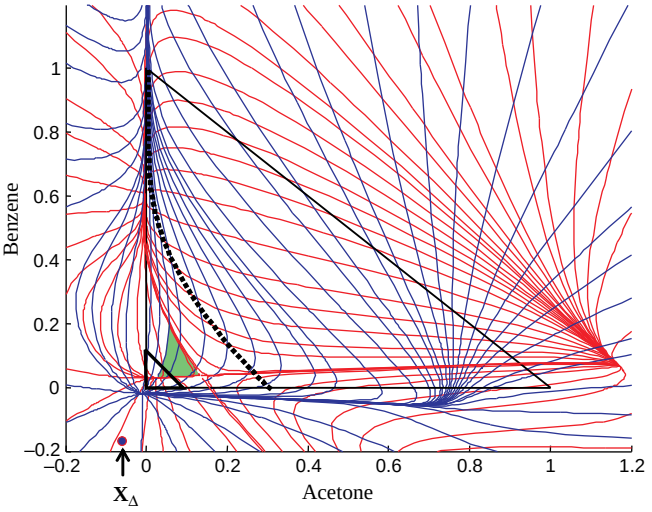


FIGURE 7.8 A possible design for the infinite reflux Petlyuk column for the acetone/benzene/chloroform system (with CS_B and CS_C at finite reflux) achieving > 90% chloroform in the sidestream.

Solution 7.1: As elucidated in the preceding text, it is necessary to identify the primary target for the intermediate stream, and then over-design the column slightly such that we can be assured that the primary target is satisfied. For this purpose, we'll again attempt to design for a sidestream composition of [0.03, 0.03]. Since CS_C is the sidestream producing CS its difference point can be determined through Equation 7.8, which is then also the operating difference point for CS_B. The difference point for both CS_B and CS_C (determined using CS_C's operating characteristics) is $\mathbf{X}_{\Delta C} = \mathbf{X}_{\Delta B} = [-0.0608, -0.1685]$. All information to plot CPMs for both CS_B and CS_C is now available; Figure 7.8 shows a superimposition of the respective CPMs, along with a green, shaded region highlighting the area where CPM profiles intersect twice (see color insert). Clearly, this shaded region has entered the area within our defined sidestream target lies, and therefore this particular design may be classified as feasible. It is also worth noting that that this particular system is in fact transgressing the distillation boundary (dashed black curve), since CS_A and CS_D are operating on RCMs and these CSs can therefore, theoretically, produce pure acetone and benzene, respectively.

7.3 GENERAL PETLYUK DESIGN

Fully thermally coupled columns can be very difficult columns to design because adjusting one variable may have multiple effects on the operation column. This was not the case in, for instance, simple columns as adjusting a parameter like the reflux ratio will only affect the profile intersection of the two applicable CSs. Thus, we will

first introduce here some general design ideas and goals of the Petlyuk column before targeting the actual design.

7.3.1 Degree of Freedom Analysis and Variable Selection

As one may infer from the structure of the Petlyuk column shown in Figure 7.1, the design procedure can be quite complex. The complication arises mainly due to the multiple degrees of freedom brought about by the thermal coupling of a prefractionating unit with a main column. Just as for the simplest of columns, these degrees of freedom can be divided into internal and external variables. External variables are generally product/feed compositions or flowrates that satisfy the overall material balance of a column. Internal degrees of freedom, on the other hand, are concerned with the inner workings of the column, such as reflux ratios or difference points in certain CSs.

Since a control volume over the Petlyuk column has one inlet stream, the feed stream, and three product streams, its external degree of freedom properties are exactly the same as other single-feed-three-product columns, such as side rectifiers or strippers (see Section 6.4.2). In Chapter 6, we concluded that there are six external variables that the designer is required to set for such columns. Now, these six variables may be set either through the flowrates or compositions of the product streams, but it is probably more pragmatic to specify all the product compositions since these are generally the most important factors in a design. Thus, in this chapter, we will choose to set $\mathbf{x}_D$, $\mathbf{x}_S$, and $\mathbf{x}_B$ which will set all six external degrees of freedom and allow us to calculate the product flowrates. Furthermore, it is assumed that the feed quality (q) is given and also that it is known whether the side-draw product stream is vapor or liquid.

The true difficulty in the design of the Petlyuk column however arises from specifying the internal degrees of freedom since these variables are inextricably linked to one another, and it is not always obvious which variables to choose such that meaningful conclusions can be drawn from the design. Generally, assuming the external degrees of freedom have been set, the Petlyuk requires that three internal flow variables be set (one for each thermally coupled junction and a reflux ratio for either CS_1 or CS_6), and one internal compositional variable, that is, a difference point of one of the internal CSs. Just as with simple columns, the total number of stages, and the position of the feed stage and side-draw stage are not considered as degrees of freedom as these may be inferred once the design is complete by tracing the value for n from a particular CS's starting and termination point.

Let us first treat the three internal flow variables required to be specified in the Petlyuk. Satisfying this requirement essentially means setting the reflux ratios in three CSs. Again it is useful to specify a reference reflux. For this purpose it is useful to specify the reflux ratio in either CS_1 or CS_6, but we will choose to set $R_{\Delta 1}$ throughout this chapter. The two remaining flow variables are thus associated with the internal CSs (2–5), and therefore require that the reflux ratios in any two of these CSs be set. This is not an easy task, because refluxes can be positive or negative, and their magnitudes are not bound. Thus, just as with side-rectifiers and

-strippers, it is convenient to use a split ratio that governs the amount of material directed to one part of the column at the thermally coupled junction. For the Petlyuk column, we shall define these distribution ratios at the uppermost thermal coupling as (refer to Figure 7.1)

$$\Phi_L = \frac{L_2}{L_1} \tag{7.9}$$

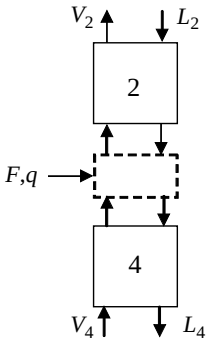
$$\Phi_V = \frac{V_2}{V_1} \tag{7.10}$$

The parameter Φ_L governs the amount of liquid in CS_1 that is directed toward CS_2 at the thermally coupled junction at the top of the column. The liquid flowrate then directed toward CS_3 is simply equal to $(1 - \Phi_L)L_1$. The parameter Φ_V dictates how much of the vapor being fed to CS_1 comes from CS_2, and again subtracting this fraction from unity gives the vapor fraction of vapor coming from CS_3. Equivalently, we could have chosen to use the actual vapor split at the thermally coupled point at the bottom of the column, but it is more convenient when constructing internal mass balances for the column to define both variables at one point. Φ_V is as such not a split ratio in a strict sense, but can be thought of as a mixing ratio. For the sake of consistency and brevity, Φ_V will however referred to as a split ratio. Importantly, with the use of the material distribution ratios, we have confined our degrees of freedom to lie within zero and one. It does not matter whether a certain CS is in rectifying or stripping mode, the appropriate Φ_L–Φ_V coordinate is still constrained to lie within these bounds. Furthermore, it is much easier to comprehend the multiple effects of this constrained parameter for design purposes than reflux values. The true value of this will become evident in the sections that follow where it will be shown how numerous variables can be represented in the Φ-space.

We have now established a convenient way of specifying and representing the internal flow variables in the column. As mentioned previously, the designer is still required to specify an internal composition variable in the column. The choice of the compositional variable will be discussed in greater detail later, but for now it will suffice to state that we will specify the difference point of CS_3 ($\mathbf{X}_{\mathbf{\Delta}3}$). The reason behind choosing this specific variable and making an intelligent choice for it will become clear in the discussions in Section 7.3.3.

7.3.2 Net Flow Patterns

The columns that have been dealt with thus far all have a commonality in that there is only one viable flow pattern to consider in the design. By flow pattern, we mean the general direction in which material flows up or down the column. For instance, in a simple one-feed-two-product column, the only possible flow pattern is that of material flowing upward in the CS above the feed, that is, the rectifying CS characterized by $\Delta > 0$, and material flowing downward in the CS below the feed, that is, the stripping CS characterized by $\Delta < 0$. Other columns can be



Overall material balance:

$$L_2 + V_4 + Fq = L_4 + V_2 + F(1-q)$$

Rearranging:

$$V_4 - L_4 + F = V_2 - L_2$$

$$\Delta_4 = \Delta_2 - F$$

FIGURE 7.9 Material balance across the Petlyuk feed stage.

interpreted similarly and it can be shown that there is only one feasible flow pattern in each of them. The Petlyuk column, however, is unique in this sense because there are multiple directions in which material can flow. Put in another way, there is not an obvious or set material flow direction in a particular CS in the Petlyuk column. CSs may operate in either rectifying or stripping mode ($\Delta > 0$ or $\Delta < 0$), and even in some instances in neither ($\Delta = 0$). With this in mind, let us start to decompose the column to identify possible flow patterns. First, consider the feed stage located between CS_2 and CS_4, as shown in Figure 7.9.

The material balance shown in Figure 7.9 indicates that the net flow in CS_2 and CS_4 is independent of the quality of the feed. This balance across the feed stage lends an important insight into why multiple flow patterns are possible in the Petlyuk column: neither CS_2 nor CS_4 produce end products, and thus the net flow in each of these CSs do not have to match any external degrees of freedom. In the case of the simple column, each CS *must* have a certain net flow value that is equal to the amount of product being drawn off from that CS. In the case of the Petlyuk column however, CS_2 or CS_4 may be either positive or negative with respect to net flow. One may consequently conceive four possible flow directions across the feed stage, summarized in Figure 7.10.

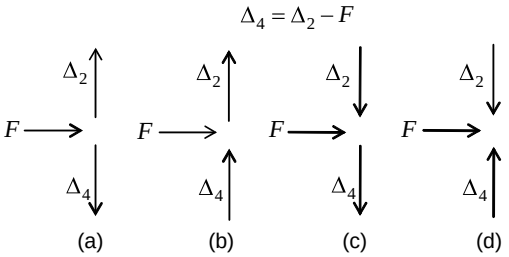


FIGURE 7.10 Feasible flow directions of the CSs across Petlyuk feed stage: (a) $\Delta_2 > 0$ and $\Delta_4 < 0$, (b) $\Delta_2 > 0$ and $\Delta_4 > 0$, and (c) $\Delta_2 < 0$ and $\Delta_4 < 0$. Infeasible flow directions: (d) $\Delta_2 < 0$ and $\Delta_4 > 0$.

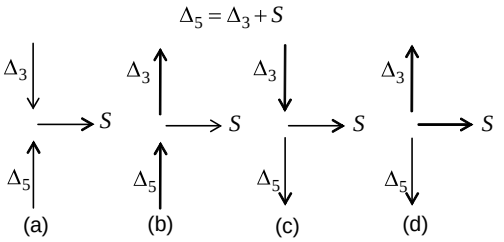


FIGURE 7.11 Feasible flow directions of the CSs across Petlyuk side-draw stage: (a) $\Delta_3 < 0$ and $\Delta_5 > 0$, (b) $\Delta_3 > 0$ and $\Delta_5 > 0$, and (c) $\Delta_3 < 0$ and $\Delta_5 < 0$. Infeasible flow directions: (d) $\Delta_3 > 0$ and $\Delta_5 < 0$.

Figure 7.10 illustrates that there are four possible flow patterns across the feed stage with different combinations of positive and negative net flows. However, the flow directions shown in Figure 7.10d are not considered feasible because this choice of flow directions violates the material balance formulated in Figure 7.9. If Δ_2 is a negative value and Δ_4 is a positive value, the result is that material has to be removed across the feed stage (and not added) because the quantity F will be negative. Depending on the phase equilibrium behavior and the objectives of the column, some of these flow patterns may hold advantages over other modes of operation, as will be highlighted in subsequent discussions.

Similarly, one may consider the material balance across the side-draw stage too. Since the side-draw product stream is not terminated by a reboiler or a condenser, there is no exact value that the net flow in either CS_3 or CS_5 is required to be. Thus, just like the CSs across the feed stage, there are multiple flow directions that may exist across the side-draw stage. These are depicted in Figure 7.11a–d.

It is no surprise that the feasible flow directions across the side-draw stage are the inverse of those across the feed stage. The flow directions shown in Figure 7.11d are infeasible because it would imply, by mass balance, that material addition is required at the side-draw stage and not material removal.

In a similar way to which feasible flow directions at the side-draw and feed stages were determined, a summary of the net flow directions at the bottommost thermally coupled point is given in Figure 7.12. By simple symmetry, the topmost thermally

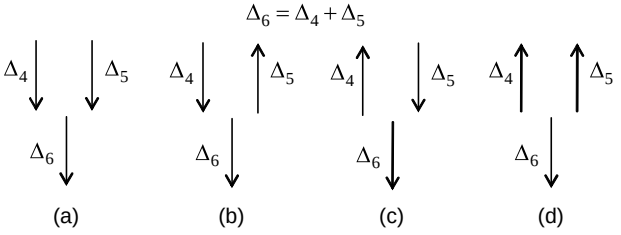


FIGURE 7.12 Feasible flow directions of the CSs at the bottommost thermally coupled point: (a) $\Delta_4 < 0$ and $\Delta_5 < 0$, (b) $\Delta_4 < 0$ and $\Delta_5 > 0$, and (c) $\Delta_4 > 0$ and $\Delta_5 < 0$. Infeasible flow directions: (d) $\Delta_4 > 0$ and $\Delta_5 > 0$.

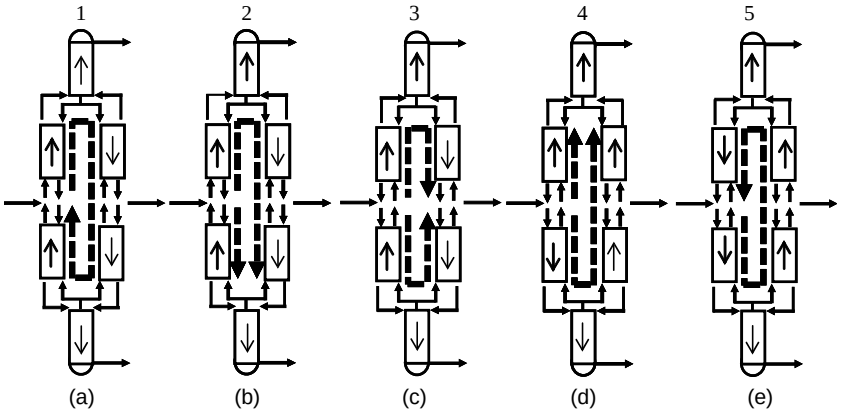


FIGURE 7.13 Five different global FPs for the Petlyuk column, labeled 1–5.

coupled point will have analogous properties. It should be noted that the flow directions of CS_1 and CS_6 do not allow the same flexibility with regard to alternate flow directions because the net flowrates in these CSs have to match the product flowrates. Thus, CS_1 is always in rectifying mode with $\Delta_1 = D$ and CS_6 is always in stripping mode with $\Delta_6 = -B$. It therefore follows that the operating flow pattern (FP) of the Petlyuk column is solely determined by the *internal* CSs (CS_{2-5}). The culmination of all the feasible flow directions illustrated in Figures 7.10–7.12 results in five global FPs in total for the Petlyuk column, shown in Figure 7.13.

FP_3 in Figure 7.13c is the only symmetric flow arrangement in the Petlyuk. We shall discuss all other flow patterns using this FP as reference. In FP_3, material is directed both upward and downward across the feed stage. This specific FP essentially divides the column into symmetrical top and bottom halves of net flow. If one were to increase the net material directed toward the bottom half of the column, FP_4 comes into existence. For this FP, material must be directed upward on the product side of the column (CS_3 and CS_5) in order to maintain the material balance constraints of the column. Conversely, by increasing the net material directed toward the top half of the column, FP_2 is achieved, and this case is the exact opposite of that in FP_4. By increasing the material directed to the top half even further, the material eventually circulates clockwise within the coupled sections, flowing upward in CS_4 instead of downward as depicted in FP_1. Similarly, if the material directed downward on the feed side is increased further, FP_5 is achieved where material is circulated in an anticlockwise direction.

It is interesting to note that for all FPs other than FP_3, the net flows in the CSs above and below the side-draw stage (CS_3 and CS_5) are in the same direction. This means that both these CSs will have the same sign for the net flow as well as reflux. This does not seem to be a problem on face value, but one needs to consider how the refluxes in these CSs come about and what their roles are. It can be shown that

TABLE 7.1 Net Flow Direction in Each CS for Different FPs

FP	Δ_1	Δ_2	Δ_3	Δ_4	Δ_5	Δ_6
1	+	+	−	+	−	−
2	+	+	−	−	−	−
3	+	+	−	−	+	−
4	+	+	+	−	+	−
5	+	−	+	−	+	−

removing a liquid side-draw product increases the absolute value of the reflux from the CS above the side-draw stage CS (CS_3) to the one below it (CS_5). If, for instance, both these refluxes are negative, the reflux of CS_5 will have a larger magnitude, that is, a large negative number, than that of CS_3, a smaller negative number. If the magnitude of the reflux of CS_3 is to be large enough to have the column operating on specification, the reflux in CS_5 must be quite high in order to compensate for this. Working one's way upward in the column from CS_3 implies that CS_1 also has to have a fairly high reflux, forcing the reflux in CS_6 to be large too. This means, from a qualitative view, that the column will be energy intensive. The same argument can be made if both refluxes are positive. However, FP_3 does not have this drawback because the reflux changes sign across the side-draw stage and is therefore likely to be the most energy efficient operating mode.

Now that we have identified the five different FPs that permit feasible Petlyuk operation and qualitatively understood each of their effects, it is now of interest to obtain a more tangible understanding. First consider then Table 7.1, which shows the net flow direction in each CS for each of the five FPs.

Table 7.1 shows that the change in one global FP to the next is caused by the net flow in a single CS changing sign. For instance, the net flow directions in each CS of FP_1 and FP_2 are the same, except for CS_4. This implies that when the net flow in CS_4 changes, the FP also changes from FP_1 to FP_2. A similar argument can be made for the transition between FP_2 and FP_3 (and all subsequent FPs), whereas in this case, the net flow in CS_5 has changed its direction. Notice again that CS_1 and CS_6 retain their net flow direction regardless of the FP. There is therefore an exact condition where FP changes occur: a change in net flow direction in CS_{2-5} has associated with it a change in the FP. The exact point of transition will occur where the net flow in the specific CS is zero, as this is the crossover point from positive to negative reflux. Using this knowledge, we can formally write net flow equations that will satisfy these conditions. Thus, starting from CS_2 and writing each equation in terms of our defined split ratios, we obtain

$$\begin{aligned} \Delta_2 &= D\Phi_V(1 + R_{\Delta 1}) - D\Phi_L R_{\Delta 1} = 0, \\ \therefore \Phi_L &= \frac{\Phi_V(1 + R_{\Delta 1})}{R_{\Delta 1}} \end{aligned} \tag{7.11}$$

$$\Delta_3 = D(1+R_{\Delta 1})(1-\Phi_V) - DR_{\Delta 1}(1-\Phi_L) = 0,$$
$$\therefore \Phi_L = \frac{(1+R_{\Delta 1})(\Phi_V - 1)}{R_{\Delta 1}} + 1 \tag{7.12}$$

$$\Delta_4 = D\Phi_V(1+R_{\Delta 1}) - F - D\Phi_L R_{\Delta 1} = 0,$$
$$\therefore \Phi_L = \frac{D\Phi_V(1+R_{\Delta 1}) - F}{DR_{\Delta 1}} \tag{7.13}$$

$$\Delta_5 = D(1+R_{\Delta 1})(1-\Phi_V) + DR_{\Delta 1}(1-\Phi_L) - S = 0,$$
$$\therefore \Phi_L = \frac{D(1+R_{\Delta 1})(\Phi_V - 1) - S}{DR_{\Delta 1}} + 1 \tag{7.14}$$

Through Equations 7.11–7.14 we now have formal conditions which dictate when changes in the global FP will occur. Notice that each of these equations is a linear function in terms of Φ_V and Φ_L and depend only on the reflux in the topmost (reference) CS ($R_{\Delta 1}$), the Distillate, Feed, and Side-draw flowrates (D, F, and S, respectively). Recall, however, that for a fixed feed flowrate, the quantities D and S are dependent on the specified product compositions one wishes to achieve. Interestingly, these net flow boundaries are independent of the feed quality or whether the side-draw is removed as a vapor or liquid product. Thus, for an arbitrary choice of product compositions and $R_{\Delta 1}$, we can represent the transition from one FP to the next in a Φ_V versus Φ_L diagram, as shown in Figure 7.14.

Representing these net flow variables in Φ-space is a very convenient way to assess which combination of Φ_V and Φ_L will result in a certain FP. The bottom-right part of the diagram below the $\Delta_4 = 0$ line represents all values of Φ_V and Φ_L that will result in FP_1. In this region, $\Delta_4 > 0$, and when one crosses the $\Delta_4 = 0$ line causing $\Delta_4 < 0$, a change in the global flow pattern occurs and the column operates in the FP_2 mode. One can see in a similar way that each subsequent crossing of these net flow boundaries will result in a different flow pattern. It is interesting note that when one chooses to operate exactly on one of these zero net flow boundaries, that particular CS will operate at infinite reflux (recall that when the $\Delta = 0$, $R_\Delta = \infty$), and thus the column profiles for these CSs will operate on the residue curves if $X^T = Y^T$. It is also important to point out that these FP boundary lines are always parallel to one another since they all have identical slopes of $(1+R_{\Delta 1})/R_{\Delta 1}$. Furthermore, the FP boundaries are unique for specific feed/product and $R_{\Delta 1}$ specifications.

7.3.3 Difference Point Behavior and Placement

7.3.3.1 Geometric Interpretation In all the structures we have investigated in the preceding chapters of the book, we have seen that the $\mathbf{X_\Delta}$'s of adjacent CSs

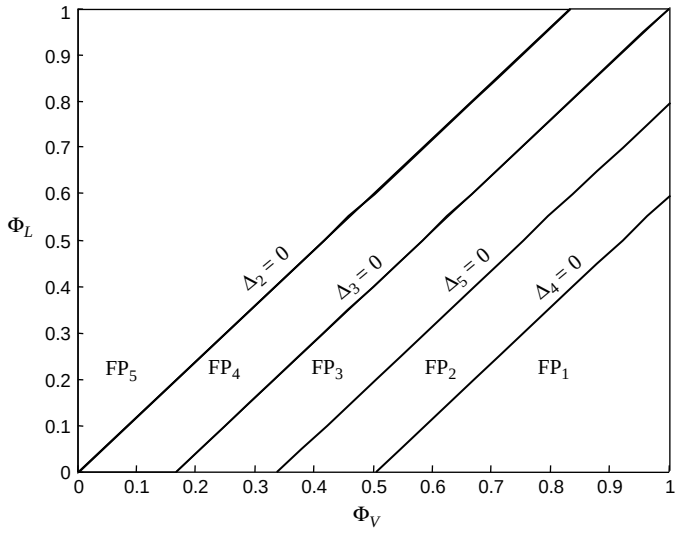
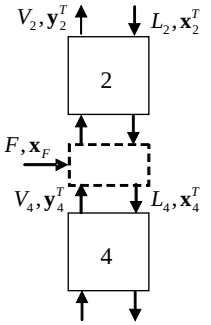


FIGURE 7.14 Representation of FP transition in Φ-space for the Petlyuk column.

behave like real compositions because there is a linear relationship between them. As one may expect, this is the case for the Petlyuk too. However, because there are different permissible FPs in this structure, different relationships between the difference points of adjacent CSs may also arise. The relationship between the difference points across the feed stage and side-draw stage are given in Figures 7.15 and 7.16 , respectively, while the mass balance around the topmost thermally coupled junction is given in Figure 7.17.

Let us first treat the difference points across the feed stage depicted in Figure 7.15. It is again important to stress that in simple columns, a similar balance can be arrived at, but the net flowrates (Δ) and difference points are fixed by the product specifications of the column. In the Petlyuk column there is no such requirement



$$L_2\mathbf{x}_2^T + V_4\mathbf{y}_4^T + F\mathbf{x}_F = V_2\mathbf{y}_2^T + L_4\mathbf{x}_4^T$$

Rearranging:

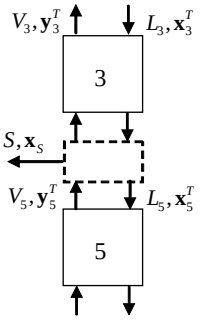
$$V_4\mathbf{y}_4^T - L_4\mathbf{x}_4^T + F\mathbf{x}_F = V_2\mathbf{y}_2^T - L_2\mathbf{x}_2^T$$

$$\Delta_4\left(\frac{V_4\mathbf{y}_4^T - L_4\mathbf{x}_4^T}{\Delta_4}\right) + F\mathbf{x}_F = \Delta_2\left(\frac{V_2\mathbf{y}_2^T - L_2\mathbf{x}_2^T}{\Delta_2}\right)$$

Therefore,

$$\Delta_4\mathbf{X}_{\Delta 4} + F\mathbf{x}_F = \Delta_2\mathbf{X}_{\Delta 2}$$

FIGURE 7.15 Magnified view of CS_2 and CS_4 with all stream definitions and a component balance for a generic feed.



$$L_3\mathbf{x}_3^T + V_5\mathbf{y}_5^T - S\mathbf{x}_S = L_5\mathbf{x}_5^T + V_3\mathbf{y}_3^T$$

Rearranging:

$$V_5\mathbf{y}_5^T - L_5\mathbf{x}_5^T - S\mathbf{x}_S = V_3\mathbf{y}_3^T - L_3\mathbf{x}_3^T$$

$$\Delta_5\left(\frac{V_5\mathbf{y}_5^T - L_5\mathbf{x}_5^T}{\Delta_5}\right) - S\mathbf{x}_S = \Delta_3\left(\frac{V_3\mathbf{y}_3^T - L_3\mathbf{x}_3^T}{\Delta_3}\right)$$

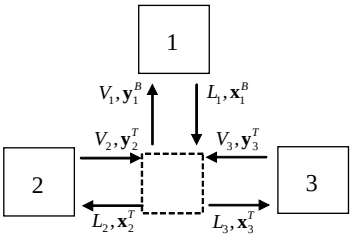
Therefore,

$$\Delta_5\mathbf{X}_{\Delta 5} - S\mathbf{x}_S = \Delta_3\mathbf{X}_{\Delta 3}$$

FIGURE 7.16 Magnified view of CS_3 and CS_5 with all stream definitions and a component balance for a sidestream product.

across the feed stage because the associated CSs are not required to produce any products although the linear relationship between the difference points still has to be maintained. We have shown in Section 7.3.2 that there are five FPs possible in a Petlyuk column where certain combinations of both positive and negative Δ values are permissible, and because of this, alternate difference points placements are also permissible, as can be inferred from Figure 7.15. It is worthy to point out from Table 7.1 that the net flow directions for the CSs across the feed stage (CS_2 and CS_4) in FPs 2, 3, and 4 are all equivalent, but are different for FP_1 and FP_5, respectively. Thus, for FP_1 and FP_5, we may expect alternate difference point behavior, which is depicted geometrically in Table 7.2.

Interestingly, FPs 2, 3, and 4 have the same properties as simple columns regarding the position of the feed composition and the difference point position on either side of it. FPs 1 and 5 however do not have this property and in these cases the feed composition lies on one side of both the difference points. This alternate placing of difference points may introduce unusual topological behavior within our system that we may want to exploit. This can be achieved by simply choosing a different FP. As one may expect, similar difference point properties exist across the side-draw stage, as inferred from the mass balance in Figure 7.16. These are summarized geometrically in Table 7.3.



$$L_1\mathbf{x}_1^B + V_2\mathbf{y}_2^T + V_3\mathbf{y}_3^T = L_2\mathbf{x}_2^T + V_1\mathbf{y}_1^B + L_3\mathbf{x}_3^T$$

Rearranging:

$$V_2\mathbf{y}_2^T - L_2\mathbf{x}_2^T + V_3\mathbf{y}_3^T - L_3\mathbf{x}_3^T = V_1\mathbf{y}_1^B - L_1\mathbf{x}_1^B$$

$$\Delta_2\left(\frac{V_2\mathbf{y}_2^T - L_2\mathbf{x}_2^T}{\Delta_2}\right) + \Delta_3\left(\frac{V_3\mathbf{y}_3^T - L_3\mathbf{x}_3^T}{\Delta_3}\right) = \Delta_1\left(\frac{V_1\mathbf{y}_1^B - L_1\mathbf{x}_1^B}{\Delta_1}\right)$$

Therefore,

$$\Delta_2\mathbf{X}_{\Delta 2} + \Delta_3\mathbf{X}_{\Delta 3} = \Delta_1\mathbf{X}_{\Delta 1}$$

FIGURE 7.17 Magnified view of the topmost thermally coupled junction CS_1, CS_2, and CS_3 with all stream definitions and a component balance.

TABLE 7.2 Geometric Description of Difference Points Across the Feed Stage

FP	Δ_2	Δ_4	Relative Difference Point Position
1	+	+	$\mathbf{X}_{\Delta 4}$ $\mathbf{X}_{\Delta 2}$ $\mathbf{x}_F$
2, 3, 4	+	−	$\mathbf{X}_{\Delta 4}$ $\mathbf{x}_F$ $\mathbf{X}_{\Delta 2}$
5	−	−	$\mathbf{X}_{\Delta 2}$ $\mathbf{X}_{\Delta 4}$ $\mathbf{x}_F$

Table 7.3 shows similar type behavior of the difference points with respect to the side-draw composition. All FPs, except for FP_3, have the property that difference points lay on either side of the side-draw composition. Table 7.4 shows the difference point placements for each FP for the thermally coupled junctions, a result of the mass balances shown in Figure 7.17.

Typical difference point placements for each of the FPs are shown in Figure 7.18a–e. These were generated by collectively looking at the four mass balances (around the feed, side-draw product, and both thermally coupled sections at the top and bottom). Each of the dotted lines represents each of these mass balances, adhering to the net flow direction of the CSs as shown in Figure 5.12. It is remarkable to note that the nonsymmetric FPs (FP_1, FP_2, FP_4, FP_5) force either $\mathbf{X}_{\mathbf{\Delta}2}$ or $\mathbf{X}_{\mathbf{\Delta}4}$ to lie in negative composition space, meaning that these FPs may lend themselves to exploiting interesting topological behavior, especially when the phase equilibrium behavior is complex. It is also entirely possible for $\mathbf{X}_{\mathbf{\Delta}3}$ or $\mathbf{X}_{\mathbf{\Delta}5}$ to be shifted into negative composition space, but this depends on the choice of the internal compositional degree of freedom, to be discussed in the following section.

7.3.3.2 Difference Point Placement Now that we have established a geometric interpretation of the effects of the FP on difference point, we turn our attention toward specifying the remaining internal degrees of freedom. When setting up the internal material balance equations for the Petlyuk it can be shown that a difference point of an internal CS needs to be specified to complete the column specification. This additional degree of freedom arises because the

TABLE 7.3 Geometric Description of Difference Points Across the Side Draw Stage

FP	Δ_3	Δ_5	Relative Difference Point Position
1, 2	−	−	$\mathbf{X}_{\Delta 5}$ $\mathbf{X}_{\Delta 3}$ $\mathbf{x}_S$
3	+	−	$\mathbf{X}_{\Delta 3}$ $\mathbf{x}_S$ $\mathbf{X}_{\Delta 5}$
4, 5	+	+	$\mathbf{X}_{\Delta 3}$ $\mathbf{X}_{\Delta 5}$ $\mathbf{x}_S$

TABLE 7.4 Geometric Description of Difference Points Across the Thermally Coupled Junctions

	Relative Difference Point Position	
FP	Top	Bottom
1	$\mathbf{X}_{\Delta 3}$ $\mathbf{X}_{\Delta 2}$ $\mathbf{X}_{\Delta 1}$	$\mathbf{X}_{\Delta 6}$ $\mathbf{X}_{\Delta 5}$ $\mathbf{X}_{\Delta 4}$
2	$\mathbf{X}_{\Delta 3}$ $\mathbf{X}_{\Delta 2}$ $\mathbf{X}_{\Delta 1}$	$\mathbf{X}_{\Delta 4}$ $\mathbf{X}_{\Delta 6}$ $\mathbf{X}_{\Delta 5}$
3	$\mathbf{X}_{\Delta 3}$ $\mathbf{X}_{\Delta 2}$ $\mathbf{X}_{\Delta 1}$	$\mathbf{X}_{\Delta 6}$ $\mathbf{X}_{\Delta 4}$ $\mathbf{X}_{\Delta 5}$
4	$\mathbf{X}_{\Delta 3}$ $\mathbf{X}_{\Delta 1}$ $\mathbf{X}_{\Delta 2}$	$\mathbf{X}_{\Delta 6}$ $\mathbf{X}_{\Delta 4}$ $\mathbf{X}_{\Delta 5}$
5	$\mathbf{X}_{\Delta 2}$ $\mathbf{X}_{\Delta 3}$ $\mathbf{X}_{\Delta 1}$	$\mathbf{X}_{\Delta 6}$ $\mathbf{X}_{\Delta 4}$ $\mathbf{X}_{\Delta 5}$

difference points of the CSs across the side-draw stage need not be equal to the side-draw specification because this stream is removed without a reboiler or a condenser. Thus, a difference point of an internal CS has to be specified, from which the remaining difference points can be calculated.

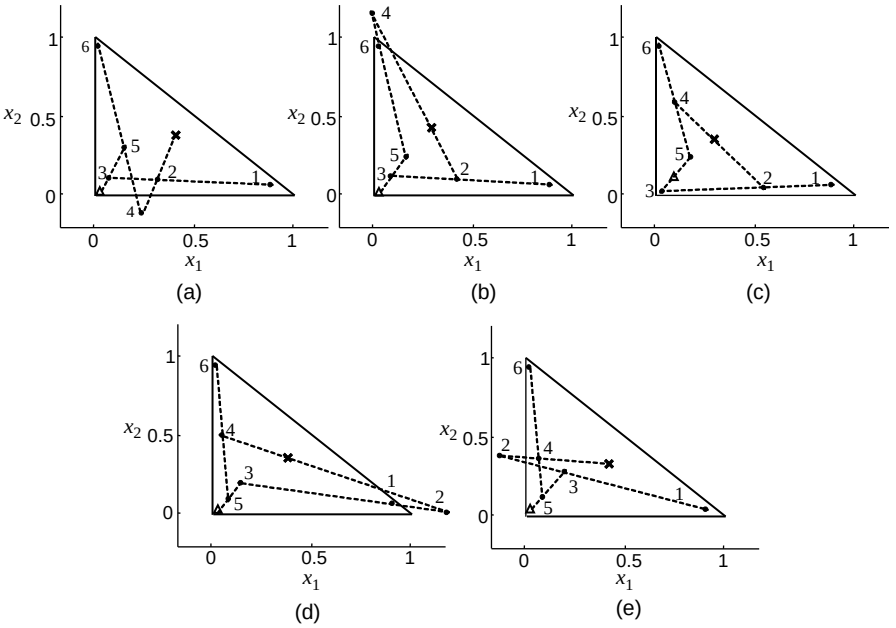


FIGURE 7.18 Difference point placements for (a) FP_1, (b) FP_2, (c) FP_3, (d) FP_4, and (e) FP_5. The labeled numbers in on each figure indicate the position of a particular CS's $\mathbf{X}_{\Delta}$ placement, and markers Δ and $\times$ indicate the side-draw and feed compositions, respectively.

Clearly, we have four possible choices for placing this variable difference point, as there are four internal CSs. This can be a very complicated matter, but we can choose to place the difference point of a CS of which we know the primary function and operation mode of. CS_3 is a very good candidate for this choice, because we know what the primary goal of CS_3 is: to transport significant quantities of intermediate-boiling component toward the side-draw stream. A similar argument can be made for CS_5. Thus, the net compositional flow in CS_3 should predominantly aid in producing a high-purity intermediate-boiling product. In terms of difference point placement, this implies that $\mathbf{X}_{\boldsymbol{\Delta}3}$ should be placed near the intermediate boiling vertex. Although it is difficult to quantify what a "high purity intermediate" actually is, or what a "high-enough purity intermediate" is, we will regard this as an additional degree of freedom which the designer can determine through trial-and-error. Nonetheless, with the arguments presented here it should be possible to, at least approximately, establish suitable difference point placements for the Petlyuk.

7.3.4 Reflux Ratios

Since the reflux ratios are, by definition, dependent on the net flow of a particular CS, the same arguments put forward in Sections 7.3.2 will hold for reflux ratios with regard to net FPs. For instance, choosing a FP that will lead to CS_2 having a negative net flow will cause the value of $R_{\Delta 2}$ to also be negative in this CS. However, because R_Δ is defined as the ratio of liquid flowrate to the net flowrate in a particular CS, the actual value of R_Δ in a particular CS depends on the quality of the feed, and whether the side-draw product is liquid or vapor. Just as we have conveniently represented net flow patterns in Φ-space, we can also then construct lines of constant reflux in the Φ-space, which will ultimately allow us to hone in on feasible designs, as will be illustrated in Section 7.4. In order to do this, it is necessary to write all our reflux equations in terms of Φ_V and Φ_L, as shown in the equations below

$$R_{\Delta 2} = \frac{\Phi_L R_{\Delta 1}}{\Phi_V(1 + R_{\Delta 1}) - \Phi_L R_{\Delta 1}}$$
$$\therefore \Phi_L = \frac{R_{\Delta 2}(R_{\Delta 1} + 1)\Phi_V}{R_{\Delta 1}(R_{\Delta 2} + 1)} \tag{7.15}$$

$$R_{\Delta 3} = \frac{R_{\Delta 1}(\Phi_L - 1)}{(1 + R_{\Delta 1})(\Phi_V - 1) - R_{\Delta 1}(\Phi_L - 1)}$$
$$\therefore \Phi_L = \frac{R_{\Delta 3}(R_{\Delta 1} + 1)\Phi_V + R_{\Delta 1} - R_{\Delta 3}}{R_{\Delta 1}(R_{\Delta 3} + 1)} \tag{7.16}$$

$$R_{\Delta 4} = \frac{DR_{\Delta 1}\Phi_L + Fq}{F + D\Phi_V(1 + R_{\Delta 1}) - DR_{\Delta 1}\Phi_L}$$
$$\therefore \Phi_L = \frac{DR_{\Delta 4}(1 + R_{\Delta 1})\Phi_V - F(q + R_{\Delta 4})}{DR_{\Delta 1}(1 + R_{\Delta 4})} \tag{7.17}$$

For a liquid side-draw

$$R_{\Delta 5} = \frac{S + DR_{\Delta 1}(\Phi_L - 1)}{D(1 + R_{\Delta 1})(\Phi_V - 1) - DR_{\Delta 1}(\Phi_L - 1) - S}$$
$$\therefore \Phi_L = \frac{DR_{\Delta 5}(R_{\Delta 1} + 1)\Phi_V - S(R_{\Delta 5} + 1) + D(R_{\Delta 1} - R_{\Delta 5})}{DR_{\Delta 1}(R_{\Delta 5} + 1)} \tag{7.18}$$

For a vapor side-draw

$$R_{\Delta 5} = \frac{DR_{\Delta 1}(\Phi_L - 1)}{D(1 + R_{\Delta 1})(\Phi_V - 1) - DR_{\Delta 1}(\Phi_L - 1) - S}$$
$$\therefore \Phi_L = \frac{DR_{\Delta 5}(R_{\Delta 1} + 1)\Phi_V - SR_{\Delta 5} + D(R_{\Delta 1} - R_{\Delta 5})}{DR_{\Delta 1}(R_{\Delta 5} + 1)} \tag{7.19}$$

$$R_{\Delta 6} = \frac{DR_{\Delta 1} + Fq}{-B} \tag{7.20}$$

Equations 7.15–7.20 are all written in terms of our "reference reflux" ($R_{\Delta 1}$), the vapor and liquid split ratios, and the product flowrates. Again, writing these variables in terms of the split ratios allows one to represent reflux ratios, similarly to the net flow for each CS, in the Φ-space, although $R_{\Delta 6}$ is not a function of either split ratio and can therefore not be represented in Φ-space. These reflux lines are linear in Φ-space, but unlike the net flow lines, they have different slopes which are always dependent on the value $R_{\Delta 1}$. Figure 7.19 shows a representation of constant reflux lines for each CS in Φ-space, illustrating the differing slopes and intercepts for the reflux in each CS for arbitrarily chosen product flowrates. We have also chosen arbitrary values for R_Δ in each CS, but we have chosen their signs such that net FP_3 is maintained. Notice that the constant R_Δ-lines do not intersect their corresponding zero net flow lines anywhere in the achievable Φ-space. This can be understood easily by remembering that the sign of the net flow in a CS, directly affects the sign of R_Δ in that CS. The constant R_Δ-line for a CS may thus only lie on one side of the corresponding zero net flow line, and it may never intersect it. The specific side on which the R_Δ line lies adjacent to its zero net flow line depends on

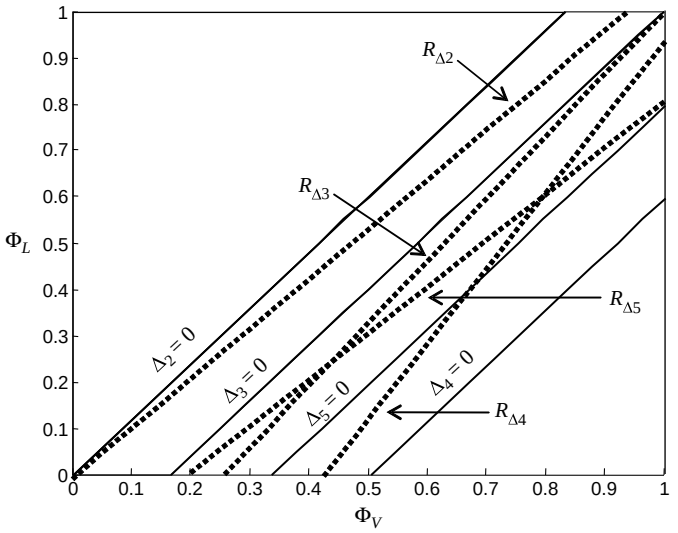


FIGURE 7.19 Representation of constant reflux lines in Φ-space for FP_3.

the net FP chosen. Although these arbitrarily chosen constant R_Δ lines chosen to construct Figure 7.19 may seem rather useless since they do not bring us any closer to finding realizable designs, it is useful for understanding the representation and effects of R_Δ in Φ-space.

7.3.5 Properties of Variables in Φ-Space

We have seen thus far that translating the internal variables of the Petlyuk into Φ-space allows one to easily assess operating conditions of the column. Overall column feasibility has not been addressed yet, but it will be shown in the section on sharp split Petlyuk design that the Φ-space allows one to construct an Attainable Region of operation. However, before dealing with this rather complicated matter, it is perhaps useful to first interpret the achievable FPs in a Petlyuk and how they might change under certain operating conditions.

It is useful to point out initially that since CS_3 or CS_5 has to produce a sidestream product, there is an automatic constraint that is placed on either of these CSs in terms of the minimum amount of material that has to flow through this CS, regardless of the FP of the Petlyuk. For example, if it is desirable to draw the sidestream as liquid stream from CS_3, then the magnitude of the liquid flowrate in CS_3 has to be at least as large as the sidestream product flowrate set by the external mass balance. This case can be expressed mathematically as

$$\begin{aligned} & L_3 \geq S \\ & \therefore \Phi_L \leq 1 - \frac{S}{DR_{\Delta 1}} \end{aligned} \tag{7.21}$$

Similarly, for the case of where we decide to draw vapor from CS_5

$$V_5 \geq S$$
$$\therefore \Phi_V \leq 1 - \frac{F}{D(R_{\Delta 1} + 1)} \tag{7.22}$$

Interestingly, neither one of these two material balance constraints are dependent on both Φ_V and Φ_L, implying that these lines are either completely horizontal (Equation 7.21) or completely vertical (Equation 7.22). An example of these lines are represented in Figure 7.20.

It is worth pointing out that there are no analogous material balance constraints for the bottoms and distillate product streams, because these constraints will always be met if a positive reflux value is chosen in CS_1. Material balance then dictates that the constraint in CS_6 is also met through Equation 7.20.

These material balance constraints are important from a design point of view because the combination of permissible Φ-values open to the design has been significantly reduced. In other words, the possible design space has been considerably reduced before we have even considered feasibility. Furthermore, upon closer inspection of Equations 7.21 and 7.22, we notice that when a large value of $R_{\Delta 1}$ is chosen, both Φ-values tend to unity. This results in a valuable conclusion: the larger $R_{\Delta 1}$ is, the larger the permissible design space becomes in the Φ-domain, and vice versa. The limit is of course when $R_{\Delta 1}$ is infinitely large, and the entire Φ-region becomes open for design.

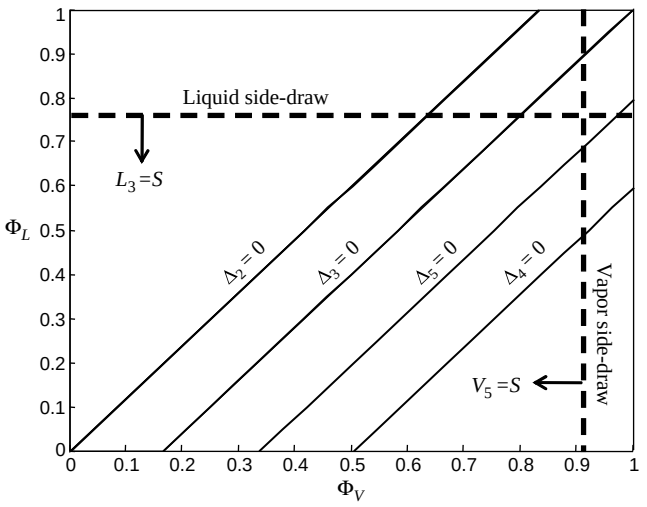


FIGURE 7.20 Representation of material balance constraints for the sidestream in Φ-space.

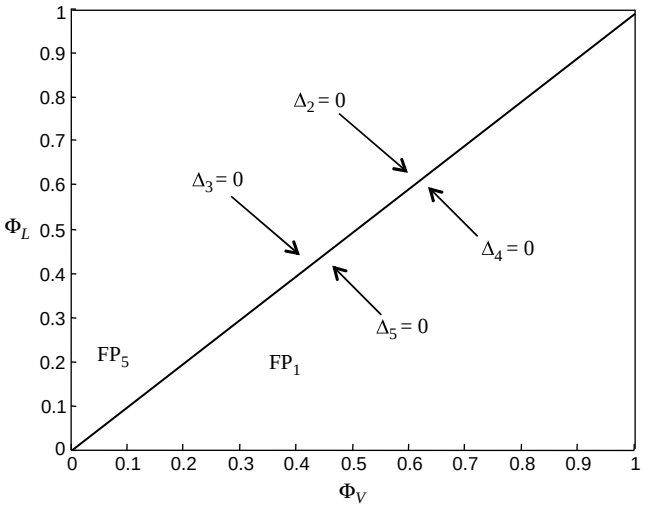


FIGURE 7.21 Collapsing of zero net flow boundaries when $R_{\Delta 1}$ is infinitely large in Φ-space.

Now that allowable design regions have been identified, we focus our attention to properties of the zero net flow boundaries in Φ-space, that is, what is the influence of adjusting certain variables on these FP boundaries. Through Equations 7.11–7.14 we have seen that these net flow boundaries are always parallel to each other because their slopes are equal. However, each of these FP boundaries may change with respect to one another since their *y*-intercept components are not the same. Let us first consider the case where CS_1 operates at infinite reflux. Equations 7.11–7.14 imply that when $R_{\Delta 1}$ is infinitely large, the *y*-intercept components are equivalent, and this intercept point is located at the origin in the Φ-space. Since their slopes are also equivalent, this means that all these zero net flow lines collapse on top of one another, as shown in Figure 7.21.

It is evident that when $R_{\Delta 1}$ is infinitely large there are essentially only two possible FPs, the outermost FP_1 and FP_5 (although the vapour and liquid flows in each CS are also infinitely large). All the other FP regions have been condensed to lie on a single line that has a slope of 1. Of course, the converse relationship is also true, the lower the value of $R_{\Delta 1}$ is, the more separated the FP boundaries are from one another because the respective y-intercepts of zero net flow equations differ considerably. The limit of $R_{\Delta 1} = 0$ in this case is meaningless because the condition implies that there is no liquid flowing in CS_1 and hence a liquid split ratio is nonsensical. Nonetheless, at very low refluxes, say 1, the FP regions become very separated, as shown in Figure 7.22.

Through Figures 7.21 and 7.22 the effect of $R_{\Delta 1}$ has been examined, but there are other factors that are also worth considering, most notably the effect of external mass balance variables *D* and *S*. By examining the $\Delta = 0$ equations for each CS (Equations 7.11–7.14), both *D* and *S* influence zero net flow y-intercepts

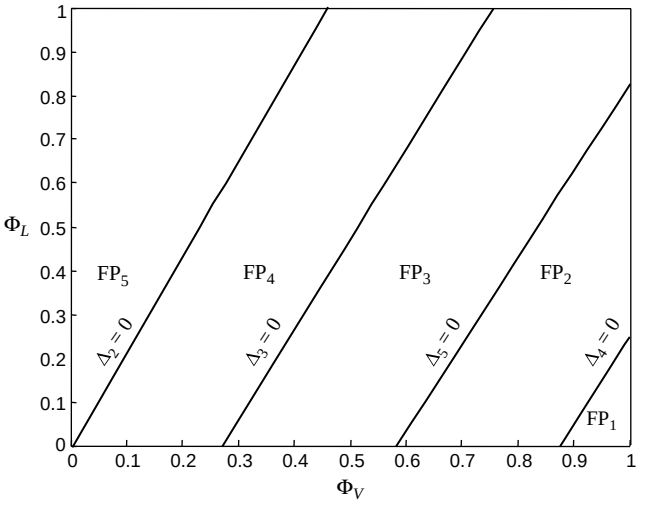


FIGURE 7.22 Separation of zero net flow boundaries when $R_{\Delta 1}$ is small in Φ-space.

of only CS_4 and CS_5, but not the other CSs. By closer inspection of Figure 7.14 or 7.22 it can be seen that the $\Delta_4 = 0$ and $\Delta_5 = 0$ lines only influence the regions of FP_1, FP_2, and FP_3, while FP_4 and FP_5 remain unchanged. To determine the effect of the external mass balance on FPs Equations 7.13 and 7.14 (the zero net flow equations of CS_4 and CS_5, respectively) can be rewritten to find the *y*-intercept value ($\Phi_V = 0$):

$$\Phi_L = \frac{-F}{DR_{\Delta 1}} \tag{7.23}$$

$$\Phi_L = \frac{-D - S}{DR_{\Delta 1}} = \frac{B - F}{DR_{\Delta 1}} \tag{7.24}$$

Equations 7.23 and 7.24 represent the *y*-intercepts for the zero net flow lines of CS_4 and CS_5, respectively. Equation 7.23 implies that if D is small with respect to F, Φ_L is a large negative number. This means that the $\Delta_4 = 0$ line is shifted to the right in the Φ-domain which in turn increases the region occupied by FP_2 in Figure 7.14, assuming that the $\Delta_5 = 0$ line remains fixed. However, the $\Delta_5 = 0$ line is also affected by the external mass balance. From Equation 7.24, it may be inferred that when $B = 0$, the intercepts of the $\Delta_4 = 0$ and $\Delta_5 = 0$ lines are equivalent, meaning that FP_2 disappears completely. A large sidestream product flowrate (S) makes the value of the *y*-intercept in Equation 7.24 a large negative number, moving this line downward and thereby increasing the FP_3 region, and vice versa. A summary of the effects of the external mass balance on the net FPs is given in Figure 7.23.

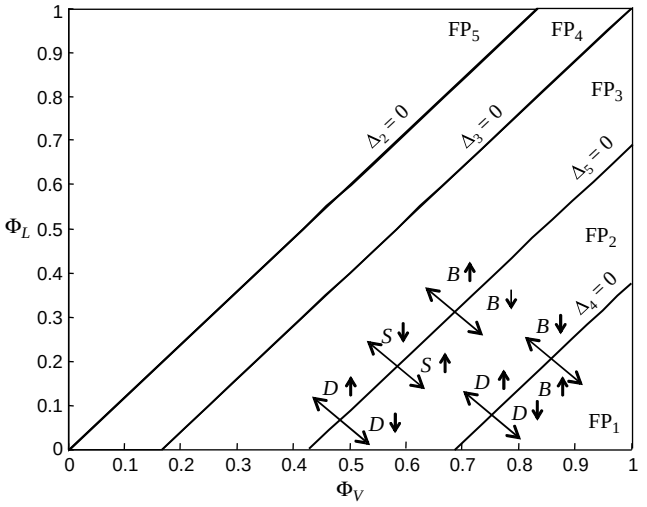


FIGURE 7.23 Summary of external mass balance effect on the net FP (↑ implies an increasing value, while ↓ implies a decreasing value).

At this moment in time it may seem rather senseless to understand the behavior of these FP regions. It will however be shown in the sections that follow, specifically in Section 7.4 on sharp split Petlyuk design using TTs, that FP_3 is the optimal FP. This may be different in other systems with nonideal behavior, but nevertheless, it is important to know how these behave and interact with one another under certain conditions.

7.3.6 Feasibility Conditions

Recall that for all our previous designs we had to satisfy the condition for all products to be connected by a set of profiles for the design to be classified as feasible. The finite reflux Petlyuk is no different, but as alluded to in the infinite reflux case, the thermal coupling in two sections means this composition matching constraint is a little more complicated. Thus, let us consider where we need to search for profile intersections in the column by systematically highlighting areas of interest.

First, at the top of the column, CS_{1-3} share a thermally coupled junction where a liquid stream is split from CS_1 to its two adjacent CSs, as shown in Figure 7.24a. Thus, CS_{1-3} all have to share the same compositions at the point where the liquid is split. It is important to stress that the profile from CS_1, a so-called termination profile that originates from the product composition, is $\mathbf{X}_{\boldsymbol{\Delta}1} = \mathbf{x}_{\boldsymbol{D}}$. Furthermore, one has the option in the Petlyuk to draw off liquid products from CS_3 or vapor products from CS_5 (one may of course decide to draw a combination of vapor and liquid products, but only these two special cases will be treated here). If the product is liquid and hence drawn from CS_3, then its profile has to originate from the side product composition, $\mathbf{x}_{\boldsymbol{S}}$ (not necessarily $\mathbf{X}_{\boldsymbol{\Delta}3}$). The intersection point of the profiles of CS_1

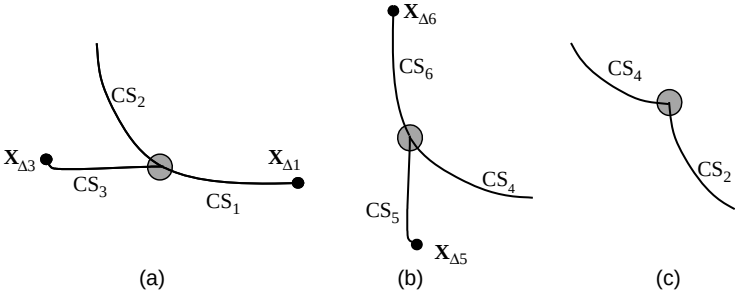


FIGURE 7.24 Areas of profile intersection in a Petlyuk column: (a) between CS_1 and CS_3, (b) between CS_4 and CS_6, and (c) across CS_2–CS_4.

and CS_3 will then be determined from where the integration will proceed for CS_2. The case where the side product is a vapor drawn from CS_5 does not change the fact the liquid compositions have to intersect one another at the top of this point, but it does mean that the initial composition from where to initiate the profile is not known. This can however be easily determined by knowing $\mathbf{X}_{\mathbf{\Delta}3}$ in Equation 7.25, through Equation 7.26:

$$\mathbf{X}_{\mathbf{\Delta}3} = \frac{V_3\mathbf{y}_3^B - L_3\mathbf{x}_3^B}{V_3 - L_3} \qquad \text{and} \qquad R_{\Delta 3} = \frac{L_3}{V_3 - L_3} \tag{7.25}$$

$$\mathbf{x}_3^B = \left(\frac{1}{R_{\Delta 3}} + 1\right)\mathbf{y}_3^B - \left(\frac{1}{R_{\Delta 3}}\right)\mathbf{X}_{\mathbf{\Delta}3} \tag{7.26}$$

where $\mathbf{y}_3^B = \mathbf{y}_5^B = \mathbf{x}_S$ for a vapor side-draw.

Second, compositions in CS_{4-6} have to match one another. As with the side rectifier shown in Chapter 6, vapor compositions have to match one another because of the vapor split between CS_{4-6} where compositions are the same (see Figure 7.24b). However, we will only consider liquid profile intersections as an approximation because the composition profiles follow each other very closely with a constant offset. Thus, the profile from CS_5 has to intersect the profile from CS_6, which is a termination profile that originates from $\mathbf{X}_{\mathbf{\Delta}6} = \mathbf{x}_B$. The starting point for CS_5's profile again depends on whether the sidestream product is a liquid or vapor stream. Once more, if a liquid product is drawn from CS_3, then this product composition is the initial profile composition since the liquid stream exiting from CS_3 is split between the product and CS_5. If the final product is vapor, then one needs to compute the initial liquid composition for constructing a profile through the definition of $\mathbf{X}_{\mathbf{\Delta 5}}$, and using the fact that $\mathbf{x}_3^B = \mathbf{x}_5^T$ (the starting point for integration in these sections). The intersection point of profiles from CS_6 and CS_5 will then serve as the initial composition for constructing CS_2's profile, which leads onto the third and final intersection criterion.

Finally, liquid profiles across the feed stage, that is, CS_2 from CS_4, have to intersect one another in order for the design to be considered feasible. Both these profiles originate from the intersection points found in neighboring CSs. The general conditions for feasibility are then essentially the same for the Petlyuk column as for any other column. The only significant difference is to establish where profiles run, originate from and terminate at, and what intersection one should be searching for.

7.3.7 Putting it all Together

So far in this chapter, we have laid down the fundamental concepts of Petlyuk column design. This stretches from net flow patterns and how they may change with different choices of vapor and liquid split ratios, to feasibility conditions, and profile intersection criteria. While these concepts are all good to know, they are only really useful when integrating them into an actual Petlyuk column design. This section will summarize the steps required to design a general Petlyuk column completely, for any given phase equilibrium behavior.

The first step in the Petlyuk, as indeed with all columns, is to specify the desired product purities or the distillate, side-draw, and bottoms streams, assuming the feed composition is known. This automatically enables one to determine the product flowrates of each stream. Of course, one could do the reverse calculation too, that is, specify the product flowrates and partial compositions and calculate the remaining compositions. Once the external mass balance properties of the column have been set, we need to shift focus toward the internal degrees of freedom of the column. From the discussion presented here it is evident that a reflux in either CS_1 or CS_6 be specified (a "reference" reflux), a split ratio for vapor and liquid streams at a thermally coupled junction, and finally a composition or difference point in one of the internal CSs. For the latter requirement, we have argued in Section 7.3.3 that it is advisable to select $\mathbf{X}_{\boldsymbol{\Delta}3}$ based on the understanding of CS_3's functions and goals. $\mathbf{X}_{\boldsymbol{\Delta}3}$ is principally responsible for transporting the intermediate-boiling component to the side-draw stage, and its elements should be selected as such.

For the first two requirements, simultaneously choosing a reflux in say, CS_1, as well as the vapor and liquid split ratios does not provide insight into flow patterns. Thus, it is advisable to choose a reflux value for CS_1 (CS_6 could also have been specified) from which one can generate net FPs in Φ-space. This will allow one to choose a Φ-coordinate within a certain FP regime. Once the Φ-coordinates have been selected in the desired flow regime, one can easily determine the vapor and liquid flowrates, reflux ratios, and difference points for all the remaining CSs. As mentioned, different FPs may hold different advantages for certain systems, depending on the specific VLE behavior and the resulting $\mathbf{X}_{\boldsymbol{\Delta}}$s. All the information to construct composition profiles in each CS is now available.

Since we know the boundary compositions and reflux values of the termination CSs, profiles can be produced for each of them. Furthermore, we know the common liquid composition in CS_3 and CS_5 (not the sidestream product composition when the side-draw is vapor, refer to Section 7.3.6), we can produce profiles in both directions from this common liquid composition for CS_3 and CS_5,

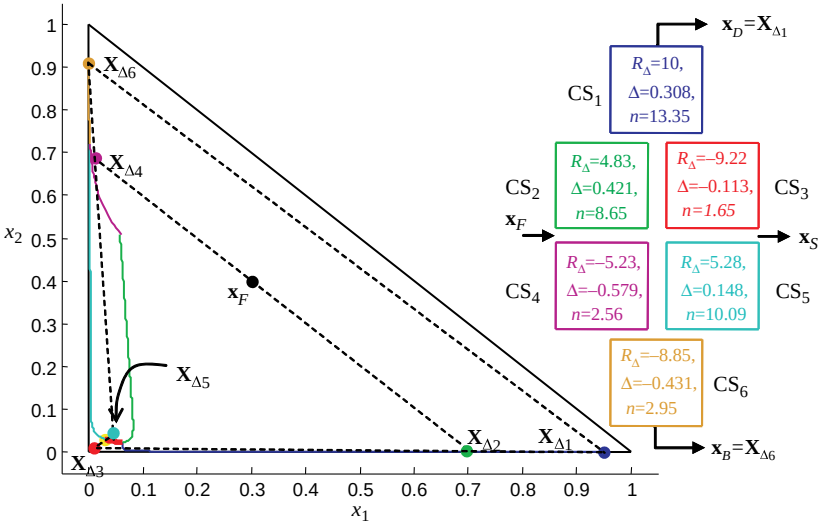


FIGURE 7.25 A typical Petlyuk column design for $\mathbf{x}_D = [0.97,\ 10^{-5}]$, $\mathbf{x}_B = [10^{-5},\ 0.91]$, $\mathbf{x}_S = [0.03, 0.03]$, $\mathbf{x}_F = [0.3, 0.4]$, $R_{\Delta 1} = 10$, $\mathbf{X}_{\Delta 3} = [0.01, 0.01]$, $\Phi_V = 0.725$, $\Phi_L = 0.660$, liquid side-draw and $\boldsymbol{\alpha} = [5,\ 1,\ 2]$.

respectively. All that remains now is to search for profile intersections. If there is an intersection between profiles from CS_1 and CS_3, as well as an intersection between profiles from CS_6 and CS_5, only an intersection across the feed stage still has to be found. By using the intersection composition between CS_1 and CS_3 as the starting point for generating profiles for CS_2, and similarly using the intersection between CS_6 and CS_5 as the starting point for CS_4, we can assess whether there is an intersection across the feed stage too. Only if all these intersection criteria are met, then a feasible Petlyuk design has been found. The feed stage, side-draw stage, thermally coupled stages at the top and bottom of the column, and the total number of stages can be easily determined by tracing the number of stages in each profile. Using this design procedure, a typical Petlyuk design for a constant relative volatility system is shown in Figure 7.25.

The color-coded design portrayed in Figure 7.25 operates in FP_3. Each colored profile represents the change in composition in a CS of the same color. Short profiles such as the one associated with CS_3 have the smallest stage requirement while the longer profiles require more stages.

As one may expect, it is possible to operate this column under the same product specifications and $R_{\Delta 1}$ value, but with alternate choices for Φ_V and Φ_L, which again suggests multiple steady states. Minimum reflux in the Petlyuk column is defined as the lowest value of $R_{\Delta 1}$ which still allows profile intersection, for any choice of Φ_V and Φ_L. Put in another way, if $R_{\Delta 1}$ is decreased any further there will be no Φ_V–Φ_L pair that will result in a feasible design.

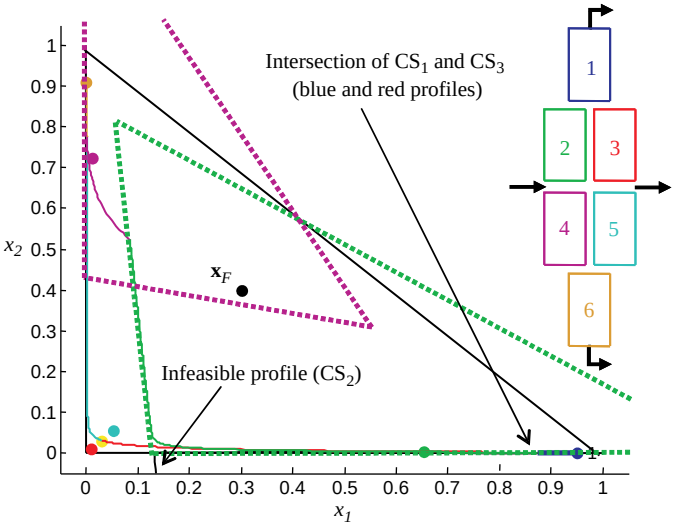


FIGURE 7.26 The application of TTs for pinch and stability analysis in the Petlyuk column.

Note too that a pinched design (infinite stages) does not necessarily have to coincide with minimum reflux (similarly to side rectifiers and strippers). A certain choice of Φ_V and Φ_L may lead to a particular CS pinching on another, meaning that one would require an infinite number of stages, even though the overall column may be far away from minimum reflux. The TTs are again quite useful in first determining proximity to pinched designs for the Petlyuk, and second in determining possible areas of instability within the column. Both these applications are elucidated in Figure 7.26 for a Petlyuk column with arbitrary operating parameters. We have only plotted the TTs for the CSs across the feed stage for the purpose of this discussion, as plotting the TTs for each of the CSs clutters the composition space and makes analysis difficult.

The TT's application to locating pinched designs in the Petlyuk column is very similar to the procedure used for distributed feed columns in Chapter 6. When the vertex of a TT of a particular CS falls exactly on a profile of a neighboring CS, the design is considered to be pinched. It can be seen in Figure 7.26 that, for the CSs across the feed stage at least, the design is still very far from being pinched since neither the green nor the purple TT's vertices fall on the adjacent profile. The designer is still quite far from approaching infinitely many stages across the feed stage, as it is still quite a long way to go before this condition occurs. However, no verdict can be made about the remaining CS's proximity to being pinched, and one would have to construct TTs for each CS to ascertain this.

As mentioned, the TTs allow us to make insightful conclusions about column stability or flexibility too. In Figure 7.26, the point where CS_2 "starts" from is where the blue, green, and red profiles all touch one another, that is, the thermally coupled

point at the top of the column. Now notice that this junction of profiles is very close to the border of CS_2's TT. Fortunately, in this design, the junction of the red and blue profiles lies inside CS_2's TT, meaning that CS_2's composition profile will move upward to intersect CS_4's profile. If however, the intersection of blue and red profiles lies outside CS_2's TT, CS_2's composition profile will in fact move into negative composition space. Under the same R_Δ and $\mathbf{X}_\Delta$ operating conditions for CS_2, but with an initial integration composition located slightly away from the blue–red profile intersection, just outside CS_2's TT, we indeed find that the profile head toward the saddle points for the TT but then swerves away toward negative compositions space, as indicated by the black profile labeled "Infeasible profile." However, it should be appreciated that a profile outside of its TT does not necessarily imply instability. Generally, saddle nodes cause this instability, so if the profile happens to lie near a TT edge, but is unaffected by, or does not approach, the saddle node, stability will not be greatly sacrificed. However, the particular column in Figure 7.26 can be considered inflexible because a small change in operating conditions in the column may lead to complete infeasibility, caused by the close proximity CS_2's to its saddle node.

Finally, the simplified infinite reflux calculations shown specifically in Figure 7.8 gives one some indication that it may be possible using the Petlyuk to overcome distillation boundaries. Figure 7.27 shows a finite reflux Petlyuk column achieving this same objective using the CPM technique, based on work done by Holland [26], for the acetone/benzene/chloroform system. Results obtained using the CPM technique were used as initialization input to Aspen Plus®, showing a remarkable agreement between the techniques. It should be noted that this particular configuration operates in the FP_4 regime with elements of $\mathbf{X}_{\Delta 2}$ lying in negative composition space.

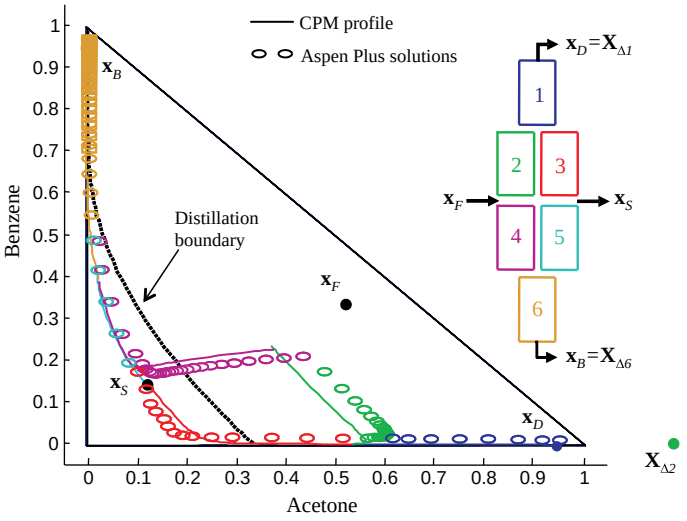


FIGURE 7.27 A Petlyuk column design for the acetone/benzene/chloroform system at $P = 1$ atm using the NRTL model.

7.4 SHARP SPLIT PETLYUK DESIGN USING TTs

By employing the techniques described above to design a complete Petlyuk column, one quickly starts to realize that that the column's feasibility is quite sensitive to changes in design parameters such as R_{Δ}, Φ_V, and Φ_L. Furthermore, it is very difficult to interpret and understand each of these design parameter's effects on each CS's profile behavior. For instance, if one finds Φ_V and Φ_L operating parameters for a system that leads to a feasible design, one still has no idea how much positive and negative deviation is allowable in these parameters before the design becomes infeasible without employing some sort of time-consuming brute-force approach to evaluate designs exhaustively. The TT phenomenon, although only applicable to sharp splits, is again very useful in designing Petlyuk columns because it allows one to rapidly construct a definitive region of feasible solutions in Φ-space. This section will outline a methodology for Petlyuk design using TTs and highlight significant conclusions.

7.4.1 Feasibility Criteria Using TTs

As is evident from all the previous designs using TTs, the sides of TTs of adjacent CSs line up with one another at sharp split, minimum reflux conditions. This property allows one to quickly assess absolute minimum operating conditions for a proposed split and perhaps more significantly, allows for a quick comparison between various structures. The preceding sections within this chapter showed the usefulness of the Φ-space for representing changes in FPs as well as constant reflux lines. Using these ideas, we will construct a feasible region in Φ-space for a particular sharp split separation, which will also allow estimating the absolute minimum reflux for the column. By sharp splits we mean that the distillate stream does not contain any high-boiling components, the bottoms stream does not contain any low-boiling components, and finally, the sidestream contains only intermediate. This directly implies then that $\mathbf{x}_S = \mathbf{X}_{\mathbf{\Delta}5} = \mathbf{X}_{\mathbf{\Delta}3}$, and will be elaborated upon in the discussion that follows.

We will start our design procedure via TTs by assuming that we have completely specified the product stream (the entire external mass balance) as well as a value for $R_{\Delta 1}$ that will lead to a feasible design. For a Petlyuk column to be considered feasible using TTs, the following conditions have to be satisfied:

1. TTs of CS_2 and CS_4 have to overlap one another (across the feed stage).
2. TTs of CS_3 and CS_5 have to overlap one another (across the side-draw stage).
3. TTs of CS_1, CS_2, and CS_3 have to overlap one another (uppermost thermally coupled junction).
4. TTs of CS_4, CS_5, and CS_6 have to overlap one another (bottommost thermally coupled junction).

These four feasibility conditions are summarized graphically in Figure 7.28. The arrows in these illustrations indicate the direction in which compositions change in a

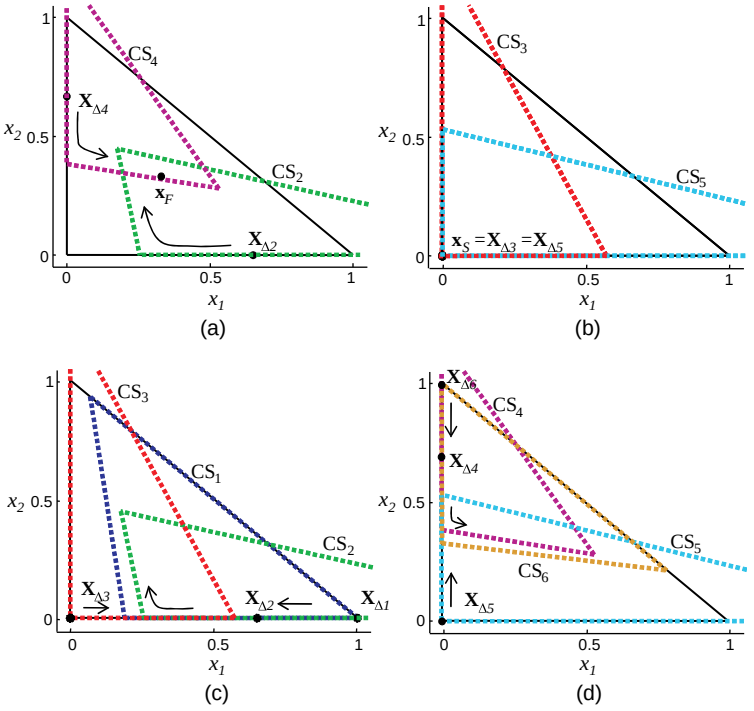


FIGURE 7.28 Summary of the four TT overlapping conditions in the Petlyuk column: (a) CS_2 and CS_4, (b) CS_3 and CS_5, (c) CS_1, CS_2, and CS_3, and (d) CS_4, CS_5, and CS_6.

particular CS, and they always move away from final products. It is important to point out that these conditions are dependent on the choices of Φ_V and Φ_L. It is apparent from illustration (c) why it is required that the sidestream does not contain impurities of either one of the other components. This is due to the fact that for the problem to be considered as a sharp split (with the TT method) $\mathbf{X}_{\boldsymbol{\Delta}2}$ and $\mathbf{X}_{\boldsymbol{\Delta}4}$ *must* lie on the edges (or their extensions) of the MBT. Furthermore, recall that, due to the linear mixing properties of $\mathbf{X}_{\boldsymbol{\Delta}}$ that $\mathbf{X}_{\boldsymbol{\Delta}1}$, $\mathbf{X}_{\boldsymbol{\Delta}2}$ and $\mathbf{X}_{\boldsymbol{\Delta}3}$ all have to lie on a straight line in composition space (see Figure 7.17). Since $\mathbf{X}_{\boldsymbol{\Delta}1}$ already lies on the edge of the MBT, it follows that $\mathbf{X}_{\boldsymbol{\Delta}3}$ is forced to lie here too. However, a similar argument can be made for $\mathbf{X}_{\boldsymbol{\Delta}4}$, $\mathbf{X}_{\boldsymbol{\Delta}5}$, and $\mathbf{X}_{\boldsymbol{\Delta}6}$. Since the side-draw composition has to lie between $\mathbf{X}_{\boldsymbol{\Delta}3}$ and $\mathbf{X}_{\boldsymbol{\Delta}5}$, the only place where $\mathbf{x}_S$ may lie in composition space to satisfy these mixing rules is on the pure intermediate vertex, which further implies that $\mathbf{x}_S = \mathbf{X}_{\boldsymbol{\Delta}3} = \mathbf{X}_{\boldsymbol{\Delta}5}$.

All the TTs in Figure 7.28 overlap one another, meaning that this design is well above minimum reflux. In order to establish minimum reflux conditions for each of the adjacent TTs, it is necessary to find a reflux value where the TT will just touch one another. There are four apparent intersection criteria to meet as illustrated by Figure 7.28a–d. However, criterion 2 is automatically fulfilled because of the aforementioned $\mathbf{X}_{\boldsymbol{\Delta}}$ arguments. In other words, criterion 2 will always hold for

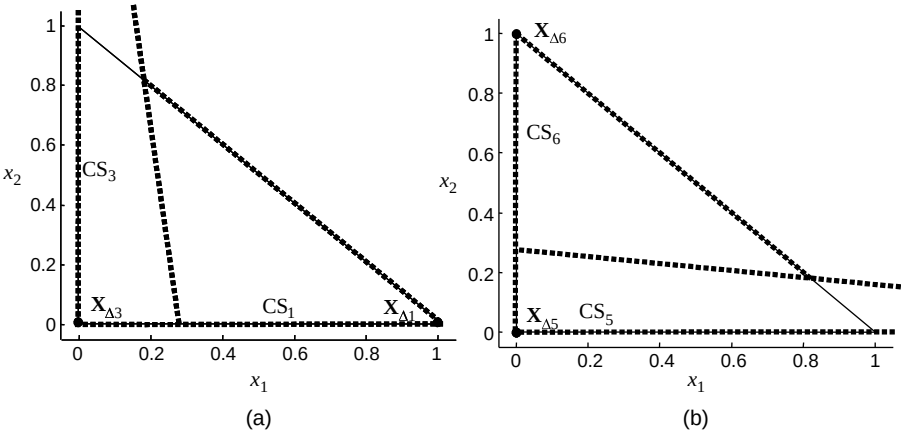


FIGURE 7.29 Minimum reflux conditions with TTs for (a) CS_1 and CS_3 and (b) CS_5 and CS_6.

any choice of Φ_V or Φ_L. Of the three remaining criteria, criteria 3 and 4 are the easiest to explain and interpret and thus will be dealt with first.

Criterion 3 specifies that the TTs of CS_1, CS_2, and CS_3 all have to overlap one another. Recall, however, that in our list of assumptions that a value of $R_{\Delta 1}$ has already been specified in the column. Since the products from the column have also been specified it is possible to draw a TT for CS_1 given that both $R_{\Delta 1}$ and $\mathbf{X}_{\mathbf{\Delta} 1}$ are known. Moreover, $\mathbf{X}_{\mathbf{\Delta} 3}$ is also known *a priori* and is fixed, but $\mathbf{X}_{\mathbf{\Delta} 2}$ is still unknown and depends on the choice of Φ_V and Φ_L. The latter fact is the main reason behind criterion 1's difficulty. In order to find the minimum reflux for CS_3, all that needs to be done is to decrease $R_{\Delta 3}$ until the TTs of CS_1 and CS_3 touch one another. This value for $R_{\Delta 3}$ will thus be the minimum reflux that $R_{\Delta 3}$ is allowed to operate at any value of $R_{\Delta 3}$ below this minimum would mean that the TTs of CS_1 and CS_3 do not overlap which implies an infeasible design. Similarly, by specifying the products and $R_{\Delta 1}$, $R_{\Delta 6}$ and $\mathbf{X}_{\mathbf{\Delta} 6}$ are also known (thus CS_6's TT is known too) and one can adjust the value of $R_{\Delta 5}$ until the TTs of CS_5 and CS_6 just touch one another (since $\mathbf{X}_{\mathbf{\Delta} 5}$ is known). These two minimum intersection criteria through TTs are presented in Figure 7.29a and b .

Using the TT method, we now quickly determined minimum bounds for the values of $R_{\Delta 3}$ and $R_{\Delta 5}$. As shown in Section 7.3.4, constant values of R_Δ for a particular CS can be conveniently represented in the Φ-domain. Using the transformation of $R_{\Delta 3}$ and $R_{\Delta 5}$ in terms Φ-values through Equations 7.16 and 7.18 or 7.19 results in a partial attainable region, as shown in Figure 7.30 though the $R_{\Delta 3\text{MIN}}$ and $R_{\Delta 5\text{MIN}}$ lines. The shaded area represents all possible combinations of Φ_V or Φ_L that will result in CS_3 and CS_5 operating above their respective minimum values. It is interesting to note that this partial attainable region occurs across a band of FPs. However, with that said, notice that at the operating conditions chosen, FP_1 (in the bottom right hand corner of Figure 5.27) is no longer feasible. This, of course, is not a general rule, but is system dependent.

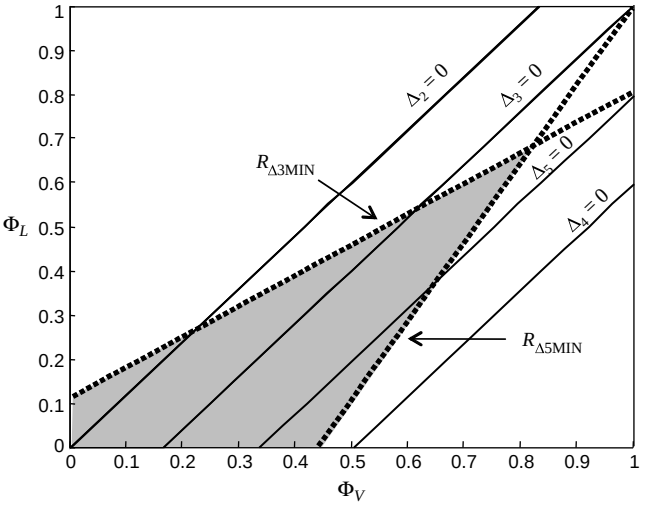


FIGURE 7.30 Partial feasible (shaded) region in the Φ-space for $R_{\Delta 3}$ and $R_{\Delta 5}$.

Through these simple co-linearity conditions the allowable choices of Φ_V or Φ_L that will result in a feasible Petlyuk column have been considerably reduced. It should however be stressed again that we have only found a partial attainable region thus far, because the overlapping conditions across the feed stage have not been met yet. Determining the overlapping conditions across the feed stage is slightly more complex than those shown previously, because both $\mathbf{X}_{\boldsymbol{\Delta}2}$ and $\mathbf{X}_{\boldsymbol{\Delta}4}$ are not fixed and vary with the choice of Φ_V or Φ_L. We are however certain that both $\mathbf{X}_{\boldsymbol{\Delta}2}$ and $\mathbf{X}_{\boldsymbol{\Delta}4}$ lie on the edges of the MBT and are therefore open to analysis using TTs. Recall from the discussions on simple columns that there are three possibilities of minimum reflux that can occur: the rectifying CS pinching on the stripping CS, the stripping CS pinching on the rectifying CS, and the double-feed-pinch case where both CSs pinch exactly on one another. These three scenarios are summarized in Figure 7.31.

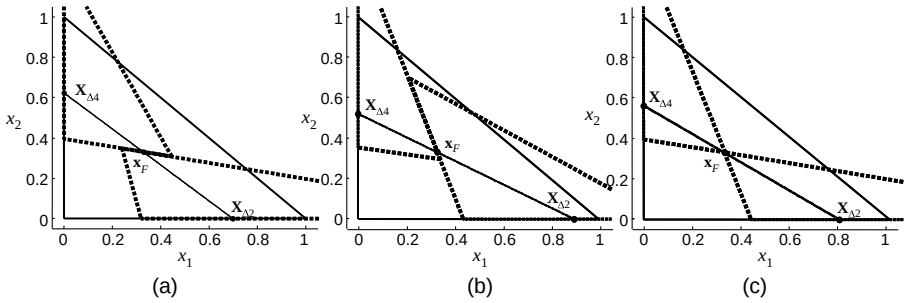


FIGURE 7.31 Three possible pinching conditions across the feed stage: (a) the rectifying CS pinching on the stripping CS, (b) the stripping CS pinching on the rectifying CS, and (c) both CSs pinch exactly on one another.

Notice that in finding $R_{\Delta 3MIN}$ and $R_{\Delta 5MIN}$ that there was only one possibility in which the TTs could touch one another since the $\mathbf{X}_{\boldsymbol{\Delta}}$'s of the respective CSs were fixed. In the case of CS_2 and CS_4 however, the difference points are variable and hence it is necessary to take account of all three of these pinching scenarios. Since a double-feed pinch case is merely the special condition where cases (a) and (b) in Figure 7.31 meet, there are essentially only two cases of minimum reflux across the feed. In order to find the minimum reflux for the CSs across the feed, it is thus necessary to consider both these cases. Holland et al. [27] treated this problem by evaluating the eigenvectors at the feed for liquid feeds only, but we will treat the general case here for any quality feed.

To start we first consider scenario (a) in Figure 7.31, where the rectifying CS pinches on the stripping CS. We notice that this scenario occurs where $\mathbf{X}_{\boldsymbol{\Delta}4}$ is very pure in the high-boiling x_2 component. By simply choosing a succession of high purity $\mathbf{X}_{\boldsymbol{\Delta}4}$ points such that the rectifying CS still pinches on the stripping CS, it is possible to successively determine the reflux of both CS_2 and CS_4 that makes the respective TTs colinear for each selection of $\mathbf{X}_{\boldsymbol{\Delta}4}$. Each reflux value that is calculated in this procedure can be again converted to a Φ-coordinate using the Φ transformations for $R_{\Delta 2}$ and $R_{\Delta 4}$ given in Equations 7.15 and 7.17. The coordinates obtained for $R_{\Delta 2}$ and $R_{\Delta 4}$ are however identical, therefore there is only one coordinate associated to a given minimum reflux. By obtaining a range of Φ-coordinates it is then possible to produce a curve in Φ-space which will effectively produce a boundary of feasibility, or a locus of minimum refluxes across the feed stage. Fortunately, the range of Φ-coordinates generated here is always a straight line in Φ-space, meaning that it is only necessary to find two Φ-coordinates to produce this boundary.

As one may have expected, the remaining minimum reflux condition at the feed can be calculated using scenario (b) in Figure 7.31. This scenario is characterized by $\mathbf{X}_{\boldsymbol{\Delta}2}$ that is very pure in the low-boiling x_1 component. Analogously, choosing a succession of high-purity $\mathbf{X}_{\boldsymbol{\Delta}2}$ points such that the stripping CS still pinches on the rectifying CS, it is possible to successively determine the reflux of both CS_2 and CS_4 that makes the respective TTs colinear for each selection of $\mathbf{X}_{\boldsymbol{\Delta}2}$. Each reflux ratio obtained here can be transported into Φ-space again, allowing one to construct a locus of minimum reflux solutions. This curve is also linear and one only needs to calculate two reflux values. These lines are represented in Figure 7.32, along with the previously calculated $R_{\Delta 3MIN}$ and $R_{\Delta 5MIN}$ lines, and are labeled as MRF_1 and MRF_2 (minimum reflux at feeds 1 and 2). Other authors have computed similar regions of feasibility using the Underwood equations, and consequently highlighted some controllability issues associated with the Petlyuk column [20,28,29]. However, using the Underwood equations it is difficult to identify the multiple FPs as shown here.

The quadrilateral shaded region shown here is the region of all possible split ratios that will result in a feasible design at a specific value for $R_{\Delta 1}$ and product specifications. Once again, this attainable region spans across multiple flow patterns. Importantly, information of the entire Petlyuk column (feasible region and net flow patterns) is contained in this relatively simple, linear diagram. For an arbitrary choice of Φ_V and Φ_L in Figure 7.32 in the FP_3 region that results in a feasible design, we can then also plot the TT of each CS as confirmation, as depicted in Figure 7.33.

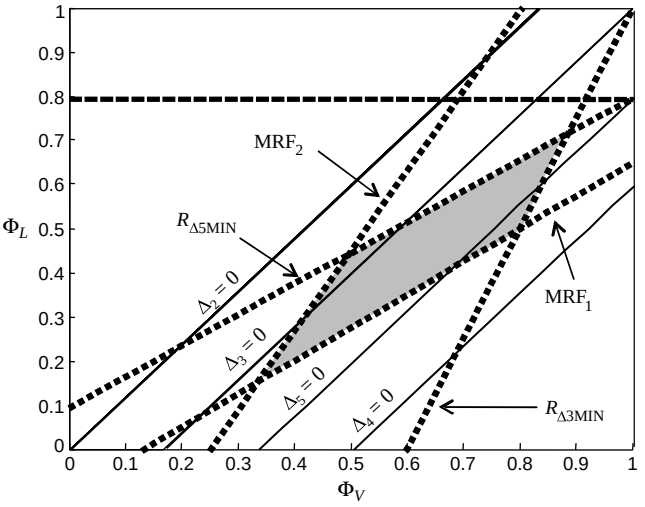


FIGURE 7.32 Attainable region for a Petlyuk column with $\mathbf{x}_F = [0.33, 0.33]$, pure product streams, a liquid side-draw, $R_{\Delta 1} = 5$ and $\boldsymbol{\alpha} = [5, 1, 2]$.

7.4.2 Design Implications

The first obvious observation from the attainable region projected in Figure 7.32 is that there is an entire region available in the Petlyuk system. This confirms our findings in the infinite reflux designs that there are multiple steady states that occur in the Petlyuk system. It is important to note that Figure 7.32 was produced for a set

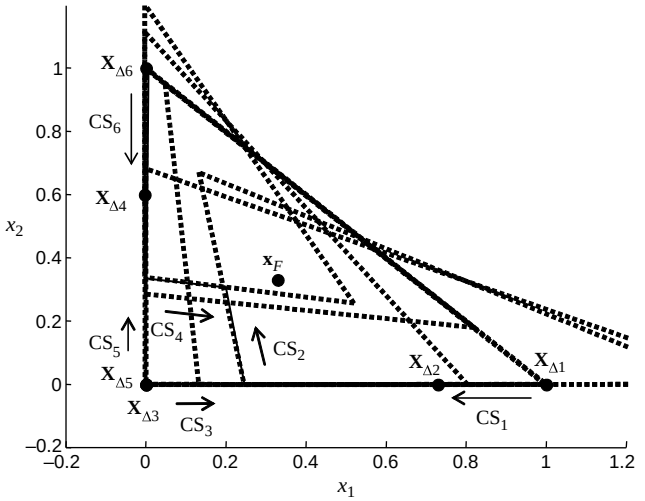


FIGURE 7.33 Feasible Petlyuk column in composition space using TTs operating with FP_3, $\mathbf{x}_F = [0.33, 0.33]$, pure product streams, a liquid side-draw, $R_{\Delta 1} = 5$ and $\boldsymbol{\alpha} = [5, 1, 2]$.

value of $R_{\Delta 1}$, or viewed differently, a set level of energy consumption. Any legitimate choice of Φ_V and Φ_L in this space will have the same reflux value and therefore the same energy expenditures. If a Φ_V and Φ_L pair is selected that happens to lie on the edge of the attainable region, two CSs will be at minimum reflux with one another. Specifically, when Φ_V and Φ_L is chosen on the $R_{\Delta 3\text{MIN}}$ boundary, the TTs of CS_1 and CS_3 will just touched one another, as portrayed in Figure 7.29a. Similarly, when Φ_V and Φ_L lie on the $R_{\Delta 5\text{MIN}}$ boundary, the TTs of CS_5 and CS_6 just touch one another, as illustrated by Figure 7.29b. Both MRF lines pertain to the last point of TT overlap across the feed stage. A selection on the MRF_1 line means the TTs at the feed will resemble Figure 7.31a and selection on line MRF_2 results in colinear TTs of the form shown in Figure 7.31b. It follows logically that when Φ_V and Φ_L are chosen to lay exactly on one of the vertices of the quadrilateral region of feasibility in Figure 7.32 that two minimum reflux conditions will have been met simultaneously. An interesting case occurs at the MRF_1–MRF_2 vertex, where the CSs across the feed stage are at the double-feed-pinch point (Figure 7.31c).

As with all distillation column designs, there are generally two points of interest from a design point of view: infinite reflux and minimum reflux. When $R_{\Delta 1}$ is infinitely large, it has been shown in Figure 7.21 that only net FP_1 and FP_5 exist because the other regions collapse to a single line. Moreover, the region of attainable Φ solutions expands as $R_{\Delta 1}$ is increased and is found to be at its largest when $R_{\Delta 1}$ is infinitely large. The region of attainable Φ-solutions for the case where $R_{\Delta 1}$ approaches infinity is shown in Figure 7.34.

Since infinite reflux is an impractical operating condition, one may think that the region shown in Figure 7.34 is only of academic interest. The region does, however, reveal a valuable property of the system: For these product specifications, the

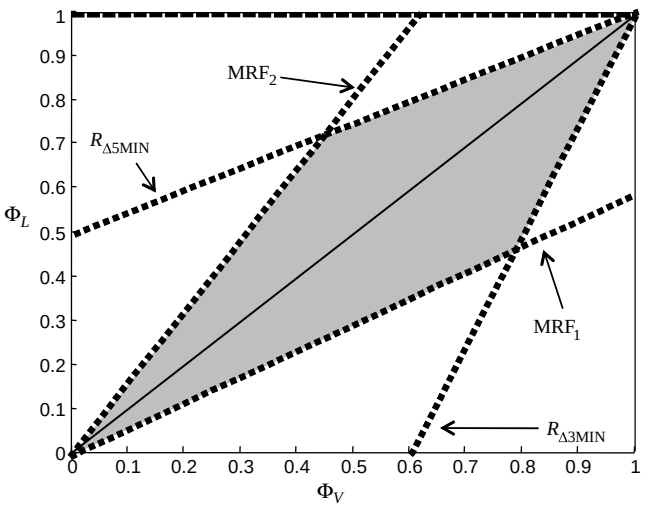


FIGURE 7.34 Attainable region for a Petlyuk column with $\mathbf{x}_F = [0.33, 0.33]$, pure product streams, a liquid side-draw, $R_{\Delta 1} = \infty$ and $\boldsymbol{\alpha} = [5, 1, 2]$.

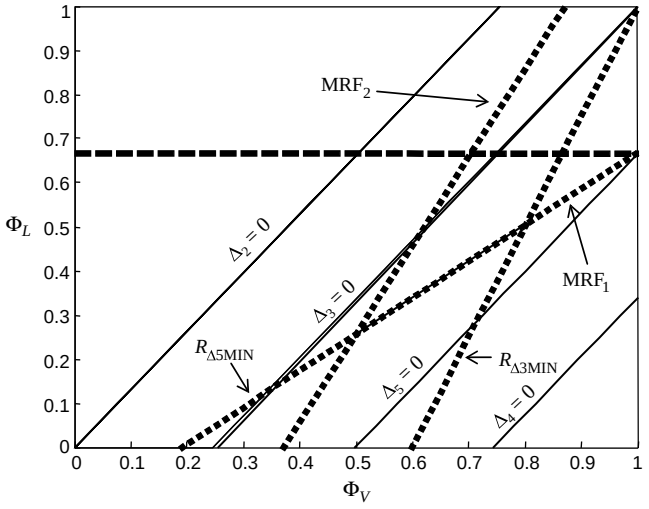


FIGURE 7.35 Collapsed attainable region for a Petlyuk column with $\mathbf{x}_F = [0.33, 0.33]$, pure product streams, a liquid side-draw, $R_{\Delta 1} = 3.08$ (minimum) and $\boldsymbol{\alpha} = [5, 1, 2]$.

enclosed feasible region at $R_{\Delta 1} = \infty$ contains all possible solutions of Φ_V and Φ_L at all possible refluxes. This means that regardless of the reflux value chosen for CS_1, solutions of Φ_V and Φ_L that bring about a feasible column will never lie outside the region shown in Figure 7.34.

As mentioned, the other interesting mode of operation is where the column operates at minimum reflux, that is, the lowest energy requirement of the Petlyuk column. We know that increasing values of $R_{\Delta 1}$ leads to an expansion of the feasible operating region. Finding the minimum $R_{\Delta 1}$ value is simply the lowest value of $R_{\Delta 1}$ where there are still Φ_V and Φ_L values open to selection. If one were to operate lower than this minimum $R_{\Delta 1}$ value, the feasible region in Φ-space is nonexistent and hence a realizable design will never be found. For the system shown thus far in Figures 7.32 and 7.34, the value of $R_{\Delta 1}$ is systematically decreased until the attainable region collapses at $R_{\Delta 1} = 3.08$. As shown in Figure 7.35, this region collapses to a single line of solutions. This line of solutions is given in this instance by the $R_{\Delta 5\text{MIN}}$ and MRF_1 lines merging with one another. The line is bound on either side by the $R_{\Delta 3\text{MIN}}$ and MRF_2 lines. It should however be noted that the convergence of these specific lines are system dependent, and another system may yield a convergence of a different set of lines at minimum reflux.

The fact that the Petlyuk column has a line of solutions at minimum reflux conditions suggests that there are multiple steady states, even at this limiting condition. Moreover, this line of minimum reflux solutions *always* occurs within the FP_3 region, implying that, for constant volatility systems, FP_3 is the optimal FP in terms of energy requirements. In other words, if any other FP is chosen as the operating FP for the column, it is certain that the design is relatively far from minimum reflux since the only feasible FP at overall minimum reflux is FP_3.

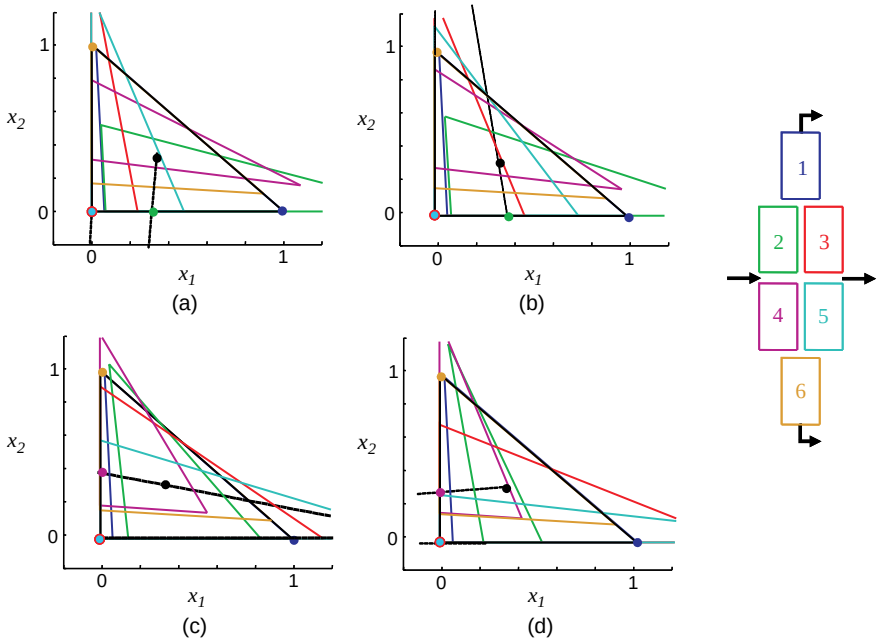


FIGURE 7.36 (a) Feasible Petlyuk column in composition space using TTs with $\mathbf{x}_F = [0.33, 0.33]$, pure product streams, a liquid side-draw, $R_{\Delta 1} = 10$ and $\boldsymbol{\alpha} = [5, 1, 2]$, for (a) FP_1, (b) FP_2, (c) FP_4, and (d) FP_5.

However, it should be kept in mind that all of the other FPs produce situations where $\mathbf{X}_{\Delta 2}$ or $\mathbf{X}_{\Delta 4}$ lie outside the MBT, which may be useful for more complex phase equilibrium behavior because CPMs may be shifted in interesting, potentially useful ways. TT designs of the remaining FPs can be seen in Figure 7.36a–d with a column reflux of 10. This choice of reflux enables the attainable region to span across all FP regimes. Notice that although the TT behavior in each of these TTs are fundamentally different, they are all still feasible designs because all the TTs overlap one another and a continuous profile path exists between all products.

As mentioned in all previous column designs using TTs, the resulting operating conditions found through this method are not necessarily representative of a practical distillation column because the products are sharp and hence require an infinite number of stages. However, simplified designs using TTs have two main uses; first as an initialization method for real, nonsharp split columns, and second for a quick design and comparison with other column configurations, especially in the early stages, the design.

Example 7.2: Design the a Petlyuk column for the benzene/*p*-xylene/toluene system that produces the following product streams: $\mathbf{x}_D = [0.98, 0.0]$, $\mathbf{x}_B = [0.0, 0.95]$, and $\mathbf{x}_S = [0.0, 0.0]$; from a feed with a flowrate of 1 mol/s and a composition of

$\mathbf{x}_F = [0.33, 0.33]$. Determine the minimum reflux, identify permissible FPs, and comment on the operability of each of the following scenarios:

(a) overall minimum reflux
(b) 1.3 times minimum reflux
(c) three times minimum reflux

Solution 7.2: It is first important to note that the benzene/*p*-xylene/toluene system may be approximated quite well with constant relative volatility behavior. Furthermore, the given product specifications are all sharp. It is therefore appropriate to use the TT approach delineated in this section. For simplicity, we shall also assume that the liquid sidestream is removed as a liquid product. It has also been shown in this section that an entire Petlyuk column operating under the aforementioned conditions can be represented with a region of feasibility in the Φ_V–Φ_L domain. This condition will be used to determine these scenarios.

1. In order to find the minimum reflux condition for this column, we successively reduce the column reflux until the region of feasibility reduces to a single line of solutions in the Φ_V–Φ_L domain. This collapsed attainable region is shown in Figure 7.37, and was found at $R_{\Delta 1} = 1.55$. This single line of solution lies only within FP_3 and this particular column may be difficult to operate because of the strict restraint of Φ_V–Φ_L coordinates.
2. Once the minimum column reflux has been determined, it is relatively easy to construct an attainable region at higher refluxes. In this particular case, the

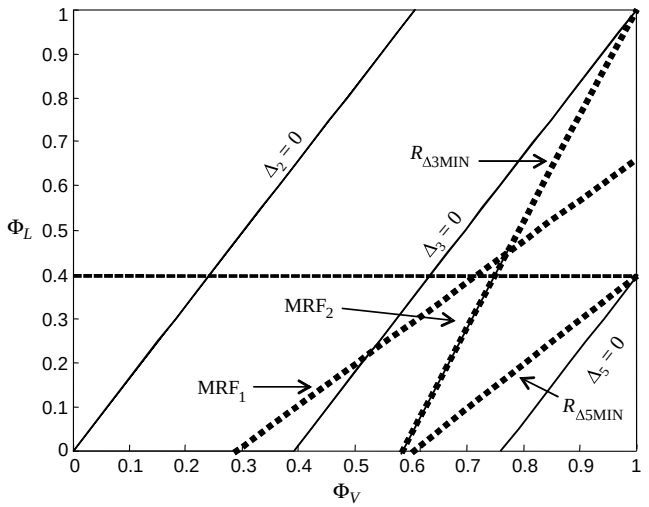


FIGURE 7.37 Collapsed attainable region for a Petlyuk column for the benzene/*p*-xylene/toluene system with $\mathbf{x}_F = [0.33, 0.33]$, a liquid side-draw and $R_{\Delta 1} = 1.55$ (minimum).

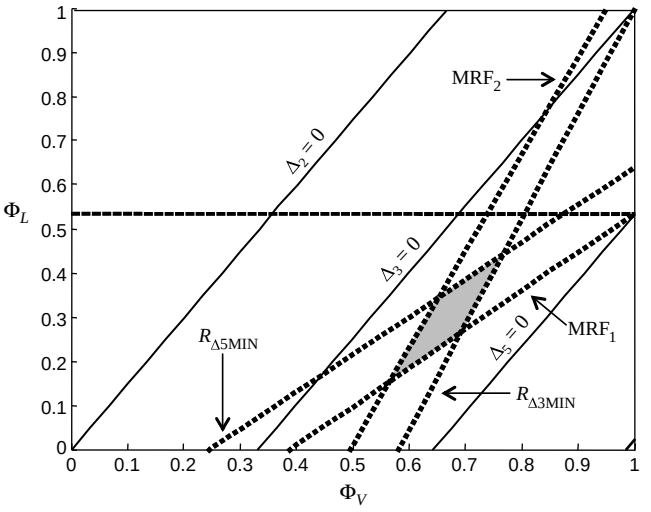


FIGURE 7.38 Attainable region for a Petlyuk column for the benzene/*p*-**x**ylene/toluene system with $\mathbf{x}_F = [0.33, 0.33]$, a liquid side-draw and $R_{\Delta 1} = 2.02$ ($1.3 \times R_{\Delta 1\text{MIN}}$).

column operates with a reflux of 2.02 and it is possible now to witness how the attainable region has grown from the minimum reflux case, shown in Figure 7.38. This attainable region however lies again only with the FP_3's bounds. This column is thought to be more operable than the one depicted in (a), since the designer has a larger region of possible Φ_V–Φ_L values from which to control the column and maintain the product specifications.

3. Finally, we construct an attainable region for the same product distribution but with $R_{\Delta 1} = 4.65$, as shown in Figure 7.39. The region depicted here is markedly bigger than the one shown in (b), and therefore an operator or controller may have more freedom or ease of operability at these conditions (although this comes at price of a high reflux). At this column reflux, the attainable region encompasses three net FPs. From an ease of operation point of view, it is thought changing from one FP to another may cause column instability.

7.5 INSIGHTS INTO KAIBEL COLUMN DESIGN

In this section, we will briefly discuss properties and insights of the four-component Kaibel column by looking at some general column properties and specifically investigating the consequences of imposing a sharp product distribution. It should be noted that this section is based largely on work of Abbas in his Ph.D. thesis (Abbas, 2011) [30]. Throughout this book, we have mainly considered ternary separation problems because they are easily presented in a 2D space which lends

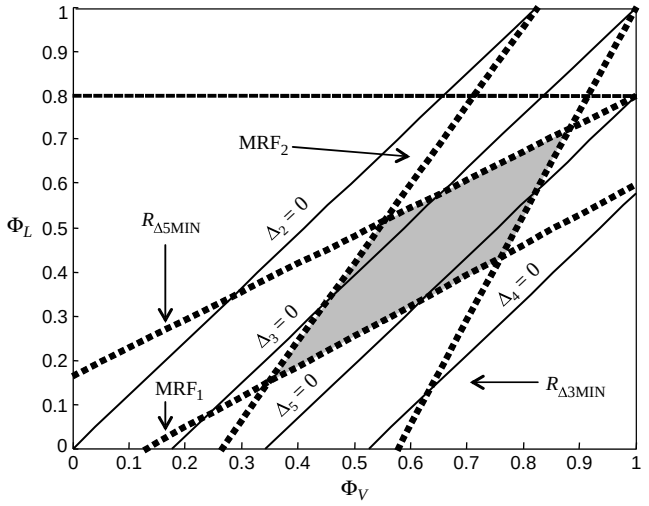


FIGURE 7.39 Attainable region for a Petlyuk column for the benzene/*p*-xylene/toluene system with $\mathbf{x}_F = [0.33, 0.33]$, a liquid side-draw and $R_{\Delta 1} = 4.65$ $(3 \times R_{\Delta 1\text{MIN}})$.

some insight. However, the CPM technique can just as easily be applied to higher order systems, although some of the useful graphical attributes of the method is somewhat lost. Since we are dealing with quaternary mixtures, it is perhaps useful to introduce a quaternary CPM, for arbitrarily chosen values for $\mathbf{X}_{\boldsymbol{\Delta}}$ and R_{Δ} as depicted in Figure 7.40.

The constant volatility quaternary CPM behaves similarly to its ternary counterpart in that there is a linear shift in topology—this time in the form of a transformed

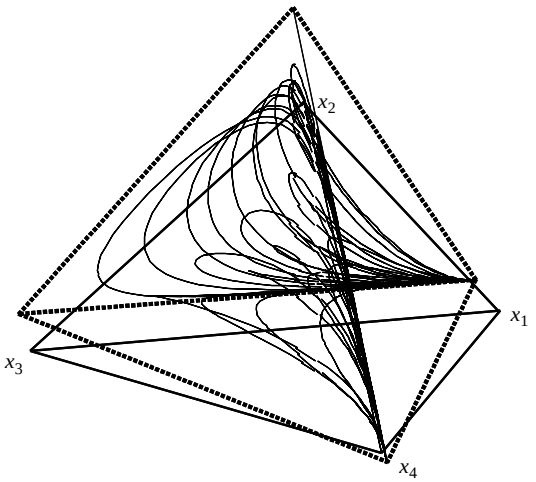


FIGURE 7.40 A quaternary CPM with $\mathbf{X}_{\Delta} = [0.3, -0.2, -0.3]$ and $R_{\Delta} = 9$, and $\boldsymbol{\alpha} = [6, 4, 2, 1]$.

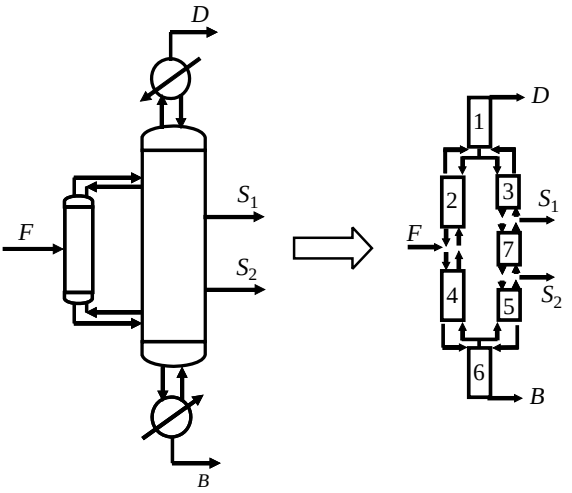


FIGURE 7.41 Column section breakdown of a Kaibel column.

tetrahedron, shown by the dashed lines in Figure 7.40. For this section, the abbreviation TT^4 will refer to a transformed tetrahedron.

7.5.1 Structure and CS Breakdown

Due to the fact that the Kaibel column falls under the same class of column as the Petlyuk column, namely fully thermally coupled columns, much of the design ideas introduced in Petlyuk design are applicable to Kaibel design too. A typical Kaibel column with its associated CS breakdown is shown in Figure 7.41. Here one can see that four products are produced for a certain feed, only requiring the use of a single reboiler and condenser set.

The fundamental difference between the Petlyuk and Kaibel columns is the removal of an additional sidestream in the Kaibel column, allowing one to theoretically obtain four pure component product streams (D, S_1, S_2, and B). The immediate consequence of removing an additional sidestream is that an extra CS is created. For the sake of consistency, we have kept the numbering format of CSs the same to that of the Petlyuk column, and simply labeled the additional CS in the Kaibel column as CS_7.

7.5.2 Similarities to the Petlyuk

The resemblance between the Petlyuk column and the Kaibel column are quite blatant from a structural point of view. The addition of another sidestream however means that there are now 12 external degrees of freedom, assuming the feed stream is known: 16 unknown material flowrates minus 4 independent material balances. This essentially requires that the compositions of each product stream be specified from

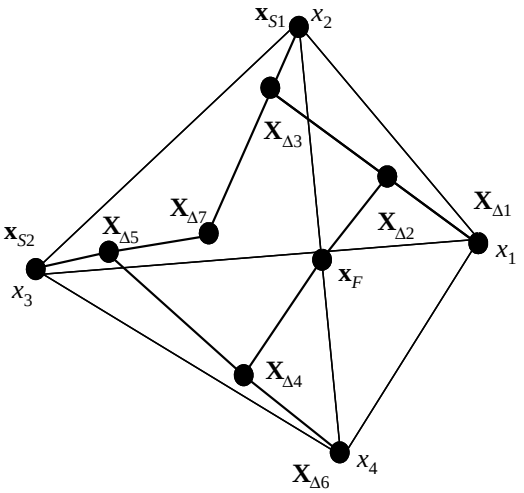


FIGURE 7.42 Typical difference point behavior for the Kaibel column.

which the respective flowrates of each product stream can be calculated, exactly the same as the three-product Petlyuk column.

Internally, there are two thermally coupled junctions at the top and the bottom of the column, splitting liquid and vapor streams, respectively. As such, we will again use the constrained variables Φ_V and Φ_L to govern the manner in which material is distributed throughout the column. Moreover, the reflux in a single CS needs to be specified as a so-called reference reflux, and $R_{\Delta 1}$ will again be used.

Finally, the designer is required to specify an internal composition variable. We elect to use $\mathbf{X}_{\mathbf{\Delta}3}$ largely because we understand the basic requirements of this CS, transporting mainly light intermediate (x_2) toward the S_1 product stream. $\mathbf{X}_{\mathbf{\Delta}3}$ should thus be chosen to lie as close to the x_2 vertex as possible. The same linear relationship between the difference points between adjacent CSs exist (by mass balance), as shown for a typical Kaibel column in Figure 7.42.

7.5.3 Net Flow Patterns

Just as we identified five potential FPs in the Petlyuk system, it is possible to rationally determine potential FPs for the Kaibel using the same directional flow arguments at the feed, sidestream, and thermally coupled points as depicted in Figures 7.10–7.12. The addition of CS_7 brings with it the possibility of an alternate FP, summing to six different FPs in total. These FPs are given graphically in Figure 7.43 and the net flow directions in each CS is summarized in Table 7.5.

The six FPs in the Kaibel column are very similar to those found in the Petlyuk column and are independent on the phase of the feed and sidestream products. In the case of the Kaibel column, there are in fact two "symmetric" FPs where material is transported to both the top and bottom halves of the column from the feed stage.

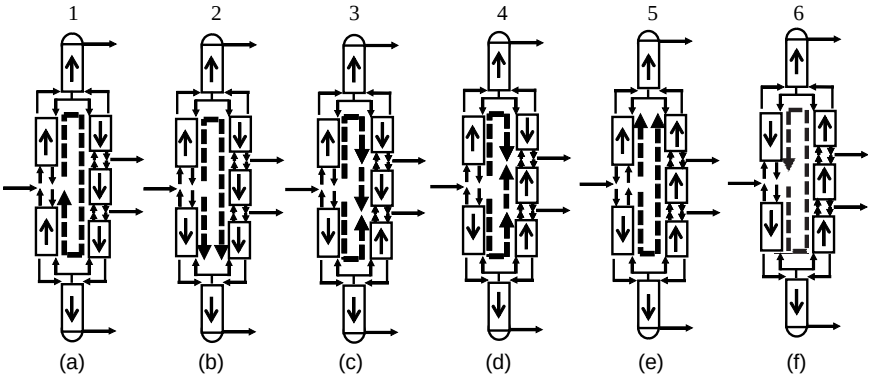


FIGURE 7.43 Six different global FPs for the Kaibel column, labeled 1–6.

The Petlyuk column has only one such FP, FP_3 in Figure 7.13c. The addition of CS_7 in the Kaibel column brings with it the possibility of material moving either up or down in this CS, hence the existence of FP_3 and FP_4. As more material is sent to the top-half the column from the feed stage the FPs progress toward FP_1, and conversely, as more material is sent to the bottom half of the column, one would eventually end up operating under FP_6. FP_1 and FP_6 are characterized by a clockwise and counter-clockwise flow of material throughout the column, respectively. It can be seen that the net FPs are completely dependent on the internal CSs of the column. Furthermore, in the Petlyuk column, qualitative arguments were made using our understanding of the effect of sidestreams on the operating reflux ratio of the column, and we concluded that FP_3 is likely to be the most efficient. The same arguments can be made to conclude that either FP_3 or FP_4 are likely to be the most efficient operating mode in the Kaibel column.

It is again possible to quantify these global net flow arguments by noting that a change in the overall FP of the column occurs where the net flow in a particular CS changes sign, or put otherwise where the net flow in a CS is equal to zero. The zero net flow equations for the internal CSs in the Kaibel column are given in Equations 7.27–7.31:

$$\begin{aligned} \Delta_2 &= (R_{\Delta 1} + 1)D\Phi_V - R_{\Delta 1}D\Phi_L = 0 \\ \therefore \Phi_L &= \frac{(R_{\Delta 1} + 1)}{R_{\Delta 1}}\Phi_V \end{aligned} \tag{7.27}$$

TABLE 7.5 Net Flow Direction in Each CS for Different FPs

FP	Δ_1	Δ_2	Δ_3	Δ_4	Δ_5	Δ_6	Δ_7
1	+	+	−	+	−	−	−
2	+	+	−	−	−	−	−
3	+	+	−	−	+	−	−
4	+	+	−	−	+	−	+
5	+	+	+	−	+	−	+
6	+	−	+	−	+	−	+

$$\Delta_3 = D(R_{\Delta 1}+1)(1-\Phi_V) - R_{\Delta 1}D(1-\Phi_L) = 0$$
$$\therefore \Phi_L = \frac{(R_{\Delta 1}+1)}{R_{\Delta 1}}\Phi_V - \frac{1}{R_{\Delta 1}} \tag{7.28}$$

$$\Delta_4 = D\Phi_V(R_{\Delta 1}+1) - R_{\Delta 1}D\Phi_L - F = 0$$
$$\therefore \Phi_L = \frac{(R_{\Delta 1}+1)}{R_{\Delta 1}}\Phi_V - \frac{F}{DR_{\Delta 1}} \tag{7.29}$$

$$\Delta_5 = D(R_{\Delta 1}+1)(\Phi_V-1) - R_{\Delta 1}D(\Phi_L-1) + S_1 + S_2 = 0$$
$$\therefore \Phi_L = \frac{(R_{\Delta 1}+1)}{R_{\Delta 1}}\Phi_V - \frac{D+S_1+S_2}{DR_{\Delta 1}} \tag{7.30}$$

$$\Delta_7 = S_1 - D(R_{\Delta 1}+1)(\Phi_V-1) + R_{\Delta 1}D(\Phi_L-1) = 0$$
$$\therefore \Phi_L = \frac{(R_{\Delta 1}+1)}{R_{\Delta 1}}\Phi_V - \frac{D+S_1}{DR_{\Delta 1}} \tag{7.31}$$

All of the zero net flow lines are again parallel to one another in the Φ-space since they have identical slopes, but their *y*-intercepts are different, as shown in Figure 7.44.

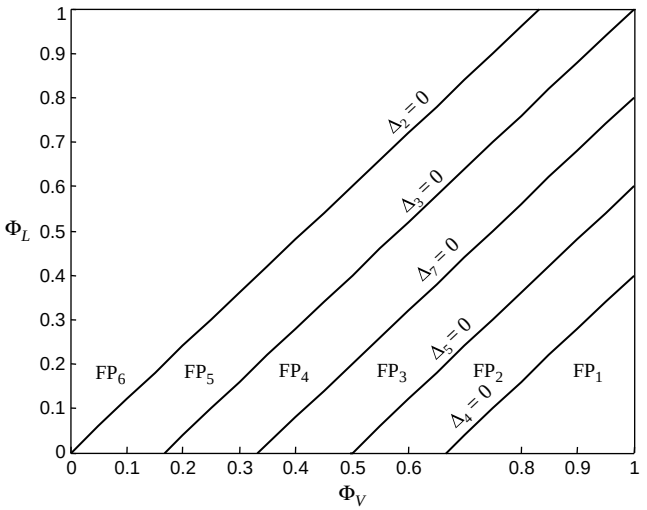


FIGURE 7.44 Representation of FP transition in Φ-space for the Kaibel column.

Similarly to the Petlyuk column, when Φ-coordinates are chosen to produce asymmetrical FPs such as FP_1, FP_2, FP_5, and FP_6, either one of the difference points across the feed stage are shifted into negative composition space, which may be especially applicable to nonideal systems.

7.5.4 Sharp Split Constraints

For the special case of a sharp split problem, we argued in the Petlyuk that if the distillate and bottoms products are confined to lie on the low and high boiling axes respectively, that the intermediate-boiling component in the sidestream should be pure, because the difference points force this (see Section 7.4.1). For the Kaibel column to be considered a sharp split problem, the difference points of the CSs across the feed stage are forced to lie on the edges of the mass balance tetrahedron (MBT^4). Specifically, $\boldsymbol{X}_{\boldsymbol{\Delta}4}$ is forced to lie on the x_3–x_4 axis (or its extension on either side), while $\mathbf{X}_{\boldsymbol{\Delta}2}$ has to lie on the x_1–x_2 axis. Due to the linear mixing properties of $\mathbf{X}_{\boldsymbol{\Delta}}$ at the topmost thermally coupled point, $\mathbf{X}_{\boldsymbol{\Delta}1}$, $\mathbf{X}_{\boldsymbol{\Delta}2}$, and $\mathbf{X}_{\boldsymbol{\Delta}3}$ all have to lie on a straight line in composition space. Since $\mathbf{X}_{\boldsymbol{\Delta}1}$ already lies on the x_1–x_2 edge of the MBT^4 due to the sharp split specification, it follows that $\mathbf{X}_{\boldsymbol{\Delta}3}$ is forced to lie on this axis too. However, a similar argument can be made for $\mathbf{X}_{\boldsymbol{\Delta}4}$, $\mathbf{X}_{\boldsymbol{\Delta}5}$, and $\mathbf{X}_{\boldsymbol{\Delta}6}$. The only way that both the requirements are met is if $\mathbf{X}_{\boldsymbol{\Delta}3}$ and $\mathbf{X}_{\boldsymbol{\Delta}5}$ lie on the x_2 and x_3 vertices, respectively, which directly implies that products in stream S_1 ($\mathbf{x}_{S1}$) and S_2 ($\mathbf{x}_{S2}$) also have to lie on these respective vertices, that is, $\mathbf{X}_{\boldsymbol{\Delta}3} = \mathbf{x}_{S1}$ and $\mathbf{X}_{\boldsymbol{\Delta}5} = \mathbf{x}_{S2}$. This also means that $\mathbf{X}_{\boldsymbol{\Delta}7}$ lies on the x_2–x_3 axis. Typical sharp split difference point behavior in the Kaibel can be seen in Figure 7.45.

Now, let us take a closer look at the material balance across the first side-draw stage. It can be shown through a similar derivation to the one given in Figure 7.9 that

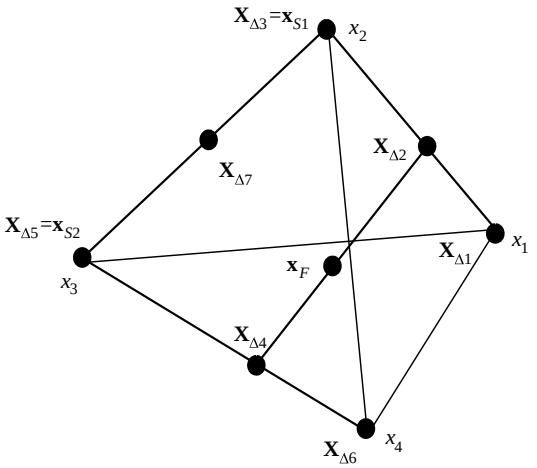


FIGURE 7.45 Difference point behavior for the sharp split Kaibel column.

the material balance at this stage reduces to

$$\Delta_7 \mathbf{X}_{\mathbf{\Delta}7} = S_1 \mathbf{x}_{S1} + \Delta_3 \mathbf{X}_{\mathbf{\Delta}3} \tag{7.32}$$

We also know from the geometric arguments above that $\mathbf{X}_{\mathbf{\Delta}3} = \mathbf{x}_{S1}$ (for sharp splits only), making Equation 7.32 reduce to

$$\Delta_7 = \frac{(S_1 + \Delta_3)\mathbf{x}_{S1}}{\mathbf{X}_{\mathbf{\Delta}7}} \tag{7.33}$$

Similarly, the material balance across the second side-draw stage with $\mathbf{X}_{\mathbf{\Delta}5} = \mathbf{x}_{S2}$ (for sharp splits only) results in

$$\Delta_7 = \frac{(\Delta_5 - S_2)\mathbf{x}_{S2}}{\mathbf{X}_{\mathbf{\Delta}7}} \tag{7.34}$$

Combining Equations 7.33 and 7.34 to eliminate $\mathbf{X}_{\mathbf{\Delta}7}$ yields Equation 7.35:

$$\Delta_7 \left(1 - \frac{(S_1 + \Delta_3)\mathbf{x}_{S1}}{(\Delta_5 - S_2)\mathbf{x}_{S2}}\right) = 0 \tag{7.35}$$

Equation 7.35 holds for all elements of $\mathbf{x}_{S1}$ and $\mathbf{x}_{S2}$. Since $\mathbf{x}_{S1} \neq \mathbf{x}_{S2}$ for certain elements (due to the product specification that have been set), the only possible solution for Equation 7.35 is

$$\Delta_7 = 0 \tag{7.36}$$

Equation 7.36 is only valid for sharp split problems. This is quite a remarkable outcome, because it means at sharp split conditions, one has to operate on the $\Delta_7 = 0$ line in Figure 7.44 regardless of the value of $R_{\Delta 1}$ or the feed composition. Conversely, it can be said that if the vapor and liquid flowrates in CS_7 are not kept equal to each other, a sharp split will never be obtained. This is true regardless of the thermodynamic properties of the system.

This result further implies that CS_7 operates at infinite reflux and because $\mathbf{X}_{\mathbf{\Delta}3} = \mathbf{x}_{S1}$ it can be shown that $\mathbf{x}_7^T = \mathbf{y}_7^T$, meaning that CS_7 will operate exactly on its RCM and that Equation 7.2 is not applicable. Moreover, this means that $\mathbf{X}_{\mathbf{\Delta}7}$ is nonexistent. It should be noted that the entire $\Delta_7 = 0$ line in Φ-space line is not open to design, only a segment of it as shown in Figure 7.46, depending on the value of $R_{\Delta 1}$. Finding the exact segment on the $\Delta_7 = 0$ line requires obtaining similar feasibility conditions as in the Petlyuk column, where the TT^4s of neighboring CSs just touch one another.

This result provides some insight into the often reported control problems of the Kaibel column. It is simply extremely difficult to obtain high purity product when the bounds on operation are so tight. Any deviation off the line in Figure 7.46 during

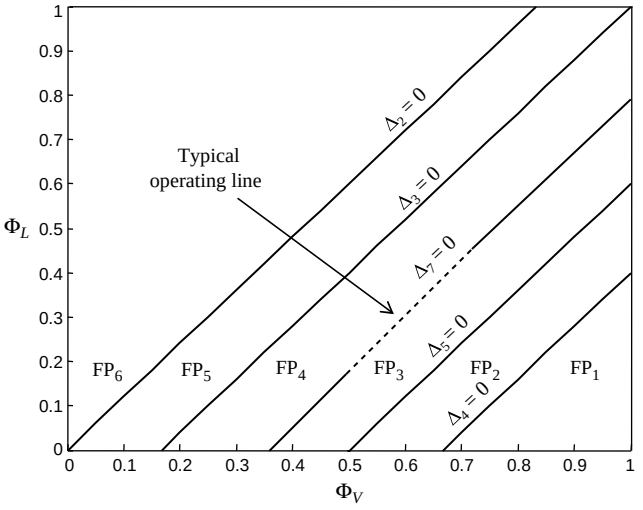


FIGURE 7.46 Typical operating line for the Kaibel column operating at sharp split condition.

process operation immediately suggests that the products will impure. It can be said that the "over-refluxed" Kaibel column operates in exactly the same way as the minimum reflux Petlyuk column. The "over-refluxed" Petlyuk column provides flexibility in this regard as there is an entire region available to the controller or operator to throttle flows such that the column remains on-spec.

7.6 SUMMARY

In this chapter, a systematic procedure has been presented to design fully thermally coupled columns. We have shown how simple infinite reflux Petlyuk columns can be designed by merely superimposing two sets of CPM on one another. The simplified infinite reflux design is very useful for determining a first estimate for feasibility, especially in nonideal systems where the behavior of phase equilibrium behavior at finite reflux is not immediately apparent. The CPM technique was also applied to the design of Petlyuk columns by searching for profile intersections. The CPM methodology allows one to easily and logically determine complex design variables such as the total number of stages, feed stage, and side-draw stage, which can be exported to process simulation packages for more rigorous results. Furthermore, the existences of multiple FPs within these fully thermally coupled columns have been pointed out and the potential for new and interesting designs that can be created through counter-intuitive placement of $\mathbf{X}_{\boldsymbol{\Delta}}$ points.

As with other complex systems, the simplified TT (or TT[4]) technique was shown to be extremely useful for analysis of sharp split systems. The TT method allows one to quickly gauge values for process variables that will result in a realizable design,

and thereby calculate the minimum energy demand for the Petlyuk column. It was also demonstrated how the TT method can be used for assessing column stability. Lastly, we have provided some valuable insights into Kaibel column design, especially for the sharp split case. It is shown that, rather counter-intuitively, the addition of a CS creates extremely stringent limits on possible selection of process variables. In both the Petlyuk and Kaibel columns, considered among the most difficult columns to design, the CPM method has proven to be a simple, insightful design technique.

REFERENCES

[1] Wright, R.O., Fractionation Apparatus. 1949: USA Patent no. 2471134.

[2] Petlyuk, F.B., V.M. Platonov, and D.M. Slavinskii, Thermodynamically optimal method for separating multicomponent mixtures. *International Chemical Engineering*, 1965, **5**(3):554–561.

[3] Kaibel, G., Distillation columns with vertical partitions. *Chemical Engineering and Technology*, 1987, **10**(1):92–98.

[4] Wenzel, S. and H.J. Röhm, Auslegung thermisch und stofflich gekoppelter Destillationskolonnen mittels Gesamtkostenoptimierung. *Chemie Ingenieur Technik*, 2003, **75**(5):534–540.

[5] Wolff, E.A. and S. Skogestad, Operation of integrated three-product (Petlyuk) distillation columns. *Industrial and Engineering Chemistry Research*, 1995, **34**(6):2094–2103.

[6] Stupin, W.J. and F.J. Lockhart, Thermally coupled distillation—a case history. *Chemical Engineering Progress*, 1972, **68**(10):71.

[7] Hendry, J.E., D.F. Rudd, and J.D. Seader, Synthesis in the design of chemical processes. *AIChE Journal*, 1973, **19**:1.

[8] Doukas, N. and W.L. Luyben, Economics of alternative distillation configurations for separation of ternary mixtures. *Industrial and Engineering Chemistry Process Design and Development*, 1978, **17**:273.

[9] Tedder, D.W. and D.F. Rudd, Parametric studies in industrial distillation: Part 1. Design comparisons. *AIChE Journal*, 1978, **24**:303.

[10] Fidkowski, Z. and L.W. Krolikowski, Minimum energy requirements of thermally coupled distillation systems. *AiChE Journal*, 1987, **33**(4):643–653.

[11] Westerberg, A.W., The synthesis of distillation based separation systems. *Computers and Chemical Engineering*, 1985, **9**(5):421.

[12] Glinos, K.N. and M.F. Malone, Design of sidestream distillation columns. *Industrial and Engineering Chemistry Process Design and Development*, 1985, **24**(3):822–828.

[13] Rudd, H., Thermal coupling for energy efficiency. *The Chemical Engineering*, 1992, p. (Supplement) S14.

[14] Triantafyllou, C. and R. Smith, The design and optimisation of fully thermally coupled distillation columns: Process design. *Transactions of the Institution of Chemical Engineers*, 1992, **70**:118–132.

[15] Westerberg, A.W. and O. Wahnschafft, Synthesis of distillation-based separation systems, in *Advances in Chemical Engineering*, L.A. John, editor. 1996, New York: Academic Press pp. 63–170.

[16] Finn, A.J., *Gas Separation and Purification*, 1996, **10**(3):169.

[17] Hernandez, S. and A. Jimenez, Controllability analysis of thermally coupled distillation systems. *Industrial and Engineering Chemistry Research*, 1999, **38**(10):3957–3963.

[18] Segovia-Hernández, J.G., S. Hernández, and A. Jiménez, Analysis of dynamic properties of alternative sequences to the Petlyuk column. *Computers and Chemical Engineering*, 2005, **29**(6):1389–1399.

[19] Hernández, S., J. Gabriel Segovia-Hernández, and V. Rico-Ramírez, Thermodynamically equivalent distillation schemes to the Petlyuk column for ternary mixtures. *Energy*, 2006, **31**(12):2176–2183.

[20] Hernández, S. and A. Jiménez, Design of energy-efficient Petlyuk systems. *Computers and Chemical Engineering*, 1999, **23**(8):1005–1010.

[21] Halvorsen, I.J. and S. Skogestad, Minimum energy consumption in multicomponent distillation. 2. Three-product Petlyuk arrangements. *Industrial and Engineering Chemistry Research*, 2003, **42**(3):605–615.

[22] Halvorsen, I.J. and S. Skogestad, Optimizing control of Petlyuk distillation: Understanding the steady-state behavior. *Computers and Chemical Engineering*, 1997. **21**(Supplement 1):S249–S254.

[23] Abdul Mutalib, M.I. and R. Smith, *Transactions of Institute of Chemical Engineering, Part A*, 1998. **76**:308.

[24] Agrawal, R. and Z.T. Fidkowski, Are thermally coupled distillation columns always thermodynamically more efficient for ternary distillations? *Industrial and Engineering Chemistry Research*, 1998, **37**(8):3444–3454.

[25] Ling, H. and W.L. Luyben, New control structure for divided-wall columns. *Industrial and Engineering Chemistry Research*, 2009, **48**(13):6034–6049.

[26] Holland, S.T., Column profile maps: A tool for the design and analysis of complex distillation systems, in *Chemical and Metallurgical Engineering*. 2005, Johannesburg: University of the Witwatersrand.

[27] Holland, S.T., et al., Complex column design by application of column profile map techniques: Sharp-split Petlyuk column design. *Industrial and Engineering Chemistry Research*, 2009, **49**(1):327–349.

[28] Halvorsen, I.J. and S. Skogestad, Optimal operation of Petlyuk distillation: Steady-state behavior. *Journal of Process Control*, 1999. **9**(5):407–424.

[29] Halvorsen, I.J. and S. Skogestad, Minimum energy consumption in multicomponent distillation. 1. $V_{\min}$ diagram for a two-product column. *Industrial and Engineering Chemistry Research*, 2003. **42**(3):596–604.

[30] Abbas, R. Utilisation of Column Profile Maps for design and optimisation of complex distillation processes, in Chemical and Metallurgical Engineering. 2011, Johannesburg: University of the Witwatersrand.

CHAPTER 8

REACTIVE DISTILLATION DESIGN USING COLUMN PROFILE MAPS

8.1 INTRODUCTION

The concept of combining a chemical reaction and separation in a single unit is by no means a new one, the concept being exploited as early as the 1920s [1–4], with Berman recognizing its potential in 1948 already [5]. This combined process, known as reactive distillation, may be implemented to replace conventional reaction-separation networks and has the potential to greatly reduce operating and capital expenditures. Taylor and Krishna [6] compiled a comprehensive review on reactive distillation and have identified several advantages, including significant savings on capital cost due to the simplification or elimination of the separation network, improved heat integration, especially if the reaction is exothermic, and an improvement in both selectivity and reactant conversion.

However, due to the fact that reaction and separation, and invariably mixing through the column reflux, occur in a single vessel, modeling of reactive distillation processes is considerably more complex than non-reactive systems. Two distinct approaches have evolved in an attempt to interpret the behavior of reactive distillation systems, namely equilibrium models, which assume that the vapor and liquid leaving or entering a stage are exactly in equilibrium, and nonequilibrium or rate-based models [7]. Although the nonequilibrium models are undoubtedly more rigorous than their equilibrium counterparts, they are often lacking in terms of the insight that may be gleaned by the simpler equilibrium model.

Understanding Distillation Using Column Profile Maps, First Edition. Daniel Beneke, Mark Peters, David Glasser, and Diane Hildebrandt.
© 2013 by John Wiley & Sons, Inc. Published 2013 by John Wiley & Sons, Inc.

In an attempt to better understand the interaction between reaction and phase equilibrium, several authors have proposed graphical techniques, in particular, using RCMs and superimposing a reaction vector field [8,9] to produce reactive residue curve maps (RRCMs). In an analogous manner, Doherty et al. also expanded their ODEs describing the change in composition in nonreactive CSs to incorporate chemical reaction using transformed variables [10–17]. In this chapter, we will show how the CPM approach can be applied to reactive systems and significantly, how quick design decisions may be made even in the presence of complex reactions or phase equilibrium behavior. In keeping with the trend of the introduction of CPMs in Chapters 2 and 3, a time-dependent batch-like system will first be discussed followed by a derivation, observations, and applications of a reactive difference point equation (RDPE) for use in reactive CSs.

8.2 SIMPLE REACTIVE DISTILLATION

8.2.1 Extending the Residue Curve Map

Analogously to batch distillation and the RCM, the simplest means of reactive distillation occurs in a still where reaction and phase separation simultaneously take place in the same unit. Additionally, we can choose to add a mixing stream to this still, and the overall process thus consists of three different phenomena: chemical reaction, vapor–liquid equilibrium, and mixing. Such a system is referred to as a simple reactive distillation setup. This setup is shown in Figure 8.1 where a stream of flowrate $\dot{F}$ and composition $\mathbf{x}_F$ enters a continuously stirred tank reactor (CSTR) in which one or more chemical reaction(s) take place in the liquid phase with a certain reaction rate $r = f(k_f, \mathbf{x}, \mathbf{v})$ where $\mathbf{v}$ represents the stoichiometric coefficients of the reaction. Reactants generally have negative stoichiometric coefficients, while products have positive coefficients. For example, the reaction $2\mathrm{A} + \mathrm{B} \rightarrow 3\mathrm{C}$ can

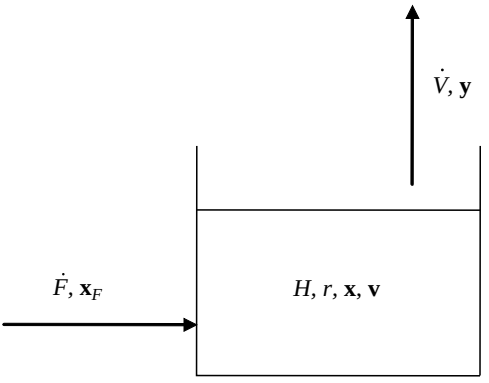


FIGURE 8.1 A CSTR with a feed stream and simultaneous phase separation.

be described by $\mathbf{v} = [v_A,\ v_B,\ v_C] = [-2,\ -1, +3]$. Furthermore, k_f represents the reaction rate constant, and $\mathbf{x}$ is the liquid composition within the reactor. While the reaction is taking place in the CSTR, volatile products are boiled off simultaneously with a flowrate of $\dot{V}$ and a composition of $\mathbf{y}$, where $\mathbf{y}$ is the vapor composition in phase equilibrium with $\mathbf{x}$. The molar holdup in the reactor is H.

Assuming that the chemical reaction proceeds in the liquid phase only and that the liquid in the still is homogenous, the chemical reaction (r) occurring in the beaker may be modeled with an appropriate reaction rate model. It is convenient to use a model which incorporates molar fractions and, for the purposes of this work, we will use an elementary rate model as shown below:

$$r = k_f \left(\prod_{i=1}^{n_R} a_i^{|v_i|} - \prod_{i=1}^{n_P} a_i^{|v_i|} / K_{\text{eq}} \right) \tag{8.1}$$

where the subscripts R and P denote the reagents and products, respectively, and where a_i is the activity of species i. The activity of a specific component i is defined as $a_i = \gamma_i x_i$, where γ_i is the activity coefficient which can be assumed to be unity for near-ideal mixtures. K_{eq} is the reaction equilibrium constant. It should be noted that r (and k_f) have units of inverted time (s^{-1}, min^{-1}, or h^{-1}). For the sake of simplicity, an ideal CSTR will be assumed, that is, the reactor is perfectly mixed and the liquid composition is exactly the same everywhere in the reactor. Through a little knowledge of chemical reaction theory, an equation describing the change that each species undergoes in the vessel due to reaction alone (ignoring first the effect of mixing and vapor boil-off) can be written as follows:

$$\frac{dH\mathbf{x}}{dt} = \text{Hvr} \tag{8.2}$$

Similarly, a material balance for the individual vapor removal and mixing process are written in Equations 8.3 and 8.4, respectively:

$$\frac{dH\mathbf{x}}{dt} = -\dot{V}\mathbf{y} \tag{8.3}$$

$$\frac{dH\mathbf{x}}{dt} = \dot{F}\mathbf{x}_F \tag{8.4}$$

Now, by performing a material balance across the entire system in Figure 8.1, taking into account all phenomena occurring simultaneously, results in Equation 8.5:

$$\frac{dH\mathbf{x}}{dt} = \dot{F}\mathbf{x}_F + H\mathbf{v}r - \dot{V}\mathbf{y} \tag{8.5}$$

Clearly, the overall process is merely a linear combination of the individual phenomena in Equations 8.2–8.4. Using the product rule for differentiation, it can be shown that

$$\frac{dH\mathbf{x}}{dt} = \mathbf{x}\frac{dH}{dt} + H\frac{d\mathbf{x}}{dt} \tag{8.6}$$

Since we are mostly interested in the change in liquid composition in the reactor, the first term on the right-hand side of Equation 8.6 needs to be eliminated. By incorporating an unsteady state, overall material balance across the reactor we obtain

$$\frac{dH}{dt} = \dot{F} - \dot{V} + Hr\sum_{i=1}^{nc} v_i \tag{8.7}$$

Finally, combining Equations 8.5–8.7 and rearranging, we find that

$$\frac{d\mathbf{x}}{dt} = \left(\frac{\dot{V}}{H}\right)(\mathbf{x} - \mathbf{y}) + \left(\frac{\dot{F}}{H}\right)(\mathbf{x}_F - \mathbf{x}) + r\left(\mathbf{v} - \mathbf{x}\sum_{i=1}^{nc} v_i\right) \tag{8.8}$$

Equation 8.8 may be further simplified in terms of a warped time variable, $d\zeta = (V/H)dt$, such that

$$\frac{d\mathbf{x}}{d\zeta} = (\mathbf{x} - \mathbf{y}) + \beta(\mathbf{x}_F - \mathbf{x}) + \theta r\left(\mathbf{v} - \mathbf{x}\sum_{i=1}^{nc} v_i\right) \tag{8.9}$$

where $\beta = \dot{F}/\dot{V}$ and $\theta = H/\dot{V}$, both of which are always positive scalar quantities. To further simplify the analysis and understanding of the interaction of simultaneous phenomena, it is convenient to substitute the θ parameter into a lumped, dimensionless parameter $\kappa = k_f H/\dot{V} = k_f\theta$, and substituting the reaction rate term (r) with $\underline{r} = r/k_f$. This dimensionless transformation allows one to write Equation 8.9 as a function of only two reactive parameters, κ and K_{eq}, instead of θ, k_f, and K_{eq}. Thus, Equation 8.9 can then be rewritten as

$$\frac{d\mathbf{x}}{d\zeta} = (\mathbf{x} - \mathbf{y}) + \beta(\mathbf{x}_F - \mathbf{x}) + \kappa\,\underline{r}\left(\mathbf{v} - \mathbf{x}\sum_{i=1}^{nc} v_i\right) \tag{8.10}$$

The right-hand side of Equation 8.10 has three separate vector terms, representing the three different phenomena present in this process: separation (**S**), mixing (**M**), and reaction (**R**), summarized as such in Equation 8.11:

$$\frac{d\mathbf{x}}{d\zeta} = \mathbf{S} + \mathbf{M} + \mathbf{R} \tag{8.11}$$

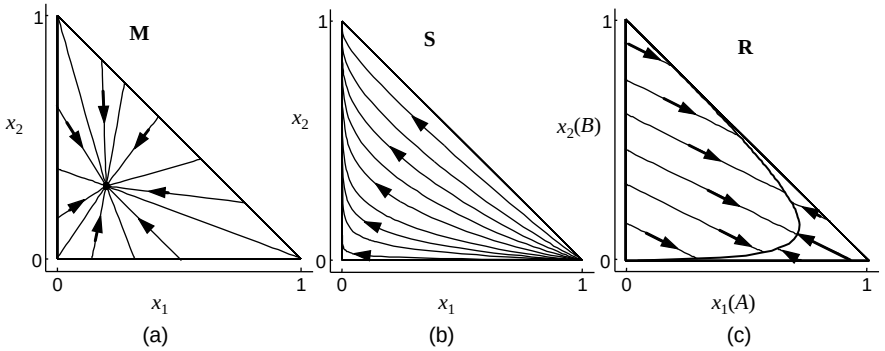


FIGURE 8.2 Phenomena vector fields for (a) mixing with $\mathbf{x}_F = [0.2, 0.3]$; (b) separation for a constant relative volatility system with $\boldsymbol{\alpha} = [5, 1, 2]$; and (c) single chemical reaction for $1B + 1C \leftrightarrow 2A$ with elementary reaction rate and $K_{eq} = 25$.

Significantly, notice that the first two terms, separation and mixing, are in a mathematical sense very similar to the DPE and may as such be interpreted similarly (refer to Section 3.6.2). Each individual phenomena has a distinct influence on the topology of a reactive distillation system and in general, mixing profiles move in a direction toward the mixing composition ($\mathbf{x}_F$), the vapor liquid-separation profiles move toward the highest boiling component in a distillation region (such as RCMs), and the reaction profiles toward the reaction equilibrium curve. All three these topological effects are shown in Figure 8.2. From this we can conclude that the overall process is merely a linear combination, in vector form, of different phenomena scaled by the appropriate process parameters, that is, the relative magnitudes of $\dot{F}$, H, and $\dot{V}$, or in terms of the simplified warped time variable, the magnitudes of β and κ.

8.2.2 Characteristics of the Reaction Vector Field

The reaction profiles depicted in Figure 8.2c are for the reaction $1B + 1C \leftrightarrow 2A$, which is described by an elementary rate law through Equation 8.1 where A, B, and C are the low, high, and intermediate components, respectively. Reaction profiles always point toward the reaction equilibrium curve, but the actual direction in which they point depends on the stoichiometric vector in the term $\mathbf{v} - \mathbf{x}\sum_{i=1}^{nc} v_i$ in Equation 8.10. Notice that when $\mathbf{v} - \mathbf{x}\sum_{i=1}^{nc} v_i = 0$ there is essentially a pinch point of the reaction profiles located where $\mathbf{x}$ satisfies this condition, where $\mathbf{x} = \mathbf{v}/\sum_{i=1}^{nc} v_i$.

Furthermore, this specific pinch point always behaves as an unstable node, meaning that *all* profiles run away from this point toward the reaction equilibrium curve, as shown specifically by Figure 8.3a. It is clear from this figure that all profiles originate from the point $\mathbf{x} = [-1, -1]$ for the $1A + 1B \leftrightarrow 3C$ reaction. Other authors have termed this point the "pole point" [18,19]. Thus, the stoichiometric vector also directly influences the direction of the reaction profiles. As shown in Figure 8.3b,

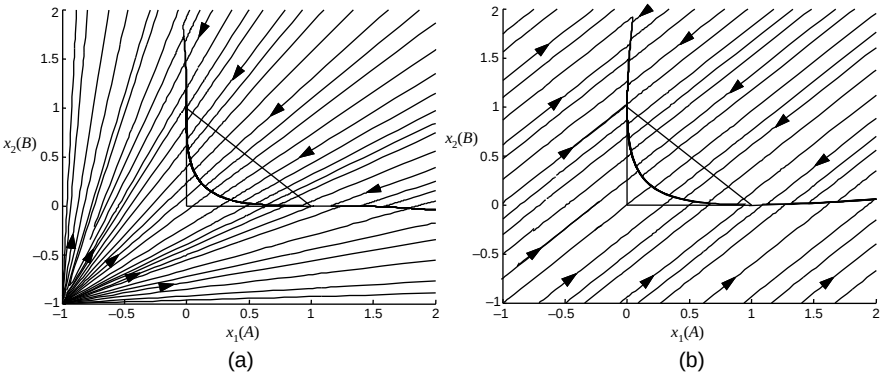


FIGURE 8.3 Reaction profiles with $K_{eq} = 25$ for the reaction (a) $1A + 1B \leftrightarrow 3C$ ($\mathbf{v} = [-1, -1, 3]$) and (b) $1A + 1B \leftrightarrow 2C$ ($\mathbf{v} = [-1, -1, 2]$).

however, for the special case where the moles are conserved in the reaction, these profiles are always parallel to one another. From a geometrical perspective, this implies that the pole point lies infinitely far away. For all other cases where the moles are not conserved, all profiles originate from this pole point, which always exists outside the MBT since stoichiometric coefficients are always such that they are greater than or equal to one.

It is further important to note the direction of the reaction. By comparing the reaction equilibrium curves in Figure 8.2c and those in Figure 8.3a and b, one can see that the curve has been rotated. This is because the reactions in each of these two figures are different: Figure 8.2c represents the $1B + 1C \leftrightarrow 2A$ reaction, while Figure 8.3b is for the $1A + 1B \leftrightarrow 2C$ reaction.

The influence of the equilibrium constant (K_{eq}) on the reaction equilibrium curve is shown in Figure 8.4. For the limiting case where $K_{eq} = \infty$, the equilibrium curve lies on the AC–BC axes and equilibrium is reached when either or either the compositions of A or B are zero. Conversely, when $K_{eq} = 0$, the reaction equilibrium curve lies on the AB diagonal of the MBT, implying that the reverse reaction in Figure 8.4, $2C \leftrightarrow 1A + 1B$, is followed irreversibly and equilibrium is reached when $C = 0$. All intermediate values of K_{eq} simply imply that chemical equilibrium is reached inside the MBT, with the equilibrium curve intersecting the reagent vertices of the MBT.

8.2.3 Overall Reactive Distillation Vector Field

It is important to realize that the individual phenomena profiles shown in Figure 8.2 are not influenced by the magnitude of process parameters β and κ. In other words, the direction of the mixing profiles in Figure 8.2a is only dependent on the feed composition and not the feed flowrate. However, when all the phenomena are combined, the magnitude of these process parameters play an important role as they scale the relative effect of each individual phenomena. To better emphasize this

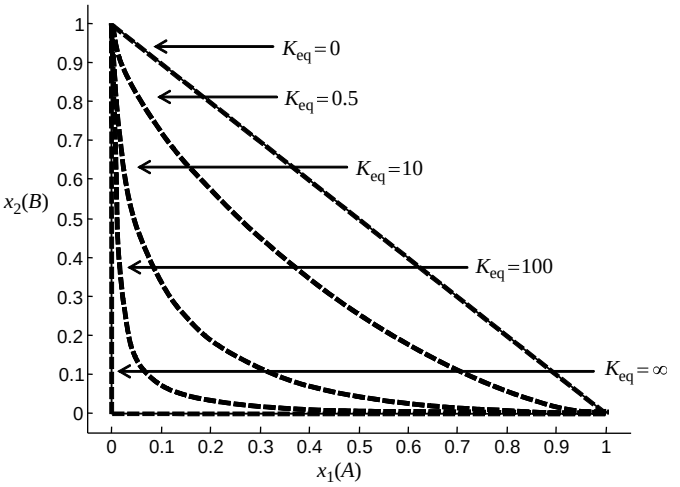


FIGURE 8.4 The influence of K_{eq} on the reaction equilibrium curve for the reaction $1A + 1B \leftrightarrow 2C$ ($\mathbf{v} = [-1, -1, 2]$).

point, consider the combination of all processes in Figure 8.2 with $\beta = 0.6$ and $\kappa = 0.9$ as shown in Figure 8.5, which we will from now on refer to as an R-RCM-M[1].

The profiles in Figure 8.5 track the liquid composition in the reactor with changing time, analogous to an RCM. In this case, however, we have additional phenomena in mixing and reaction, but the general interpretation remains the same. Notice that all the profiles run toward a single point, a stable node. At this point, the composition inside the reactor is no longer changing, and the process has reached a compositional steady state, represented by Equation 8.12. This is an important point from a design perspective, as this steady state can be reached independently of the initial conditions within the reactor.

$$\frac{d\mathbf{x}}{d\zeta} = 0 = \mathbf{S} + \mathbf{M} + \mathbf{R} \tag{8.12}$$

In the nonreactive cases presented thus far in the book, there were only two vector fields to consider. At a pinch point, these two vector fields can be seen as two equal forces "pulling" in opposite directions. When a third vector field is added, like reaction, a pinch again occurs where these forces cancel one another out, as qualitatively explained in Figure 8.6.

It is also interesting to observe that versions of the scaled vector fields represented in Equation 8.12 are found elsewhere in process engineering too [20]. For instance, the case where only the **S** and **M** vector fields are present is found in pinched

[1] The abbreviation RCM refers to the classical residue curve map discussed in Chapter 2. When a reaction is introduced, the equivalent map is known as a reactive residue curve map, abbreviated as R-RCM, while the addition of mixing phenomena will result in a reactive residue curve map with mixing (R-RCM-M)

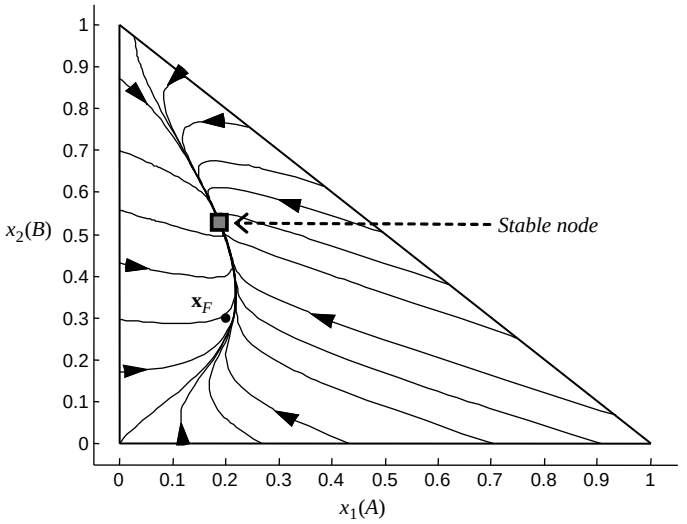


FIGURE 8.5 A reactive distillation process with mixing (R-RCM-M) indicating the stable node and the feed composition $\mathbf{x}_F = [0.2, 0.3]$ for the reaction $1B + 1C \leftrightarrow 2A$, with $K_{eq} = 10$, $\boldsymbol{\alpha} = [5, 1, 2]$, $\beta = 0.6$, and $\kappa = 0.9$.

distillation columns, as discussed extensively throughout this book. The $\mathbf{S} + \mathbf{R} = 0$ case is characteristic of a pinch point in batch reactive distillation systems used to plot RRCMs [10], while the $\mathbf{M} + \mathbf{R} = 0$ scenario is found in CSTRs at steady state.

Perhaps the most important highlight is that the topology of the overall processes in Figure 8.5 is just a summation of three phenomena. For example, if we were to choose a feed flowrate $(\dot{F})$ that is infinitely large (equivalent to making β infinitely large), the reaction and phase equilibrium phenomena will appear insignificant and the process will reduce to just the mixing process. Similarly, choosing an infinitely large holdup (H) in the reactor (equivalent to making κ infinitely large) leads to a process that resembles only the reaction profiles. Finally, if one chooses to reduce the

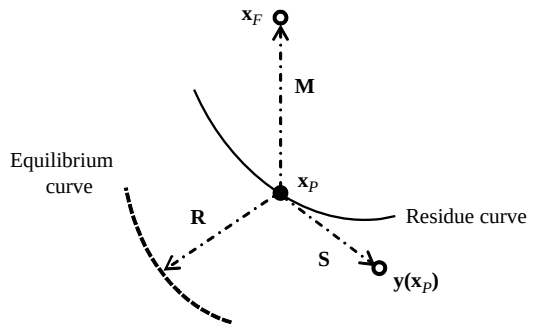


FIGURE 8.6 An illustration of the vectors at a pinch point.

feed input and the reactor holdup to zero, (equivalent to setting both κ and β near-zero), the result in the overall process will resemble only the particular set of components' RCM, that is, only the separation term is significant. The manner in which the profiles behave and where they pinch for the overall process is thus just a matter of how the scalar parameters β and κ are balanced relative to one another.

It should be noted that the value of β and κ are assumed to be constant in these analyses. Of course, they need not be (and most likely aren't) constant during the course of an experiment. For example, κ is a function of the reaction constant (k_f), which for most reactive systems is a strong function of temperature through the Arrhenius equation. Thus, as boiling proceeds and the temperature rises in the still, so too will the value of k_f and κ change. Thus, the plots shown throughout this chapter where β and κ are assumed to be constant and can be seen simply as a "snapshot" of how the experiment behaves at a particular instant. It is however reasonably straightforward to accommodate these temperature effects in the governing differential equations.

8.2.4 Simple Reactive Distillation Design

Gaining an understanding of the influence of each phenomenon on the overall process behavior allows one to qualitatively assess the process. However, one may wonder what the theory presented so far says about the actual design of a simple reactive distillation process. Just like one may deliberately choose parameters to accomplish certain separations in CPMs in Chapter 3, one can also choose parameters in the simple reactive distillation operation to obtain a certain product specification. Also, with CPMs we have seen that expanding the topological space to encompass negative compositions had significant benefits when analyzing CPMs, as the designer is free to position topology even outside the physically realizable composition space. To illustrate this, consider the R-RCMs in Figure 8.7a and b where we have arbitrarily chosen, for simplicity, that there is no feed stream addition ($\beta = 0$), the phase equilibrium behavior can be modeled with constant volatilities of

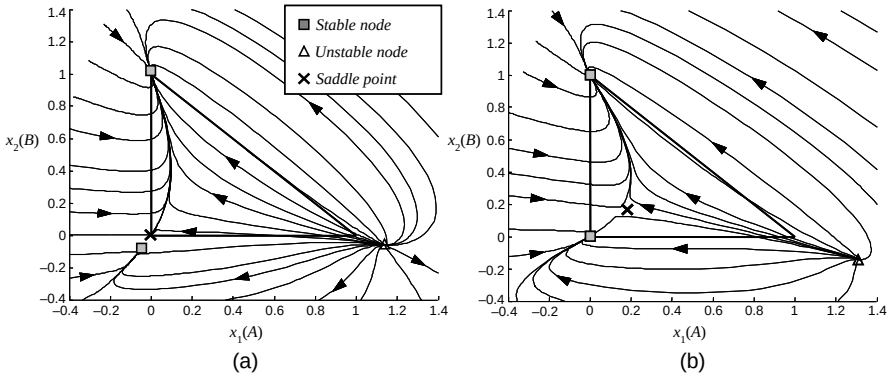


FIGURE 8.7 An R-RCM for the reaction 1B + 1C↔2A, with $K_{eq} = 10$, $\boldsymbol{\alpha} = [5, 1, 2]$ and (a) $\kappa = 0.4$, (b) $\kappa = 0.8$.

5 and 2 for the low- and intermediate-boiling components with respect to the high-boiling component, and a reaction of $1B + 1C \leftrightarrow 2A$ following an elementary reaction rate with $K_{eq} = 10$. This is the same set of process parameters as shown in the R-RCM-M in Figure 8.5, barring feed addition. In Figure 8.7a, the parameter κ has been chosen as 0.4, while in Figure 8.7b, it has a value of 0.8.

As with the CPMs, permitting the analysis of negative compositions aids in understanding the overall process. Due to the nature of the reaction rate model (Equation 8.1), additional nodes have been introduced to the composition space. For this particular example, there are in fact five different stationary points, but only four can be identified here due to the scope of our view of the composition space. As with azeotropic systems which also contain additional stationary points, both inside and outside composition space, the presence of additional nodes can give one more freedom or options in finding a suitable design.

Notice in Figure 8.7a that there is a stable node outside the positive composition space near the intermediate boiling vertex, with a saddle point located on the intermediate boiling vertex. At this particular choice of κ, the profiles loosely resemble this particular system's RCM since the effect of the reaction is relatively small. However, increasing the effect of reaction, as in Figure 8.7b, the curves within the mass balance triangle have been changed considerably, with the saddle node now having moved inside the mass balance triangle, and the stable node (which was previously in negative composition space in Figure 8.7a) now lays on the intermediate boiling vertex. In effect, the stable node in Figure 8.7a has "bumped" and replaced the saddle point from its position on the intermediate boiling vertex. The saddle point that is now in the MBT can be seen in a similar light as an azeotrope in a classical RCM, it has in fact been termed a "reactive azeotrope" by other researchers [18]. By increasing the effect of reaction even more, the curves will eventually reduce to the reaction-only profiles shown in Figure 8.2c.

Note from Figure 8.7a and b that by allowing negative compositions, the so-called reactive azeotrope can be predicted. If one were to be constrained by only positive compositions, the appearance of a node in the MBT, as shown in Figure 8.7b, would have been somewhat surprising. This illustration thus again affirms expanding the view of composition profiles to include those found outside the MBT.

An interesting aspect of Figure 8.7a and b is that, for this particular system, there are *always* nodes fixed to the high- and intermediate-boiling vertices, although their nature may differ. These nodes are termed "locked nodes." This occurs because both the individual separation and reaction processes (illustrated in Figure 8.2b and c, respectively) have nodes on these vertices, and consequently, the combined process must have the same property. If however, we were to add a feed stream to this process, where the only node is at the feed composition (as in Figure 8.2a), the process would not have this locked node property since one of the individual phenomena does not exhibit nodes in the same locations as the others (unless the feed stream has the same composition as the locked nodes). The effect of adding mixing phenomena to the process shown in Figure 8.7 is that stationary points will be drawn closer to the mixing composition, as illustrated in Figure 8.8 a and b. Notice too that in both these illustrations that there is not a node on any pure component vertex, that is, no node locking behavior.

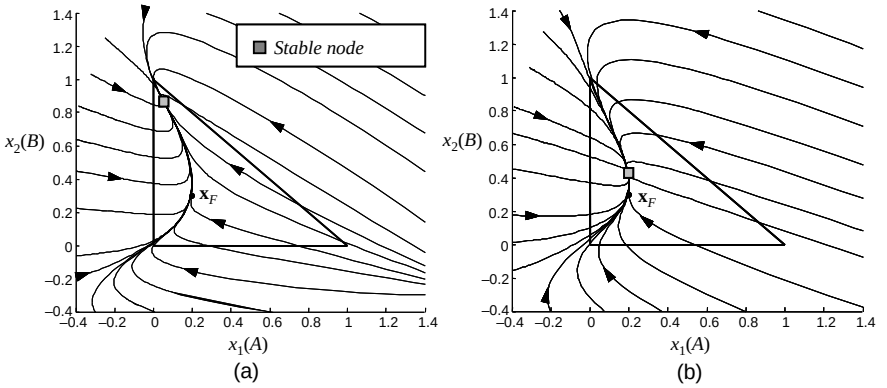


FIGURE 8.8 An R-RCM-M for the reaction 1B + 1C↔2A, with $K_{eq} = 10$, $\kappa = 0.8$, $\boldsymbol{\alpha} = [5, 1, 2]$, $\mathbf{x}_F = [0.2, 0.3]$, and (a) $\beta = 0.05$, (b) $\beta = 0.8$.

Figure 8.8a and b shows that increasing the effect of feed stream addition "pulls" profiles toward the feed composition. Topologically, Figure 8.8a is not too different from Figure 8.7b because the effect of feed addition is relatively small. When comparing Figure 8.8a with Figure 8.8b it was found that the stable node in Figure 8.8b has moved closer to the feed composition due to the increased effect of feed addition. The roles of each individual phenomenon can now be rather quickly and efficiently assessed. However, one might wonder if and/or how we can use these maps for synthesis, the same way in which we synthesized CSs using CPMs by placing nodes in composition space, that is, can we design an experiment so as to produce a certain product? This is illustrated in the following example.

Example 8.1: In the reaction system 1A + 1C↔3B and $K_{eq} = 15$, we would like to determine whether it is possible to design a batch reactive distillation system that will produce a composition of $\mathbf{x}_{desired} = [0.02, 0.93]$. It has been predetermined that the feed to the system should be $\mathbf{x}_F = [0.4, 0.2]$, the relative volatilities to the system are $\boldsymbol{\alpha} = [\alpha_A, \alpha_B, \alpha_C] = [6, 1, 3]$, and the reaction rate is elementary. If the system is indeed possible, produce the relevant R-RCM-M and comment on the system's behavior.

Solution 8.1: In the problem statement all data has been provided, except for a reactor size variable (κ) and vapor boil-off rate variable (β). Since we are interested in producing a particular product with a composition of $\mathbf{x}_{desired} = [0.02, 0.93]$, we can calculate through the steady state version of Equation 8.10 ($d\mathbf{x}/d\zeta = 0$) what values of κ and β will result in a pinch point at $\mathbf{x}_{desired}$. The vapor in equilibrium with $\mathbf{x}_{desired}$ can be calculated through a constant volatility model as $\mathbf{y} = [0.100, 0.775]$. Similarly, $\underline{r}$ (where $\underline{r} = r/k_f$) can be calculated through the elementary rate law equation in Equation 8.1 to be –0.0526, and $\sum_{i=1}^{nc} v_i = 1$. Thus, for components A and B, the pinched versions of Equation 8.10 can be written as

$$0 = 0.38\beta + 0.0537\kappa - 0.08 \tag{8.13}$$

for component A, and

$$0 = -0.73\beta - 0.1089\kappa + 0.155 \tag{8.14}$$

for component B. Equations 8.13 and 8.14 are reasonably simple, linear equations that are only dependent on κ and β. Solving simultaneously for κ and β, it is found that $\kappa = 0.2262$ and $\beta = 0.1786$. Both of these values are positive, and therefore this process is theoretically achievable. An R-RCM-M operating with these calculated values for κ and β is shown in Figure 8.9. Here it shown that there is indeed a pinch point at $\mathbf{x}_{\text{desired}}$, specifically a stable node. Thus, regardless of the initial composition within the reactor, $\mathbf{x}_{\text{desired}}$ will be obtained if the process is in operation for long enough (assuming κ and β are maintained throughout).

Example 8.1 illustrates how one may go about synthesizing a simple reactive distillation process, or at the very least allows one to assess whether the proposed process is at all feasible. It should be noted that if either κ or β turned out to be negative, the proposed process would be infeasible since these parameters only have realistic meaning when they are positive quantities. Moreover, if the κ and β were found to be positive but the node at the desired composition is found to be an unstable node, the simple process would not be feasible either. If a saddle node were found, one has to be certain of the initial composition within the reactor because there is only a single profile which will end at the desired composition. Any other initial composition would result in an entirely different ending composition because the profile will veer away from the saddle point. Lastly, the reader should also be aware that, in the case of the three component system, there are two independent equations that may be written, implying that one may solve for two unknown process

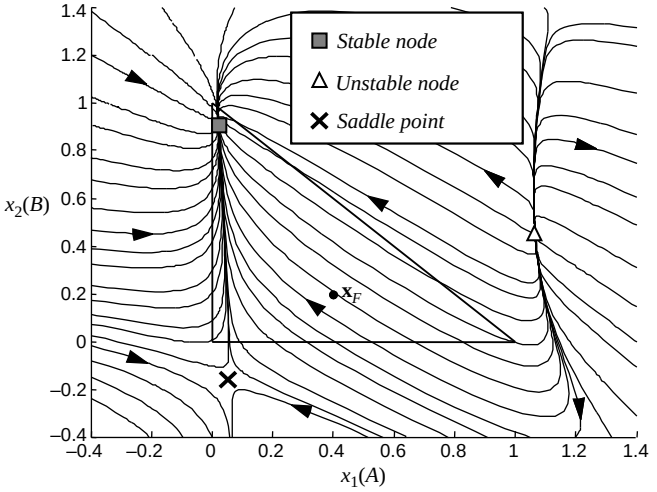


FIGURE 8.9 An R-RCM-M for the reaction 1A + 1C↔3B, with $K_{\text{eq}} = 15$, $\kappa = 0.2262$, $\beta = 0.1786$, $\mathbf{x}_F = [0.4, 0.2]$, and $\boldsymbol{\alpha} = [6, 1, 3]$.

parameters. Which two unknown process parameters are to be solved for is of course up to the designer or the process requirements. Example 8.1 could just as easily been asked as: "Given a system with all reaction and phase equilibrium properties known, as well as κ and β, calculate what feed composition would result in a certain end-product." Similarly, if this calculated feed composition is nonsensical, then the resulting process would also be infeasible.

8.2.5 Zero-Order Reactions—An Interesting Analogy

Consider the special case where the chemical reaction is of zero order ($r = k_f$ or $\underline{r} = 1$), that is the reaction rate is independent of the concentrations of species present in the system. We will furthermore impose restrictions on the system such that the moles are conserved in the reaction $\left(\sum_{i=1}^{nc} v_i = 0\right)$, and the mixing term has a magnitude of zero ($\beta = 0$). For this special case, the unsteady state mass balance, in warped time, for such a process reduces to

$$\frac{d\mathbf{x}}{d\zeta} = (\mathbf{x} - \mathbf{y}) + \kappa\mathbf{v} \tag{8.15}$$

where κ has the same meaning as defined previously. As the reaction term in Equation 8.15 is now independent of composition, Equation 8.15 simply reduces to a linear transformation of the conventional residue curve equation for distillation ($d\mathbf{x}/d\zeta = \mathbf{x} - \mathbf{y}$) discussed in Chapter 2. Thus, the same number of nodes present in the nonreactive RCM will also be present in the zero-order R-RCM because the reactive term is independent of composition. In order to illustrate this, consider such a zero-order system as described by Equation 8.15 where the reaction is given by $1A + 1B \leftrightarrow 2C$ with $\kappa = 0.1$; and constant relative volatilities of 5 and 2. A classical RCM (i.e., $\kappa = 0$) and its associated zero-order R-RCM is then shown in Figure 8.10 a and b, respectively.

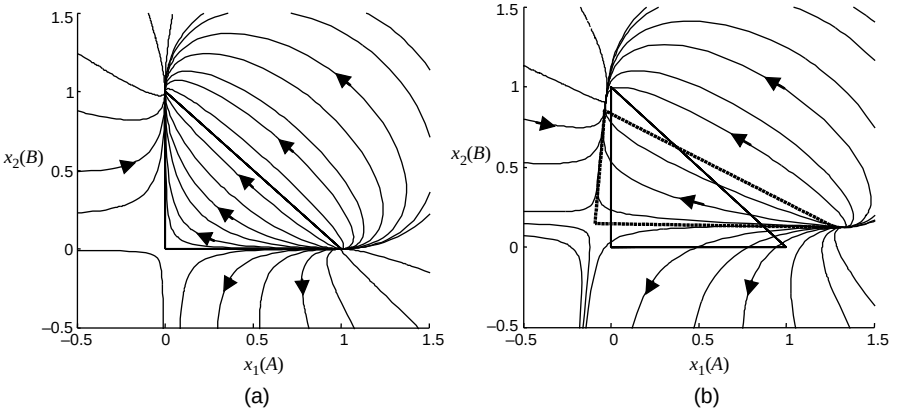


FIGURE 8.10 (a) A RCM extended beyond the positive composition space and (b) an R-RCM for the zero-order $1A + 1B \leftrightarrow 2C$ chemical reaction with $\kappa = 0.1$. $\boldsymbol{\alpha} = [5, 1, 2]$.

Figure 8.10a and b shows that the topological constellation for the RCM and the zero-order R-RCM are similar, as both display the same number of stationary points. However, stationary points have been shifted in the composition space. In fact, Figure 8.10b shows that the resulting R-RCM's nodes are connected by straight lines to yield a TT (see Chapter 3). Significantly, the stationary points have been shifted in such a way that no singularities occur within the MBT, implying that a process operating under these conditions does not reach a compositional steady state anywhere within the MBT. It is however quite obvious that different choices for the $\kappa\mathbf{v}$ term in Equation 8.15 will give rise to different movement of fixed points in composition space. The effect of both κ and $\mathbf{v}$ on the movement of stationary points is summarized conveniently in the pinch point loci in Figure 8.11a–c.

Note that for a ternary reactive system for which the moles are conserved, there are essentially six different reactions that may be conceived. However, as shown in Figure 8.11, by pairing reactions with respect to the absolute magnitude of their stoichiometric coefficients, three distinctive, continuous loci may be constructed. Essentially this implies that the direction in which the reaction proceeds shifts stationary points such as stable and unstable nodes in qualitatively opposite directions. Thus, it is not necessarily the magnitude of reaction (κ) that occurs that has a major impact on the design, but more the direction in which the reaction proceeds. Furthermore, notice specifically that when the reaction proceeds either toward or away from the intermediate boiling component (Figure 8.11b), there are no pinch points located within the MBT, which implies there is not one single composition that would lead to a compositional steady state or pinched behavior within the reactor.

An interesting analogy to the zero-order problem described above is that of the thermally coupled Petlyuk column operating at infinite reflux, in particular for the special case where the vapor and liquid compositions at the top (T) of the column are different ($\mathbf{y}^T \neq \mathbf{x}^T$), as discussed in Chapter 7 (see Figure 7.3). Also, as shown in Chapter 7, the differential equation describing this system was shown to be

$$\frac{d\mathbf{x}}{dn} = (\mathbf{x} - \mathbf{y}) + \boldsymbol{\delta}^T \qquad \text{where} \qquad \boldsymbol{\delta}^T = \mathbf{x}^T - \mathbf{y}^T \tag{8.16}$$

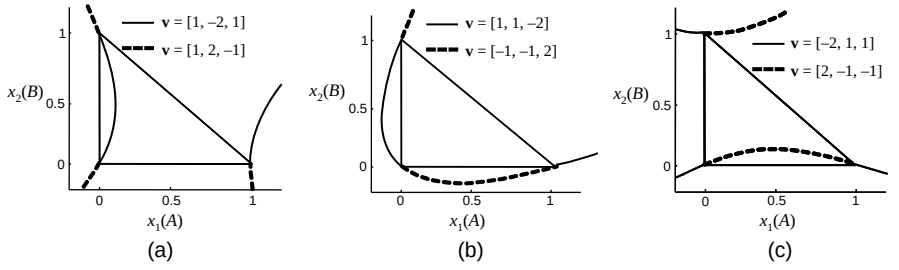


FIGURE 8.11 Pinch point loci with varying κ with a stoichiometric vector of: (a) $\mathbf{v} = \pm[-1, 2, -1]$, (b) $\mathbf{v} = \pm[-1, -1, 2]$, and (c) $\mathbf{v} = \pm[2, -1, -1]$.

Notice that Equation 8.16 is also a linear transform of the residue curve equation, as the difference vector ($\boldsymbol{\delta}^T$) is not a function of the column's internal liquid composition ($\mathbf{x}$). Hence, the mathematics describing the zero-order reactive distillation system is in fact identical to the infinite reflux Petlyuk column, even though the phenomena and equipment involved in the process are very different.

8.3 REACTIVE COLUMN SECTIONS

8.3.1 Definition

Although the preceding sections in this chapter are useful for synthesizing simple reactive distillation systems, we have yet to formulize a tool for designing continuous reactive distillation columns. With this in mind, we introduce here the concept of a reactive column section (RCS). As with nonreactive CSs discussed previously in this book, in a RCS there is a continuous, counter current flow of vapor and liquid streams. However, as the name implies, in addition to the separation and mixing occurring, there is also a chemical reaction occurring in this length of column.

Consider the column configuration shown in Figure 8.12a, with the reaction zone as indicated. Reaction only proceeds in this zone, where the necessary catalyst is appropriately placed in the column. The rest of the column behaves as a normal, nonreactive column. Thus, apart from the reaction zone, identification of the remaining CSs is trivial, as previously discussed and shown in preceding chapters (specifically Chapter 3). Within the reaction zone, there is a combination of reaction, separation, and mixing occurring simultaneously, very similarly to the simple experiment in Figure 8.1. One should take cognizance of the fact that as reaction proceeds in a particular RCS, moles may be created, lost, or remain constant

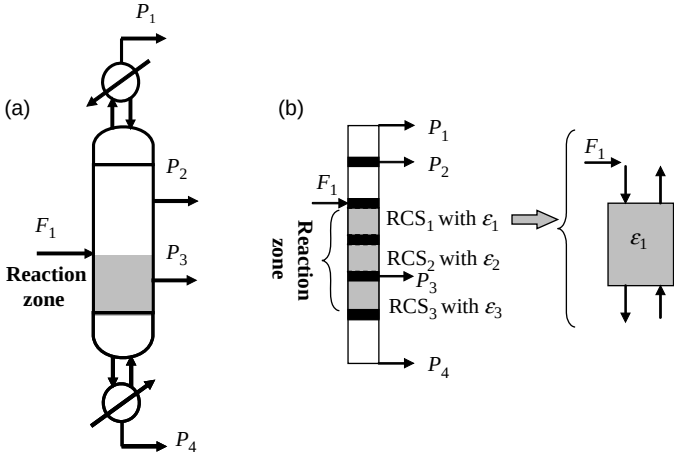


FIGURE 8.12 (a) An arbitrarily specified reactive distillation column and (b) its associated CS and RCS breakdown.

depending on the reaction stoichiometry, and how far the reaction proceeds. Moreover, if the heat of reaction is significant, one may need to account for these additional vaporization/condensation effects. Consequently, taking all these factors into account, the operating mode (and therefore the parameters describing the process) in a particular RCS will change. All of these factors have to be accounted for in the definition of the RCS. Therefore, in accordance with the definition of a nonreactive CS in Chapter 3, we formulate the definition for a RCS as*: a length of column within a "reaction zone" where a reaction occurs with a certain reaction extent (ε), or between points of material addition or removal.*

We use the concept of reaction extent to account for how far the reaction proceeds. For example, suppose the reaction $1A + 2B \leftrightarrow 3C$ is occurring in a particular RCS. If there are initially n_{A0}, n_{B0}, and n_{C0} number of moles present (before the reaction starts), then the number of moles of components A and B remaining after the reaction has taken place (n_A and n_B):

$$n_A = n_{A0} - 1\varepsilon \tag{8.17}$$

$$n_B = n_{B0} - 2\varepsilon \tag{8.18}$$

And the number of moles of C created through the reaction are (n_C)

$$n_C = n_{C0} + 3\varepsilon \tag{8.19}$$

In general for any component K, it can be said that

$$n_K = n_{K0} + \nu_K \varepsilon \tag{8.20}$$

Thus, using this definition of an RCS and reaction extent, a typical RCS can be seen in Figure 8.12b. It can be seen that each RCS operates with a unique reaction extent. Material addition or removal within the reaction zone also leads to the formation of a new RCS, as shown by the removal of stream P_3.

8.3.2 The Reactive Difference Point Equation

Once the RCS has been defined, it is now possible to also derive a RDPE, in much the same way as we have derived the nonreactive DPE in Chapter 3. For the sake of completeness and clarity in the derivation, consider a magnified view of the RCS in Figure 8.13 with the appropriate stream definitions.

In Figure 8.13, the streams at the bottom of the RCS are known, while those at the top are stage-dependent and therefore change down the length of the column. The reaction is assumed to take place from the top of the RCS downward, and only occurs in the liquid phase. Gas phase reactions can also be taken into account, but we shall not consider such reactions in this book. Thus, a molar component balance over the RCS gives

$$L^T\mathbf{x}^T - V^T\mathbf{y}^T - L^B\mathbf{x}_{n-1} + V^B\mathbf{y}_n + \varepsilon\mathbf{v} = 0 \tag{8.21}$$

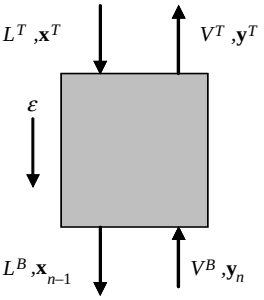


FIGURE 8.13 A magnified view of an RCS with stream definitions.

Since there may be a change in the number of moles due to reaction, we cannot simply apply the constant molar overflow assumption as with nonreactive CSs. An overall molar material balance over the RCS thus yields

$$L^T - V^T - L^B + V^B + \varepsilon \sum_{i=1}^{nc} v_i = 0 \tag{8.22}$$

Superscripts T and B signify the top and bottom of the RCS, respectively. In accordance with the conventional DPE, it is useful to define parameters $\mathbf{X}_{\mathbf{\Delta}T}$ and Δ_T, where the subscript T also denotes the top of the RCS:

$$\mathbf{X}_{\mathbf{\Delta}T} = \frac{V^T\mathbf{y}^T - L^T\mathbf{x}^T}{V^T - L^T} = \frac{V^T\mathbf{y}^T - L^T\mathbf{x}^T}{\Delta_T} \tag{8.23}$$

Although it will become apparent in discussions that follow, it is useful to mention here that $\mathbf{X}_{\mathbf{\Delta}B} \neq \mathbf{X}_{\mathbf{\Delta}T}$, where the subscript B denotes the bottom of the RCS. This is because vapor and liquid flowrates at the top and bottom of the RCS may not be constant as was the case with constant molar overflow CSs. This may be deduced from Equation 8.21.

Using the definition of $\mathbf{X}_{\mathbf{\Delta}T}$ in Equation 8.23 and eliminating L^B from Equation 8.21 through substitution of Equation 8.22 gives

$$\mathbf{x}_{n-1} = \left(\frac{1}{V^B - \Delta_T + \varepsilon \sum_{i=1}^{nc} v_i} \right) \left(-\Delta_T \mathbf{X}_{\Delta T} + \varepsilon \mathbf{v} + V^B \mathbf{y}_n \right) \tag{8.24}$$

Notice that there still remains a V^B term in Equation 8.24, implying that the vapor flowrate (and therefore the liquid flowrate) is changing as reaction proceeds, which may be a significant effect in the RCS and should be accounted for. The fundamental difference between the nonreactive DPE and the RDPE is that the assumption of

constant molar overflow is not necessarily a good one in the reactive case, specifically when the moles of the reaction are not conserved ($\Sigma v_i \neq 0$), as can be inferred from Equation 8.22. Thus, in order to eliminate V^B from Equation 6.14, we need to incorporate an additional equation, in the form of the energy balance, which will allow us to gauge to what degree flowrates are changing in the RCS. A reactive energy balance over the RCS gives

$$H_L^T L^T - H_V^T V^T - H_L^B L^B + H_V^B V^B + \varepsilon \Delta H_{\text{RXN}} = 0 \tag{8.25}$$

where H represents the molar enthalpy of a specific stream and ΔH_{RXN} is the molar heat of reaction at 298 K. Using the form of the reactive energy balance in Equation 8.25 requires that enthalpies of all components at a reference state (in this chapter taken to be a liquid at 1 atm and 298 K) are set to zero because the actual formation enthalpies are taken into account in the ΔH_{RXN} term. As with nonreactive CSs, we can assume that heating effects are negligible when compared to the heat of reaction and the heat of vaporization, that is, $\int C_P dT \approx 0$, and that there are no (or negligible) heat losses through the column walls or mixing effects. These assumptions are equivalent to the constant molar overflow assumptions in nonreactive CSs. These assumptions thus imply

$$H_L^B = H_L^T \simeq 0 \tag{8.26}$$

$$H_V^B = H_V^T \simeq \Delta H_{\text{VAP}} \tag{8.27}$$

where ΔH_{VAP} is the average molar heat of vaporization of all components. Using these assumptions, the only significant enthalpy quantities left in Equation 8.25 are now the heat of reaction and the heat of vaporization. Thus, Equation 8.25 reduces to

$$V^B = V^T - \varepsilon \frac{\Delta H_{\text{RXN}}}{\Delta H_{\text{VAP}}} \tag{8.28}$$

At this point, it is convenient to define a ratio of enthalpies such that $\tau = \frac{\Delta H_{\text{RXN}}}{\Delta H_{\text{VAP}}}$. This ratio then governs by how much the flowrates are changing in the RCS due to simultaneous vaporization and reaction heating effects. When ΔH_{RXN} is comparatively large relative to the heat of vaporization, a large change in the vapor flowrates can be expected from the bottom of the column to the top. Conversely, when the heat of reaction term is small in comparison to the vaporization term, there will be very little change in the vapor flowrates of the RCS. Notice too that the quantity τ can be both negative and positive depending on whether the reaction is exothermic or endothermic, and hence vapor flowrates can either increase or decrease along the length of the RCS. A more detailed account of the influence of the ratio of enthalpies on the net flow in a RCS is given in the section on RCS transition (Section 8.3.3).

We now have a relatively simple expression for the quantity V^B, which can be substituted into Equation 8.24, resulting in

$$\mathbf{x}_{n-1} = \left(L^T + \varepsilon \left[\sum_{i=1}^{nc} v_i - \tau \right] \right)^{-1} \left(-\Delta_T \mathbf{X}_{\mathbf{\Delta}T} + \varepsilon \mathbf{v} + \left(V^T - \varepsilon\tau \right) \mathbf{y}_n \right) \tag{8.29}$$

Now, as was done in the derivation of the nonreactive DPE in Chapter 3, expanding $\mathbf{x}_n$ around stage n using a Taylor series gives

$$\mathbf{x}_n = \mathbf{x}_{n-1} + \frac{d\mathbf{x}}{dn}\Delta n + \frac{d^2\mathbf{x}}{dn^2}\Delta n^2 + \cdots \tag{8.30}$$

Assuming again that only the first-order derivative is significant [21,22] and noting that $\Delta n = n-(n-1) = 1$, Equation 3.7 reduces to

$$\frac{d\mathbf{x}}{dn} = \mathbf{x}_n - \mathbf{x}_{n-1} \tag{8.31}$$

Finally, replacing $\mathbf{x}_{n-1}$ in Equation 8.29 leads to a differential equation

$$\frac{d\mathbf{x}}{dn} = \left(L^T + \varepsilon \left[\sum_{i=1}^{nc} v_i - \tau \right] \right)^{-1} \left[(V^T - \varepsilon\tau)(\mathbf{x} - \mathbf{y}) + \Delta_T (\mathbf{X}_{\mathbf{\Delta}\mathrm{T}} - \mathbf{x}) + \varepsilon \left(\mathbf{x} \sum_{i=1}^{nc} v_i - \mathbf{v} \right) \right] \tag{8.32}$$

Equation 8.32 is remarkably similar to the nonreactive version because it contains both mixing ($\mathbf{X}_{\mathbf{\Delta}T} - \mathbf{x}$) and separation ($\mathbf{x} - \mathbf{y}$) terms. Notice that this equation may however be simplified even further because the scalar term in front of the square brackets on the right hand side of the equation does not influence the direction of profiles in composition space, because it is not a function of composition. It is thus possible to rewrite Equation 8.32, ultimately yielding what is known as the RDPE:

$$\frac{d\mathbf{x}}{d\mu} = (V^T - \varepsilon\tau)(\mathbf{x} - \mathbf{y}) + \Delta_T (\mathbf{X}_{\mathbf{\Delta}\mathrm{T}} - \mathbf{x}) + \varepsilon \left(\mathbf{x} \sum_{i=1}^{nc} v_i - \mathbf{v} \right) \tag{8.33}$$

where $d\mu = \left(L^T + \varepsilon \left[\sum_{i=1}^{nc} v_i - \tau \right] \right)^{-1} dn$ is a simple variable transformation for the independent integration variable *n,* and can be seen as a position coordinate for the RCS signifying the amount of catalyst to be loaded in the RCS.

It is again possible to identify three distinct terms in the RDPE, essentially representing VLE separation, mixing, and reaction phenomena (in much the same way as we interpreted the simple experiment in Equations 8.10 and 8.11). It is important to point out that when the reaction is turned off, that is, $\varepsilon = 0$, that the RDPE is exactly equivalent to the nonreactive DPE of Chapter 3, as expected.

Unfortunately however, because flowrates are changing the RCS, one has to specify actual values for terms such as L^T and V^T in the RDPE so that these changes in flows can be accounted for. Recall that actual flowrates do not need to be specified in the non-reactive DPE.

Furthermore, since the flowrates are changing along the RCS as reaction occurs, so do the components of $\mathbf{X}_{\boldsymbol{\Delta}}$; in other words, $\mathbf{X}_{\boldsymbol{\Delta}}$ does not remain constant as in the nonreactive case. $\mathbf{X}_{\boldsymbol{\Delta}}$ changes from the top (T) of the RCS to the bottom (B) as follows:

$$\mathbf{X}_{\boldsymbol{\Delta}B} = \frac{\Delta_T \mathbf{X}_{\boldsymbol{\Delta}T} - \varepsilon \mathbf{v}}{\Delta_T - \varepsilon \sum v} \tag{8.34}$$

Through these equations, it is thus possible to relate the bottom and the top of the RCS with one another. It is also important to note from the RDPE, that its topological constellation still contains the same number of stationary points as there are components (like the constant relative volatility RCM and CPM), as the reaction term does not introduce any new roots or nodes. Thus, the RDPE is fully reconcilable with "transformed triangle" ideas discussed throughout this book. To illustrate this, a reactive column profile map (RCPM) is shown in Figure 8.14 for a RCS with constant relative volatilities of [5, 1, 2] for the high-, low-, and intermediate-boiling components. The reaction has stoichiometric coefficients of $\mathbf{v} = [-1, -1, 2]$, the extent of the reaction is $\varepsilon = 0.05$ mol/s, the ratio of enthalpies is $\tau = 1.25$, and finally, $V^T = 1.2$ mol/s, $L^T = 1$ mol/s, and $\mathbf{X}_{\boldsymbol{\Delta}T} = [0.3,\ 0.3]$. $\mathbf{X}_{\boldsymbol{\Delta}B}$ can be determined from Equation 8.34, but it is not necessary for producing a single RCPM.

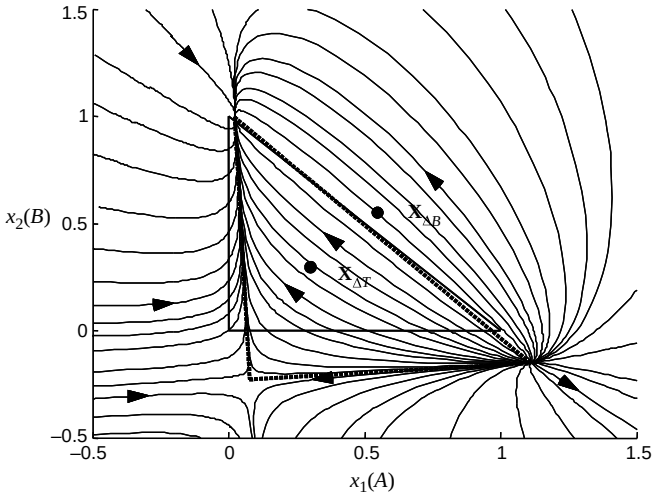


FIGURE 8.14 A RCPM with accompanying TT for the reaction with $\mathbf{v} = [-1, -1, 2]$, $\varepsilon = 0.05$ mol/s, $\tau = 1.25$, and $V^T = 1.2$ mol/s, $L^T = 1$ mol/s, and $\mathbf{X}_{\boldsymbol{\Delta}T} = [0.3,\ 0.3]$.

8.3.3 RCS Transition

The design of both nonreactive and reactive CSs is due to the similarities of the respective DPEs, very much the same. In reactive columns, the goal is again to link up all CSs (both reactive and nonreactive) with one continuous profile path. However, as one may expect, there are some considerations to take into account when adding a reaction. A subtle, yet very important, assumption in the derivation of the RDPE is that there is only a single extent of reaction assigned to a particular RCS. This implies that the entire reaction occurs instantaneously at the top of the RCS (on the first stage), rather than happening progressively along the entire length of the RCS, as one would realistically expect. If this sudden occurrence of reaction was true, then the entire reaction zone's composition profile can be generated using a single integration of the RDPE. An example of this is given in Figure 8.15a, where the entering liquid composition taken as $\mathbf{x}^T$, and the extent is assumed to be $\varepsilon = 1$mol/s. All subfigures in Figure 8.15 were generated for the following

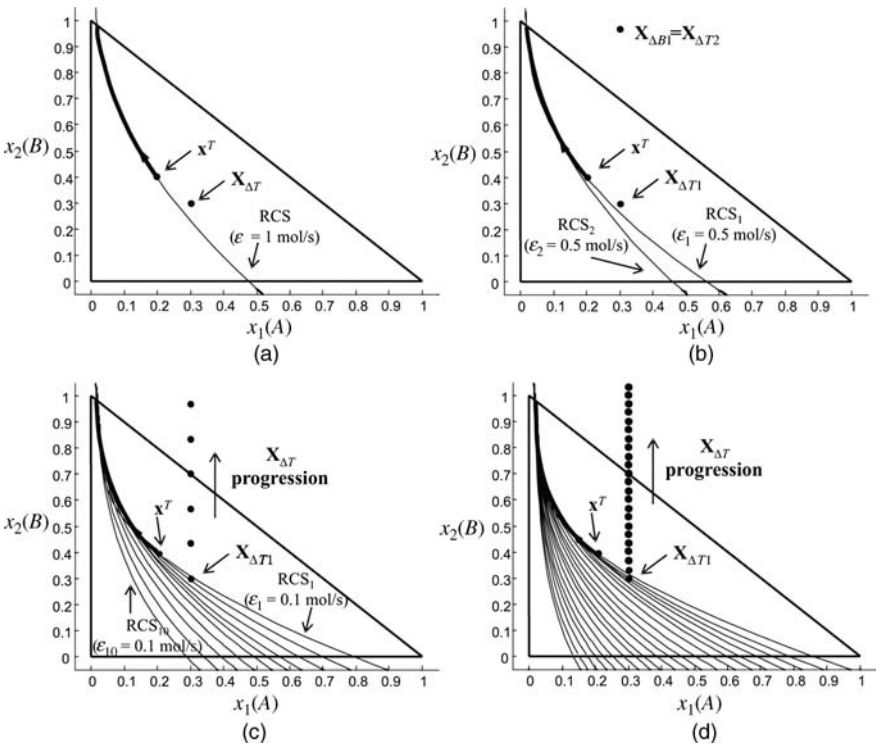


FIGURE 8.15 Reaction zone profiles with conditions $\mathbf{v} = [0, -1, 1]$, $\boldsymbol{\alpha} = [5, 1, 2]$, $L^T = 1.5$ mol/s; $V^T = 2.25$ mol/s and $\mathbf{X}_{\boldsymbol{\Delta}T} = [0.3, 0.3]$ and $\tau = -2$ for (a) instantaneous reaction in a single RCS with $\varepsilon = 1$mol/s. (b) Reactions in two RCSs each with $\varepsilon_1 = \varepsilon_2 = 0.5$mol/s. (c) 10 RCSs with $\varepsilon_i = 0.1$mol/s for each section. (d) Infinitely many RCSs with $\varepsilon \to 0$ for each section.

conditions: $\mathbf{v} = [0, -1, 1]$, $\boldsymbol{\alpha} = [5, 1, 2]$, $L^T = 15$ mol/s; $V^T = 22.5$ mol/s and $\mathbf{X}_{\Delta T} = [0.3, 0.3]$ and $\tau = -2$.

Now consider the scenario where the reaction does not happen instantaneously, but occurs at various increments along the length of the reaction zone. In other words, the reaction is now occurring at discrete points along the reaction zone instead of in a single, instantaneous step. Note that irrespective of the number of RCSs in the reaction zone, the extents in each RCS sum to that required by the column's product specifications. Figure 8.15b depicts a situation where the reaction took place in two steps, each of equal extent, $\varepsilon = 0.5$ mol/s. The overall reaction extent from the two RCSs is thus still 1 mol/s. Also, the resulting liquid from the first RCS in Figure 8.15b is the feed to the second RCS, and thus the profile path is altered as shown in Figure 8.15b. Since the reaction extent in each individual RCS in Figure 8.15b is different to the single RCS in Figure 8.15a, the RCPMs can be expected to be different for these RCSs. The full profiles for each RCS are shown, with the actual resulting reactive profile path followed with a thicker curve. The actual reacting profile (thicker line) initially follows the profile for RCS_1, and thereafter follows that of RCS_2, resulting in a different trajectory followed than in Figure 6.13a.

Figure 8.15c shows a case where the reaction extent is divided into 10 equivalent RCSs. Again, the resulting path that the reaction zone follows is very similar to that in Figure 8.15a and b. Finally, Figure 8.15d shows the extreme scenario where the RCSs in the reaction zone approach infinity, each with an infinitely small reaction extent.

The reactive zones modeled in each scenario displayed in Figure 8.15a–d produce identical liquid and vapor flowrates at the top and bottom end of the reactive zone, as well as overall reaction extents. Although the exiting liquid composition from the reaction zone are different, the only fundamental difference between each of the reactive zones is that the reaction occurs more gradual as the number of RCSs is increased.

Figure 8.15a–d also shows that the general form of the change in composition in the reactive zone is quite similar regardless of the number of RCSs used and how the reaction is distributed along the reaction zone. Producing profiles for each one of these incremental RCSs can be quite a tedious process, and using an abrupt, single RCS should be sufficient for quick design estimates as the general behavior and profile curvature is very similar. This may of course have an impact on the eventual minimum reflux and feasibility calculations of a reactive distillation column when trying to match profiles of neighboring RCSs/CSs. As mentioned, a better model is probably where the reaction proceeds incrementally requiring several RCS. It should also be noted that we have simply assumed that the reaction occurs with a fixed reaction extent in a RCS. A more accurate method would be the inclusion of an appropriate kinetic model to describe how ε is changing down the length of the reaction zone as temperature and concentrations change.

As highlighted in Equation 8.34, the difference point changes from one end of an RCS to the other. The "new" difference point that is generated in a RCS due to the reaction extent ($\mathbf{X}_{\Delta B}$) is then the starting difference point to the RCS below ($\mathbf{X}_{\Delta T}$). This is exactly analogous to the ideas expressed in Chapter 5, where adding or

removing a stream essentially does exactly this—it changes the difference point from one CS to the next. Mathematically, this can be expressed as

$$\mathbf{X}_{\Delta T}|_{\mathrm{RCS}(k)} = \mathbf{X}_{\Delta B}|_{\mathrm{RCS}(k-1)} \tag{8.35}$$

where the RCSs are numbered from the top.

Thus, a reaction will have the same effect, topologically speaking, as adding or removing streams. It has been shown in Chapter 5 that this effect can be extremely beneficial in terms of stage and reflux reductions with a distributed feed column. Here, the difference points also progress linearly as the reaction proceeds. A typical progression of the difference point as the reaction proceeds is depicted in Figure 8.16 for a RCS with $\mathbf{v} = [-1, -1, 2]$. Figure 8.15c and d also depicts the progression of difference points in the reaction zone for the reaction described by $\mathbf{v} = [0, -1, 1]$, showing that the coordinates of each successive $\mathbf{X}_{\Delta T}/\mathbf{X}_{\Delta B}$ are more and more alike the more RCSs one chooses to have in the reaction zone. Each RCS in this reaction zone operates with a unique reaction extent.

An important insight from Figure 8.16 is that the direction of the reaction (the stoichiometric vector, $\mathbf{v}$) in essence determines what the direction of progression of $\mathbf{X}_{\Delta T}/\mathbf{X}_{\Delta B}$ is to be (evident from Equation 8.34). Thus, when $\mathbf{v} = [1, 1, -2]$ (the reverse reaction of Figure 8.16), the $\mathbf{X}_{\Delta T}/\mathbf{X}_{\Delta B}$ progression will proceed in the opposite direction of that shown in Figure 8.16. Notice too that, as with all other complex columns with multiple CSs, difference points are linearly linked to one another.

Since the RDPE cannot be written in terms of a unified flow variable such as the reflux ratio, it is slightly more difficult to comprehend the effects of the net flow in a RCS as the reaction proceeds. However, by examining our equations more closely it

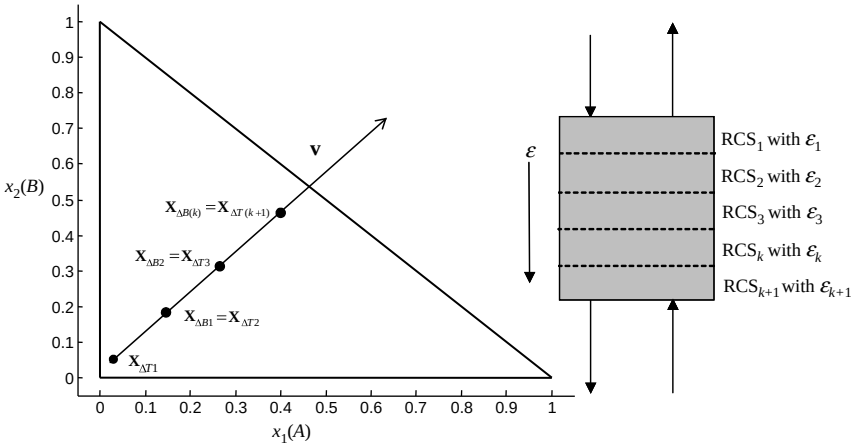


FIGURE 8.16 The progression of $\mathbf{X}_{\Delta}$ in the reaction zone as the reaction with $\mathbf{v} = [-1, -1, 2]$ proceeds.

is still possible to obtain a reasonable idea regarding the change in flowrates in RCSs. We know from Equation 8.28 that the change in the vapor flowrate is only dependent on the ratio of enthalpies and the extent of the reaction. When the extent is zero, the flowrates reduce to the standard constant molar overflow balances where both liquid and vapor flowrates remain the same in the CS. In general, it can be said that the greater the extent of reaction in a RCS, the greater the changes in vapor and liquid flowrates are. When the reaction is exothermic ($\Delta H_{\mathrm{RXN}} < 0$ and thus $\tau < 0$, since ΔH_{VAP} is always positive) the vapor flowrate will be less at the top of the RCS than it is at the bottom. This means that in simple terms that some of the heat being generated through the reaction is being used for vaporization of liquid. Conversely, when the reaction is endothermic, the vapor flowrate at the top of the RCS will be greater than the vapor flowrate at the bottom, implying that a portion of heat being added to the column (usually via the reboiler) is being used not only for vaporization of liquid, as in simple distillation, but also for the reaction. It is noteworthy that the change in vapor flowrate is *not* governed by the reaction stoichiometry but only by τ. For the special case where the heat of reaction is very low $\tau \approx 0$, the vapor flowrate remains exactly the same throughout the RCS, regardless of how far the reaction proceeds.

The liquid flowrate, on the other hand, is a function of the reaction stoichiometry and extent as well as the ratio of enthalpies. This can be seen by substituting Equation 8.28 into Equation 8.22, to obtain

$$L^B = L^T + \varepsilon\left(\sum_{i=1}^{nc} v_i - \tau\right) \tag{8.36}$$

In Equation 8.36, it is evident that the liquid flowrate will be at its largest at the top of each RCS if $\tau > \sum_{i=1}^{nc} v_i$, and vice versa, since ε is assumed to be a positive quantity. Equations 8.28 and 8.36 thus relates the flowrates at the top of each RCS to the bottom, and similarly to the behavior of the difference points in the reaction zone, the liquid and vapor flowrates at the top of a RCS will be the liquid and vapor flowrates at the bottom of the CS, or RCS, attached on top of it.

It is worthy to note that a special condition arises here when $\tau \approx \sum_{i=1}^{nc} v_i$, as the liquid flowrate does not change in the RCS, regardless of the reaction progression. The vapor flowrate will still change however, providing that $\tau \neq 0$. This special condition essentially implies that each mole formed in the liquid phase through the reaction is being vaporized to the vapor phase.

8.3.4 Conserved Moles and Low Reaction Heat—A Simplified Case

The properties of several important industrial reactions, such as metathesis [23] and disproponation [24] reactions, allow for a significant simplification of the RDPE because their moles stay conserved in the reaction (i.e., $\sum v = 0$) and the heat of reaction is near zero ($\tau \approx 0$). These properties allow for an elegant form of the RDPE that exactly resembles the DPE for nonreactive systems from a mathematical point of

view, as shown in Equation 8.37:

$$\frac{d\mathbf{x}}{dn} = \left(1 + \frac{1}{R_\Delta}\right)(\mathbf{x} - \mathbf{y}) + \left(\frac{1}{R_\Delta}\right)(\mathbf{X}_{\boldsymbol{\Delta}\mathrm{RXN}} - \mathbf{x}) \tag{8.37}$$

where $\mathbf{X}_{\boldsymbol{\Delta}\mathrm{RXN}} = \mathbf{X}_{\boldsymbol{\Delta}T} - \frac{\varepsilon\mathbf{v}}{\boldsymbol{\Delta}}$. $\mathbf{X}_{\boldsymbol{\Delta}\mathrm{RXN}}$ is the reactive difference point and consists of two terms: the classical definition of $\mathbf{X}_{\Delta T}$, and a reaction term taking into account the stoichiometry and extent of the reaction. Notice specifically in this simplified case that, in fact, $\mathbf{X}_{\boldsymbol{\Delta}\mathrm{RXN}} = \mathbf{X}_{\boldsymbol{\Delta}B}$. This simplified case makes for an easier understanding of the interaction between reaction, mixing, and separation. $\mathbf{X}_{\boldsymbol{\Delta}\mathrm{RXN}}$ can be placed in composition space in exactly the same way as the classical $\mathbf{X}_{\boldsymbol{\Delta}}$ variable was placed in nonreactive systems to achieve certain topological effects. Moreover, these simplifications mean that there is no change in the absolute flowrates in the RCS because firstly the moles are conserved, thereby the liquid stream does not lose or gain moles, and secondly because the reaction heat is near zero, meaning that the reaction heat does not prevent or accelerate vaporization. One can now relatively simply, using the ideas of classic CPMs developed through this book, construct RCPMs and also position topology. Note also that in this simplified version of the RDPE that it is possible to simply specify R_Δ and not actual vapor and liquid flowrates because vapor and liquid flowrates remain unchanged in this scenario.

8.3.5 Column Design

As mentioned in Section 8.1, there are numerous techniques available in the literature for continuous reactive distillation column design. Many of these methods are however quite complex and one often needs extensive experience with the proposed method to gain any insight at all. Using the CPM technique for design is however a simple extension of the design of nonreactive cases. As with all other separation problems dealt with thus far, the designer is required to propose a column structure from which a CS breakdown can be taken. A typical reactive distillation column is shown in Figure 8.17, with the reaction zone highlighted.

In Figure 8.17 we have arbitrarily assumed that the feed stream enters the column above the reaction zone and the column is only reactive in the middle of the column, that is, no reaction is occurring in the top and bottommost parts of the column attached to the condenser and reboiler, respectively. This is of course just one configuration of a reactive distillation column and the designer is free to specify the relative position of the feed stage, reactive and nonreactive zones, and so on. Each of these choices will also ultimately affect the CS breakdown of the structure. The RCPM technique is of course applicable regardless of the column structure that is chosen. A good review of choices of reactive distillation structures for different sets of process chemistry, feed/product conditions, and so on, is given in Reactive Distillation Design and Control by Luyben and Yu [25].

Once there is certainty regarding the number of feed/product streams in the column, we may turn our attention to determining the external mass balance for the

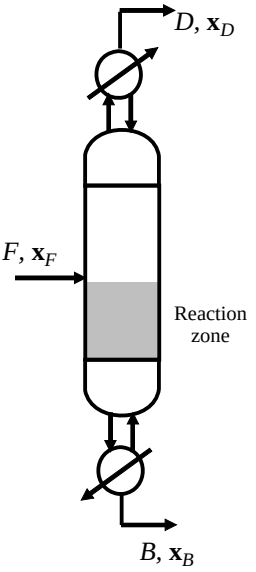


FIGURE 8.17 A simple two product-single feed reactive distillation column.

reactive column. A molar balance for the simple two product-single feed column depicted in Figure 8.17, in vector form, yields

$$F\mathbf{x}_F = D\mathbf{x}_D + B\mathbf{x}_B - \mathbf{v}\varepsilon_{\text{Tot}} \tag{8.38}$$

Notice from Equation 8.38 that there is the same number of independent equations as there are components in the system, just as the nonreactive case. In a ternary system with two product streams, assuming the feed flowrate, feed composition, and reaction stoichiometry are known, there are thus three independent equations and seven free variables. The designer is required to specify four of these variables, which can be achieved by completely specifying the product compositions, allowing one to determine the total reaction extent across the column (ε_{Tot}) and product flowrates. The choices of which variables are to be specified in the external balance are of course arbitrary, one could have just as simply specified the reaction extent with three product composition/flowrates. The advantage of specifying the product specifications is that we are able to calculate perform the design from a "boundary value method" point of view, meaning that we can determine what the operating conditions of the column should be, that is, minimum reflux ratios, stage numbers, and so on, that will result in these product specifications being met precisely. Thus, completely specifying the product stream enables one to determine all the product stream flowrates as well as the overall extent of reaction.

As mentioned earlier, the reaction in the RDPE takes place instantaneously on the first stage of a RCS and that a more realistic model would be one where the extent takes place gradually. This is easily achievable by simply dividing the reaction zone

into a set of smaller RCSs (instead of a single RCS) of which the reaction extents in each RCS sum to the column's overall reaction extent calculated in Equation 8.38. The change in $\mathbf{X}_{\Delta T}$ and liquid and vapor flowrates in each subsequent RCS may then be determined from Equations 8.34, 8.35, 8.28, and 8.36. The number of RCSs used to make up the overall reaction extent can thus be seen as another degree of freedom to be specified by the designer, although as mentioned earlier, only one RCS may still be sufficient for quick design approximates. Furthermore, for the column depicted here, there is only one internal variable: a reflux ratio of a single CS (or a vapor/liquid flowrate in a RCS). Once this internal variable has been specified, all the other flow variables may be subsequently calculated for all remaining CSs and RCSs.

Finally, the aim is again to produce a continuous path of column profiles that originate from the product specifications. A reactive distillation column is in a way not too dissimilar from a distributed feed column because reflux ratios and difference points change as the reaction proceeds. To illustrate a feasible design, consider the column structure and associated profiles in Figure 8.18. In this illustration, the reaction 1B→1C occurs in the reaction zone in three separate RCSs (RCS_1–RCS_3). We have assumed a negligible reaction heat, with feed, bottoms, and distillate compositions of [0.5, 0.5], [0.95, 0.001], and [0.001, 0.7], respectively, and a constant relative volatility model with $\boldsymbol{\alpha} = [5, 1, 2]$. These assumptions mean that this problem is in fact the simplified case highlighted in Section 8.3.4. The reflux in the topmost rectifying section is 2.

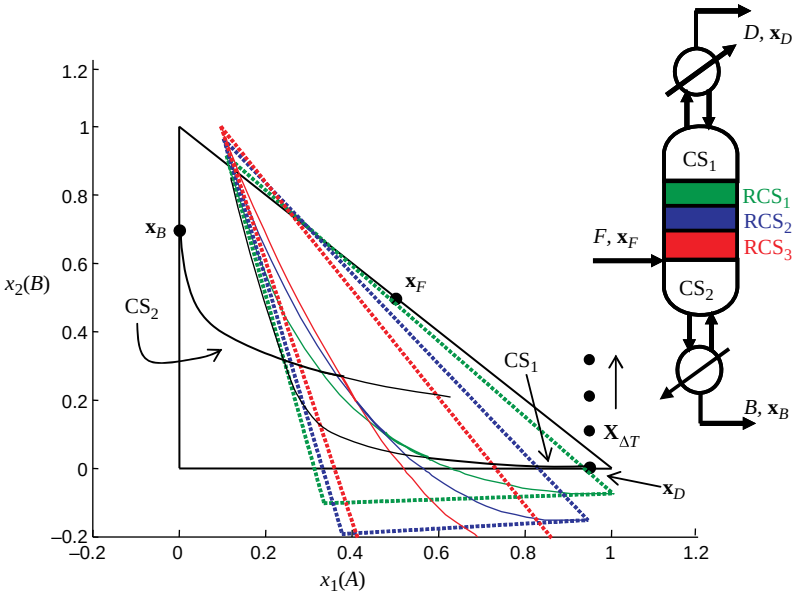


FIGURE 8.18 A feasible design using for the two product-single feed reactive distillation column, with $R_{\Delta CS1} = 2$, $\mathbf{x}_F = [0.5, 0.5]$, $\mathbf{x}_D = [0.95, 0.001]$, and $\mathbf{x}_B = [0.001, 0.7]$, $\mathbf{v} = [0, -1, 1]$, and $\boldsymbol{\alpha} = [5, 1, 2]$.

Figure 8.18 shows the two nonreactive profiles (CS_1 and CS_2) originating from the product specifications and are connected by profiles of the internal RCSs. The two nonreactive profiles are thick black lines, while the reactive profiles that the column follows are represented by thick colored lines, coordinated with the colored column structure in Figure 8.18. All profile continuations are represented by thinner lines. It is interesting to note that the nonreactive CSs actually intersect one another in this design (note the profile intersections). The intersection of nonreactive profiles in a reactive column like this is however senseless, because this design absolutely requires the reactive zone. Thus, in this case, the nonreactive profiles that terminate the column at either end need to be joined up by *all* the reactive profiles.

The TT of each RCPM has also been included in Figure 8.18 and color coordinated. The design shown here is of course only one possible profile path that the RCSs may follow. We may in fact choose any one of the profiles in the RCPMs to bring forth a feasible design. The TTs in the RCSs are useful in this regard because they give an indication of how other designs may look like, and visualizing the trend of the RCSs as reaction proceeds.

One can also see that the TT vertices are well away from the area of interest where profile intersections occur; implying that this particular design is far from being pinched. Thus, minimum reflux is still far away. Because there are such a plethora of different reaction chemistry and mechanisms, it is hard to formulate a general minimum reflux condition using only the TTs (see for instance Figure 8.19). It is therefore necessary to plot each profile of the RCS to determine minimum reflux. Recall that the minimum reflux of a particular column is an overall column reflux below which a continuous connection between product specifications does not exist, or in other words, where one CS/RCS pinches exactly on another. The minimum reflux case for the aforementioned design can be seen in Figure 8.19, where the reflux in the top rectifying CS (CS_1) is 0.68.

Notice in Figure 8.19 that the reaction zone is small in comparison with the non reactive profiles. The TTs are not shown here because for this design, the pinch points for all the RCS are complex, that is, the TT do not exist in real space. The profiles however are completely valid. Both the rectifying and stripping nonreactive profiles are virtually pinched and only a small reactive zone is required to connect these two profiles. Reducing the reflux in CS_1 to lower than 0.68 will not lead to a continuous profile path.

Upon looking for feasible designs, the designer should take cognizance of the direction of profiles, as when searching for feasible designs in distributed feed type columns. The direction of the profiles should consistently point in the same direction. Put differently, when designing the column from the top downward, integration should always be in the positive direction and in the direction of each CS/RCS's stable node. Conversely, if one elects to perform the design from the bottom-up, integration should always be in the negative direction and in the direction of each CS/RCS's unstable node. This criterion has clearly been maintained in Figures 8.18 and 8.19. An infeasible design is shown in Figure 8.20, where the reflux in the topmost CS is taken as 0.5. The bundle of profiles for the reactive zone on the left-hand side does indeed intersect the bottommost stripping and topmost rectifying

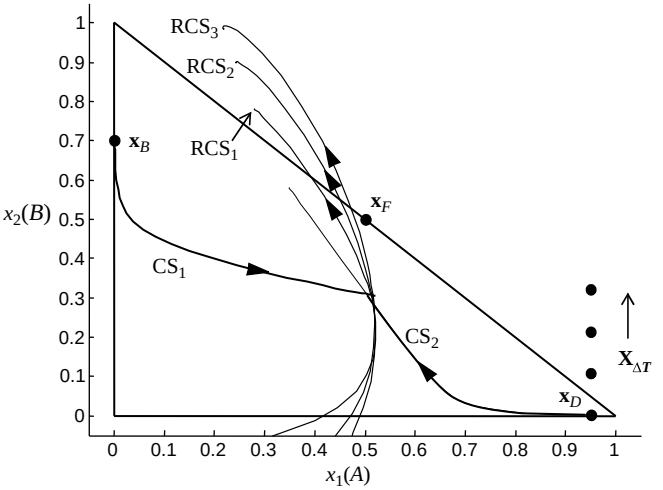


FIGURE 8.19 A minimum reflux design for the two product-single feed reactive distillation column, with $R_{\Delta CS1} = 0.68$, $\mathbf{x}_F = [0.5, 0.5]$, $\mathbf{x}_D = [0.95, 0.001]$, and $\mathbf{x}_B = [0.001, 0.7]$, $\mathbf{v} = [0, -1, 1]$ and $\boldsymbol{\alpha} = [5, 1, 2]$.

profile, but the profiles are aligned incorrectly. The bundle of profiles on the right-hand side shows that a feasible design cannot be achieved if the integration direction is consistent; hence, the design is not realizable.

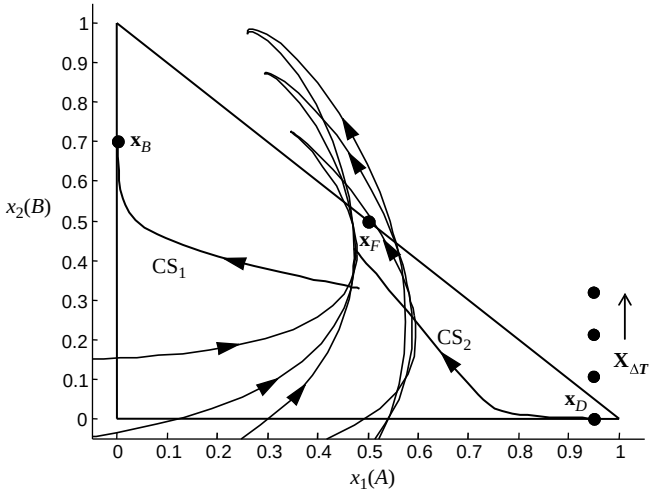


FIGURE 8.20 An infeasible design for the two product-single feed reactive distillation column, with $R_{\Delta CS1} = 0.68$, $\mathbf{x}_F = [0.5, 0.5]$, $\mathbf{x}_D = [0.95, 0.001]$ and $\mathbf{x}_B = [0.001, 0.7]$, $\mathbf{v} = [0, -1, 1]$ and $\boldsymbol{\alpha} = [5, 1, 2]$.

Although the TTs are a useful means of assessing the design characterizes of a column as shown in Figure 8.18, it is of course only applicable to constant relative volatility systems. The general ideas outlined in the preceding discussions and examples are however not limited to constant relative volatility systems only. One may very easily introduce nonideal phase equilibrium behavior, just as with conventional CSs, although the TT technique is not applicable. The general design strategy remains the same, but instead of producing TTs, it is necessary to actually plot profiles and scan for profile intersections. A nonideal example is shown below for the DME/water/methanol system.

Example 8.2: Dimethyl ether (DME) has long been touted by several researchers as an alternative fuel for transportation, largely due to is similarities to current fuels and its favorable environmental properties. One method of DME synthesis is to transform raw feeds such as coal or natural gas to methanol (MeOH), which can in turn be converted to DME via the following reaction:

$$2\text{MeOH} \rightarrow 1\text{H}_2\text{O} + 1\text{DME}$$

If DME is to be used as a fuel it needs to be of high purity ($\geq$99.9 mol%), and thus the accompanying separation step to this problem is very important. This seems like a good fit for a reactive distillation type problem since we could potentially perform the reaction and separation in a single step. An et al. [26] have designed a small scale version of such a reactive distillation column through catalyst testing and rigorous modeling with Aspen Plus®, and concluded that reactive distillation is not only possible, but also economically favorable with regards to the classic reactor-separation process. They suggested operating the column with the same structure shown in Figure 8.17 at $\sim$8 atm pressure, with a pure methanol feed and producing DME and water as high purity distillate and bottoms products, respectively. Using this as a guideline, suppose you are the chief design engineer for a company looking to exploit the upcoming DME market and that you have been instructed to design, relatively quickly, a preliminary reactive distillation column for this process, by using the following specifications:

- Feed stream purity: [0, 0]; [DME, H_2O, MeOH] at 1 mol/s
- DME stream purity: [0.999, 5×10^{-5}];
- Water stream purity: [5×10^{-9}, 0.999];
- $\Delta H_{\text{RXN}} = -20$ kJ/mol, $\Delta H_{\text{VAP}} = 32$ kJ/mol
- NRTL to be used as phase equilibrium model (nonideal zeotropic system).

Solution 6.2: We shall perform this approximate design by assuming the reactive zone consist of five RCSs, as shown in Figure 6.19, each one operating with the same reaction extent which sum to the total column reaction extent. Important properties that need be known are: the ratio of enthalpies, τ, easily calculated to be -0.625, and using Equation 8.38 the total extent of the reaction is determined to be 0.4995 mol/s (implying that virtually all the methanol has been reacted). We also know the $\mathbf{X}_{\boldsymbol{\Delta}}$'s

in the uppermost and bottommost nonreactive CSs, since they are just the corresponding product specifications. The relevant $\boldsymbol{\Delta}$'s of each RCS and CS can the also be subsequently determined as

$$\Delta_{\mathrm{CS1}} = D \tag{8.39}$$

$$\Delta_{T,\mathrm{RCS1}} = \Delta_{\mathrm{CS1}} - F \tag{8.40}$$

$$\Delta_{T,\mathrm{RCS}(k+1)} = \Delta_{B,\mathrm{RCS}(k)} = \Delta_{T,\mathrm{RCS}(k)} - (1/5)\varepsilon \sum v_i \tag{8.41}$$

$$\Delta_{\mathrm{CS2}} = \Delta_{B,\mathrm{RCS5}} - B \tag{8.42}$$

The $\mathbf{X}_{\boldsymbol{\Delta}}$'s for the each RCS can also be determined by mass balance:

$$\mathbf{X}_{\boldsymbol{\Delta},\mathrm{CS1}} = \mathbf{x}_D \tag{8.43}$$

$$\mathbf{X}_{\boldsymbol{\Delta}T,\mathrm{RCS1}} = \frac{\Delta_{\mathrm{CS1}}\mathbf{X}_{\boldsymbol{\Delta}\mathrm{CS1}} - F\mathbf{x}_F}{\Delta_{\mathrm{CS1}} - F} \tag{8.44}$$

$$\mathbf{X}_{\boldsymbol{\Delta}T,\mathrm{RCS}(k+1)} = \mathbf{X}_{\boldsymbol{\Delta}B,\mathrm{RCS}(k)} = \frac{\Delta_{T,\mathrm{RCS}(k)}\mathbf{X}_{\boldsymbol{\Delta}T,\mathrm{RCS}(k)} - (1/5)\varepsilon\mathbf{v}}{\Delta_{T,\mathrm{RCS}(k)} - (1/5)\varepsilon \sum v_i} \tag{8.45}$$

$$\mathbf{X}_{\boldsymbol{\Delta},\mathrm{CS2}} = \mathbf{X}_{\boldsymbol{\Delta}B,\mathrm{RCS5}} = \mathbf{x}_B \tag{8.46}$$

All that remains now is for the designer to examine feasibility by finding a continuous profile path. For this, it is necessary to specify a value for $R_{\Delta\mathrm{CS1}}$ such that all subsequent net flows and difference points may be calculated. Figure 8.21 shows such a feasible design where the reflux in the nonreactive rectifying section ($R_{\Delta\mathrm{CS1}}$) is 7, resulting in a nonreactive stripping section reflux ($R_{\Delta\mathrm{CS2}}$) of -9.623. These conditions were chosen in accordance with work done by An et al. [26].

Figure 8.21 implies that a reactive distillation column for DME synthesis via methanol is indeed feasible, and certainly warrants further investigation. The black, solid profiles signify nonreactive rectifying and stripping CSs, originating from $\mathbf{x}_D$ and $\mathbf{x}_B$, respectively. The RCS profiles are color coordinated to match the accompanying column in Figure 8.21 and serve to link the two nonreactive profiles with one another. The black circles indicate where a transition from one RCS/CS to the next occurs. This is of course permitting catalyst activity at the VLE temperatures in the reactive zone although An et al. [26] seem to suggest that for this system it is realizable. In fact, the design shown here is remarkably similar to the one given by An et al. through a rigorous Aspen simulation.

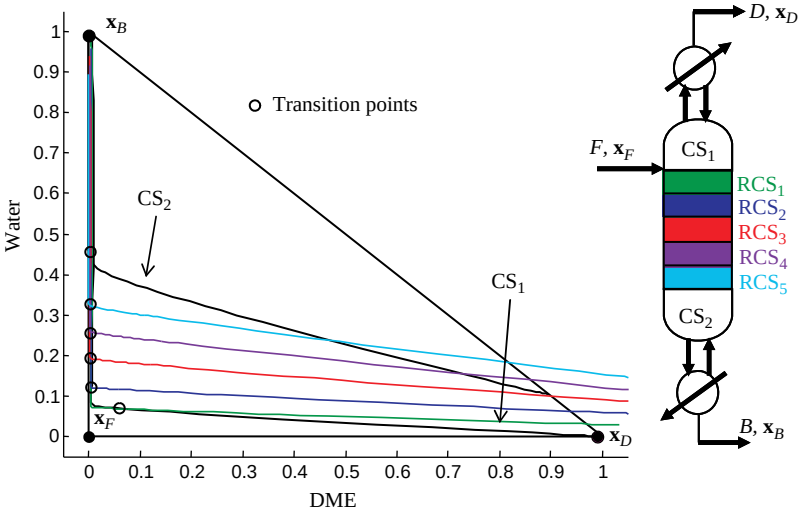


FIGURE 8.21 Feasible design for the reactive DME/water/methanol system with a reflux in the rectifying section ($R_{\Delta CS1}$) of 7. The NRTL model was used at $P = 8$ atm.

Although we have chosen not to determine the exact location of the feed stage and the beginning of the reactive zone from either end, it is easily inferable by tracing the number of stages until an intersection of profiles is reached. It should also be noted that the profile path chosen here (from one profile transition to another) is only one of many that could have been chosen. Each RCS has a RCPM associated to it, and any profile within that RCPM may be chosen to realize the design.

8.3.6 Column Stability

The work in this chapter has thus far demonstrated that the general CPM theory can very easily be adapted to encompass reactive distillation design. Although a design is feasible because neighboring profiles intersect one another, only viewing a single profile may not tell the designer the full story. Plotting a RCPM for a particular RCS allows one to assess whether the column will reliably operate as originally designed. Figure 8.22 is the same design as that shown in Figure 8.21, but in this instance only the full RCPM of RCS_1 is shown. Interestingly, the RCPM exhibits a saddle point (labeled SP) near a critical point in the column. Upon closer inspection one can conclude that if something were to change in this particular RCS, perhaps catalyst deactivation or a disruption in the vapor or liquid flowrates, the RCS's profiles may fall on the wrong side of the saddle point causing the profile to move downward and not toward CS_2's profile. Also, if the CS_1–RCS_1 transition point (see Figure 8.21) is too high up in CS_1, the RCS_1 profile may very well veer to the wrong direction. Thus, one can see that an RCPM gives valuable insight into the operability of a reactive distillation column.

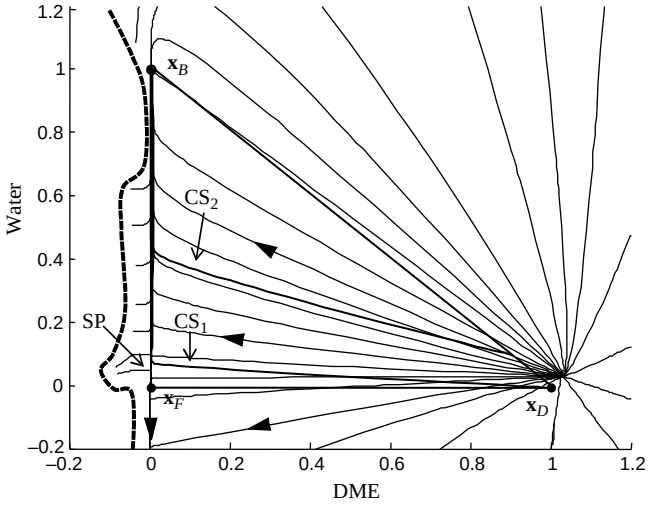


FIGURE 8.22 The design shown in Figure 8.21 with an RCPM for RCS_1 only.

8.4 SUMMARY

In this chapter, we have extended the ideas of CPM design for nonreactive systems to encompass reacting systems. Simple reactive systems can be designed relatively easily and quickly, and plotting composition profiles allows one to easily assess the topographical influences of mixing, reaction, and separation phenomena. Nodes can be placed almost at will in these systems, and one now has the tools to devise an experiment to suit the exact needs of the problem at hand. An interesting case has also been highlighted about a somewhat counter-intuitive relationship between a simplified Petlyuk column and a zero-order chemical reaction in a batch still.

The continuous reactive distillation column has also been treated with the derivation and application of a reactive DPE, or RDPE. Column design using this RDPE is in many ways similar to nonreactive column design, as the RDPE is merely an extension of the DPE to encompass reactive systems. In reactive systems, however, there are flow variations in liquid and vapor streams that need to be considered that were assumed negligible for nonreactive column design. The designer has to account for the effect of creating/reducing moles due to reaction stoichiometry, as well as considering the simultaneous effects of reaction heat and the latent heat of vaporization. The tools presented in this chapter allow one to take into account of the change in flowrates along a CS due to reaction. Using the TT ideas for ideal systems, and profile intersection for rigorous design, continuous reactive distillation columns can be synthesized and important parameters such as the stage and catalyst requirement and column reflux ratio can also be gauged, as well as the interaction between these parameters. Admittedly, these models may be too simplified for the complex behavior occurring in a reactive distillation column, but the idea for these methods is to give a designer a good approximation and understanding of such a column's characteristics and operability.

REFERENCES

[1] Backhaus, A.A., Continuous processes for the manufacture of esters, 1921, USA.

[2] Backhaus, A.A., Apparatus for producing high grade esters, 1922, USA.

[3] Backhaus, A.A., Process for producing high grade esters, 1923, USA.

[4] Backhaus, A.A., Process for esterification, 1923, USA.

[5] Berman, S., et al., Esterification. Continuous production of dibutyl phthalate in a distillation column. *Industrial and Engineering Chemistry*, 1948, **40**:2139–2148.

[6] Taylor, R. and R. Krishna, Modeling reactive distillation. *Chemical Engineering Science*, 2000. **55**:5183–5229.

[7] Taylor, R. and R. Krishna, Modelling reactive distillation. *Chemical Engineering Science*, 2000, **55**(22):5183–5229.

[8] Venimadhavan, G., et al., Effect of kinetics on residue curve maps for reactive distillation. *AIChE Journal*, 1994, **40**(11):1814.

[9] Jiménez, L., O.M. Wanhschafftb, and V. Julka, Analysis of residue curve maps of reactive and extractive distillation units. *Computers and Chemical Engineering*, 2001, **25**(4–6):635–664.

[10] Barbosa, D. and M.F. Doherty, The simple distillation of homogeneous reactive mixtures. *Chemical Engineering Science*, 1988, **43**(3):541–550.

[11] Barbosa, D. and M.F. Doherty. *Synthesis and Analysis of Multicomponent Reactive Distillation Systems*. 1986, Miami, FL, USA: AIChE.

[12] Barbosa, D. and M.F. Doherty. *Design of multicomponent reactive distillation columns*. 1987. Brighton, UK: European Federation of Chemical Engineering, Amarousion-Pefki, Greece.

[13] Barbosa, D. and M.F. Doherty, Design and minimum reflux calculations for single-feed multicomponent reactive distillation columns. *Chemical Engineering Science*, 1988, **43**:1523–1537.

[14] Buzad, G. and M.F. Doherty, Design of three-component kinetically controlled reactive distillation columns using fixed-points methods. *Chemical Engineering Science*, 1994, **49**(12):1947–1963.

[15] Chen, F., et al., Multiple steady states in reactive distillation: Kinetic effects. *Computers and Chemical Engineering*, 2002, **26**(1):81–93.

[16] Chen, F., et al., Simulation of kinetic effects in reactive distillation. *Computers and Chemical Engineering*, 2000, **24**(11):2457–2472.

[17] Okasinski, M.J. and M.F. Doherty, Design method for kinetically controlled, staged reactive distillation columns. *Industrial and Engineering Chemistry Research*, 1998, **37** (7):2821–2834.

[18] Doherty, M.F. and M.F. Malone, *Conceptual Design of Distillation Systems, ed. C.E. Series*. 2001, New York, NY, USA: McGraw-Hill. 568.

[19] Hauan, S. and K.M. Lien, Phenomena based design approach to reactive distillation. *Chemical Engineering Research & Design, Transactions of the Institute of Chemical Engineers, Part A*, 1998, **76**(A3):396–407.

[20] Hauan, S., A.W. Westerberg, and K.M. Lien, Phenomena-based analysis of fixed points in reactive separation systems. *Chemical Engineering Science*, 2000, **55**(6):1053–1075.

[21] Van Dongen, D.B. and M.F. Doherty, Design and synthesis of homogeneous azeotropic distillations. 1. Problem formulation for a single column. *Industrial and Engineering Chemistry, Fundamentals*, 1985, **24**(4):454–463.

[22] Levy, S.G., D.B.Van Dongen, and M.F. Doherty, Design and synthesis of homogeneous azeotropic distillations. 2. Minimum reflux calculations for nonideal and azeotropic columns. *Industrial and Engineering Chemistry, Fundamentals*, 1985, **24**(4):463–474.

[23] Hoffmaster, W.R. and S. Hauan, Using feasible regions to design and optimize reactive distillation columns with ideal VLE. *AIChE Journal*, 2006, **52**(5):1744–1753.

[24] Stitt, E.H., Reactive distillation for toluene disproportionation: A technical and economic evaluation. *Chemical Engineering Science*, 2002, **57**(9):1537–1543.

[25] Luyben, W.L. and C.-C. Yu, *Reactive Distillation Design and Control*. 2008, Hoboken, NJ: Wiley: AIChE. xxi, 574 p.

[26] An, W., K.T. Chuang, and A.R. Sanger, Dehydration of methanol to dimethyl ether by catalytic distillation. *The Canadian Journal of Chemical Engineering*, 2004, **82**(5): 948–955.

CHAPTER 9

APPLICATION OF COLUMN PROFILE MAPS TO ALTERNATIVE SEPARATION PROCESSES: MEMBRANE PERMEATION

9.1 INTRODUCTION

In this book, novel and innovative design techniques for distillation systems have been explored and discussed. A wide range of distillation configurations, from simple batch boiling through to complex columns, and even reactive distillation, were successfully synthesized and designed using CPMs. By this point, what should be evident is that any distillation structure, no matter how complex in form, can be broken down into CSs and the CPM method can be applied to assess its feasibility, as well as give insight into the structure's operation and controllability. Thus, from a distillation perspective, the CPM technique has shown its versatility and relevance.

A logical question that arises at this point is whether CPM theory can be applied to other separation systems. In an effort to illustrate this, we will consider membrane permeation because of its striking difference from distillation. By the nature of its operation, membrane separation is fundamentally different: while in distillation, the separation is achieved by differences in boiling points, the driving force in membrane permeation is a difference between chemical potentials in the two phases. One of the most important consequences of this is that the constant molar overflow assumption, in general, cannot be employed in membrane permeating systems.

Understanding Distillation Using Column Profile Maps, First Edition. Daniel Beneke, Mark Peters, David Glasser, and Diane Hildebrandt.
© 2013 by John Wiley & Sons, Inc. Published 2013 by John Wiley & Sons, Inc.

The CPM method derived for distillation was done so with CMO as an underlying assumption, and thus relaxing this will become a major focal point of this chapter.

In this chapter, the development of a novel graphical method of analyzing continuous membrane separation systems will be shown. The method is applicable to all counter- and co-current membrane modules—single-stage, cascades, and membrane columns. All configurations can be broken down into "membrane column sections (MCSs)," no matter how complex the arrangement. Each MCS, which resembles a typical single-stage separator, is modeled using the difference point equation. The difference point equation, when applied to membrane permeation, tracks the change in the retentate (nonpermeating stream) composition down the length of the MCS.

For demonstration purposes, a simple constant relative permeability flux model is employed to determine the continually changing retentate flow. Various possible operating conditions of a CS are explored. Using the difference point equation, column profiles for each condition can be plotted. The behavior of the profiles is discussed both mathematically and graphically. This innovative way of investigating membrane processes provides a unique way of synthesizing and designing them.

Furthermore, being able to analyze membrane separation with the same tools as distillation now places one in a very unique position that we are able to design hybrid configurations of the two processes with relative ease. An example of this will be given at the end of this chapter (see Section 9.8). In this example, a complex and highly selective membrane is used to show the versatility and adaptability of the method.

The work presented in this chapter is an abridged version of some of the material in the book *Membrane Process Design Using Residue Curve Maps* and has been reproduced with permission from John Wiley & Sons, Inc. [1]. The reader is referred to that book for a more detailed appraisal of membrane design.

Notation used in this chapter: To avoid confusion with the various symbols, some of the notation used in this chapter may not conform to that used in the rest of the book. Most notably, since R is used to denote retentate flow, then reflux ratio will be defined noncapitalized as r_Δ. Also, the symbol π will be used for total pressure (unlike the usual symbol of P). This has been done since P (and many of its derivatives) has been or will be used for other parameters.

9.2 MEMBRANE PERMEATION

Novel separation methods and techniques have been the focus for engineers in recent decades. Although traditional separation procedures have established their industrial value, innovative methods have been emerging in recent years. These fresh approaches have come about in the pursuit of more economical and environmentally attractive processes. Membrane-based separation procedures are one of many alternatives proving to be a viable option.

A vast array of different types of membranes, ranging from reverse osmosis to ultrafiltration, has been developed for various applications [2]. An immense amount

of research into permeation modeling has been completed [3–5]. As will be evident, the nature of the work given in this chapter is general and can be applied to any membrane, and its associated flux model. For demonstration purposes, however, only diffusion membranes (i.e., gas separation and pervaporation) will be discussed here. The driving force for separation in diffusion membranes is the difference in partial pressures for each component on either side of the membrane. The work can then further be extended and applied to other membrane types.

Consider some of the unit operations used for continuous membrane separation. A conventional separator consists of a single feed (F) mixture entering a membrane unit. The mixture is separated into two product streams, namely the permeate (P) and retentate (R). Numerous possibilities in flow regimes have been proposed for such a separator, with the countercurrent option being the most efficient [6]. Various external flow arrangements, using a single unit, are also possible, such as recycling the retentate to the feed, or even to the permeate side.

In some cases, a single unit may not be sufficient. In order to achieve a desired degree of separation, several single-stage modules connected in series are often advantageous [7]. This is known as cascading. There are numerous configurations that can be employed when cascading, but it can be shown that the simple countercurrent recycle cascade is most effective. Such an arrangement of units is what is typically used in solvent (liquid) extraction circuits. Furthermore, the same configuration of interconnected flash stages is equivalent to a distillation column [7]. It is therefore logical that this same analogy be applied for membrane systems. A continuous membrane column, displayed in Figure 9.1a, was first identified by Hwang and Thorman [8].

The column is filled with hollow-fiber membranes, resembling the design of a shell-tube heat exchanger. A high pressure is maintained on one of side in order to allow permeation through the membrane to the low-pressure side. To allow the recycle streams to flow, a compressor is necessary. It is claimed that complete separation of a binary mixture into pure products is achievable in a finite area [8].

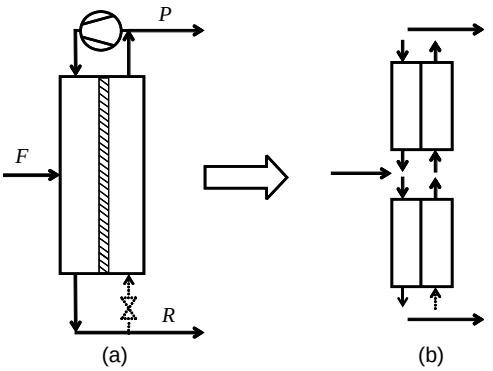


FIGURE 9.1 (a) A continuous membrane column. (b) Membrane column section breakdown [1].

The original proposition of a membrane column did not include a retentate recycle; however, it has been reported that the inclusion of the recycle has assisted separation in some cases [9].

9.3 GENERALIZED MEMBRANE COLUMN SECTIONS

Consider the membrane column given in Figure 9.1a. Analyzing the entire column as a whole limits one's possibilities to only that particular configuration. This is not useful when it comes to synthesizing a separation sequence, especially if it is intended to be optimal. Therefore, a different approach is taken: any general column or cascade can be divided into MCSs, analogous to the distillation-only columns shown in preceding chapters.

A generalized MCS is defined as "a length of column between points of addition and removal of material and/or energy" [10]. This definition is general and applicable to most, if not all, counter- and co-current applications, such as distillation, absorption, and stripping. Although unique in its operation, membrane permeation is no exception to this. Figure 9.1b shows an example of a MCS breakdown for the membrane column given in Figure 9.1a. Similar breakdowns can be done for any other arrangement. Analysis of each of the CSs in Figure 9.1b reveals that each one resembles a single unit. Thus, provided the assumptions of operation are clear and defined, a MCS introduces a novel way of investigating membrane separations.

The section that follows adapts and extends the CPM concepts to the specific case of an MCS. It is crucial to note that the specific case of the MCS differs from the general case for distillation presented elsewhere in this book in that the flowrates are not constant in an MCS. This means that the reflux ratio (r_Δ) is not constant down the length of the column. All CPMs drawn up to this point have made use of the constant flow assumption, and the following section will discuss the changes that arise in the absence of this assumption.

9.4 THEORY

9.4.1 Membrane Column Sections

A schematic representation of a countercurrent MCS is shown in Figure 9.2.

It is assumed that

- All flows and compositions at the top (T) of a CS are known and fixed. This assumption can be altered accordingly, if necessary.
- The permeate pressure is set sufficiently close to vacuum ($\pi_P \approx 0$), thus, permeation will be monodirectional from the retentate to the permeate side.
- Permeation occurs through the membrane only in a direction that is perpendicular to the flow of the retentate stream, as indicated in Figure 9.2.

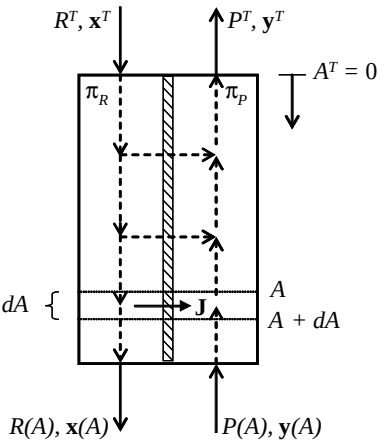


FIGURE 9.2 A generalized membrane column section (MCS). Material moves through the membrane from the high pressure (π_R) retentate (R) side to the low pressure (π_P) permeate (P) side [1].

The actual area of the membrane is not used directly, but is rather embedded within the flux modeling, as will be shown later. A dimensionless area is incorporated for locating a position within the column, without being restricted to exact dimensions. However, the dimensionless area is related to the real area. As a boundary condition, the membrane area is zero at the top of the column. It increases down the length of the column, until the MCS is terminated.

9.4.2 The Difference Point Equation for an MCS

By combining the overall and component material balances around the top of the MCS and any point down the membrane length (refer to Figure 9.2), it can be shown that the change in retentate composition, **x**, along the MCS can be modeled using a slightly modified version of the DPE, as shown in Equation 9.1, and will be referred to as the membrane difference point equation (MDPE). The reader is referred to Peters et al. [1] for a detailed proof:

$$\frac{d\mathbf{x}}{dA} = \left[\frac{\Delta}{R(A)} + 1\right] \cdot [\mathbf{x} - \mathbf{y}(\mathbf{x})] + \frac{\Delta}{R(A)}[\mathbf{X}_{\boldsymbol{\Delta}} - \mathbf{x}] \tag{9.1}$$

where

A is the dimensionless membrane area,
$R(A)$ is the retentate flowrate as a function of position (mol/s),
$P(A)$ is the permeate flowrate as a function of position (mol/s),
x is the mole fraction of the retentate phase, and
y is the mole fraction of the permeate phase.

Δ is the net molar flow, as with distillative systems, and for an MCS is defined as

$$\Delta = P(A) - R(A) \tag{9.2}$$

Also, $\mathbf{X_\Delta}$ is the net molar composition within the MCS, defined as

$$\mathbf{X_\Delta} = \frac{P(A) \cdot \mathbf{y}(A) - R(A) \cdot \mathrm{x}(A)}{\Delta}; \quad \Delta \neq 0 \tag{9.3}$$

As with distillative separations, $\mathbf{X_\Delta}$ is commonly referred to as the difference point, and is the vector of the net molar flowrates for all components divided by the total net molar flow.

It is worth noting that the direction of permeate flow, $P(A)$, is taken to be the positive direction. Additionally, the resulting MDPE for an MCS is mathematically similar to the general DPE derived in Section 3.3.3. This is quite a remarkable result: two fundamentally different pieces of separation equipment operating with different driving forces and mechanisms are modeled with mathematically analogous equations. The reason for this is that the DPE (for any separation system) is merely a combination of mass balances, and the derivation thereof does not require knowledge of the details of the separation. This is what makes the DPE a general equation, with countless applications. Of course, solving the DPE for a particular type of separation requires knowledge of its mechanism. This is discussed in the next section for membrane permeation.

9.4.3 Permeation Modeling

In order to solve the MDPE in Equation 9.1, it is necessary to understand how $\mathbf{y}$ is related to $\mathbf{x}$. There are numerous methods of describing this relationship. Gas separation involves the diffusion of a gaseous mixture through the membrane material. The rate at which a gas, or particular component of a gas mixture, moves through a membrane is known as the flux (total or individual). In order to obtain a general flux model for a gas separation membrane, the fundamental thermodynamic approach incorporating the solution-diffusion model [11] will be used at vacuum permeate conditions ($\pi_P \approx 0$):

$$J_i = \frac{P_i'(\pi_R x_i)}{\delta} \tag{9.4}$$

where

J_i is the flux of component i through the membrane $\left(\frac{\text{mol}}{\text{s m}^2}\right)$,

P_i' is the permeability of component i (which is equal to the product of solubility and diffusivity through the membrane material) $\left(\frac{\text{mol m}}{\text{s m}^2 \text{ Pa}}\right)$,

π_R is the (high) retentate pressure (Pa),

x_i is the mole fraction of component i in the retentate phase,

δ is the effective thickness of the membrane (m).

Since the flux of any component is the amount of material that permeates through the membrane per unit time per unit area, one may also write

$$J_i = \frac{Py_i}{A} \tag{9.5}$$

where y_i is the mole fraction of component i in the permeate phase.

It can be shown that by combining Equations 9.4 and 9.5, for a gas separation membrane

$$y_i = \frac{\alpha_{ij}^M x_i}{\sum_i \alpha_{ij}^M x_i} \tag{9.6}$$

where α_{ij}^M is known as relative membrane permeability of component i to component j, defined as

$$\alpha_{ij}^M = \frac{P_i'}{P_j'} \tag{9.7}$$

It is agreed that the permeabilities of the components may not be constant, but rather depend on a number of factors, such as the retentate and/or permeate composition(s), and mass transfer through the membrane can be quite complex. However, for demonstration purposes, a simplified approach will be followed. For this reason, constant relative permeabilities have been assumed, resulting in what is known as a Knudsen membrane [12].

In order to solve the MDPE, it is further required to model how the retentate flow (R) is changing as a function of position, since material is being transferred monodirectionally (from R to P only). Note that in distillation, transfer between phases occurs bidirectionally as liquid evaporates to the vapor stream and vapor condenses in the liquid stream. Consider a strip membrane area, as shown in Figure 9.2, where $\mathbf{J}$ is a vector containing the fluxes of all the components. It can be shown that

$$dR(A) = dP(A) \tag{9.8}$$

For the counter-current operation displayed in Figure 9.2, one can deduce that both $R(A)$ and $P(A)$ have their largest values at the top of the MCS.

For a simple gas separation membrane, with constant relative permeabilities (α_{ij}^M), the following expression can be derived (refer to Equation 9.11):

$$\frac{dR(A)}{dA_n} = -\sum_i \alpha_{ij}^M x_i \tag{9.9}$$

where $A_n = A\frac{\pi_R P'_{\text{ref}}}{\delta}$ is a normalized form of A, and has units of mol/s.

For any other membrane (i.e., nanofiltration, reverse-osmosis, and so on), manipulation of the appropriate flux model should replace the right-hand side of Equation 9.9. The subscript "ref" denotes a chosen reference component. In Sections 9.5 and 9.6, component 2 is the reference component, and the following relative permeabilities have been assumed throughout: $\alpha_{12}^{M} = 3$, $\alpha_{22}^{M} = 1$, and $\alpha_{32}^{M} = 1.5$. Similarly to previous chapters, these permeabilities can be arranged in a vector format such that $\boldsymbol{\alpha}^{M} = \left[\alpha_{12}^{M}, \alpha_{22}^{M}, \alpha_{32}^{M}\right] = [3,\ 1,\ 1.5]$. This is known as a nonselective membrane, since all species are allowed to move through the membrane, but at different rates, or fluxes.

Using Equations 9.9 and 9.6 in the MDPE, one can solve for and graphically interpret the retentate profile for a specified CS.

9.4.4 Properties of the MDPE

The MDPE is derived on a mass balance basis, and is not dependent on the type of membrane used (i.e., diffusion, filtration, reverse osmosis, and so on). Whereas solving it requires knowledge of the membrane flux, the actual form of the MDPE is general.

The net flow (Δ) and net composition ($\mathbf{X}_{\boldsymbol{\Delta}}$) are constant throughout a MCS. This can be easily deduced by overall and component mass balances (refer to Figure 9.2):

$$\Delta = P(A) - R(A) = P^{T} - R^{T} \tag{9.10}$$

And

$$\mathbf{X}_{\boldsymbol{\Delta}} = \frac{P(A)\mathbf{y}(A) - R(A)\mathbf{x}(A)}{\Delta} = \frac{P^{T}\mathbf{y}^{T} - R^{T}\mathbf{x}^{T}}{\Delta} \tag{9.11}$$

Equations 9.10 and 9.11 present very interesting results: they indicate that there remains a constant difference in flows and composition between any two points along a horizontal cross-section in the MCS. This occurs despite the continual change in retentate and permeate flowrates down the length of the MCS.

The physical implication of Δ is that since the direction of flow of $P(A)$ is taken as positive, $\Delta > 0$ results in more material moving up the MCS than downward, as sketched in Figure 9.2 (i.e., $P(A) > R(A)$). The opposite is true for $\Delta < 0$.

The product $\Delta\mathbf{X}_{\boldsymbol{\Delta}}$ is the vector of net flows for individual components. A positive element in this vector corresponds to a net flow of that component up the MCS, and vice versa.

A further generality of the MDPE is that knowledge of the actual shape and geometry of the membrane within the MCS is not necessary. The equation is not restricted, and can be applied to any chosen shape (plate module, hollow fiber, spiral wound, and so on).

There are four possible operating conditions that can be identified for an MCS. These are a result of the either the equality or inequality relationships that may arise

between R^T and P^T, as well as $\mathbf{x}^T$ and $\mathbf{y}^T$. All these possibilities are detailed in Peters et al. [1]; however, in this abridged section we will look at the total reflux scenario (Section 9.5) and the finite reflux cases (Section 9.6).

9.5 MCS PROFILES: TOTAL REFLUX

9.5.1 Operating Conditions

Let us consider a special case of operation of the MCS shown in Figure 9.2 where

$$P^T = R^T \qquad \text{and} \qquad \mathbf{y}^T = \mathbf{x}^T \tag{9.12}$$

Equation 9.12 implies that both flows and compositions are the same at the top of the MCS. This is equivalent to describing a total reflux column, and also sufficiently expresses an infinite reflux column, as discussed by Peters et al. [13]. Refer to Chapter 2 (Section 2.6) for the equivalent discussions on total and infinite reflux in simple distillation columns.

9.5.2 Mathematics

The conditions of total reflux result described in Equation 9.12 lead to

$$\Delta = 0 \tag{9.13}$$

and thus the MDPE reduces to

$$\frac{d\mathbf{x}}{dA} = \mathbf{x} - \mathbf{y}(\mathbf{x}) \tag{9.14}$$

It is interesting to note that Equation 9.14 is mathematically similar to the residue curve equation for distillation processes (refer to Equation 2.8). As one may recall from preceding chapters, this simplification of the MDPE under total reflux conditions is comparable to the simplification of the distillation-based DPE under infinite reflux conditions.

9.5.3 Membrane Residue Curve Map

Equation 9.14 is the membrane residue curve equation as identified by Peters et al. [14]. It is mathematically analogous to the residue curve equation derived in Chapter 2 for distillation processes. While the residue curve equation was derived

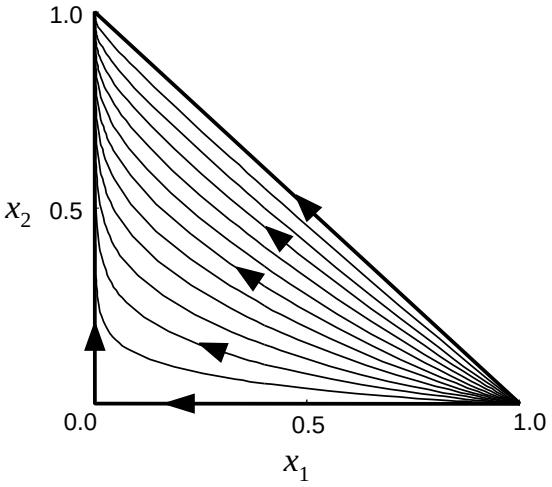


FIGURE 9.3 M-RCM for an ideal system with $\boldsymbol{\alpha}^M = [3, 1, 1.5]$ [1].

for a simple batch boiling scenario, a similar experiment can be set-up for batch permeation [14]. In both situations, the resulting equations are merely material balances, and the combination of these equations result in the residue curve equation. The variable of integration depends on the operating conditions: a batch process will have a time variable, while a continuous process (such as the one shown in Figure 9.2) will be position dependent.

Traditionally, it was believed that RCMs were only suitable for *equilibrium-based* separations and could not be used for the representation of kinetically based processes [15]. However, the differential equations which describe a residue curve are simply a combination of *mass balance equations*. Because of this, the inherent nature of RCMs is such that they can be used for equilibrium- as well as non-equilibrium-based processes. This now allows one to consider kinetically based processes, such as reactive distillation (see Chapter 8) as well as membrane separation processes.

Solving this set of equations in Equation 9.14, in conjunction with the flux model (Equation 9.6), for a range of initial conditions ($\mathbf{x}^{\mathbf{o}}$) allows one to produce a membrane residue curve map (M-RCM) as shown in Figure 9.3.

From any given initial condition ($\mathbf{x}^{\mathbf{o}}$), integration of Equation 9.14 can occur in two directions.

(i) ***Positive integration*** ($A \rightarrow +\infty$) corresponds to determining the retentate composition from the top of the MCS to the bottom (i.e., $\mathbf{x}^{\mathbf{o}} = \mathbf{x}^{\boldsymbol{T}}$)

(ii) ***Negative integration*** ($A \rightarrow -\infty$) performs the reverse direction, integrating from bottom to top (i.e., $\mathbf{x}^{\mathbf{o}} = \mathbf{x}^{\boldsymbol{B}}$).

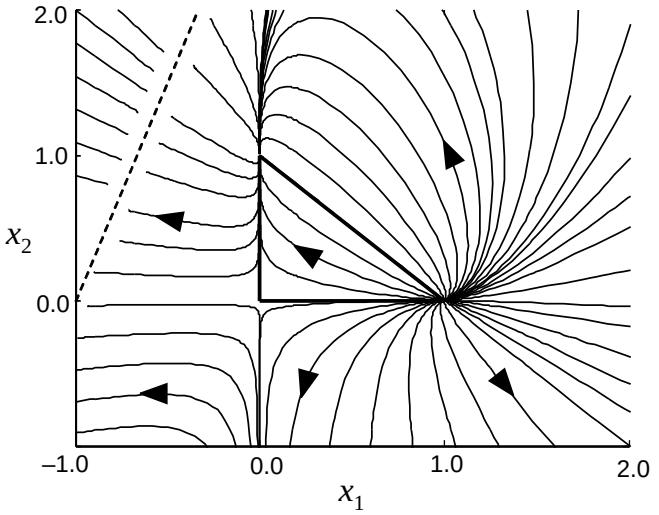


FIGURE 9.4 Global M-RCM for an ideal system with $\boldsymbol{\alpha}^M = [3, 1, 1.5]$ [1].

It is customary to indicate the direction of the positive integration on such maps as is done throughout this book and is shown in Figure 9.3 too. As discussed in Section 2.8, the x_1–x_2 space is, from a mathematical point of view, not limited to only positive profiles. It is possible to populate the entire x_1–x_2 space with curves as shown in Figure 9.4.

As with the distillation RCMs, the profiles lying outside the MBT may not be physically achievable, but the relevance of this global map is very important, and will be highlighted in subsequent sections. Note that it is also possible to identify stable, unstable, and saddle nodes, and each of these stationary points' nature and location provide insight into the behavior of the curves (refer to Section 2.5.2).

Figures 9.3 and 9.4 closely resemble the RCMs generated in Chapter 2 because the mathematical form of the flux model is the same as that of the model used in the distillation case. However, differences will arise under finite reflux conditions in the absence of the constant flow assumption. The initial similarity will serve to highlight these differences.

9.6 COLUMN SECTION PROFILES: FINITE REFLUX

9.6.1 Operating Conditions

The total reflux scenario discussed in Section 9.5 displays a more theoretical operation of a MCS, and is unlikely to find any relevance in the commercial sector. Operation of a MCS at finite reflux, however, presents situations that are of far more

practical use. These can be classified according to the following flow and composition relationships:

(a) Finite reflux case 1:

$$P^T \neq R^T \quad \text{and} \quad \mathbf{y}^T = \mathbf{x}^T \tag{9.15}$$

(b) Finite reflux case 2:

$$P^T \neq R^T \quad \text{and} \quad \mathbf{y}^T \neq \mathbf{x}^T \tag{9.16}$$

Case 1 would represent, for example, the terminating sections (e.g., rectifying) of an entire membrane column configuration. Case 2, alternatively, would be a general MCS placed anywhere within the membrane column or cascade.

9.6.2 Mathematics

Consider the conditions of operation for Case 1. Substituting these into Equation 9.11 yields

$$\mathbf{X}_{\boldsymbol{\Delta}} = \mathbf{x}^T \tag{9.17}$$

This results in the following MDPE for Case 1:

$$\frac{d\mathbf{x}}{dA} = \left[\frac{1}{r_\Delta} + 1\right][\mathbf{x} - \mathbf{y}(\mathbf{x})] + \frac{1}{r_\Delta}\left[\mathbf{x}^T - \mathbf{x}\right] \tag{9.18}$$

where r_Δ is known as the (local) reflux ratio, defined as

$$r_\Delta = \frac{R(A)}{\Delta} \tag{9.19}$$

In Case 2, there is no simplification possible, and the MDPE is

$$\frac{d\mathbf{x}}{dA} = \left[\frac{1}{r_\Delta} + 1\right][\mathbf{x} - \mathbf{y}(\mathbf{x})] + \frac{1}{r_\Delta}[\boldsymbol{X}_\Delta - \mathbf{x}] \tag{9.20}$$

Notice that the DPEs describing the scenarios in Cases 1 and 2 (Equations 9.18 and 9.20) are mathematically similar to each other. Each comprise of the addition of two vectors, namely: the separation vector, $\mathbf{S} = \mathbf{x} - \mathbf{y}$, and the mixing vector, $\mathbf{M} = \mathbf{X}_{\boldsymbol{\Delta}} - \mathbf{x}$. The only difference between the two cases is that the difference point ($\mathbf{X}_{\boldsymbol{\Delta}}$) is equal to the composition of the product being removed in Case 1. To avoid repetition, these two cases will be discussed simultaneously, due to the similar nature of their equations.

Now, Δ is pseudo-flowrate, and does not actually exist, except in Case 1 where a product is being withdrawn from a MCS. Since Δ is a difference in two flows, it is

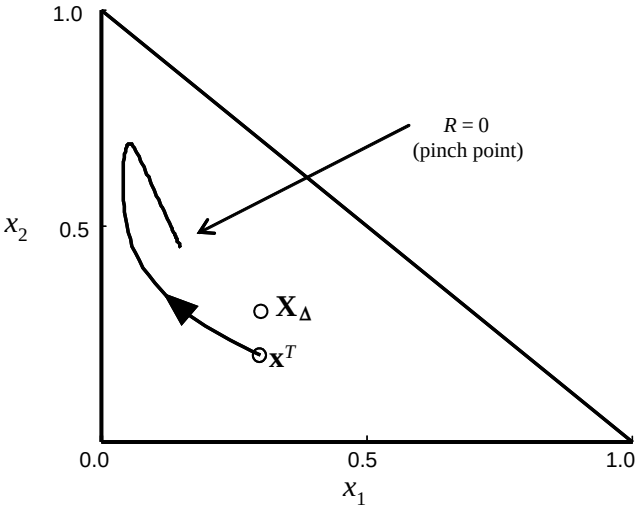


FIGURE 9.5 Membrane column profile for finite reflux and integration in a positive direction. $\mathbf{X}_\Delta = [0.3,\ 0.3]$, $\mathbf{x}^T = [0.3,\ 0.2]$, $\Delta = 20$ mol/s, and $R^T = 120$ mol/s. $\boldsymbol{\alpha}^M = [3,\ 1,\ 1.5]$ [1].

possible for it to have a positive or even negative sign. The individual elements of $\mathbf{X}_\Delta$ are viewed in a similar light, which is simply composition of the net flow stream within a MCS. Refer to earlier discussions about these parameters in Section 3.5.

9.6.3 Membrane Column Profile

The conditions of Case 1 compel all the entries of $\mathbf{X}_\Delta = \mathbf{x}^T$ to be positive, that is, to lie within the bounds of the MBT. Case 2, on the other hand, allows $\mathbf{X}_\Delta$ to exist anywhere in the x_1–x_2 space, both inside and outside the MBT. For this reason, we will select an $\mathbf{X}_\Delta$ within the MBT, thereby covering columns profiles for both cases concurrently.

Consider the following arbitrary conditions of operation (for Case 2): $\mathbf{X}_\Delta = [0.3,\ 0.3]$, $\mathbf{x}^T = [0.3,\ 0.2]$, $\Delta = 20$ mol/s, and $R^T = 120$ mol/s. (Note: for Case 1, one would have to ensure that $\mathbf{X}_\Delta = \mathbf{x}^T$). Integrating the MDPE for Case 2 down the length of the MCS yields the plot shown in Figure 9.5.

The curve is terminated when the retentate flow equals zero, as indicated in Figure 9.5. This will be discussed in the section that follows. Furthermore, although not shown here, it is possible to determine at what value of area, A, the curve pinches.

9.6.4 Pinch Point Loci

It is important to recognize that every point on the retentate column profile has two parameters associated with it, namely

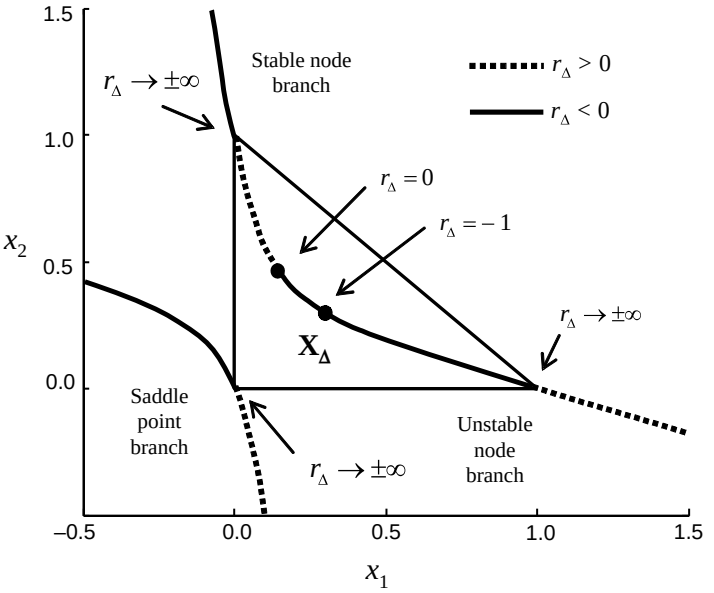


FIGURE 9.6 Pinch point loci for $\mathbf{X}_\Delta = [0.3, 0.3]$ [1].

- the composition, **x**, and
- the reflux, r_Δ.

This is different from the distillation profiles generated earlier in this book, where the CMO assumption was employed: those profiles had only **x** associated with every point. The reflux was held constant, and did not change down the length of the CS. In this scenario, however, both compositions and flows change down the length of the MCS. Hence, both **x** and r_Δ change along a membrane column profile.

Moreover, for a fixed flux model and $\mathbf{X}_\Delta$ (or $\mathbf{x}^T$), each r_Δ has associated with it a set of stationary or pinch point locations (refer to Section 3.6.). The pinch points are defined by equating the MDPE to zero, that is, when the composition is no longer changing down the length of the MCS. As r_Δ changes, so do the positions of the pinch points. It is therefore possible to generate pinch point loci, as shown in Figure 9.6, to visualize the movement of each node.

A property of the pinch point loci, which can be mathematically proven, is that one branch will always pass through $\mathbf{X}_\Delta$ at $r_\Delta = -1$. More details on the nature and behavior of pinch point loci can be found in Section 3.7.

9.6.5 Analysis of Column Profile

The behavior of the profile in Figure 9.5 can be understood by performing a mathematical analysis on the MDPE for Cases 1 and 2. As mentioned before, the MDPE is a combination of two vectors, **S** and **M**. Each vector is preceded by a

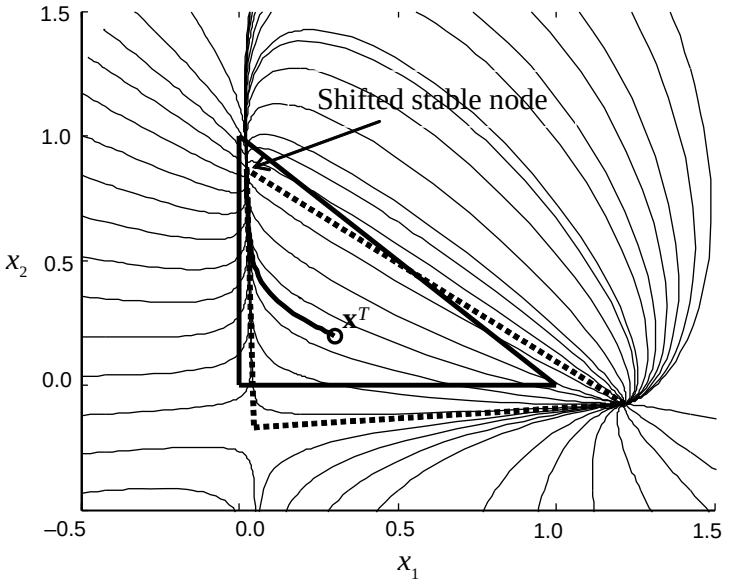


FIGURE 9.7 Shifted M-RCM. The solid triangle represents the MBT, the dashed triangle shows the TT. $\mathbf{X}_{\boldsymbol{\Delta}} = [0.3, 0.3]$, $\mathbf{x}^T = [0.3, 0.2]$, $r_\Delta = 6$. Actual membrane profile (see Figure 9.5) is tangent to the bold profile at the point indicated [1].

scalar, both involving r_Δ. Now, r_Δ is continually changing: it has its maximum value at the top of the MCS (since $R(A)$ has its maximum value at this point), and diminishes to zero as material permeates (refer to Equation 9.19). In the example discussed above, the maximum value of r_Δ is

$$r_\Delta = \frac{120}{20} = 6 \tag{9.21}$$

Figure 9.7 shows the shifted M-RCM (equivalent to a CPM) that was generated using this value of r_Δ.

The very first retentate composition, namely $\mathbf{x}^T$, will have the maximum r_Δ value associated with it. This implies that at the instant permeation begins at the top of the MCS, the retentate profile is seeking the stable pinch point that is associated with $r_\Delta = 6$, as shown in Figure 9.7. Since it is seeking this pinch point, the curve will be moving in a direction that is tangent to the profile passing through $\mathbf{x}^T$ and that has a constant r_Δ-value of 6.

However, a slight way down the MCS, some material has permeated, therefore changing $\mathbf{x}$ as well as reducing the magnitude of r_Δ. As this happens, the retentate curve now seeks a new stable node associated with the new value of r_Δ. Yet again, the column profile is tangent to the "constant r_Δ" profile that passes through $\mathbf{x}$ at this point, having the same r_Δ. Figure 9.8 shows this tangency effect at arbitrarily chosen discrete points on the column profile.

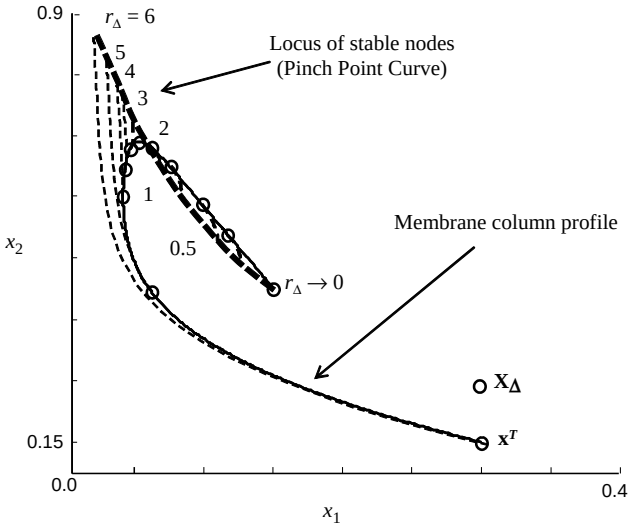


FIGURE 9.8 Tangency of curves to the column profile. Each curve corresponds to a different r_Δ- value, and is allowed to run to its stable pinch point [1].

Analysis of Figure 9.8 gives the understanding necessary to explain the behavior of the profile. Each point on the profile is seeking its stable node. The stable node itself is continually moving as r_Δ changes. This implies that the column profile has to adjust itself accordingly so as to move in the appropriate direction in order to seek the mobile stable node. It will continue to do this until the retentate has run out of material, at which point the profile will terminate.

One can see from Figure 9.8 that the profile intersects the pinch point locus at an r_Δ value of about 2. However, it is evident that the profile does not pinch at this point. The reason for this is that there is still material present in the retentate for permeating. Even though there is an intersection between the profile and the locus, this is only instantaneous. A moment later (down the length of membrane), the r_Δ value will decrease, and thus search for another stable node. Therefore, the profile does not terminate if it intersects with the pinch point locus, unless r_Δ has gone to zero.

9.6.6 Pinch Points

By definition of a pinch:

$$\frac{d\mathbf{x}}{dA} = 0 \tag{9.22}$$

Thus, using Equations 9.18 or 9.20 at $r_\Delta = 0$, and simplifying

$$\mathbf{y}(\mathbf{x}) = \mathbf{X_\Delta} \tag{9.23}$$

This means that when the retentate runs out of material, the very last permeate composition will be that of $\mathbf{X}_{\boldsymbol{\Delta}}$ (or $\mathbf{x}^T$). This result is intuitive, since all the material has transferred through the membrane. One can simply use the permeation model to determine the composition of the last drop of retentate (refer to Equation 9.6). Using the $\boldsymbol{\alpha}^M$-values selected and $\mathbf{X}_{\boldsymbol{\Delta}} = [0.3, 0.3]$, the pinch will occur at $\mathbf{x}^p = [0.15, 0.45]$. This corresponds to the last point on the curve in Figure 9.8. The position of the pinch is fixed for a chosen $\mathbf{X}_{\boldsymbol{\Delta}}$ and flux model. All curves will terminate at this point, irrespective of $\mathbf{x}^T$ (see Section 9.6.7).

9.6.7 Further Column Profiles

Arbitrarily chosen values for $\mathbf{x}^T$ and r_Δ are used in order to demonstrate a membrane column profile for Cases 1 and 2. However, any positive flowrate, R^T, is feasible, as is any point within the MBT a possible top retentate composition. Figure 9.9a displays column profiles for a fixed $\mathbf{x}^T = [0.3, 0.2]$, varying r_Δ as indicated. Figure 9.9b, on the other hand, shows a range of column profiles for select $\mathbf{x}^T$'s at a constant $r_\Delta = 6$.

Notice in Figure 9.9a that increasing the r_Δ at the top of the MCS does not alter the termination or pinch point location of each curve. This was discussed previously. The actual path mapped out by the profiles do, however, change. The path followed is a function of a stable pinch point locus. The larger r_Δ is at the MCS top, the closer the curve will begin to approximate an infinite reflux profile (see Figure 9.4). However, as r_Δ reduces substantially, the curve is forced to redirect its path so as to search for the mobile stable node.

The profiles in Figure 9.9b exhibit the same properties. Irrespective of their starting point, their trajectories are dictated by the stable node pinch point locus, with all curves ultimately pinch at the same point.

9.6.8 Variations in $\mathbf{X}_{\boldsymbol{\Delta}}$ and r_Δ

As with distillation CSs, it is perfectly legitimate for r_Δ, and elements of the vector $\mathbf{X}_{\boldsymbol{\Delta}}$ to assume negative values. Consider the possible variations on $\mathbf{X}_{\boldsymbol{\Delta}}$ and their effect on column profiles.

- Analysis and visualization of the pinch point loci associated with each $\mathbf{X}_{\boldsymbol{\Delta}}$ gives insight into the trajectory followed by a profile. This is evident from the above discussions.
- Now, for a three-component system $\mathbf{X}_{\boldsymbol{\Delta}}$ has three entries, each of which can have a possibility of two signs (+ or −). This means that there are eight possible directions that $\mathbf{X}_{\boldsymbol{\Delta}}$ can have. However, $\mathbf{X}_{\boldsymbol{\Delta}}$ has the property that all its entries have to sum to 1. Therefore, the combination where all entries are negative is not valid. So seven possibilities remain.
- Tapp et al. graphically identified these seven possibilities as regions within the entire $x_1 - x_2$ space [10] (see Figure 2.17a). They showed that the pinch point

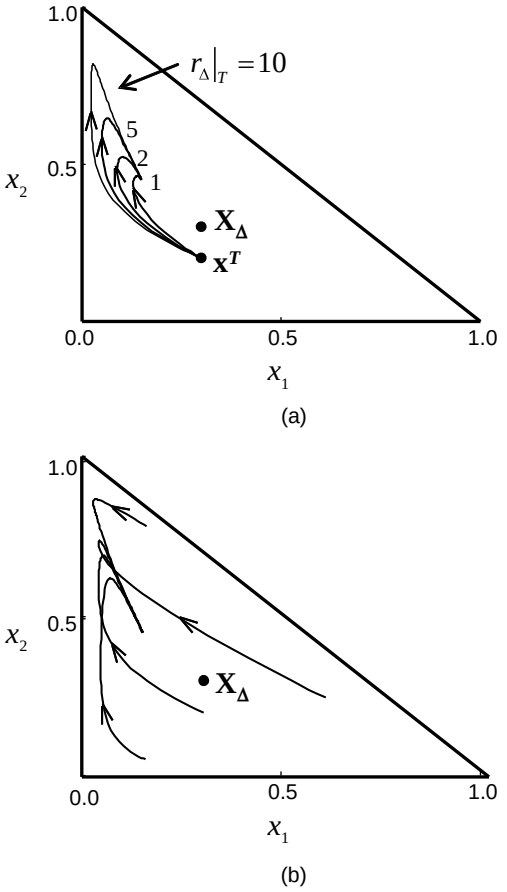


FIGURE 9.9 Column profiles for selected values of (a) various initial r_Δ- values with $\mathbf{x}^T = [0.3, 0.2]$, and (b) various $\mathbf{x}^T$ with an initial $r_\Delta = 6$ [1].

loci for an $\mathbf{X}_\Delta$ in each region were different from that in any other region. However, they concluded that the general shape of the pinch point loci for an $\mathbf{X}_\Delta$ in a given region was the same, irrespective of where $\mathbf{X}_\Delta$ was placed in the region. Refer to Section 3.7 (Figure 3.20) for the graphical representation of these pinch point loci.

r_Δ can either be positive or negative, but either way will ultimately tend toward zero as permeation proceeds. A column profile moves in such a way so as to find its associated stable node. However, the stable node pinch point locus has two branches to it, one for each sign of r_Δ (see Figure 9.6). Therefore, the sign of r_Δ determines which branch the column profile will follow. An example is shown in

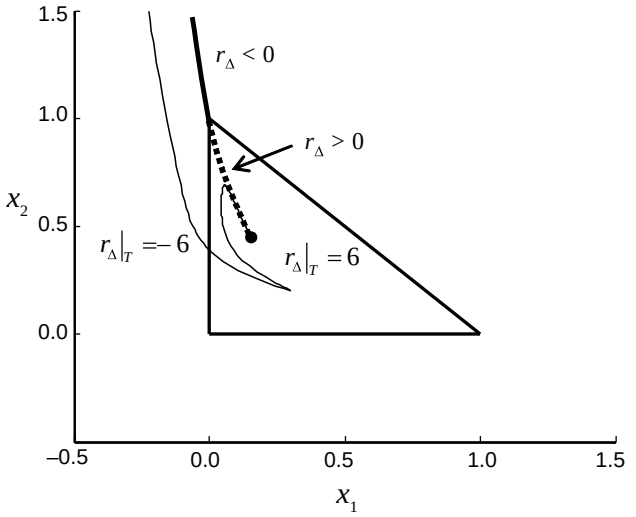


FIGURE 9.10 Effect of the sign of r_Δ on the trajectory of the profile. Each profile is influenced by its associated stable pinch point locus [1].

Figure 9.10, where it can be seen that the profile with $r_\Delta|_T = -6$ maps out a path that follows the negative branch of the stable node locus.

9.7 CONCLUSIONS

A novel graphical method of analyzing alternative separation processes using the CPM approach has been presented. This was done for continuous membrane systems. It has been shown that any configuration of membrane separators, no matter how complex in its arrangement, can be broken down into CSs. Each MCS is modeled using the MDPE. The MDPE tracks the change in the retentate composition down the length of the MCS. Various operating conditions of a CS were explored. Each condition is a result of the relationships between the flows and compositions at the top of a MCS. Using the MDPE, column profiles for each condition were plotted. The behavior of the profiles was discussed both mathematically and graphically. The profiles generated provide valuable insight into the operation of all membrane processes, even the simplest single-stage module. Being able to graphically visualize the change in the retentate composition assists a design engineer in making informed decisions. Although complex in their behavior, the nature of the profiles can be understood and explained. With this novel method, one is now able to synthesize and design more informed and creative configurations. Being able to break down any membrane arrangement to its simplest form allows one to isolate and evaluate the individual building blocks, thereby permitting an optimal design to emerge. This method is also very useful in the design of hybrid systems involving membrane separators, as shown in the next section.

9.8 EXAMPLE: DESIGN OF HYBRID SYSTEMS USING DISTILLATION-MEMBRANE PROCESSES

The example presented in this section is a condensed version of a study detailed in the book *Membrane Process Design Using Residue Curve Maps* [1] and has been reproduced with permission from John Wiley & Sons, Inc. The example is included here to demonstrate the versatility and adaptability of the techniques discussed throughout this book.

9.8.1 Introduction

The techniques developed throughout this book enable one to produce column profiles for distillation processes, including batch boiling curves, as well as continuous CSs. Further, it is possible to display a sequence of column profiles on the same map, thus graphically interpreting a system of CSs in an efficient manner. With the analogous theory that was developed for membrane separation process in this chapter, it is now possible to do this for a CS of any separation type, offering an efficient technique for the analysis of hybrid systems. The method generates an attainable region (AR) for a chosen configuration and also informs the designer of parameters such as membrane area and number of distillation stages required.

As an example, the separation of a butene/methanol/MTBE system is investigated. Methyl tertiary-butyl ether (MTBE) is the desired product, and hence needs to be efficiently recovered from a reactor output. Difficulty arises when separating such a mixture with conventional distillation processes, because of the binary azeotropes that exist between methanol and MTBE, as well as between methanol and butene. The driving force for separation in membrane processes differs from that in distillation, thus a membrane process will not exhibit the same azeotropic behavior. Thus, the limitations on distillation processes can be overcome by using a membrane unit.

Distillation remains the most widely used of all separation processes, in spite of its relative inefficiencies and high energy consumption. However, a number of alternative separation techniques have been explored, each with its own unique characteristics. Any single type of separation process is subject to limitations that could be overcome with the use of hybrid designs. For example, a selective membrane such as PERVAP 1137 (manufactured by Sulzer Chemtech®) can obtain a single pure component for the system of interest, namely methanol. The necessary flux data for this membrane can be found elsewhere [1,16]. Distillation processes, on the other hand, are often restricted by the existence of azeotropes. An additional difference between these two processes is that equimolar overflow, which is often assumed in distillation (as was done for the most part of this book), results in constant flowrates down a distillation column, whereas in a membrane unit, the retentate flow is depleted as it progresses down the column, resulting in a diminishing local reflux ratio. Even in those cases where equimolar overflow is not a valid assumption, the change in the flowrates in distillation is relatively small in comparison to that which occurs in membrane separation, where any portion of the retentate flow may be

permeated. This results in the two process types exhibiting different column profile behavior. This was highlighted in Section 9.6.

In seeking the most efficient process possible, a designer will wish to explore a wide range of feasible designs. To make this possible, an efficient method for the synthesis and assessment of any hybrid separation process has been developed. Since both processes have been analyzed using similar mathematical backgrounds, it is possible to use residue curve maps and column profile maps for both distillation and membranes to design hybrid systems of the two.

This section will look at hybrid processes featuring distillation and membrane units exclusively. Even when limited to these two types of separation techniques, a wide variety of configurations are available so the reader is advised to take note that the configuration selected and analyzed is by no means an optimal process and has merely been used to illustrate the methods. A rigorous design should consider several configurations and seek to optimize the design by taking into account considerations such as capital cost, running costs, and environmental impact.

The flexibility of hybrid configurations allows a designer greater freedom in optimizing an overall process and provides the option of overcoming deficiencies in any single process. Analysis of the properties and behavior of the respective maps for distillation and membranes equips one with the necessary tools to graphically configure a hybrid process. To facilitate the construction of a hybrid design, it is important to sequence the separation units such that each unit operates in the region of the composition space where its separation ability is best suited and most effective.

9.8.2 The Methanol/Butene/MTBE System

MTBE has found extensive use as a fuel additive. Its demand had increased due to an environmental drive to phase-out lead-compound emissions in fuels. MTBE is produced industrially in the conventional Hüls process [1]. It is formed by the reaction between methanol and *i-butene*. *i-Butene* arises from a cracking plant, and arrives at the reactor as part of a C_4 hydrocarbon stream. For simplicity, it is assumed that the C_4 stream contains only *i-butene* and 1-butene. The reaction is equilibrium limited, and in order to obtain high conversions of *i-butene*, methanol is fed in excess [17]. It is further assumed that the ratio of methanol to *i-butene* is such that all the *i-butene* is converted. The reactor product, therefore, consists of recently formed MTBE, unconverted methanol as well as inert 1-butene (from now on referred simply as butene).

The reactor product needs to be efficiently separated. Figure 9.11a shows the distillation residue curve map (referred to here as D-RCM, to avoid confusion) for the system at 6 bar. A two-column sequence is used, with the first column operating at a pressure of 6 bar. The distillate composition is nearly that of the butene/methanol azeotrope. This stream is sent back to the cracking plant from where the C_4 stream originated. The bottoms stream is sent to a second column where pure MTBE is produced, as well as an azeotropic mixture of methanol and MTBE. To avoid too much MTBE reporting to the azeotropic mixture, the pressure in the second column

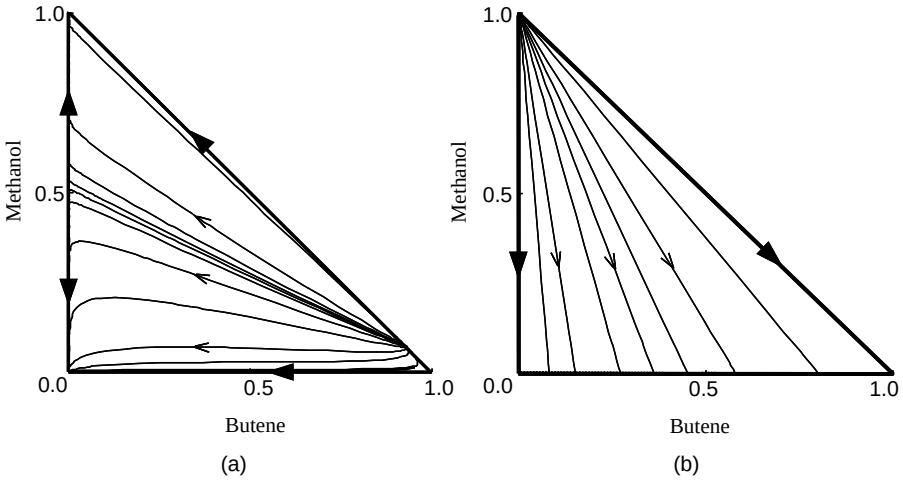


FIGURE 9.11 Butene/methanol/MTBE system. (a) D-RCM at $P = 6$ bar. (b) M-RCM at $\pi_P = 0$ [1].

is increased to 12 bar. The MTBE is the desired product, while the methanol (containing some MTBE) is recycled back to the reactor

The need for compression to 12 bar requires that substantial work be added to the process. Further, the mixture has to be heated to saturation temperature at 12 bar, resulting in increased heat duty on the reboiler. Thus, the overall process is unnecessarily energy intensive, warranting the consideration of alternative processes.

This section focuses on the use of a distillation–membrane hybrid as an alternative to the Hüls process. Such an alternative is not something new, but has been researched before [16,18,19]. What will be proposed in this section, however, is a novel graphical method of designing such systems. Lu et al. design a hybrid process using rigorous mathematical calculations, but their method does not enable them to examine other configurations [16]. Hommerich and Rautenbach examine the feasibility of various process configurations. They design each of these using Aspen Plus® with a FORTRAN subroutine for the membrane unit [19]. Bausa and Marquardt utilize shortcut methods for the design of both the distillation and membrane units. This enables them to design the hybrid process graphically. However, the reflux and reboil ratios, as well as the number of theoretical trays, needed are not so easily accessible. They do furnish the reader with a method to obtain the minimum membrane area required [18].

Various membranes have been developed for the separation of butene/methanol/MTBE [16,18,19]. The chosen membrane used here has its associated M-RCM shown in Figure 9.11b. This membrane cannot be employed as a stand-alone unit to produce pure MTBE. Using that particular membrane, it is only possible to obtain a pure methanol stream. As discussed by Peters et al., each of the curves in the M-RCM ($\pi_P = 0$) terminate when they reach the MTBE/butane binary since it

can be shown that the flux of each component goes to zero at that point [14]. Thus, pure MTBE or butane cannot be obtained from the membrane, unless the curve followed is either the binary MTBE/methanol boundary or the butane/methanol boundary, which is very unlikely. For this reason, the membrane needs to be used in conjunction with either a different membrane (capable of removing MTBE from the mixture), or with a distillation column.

Furthermore, since the membrane selected is highly selective to methanol, it becomes insensitive to the operating conditions. In other words, the permeate stream will always be pure methanol irrespective of the flowrate and composition entering the membrane unit. This is different from the nonselective membrane discussed earlier in this chapter. For this reason, one may regard the profiles in the M-RCM as actual operating profiles, since they would not vary too much under finite reflux conditions.

9.8.2.1 Design Requirements The feed to the separation system arising from the reactor has a composition of [butene, methanol, MTBE] = [0.09, 0.45, 0.46]. The required products from the hybrid separation are as follows.

- An essentially pure MTBE stream, of composition [10^{-7}, 0.001, 0.998999].
- A pure methanol stream, which will be recycled back to the reactor. With the nature of the membrane, it is possible to obtain pure methanol of [0, 1, 0].
- A butene-rich stream, with composition [0.925, 0.07, 0.005], which will be returned back to the plant from which it originated.

The D-RCM for the butene/methanol/MTBE system is shown in Figure 9.11a. The D-RCM reveals the presence of two binary azeotropes, which in turn create a distillation boundary, suggesting that separation by distillation only is a complex matter.

Analysis of the properties and behavior of the D-RCM in conjunction with that of the M-RCM equips one with the necessary tools to initially graphically configure a hybrid process. The different topologies of these two maps give a designer greater freedom in selecting column profiles, in order to achieve a desired product composition, allowing each unit to operate in the region of the composition space where its separation ability is best suited and most effective.

Numerous hybrid configurations can be investigated, such as membrane placement either upstream or downstream from the column. One could also side-connect the membrane to the column in various ways, thereby creating a recycle with the column. For illustration purposes, in this section, only one particular configuration will be examined.

9.8.3 Design of a Hybrid Configuration

Consider the hybrid configuration shown Figure 9.12a. This particular process has been proposed to perform the required separation. Using the appropriate maps, the

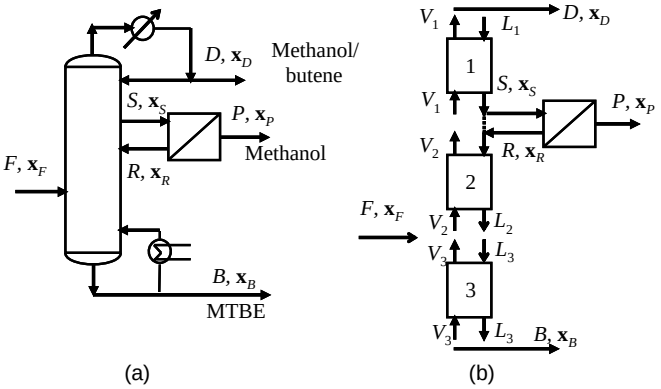


FIGURE 9.12 (a) A possible hybrid configuration. (b) The CSs for the hybrid system [1].

feasibility of this design can be verified. Since such a design would probably entail modifying an existing plant, rather than building a new one, the operating conditions of the distillation column will be kept at its original design values. For this reason, the pressure in the distillation column will be assumed to be 6 bar. Note that this is just one of many possible configurations, and is not necessarily an optimal process. It is arbitrarily chosen, and is used for demonstration purposes.

The design in Figure 9.12a can be divided into CSs as shown in Figure 9.12b. Each of the distillation column sections (DCSs 1–3) has its own unique profile described by the difference point equation (DPE)—refer to Section 3.3. As previously discussed, the DPE describes how the liquid composition changes down the length of a DCS. The profile for each DCS depends on the $\mathbf{X}_{\boldsymbol{\Delta}}$- and r_{Δ}-values for that particular section. With these values set, a CPM can be generated.

We have shown in this book that any distillation configuration, no matter how complex, can be modeled using CPMs. The example shown here is an extension of this work. While previous Chapters 5–7 focused on distillation only, we include the addition of a membrane unit connected to CSs.

When designing a hybrid system, such as the one displayed in Figure 9.12, one would like to have available all possible concatenations for a chosen configuration. This would then allow for an easy screening process during optimization.

Regardless of the configuration of the hybrid process, the objective is to meet the separation requirements. By specifying the feed and product compositions, the product flows can be determined for a set feed flowrate. It is assumed that the feed rate is 100 mol/s.

9.8.3.1 Degrees of Freedom In the arrangement chosen (refer Figure 9.12), one can concatenate the various sections in numerous ways. A "top-down" method is utilized here, but can easily be adapted for other methods, that is, "bottom-up." Beginning with the top section (CS_1), the net flow (Δ_1) and difference point ($\mathbf{X}_{\boldsymbol{\Delta}1}$) can be calculated. The reflux ratio ($r_{\Delta 1}$), on the contrary, is a choice of the designer—it is the first of 3 degrees of freedom in this design problem. It does, however, have

TABLE 9.1 Design Variables in Hybrid Configuration (Refer to Figure 9.12)

	Δ	$\mathbf{X}_{\Delta}$	r_{Δ}	L	V
CS_1	D	$\mathbf{x}_D$	$r_{\Delta 1}$	$D \cdot r_{\Delta 1}$	$D \cdot (r_{\Delta 1} + 1)$
CS_2	$P + D$	$\dfrac{(P \cdot \mathbf{x}_P + D \cdot \mathbf{x}_D)}{P + D}$	$\dfrac{(D \cdot r_{\Delta 1} - P)}{P + D}$	$D \cdot r_{\Delta 1} - P$	$D \cdot (r_{\Delta 1} + 1)$
CS_3	$-B$	$\mathbf{x}_B$	$\dfrac{(D \cdot r_{\Delta 1} - P)}{-B}$	$D \cdot r_{\Delta 1} - P$	$D \cdot (r_{\Delta 1} + 1) - F$

$r_{\Delta 1}$ is a degree of freedom.

constraints that have to be met—these will be discussed later in this section. The liquid (L_1) and vapor (V_1) flows can also be determined. All these values are constant throughout CS_1 under the previously mentioned assumption of constant molar overflow (CMO) for distillation CSs. Performing the necessary material balances around the feed (F), as well as the membrane permeate (P), enables one to define all the process variables for CS_2 and CS_3 in terms of $r_{\Delta 1}$. The feed is assumed to be all vapor. All these values are summarized in Table 9.1.

It can be seen that once an $r_{\Delta 1}$-value is set, all the values in Table 9.1 are known. However, setting $r_{\Delta 1}$ alone does not fully specify the entire hybrid system. Another degree of freedom is the amount of liquid that enters the membrane unit from the end of CS_1. Only liquid is drawn off since a pervaporation membrane is incorporated. The split ratio,

$$\Phi = \frac{S}{L_1}, \tag{9.24}$$

is defined as the fraction of liquid from the end CS_1 that reports to membrane module.

Although the range of Φ-values has to lie between 0 and 1, the design is only feasible over a narrower, more restricted range. This is to ensure that there is sufficient amount of methanol being drawn off from the end of CS_1 required to produce the desired rate and purity of methanol in the permeate product. Thus, it can be shown that

$$\Phi_{\min} = \frac{P}{D \cdot r_{\Delta 1}} \cdot \frac{\mathbf{x}_P}{\mathbf{x}_S} \quad \text{and} \quad \Phi_{\max} = 1 \tag{9.25}$$

where $\mathbf{x}_S$ is the composition of the side-draw stream. This is the same as the liquid composition leaving CS_1, $\mathbf{x}_1^B$.

When operating at $\Phi_{\min}$, the amount of methanol that enters the membrane exactly matches the amount being drawn off in the permeate stream (Note: $0 < \Phi_{\min} < 1$). Operating at values smaller than $\Phi_{\min}$ creates an infeasible retentate composition. $\Phi_{\max}$; on the other hand, it allows all the liquid leaving CS_1 to be fed into the membrane module.

Now, $\mathbf{x}_S$ is a function of $r_{\Delta 1}$ as well as n_1 (the number of stages in CS_1), among others. As $r_{\Delta 1}$ changes, so the profile trajectory for CS_1 is altered. As n_1 changes, so the termination point of CS_1 moves. Thus, it can be seen that $\Phi_{\min}$ is not a constant for the system, but rather depends on these factors.

Another important composition is that of the liquid entering CS_2:

$$\mathbf{x}_2^T = \frac{D \cdot r_{\Delta 1} \cdot \mathbf{x}_S - P \cdot \mathbf{x}_P}{D \cdot r_{\Delta 1} - P} \tag{9.26}$$

This is calculated by mixing the retentate stream with remaining liquid from CS_1 that did not go to the membrane. Notice that $\mathbf{x}_2^T$ does not depend on Φ. This implies that once $r_{\Delta 1}$ and n_1 are set, the location of is fixed. It is obvious that $0 < \mathbf{x}_2^T < 1$, thereby restraining $r_{\Delta 1}$ to set ranges. For this to hold true, it can be shown that

$$r_{\Delta 1} > \frac{P \cdot \mathbf{x}_P}{D \cdot \mathbf{x}_S}, \quad \text{or} \quad r_{\Delta 1} < 0 \tag{9.27}$$

This is diagrammatically represented in Figure 9.13.

The second inequality in Equation 9.27 is impossible since CS_1 operates in rectifying mode, and $r_{\Delta 1}$ has to be positive by definition. Therefore, $r_{\Delta 1}$ has to adhere to the first constraint in Equation 9.27 only. This would be the minimum value that $r_{\Delta 1}$ can have, and would necessitate that the fraction of methanol in the distillate stream be zero. $r_{\Delta 1,\min}$ is not set for the system, but does depend on n_1, as discussed previously for $\Phi_{\min}$.

Thus, it can be concluded that this design has 3 degrees of freedom, namely

- $r_{\Delta 1}$,
- n_1, and
- Φ.

each having to operate within their respective bounds.

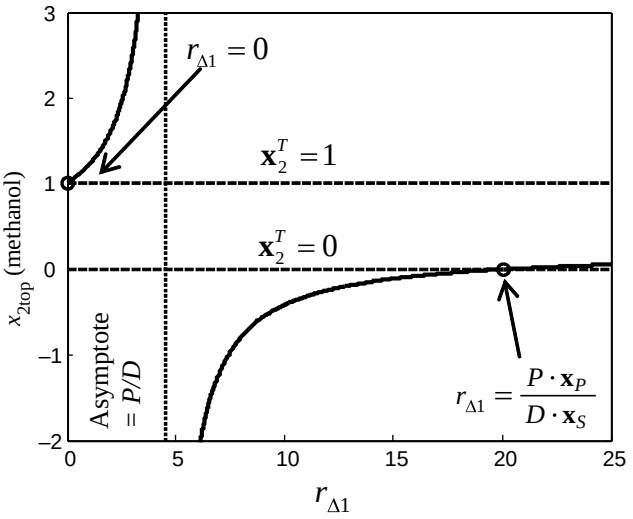


FIGURE 9.13 Feasibility ranges for $r_{\Delta 1}$ $(0 < \mathbf{x}_2^T < 1)$ [1].

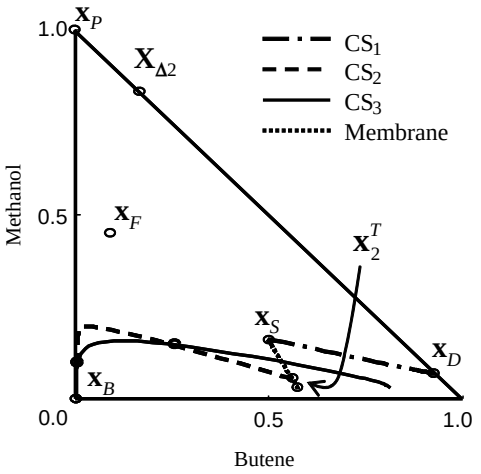


FIGURE 9.14 Column and membrane profiles for the hybrid design in Figure 9.12 with $r_{\Delta 1} = 40$ and $n_1 = 5$ [1].

9.8.3.2 Generating Profiles for Hybrid Column For demonstration purposes, it will initially be assumed that operation will occur at $\Phi = 0.8$. In order to display the profiles obtainable for this design, $r_{\Delta 1}$- and n_1-values were arbitrarily chosen. Furthermore, for the design to be feasible, it is required that the profiles of each section, including the membrane, intersect in the same order and direction as that of liquid flow in the system. Figure 9.14 shows the column and membrane profiles for operation at $r_{\Delta 1} = 40$ with $n_1 = 5$.

Since the feed is a vapor, an intersection of the (liquid) profiles for CS_2 and CS_3 signifies the end of CS_2 and beginning of CS_3. This is because the composition of the liquid leaving CS_2 will not be altered by the addition of a vapor feed. It is clear in Figure 9.14 that the profiles for CS_2 and CS_3 intersect twice (at $x_{\text{methanol}} = 0.1$ and 0.16). Thus, the termination of CS_2 can occur at either of these points. Figure 9.15a and b shows the possible concatenations of the sections in the hybrid.

9.8.3.3 Comparing Feasible Design Options To compare these two options one would like to have necessary design parameters easily accessible. With this novel method of design, values such as the number of stages in each CS and the membrane area can be determined with relative ease. This has been done for the two options proposed above and the results tabulated in Table 9.2. The numbers of stages were calculated from the distillation DPE (Equation 3.10) and are theoretical. The membrane area was sought via the methods described Peters et al. [1] using the appropriate flux model. (Note: while it may appear that the membrane area is somewhat large, it is not the aim here to calculate an exact area, but rather to convey an understanding of the simple yet effective methods used.)

TABLE 9.2 Design Parameters for the Different Cases in Figure 9.15

Parameter	Option (a)	Option (b)
n_1	5	5
n_2	0.6	5.7
n_3	4.8	3.3
A (m^2)	4746.6	4746.6

9.8.3.4 Attainable Region The diagram in Figure 9.14 shows only one possible profile arrangement for the chosen hybrid design. However, there are numerous ways in which one can configure this design based on the degrees of freedom discussed above. A parametric study has been performed that allows for design flexibility. It is therefore possible to generate "attainable regions" (ARs) which integrates the degrees of freedom. It should, however, be appreciated that the ARs generated here are **not** the entire AR, but rather a select part of it. The complete AR can be produced, but is detailed and is not done here as it is out of the scope of this chapter.

For the select ARs, it was assumed that the split ratio, Φ, is set at its minimum value (refer to Equation 9.25). Remember, the split ratio only influences the amount of material that goes to the membrane (and hence the membrane area), but does not affect the location of any of the compositions within the MBT, except $\mathbf{x}_R$. Thus, two types of ARs can be produced: varying $r_{\Delta 1}$ for a set n_1 and vice-versa.

Figure 9.16 shows the AR for a variable $r_{\Delta 1}$ and a set $n_1 = 4$. As discussed previously, $r_{\Delta 1}$ has a minimum value that depends on $\mathbf{x}_S$ (refer to Equation 9.27). It can be shown that for this case, $r_{\Delta 1,\min} = 41.77$.

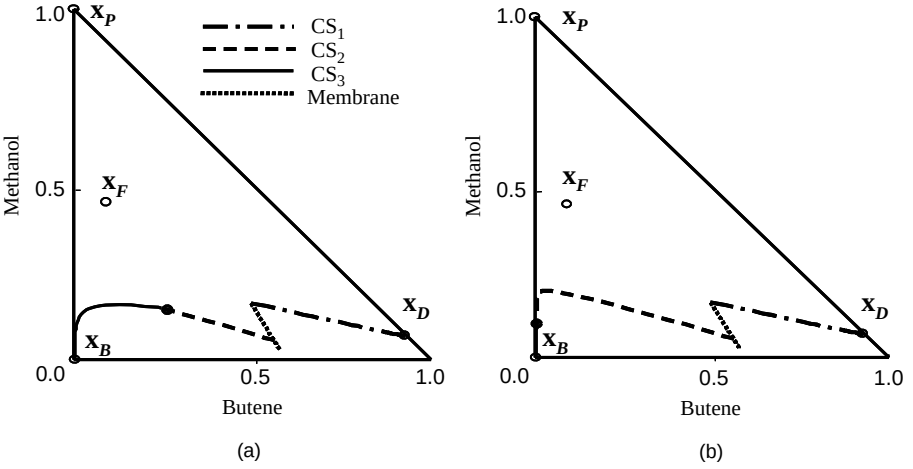


FIGURE 9.15 Profile options (a) and (b) for the hybrid design in Figure 9.12 with $r_{\Delta 1} = 40$ and $n_1 = 5$ [1].

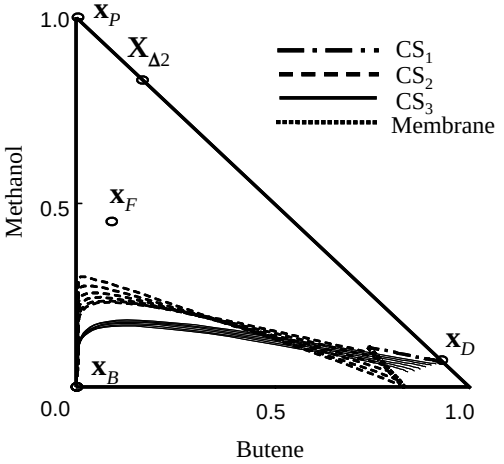


FIGURE 9.16 Attainable region for $n_1 = 4$, operating at $r_{\min}$. Select $r_{\Delta 1}$-values between 41.77 and 250 have been chosen [1].

Although not apparent from Figure 9.16, the profile for CS_1 is changing as $r_{\Delta 1}$ changes. The various CS_1 profiles have similar trajectories, making it impossible to distinguish on the given scale. Furthermore, there is definite intersection between the profiles for CS_2 and CS_3 for each $r_{\Delta 1}$. Thus, we can conclude that, for a set n_1, the design is feasible provided that $r_{\Delta 1} > r_{\Delta 1,\min}$. Similar plots would be obtained for other values of n_1.

Figure 9.17a , on the other hand, shows the AR for a set value of $r_{\Delta 1} = 70$. The number of stages in CS_1 was varied from 2 to 7 in various increments. A high $r_{\Delta 1}$-value was chosen so as to ensure that it is well above the minimum required for each n_1. For clarity purposes, Figure 9.17b and c shows zoomed in versions of Figure 9.17a, as indicated by their axes. Of course, for a set $r_{\Delta 1}$, there is a set $r_{\Delta 2}$ and $r_{\Delta 3}$ (refer to Table 9.1). This in turn fixes the profiles for CS_1 and CS_3, as well as the CPM for CS_2. Hence, there is only one possible profile for CS_1 as well as CS_3, as shown. The profile for CS_2 depends on $x_{2\text{top}}$, which changes with each n_1 (or x_S). But it should be appreciated that all the profiles obtained for CS_2 belong to the same CPM since both $\mathbf{X}_{\boldsymbol{\Delta 2}}$ and $r_{\Delta 2}$ are constant.

For each chosen n_1, the membrane profile intersects with that of CS_1, as does CS_2's profile with the membrane profile. However, it can be seen in Figure 9.17b that the profiles for CS_2 and CS_3 do not intersect for all n_1. For example, when $n_1 = 2$, there is no intersection indicating an infeasible design. It has been determined that the first point of intersection occurs when $n_1 = 2.63$. This is the minimum number of theoretical stages that CS_1 has to have for $r_{\Delta 1} = 70$ in order for a feasible design!

It is further noticed, in Figure 9.17c, that some profiles of CS_2 curves again do not intersect with the profile for CS_3 (for $n_1 = 6.75$ and $n_1 = 7$). This means that there are a maximum number of stages that CS_1 can have as well. This maximum occurs at $n_1 = 6.52$, where profile 2 is tangent to profile 3. While it may be thought that adding

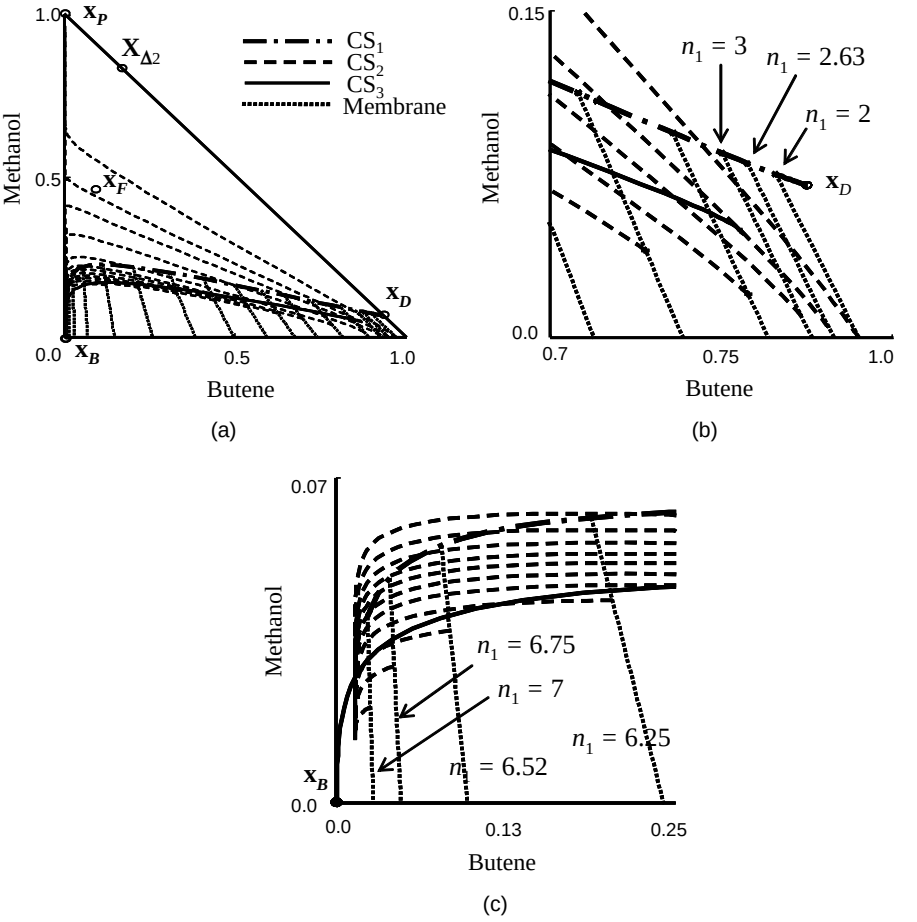


FIGURE 9.17 (a) Attainable region for $r_{\Delta 1} = 70$, operating at $r_{\min}\ 2 < n_1 < 7$. (b) Minimum n_1 and (c) maximum n_1 tangent to CS_3 profile [1].

an excess amount of stages in a column is beneficial, this result is very interesting as it proves that adding too many stages in CS_1 may result in an infeasible design!

Of course the maximum and minimum n_1 values depend on $r_{\Delta 1}$, but can easily be sought for each $r_{\Delta 1}$-value. Similar plots to the one in Figure 9.17a can be generated for different $r_{\Delta 1}$-values.

9.8.4 Conclusion

Using membrane profiles in conjunction with column profile maps allows one to graphically interpret hybrids in an efficient manner. Furthermore, by focusing on the membrane in *isolation*, one is not limited to a single hybrid configuration,

making the possibilities infinite. A method of design that can be used to quickly evaluate feasible options for a particular design has been discussed. Using the graphical method not only makes the design easier to visualize and understand, but it also does provide the designer with useful and necessary design parameters. The operating ranges of the reflux ratios result, as do the number of stages in each section. Using earlier discussed techniques, the membrane area can also be determined in each scenario. The method can be adapted accordingly for other process configurations, with the ultimate design chosen by a screening or optimization procedure.

REFERENCES

[1] Peters, M., et al., *Membrane Process Design Using Residue Curve Maps* 2011, *New York*: Wiley. p. 224.

[2] Rautenbach, R. and R. Albrecht, *Membrane Processes*. 1st ed. 1989, New York: Wiley. 490.

[3] Marriott, J. and E. Sørensen, A general approach to modelling membrane modules. *Chemical Engineering Science*, 2003, **58**(22):4975–4990.

[4] Marriott, J. and E. Sørensen, The optimal design of membrane systems. *Chemical Engineering Science*, 2003, **58**(22):4991–5004.

[5] Rautenbach, R. and R. Albrecht, The separation potential of pervaporation: Part 2. Process design and economics. *Journal of Membrane Science*, 1985, **25**(1):25–54.

[6] McCandless, F.P., A comparison of membrane cascades, some one-compressor recycle permeators, and distillation. *Journal of Membrane Science*, 1994, **89**(1–2):51–72.

[7] Seader, J.D. and E.J. Henley, *Separation Process Principles*. 2nd ed. 2006, Hoboken, NJ: Wiley. p. 756.

[8] Hwang, S. and J.M. Thorman, The continuous membrane column. *AIChE Journal*, 1980, 26.

[9] Tsuru, T. and S.-T. Hwang, Permeators and continuous membrane columns with retentate recycle. *Journal of Membrane Science*, 1995, **98**(1–2):57–67.

[10] Tapp, M., et al., Column profile maps. 1. Derivation and interpretation. *Industrial and Engineering Chemistry Research*, 2004, **43**(2):364–374.

[11] Wijmans, J.G. and R.W. Baker, The solution–diffusion model: A review. *Journal of Membrane Science*, 1995, **107**(1–2):1–21.

[12] Huang, Y.-S., et al., Residue curve maps of reactive membrane separation. *Chemical Engineering Science*, 2004, **59**(14):2863–2879.

[13] Peters, M., et al., Application of membrane residue curve maps to batch and continuous processes. *Industrial and Engineering Chemistry Research*, 2008, **47**(7):2361–2376.

[14] Peters, M., et al., Derivation and properties of membrane residue curve maps. *Industrial and Engineering Chemistry Research*, 2006, **45**(26):9080–9087.

[15] Fien, G.-J.A.F. and Y.A. Liu, Heuristic synthesis and shortcut design of separation processes using residue curve maps: A review. *Industrial and Engineering Chemistry Research*, 1994, **33**(11):2505–2522.

[16] Lu, Y., et al., Hybrid process of distillation side-connected with pervaporation for separation of methanol/MTBE/C4 mixture. *Desalination*, 2002, **149**(1–3):81–87.

[17] Rehfinger, A. and U. Hoffmann, Kinetics of methyl tertiary butyl ether liquid phase synthesis catalyzed by ion exchange resin—I. Intrinsic rate expression in liquid phase activities. *Chemical Engineering Science*, 1990, **45**(6):1605–1617.

[18] Bausa, J. and W. Marquardt, Shortcut design methods for hybrid membrane/distillation processes for the separation of nonideal multicomponent mixtures. *Industrial and Engineering Chemistry Research*, 2000, **39**(6):1658–1672.

[19] Hömmerich, U. and R. Rautenbach, Design and optimization of combined pervaporation/distillation processes for the production of MTBE. *Journal of Membrane Science*, 1998, **146**(1):53–64.

CHAPTER 10

CONCLUDING REMARKS

10.1 OVERALL CONCLUSIONS

The work presented in this book is a culmination of the research efforts of the COMPS separation group in the past decade or so. Many of the problems and structures that have been discussed throughout this book have been chosen because they are relevant problems or have interesting aspects that we, the authors, felt are essential for the reader's enrichment. However, we would like to stress that these problems are merely to show how the CPM technique can be applied. The real crux of the book is not the specific problems discussed, but more the presentation and elucidation of a new design technique. We hope that the reader is encouraged to use the mathematical and graphical tools presented here to synthesize and design their own column structure to suit some sort of separation need (breaking azeotropes, reducing energy or capital expenditures, improving operation, and so on).

It is hoped that, although simple in its nature, the importance of analyzing the individual, stand-alone, and generalized CS is now apparent. Intuitively, it is seemingly obvious to examine distillation systems in this manner of breaking them down to their simplest structures, yet the general CPM displayed in this text, to the best of the authors' knowledge, appears to be the only such method. We have aimed to show the method's versatility in that it can be applied to the design of virtually any distillation structure, regardless of its complexity or even the presence of chemical reactions. Even seemingly unrelated separation methods such as membrane permeation have also been modeled and explained using these very ideas. The tools allow one to examine a column's stability and lend an intuitive

Understanding Distillation Using Column Profile Maps, First Edition. Daniel Beneke, Mark Peters, David Glasser, and Diane Hildebrandt.
© 2013 by John Wiley & Sons, Inc. Published 2013 by John Wiley & Sons, Inc.

insight into separation problems that more complex models may not. It has also been shown how one may, relatively simply, reproduce column profiles experimentally to assess and validate the workings of a *real* column.

The original development of the difference point equation (DPE) relied upon an assumption of constant molar overflow (CMO). This assumption can be relaxed with the inclusion of the appropriate energy balance. Although this was never shown in the text, it is hoped that the reader can infer this by the methods shown in Chapter 9 on membrane permeation, for example, where this assumption is not justified. Thus, with the necessary modeling, the DPE and hence the CPM method show great versatility and adaptability.

By constructing column profiles one is able to infer variables like the feed stage, total number of theoretical stages, side-draw stage, and so on. These variables are often difficult to predict using other design techniques. This concept can also be readily extended to reactive and membrane permeation systems where one can infer, or at least obtain a good guess of, either the catalyst requirement or the membrane permeation area, respectively. Further, we have also shown a simplified a transformed triangle technique: although only applicable to ideally-behaved systems, it does give great insight into the nature and location of pinch points. Furthermore, the use of transformed triangles in designing columns is extremely useful for sharp splits. It is possible to design highly complex structures with this technique and construct regions of feasibility. Solutions obtained with this simplified technique can be used as a starting point for more rigorous designs with profiles with surprising efficacy.

Finally, and perhaps most importantly, the technique gives insight into problems that are often poorly understood. For instance, in Chapter 2 we showed RCMs for the acetone/ethanol/methanol system at pressure 1 and 10 atm, both using Aspen Plus® and through profile integration (Figures 2.8 and 2.9). There is clearly a difference in the system's behavior at these two pressures. However, by not permitting the global topological view that has been advocated in this book, there is no way of knowing why the system is different at these pressures, or where these differences have originated from. It is clear from Figures 2.19 and 2.20 that the nodes do not just "appear" and "disappear." These nodes were in fact part of the system all along; they have merely been shifted to a different location. Thus, the designer has *a priori* knowledge of how a system may behave. Similar instances were shown for reactive distillation in Chapter 8. These insights may be extremely useful when new columns are being synthesized.

10.2 LIMITATIONS

Although we firmly believe that the CPM technique is an invaluable distillation synthesis tool, we would like to point out a shortcoming of the method, namely the ability to deal with higher order systems. The vast majority of problems discussed in this book deal with ternary systems. Ternary systems allow one to visualize the problem graphically and many conclusions can be drawn from this analysis. However, when more components are introduced, the problem becomes exceedingly difficult and insights are diminished. Although a four-component system can be

analyzed graphically, even this is a challenge. For large systems such as those found in crude refining, one has to draw on the ideas and methods developed for ternary systems, and use the necessary traits and understanding when not being able to visualize the profiles graphically. One would also find the need to incorporate mathematical tools such as those presented by Linninger and coworkers [1–6].

10.3 EXTENSIONS AND THE WAY FORWARD

We are of the opinion that the tools in this book are applicable to various other topics in separation science. If one examines a liquid–liquid extraction process, one quickly realizes that it is not that dissimilar to distillation: in a particular separation stage in the process, there is contact between two phases that can be assumed to be in equilibrium with each other. Piecing these stages together eventually constitutes the liquid–liquid extraction process, in much the same way as an array of separation stage constitutes a distillation column. Naturally, the problem may not be this simple and one may need to take into account additional effects, but the principles remain the same. Creating hybrid designs involving various types of separation (distillation, membrane, liquid extraction, and so on) is merely an extension of the work presented in this book, and can be easily applied.

Additionally, we have shown that allowing negative compositions can be very enlightening, even though they have no practical significance. The reader is urged to employ some of this "out of the box" thinking to other engineering or scientific fields. It may not be negative compositions, but very well negative absolute temperatures or pressures, or indeed any other parameters that may be impractical but allowable from a theoretical point of view.

REFERENCES

[1] Kim, S.B. and A.A. Linninger, Rigorous separation design. 2. Network design solutions for mixtures with various volatility differences and feed compositions. *Industrial and Engineering Chemistry Research*, 2010, **49**(18):8670–8684.

[2] Kim, S.B., G.J. Ruiz, and A.A. Linninger, Rigorous separation design. 1. Multicomponent mixtures, nonideal mixtures, and prefractionating column networks. *Industrial and Engineering Chemistry Research*, 2010, **49**(14):6499–6513.

[3] Ruiz, G.J., et al., Design and optimization of energy efficient complex separation networks, in *7th International Conference on the Foundations of Computer-Aided Process Design*. 2009, New York: Taylor & Francis Group.

[4] Ruiz, G.J., et al., Robust thermodynamically-guided algorithms for synthesis of energy efficient separation networks, in *Computer Aided Chemical Engineering*, S. Pierucci and G.B. Ferraris, Editors. 2010, Amsterdam, The Netherlands: Elsevier. pp. 1117–1122.

[5] Zhang, L. and A.A. Linninger, Towards computer-aided separation synthesis. *AIChE Journal*, 2006, **52**(4):1392–1409.

[6] Zhang, L. and A.A. Linninger, Temperature collocation algorithm for fast and robust distillation design. *Industrial and Engineering Chemistry Research*, 2004, **43**(12):3163–3182.

APPENDIX A

DODS SOFTWARE PACKAGE

A.1 BACKGROUND TO THE DODS PACKAGE

The DODS software package can be used to complete most of the examples and tutorials in this book. The package has been written in Matlab, but has been complied such that it may be used on a computer without Matlab installation. It is also useful as an independent design tool and, as shown in the examples in the book, the results obtained can be used as initialization to rigorous simulation packages such as Aspen Plus®. The DODS package consists of five independent packages:

1. *DODS-ProPlot*. This is a comprehensive profile plotting package which allows the user to plot single profiles, entire CPMs and RCMs, and their associated pinch points. There are 13 systems to choose from, each of which may be modeled either with a modified Raoult's law and the NRTL activity coefficient model, or with the ideal Raoult's law (does not model azeotropes), or with a constant relative volatility approximation where the software automatically determines the relative volatilities between components (this model also cannot account for azeotropic behavior). One also has the option to insert one's own constant volatilities. It is possible to plot the full DPE, the shortened DPE at infinite reflux (shown in Chapter 7) or the classic residue curve equation. Depending on the equation chosen, the user is free to specify any relevant parameters such as an R_Δ value, difference points, system

Understanding Distillation Using Column Profile Maps, First Edition. Daniel Beneke, Mark Peters, David Glasser, and Diane Hildebrandt.
© 2013 by John Wiley & Sons, Inc. Published 2013 by John Wiley & Sons, Inc.

pressure, and the integration coordinate (n). Further, the program allows one also to rapidly find pinch points for any system at any conditions for any of the thermodynamic models.

2. *DODS-SiCo.* DODS-SiCo allows the user to graphically design ternary simple columns through either profile intersections for nonsharp splits or through TT alignment for sharp splits. When designing for finite-sized nonsharp split columns, the user is informed whether the design is feasible and the number of rectifying and stripping stages for a chosen column reflux. There are again 13 preloaded systems available and the designer may choose various models to describe the system. For sharp splits, a minimum reflux calculation is performed using TTs and the calculated minimum reflux value is returned (only available for constant relative volatility systems). In both instances the user can specify product specifications, a feed flowrate and quality, and the software automatically determines the column mass balance.
3. *DODS-DiFe.* As an introduction to complex column design, the DODS-DiFe allows the user to graphically design ternary distributed feed columns through either profile intersections for nonsharp splits or through TT alignment for sharp splits. The software has been limited to only account for three feed inputs with differing vapor fractions, but all feed streams have the same composition. Only a user-defined constant volatility model is available for this package. The purpose of the DODS-DiFe package is thus not intended specifically for column design, but more as a complex column design teaching tool.
4. *DODS-SiSt.* The DODS-SiSt toolbox allows one to design side-stripper columns through profile intersections by specifying a single CS reflux and a liquid split ratio. If the design is feasible, DODS-SiSt gives all stage number in all CS, as well as the operating refluxes. One may find that it is quite difficult finding a feasible design using profile intersections alone, and we suggest using the TT method as either a reliable guide for finding profile intersections, or as a conservative yet rapid design estimate. When using the TT design method, an attainable region is constructed, which prompts the user to choose a suitable operating condition.
5. *DODS-SiRe.* The DODS-SiRe toolbox for side-rectifier design is exactly equivalent to the SiSt package, and allows one to design side-rectifier columns through either profile intersections by specifying a single CS reflux and a vapor split ratio. Also, equivalently to the SiSt package, the TT conditions can be used for quick design estimates.

A.2 SYSTEM REQUIREMENTS

Windows XP or newer (64-bit). A subsequent release will include a 32-bit version.

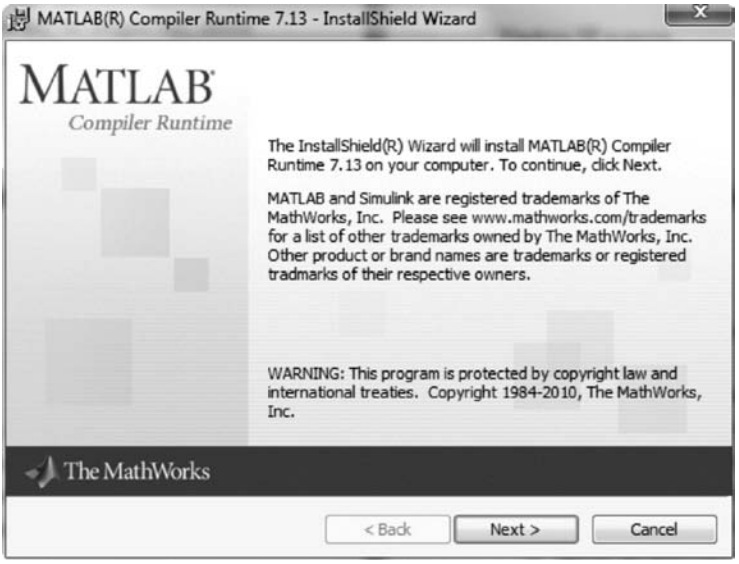

MATLAB(R) Compiler Runtime 7.13 - InstallShield Wizard
MATLAB
Compiler Runtime
The InstallShield(R) Wizard will install MATLAB(R) Compiler Runtime 7.13 on your computer. To continue, click Next.
MATLAB and Simulink are registered trademarks of The MathWorks, Inc. Please see www.mathworks.com/trademarks for a list of other trademarks owned by The MathWorks, Inc. Other product or brand names are trademarks or registered tradmarks of their respective owners.
WARNING: This program is protected by copyright law and international treaties. Copyright 1984-2010, The MathWorks, Inc.
The MathWorks
< Back
Next >
Cancel

FIGURE A.1 MCR window.

A.3 INSTALLATION

None of the DODS programs require installation per se, as all of them are available as executable .exe files. However, for any of these programs to be fully operational, the user is required to first install the Matlab Component Runtime (MCR), version 7.13. This is available as freeware from Mathworks, the creators of Matlab, but it has also been provided here. Thus to commence installation (Figure A.1):

1. Double-click on the MCRInstaller-7.13 executable file.
2. The Windows InstallShield Wizard window will appear and the user will be prompted with a window for language preference. Select English (US) and click "OK."
3. The user will be prompted with an "Install" window. Click "Install."
4. A MCR window is presented, shown in Figure A.1. Click "Next."
5. A window requesting the User Name and Organization is presented. Once information has been entered, click "Next."
6. A window requesting the location where the MCR should be saved is presented, shown in Figure A.2. Simply use the default location given, or browse for a new location. Once the location has been selected, click "Next."
7. A window is presented for the installation of MCR, shown in Figure A.3. Click "Install," which will commence the installation procedure.
8. Wait until installation is complete and until Figure A.4 appears. Click "Finish."
9. Installation is complete and the user can now open any of the DODS packages.

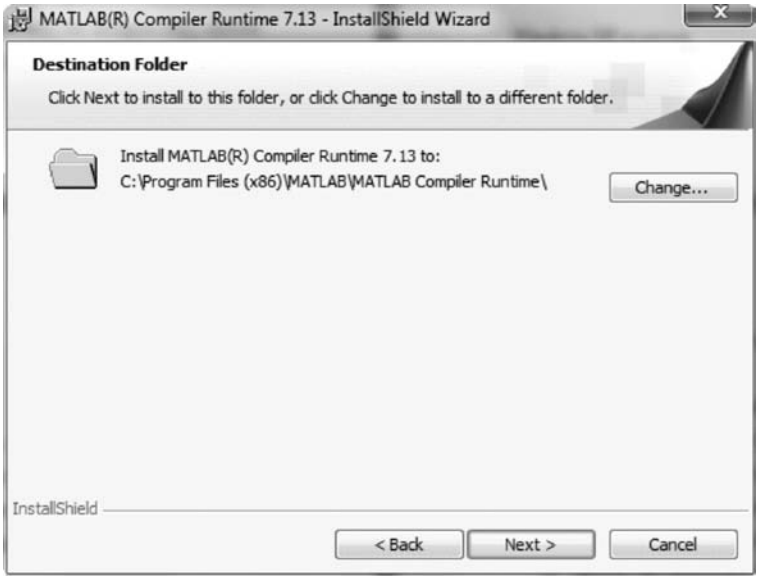

MATLAB(R) Compiler Runtime 7.13 - InstallShield Wizard
Destination Folder
Click Next to install to this folder, or click Change to install to a different folder.
Install MATLAB(R) Compiler Runtime 7.13 to:
C:\Program Files (x86)\MATLAB\MATLAB Compiler Runtime\
Change...
InstallShield
< Back
Next >
Cancel

FIGURE A.2 MCR destination location.


MATLAB(R) Compiler Runtime 7.13 - InstallShield Wizard
Ready to Install the Program
The wizard is ready to begin installation.
Click Install to begin the installation.
If you want to review or change any of your installation settings, click Back. Click Cancel to exit the wizard.
InstallShield
< Back
Install
Cancel

FIGURE A.3 MCR installation window.

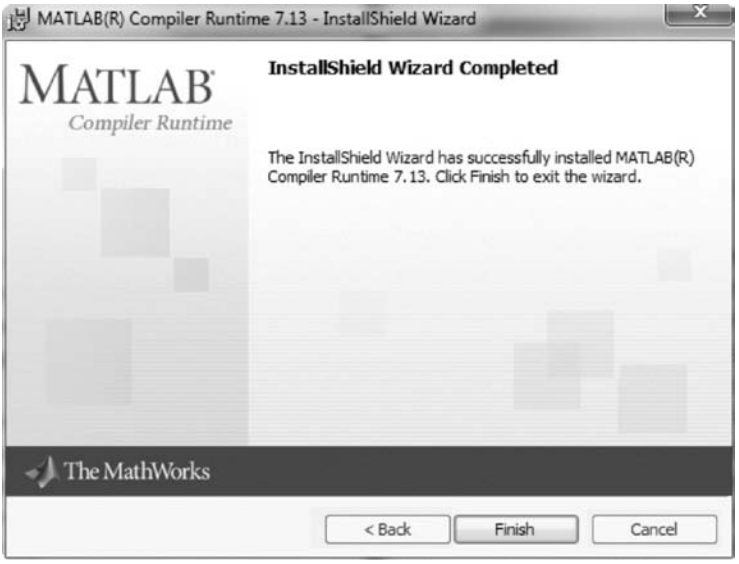


FIGURE A.4 MCR complete installation window.

A.4 DODS-ProPlot

Upon successful installation of the ProPlot package, the user will be presented with a screen shown in Figure A.1. Once this screen is seen, the user can immediately start plotting profiles and pinch points once the appropriate parameters have been set. If these parameters are not set or specified illogically, ProPlot will return an error. Below is a description of the function and workings each of the labeled points in Figure A.5.

1. *Select a Thermodynamic Model.* The user is free to choose (i) the NRTL model for highly nonideal systems, (ii) the ideal model obeying Raoult's law, (iii) a constant volatility model whereby ProPlot automatically computes the volatilities between components, or (iv) his/her own constant volatilities. Note that when options (i)–(iii) are selected, the user is required to select one of the predefined systems in (b). When option (iv) is selected, the user is required to enter volatilities in the form [L,H,I] for the Low, High, and Intermediate boiling components, respectively.
2. *Select a Predefined System.* There are 13 preprogrammed ternary systems that the user may choose from in the dropdown menu. These systems have either been shown in the book, are industrially relevant, or are simply interesting from a topological perspective.
3. *Specify the Reflux Ratio.* Any value for R_Δ may be selected, except for the co-current range where $-1<R_\Delta<0$. Note that the R_Δ input is disabled/enabled when the appropriate equation in (g) is selected.

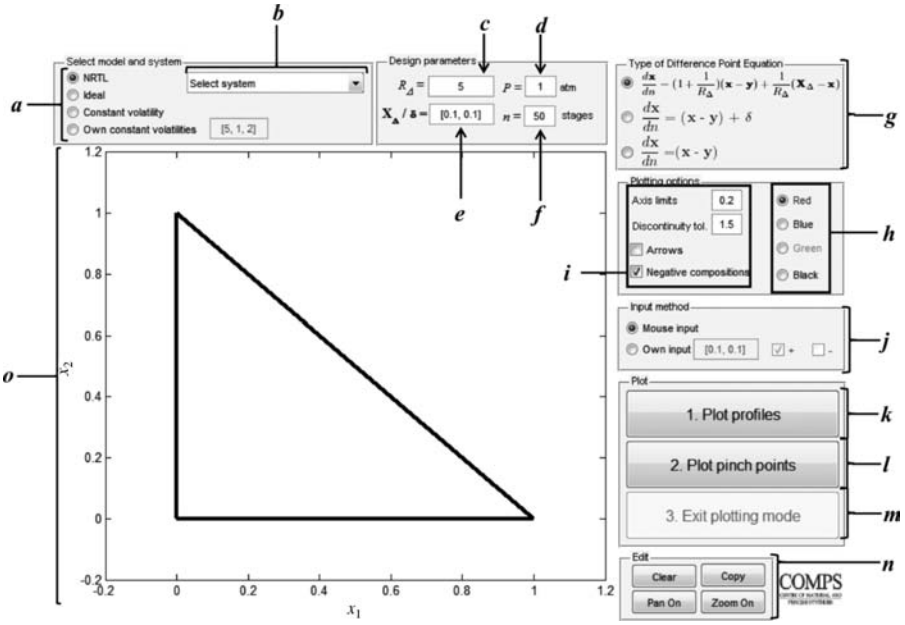


FIGURE A.5 The DODS-ProPlot package labeled a–o.

4. *Specify the System Pressure.* Merely specify a positive, scalar value for the system pressure. This parameter will influence VLE behavior.
5. *Specify the Difference Point.* A two-row vector is required with logical input for the difference points of the L and H. This block serves as both the X_Δ and δ input, depending on the equation selected in (g). Note that the X_Δ/δ input is disabled/enabled when the appropriate equation in (g) is selected.
6. *Specify the Final Integration Limit.* A positive scalar value is required to specify the final point of integration. It is set to 50 by default, and is generally sufficient to plot profiles all the way to their pinch points.
7. *Specify the Equation.* In this panel, the user is required to select an equation: (i) the entire DPE, (ii) a shortened DPE with the difference vector (see Chapter 7 for use and application), or (iii) a residue curve equation.
8. *Specify a Plot Color.* Simply specify the color in which you wish to produce your figure.
9. *Specify Plot Properties.* Allows one to set
   (i) The axis limits, that is, the scope beyond the MBT (a value of 0.2 thus means that plot view is a box with lower and upper x and y limits of -0.2 and 1.2). Must be a positive, scalar quantity.
   (ii) The discontinuity tolerance, that is, the absolute difference between **x** and **y** compositions. The integration procedure will terminate once this

difference has been reached. The larger this number is the longer it will take for integration to terminate, but profiles will approach the discontinuity much closer. This value must be positive and greater than 1.

(iii) Arrows checkbox, that is, whether the user would like to include arrows on profiles showing the direction toward a stable node.

(iv) Negative composition checkbox, that is, whether negative composition should be allowed. When checked, the MBT is disregarded and integration will continue past its boundaries. When unchecked, the user will not be able to select negative compositions for integration initialization and integration will be terminated once a negative composition is obtained.

10. *Specify the Input Method.* The user is allowed to specify the initial integration composition either via mouse input, or via a specified, exact input. Selecting the latter option requires a two-row vector field as input in the form [L, H] (I is implied through unity summation). One may also select the direction of integration by checking the (+) or (−) boxes. Selecting the mouse input option activates the plotting area (o) once the profile plotting button has been clicked (k).
11. *Profile Plotting.* When all parameters have been appropriately and correctly specified, the user can press this button to start plotting profiles. Once this button is pressed, plotting starts immediately. Note that the plotting differs depending on the initial composition input method (j).
12. *Pinch Point Plotting.* Clicking on this button allows the user to plot pinch points for each system. For all thermodynamic models except the NRTL model, the ProPlot package automatically finds *all* pinch points associated to that particular system's operating conditions. For the NRTL model, the user will be asked to click near a pinch point. Clicking near a pinch point serves as an initial guess and deploys a numerical algorithm to identify the pinch composition and temperature.
13. *Exit Plotting Mode.* When either plotting profiles or fining pinch points via mouse input, the user may click on this button to exit plotting mode. This button is disabled by default, but is enabled when the user needs to exit a mouse input method.
14. *Editing Panel.* There are four buttons in this panel, for clearing the plot area, copying, zooming, and panning. The clear button clears all previous plotted data from the plotting area. Upon pressing the copy button, all graphical information currently in the ProPlot window will be placed on the clipboard. The zoom button allows one to zoom into a particular area of interest in the plotting area, while the pan button allows one to move the plot around, as desired.
15. *Plotting Area.* This is the main area where all plotting of profiles and pinch points takes place.

A.5 DODS-SiCo

Upon successful installation of the SiCo package, the user will be presented with a screen shown in Figure A.2. Once this screen is seen, the user can immediately begin to design a simple column once the appropriate parameters have been set and subsequently clicking the "Design!" button. If any parameters are not set or specified illogically, SiCo will return an error. Below is a description of the function and workings of each of the labeled points in Figure A.6.

1. *Select a Thermodynamic Model.* The user is free to choose (i) the NRTL model for highly nonideal systems, (ii) the ideal model obeying Raoult's law, (iii) a constant volatility model whereby SiCo automatically computes the volatilities between components, or (iv) his/her own constant volatilities. Note that when options (i)–(iii) are selected, the user is required to select one of the predefined systems in (b). When option (iv) is selected, the user is required to enter volatilities in the form [L, H, I] for the Low, High, and Intermediate boiling components, respectively.
2. *Select a Predefined System.* There are 13 preprogrammed ternary systems that the user may choose from in the dropdown menu. These systems have either been shown in the book, are industrially relevant, or are simply interesting from a topological perspective.

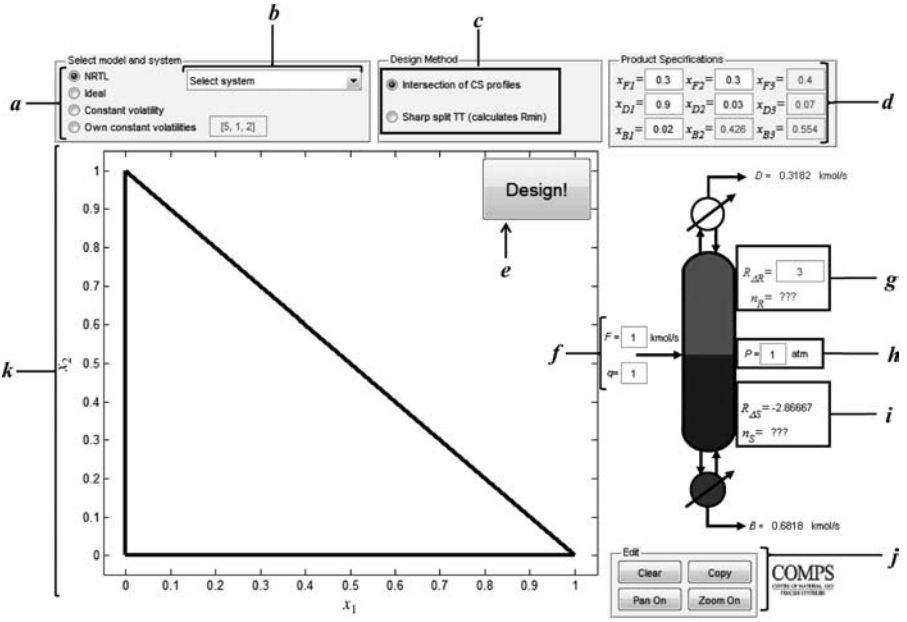


FIGURE A.6 The DODS-SiCo package labeled a–i.

3. *Specify the Design Method.* Simple column design can be performed either through searching for profile intersections or by calculating minimum reflux for a sharp split problem using TTs. When the TT method is selected, product specifications are automatically set to sharp, and upon pressing the "Design!" (e) button will a minimum reflux value will be returned in the $R_{\Delta R}$ textbox in (g). Note that the stage numbers in (g) and (i) are automatically set to infinity. When opting for a design via profile intersection, the user is required to also enter a $R_{\Delta R}$-value in (g). Upon pressing the "Design!" button, profiles will be generated from the product specifications in (d) and column data will be returned to (g) and (i) if the design is feasible.
4. *Specify the Feed/Product Composition.* The user can specify any feed composition and product distribution. All entries must be greater than 0 and less than 1. When a value is changed in this panel, the column mass balance is automatically updated.
5. *Designing the Column.* Once all column parameters have been appropriately set, the user can press the "Design!" button to generate profiles/TTs. Once the design is complete, the user will be informed whether the design is feasible and if so, what the rectifying and stripping stage numbers are.
6. *Specify the Feed Conditions.* Here the user is able to set the feed flowrate to the column, as well as the feed quality. If either one of these properties are adjusted, the column mass balance automatically changes.
7. *Rectifying Section Operating Conditions.* Here, all data regarding the rectifying section is displayed ($R_{\Delta R}$ and n_R). When the TT method is selected in (c), the $R_{\Delta R}$ textbox is disabled. If the profile intersection method is selected in (c), the user is required to specify a positive, scalar value in the $R_{\Delta R}$ textbox.
8. *Specify the System Pressure.* Merely specify a positive, scalar value for the system pressure. This parameter will influence VLE behavior.
9. *Stripping Section Operating Conditions.* Here, all data regarding the stripping section is displayed ($R_{\Delta S}$ and n_S). The user is not required to specify anything here.
10. *Editing Panel.* There are four buttons in this panel, for clearing the plot area, copying, zooming, and panning. The clear button clears all previous plotted data from the plotting area. Upon pressing the copy button, all graphical information currently in the SiCo window will be placed on the clipboard. The zoom button allows one to zoom into a particular area of interest in the plotting area, while the pan button allows one to move the plot around, as desired.
11. *Plotting Area.* This is where the profiles pertaining to the design are given, and where the user is informed about the feasibility of the design.

A.6 DODS-DiFe

Upon successful installation of the DiFe package, the user will be presented with a screen shown in Figure A.3. Once this screen is seen, the user can immediately begin

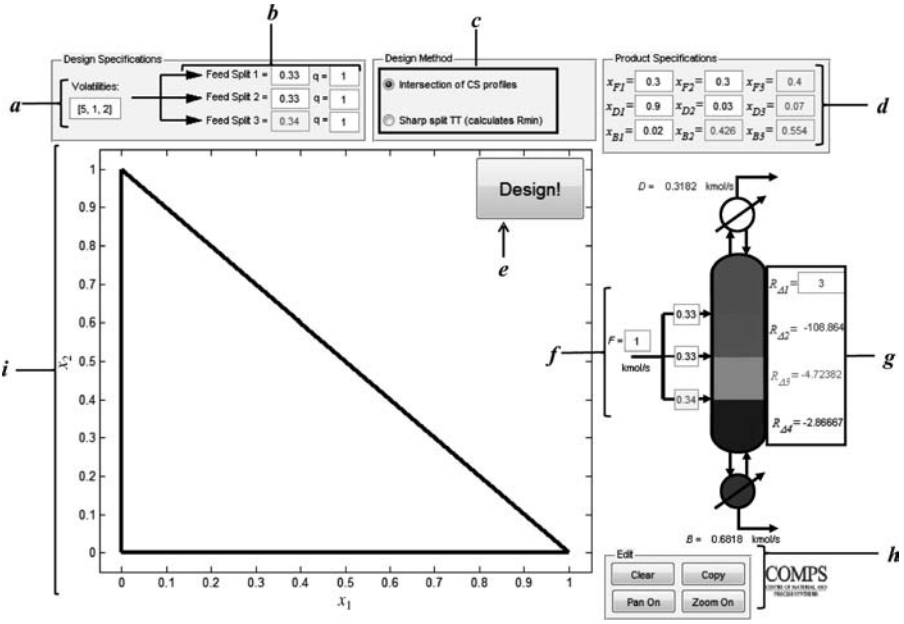


FIGURE A.7 The DODS-DiFe package labeled a–i.

to design a distributed feed column once the appropriate parameters have been set and subsequently clicking the "Design!" button. If these parameters are not set or specified illogically, DiFe will return an error. Below is a description of the function and workings each of the labeled points in Figure A.7.

1. *Specify Constant Relative Volatilities.* In the DiFe package, only constant relative volatility systems are allowed. Here, the user should specify volatilities in the form [L, H, I] for the Low, High, and Intermediate boiling components, respectively.
2. *Specify the Feed Distribution/Quality.* The DiFe package limits the user to only three feed distributions. The fractions of feed split to each part of the column can be set here, along with the quality of that particular feed stream. Each split fraction must be greater than 0 and less than 1, and they must sum to 1. The feed fractions in (b) are equivalent to the feed fraction in (f). Both are linked, so setting a feed fraction at (f) will change the values in (b), and vice versa. Feed qualities should simply be positive scalar quantities.
3. *Specify the Design Method.* Distributed feed column design can be performed either through searching for profile intersections or by calculating minimum reflux for a sharp split problem using TTs. When the TT method is selected, product specifications are automatically set to sharp, and upon pressing the "Design!" button (e) a minimum reflux value will be returned in the $R_{\Delta 1}$ value in the textbox in (g). When opting for a design via profile intersection, the user

is required to also enter a $R_{\Delta R}$ value in (g). Upon pressing the "Design!" button, blue and red profiles will be generated for CS_1 and CS_4, originating from their respective product specifications, and CPMs with multiple profiles for the internal CSs. No information regarding design feasibility or the stage numbers required in each section is given in the DiFe package.

4. *Specify the Feed/Product Composition.* The user can specify any feed composition and product distribution. All entries must be greater than 0 and less than 1. When a value is changed in this panel, the column mass balance is automatically updated.
5. *Designing the Column.* Once all column parameters have been appropriately set, the user can press the "Design!" button to generate profiles/TTs. In the DiFe package, no indication is given on the feasibility of the design, nor is the stage requirement of each CS given.
6. *Specify the Feed Overall Feed Flowrate and Distribution.* The user is able to set the overall feed flowrate which automatically.
7. *Individual CS Reflux Ratios.* Each CSs refluxes are displayed here. When the designer chooses to do the design by profile intersection, an input value for $R_{\Delta 1}$ is required. If the TT method is selected, the $R_{\Delta 1}$ textbox is disabled, as the $R_{\Delta 1}$-value will be calculated. The reflux values for each of the CSs are automatically updated once a value for $R_{\Delta 1}$ is specified/calculated.
8. *Editing Panel.* There are four buttons in this panel, for clearing the plot area, copying, zooming, and panning. The clear button clears all previous plotted data from the plotting area. Upon pressing the copy button, all graphical information currently in the DiFe window will be placed on the clipboard. The zoom button allows one to zoom into a particular area of interest in the plotting area, while the pan button allows one to move the plot around, as desired.
9. *Plotting Area.* This is where the profiles pertaining to the design are given.

A.7 DODS-SiSt AND DODS-SiRe

Since the SiSt and SiRe packages are very similar, only the SiSt module will be discussed. The only fundamental difference is that instead of specifying $R_{\Delta 1}$ and Φ_L in SiSt package, the user is required to specify $R_{\Delta 3}$ and Φ_V in SiRe package. Upon successful installation of the SiSt packages, the user will be presented with a screen shown in Figure A.3. Once this screen is seen, the user can immediately begin to design a side-stripper column once the appropriate parameters have been set and subsequently clicking the "Design!" button. If these parameters are not set or specified illogically, DiFe will return an error. Below is a description of the function and workings of each of the labeled points in Figure A.8.

1. *Select a Thermodynamic Model.* The user is free to choose (i) the NRTL model for highly nonideal systems, (ii) the ideal model obeying Raoult's law, (iii) a constant volatility model whereby SiSt automatically computes the volatilities between components, or (iv) his/her own constant volatilities.

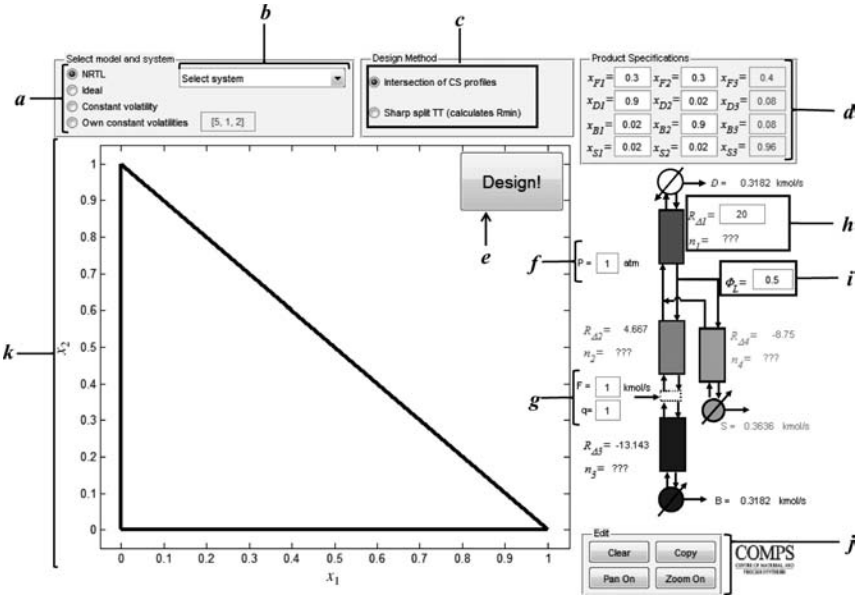


FIGURE A.8 The DODS-SiSt package labeled a–i.

Note that when options (i)–(iii) are selected, the user is required to select one of the predefined systems in (b). When option (iv) is selected, the user is required to enter volatilities in the form [L, H, I] for the Low, High, and Intermediate boiling components, respectively.

2. *Select a Predefined System.* There are 13 preprogrammed ternary systems that the user may choose from in the dropdown menu. These systems have either been shown in the book, are industrially relevant, or are simply interesting from a topological perspective.
3. *Specify the Design Method.* Simple column design can be performed either through searching for profile intersections or by calculating minimum reflux for a sharp split problem using TTs. When the TT method is selected, product specifications are automatically set to sharp, and upon pressing the "Design!" (e) button will a minimum reflux value will be returned in the $R_{\Delta R}$ textbox in (g). Note that the stage numbers in (g) and (i) are automatically set to infinity. When opting for a design via profile intersection, the user is required to also enter a $R_{\Delta R}$ value in (g). Upon pressing the "Design!" button, profiles will be generated from the product specifications in (d) and column data will be returned to (g) and (i) if the design is feasible.
4. *Specify the Feed/Product Composition.* The user can specify any feed composition and product distribution. All entries for the product specifications must be greater than or equal to 0 and less than or greater than 1. It should be noted that only ternary problems can be dealt with in this version of SiSt, so all feed composition have to be greater than 0 and less than 1. When a

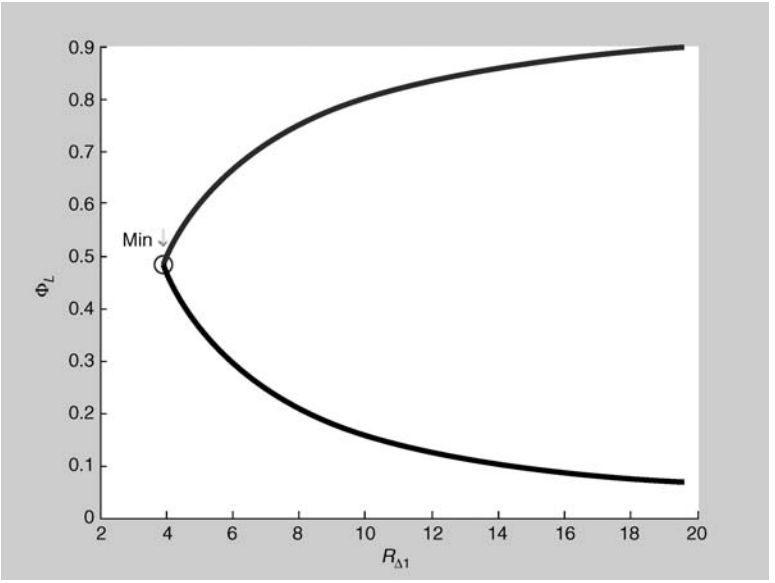


FIGURE A.9 Attainable region figure for the SiSt package.

value is changed in this panel, the column mass balance is automatically updated.

5. *Designing the Column.* Once all column parameters have been appropriately set, the user can press the "Design!" button to generate a design by profiles/TTs. When the TT method is chosen, the user is presented with a figure with an attainable region in $R_{\Delta 1}$–Φ_L space, shown in Figure A.9, where a $R_{\Delta 1}-\Phi_L$ coordinate must be selected by a click action. Once the design is complete, the user will be informed whether the design is feasible and if so, what the rectifying and stripping stage numbers are.
6. *Specify the System Pressure.* Merely specify a positive, scalar value for the system pressure. This parameter will influence VLE behavior.
7. *Specify the Feed Conditions.* Here the user is able to set the feed flowrate to the column, as well as the feed quality. If either one of these properties are adjusted, the column mass balance automatically changes.
8. *Rectifying Section Operating Conditions.* Here, all data regarding the rectifying section is displayed ($R_{\Delta 1}$ and n_1). When the TT method is selected in (c), the $R_{\Delta 1}$ textbox is disabled. If the profile intersection method is selected in (c), the user is required to specify a positive, scalar value in the $R_{\Delta 1}$ textbox.
9. *Liquid Split Ratio.* Adjusting the Φ_L value automatically updates the R_Δ's for the entire column. When the TT method is selected in (c), the $R_{\Delta 1}$ textbox is disabled. If the profile intersection method is selected in (c), the user is required to specify a positive, scalar value in the Φ_L textbox that is greater than zero and less than 1.

10. *Editing Panel.* There are four buttons in this panel, for clearing the plot area, copying, zooming, and panning. The clear button clears all previous plotted data from the plotting area. Upon pressing the copy button, all graphical information currently in the SiSt window will be placed on the clipboard. The zoom button allows one to zoom into a particular area of interest in the plotting area, while the pan button allows one to move the plot around, as desired.
11. *Plotting Area.* This is where the profiles pertaining to the design are given, and where the user is informed about the feasibility of the design.

APPENDIX B

NRTL PARAMETERS AND ANTOINE COEFFICIENTS

Tables B.1, B.2, and B.3 give binary interaction parameters (a, b, and c, respectively) for the NRTL equation (Equations B.1 and B.2) for systems that have been used and discussed extensively throughout the book. All parameters are regressed values from the Dortmund databank, obtained from Aspen Plus®.

$$\gamma_i = \exp\left[\frac{\sum_j x_j \tau_{ji} G_{ji}}{\sum_k x_k G_{ki}} + \sum_j \frac{x_j G_{ij}}{\sum_k x_k G_{kj}}\left(\tau_{ij} - \frac{\sum_m x_m \tau_{mj} G_{mj}}{\sum_k x_k G_{kj}}\right)\right] \tag{B.1}$$

$$\text{where } \tau_{ij} = a_{ij} + b_{ij}/T(K) \quad \text{and} \quad G_{ij} = \exp(-c_{ij}\tau_{ij}) \tag{B.2}$$

Example of Using Tables B.1–B.3

Suppose the binary interaction coefficients are being sought for the benzene–water system. We shall designate benzene as component i and water as component j. Then, in Table B.1, progress down the first column until component i is found (benzene). Then, progress down the row where component i has been found and search for the cell intersection with component j in the first row. It can be seen that $a_{ij} = 45.191$. To find a_{ji}, repeat the procedure, but search for component j in the first column, and then for the cell intersection with component i in the first row. In this

Understanding Distillation Using Column Profile Maps, First Edition. Daniel Beneke, Mark Peters, David Glasser, and Diane Hildebrandt.
© 2013 by John Wiley & Sons, Inc. Published 2013 by John Wiley & Sons, Inc.

TABLE B.1 Binary Interaction Parameter a_{ij} for the NRTL Model for Selected Components

	Methanol	Ethanol	Benzene	*p*-Xylene	Toluene	Chloroform	Water	Acetone
Methanol	0.000	4.712	−1.709	0.678	0.000	0.000	−0.693	0.000
Ethanol	−2.313	0.000	0.569	4.075	1.146	0.000	−0.801	−1.079
Benzene	11.580	−0.916	0.000	0.000	−2.885	0.000	45.191	0.422
p-Xylene	−3.259	−5.639	0.000	0.000	0.000	0	2.773	0.000
Toluene	0.000	−1.722	2.191	0.000	0.000	0.000	−247.879	−1.285
Chloroform	0.000	0.000	0.000	0	0.000	0.000	−7.352	0.538
Water	2.732	3.458	140.087	162.477	627.053	8.844	0.000	0.054
Acetone	0.000	−0.347	−0.102	0.000	1.203	0.965	6.398	0.000

TABLE B.2 Binary Interaction Parameter b_{ij} for the NRTL Model for Selected Components

	Methanol	Ethanol	Benzene	*p*-Xylene	Toluene	Chloroform	Water	Acetone
Methanol	0.0	−1162.3	892.2	295.5	371.1	−71.9	173.0	114.1
Ethanol	483.8	0.0	−54.8	−1202.4	−113.5	−148.9	246.2	479.1
Benzene	−3282.6	882.0	0.0	122.7	1124.0	−375.4	591.4	−239.9
p-Xylene	1677.6	2504.2	−136.5	0.0	75.9	−17.7	296.7	173.6
Toluene	446.9	992.7	−863.7	−91.1	0.0	−57.0	14759.8	630.1
Chloroform	690.1	690.3	313.0	−120.2	−25.2	0.0	3240.7	−106.4
Water	−617.3	−586.1	−5954.3	−6046.0	−27269.4	−1140.1	0.0	420.0
Acetone	101.9	206.6	306.1	83.2	−400.5	−590.0	−1809.0	0.0

TABLE B.3 Binary Interaction Parameter c_{ij} for the NRTL Model for Selected Components

	Methanol	Ethanol	Benzene	*p*-Xylene	Toluene	Chloroform	Water	Acetone
Methanol	0.0	0.3	0.4	0.5	0.3	0.3	0.3	0.3
Ethanol	0.0	0.0	0.3	0.3	0.3	0.3	0.3	0.3
Benzene	0.0	0.0	0.0	0.3	0.3	0.5	0.2	0.3
p-Xylene	0.0	0.0	0.0	0.0	0.3	0.3	0.2	0.3
Toluene	0.0	0.0	0.0	0.0	0.0	0.3	0.2	0.3
Chloroform	0.0	0.0	0.0	0.0	0.0	0.0	0.2	0.3
Water	0.0	0.0	0.0	0.0	0.0	0.0	0.0	0.3
Acetone	0.0	0.0	0.0	0.0	0.0	0.0	0.0	0.0

TABLE B.4 Antoine Equation Coefficients for Selected Components

	Methanol	Ethanol	Benzene	*p*-Xylene	Toluene	Chloroform	Water	Acetone
A	8.07240	8.1122	6.90565	6.99052	6.95464	6.93710	8.01767	7.23160
B	1574.990	1592.864	1211.033	1453.430	1344.800	1171.200	1715.7	1277.030
C	238.870	226.184	220.790	215.307	219.482	227.000	234.268	237.230

example, $a_{ji} = 140.087$. Using a similar procedure, values for parameters b and c can also be found.

The Antoine equation for calculating vapor pressure is given in Equation B.3, with the relevant constants in Table B.4.

$$\ln\left(P_i^{\mathrm{VAP}}\right) = A_i - \frac{B_i}{T + C_i} \tag{B.3}$$

INDEX

Absorbers, 117
  design of, 118–124
Activity coefficient, 10
  NRTL model, 10–11, 345–347
Antoine equation
  see Vapor pressure
Apparatus
  batch, 94–95
  continuous, 106–112
Attainable regions
  see Feasible designs
Azeotrope, 11, 28, 30
  See also Stationary points

Batch boiling
  reactive systems, 262–263
  rectifying profiles, 92–98, 103–105
  residue curves, 16–17, 22, 24
  stripping profiles, 98–103
Binary systems, 8, 10, 11
Bottoms product, 2, 99–101
Boundary value method, 3, 117, 128
Bow-tie regions, 35–38, 129–130
  See also Direct split mass balance; Indirect split mass balance; Infinite reflux columns

Chemical reaction
  see Reaction
Column profile maps
  history, 4
Condenser, 5
Column internals, 5, 117
Column profile, 55–56
  application to absorbers, 122–123
  application to distributed feed columns, 162–175
  application to side rectifiers, 190–194
  application to side strippers, 190–194
  direction of, 163
  membrane systems, 308, 312–314
  reactive systems, 281, 287, 289, 292–293
  validation, 64–65, 141, 151–153

Understanding Distillation Using Column Profile Maps, First Edition. Daniel Beneke, Mark Peters, David Glasser, and Diane Hildebrandt.

© 2013 by John Wiley & Sons, Inc. Published 2013 by John Wiley & Sons, Inc.

Column profile maps, 48–90
  applications, 103–105, 122–123, 132–137, 162–175, 175–184, 209–216
  constant relative volatility systems, 55–59
  coupled column sections, 210–216
  experimental measurement of, 91–114
  mathematical aspects, 80–84
  nonideal systems, 59–60, 87, 97, 103
  pinch points, 69–71
  plotting of, 54–60
  profile intersection, 135
  properties of, 67–75
  reactive systems, 280, 287, 289, 292–293
  relation to residue curve maps, 57, 67–68
  See also Column section
Column section(s)
  definition, 49
  distributed feed columns, 158–159
  fully thermally coupled columns, 207–208, 252
  generalized, 51, 117, 118, 123, 159
  in parallel, 208–209
  membrane systems, 299–300
  reactive, 275–293
  side-draw columns, 173–175
  side rectifiers,185–186
  side strippers, 185–186
  simple columns, 131
Column section breakdown
  see Column section
Column stability, 85–87
  reactive systems, 292–293
Complex columns, 6
  design of, 157–205
  See also Distributed feed columns; Side withdrawal columns; Thermally coupled columns
Condenser
  total, 138–139
Constant molar overflow, 52, 118
Constant relative volatility systems
  column profile maps, 55–59
  minimum reflux in simple columns, 145–153
  residue curve maps, 21, 40
  stationary points, 27
  vapor-liquid equilibrium, 7–8, 21
Coupled column sections, 208–216
  See also Transformed triangles
Crystallization, 1

Degrees of freedom
  simple columns, 129
  thermally coupled columns, 186, 217–218
Design
  of absorbers, 118–124
  of distributed feed columns, 158–175
  of hybrid processes, 314–325
  of membrane systems, 296–314
  of reactive distillation columns, 261–295
  of side rectifiers, 186–205
  of sidestream withdrawal columns, 175–184
  of side strippers, 186–205
  of simple columns, 128–156
  of strippers, 124–128
  of thermally coupled columns, 206–260
Difference point, 53, 62–66
  coupled column sections, 213
  distributed feed columns, 160–162
  fully thermally coupled columns, 223–228
  general column sections, 63–65, 66, 119, 125
  membrane systems, 301, 303, 307, 312–314
  reactive systems, 277, 280, 281–285
  rectifying column sections, 63, 93, 129
  side rectifiers, 186–187
  side strippers, 186–187
  sidestream withdrawal columns, 176–177
  stripping column sections, 63, 129
  See also Pinch point loci
Difference point equation, 51–54, 118
  for coupled column sections at infinite reflux, 209
  derivation, 52
  for membrane permeation, 299–301, 307
  numerical integration of, 54, 119
  reactive systems, 276–280
  rectifying column sections, 92
  stripping column sections, 99
  for vapor compositions (strippers), 124–125
  See also Column section

Difference vector
in coupled column sections, 210
definition, 209
Dimensionless time, 20, 32, 264
Direct split mass balance, 34
See also Infinite reflux columns
Discontinuity in residue curve map, 43
Distillate product, 2, 93, 94
Distillation
capital costs, 2, 6
definition, 1
energy costs, *see* Distillation, operating costs
energy inputs in US, 2
heating requirements, 1
operating costs, 2, 5
power consumption in US, 2
simple columns, *see* Simple distillation columns
Distillation boundary, 24
crossing of, 143–145
Distillation region, 24, 27
See also Distillation boundary
Distributed feed columns, 6, 158
benefits, 166
design of, 158–175
limitations, 166, 171–173
Double-feed pinch, 135–136, 149–151

Enthalpy
of reaction, 278
of vaporization, 204, 278
Eigenvalues, 80–82
Eigenvalue map, 82
Eigenvectors, 82–83
minimum reflux, 153–154
Eigenvector map, 83
Equilibrium models, 3
Experimental measurement of CPMs, 91–114
Extent
see Reaction

Feasible designs
coupled column sections, 212, 214–216
definition, 136
distributed feed columns, 162–166, 170–171
fully thermally coupled column sections, 240–250
hybrid processes, 323–325
side rectifiers, 190–194
side strippers, 190–194
simple columns, 132–133, 145
Feed quality
effect on profile intersection, 135–137
liquid fraction of, 131, 197–198
Feed stage, 6
distributed feed columns, 159–162
fully thermally coupled columns, 218–219
simple columns, 130–131, 138–141, 151–153
Finite reflux
see Design
Flow patterns
Kaibel columns, 253–256
Petlyuk columns, 221–223
Flux
see Permeation modeling

Gibbs triangle,
see Mass balance triangle
Graphical design methods,
distillation line maps, 3
McCabe-Thiele, 3
residue curve maps, *see* Residue curve maps

Heat duty
in side rectifiers and side strippers, 203–205
Henry's Law, 7, 119
HETP, 51, 117
Hybrid membrane-distillation columns, 6, 314–325

Ideal systems
see Vapor-liquid equilibrium
Indirect split mass balance, 35
See also Infinite reflux columns
Infeasible designs
side rectifier, 193–194
simple columns, 133–134, 148
Infinite reflux, 33–35
column sequencing, 38–39, 135
fully thermally coupled columns at, 208–216

Infinite stages
  simple design (minimum reflux), 135, 146
Isotherms, 29–30, 71–72, 113–114
Intersection of column profiles
  see Column profiles (direction); Feasible designs

Kaibel columns
  see Thermally coupled columns

Liquid extraction
  see Solvent extraction
Liquid split ratio
  for fully thermally coupled columns, 218, 222–223, 230–234, 254–255, 257
  for side-stripper, 189, 199, 200–201
Liquid-liquid equilibrium, 103–104
Liquid-phase activity,
  see Activity coefficient

Mass balance triangle, 17–19, 40, 58, 73–74
McCabe-Thiele method
  see Graphical design methods
Membrane column, 298
Membrane column section
  see Column section
Membrane separation, 296–325
  separation process, 1, 297–298
  flux modeling, 301–303
Minimum reflux
  distributed feed columns, 173–175
  side rectifiers, 192, 193–199
  side strippers, 192, 193–199
  simple columns, 134–135, 137
  using eigenvectors, 153–154
  using transformed triangles, 145–153, 193–199
Mixing vector, 69, 70, 264–265, 267–269
Multiple feed columns
  see Distributed feed columns

Net flow, 52, 61–62, 128
  coupled columns, 187–190, 213, 218–223, 253–256
  membrane systems, 301, 303
  reactive systems, 277
  rectifying mode, 61, 130, 218
  stripping mode, 62, 130, 218
Nonequilibrium models, 3
  in negative space, 43–44
Nonideal systems
  column profile maps, 59–60, 71, 79, 86, 87
  distributed feed column design, 170–171
  reactive systems, 290–293
  residue curve maps, 23–24, 28–29, 41
  simple column design, 141–145
  See also Vapor-liquid equilibrium; Experimental measurement of CPMs

Parallel column sections, 208–216
Permeation modelling, 301–303
Petlyuk columns
  see Thermally coupled columns
Pinch points
  see Stationary points
Pinch point loci, 75–80, 144, 210, 274, 308–311, 314

Quaternary systems, 251–259

Raoult's Law, 8, 10, 132
Reaction, 1, 261
  equilibrium, 263, 266–267
  extent, 275–280, 281–285
  rate, 262–269, 273
  See also Reactive distillation
Reaction vector, 264–269
Reaction zone, 275, 285–286
Reactive azeotrope, 270
Reactive column profile maps
  see Column profile maps
Reactive column section, 276–280
  energy balance, 278
  See also Column section
Reactive distillation, 6, 261–295
Reactive residue curve maps, 267–275
Reboiler, 5
  partial, 138–139
Reboil ratio, 131
  relation to general reflux ratio, 131
Rectifying section, 49–50, 61, 63, 66, 73, 77–78
  experimental profiles of, 92–98, 103–105
Reflux
  see Reflux ratio

Reflux ratio
  definition, 5
  distributed feed columns, 159–160, 166, 169
  fully thermally coupled columns, 228–230
  generalized, 53, 66–67, 118, 125
  membrane systems, 307, 309–311, 312–314
  minimum, 5
  rectifying column sections, 66, 93, 96, 130
  side rectifiers, 187–190, 200–205
  side strippers, 187–190, 200–205
  sidestream withdrawal columns, 176–177
  simple columns, 131
  stripping column sections, 67, 130
  See also Finite reflux; Infinite reflux; Minimum reflux; Pinch point loci
Residue curve equation, 19–21
  derivation, 19–20
  membrane systems, 304
  reactive systems, 262–265, 273–275
Residue curve maps, 3, 15–47
  applications, 30–39, 80
  constant relative volatility systems, 21
  discontinuity, 43
  extending axes, 40–42
  limitations of, 39–40
  membrane systems, 304–306
  negative space, 43–46
  nonideal systems, 24
  numerical integration, 24
  plotting of, 21–25
  properties of, 25–30
  reactive systems, 262–275
  See also Batch boiling; Infinite reflux columns; Reactive residue curve maps; Residue curve equation; Total reflux columns

Saddle points
  see Stationary points
Separations
  processes, 1
Separation vector, 25, 68, 69–70, 264–265, 267–269
Sharp splits, 3, 88–89
  in distributed feed columns, 171–175
  in fully thermally coupled column sections, 240–250, 256–258
  in side rectifiers, 202–203
  in side strippers, 202–203
Side-draw columns, 6
  design of, 175–184
Side-draw stage
  fully thermally coupled columns, 219–220
Side rectifiers
  see Thermally coupled columns
Side strippers
  see Thermally coupled columns
Simple distillation columns, 2
  design of, 128–156
Solvent extraction, 1
Stable nodes
  see Stationary points
Stages
  determination of amount, 137–141, 151–153, 169–171
  See also Infinite stages
Stationary points, 26–29, 144–145
  classification, 80–83
  constant relative volatility systems, 27
  definition, 26, 70
  experimentally measured, 96, 97–98
  locked nodes, 270
  membrane systems, 311–312
  nature of, 83–84
  nonideal systems, 41, 144
  placement, 87–88
  reactive systems, 267–275
  See also Azeotrope; Pinch point loci; Transformed triangle
Strippers, 117
  design of, 124–128
Stripping section, 49–50, 61, 63, 67, 73, 77–78
  experimental profiles of, 98–103
Stoichiometric vector, 262–265, 281–285

Temperature inversion
  see Temperature profile
Temperature profile, 32
  experimental, 113–114
Ternary systems, 17, 62–63, 129
Thermally coupled columns, 6
  fully thermally coupled, 6–7, 206–260
  side-rectifiers, 6–7, 183–205
  side-strippers, 6–7, 183–205

Total reflux columns, 30–33
membrane systems, 304–306
Transformed tetrahedron, 252–259
Transformed triangle, 57–58, 72–75, 88–89, 124
coupled column sections, 211–216
design of distributed feed columns, 162–175
design of fully thermally coupled column sections, 240–250
design of side rectifiers, 200–205
design of side strippers, 200–205
minimum reflux design, 145–153, 193–199
reactive systems, 280, 285–290
See also Constant relative volatility systems; Difference point; Ideal systems; Minimum reflx; Reflux ratio; Stationary points

Underwood equations, 3
See also Minimum reflux; Reflux
Unstable nodes
see Stationary points

Vapor-liquid equilibrium, 7–12, 17, 119
constant relative volatility, 7–8, 21
ideal solutions, 7, 8–10, 24, 132
nonideal solutions, 7, 10–12, 24
Vapor pressure, 7, 9
Vapor split ratio
for fully thermally coupled columns, 218, 222–223, 254–255, 257
for side-stripper, 189, 190, 199, 201–202

Warped time
see Dimensionless time

x-y diagrams
see Binary systems